# Comportement biogéochimique d'antimoine (Sb) et de tellure (Te) dans le milieu côtier : vers des scénarios de dispersion des radionucléides de Sb et de Te en cas de rejets accidentels de centrales nucléaires (projet AMORAD, ANR-11-RSNR-0002)

Teba Gil-Díaz

▶ **To cite this version:**

Teba Gil-Díaz. Comportement biogéochimique d'antimoine (Sb) et de tellure (Te) dans le milieu côtier : vers des scénarios de dispersion des radionucléides de Sb et de Te en cas de rejets accidentels de centrales nucléaires (projet AMORAD, ANR-11-RSNR-0002). Géochimie. Université de Bordeaux, 2019. Français. NNT : 2019BORD0004 . tel-02275552

**HAL Id: tel-02275552**
**https://theses.hal.science/tel-02275552**

Submitted on 31 Aug 2019

**HAL** is a multi-disciplinary open access archive for the deposit and dissemination of scientific research documents, whether they are published or not. The documents may come from teaching and research institutions in France or abroad, or from public or private research centers.

L'archive ouverte pluridisciplinaire **HAL**, est destinée au dépôt et à la diffusion de documents scientifiques de niveau recherche, publiés ou non, émanant des établissements d'enseignement et de recherche français ou étrangers, des laboratoires publics ou privés.

université de BORDEAUX

# THÈSE

Présentée à

## L'UNIVERSITÉ DE BORDEAUX

École Doctorale Sciences et Environnements


## Par M$_{me}$ Teba GIL-DÍAZ


Pour obtenir le grade de

## DOCTEUR

Label de Doctorat Européen

Spécialité : Géochimie et Écotoxicologie

---

# Comportement biogéochimique d'antimoine (Sb) et de tellure (Te) dans le milieu côtier : vers des scénarios de dispersion des radionucléides de Sb et de Te en cas de rejets accidentels de centrales nucléaires

(PROJET AMORAD, ANR-11-RSNR-0002)

---

Soutenue le 11 Janvier 2019

Devant la commission d'examen formée de :

| | |
|---|---|
| M. Nestor Etxebarria, Professeur, Université du Pays Basque, Espagne | Rapporteur |
| M. Andrew Cundy, Professeur, Université de Southampton, UK | Rapporteur |
| Mme. Montserrat Filella, Enseignant-chercheur, Université de Genève, Suisse | Examinatrice |
| M. Thierry Corrège, Professeur, Université de Bordeaux | Président |
| Mme. Elisabeth Eiche, Enseignant-chercheur, KIT, Karlsruhe, Allemagne | Invitée |
| M. Jörg Schäfer, Professeur, Université de Bordeaux | Directeur |
| Mme. Frédérique Eyrolle, Chercheur HDR, IRSN Cadarache | Co-directrice |

**- 2019 -**

# Coastal biogeochemical behaviour of antimony (Sb) and tellurium (Te): an approach to Sb and Te radionuclide dispersal scenarios in case of accidental nuclear power plant releases

(AMORAD PROJECT, ANR-11-RSNR-0002)

Directed by:

Jörg Schäfer, Université de Bordeaux

Frédérique Eyrolle, IRSN Cadarache

**Coastal biogeochemical behaviour of antimony (Sb) and tellurium (Te): an approach to Sb and Te radionuclide dispersal scenarios in case of accidental nuclear power plant releases**

Antimony (Sb) and tellurium (Te) are relatively uncommon contaminants (stable isotopes) and may form short-lived fission products (radionuclides) released into the environment during nuclear power plants accidents. Little is known about their respective biogeochemical behaviours, necessary for general contamination studies and post-accidental radiological risk assessment.

This work provides original knowledge on Sb and Te biogeochemical behaviour in highly dynamic continent-ocean transition systems: the Gironde Estuary and the Rhône River. Concentrations, spatial/temporal variations, solid/liquid partitioning (Kd), and fluxes are studied from long-term records at the watershed scale. Four estuarine sampling campaigns during contrasting hydrological conditions show higher Sb solubility and Te particle affinity in the estuary than in the upstream fluvial reaches. Historical records (1984-2017) in wild oysters from the estuary mouth do not show clear trends of past or recent contamination, but measurable bioaccumulation suggests that potential uptake of radionuclides is likely to occur. Combined adsorption experiments using isotopically-labelled (spiked) Sb and Te, and subsequent selective extractions of carrier phases from suspended particulate matter (SPM) suggest that spiked Sb and Te are more mobile and potentially bioaccessible than their environmental (inherited) equivalents. Radiotracer adsorption experiments using environmentally representative concentrations of both Gironde and Rhône systems underpin that highly soluble elements may show contrasting reactivity between inherited and spiked forms.

Radionuclide dispersion will greatly depend on (i) the geographical position of the source (Rhône) and/or the maximum turbidity zone (MTZ; Gironde fluvial-estuarine system), (ii) the succession of hydrological situations during and after the accident, and (iii) the biogeochemical reactivity and half-lives of the radionuclides. First scenarios on hypothetical dissolved radionuclide dispersion in the Gironde Estuary suggest (i) low sorption of Sb to the SPM, implying a transport of radionuclides in dissolved phase towards the coast, and (ii) high retention of Te within the MTZ, especially for accidental releases during flood conditions, linking the fate of radioactive Te to long estuarine SPM residence times (1-2 years). Potential upstream migration of Te radionuclides in the MTZ towards the city of Bordeaux during the following summer season and Te decay into radioactive iodine warrants further evaluation of the associated potential radiotoxicity.

***Keywords:*** *antimony, tellurium, Gironde Estuary, solid/liquid partitioning (Kd), selective extractions*

**Comportement biogéochimique d'antimoine (Sb) et de tellure (Te) dans le milieu côtier : vers des scénarios de dispersion des radionucléides de Sb et de Te en cas de rejets accidentels de centrales nucléaires**

Antimoine (Sb) et tellure (Te), sont des contaminants peu étudiés (isotopes stables) et leurs radionucléides artificiels peuvent être rejetés dans le milieu aquatique lors des accidents nucléaires. La connaissance de leurs comportements biogéochimiques respectifs est nécessaire à l'évaluation du risque radiologique post-accidentel.

Ce travail présente des données originales sur le comportement biogéochimique de Sb et de Te dans les systèmes de transition continent-océan, tels que l'estuaire de la Gironde et la rivière du Rhône. Un suivi de 14 ans et des campagnes océanographiques dans le bassin versant de l'estuaire de la Gironde ont permis d'identifier des concentrations, des flux, et des réactivités (variabilités spatio-temporelles et distribution solide/liquide) plus élevés pour Sb que pour Te, mettant en évidence un comportement additif pour Sb et de soustraction pour Te le long des gradients de salinité et de turbidité estuariennes. Des expériences couplant l'adsorption d'isotopes marqués sur des matières en suspension (MES) et des extractions sélectives des phases porteuses, suggèrent que les formes apportées de Sb et de Te sont plus mobiles et potentiellement plus biodisponibles que leurs équivalents naturels. De plus, l'observation de la bioaccumulation non-négligeable de Sb et de Te naturels dans les huîtres sauvages à l'embouchure de l'estuaire permet d'envisager une absorption potentielle de leurs homologues radioactifs.

Ainsi, le développement de scenarios de dispersion de radionucléides rejetés dans les zones de transition dépendra (i) de la position géographique de la source (Rhône) et/ou de la zone de turbidité maximale (ZTM; système fluvio-estuarien de Gironde), (ii) de la situation hydrologique pendant et post accident, ainsi que (iii) de la réactivité biogéochimique et des temps de demi-vies des radionucléides. Les premiers scénarios de dispersion de radionucléides dans l'estuaire de la Gironde suggèrent (i) un transport préférentiel de Sb dissous vers la zone côtière, et (ii) une forte rétention de Te radioactif dans la ZTM si la dernière est présente en aval du site d'accident, impliquant le risque de migration saisonnière de la radioactivité vers la ville de Bordeaux pendant l'étiage suivant. Ainsi, la dynamique intra estuarienne (marée, débit et migration de la ZTM) sera le facteur prédominant dans le devenir de Te radioactif, depuis son rejet jusqu'à sa désintégration complète en iode radioactif. L'ensemble de ce travail met en évidence la nécessité d'une évaluation plus approfondie de la radiotoxicité potentielle de Sb et Te lors de leurs rejets en milieu aquatique.

***Mots clés :*** *antimoine, tellure, estuaire de la Gironde, partition solide/liquide (Kd), extractions sélectives*

This work is a scientific contribution to the French National Project AMORAD (ANR-11-RSNR-0002) from the National Research Agency, allocated in the framework programme “Investments for the Future”.

Partial funding by the ANR Programme TWINRIVERS (ANR-11-IS56-0003) and the FEDER Aquitaine-1999-Z0061 are greatly acknowledged. Support from “l’Agence de l’Eau Adour-Garonne” and the European Project SCHEMA (EU FP7-OCEAN 2013.2-Grant Agreement 614002) are also acknowledged.

This work has benefited from environmental samples (i) from the RNO/ROCCH oyster sample bank (Ifremer Centre Atlantique, Nantes), and (ii) from the IRSN mussel sample bank and SORA Station (Arles).

# Remerciements - Acknowledgements

J'ai le grand plaisir de faire un récapitulatif de toutes les personnes qui ont eu un rôle significatif, voire très important, au cours de ma thèse pour arriver aujourd'hui à avoir ce travail de trois ans de vie. Personnellement, c'est la meilleure trace écrite que j'aurai dans l'avenir pour déclencher ma joie et des larmes de nostalgie à chaque fois que j'y reviendrai pour me rappeler de toutes les belles expériences vécues et les personnes inoubliables de ces dernières années… car si on avance dans la science c'est parce qu'on n'est pas seul.

Tout d'abord, je voudrais remercier les membres de mon jury de thèse d'avoir accepté de corriger et d'évaluer ce travail. I am very grateful to Nestor ETXEBARRIA, Andrew CUNDY, Montserrat FILELLA and Thierry CORRÈGE for their availability and interest in reviewing this work.

Un grand merci à mes directeurs de thèse Jörg SCHÄFER et Frédérique EYROLLE-BOYER pour m'avoir donné ce sujet de thèse et le travail associé, qui avait déjà commencé pendant mon stage de master M2. Depuis ce temps et grâce à eux, j'ai eu énormément d'opportunités pour profiter de leur expertise en géochimie et radioactivité environnementale et beaucoup de plaisir à partager mes travaux sous leur direction dans plusieurs conférences et réunions du projet AMORAD. Je vous remercie d'avoir toujours cru en mes compétences, d'avoir partagé votre joie scientifique à chaque découverte le long du chemin et d'avoir toujours soutenu l'objectif de cette thèse malgré les adversités. Merci Jörg pour la liberté et le soutien scientifique, toujours présents.

Je voudrais remercier Alexandra COYNEL pour tous ses bonnes remarques et corrections dans les publications qu'on a en commun et surtout de m'avoir donné l'opportunité de commencer ma carrière dans le monde de l'enseignement pendant ma troisième année de thèse à plusieurs niveaux de l'éducation universitaire (licence et master). Surtout, merci de m'avoir transmis qu'en science et dans l'enseignement il faut toujours viser à bien faire les choses, et de m'avoir appris dès le début qu'une thèse « n'est pas un sprint mais un marathon » … merci d'avoir veillé au soutien financier des trois derniers bornes.

Je remercie Gérard BLANC pour sa bonne humeur et les sourires de chaque jour. On n'a pas eu l'opportunité de travailler beaucoup ensemble mais je vous remercie de m'avoir accepté et bien accueilli dans l'équipe pendant tout ce temps.

Merci beaucoup Fred FAURE-POUGNET pour un milliard de choses, entre lesquelles je garde précieusement : ta force en esprit (dans le personnel et professionnel), pour tous ces années au bureau, d'avoir partagé avec moi ta connaissance sur la dynamique de l'estuaire et le comportement du Cd et des butyl-Sn, de m'avoir permis d'échantillonner avec toi pendant MGTS 3, de m'avoir laissé analyser tous tes échantillons de MGTS en cherchant les comportements environnementaux de Sn, de

Sb, et de Te, de me transmettre comment toujours travailler en sécurité dans le labo et le terrain, et d'être là jusqu'à la fin…

Merci beaucoup Mélina ABDOU aussi pour plein de choses : d'être là pour m'aider à ne rien oublier et préparer les colis d'échantillons à chaque fois que je partais en stage en Allemagne, d'avoir partagé avec moi 5 campagnes océanographiques dans plusieurs endroits européens (avec la préparation du mathos et tout l'expertise inclus), d'avoir vécu les adversités environnementales implicites dans chaque mission (p.e. l'attaque d'une centaine d'insectes volants sur le bateau à 4h du matin !), d'avoir partagé aussi tes découvertes sur le comportement du Pt en milieu aquatique, d'avoir assisté à plus de 5 conférences ensemble, sans manquer $>10^5$ sourires et rigolades au cours de tous ces moments !!

Ne t'inquiètes pas Antoine LERAT, j'ai aussi beaucoup à te remercier ! Pour tous ces années de partage de bureau aussi, nous permettant d'avoir plusieurs discussions sur tous les sujets (sur la vie du labo, nos travaux, l'enseignement), toujours « scientifiquement pertinentes » bien sûr ! Merci d'avoir partagé avec moi tes joies et challenges avec le Gd, toujours enrichissants ! de m'avoir laissé afficher mes posters sur ta partie du mur :P et d'avoir veillé sur moi pendant les dernières mois de rédaction.

Je voudrais remercier Clément PERETO, pour son aide précieuse avec le traitement de données ICP-OES, les discussions scientifiques de bureau sur les transferts des métaux vers le biote, la dernière sortie Decaz en Août 2018, et les moments de détente au Carpe. A Mathilde MYKOLAZYCK et Ane REMENTERIA pour toutes leurs expertises en manipulation d'huîtres sauvages et l'assimilation en Cd et Ag. A Guia MORELLI pour son soutien moral et le travail sur les carottes estuariennes. A Stéphane AUDRY pour son aide indirect grâce à sa thèse au sein de l'équipe TGM sur les extractions sélectives en métaux classiques ainsi que de Sb et As.

A Lionel DUTRUCH et Cécile BOSSY, sans lesquels je n'aurai jamais su traiter les échantillons (attaques, acidifications), doser tous les éléments que j'ai étudié, utiliser tous les techniques analytiques (dilution gazeuse, iCAP), faire les bons *calcouls* de traitement de données, commander les bons matériaux de labo, faire une grande partie des missions Decaz, etc. Merci beaucoup d'avoir toujours répondu à absolument toutes mes questions de labo, en personne et par email, toujours avec des réponses « techniquement correctes » !

Merci Hervé DERRIENNIC, Marie BILLA et Eric MANEUX qui ont fait partie de ma vie quotidienne de labo. Je remercie aussi à mes stagiaires au cours des années : Linda, Thomas, Ruoyu, Khalil, Virginia, JB et Madhushri. Travailler avec vous a été souvent une expérience très stimulante, merci de votre aide et enthousiasme inépuisable pour le travail de labo.

I have a warm thanks to all the AGW KIT team that hosted me during the internship of my second year of PhD in Karlsruhe (Germany). Thank you Eli EICHE for integrating me so naturally in the team and for your resourcefulness in equipment and Se contacts. I will always recall your constant impulse, good advice and optimism despite the « challenging » water and sediment samples that I brought to you. After all, Se was indeed an « analytical chemist's nightmare » but we managed to advance and characterise its behaviour and concentrations in some of my sample matrices. I thank Markus LENZ for accepting the challenge to double-check Se and Te concentrations in the freshwater and some sediment-digested samples with his new triple-quad ICP-MS in Basel (Switzerland). I also thank very much Gesine PREUB and Claudia MÖBNER, for spending some time sharing their enthusiasm, working precision and knowledge on GF-AAS and ICP-MS at KIT. Thanks to Beate OETZEL for her help in milling and preparing the samples for ED-XRF and XRD measurements. Many thanks to Utz KRAMAR and Andreas HOLBACH for their guidance in ED-XRF world as well as Kirsten DRÜPPEL for her help in the XRD interpretations. Many thanks to Andrea FRIEDRICH for all her paperwork assistance, Gerhard OTT for connecting my French PC to the network and printers in the lab and to Ralf WACHTER for fixing every machine (microwave, stove, water tank) that gave problems. I also thank Alexandra NOTHSTEIN and Helena BANNING for their help in HG method and performance. My office and lunch-mates, Andrew THOMAS and Flavia DIGIACOMO, thanks for making me discover the Mensa and the AKK. From the personal point of view, I owe a big thanks to Sandra KLINGLER, Christine BRAUN, Eugen BLUM and the BURY's family for being so kind and helpful, for showing me new places in the region and for making my stay in Germany possible, enjoyable and unforgettable; Vielen Dank.

I also have a special thanks to Frank HEBERLING for giving me a second chance to come back to Karlsruhe during my last year of PhD to measure sorption kinetics of radioactive elements ($^{113}$Sn and $^{75}$Se) at the INE KIT in the Northern Campus. I'm very grateful for this opportunity and for all the advices on practical and theoretical knowledge about radioactive handling and decay. Thank you for always being positive, patient and willing to help. I would also like to thank Bernd BUMMEL and Andreas BAUER for all their help allowing me to getting started (and the bike!), as well as Melanie BÖTTLE and Markus FUSS for the gamma spectroscopy measurements and explanations on HPGe detectors. I greatly acknowledge Christian MARQUARDT for arranging all the paperwork for the $^{113}$Sn and $^{75}$Se stock solutions, Tanja KISELY for supplying the clothes and all labware every time I asked for it, David FELLHAUER for all the advices on good practices in the controlled-area, and a special thanks to Gerhard CHRISTILL for being patient when I had to sample near the closing time and allowing me to take pictures of my experimental setup. Many thanks to Frank BECKER for his help with radioactive decay chains and understanding of fission yields, and to all the team from INE (including all the PhD and master students: Fabian, Jurij, Nese, Nicoletta, Tims, ...) for their smiling Gütten Morgen and nice meals together every day.

Je remercie Franck GINER de l'IRSN pour l'effort d'échantillonnage à SORA et l'envoi des échantillons de MES du Rhône, toujours présent par email pour répondre à mes questions sur le Rhône et pour résoudre les défis de la poste concernant la réception des colis à Bordeaux. Je remercie également Sabine CHARMASSON de l'IRSN - Centre IFREMER de la Méditerranée pour l'envoi des échantillons de moules de la banque biologique de la Méditerranée, et surtout pour son soutien et bienveillance tout le long du projet AMORAD en tant que responsable scientifique de l'axe de recherche Marin.

Je remercie énormément Nicolas BRIANT, Teddy SIREAU et Jöel KNOERY du Centre Atlantique IFREMER d'avoir partagé avec nous les échantillons d'huîtres du suivi RNO/ROCCH. Merci beaucoup de m'avoir accueilli très chaleureusement pendant mon séjour de <24h à Nantes, de votre bienveillance pendant les minéralisations et merci pour les corrections apportées au travail final avec les résultats de Te.

Je tiens à remercier toutes les personnes que j'ai pu rencontrer et avec lesquels j'ai eu la chance de partager des journées enrichissantes pendant les missions terrain. Je pense particulièrement aux personnes du Projet SCHeMA (Mary-Lou, Abra, Silvia, Lukas, Marianna, Maria, Nadia, Miguel, Michaela, Francesco) et à celles du PiE à Plentzia (Ionan, Manu, Urtzi, Tifanie, …).

I thank the MER family (Fouzia, Pauline, Kiyo, Marina, Ankje, Tamer, Niko, Whollie) for always being there, on the other side of the screen during our skype group calls, ready to share and listen all our worldwide adventures no matter how early in the morning your local time slots had to be. I also thank my friends and flat mates (Arielle IKI, Chris BOEIJE, Alberto ADÁN, Luca PERUZZO, Irene TONELATO, Daniela ROSSO, Tamara MAURY and Corentin DETRE) for all the trips, games, movies, dinners and birthdays, every moment duly flavoured with good cider and many laughs.

Y ya que se están convirtiendo en unos agradecimientos internacionales no podía terminar de otra manera. A las chicas de CCMar (Marta, Nadia, Lourdes, Jesenia), porque a pesar de las vueltas que da la vida, el tiempo no pasa para nosotras. A Sele y Óscar, por apuntar en el calendario todas las fechas en las que vuelvo a casa. A Aída, Fernando y mis padres, porque sin vuestro apoyo y confianza no habría llegado hasta aquí.

A todos, gracias.

*“The misconceptions about the effects of radiation and the psychological effect of not understanding the risks are far greater than the radiation risk itself”*

*Prof. Gerry Thomas (Imperial College)*

# Table of contents


## GENERAL INTRODUCTION

**I. CONTEXT ..... 1**

1. **WORLDWIDE ENERGY DEMAND: THE REASON FOR NUCLEAR ENERGY PRODUCTION** ..... 1
2. **EUROPEAN CONCERN ON THE NUCLEAR ENERGY INDUSTRY: A FOCUS ON RADIOECOLOGY** ..... 4

**II. THE RESEARCH QUESTION ..... 6**

1. **NUCLEAR ENERGY IN FRANCE: CURRENT STATUS AND FUTURE PLANS** ..... 6
2. **IMPROVED FRENCH APPROACH TO POST-ACCIDENTAL MANAGEMENT: THE AMORAD PROJECT** ..... 7

**III. THESIS OBJECTIVES AND CHAPTER DISTRIBUTION ..... 12**

## CHAPTER 1: SCIENTIFIC CONTEXT

**I. INTRODUCTION ..... 16**

**II. ISOTOPES AND RADIOACTIVITY ..... 17**

1. **ATOMIC DEFINITIONS, ELEMENTAL ABUNDANCE AND ISOTOPE STABILITY** ..... 17
2. **DECAY MODES** ..... 20
3. **ENERGY AND RADIOACTIVITY UNITS** ..... 22
4. **EXPOSURE TO RADIATION AND BIOLOGICAL IMPLICATIONS** ..... 22

**III. RADIONUCLIDES FROM NUCLEAR POWER PLANTS (NPP) ..... 26**

1. **NUCLEAR FISSION PRINCIPLES AND NPP ELECTRICITY PRODUCTION** ..... 26
2. **CAUSES OF PAST NPP ACCIDENTAL EVENTS** ..... 28
3. **EXAMPLES OF NPP INCIDENTS IN FRANCE** ..... 30
4. **ENVIRONMENTAL LESSONS FROM PAST NPP ACCIDENTAL EVENTS: CASE OF CS IN AQUATIC SYSTEMS** ..... 31

**IV. RADIOACTIVE AND STABLE ISOTOPES OF ANTIMONY AND TELLURIUM ..... 34**

1. **RADIOACTIVE ANTIMONY (SB) AND TELLURIUM (TE)** ..... 34
   1.1. Radionuclides of Sb and Te in NPPs ..... 34
   1.2. Knowledge on Sb and Te radionuclide environmental releases ..... 35
   - Radioactive Sb ..... 35
   - Radioactive Te ..... 37

   1.3. Antimony and tellurium radioactive decay chains ..... 39
2. **STABLE ANTIMONY (SB) AND TELLURIUM (TE)** ..... 44
   2.1. Sources, applications, chemical properties, concentrations and toxicity of stable Sb ..... 45
   2.1.1. Anthropogenic sources and applications ..... 45
   2.1.2. Environmental speciation and redox dynamics ..... 47
   2.1.3. Environmental concentrations and biogeochemical behaviour ..... 60
   2.1.4. Biological uptake and toxicity ..... 71
   2.2. Sources, applications, chemical properties, concentrations and toxicity of stable Te ..... 72
   2.2.1. Anthropogenic sources and applications ..... 72
   2.2.2. Environmental speciation and redox dynamics ..... 76
   2.2.3. Environmental concentrations and biogeochemical behaviour ..... 78
   2.2.4. Biological uptake and toxicity ..... 80

**V. CONCLUSION ..... 82**

# CHAPTER 2: MATERIALS AND METHODS


**I. INTRODUCTION ..... 83**

**II. AREAS OF STUDY AND SAMPLING SITES ..... 84**

1. **AREAS OF STUDY** ..... 84
   1.1. The Lot-Garonne-Gironde fluvial estuarine system ..... 84
      1.1.1. The Lot River watershed ..... 85
      1.1.2. The Gironde Estuary ..... 86
      1.1.3. Nuclear power plants ..... 88
   1.2. The Rhône River ..... 90
      1.2.1. Nuclear power plants ..... 91
2. **ENVIRONMENTAL MONITORING: FLUVIAL AND ESTUARINE SAMPLING SITES** ..... 92
3. **SPORADIC SAMPLING: COLLECTION OF SPECIFIC ENVIRONMENTAL MATRICES** ..... 94

**III. SAMPLING STRATEGIES ..... 96**

1. **LABWARE PRE-CONDITIONING, SAMPLED PHASES AND FIELD WORK APPROACH** ..... 96
2. **RIVER DISCHARGES, SPM CONCENTRATIONS AND PHYSICAL-CHEMICAL PARAMETERS** ..... 100
3. **COLLECTION OF WATER AND SPM SAMPLES** ..... 100
4. **COLLECTION OF BIOLOGICAL SAMPLES** ..... 101

**IV. EXPERIMENTAL DESIGNS ..... 102**

1. **ISOTOPICALLY-LABELLED KINETIC EXPERIMENTS** ..... 102
   1.1. Adsorption kinetics and isotherms of stable $^{125}$Te and $^{77}$Se ..... 102
   1.2. Adsorption/desorption kinetics of $^{75}$Se and $^{113}$Sn radiotracers ..... 104
2. **ADSORPTION OF ISOTOPICALLY-LABELLED SPIKES FOR PARALLEL SELECTIVE EXTRACTIONS** ..... 107

**V. SAMPLE PRE-TREATMENT ..... 108**

1. **SAMPLE DRYING** ..... 108
   1.1. Sediments ..... 108
   1.2. Biological materials ..... 108
2. **BULK SEDIMENT MINERALOGY PREPARATIONS** ..... 109
3. **DIGESTIONS AND SELECTIVE EXTRACTIONS OF SEDIMENTS** ..... 110
4. **DIGESTIONS OF BIOLOGICAL MATRICES** ..... 114

**VI. ANALYTICAL METHODS ..... 117**

1. **BULK MINERALOGY** ..... 117
   1.1. Principle of X-Ray Powder Diffraction (XRD) analysis ..... 117
2. **ANALYSES OF STABLE TRACE ELEMENT CONCENTRATIONS** ..... 118
   2.1. Principle of mass spectrometry (ICP-MS) ..... 118
   2.2. Single vs triple quadrupole ICP-MS performance ..... 120
   2.3. Quantification methods ..... 124
      2.3.1. External calibration ..... 124
      2.3.2. Isotopic dilution (ID) ..... 126
   2.4. Analytical quality control ..... 127
   2.5. Applied analyses for Sb, Te and Se quantification ..... 128
3. **ANALYSES OF RADIONUCLIDE ACTIVITIES** ..... 130
   3.1. Principle of gamma-ray spectroscopy ..... 130
   3.2. High Purity Germanium detectors ..... 131
   3.3. Quantification of $^{113}$Sn and $^{75}$Se ..... 133

**VII. DATA TREATMENT ..... 134**

1. **STATISTICAL APPROACH** ..... 134
   1.1. Temporal series: trends and seasonal components ..... 134
   1.2. Dissolved and particulate annual fluxes ..... 135
2. **TRACE ELEMENT SOLID/LIQUID EQUILIBRIUMS** ..... 138
   2.1. Sorption isotherms ..... 138
   2.2. Solid/liquid partition coefficient (Kd) ..... 140
3. **ENRICHMENT FACTORS** ..... 142
   3.1. Geoaccumulation index (I'geo) ..... 142
   3.2. Bioaccumulation factor (BAF) ..... 143

**VIII. CONCLUSION ..... 145**

## CHAPTER 3: Biogeochemical behaviour of antimony in the Lot-Garonne-Gironde fluvial estuarine system

**I. INTRODUCTION ..... 146**

1. **BIOGEOCHEMICAL BEHAVIOUR OF ANTIMONY IN THE FRESHWATER DOMAIN OF THE GIRONDE ESTUARY.** . 148
2. **BIOGEOCHEMICAL BEHAVIOUR OF ANTIMONY IN THE SALINITY AND TURBIDITY GRADIENT OF THE GIRONDE ESTUARY.** ..... 182

**II. CONCLUSION ..... 208**

## CHAPTER 4: Particulate carrier phases of Sb, a fractionation approach

**I. INTRODUCTION ..... 210**

1. **SELECTIVE EXTRACTION METHODS** ..... 211
   1.1. Origin and evolution of most known selective extraction methods ..... 211
   1.2. Important known modes of action of reducible (Fe/Mn oxide) fraction methods ..... 218
   1.3. Parallel selective extractions and total digestions: overview of bulk sediment carrier phases ..... 222
2. **PARALLEL SELECTIVE EXTRACTIONS ON PARTICULATE ANTIMONY** ..... 225

**II. CONCLUSION ..... 245**

## CHAPTER 5: Biogeochemical behaviour of tellurium in the Lot-Garonne-Gironde fluvial estuarine system

**I. INTRODUCTION ..... 247**

1. **BIOGEOCHEMICAL BEHAVIOUR OF TELLURIUM IN THE FRESHWATER DOMAIN OF THE GIRONDE WATERSHED**.... ..... 248
2. **BIOGEOCHEMICAL BEHAVIOUR OF TELLURIUM IN THE SALINITY AND TURBIDITY GRADIENT OF THE GIRONDE ESTUARY** ..... 277

**II. CONCLUSION ..... 300**

## CHAPTER 6: Trace element reactivity of Sn and Se in contrasting fluvial-estuarine systems – a comparative approach between the Gironde Estuary and the Rhône River


**I. INTRODUCTION ..... 302**

1. **REACTIVITY OF TIN AND SELENIUM RADIONUCLIDES WITH PARTICLES FROM THE GIRONDE AND RHÔNE FLUVIAL-ESTUARINE SYSTEMS IN SIMULATED CONTRASTING ESTUARINE CONDITIONS** ..... 303
2. **TRANSFER OF SN AND SE TO WILD LIVING BIVALVES** ..... 322
   2.1. Bioaccumulation in wild oysters and mussels ..... 322
   2.2. Organotropism in wild oysters from the Gironde Estuary ..... 325

**II. CONCLUSION ..... 327**


## DISCUSSION


**I. FUNDAMENTAL PARAMETERS FOR RADIONUCLIDE DISPERSION SCENARIOS ..... 328**

1. **INHERITED VS SPIKED SOLID/LIQUID PARTITIONING (KD)** ..... 328
2. **TEMPORAL COUPLING BETWEEN RADIONUCLIDE DECAY TIME SCALES AND HYDROLOGICAL PROCESSES** ..... 329

**II. MULTI-ELEMENT RADIONUCLIDE DISPERSION SCENARIOS IN THE GIRONDE ESTUARY ..... 333**


## GENERAL CONCLUSIONS AND PERSPECTIVES


**I. GENERAL CONCLUSIONS ..... 344**

**II. PERSPECTIVES ..... 350**


## RESUME ETENDU


**..... 355**


## REFERENCES


**..... 364**


## SCIENTIFIC PRODUCTION


**..... 393**

# List of figures

## GENERAL INTRODUCTION

***Figure 1. Worldwide largest electricity end uses*** *(Australia, Austria, Canada, Czech Republic, Finland, France, Germany, Greece, Ireland, Italy, Japan, Korea, New Zealand, the Netherlands, Spain, Sweden, Switzerland, the United Kingdom and the United States). Other industries include agriculture, mining and construction. Passenger cars include cars, sport utility vehicles and personal trucks (IEA 2017).* ..... 1
***Figure 2. Worldwide statistics on: (a) electricity generation by fuel type (1971-2015), (b) source shares of electricity generation (1973 and 2015 as examples), (c) nuclear electricity production by region (1971-2015), and (d) outlook to 2040's total primary energy supply by fuel type and socio-economic predicted scenario.*** *Countries are classified according to their attachment to the Organisation for Economic Co-operation and Development (OECD; IEA 2017).*..... 2
***Figure 3. Spatio-temporal phases after a nuclear incident/accident.*** *(Modified from IRSN 2014).*..... 5
***Figure 4. French Nuclear Power Plant (NPP) network.*** *Range of operating starting year for all reactors per NPP (brackets). Legend shows reactor differences by energy generating capacity (Megawatts electric, MWe) and reactor characteristics: single wall lined reactor with steel sealing skin (CP0 and CPY, red), double concrete reinforcement for accident prevention (P4 and P'4, yellow), compact steam generator with higher reliance on computer software (N4, blue), and new generation reactor under construction (EPR, pink). (Modified from ANS 2016).* ..... 6
***Figure 5. Post-accidental approach to evaluating the radiological risk and dosimetry consequences of a nuclear accident in the environment (left) together with the role of the AMORAD project in such approach (right).*** *The central question of the AMORAD project (in quotes) and the two main research domains including (i) environmental interfaces (MARIN, CONTI, ATMO), and (ii) consequences on the biosphere (ECOTOX), are also shown*..... 10

## CHAPTER 1: SCIENTIFIC CONTEXT

***Figure 6. Binding energy as a function of mass number****, showing the three main regions determining nuclear stability, indicating which elements are used in nuclear fission and which in nuclear fusion processes. (Adapted from UiO Chemical Institute).*..... 18
***Figure 7. Segré Diagram Chart of radionuclides.*** *(Sonzogni et al. 2013).*..... 19
***Figure 8. Main environmental pathways of human radiation exposure*** *(IAEA 1991).* ..... 25
***Figure 9. Smoothed probability distribution of fission products produced from $^{233}U$, $^{235}U$ and $^{239}Pu$ thermal neutron induced fission*** *(Adapted from Seaborg and Loveland 1990).* ..... 26
***Figure 10. General scheme of a Pressurised-Water Reactor (PWR) in a NPP*** *(Miller 2012)* ..... 27
***Figure 11. International Nuclear and Radiological Event Scale, INES*** *(IAEA 2017).*..... 28
***Figure 12. Summary of breakdown declared incidents in French NPPs in the year 2005*** *concerning (a) safety and (b) environmental incidents, classified according to main cause. (ASN Annual Report).*..... 31
***Figure 13. Decay chains of Sb and Te radionuclides.*** *Information on corresponding half-lives (below each isotope $^{A}X$), decay modes (electron capture-EC, beta decay-$\beta^-$, isomeric transitions-IT), decay direction (red arrows), decay probability (from 0 to 1) and independent fission yields (FY) for $^{235}U$/$^{239}Pu$ fuels (above each isotope $^{A}X$) are given. Metastable nuclides (in orange) and respective half-lives are also shown when appropriate, not specifying their probability of being formed. Empty arrows on the right (blue) denote the decay lines containing the most followed-up Sb and Te radionuclides after NPP accidental events. (The above decay chains have been assembled using available data from Element Collection Inc., and Sonzogni 2013).* ..... 43
***Figure 14. Schematic example of environmental compartments considered in geochemical cycling models.*** *Global biogeochemical cycles of trace elements consider several main reservoirs (in capital letters) interacting by fluxes (arrows). Estuaries are highlighted in a red box (Austin and Millward 1967).* ..... 44
***Figure 15. Atmospheric Sb trends by sectors*** *(Tian et al. 2014)*..... 46
***Figure 16. Worldwide Sb production*** *between 1900 and 2015 (Mlynarski 1998).*..... 46
***Figure 17. Common environmental chemical species of Sb.*** *(Modified from Herath et al. 2017)*..... 48

***Figure 18. Eh-pH (Pourbaix) diagram of aqueous speciation of Sb**. Modelling conditions include concentrations of total dissolved Sb of $10^{-9}$ mol $L^{-1}$ at 25ºC, showing with shaded areas the exceeding solubility of Sb relevant solids (Krupka and Serne 2002).* ..... 50
***Figure 19. Separation of metal ions and metalloid ions (As(III) and Sb(III)) into Pearson's modified classification**: class A, borderline and class B. This classification is based on indices where $\chi_m$ is the metal-ion electronegativity (Pauling's units), r is the ionic radius (crystal IR in angstrom units) and Z its formal charge. Specified oxidation states of Pb, As, Sb and Sn imply that simple cations do not exist even in acidic aqueous solutions. Elements of interest for this work have been highlighted (red). Tellurium (IV) has been added to the original image. (Modified from Nieboer and Richardson 1980).* ..... 52
***Figure 20. Antimony dissolved** (µg $L^{-1}$, 0.45 µm filtered, N = 807; a) **and particulate** (mg $kg^{-1}$, <63 µm grain-size, N = 848; b) **concentrations in European streams** sampled between 1998 and 2001 and analyzed between 1999 and 2003 (Salminen et al. 2005).* ..... 61
***Figure 21. Worldwide Sb dissolved concentrations** (ng $L^{-1}$) analysed since 1980's to 2000 for several rivers, groundwater and tap water samples (data compilation from Filella et al. 2002a) distributed by countries: Canada (CA), United States (US), Amazon River (Amazon), United Kingdom (UK), Sweden (SE), Netherlands (NL), Germany (DE), France (FR), Portugal (PT), Spain (ES), Poland (PO), Japan (JP) and other Asian countries (Taiwan, Indonesia, etc.). Published worldwide average freshwater concentration ranges (shaded in grey area). Noteworthy the change in scale to distinguish concentrations from highly polluted sites (a) and natural concentrations (b). Most commonly observed dissolved Sb estuarine behaviours along the salinity gradient (c) are also shown for the Tamar Estuary (UK; van den Berg et al. 1991), the Tama Estuary (JP; Byrd 1990), the Scheldt Estuary (NL; van der Sloot et al. 1985), the Tagus Estuary (PT; Andreae et al. 1983) and the St. Mary's Estuary (US; Byrd 1990). Surface seawater endmember (sw; Filella et al. 2002a) is also depicted at a random salinity of S = 40.* ..... 62
***Figure 22: Surface seawater total dissolved Sb concentrations published between 1960 and 2000**. Average and standard deviation deduced for the last 15 years is also shown (Filella et al. 2002a).* ..... 70
***Figure 23. Worldwide Te production** (t $y^{-1}$) between 1900 and 2015 (Mlynarski 1998).* ..... 73
***Figure 24.** Periodic Table highlighting assigned **Technology Critical Elements** (red)**.** Tellurium is denoted by a black square. (Modified from Cobelo-García et al. 2015).* ..... 74
***Figure 25. Common environmental chemical species of Te** (compilation from Belzile and Chen 2015, Wang 2011 and references therein. Humble Te speciation in aqueous media adapted from Brookins 1988).* ..... 77
***Figure 26. Eh-pH (Pourbaix) diagram of aqueous speciation of Te**. Modelling conditions include concentrations of total dissolved Te of $10^{-6}$ mol $L^{-1}$ at 25ºC (Lombi and Holm 2010).* ..... 78
***Figure 27. Environmental concentrations of dissolved Te** in (a) European streams sampled between 1998 and 2001 and analysed between 1999 and 2003 (µg $L^{-1}$, 0.45 µm filtered, N = 807; Salminen et al. 2005), and (b) in surface seawater between 1980 and 2010 (ng $L^{-1}$), with (c) a zoom in box for data <1 ng $L^{-1}$ before 1990 (Modified from Filella 2013).* ..... 79
***Figure 28. Dissolved Te reactivity along salinity gradients** of the Scheldt Estuary (total Te; van der Sloot et al. 1985) and the Changjiang River Estuary (speciation; modified from Wu et al. 2014).* ..... 80

## CHAPTER 2: MATERIALS AND METHODS

***Figure 29. The Lot-Garonne-Gironde fluvial estuarine system.** Rock composition along the watershed is denoted by the colour code legend (Adapted from BRGM 2014). Information on the location of the upstream historical industrial site (industrial icon), the city of Bordeaux (black circle) constituting the kilometric point zero, the assigned estuarine kilometric points (KP) and the two nuclear power plants in the area (Blayais and Golfech) are also shown.* ..... 84
***Figure 30. Water discharge trend (1959-2017) in the Garonne and Dordogne Rivers**. (Adapted from DIREN) .* 85
***Figure 31. Natural lithology and presence of anthropogenic tailings in the Riou Mort River watershed.** Location of the historical industrial activities in Decazeville area is also presented (adapted from Coynel et al. 2007a)...* 86
***Figure 32. Vertical turbidity gradient of the maximum turbidity zone (MTZ) in the water column of the Gironde Estuary.** SPM: suspended particulate matter. (Modified from Audry et al. 2006, after Abril et al. 1999 and Robert et al. 2004).* ..... 87
***Figure 33. Golfech and Blayais NPPs in the Garonne-Gironde fluvial estuarine system.*** ..... 88
***Figure 34. Sources and associated events causing potential flooding of the Blayais NPP.** Failure of NPP structures (red crosses) and water overflowing into the NPP (arrows) are depicted (IRSN View-point Report 2007).* ..... 89

***Figure 35. The Rhône River system.*** *Major cities (black squares), monitoring sites (black circle) and nuclear facilities (power plants and fuel reprocessing plant) are shown. Rock composition along the watershed is denoted by the colour code legend (Adapted from Ollivier et al. 2010).* ..... 90
***Figure 36. Current NPPs in the Rhône River watershed.*** ..... 91
***Figure 37. Diagram of a steam generator of a PWR.*** *The effect of tube plate clogging is also represented. (Adapted from IRSN View-point Report 2007 and Yang et al. 2017).* ..... 92
***Figure 38. Sampling sites in the Lot-Garonne-Gironde fluvial estuarine system.*** *Sampling sites are shown for the long-term monitoring programmes in the (i) upstream Lot-Garonne watershed (white squares), and (ii) estuary mouth (star), as well as for historical sediment records from hydroelectric reservoir lakes in Cajarc and Marcenac (black rectangles), sporadic samplings in Portets and Arcachon (black triangles) and from oceanographic campaigns (white and black crosses).* ..... 93
***Figure 39. Size distribution of particles and colloidal compounds in aquatic environmental samples.*** *(Adapted from Buffle and Van Leeuwen 1992).* ..... 97
***Figure 40. Diagram of sampling sites and sample collection in the Lot-Garonne-Gironde fluvial estuarine system.*** ..... 99
***Figure 41. Materials for measuring SPM concentrations and physical-chemical parameters.*** *(a) Filtration unit and pump, (b) dried filters showing contrasting SPM loads from different monitoring sites, and (c) in situ quantification of physical chemical parameters.* ..... 100
***Figure 42. Example of (a) fluvial water and SPM collection, (b) water collection in the Gironde Estuary and (c) on board water sampling and storage.*** ..... 101
***Figure 43. Summary of preparation steps for Te and Se isotopically-labelled adsorption kinetic and isotherm experiments****. (a-b) Matrix preconditioning, (c) spike equilibration, (d) experimental mixtures, (e) temporal sampling.* ..... 103
***Figure 44. Fume hood radiotracer experimental conditions.*** *(a) experimental disposition and (b) sample collection.* ..... 105
***Figure 45. Experimental design for Se and Sn adsorption kinetics in contrasting estuarine conditions representing the Gironde Estuary and the Rhône River systems.*** ..... 106
***Figure 46. Preparation of wet SPM isotopically-labelled spikes for parallel selective extractions.*** ..... 107
***Figure 47. Preparations for mineralogical analysis.*** *Suspended particulate matter from the Garonne-Gironde fluvial estuarine system (light brown) and the Rhône River (dark brown).* ..... 109
***Figure 48. Hotplate total extraction protocol for sediment digestions****. Described and validated for fluvial sediments and SPM in Schäfer et al. (2002).* ..... 111
***Figure 49. Required materials for microwave-assisted digestions.*** *(a) direct sample weighing, (b) teflon vessels and (c) microwave START 1500 (MLS GmbH).* ..... 112
***Figure 50. Protocols of applied parallel selective extractions*** *(described in Audry et al. 2006).* ..... 113
***Figure 51. Example of selective extraction slurries and blanks after (a) ascorbate and (b) HCl extractions.*** . 114
***Figure 52. Scheme of applied mussel sample pre-treatment steps before analysis.*** ..... 115
***Figure 53. Principle of X-Ray Powder Diffraction (XRD) measurements.*** *(a) Bragg's law and simplistic model, (b) XRD Bruker D8 DISCOVER instrument, and (c) example of a polycrystalline diffractogram. Abbreviations: normal plane [hkl], diffraction vector s, incident angle (ω) and diffraction angle (2ϑ). (Speakman, MIT).* ..... 117
***Figure 54. Principle of single quadrupole ICP-MS technique.*** *("An overview of ICP-MS" in dnr.wi.gov)*..... 119
***Figure 55. ICP-MS Thermo Fisher Scientific®.*** *(a,b) Single quadrupole ICP-MS X-Series 2 and (c,d) triple quadrupole ICP-MS iCAP TQ.* ..... 120
***Figure 56. Analysing modes for single and triple quadrupole ICP-MS.*** *(Adapted from Kate Jones www.slideshare.net/KateJones7/142-wahlen).* ..... 123
***Figure 57. Methodology used to determine $Sb_{ex}$ and $Sb_{nat}$ concentrations from BATCH sediment samples.*** . 125
***Figure 58. Principle of isotopic dilution (ID)*** *(adapted from Castelle 2008)..* ..... 126
***Figure 59. Analytical scheme to quantify Sb, Te and Se in several environmental samples.*** *Acronyms: QQQ-ICP-MS (triple-quadrupole ICP-MS), ID (isotopic dilution), CRM (certified reference material), LOD (limit of detection).* ..... 129
***Figure 60. The electromagnetic spectrum.*** ..... 130
***Figure 61. Diagram of main interactions between gamma-rays and matter*** *(left): photoelectric absorption, Compton scattering, and pair production. The importance of the three interactions according to the photon energy (from the gamma emission) and the atomic number of the interacting element (constituting the matter in the detector) are shown (right). Lines show cases where there is equal probability of showing boundary interaction properties. (Rizzi et al. 2010).* ..... 131

***Figure 62. Diagram of a HPGe detector.*** *(www.radek.ru and Saegusa et al. 2000)* ..... 132
***Figure 63. Graphical representation of mathematical breakdown of temporal series.*** *(Modified from Esparza Catalán).* ..... 135
***Figure 64. Maximum error percentages for simulated SPM annual fluxes (1994 to 2002) in the Garonne River (G) as a function of sampling frequency (log scale).*** *$F_{ref}$ is the annual SPM reference flux calculated from hourly-based sampling frequencies. (Modified from Coynel et al. 2004).* ..... 136
***Figure 65. Total annual fluxes of Sb and Te metalloids in the Lot-Garonne River system.*** *(a) Sb (2003-2016) and (b) Te (2014-2017).* ..... 138
***Figure 66. Examples of Langmuir isotherms.*** *Modified from (a) Sorption.ppt (University of Vermont) and (b) Weber and Chakravorti (1974).* ..... 139
***Figure 67. Example of Freundlich isotherms.*** *(Modified from Sorption.ppt, University of Vermont)* ..... 140
***Figure 68. Solid/liquid partition coefficient or distribution coefficient (Kd).*** ..... 141
***Figure 69. Terminology of trace element transfer from particles and water into organisms.*** ..... 144

## CHAPTER 4: Particulate carrier phases of Sb, a fractionation approach

***Figure 70. Known modes of action of acid-based (a), oxalate-based (b,c,d) and ascorbate-based solutions (e) in selective extractions.*** *The oxalate solution shows different responses if the extraction is performed in the presence of Fe(II) minerals (b), with light (c) or in the dark (d). (Adapted from Stumm and Sulzberger 1992).* ..... 220
***Figure 71. Overview of mechanisms of oxidative and anaerobic degradation of ascorbic acid.*** *Structures with bold lines represent primary sources of vitamin C. Abbreviations: fully protonated ascorbic acid ($AH_2$), ascorbate monoanion ($AH^-$), semidehydroascorbate radical ($AH^\bullet$), dehydroascorbic acid (A), 2-furonic acid (FA), 2-furaldehyde (F), 2,3-diketo-l-gulonic acid (DKG), 3-deoxypentosone (DP), xylosone (X), metal catalyst ($M^{n+}$), perhydroxyl radical ($HO_2$). (Fennema 1996).* ..... 222

## CHAPTER 6: Trace element reactivity of Sn and Se in contrasting fluvial-estuarine systems – a comparative approach between the Gironde Estuary and the Rhône River

***Figure 72. Sampling sites used for comparison between Cs, Sn and Se bioaccumulation in wild organisms:*** *two sites in the Atlantic Ocean (La Fosse in the Gironde Estuary mouth and Comprian in the Arcachon Bay) and two sites in the Mediterranean Sea (St. Maries de la Mer in the Petit Rhône River mouth and Faraman in the Grand Rhône River mouth). Condition indexes (CI) are also given.* ..... 322
***Figure 73. Identification of oyster organs in a sample of Crassostrea gigas.*** ..... 325
***Figure 74. Organotropism of Cs, Sn and Se.*** *Trace metal content in organs (gills, digestive gland, mantle and muscle) from a pool of wild oysters (N=5) from La Fosse (Gironde Estuary mouth, April 2014). Percentages indicate the relative contribution of each fraction to total metal content.* ..... 326
***Figure 75. Sb-Te radionuclide persistence after an instantaneous emission (t=0) up to ~1 year forecast from $^{235}U$ in NPPs.*** *Each panel is a zoom of the lower scale of the previous graph. Radionuclides generally followed after NPP accidents are marked in red boxes. Hydrologically relevant time scales such as tidal semi-diurnal variability (top) or general 3-month seasonal variations (yellow-pink degraded background shading) are also shown.* ... 331
***Figure 76. Diagrams of proposed scenarios for accidental releases in low discharge conditions (Scenario A).*** *Each panel represents (from top to bottom) foreseen situations (i) during the first 5h, (ii) for the following dry/wet season, and (iii) one year after the accidental release.* ..... 340
***Figure 77. Diagrams of proposed scenarios for accidental releases in high discharge conditions (Scenario B).*** *Each panel represents (from top to bottom) foreseen situations (i) during the first 5h, (ii) for the following dry/wet season, and (iii) one year after the accidental release.* ..... 341

# List of tables

## GENERAL INTRODUCTION

***Table 1. Worldwide 2015 statistics for global nuclear energy production (left) and relevance in domestic application (right) per country*** *(IEA 2017).* ..... 3
***Table 2. Worldwide 2015 electricity net exporter and importer countries*** *(IEA 2017).* ..... 4

## CHAPTER 1: SCIENTIFIC CONTEXT

***Table 3. Characteristics of the subatomic particles constituting elements in the physical universe.*** ..... 17
***Table 4. Common modes of nuclear decay*** *(Averill and Eldredge 2012).* ..... 20
***Table 5. Examples of $^{238}U$, $^{235}U$ and $^{232}Th$ natural decay chains****, showing associated daughter radionuclides and corresponding half-lives. Colours represent particle reactivity (for more information see Ah and Car 2016).* ..... 22
***Table 6. Public exposure to natural radiation*** *(WNA 2018)* ..... 23
***Table 7. Comparative whole-body radiation doses and observed effects*** *(WNA 2018)* ..... 23
***Table 8. Nuclear power plants in commercial operation*** *(WNA 2018)* ..... 28
***Table 9. Examples of activity levels emitted to the atmosphere and ocean after Chernobyl (CNPP) and Fukushima Daiichi (FDNPP) nuclear power plant accidents.*** *Elements of interest for this work are highlighted (red). *1PBq = $10^{15}$ Bq* ..... 32
***Table 10. Class A/B and borderline metal-binding ligands encountered in biological systems*** *(upper table)* ***and specific amino acid functional groups*** *(bottom table). Symbol R represents any alkyl radical (e.g., $CH_3$- ) or aromatic moiety (e.g., phenyl ring). Class A metal ions bind preferentially to ligands in column I, class B to ligands in III and some in II but borderline metals can interact with all types of ligands. (Nieboer and Richardson 1980).* ..... 53
***Table 11. Examples of redox reactions involved in natural diagenetic systems including Sb species (red)****. Reactions are presented in preferential order concerning energy consumption. (Modified from Wilson et al. 2010)* ..... 57
***Table 12: Advantages and disadvantages of selective extraction methods in sequential vs parallel protocols*** ..... 59
***Table 13. Some examples of Sb behaviour in worldwide estuaries****. Both dissolved ($Sb_d$) trend and particulate ($Sb_p$) descriptions are shown when available from the same study* ..... 64
***Table 14. Criteria for distinguishing clay minerals.*** *(Nelson 2014)* ..... 110
***Table 15. Biological concentrations (µg $kg^{-1}$) of Te, Sb and Se in wild mussels (Mytilus galloprovincialis) from Arriluze (N=20).*** *Errors correspond to standard deviations (SD). Abbreviations: Limit of Detection (LOD).* ..... 116
***Table 16. List of interferences in ICP-MS for targeted elements (Sb, Te and Se).*** *Isotopes that were not used in this work due to low abundance or high interference effects are presented in grey font.* ..... 121

## CHAPTER 4: Particulate carrier phases of Sb, a fractionation approach

***Table 17: Summary of most commonly used reagents and identified artefacts/remarks in cation- and anion-adapted (mostly sequential) selective extractions*** ..... 213

## CHAPTER 6: Trace element reactivity of Sn and Se in contrasting fluvial-estuarine systems – a comparative approach between the Gironde Estuary and the Rhône River

***Table 18. Analytical performance of Cs, Sn and Se in dissolved (freshwater NIST 1643f) and particulate/biological (stream sediment NCS DC 73307 and oyster tissue NIST 1566b) certified reference***

***materials (CRM).*** *Averages ± standard deviations (SD) are given for certified and measured values. Analytical limits of detection (LOD = 3·SD (n=10 blanks)).* ..... 323
***Table 19. Total concentrations (µg kg$^{-1}$) of Cs, Sn and Se in wild oysters*** *(Crassostrea gigas, cf. Magallana gigas) from the La Fosse (Gironde Estuary mouth, N=20) and Comprian (Arcachon Bay, N=20) sites in the Atlantic coast, as well as wild mussels (Mytilus galloprovincialis) from the St. Maries de la Mer ("Petit" Rhône River mouth, N=80) and Faraman ("Grand" Rhône River mouth, N=80) sites in the Mediterranean coast. Errors correspond to standard deviations (SD).* ..... 324

## DISCUSSION

***Table 20. Example of coupled timescales for Sb and Te radionuclide dispersion scenarios in the Gironde Estuary.*** *Assumed solid/liquid equilibrium times ($t_{S/L(eq)}$) for Te isotopes are ~5h in 1000 mg L$^{-1}$ (i.e., MTZ) and ~4 days in 100 mg L$^{-1}$ (i.e., average estuarine SPM), deduced from Te sorption kinetics (Chapter 5). Predicted fate is based on a single discharge, thus, scenarios for continuous/intermittent NPP discharges would, at least partly derive from the following:*..... 334

# List of abbreviations

| | |
|---|---|
| **AEAG** | Agence de l'Eau Adour Garonne |
| **AMORAD** | Amélioration des Modèles de prévision de la dispersion et d'évaluation de l'impact des RADionucléides au sein de l'environnement |
| **ANR** | Agence Nationale de la Recherche |
| **$As_{d/p}$** | Arsenic $_{dissolved/particulate}$ |
| **BAF** | BioAcumulation Factor |
| **BWR** | Boiling Water Reactor |
| **Chl-a** | Chlorophyll a |
| **CNPP** | Chernobyl Nuclear Power Plant |
| **DOC** | Dissolved Organic Carbon |
| **Eh** | Redox potential |
| **POC** | Particulate Organic Carbon |
| ***cf.*** | "compared to" |
| **CRM** | Certified Reference Material |
| **DIREN** | DIrection Régional de l'Environnement |
| **EDF** | Éléctricité De France |
| **EPOC** | Environnements et Paléoenvironnements Océaniques et Continentaux |
| **ex** | "experimental" or spiked |
| **FDNPP** | Fukushima Daiichi Nuclear Power Plant |
| **FOREGS** | FORum of European Geological Surveys |
| **FY** | Fission Yield |
| **HCl** | Hydrochloric acid |
| **HF** | Hydrofluoric acid |
| **$HNO_3$** | Nitric acid |
| **HOAc** | Acetic acid |
| **IAEA** | International Atomic Energy Agency |
| **ICP-MS** | Inductively Coupled-Plasma Mass-Spectrometre |
| **IEA** | International Energy Agency |
| **Ifremer** | L'Institut Français de Recherche pour l'Exploitation de la Mer |
| **I'geo** | modified geoaccumulation Index |
| **INES** | International Nuclear and radiological Event Scale |
| **IRSN** | Institut de Radioprotection et de Sûreté Nucléaire |
| **Kd** | solid/liquid partitioning coefficient |
| **KED** | Kinetic Energy Discrimination |

| | |
|---|---|
| **KP** | Kilometric Point |
| **LOD** | Limit of Detection |
| **MGTS** | Métaux Gironde Transfert et Spéciation |
| **MOX** | Mixed OXide fuel |
| **MTZ** | Maximum Turbidity Zone |
| **nat** | "natural" or inherited |
| **NPP** | Nuclear Power Plant |
| **PBq** | Peta Becquerel |
| **pH** | Hydrogen potential |
| **PWR** | Pressurised Water Reactor |
| **Q** | water discharge |
| **RNO/ROCCH** | Réseau National d'Observation/Réseau d'Observation de la Contamination Chimique du littoral |
| **S** | Salinity |
| **$Sb_{d/p}$** | Antimony $_{dissolved/particulate}$ |
| **SCHeMA** | integrated in Situ Chemical Mapping probes |
| **$Se_{d/p}$** | Selenium $_{dissolved/particulate}$ |
| **$Sn_{d/p}$** | Tin $_{dissolved/particulate}$ |
| **SOGIR** | Service d'Observation de la GIRonde |
| **SORA** | Station Observatoire du Rhône en Arles |
| **SPM** | Suspended Particulate Matter |
| **Sv** | Sieverts |
| **$t_{1/2}$** | Half-life |
| **TCE** | Technology Critical Element |
| **$Te_{d/p}$** | Tellurium $_{dissolved/particulate}$ |
| **TGM** | Transferts Géochimiques des Métaux à l'interface continent-océan |
| **$Th_p$** | Thorium $_{particulate}$ |
| **USEPA** | U.S. Environmental Protection Agency |
| **USGS** | U.S. Geological Survey |
| **WHO** | World Health Organisation |
| **WNA** | World Nuclear Association |

# GENERAL INTRODUCTION

# I. CONTEXT

## 1. Worldwide energy demand: the reason for nuclear energy production

Global development of modern socio-economies has been widely enhanced since the discovery and mastering of electricity. The use of electricity has become intrinsic to our individual daily activities to such an extent that electrical power and its availability appear as ubiquitous and granted. Accordingly, we tend to lose the awareness of our dependence on its production. Supporting evidence from the International Energy Agency (IEA) indicates that almost 40% of total electricity production worldwide is destined to residential and personal transport uses (***Figure 1***).

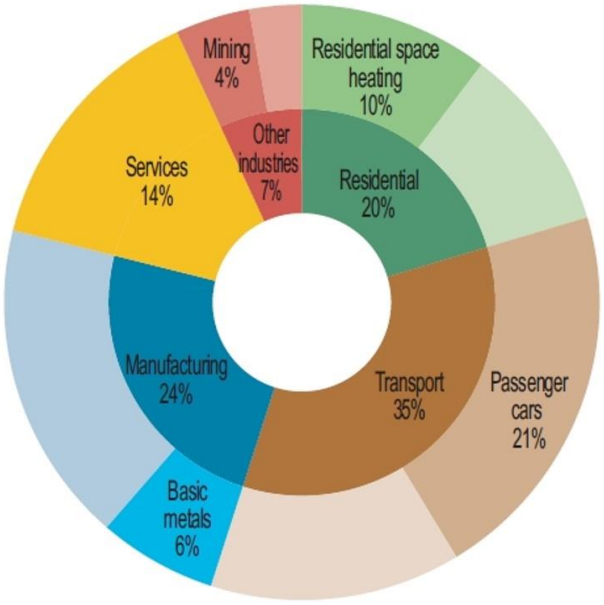


**Figure 1. Worldwide largest electricity end uses** (Australia, Austria, Canada, Czech Republic, Finland, France, Germany, Greece, Ireland, Italy, Japan, Korea, New Zealand, the Netherlands, Spain, Sweden, Switzerland, the United Kingdom and the United States). *Other industries* include agriculture, mining and construction. *Passenger cars* include cars, sport utility vehicles and personal trucks (*IEA 2017*).

This electricity is produced from several sources which can be briefly classified into:

- Fossil fuels (coal, petroleum and natural gas) and biofuels
- Renewable energies: based on wind/water motion on Earth or from solar radiation
- Nuclear energy (enriched radioactive materials in nuclear fission and future nuclear fusion)

Despite the different energy sources and their well-known advantages (e.g., green-technology, continuous supply, cheap production, etc.) and disadvantages (e.g., $CO_2$ emissions, instability for the grid, consumable sources, etc.), the trend of worldwide electricity generation has been increasing (***Figure 2a***) ever since a record exists (i.e., 1970's, IEA 2017). Noteworthy, during this time (1970's to 2010's) a parallel development in the nuclear energy sector has also increased, accounting in 2015 for almost 11% of the world's electricity production (***Figure 2b***).

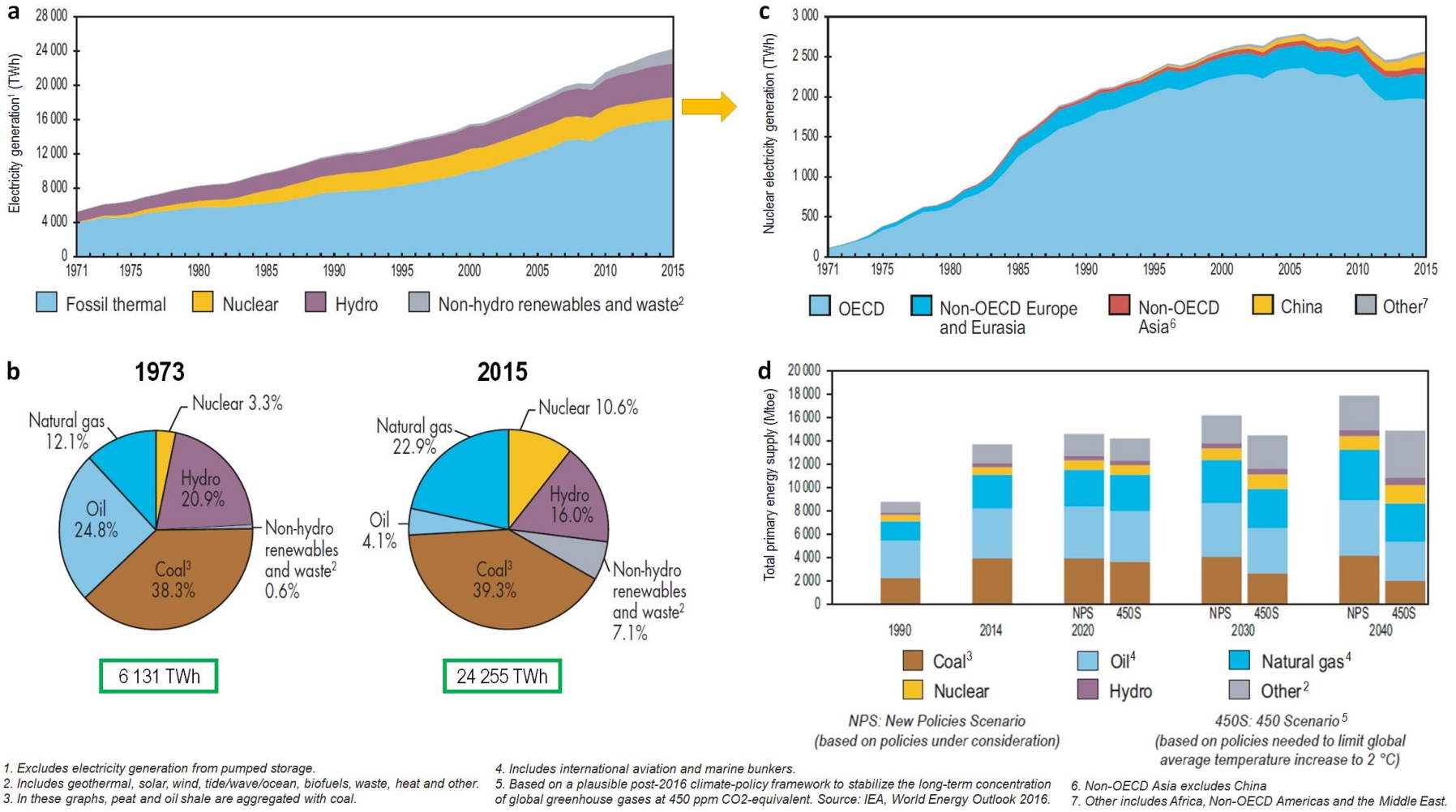


**Figure 2. Worldwide statistics on: (a) electricity generation by fuel type (1971-2015), (b) source shares of electricity generation (1973 and 2015 as examples), (c) nuclear electricity production by region (1971-2015), and (d) outlook to 1940's total primary energy supply by fuel type and socio-economic predicted scenario.** Countries are classified according to their attachment to the Organisation for Economic Co-operation and Development (OECD; *IEA 2017*).

In fact, nuclear energy constitutes a low-cost and continuous mean for electricity generation (WNA 2015) exempted from current large scale $CO_2$ emission-issues (i.e., Climate Change and consequences; IPCC 2017). Furthermore, despite the slight decrease in production in ~2011 (i.e., Fukushima Dai-ichi Nuclear Power Plant accident) followed by a current stabilisation (***Figure 2c***), nuclear energy is still considered an adequate alternative for future electricity demands (***Figure 2d***), expected to increase by more than two-thirds by 2035 (WNA 2015, 2018).

In the worldwide ranking of nuclear energy production by countries (***Table 1***), the United States of America are in the lead, producing ~32% of global nuclear energy (N ~100 reactors), spending <20% in domestic use (IEA 2017). The second nuclear energy producing country is France, with a global production of 17%, mostly invested in domestic use (>77%) and exportation (***Table 2***). This means that France is the European country with the highest local nuclear energy production, important nuclear management facilities and the highest nuclear dependence in the power supply (as nuclear energy accounts for ~75% of the total energy share; WNA 2015).

**Table 1. Worldwide 2015 statistics for global nuclear energy production (left) and relevance in domestic application (right) per country** (*IEA 2017*).

| Producers | TWh | % of world total | Top ten countries | % of nuclear in total domestic electricity |
|---|---|---|---|---|
| United States | 830 | 32.3 | France | 77.6 |
| France | 437 | 17.0 | Ukraine | 54.1 |
| Russian Federation | 195 | 7.6 | Korea | 30.0 |
| China | 171 | 6.7 | United Kingdom | 20.9 |
| Korea | 165 | 6.4 | Spain | 20.6 |
| Canada | 101 | 3.9 | United States | 19.3 |
| Germany | 92 | 3.6 | Russian Federation | 18.3 |
| Ukraine | 88 | 3.4 | Canada | 15.1 |
| United Kingdom | 70 | 2.7 | Germany | 14.3 |
| Spain | 57 | 2.2 | China | 2.9 |
| Rest of the world | 365 | 14.2 | Rest of the world* | 7.2 |
| **World** | **2571** | **100** | **World** | **10.6** |

**excluding countries that do not produce nuclear energy*

**Table 2. Worldwide 2015 electricity net exporter and importer countries** (*IEA 2017*).

| Net exporters | TWh | Net importers | TWh |
|---|---|---|---|
| France | 64 | United States | 67 |
| Canada | 60 | Italy | 46 |
| Germany | 48 | Brazil | 34 |
| Paraguay | 41 | Belgium | 21 |
| Sweden | 23 | United Kingdom | 21 |
| Norway | 15 | Finland | 16 |
| Czech Republic | 13 | Hungary | 14 |
| China | 12 | Thailand | 12 |
| Russian Federation | 12 | Hong Kong. China | 11 |
| Bulgaria | 11 | Iraq | 10 |
| Others | 39 | Others | 112 |
| **Total** | **338** | **Total** | **364** |

## 2. European concern on the nuclear energy industry: a focus on radioecology

The European Research Area (ERA) was formed in 2000 to coordinate and favour European co-evolution in research-and-development (R&D) and scientific excellence, supporting several projects within succeeding Framework Programmes (e.g. FP6, FP7, H2020) on different research topics and subjects of socio-economic impact. Within the European interests, the EURATOM project was designed to coordinate the European development of the nuclear industry as, in the future, energy supply (i.e., nuclear fusion and fission), waste disposal and nuclear safety are a matter of European concern.

In standard working conditions, the population is exposed to very low ionising radiation (~0.3 µSv $y^{-1}$; 1%) coming from Nuclear Power Plants (NPPs). This contrasts with the 85% of natural background radiation (e.g., 200 µSv $y^{-1}$ from radon in houses or 1000 Bq $kg^{-1}$ of granite rock) and 14% from medical use (e.g., average 370 µSv $y^{-1}$ from medical chest X-ray, corresponding to 70 million Bq; WNA 2015). However, during NPP accidents, i.e. Chernobyl (CNPP, Ukraine 26$^{th}$ April 1986) and Fukushima Dai-ichi (FDNPP, Japan 11$^{th}$ March 2011), atmospheric radiation levels (i.e., iodine-131 equivalent) increased up to 5300 PBq and 520 PBq, respectively, with 20 mSv $y^{-1}$ established as the maximum dose threshold to delimit the evacuation zone in case of a FDNPP accident (Steinhauser et al. 2014; WNA 2015). These extremely high radiation levels entail potential risks in causing at long term cancers and leukaemia (mostly due to internal radioactive exposure) and relevant psychological disturbances on public health (due to lack of radiological/environmental knowledge; Steinhauser et al. 2014).

The use of current nuclear facilities implies the risk of potential accidents such as those of CNPP and FDNPP, with hypothetically non-negligible large-scale impacts. Nevertheless, there is still high uncertainty on radioactive environmental dispersion, activity levels and consequences for humans and organisms. For this reason, the COMET project (COordination and iMplementation of a pan-European instrumenT for radioecology) was launched within the FP7-EURATOM-Fission in 2013 to coordinate the studies on radioecology (i.e., the environmental behaviour/processes and transport of natural and anthropogenic radiation, its transfer towards organisms along the human food chains and the transgenerational effects in radiosensitive species). Such studies are a prerequisite for nuclear risk assessment, as decision making for nuclear safety requires precise knowledge on exposure pathways and environmental dispersion.

Nuclear risk assessment follows several phases at different spatial and temporal scales, applicable to all types of incidents and accidental magnitudes (***Figure 3***). The first phase is the crisis or emergency phase, subdivided into menace phase (anomalous event compromising environmental levels), discharge phase (external detection of radioactivity from the NPP installations) and end of the emergency phase (when the NPP installation has returned to a safe status). The second one is the post-accidental phase subdivided in the transition (first months to years, with intense measuring campaigns) and long-term phases (environmental sampling campaigns are pursued and allow, together with modelling, to achieve an increased knowledge on contamination fate). The idea is to react efficiently and in an organised manner to a nuclear release, improving actions in future events based on the knowledge from direct measurements and experiences. Such knowledge on radiological risk assessment is essential for decision making of authorities at all levels (e.g., the Nuclear Safety Authority-ASN, prefects, ministries, amongst others).

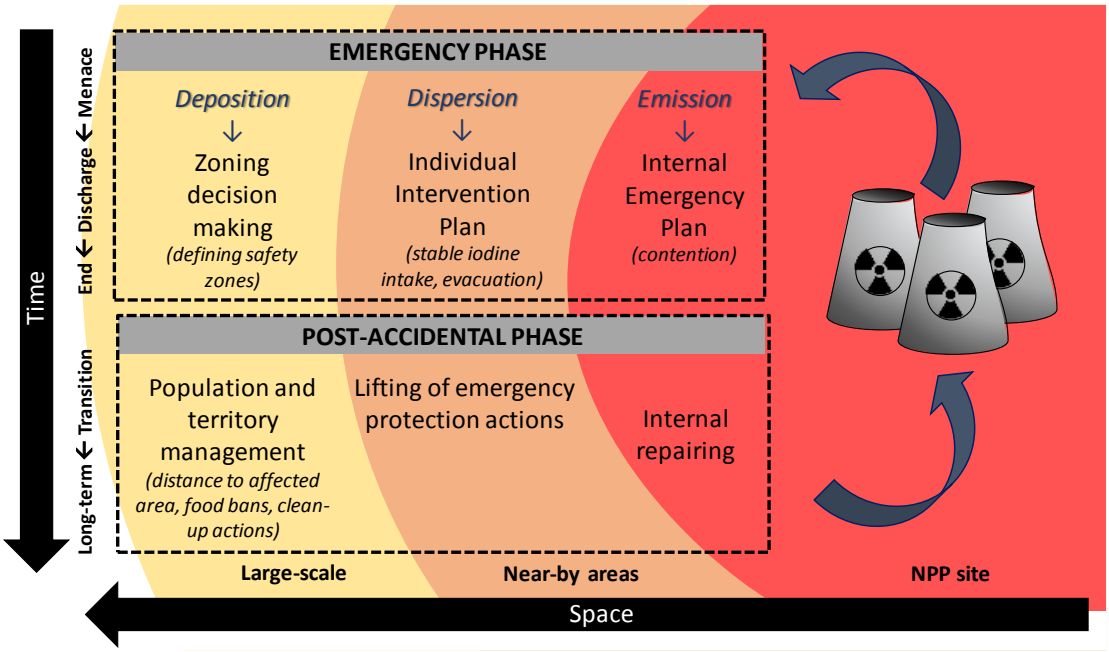


**Figure 3. Spatio-temporal phases after a nuclear incident/accident.** *(Modified from IRSN 2014).*

## II. THE RESEARCH QUESTION

### 1. Nuclear energy in France: current status and future plans

The French NPP network, operated by the electrical company Electricité de France (EDF), consists of 19 NPPs distributed over the metropolitan territory; 14 NPPs associated to streams and 5 NPPs located on the coast (***Figure 4***). There is a total of 58 pressurised water reactors (PWR; WNA 2015) with a net total power production of ~63 GWe. Since 2005, a 59$^{th}$ new generation Evolutionary Pressurised Water Reactor type (EPR) is under construction in Flamanville, expected to contribute 1.6 GWe (ANS 2016).

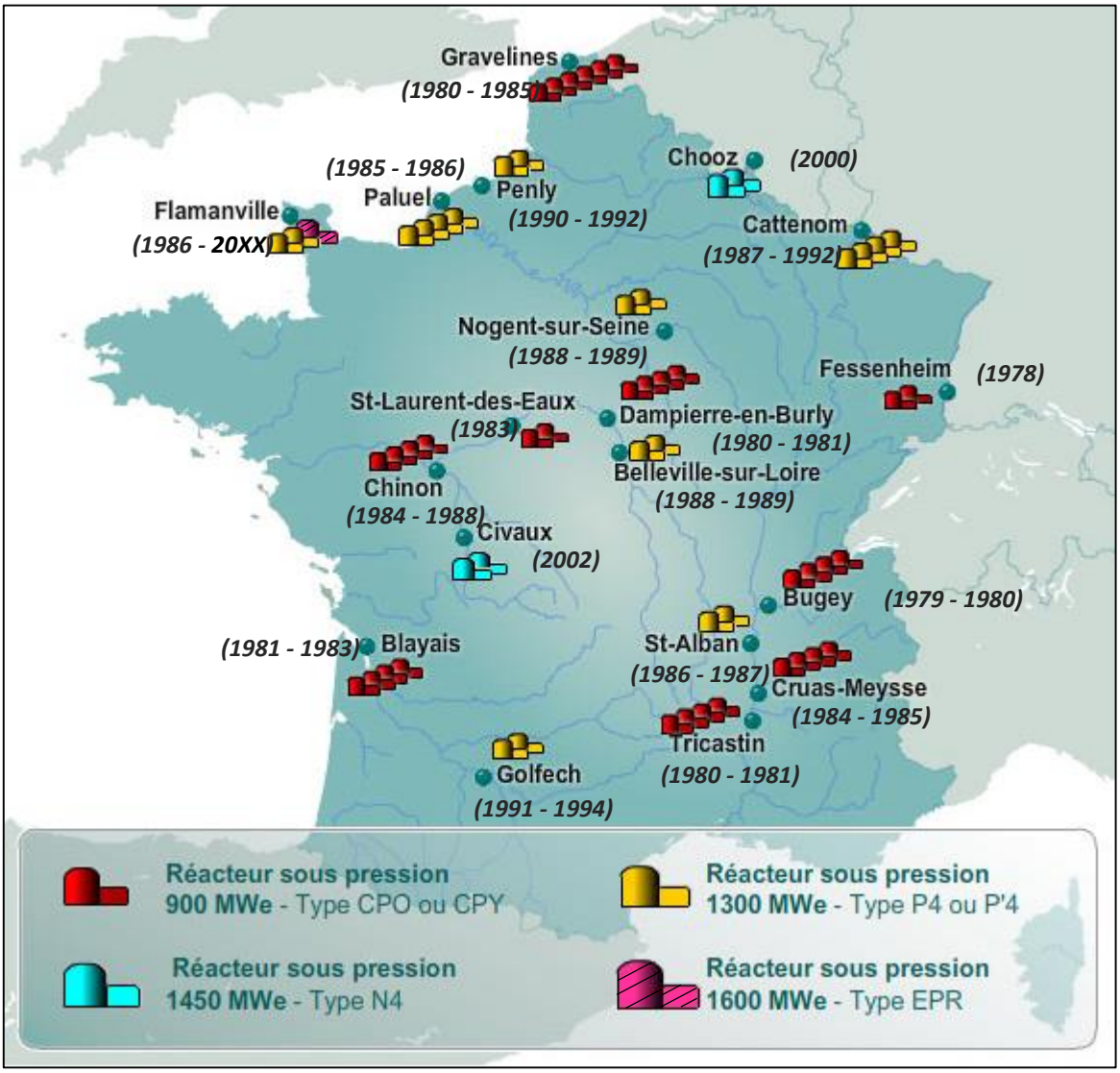


**Figure 4. French Nuclear Power Plant (NPP) network.** Range of operating starting year for all reactors per NPP (brackets). Legend shows reactor differences by energy generating capacity (Megawatts electric, MWe) and reactor characteristics: single wall lined reactor with steel sealing skin (CP0 and CPY, red), double concrete reinforcement for accident prevention (P4 and P'4, yellow), compact steam generator with higher reliance on computer software (N4, blue), and new generation reactor under construction (EPR, pink). *(Modified from ANS 2016).*

The origin of such strong NPP development dates back to 1974, when the French government decided to expand the country's nuclear power potential (WNA 2018): (i) as a response to the first oil shock at that time (to secure future energy crises), and (ii) as a logical step given the important engineering expertise of the country and the advantageous low costs of nuclear fuel importation compared to other energy sources. However, the Fukushima Dai-ichi NPP accident in 2011 has raised many new questions and doubts worldwide concerning nuclear safety in the 21$^{st}$ century; from non-negligible accidental dispersion extents (already observed for the Chernobyl accident) to unexpected impacts in different environmental compartments, notably in ocean/aquatic systems. In fact, the Dai-ichi accident has entailed direct and massive contamination of seawater, used for urgency reactor cooling, and huge leakages of radioactive seawater, unforeseen as a likely scenario.

In August 2015, France defined new objectives in favour of a national energetic transition scheme called "The Energy Transition for Green Growth bill", designed to reinforce French energy independence and economic competitiveness, preserving human and environmental health whilst continuing to fight against Climate Change (Law n° 2015-992, 2015). These objectives aim at: (i) a 40% reduction in greenhouse gas emissions by 2030 compared to 1990 levels (decreasing by 75% by 2050), (ii) an increase in renewable energies by 32% of the final energy consumption by 2030 (final energy consumption should decrease by half in 2050 compared to reference consumptions in 2012), and (iii) a maximum nuclear energy production of 63.2 GW (fixing the nuclear contribution to 50% of the national energy share by horizon 2025).

Furthermore, in March 2016, Areva (a multinational group focused on the nuclear fuel cycle, renamed Orano since January 2018), EDF and the Atomic Energy Commission (CEA) formed the tripartite French Nuclear Platform (PFN) to coordinate the medium- and long-term fate of the French nuclear industry (WNA 2018). Some of their goals are: (i) the review of the new EPR technological options/changes and R&D, (ii) the future of fuel reprocessing in France, (iii) nuclear waste deep geological repository, and (iv) the development of dismantling know-how. All of this locates France in an energetic context of high nuclear reactor density and dismantling activities within the metropolitan territory for the coming years.

## 2. Improved French approach to post-accidental management: The AMORAD Project

The current procedure for the evaluation of radiological risk and dosimetric consequences from major nuclear events relies on post-accidental measurements and/or modelling (to estimate unmeasured parameters or forecast future situations, ***Figure 5***). However, this radioprotection procedure remains at present an unreliable tool as it has several limitations (IRSN 2014): (i) model spatio-temporal resolution for radioactive concentrations and mobility between different

environmental compartments, (ii) unaccounted process variability, and (iii) unknown chronical effects at ecosystem level.

The French National project AMORAD (« Amélioration des MOdèles de prévision de la dispersion et d'évaluation de l'impact des RADionucléides au sein de l'environnement »; ANR-11-RSNR-0002) of the French Excellence Initiative "Investments for the Future" (Investissements d'Avenir, funded by the French Government) is englobed in the COMET project and was also launched in 2013 with the support of the National Research Agency (ANR). AMORAD was designed as a 6-year-research project (2014-2019) that aims at overcoming technical obstacles in spatial-temporal resolution of radioactive concentrations, dispersion (transfer/fluxes) and impacts on humans and environmental compartments, by discovering means for accurate evaluation of radioactive contamination (IRSN 2018). This study is expected to provide operational tools to improve current use and knowledge on radionuclide modelling to reinforce radiological risk evaluation and decision making (***Figure 5***). The results from the project are foreseen to be useful in nominal radioactive discharges and management of contaminated sites. For the latter, a computational tool will be further developed in the 3-year extension of the project (AMORAD-II), including the socio-economic consequences of nuclear accidents.

The AMORAD project is structured in two main research domains concerning:

**(i)** the radionuclide dispersion between environmental compartments (interfaces), constituted by three main research axes focusing on three environmental compartments, each with specific objectives:

- *ATMO (Atmosphere)*: this research axis aims at improving existing tools for the evaluation of atmospheric deposition of radionuclides (in gaseous or aerosol forms) and the effect of short/long temporal (e.g., seasonal influences on wet/dry deposition) and spatial variables (e.g., within <10km of the NPP and beyond) on radionuclide dispersion to model possible uncertainties in atmospheric transport for French NPPs.

- *MARIN (marine environment):* this compartment has the greatest unknowns as massive release of radionuclides into coastal water during nuclear crises was not foreseen before the FDNPP accident. Improving knowledge on radionuclide dispersion in the marine environment implies (i) studying water mass transport of radionuclides, (ii) determining water-continent interface processes and particulate transport at different spatial-temporal scales, and (iii) understanding radionuclide adsorption and bioaccumulation in the trophic chains (unveiling the sensitivity and vulnerability of the impacted ecosystems). These results will allow to (i) produce maps of contamination risk, and (ii) anticipate socio-economic consequences of

nuclear accidents (e.g., controlling human sea food consumption). Specifically, this axis considers four areas of study ("zones ateliers"):

- Fukushima (focusing on the area in Japan directly affected by the FDNPP)
- English Channel (hosting several French NPPs and a nuclear-fuel treatment plant)
- Bay of Biscay, in the Atlantic Ocean (receiving liquid and solid fluxes from the Garonne Gironde fluvial-estuarine system hosting two NPPs)
- Gulf of Lions, in the Mediterranean Sea (receiving liquid and solid discharges from the Rhône River, also hosting several NPPs)

- *Continental environment (CONTI)*: aims at acquiring better knowledge on dose-related impact on human populations in post-accidental situations from a multidisciplinary view-point (i.e., combining hydrology, ecophysiology, biogeochemistry and soil sciences). The results from this field will allow to better determine post-accidental areas of control:
  - the "population protection zone" (ZPP) concerning the delimited area, where management priorities aim to reduce susceptible radionuclide exposure to people living within the zone, and
  - the "zone of enhanced territorial surveillance" (ZST), where specific surveillance will control that foodstuffs and agricultural products intended for marketing do not surpass regulated radioactive levels.

**(ii)** the impacts to the biosphere, concerning a single project axis devoted to *ecotoxicology (ECOTOX)*. The aim is to characterise the radiological sensitivity of ecosystems, focusing on physiological aspects and transgenerational effects on organisms from exclusion zones in Fukushima, Chernobyl or laboratory experiments. Biomonitoring aspects (genotoxic or epigenetic effects) and validation of bioassays are also addressed in this axis.

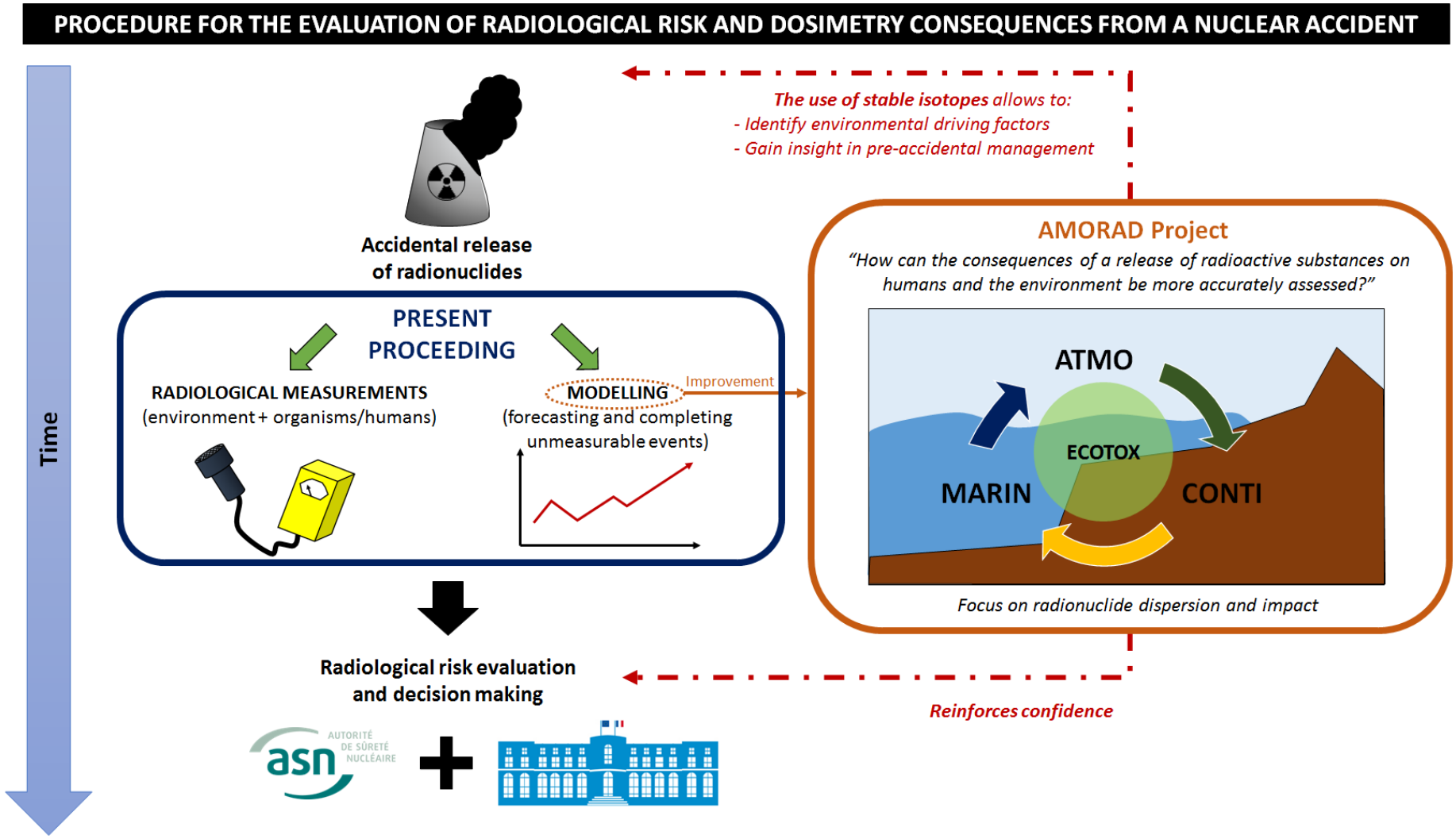


**Figure 5. Post-accidental approach to evaluating the radiological risk and dosimetry consequences of a nuclear accident in the environment (left) together with the role of the AMORAD project in such approach (right).** The central question of the AMORAD project (in quotes) and the two main research domains including (i) environmental interfaces (MARIN, CONTI, ATMO), and (ii) consequences on the biosphere (ECOTOX), are also shown.

As the scope of the AMORAD project is to improve spatial-temporal resolutions of NPP accidents, all types of emitted radionuclides must/should be taken into account. This includes most commonly studied radionuclides (i.e., iodine-I, due to its importance in organism health status, and caesium-Cs, with long-term environmental persistence and strong radioactive decay activities; e.g., Steinhauser et al. 2014) as well as those which are generally not followed up (due to shorter environmental persistence but with unknown behaviour/effects). This is of particular interest in the continental-ocean interface, where water and sediment dynamics can delay radionuclide transport to the ocean at various timescales (from tidal scale to seasons and years). Furthermore, this also implies that the historic sites affected by NPP accidents (e.g., CNPP and FDNPP areas) no longer present these fast-decaying radionuclides. Thus, their current post-accidental measurements are no longer available or very low, hindering the study of the biogeochemical behaviours of the released short- and medium-decay radionuclides (compared to longer-lived radionuclides like $^{137}$Cs). Therefore, the AMORAD approach to fast-decaying radionuclides relies on the expected analogous chemical behaviour (e.g., solubility, speciation, etc.) between stable isotopes and radionuclides of the same chemical element. This assumption allows simulating and learning about the environmental behaviour of the radioactive isotopes, without them being present in the environment, by studying their stable analogues.

## III. THESIS OBJECTIVES AND CHAPTER DISTRIBUTION

This thesis is co-directed by researchers of the University of Bordeaux and the Institute for Radioprotection and Nuclear Safety (IRSN) in Cadarache, within the MARIN research field of the AMORAD project. The general aim is to develop dispersion scenarios of poorly known antimony (Sb) and tellurium (Te) radionuclides for two main continent-ocean transition study areas in southern France. These study areas discharge water and particle fluxes from: (i) the Garonne-Gironde fluvial-estuarine continuum (largest estuary in southwest Europe) into the Bay of Biscay in the Atlantic Ocean, and (ii) the Rhône River to the Gulf of Lions (main freshwater input to the Mediterranean Sea). Furthermore, this work is based on the hypothesis of similar biogeochemical behaviour between stable and radioactive isotopes. The focus will be on producing knowledge on qualitative and quantitative aspects of stable Sb and Te coastal/estuarine dynamics (transport and fluxes) and physical-chemical transfers (partitioning and potential bioavailability), knowing that their current biogeochemical cycles in coastal aquatic and biological compartments are actually quite unknown. The approach implies handling challenges related to limitations in current analytical techniques (trace to ultra-trace concentration levels, seawater matrices, etc.). Occasional comparisons along the thesis between the biogeochemical behaviour of Sb and Te, and their better documented respective geochemical pairs, arsenic (As) and selenium (Se), on the one hand, as well as the well-studied caesium (Cs) and the parent radionuclide of Sb, tin (Sn), on the other, complete the approach.

The specific **objectives** of this thesis are to:

- Characterise the dissolved and particulate concentrations and fluxes of Sb and Te in the Gironde watershed and along the turbidity and salinity gradients of the Gironde Estuary to understand their natural distribution/behaviour.
- Determine the kinetics and transfer rates between dissolved and particulate phases for Te, Se and Sn under different salinities and suspended particulate matter (SPM) concentrations to evaluate the fate of accidentally released dissolved radionuclides from NPPs in the estuarine gradients.
- Define Sb, Te and Se association to the heterogeneous sediment components by selective extractions, to determine major particulate carrier phases and foresee potential roles of these carrier phases in different environmental conditions.
- Document and compare Sb, Te, Se and Sn concentrations in wild oysters (*Crassostrea gigas, cf. Magallana gigas*) and mussels (*Mytilus edulis*), often used as biomonitoring organisms of metal contamination, to assess potential transfer to the marine food chain.

- Develop conceptual and qualitative models (scenarios) for the Garonne-Gironde fluvial-estuarine system and the Rhône River as a first step to predict the dispersion and fate of potential radionuclide emissions from the NPP along the river-estuary continuum.
- Provide fundamental know-how on the estuarine biogeochemistry of Sb and Te as a support for similar approaches to radionuclide dispersion in other systems with existing or scheduled nuclear energy production.

The answers to these objectives have been distributed in the following **chapters**:

A first introductory chapter (**Chapter 1**) states the link between radioactive and stable elements and the current situation/knowledge of both research fields. This chapter starts with a quick reminder and pseudo-glossary of atomic stability and radioactive terminology, useful to: (i) back-up/justify the hypothesis of analogous environmental behaviour assumed for stable and radioactive isotopes, (ii) understand potential elemental releases (forms, species, etc.) in hypothetical NPP accidents from current NPP designs and performances, and (iii) present the link between Sb and Te radionuclides. A brief review on the state-of-the-art of the environmental behaviour of both radioactive and stable Sb and Te highlights knowledge gaps and sets the background conditions of this thesis.

A summary of the materials and methods used in this work (**Chapter 2**) is compiled in a single chapter to provide an overview of all the analytical techniques performed during this work. Specific parts of the methodology may re-appear in condensed versions within the Material and Methods sections of the different publications in the following chapters.

The **Chapter 3** addresses the environmental biogeochemical behaviour of **antimony** in the Lot-Garonne-Gironde fluvial-estuarine system. In fact, both long-term and watershed scale Sb dynamics and partitioning are studied through a 14-year record (2003-2016) at five strategic sampling points in the watershed for both dissolved (<0.2 µm and some years completed by <0.02 µm filter-passing fractions) and particulate Sb concentrations. This study is completed by the first results on Sb reactivity in the Gironde Estuary obtained from three oceanographic sampling campaigns in 2014-2015 covering contrasting hydrological conditions (from dry to flood) and variable estuarine salinity and turbidity dynamics and water/particle residence times. The obtained Sb concentrations are compared with other French river-estuarine systems such as the Loire, Seine and Rhône Rivers to identify potential watershed particularities. The latter study also proposes preliminary scenarios of Sb radionuclide transport/retention for the Gironde Estuary.

The **Chapter 4** is dedicated to **solid partitioning of Sb** in natural sediments. The application of several selective extraction protocols to sediments from the Gironde and Rhône systems aims at the determination of particulate carrier phases and the identification of methodological artefacts in

particulate Sb fractionation. A second approach focuses on the potential differences between inherited Sb and spiked Sb solid fractionation by applying common selective extraction methods to isotopically-labelled sediments of the Gironde Estuary. Both studies provide better insights into particulate Sb carrier phases, thus, information on Sb environmental reactivity and potentially bioaccessible fraction in sediments from the Gironde and the Rhône systems (cf. within the scope of high resolution studies of the AMORAD Project).

**Tellurium** and caesium radionuclides are two major components released during NPP accidents and highly followed due to their relevant radiation doses. Given that there is little (or no) information available on their transport from the watershed to the coastal areas (i.e., goal of AMORAD-related research studies), **chapter 5** focuses on temporal and spatial variability of dissolved and particulate Te concentrations and fluxes in the Lot-Garonne-Gironde fluvial-estuarine system (2013-2017), along the salinity and turbidity gradients of the Gironde Estuary (2014-2017) and from a long-term record (1984-2017) of oyster soft tissues (RNO/ROCCH) at the estuary mouth. In the second part of this chapter, an experimental study focuses on Te reactivity (sorption kinetics and isotherms) in simulated estuarine salinity and turbidity gradients, compared to that of Se. These results allow to propose preliminary dispersion scenarios for potentially released radioactive Te and Se in the Gironde Estuary.

An important factor when studying trace element reactivity in continent-ocean transition systems is the analytical challenge of determining trace to ultra-trace concentrations in complex matrices such as seawater. **Chapter 6** presents an experimental study on Sn and Se radionuclide adsorption and desorption experiments applied to sediments from both the Gironde and Rhône systems in contrasting salinity and turbidity concentrations, performed in the controlled area of the Karlsruhe Institute of Technology (Germany). This approach allows to compare both continent-ocean transition systems at environmentally representative concentrations. The second part of this chapter compares the obtained results on Sn and Se reactivity with environmental concentrations of Sn and Se in wild organisms such as oysters from the Gironde Estuary mouth and mussels from the Rhône River mouth. These results, potentially comparable to Te and Sb, broaden the view to the development of radionuclide dispersion scenarios concerning experimental representativity and potential biotransfer.

This thesis ends with a **Conclusions and perspectives** section compiling the developed dispersion scenarios for hypothetical releases of Sb and Te radioactive elements in transition-water systems presenting important salinity and turbidity gradients and/or characteristic sediment properties and dynamics. The thesis conclusions provide a comprehensive view of radionuclide dispersion, transport and interactions between water-sediment-biota, all integrated in a temporal scheme that considers both watershed scale environmental dynamics (tidal and seasonal hydrodynamics) and radionuclide decay (half-lives and element transformations). This original approach matches the focus of the

extended AMORAD-II Project to produce a scientific basis for further application in managing medium/long-term socio-economic consequences of the hypothetically impacted areas. Furthermore, the obtained natural solid/liquid partitioning coefficients (Kd) contribute to field and laboratory values for current radionuclide databases from the International Atomic Energy Agency (IAEA 2004), requiring more accurate values, as foreseen within the milestones of the AMORAD-II Project. The final perspectives provide an outlook on how to improve the proposed scenarios and encourage future lines of research.

# CHAPTER 1:

# SCIENTIFIC CONTEXT

# I. INTRODUCTION

The development of radionuclide dispersion scenarios in aquatic environments from nuclear power plant accidental releases, based on the hypothesis of similar behaviour between radioactive and stable isotopes, requires a background knowledge on both, radioactive and stable element production and known geochemical dynamics in aquatic systems. The aim of this chapter is to present existing studies on (i) antimony (Sb) and tellurium (Te) radionuclide releases from nuclear facilities, and (ii) the biogeochemical behaviours of Sb and Te stable isotopes in aquatic environments.

The first part of this chapter compiles basic knowledge on radioactivity, including element abundance, stability, and decay modes, as well as general biological implications of exposure to radiation. Radionuclide production in nuclear power plant reactors, causes of historical nuclear power plant accidental events and evidence of aquatic dispersion of known Sb and Te radionuclides from both, nuclear fuel reprocessing plants and/or past accidental nuclear power plant releases, are also reported in this section.

The second part of the chapter presents available data concerning stable Sb and Te, including known sources, anthropogenic uses, environmental chemistry and aquatic biogeochemical behaviour, mainly focused in coastal environments. Information on Sb and Te biological toxicity and exposure pathways resulting in human assimilation are also considered as a first approach to estimate the potential relevance of an environmental release of Sb and Te radionuclides.

The present review will allow to better understand the scientific context of the thesis and to establish a background level from which preliminary dispersion scenarios of Sb and Te radionuclides in continent-ocean transition systems can be built.

## II. ISOTOPES AND RADIOACTIVITY

### 1. Atomic definitions, elemental abundance and isotope stability

Since E. Rutherford´s experience in 1911, the simplest atomic model accepted nowadays is that formed by subatomic particles which are rearranged in a nucleus containing uncharged ***neutrons (n)*** and positively charged ***protons (p)***, surrounded by electron orbitals, which are high probability areas of negatively charged spinning ***electrons ($e^-$)*** (***Table 3***). The ***atomic number (Z)***, i.e., the number of protons in a nucleus, is characteristic of each fundamental substance/***element (X)*** that composes matter in the physical universe and serves to organise all elements in Mendeleev's Periodic Table. However, the same element can have several ***isotopes***, as the element can show different number of neutrons in a nucleus. Isotopes of an element *X* are represented as $^{A}_{Z}X$, with the ***mass number (A)*** being the sum of the number of protons and neutrons in the nucleus. The general term ***'nuclide'*** is used when referring to atoms with a specific number of protons and neutrons. The stability of each nucleus and the physical properties of the element (e.g., freezing-boiling-melting points, density, etc.) are defined by the weight of the nucleus, also known as **atomic mass** (i.e., $Z \cdot u_p + (A\text{-}Z) \cdot u_n + e^- \cdot u_{e^-}$, ***Table 3***). The number of electrons from the external orbitals (***electrons of valence***) determine the ionised state or charge of the element by either forming electrically neutral (i.e., $e^- = Z$) or ionic species (i.e., $Z < e^-$ or $e^- < Z$). Therefore, theoretically, all isotopes of the same element should show identical chemical properties (e.g., reactivity, toxicity, oxidation properties, speciation, etc.) given their common redox/ionised state in specific environmental conditions.

**Table 3. Characteristics of the subatomic particles constituting elements in the physical universe**.

| | Proton (p) | Neutron (n) | Electron ($e^-$) |
|---|---|---|---|
| **Electric charge** | + | 0 | - |
| **Mass (u)** | 1.007 | 1.009 | 0.001 |
| **Mass (MeV)** | 938 | 940 | 0.51 |
| **Mass (kg)** | $1.67.10^{-27}$ | $1.68.10^{-27}$ | $9.11.10^{-31}$ |

u: "atomic mass units", 1 u = $1.66054.10^{-27}$ kg, MeV: Megaelectron volts

Element abundance on Earth depends on formation mechanisms and binding energies. Formation mechanisms are related to the history of the Universe (i.e., big bang fusion, merging of neutron stars, dying of low mass stars, exploding massive stars, etc.; ESA/NASA/AASNOVA), explaining nuclear synthesis by fusion and neutron capture processes. ***Fusion*** are energetic processes related to stellar reactions at extremely high temperatures (up to ~$3.10^9$ ºK) that bind subatomic particles together forming heavier nuclides, producing new elements (from H to Fe). Higher mass elements are produced by ***neutron capture***, which are less energetic processes implying neutron inclusion into the nuclei before or after the neutron-to-proton decay occurs.

***Binding energies*** reflect the energy required to disassemble the nucleus of an atom and it corresponds to the amount of energy released when the nucleus was formed. This binding energy appears as extra mass due to the ***mass defect*** or mass difference encountered between the predicted atomic mass (i.e., $Z \cdot u_p + (A-Z) \cdot u_n + e^- \cdot u_{e^-}$, using the stated values in ***Table 3***) and the actual nuclide atomic mass, obtained experimentally (i.e., present in the Periodic Table); with the predicted mass being always higher than the experimental one. This mass defect is transformed into energy with the mass-energy equation of A. Einstein's Theory of Relativity ($E = \Delta M \cdot c^2$), stating that the energy released (*E*, in Jules (J)) equals the mass difference (*ΔM*, in kg) times the speed of light (*c*, ~$3.10^8$ m $s^{-1}$). Energy units can be converted from Jules to electronvolts (eV) as 1eV = $1.602176.10^{-19}$ J. In any case, binding energies vary in a convex relation to *A* (***Figure 6***) and reflect all the processes that determine nucleus stability:

1. *Spin pairing* and *shell binding* – Nuclide stability is achieved when there is equal or a similar amount of protons and neutrons in the nucleus (especially when they both show even numbers and have filled nuclear/orbital shells).

2. *Surface/volume ratio or nuclear force saturation* – Nuclear interactions of peripheral neutrons and protons do not act to their maximum capacity in atoms with high surface/volume ratio (i.e., the lower the ratio, the higher the tension, thus more stable).

3. *Coulomb repulsion* – Nuclides with high number of protons (positive charge) have higher internal repulsion, thus, increasing the number of neutrons would diminish such electrostatic repulsions, favouring nucleus stability.

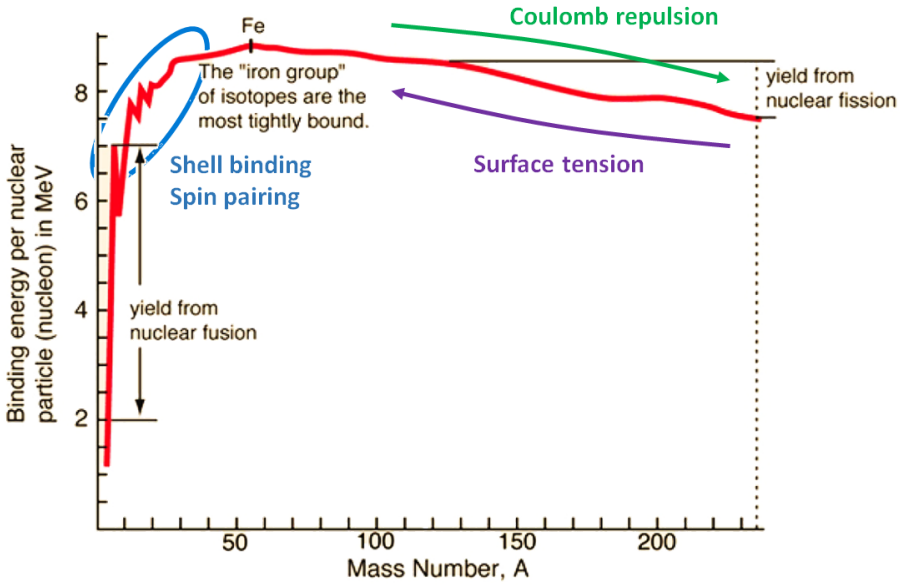


**Figure 6. Binding energy as a function of mass number**, showing the three main regions determining nuclear stability, indicating which elements are used in nuclear fission and which in nuclear fusion processes. *(Adapted from UiO Chemical Institute).*

There is a total of 90 natural elements (from $1 \leq Z \leq 92$, except $_{43}$Tc-Technetium and $_{61}$Pm-Promethium) with 331 natural nuclides (256 stable and 75 unstable or ***radioactive***) and 2700 artificial nuclides which are re-generated over time by human kind or cosmic rays, all unstable (***Figure 7a***). Light weighted elements can show both stable and radioactive isotopes but all elements with $Z > 83$ are radioactive. Such instability is reflected by spontaneous changes in the nucleus structure resulting in ***radiation*** emissions towards a more stable nuclei state. These changes to remove energy excess can be performed under different mechanisms or ***decay modes*** which are related to the amount of $Z$ and $n$ (***Figure 7b***)

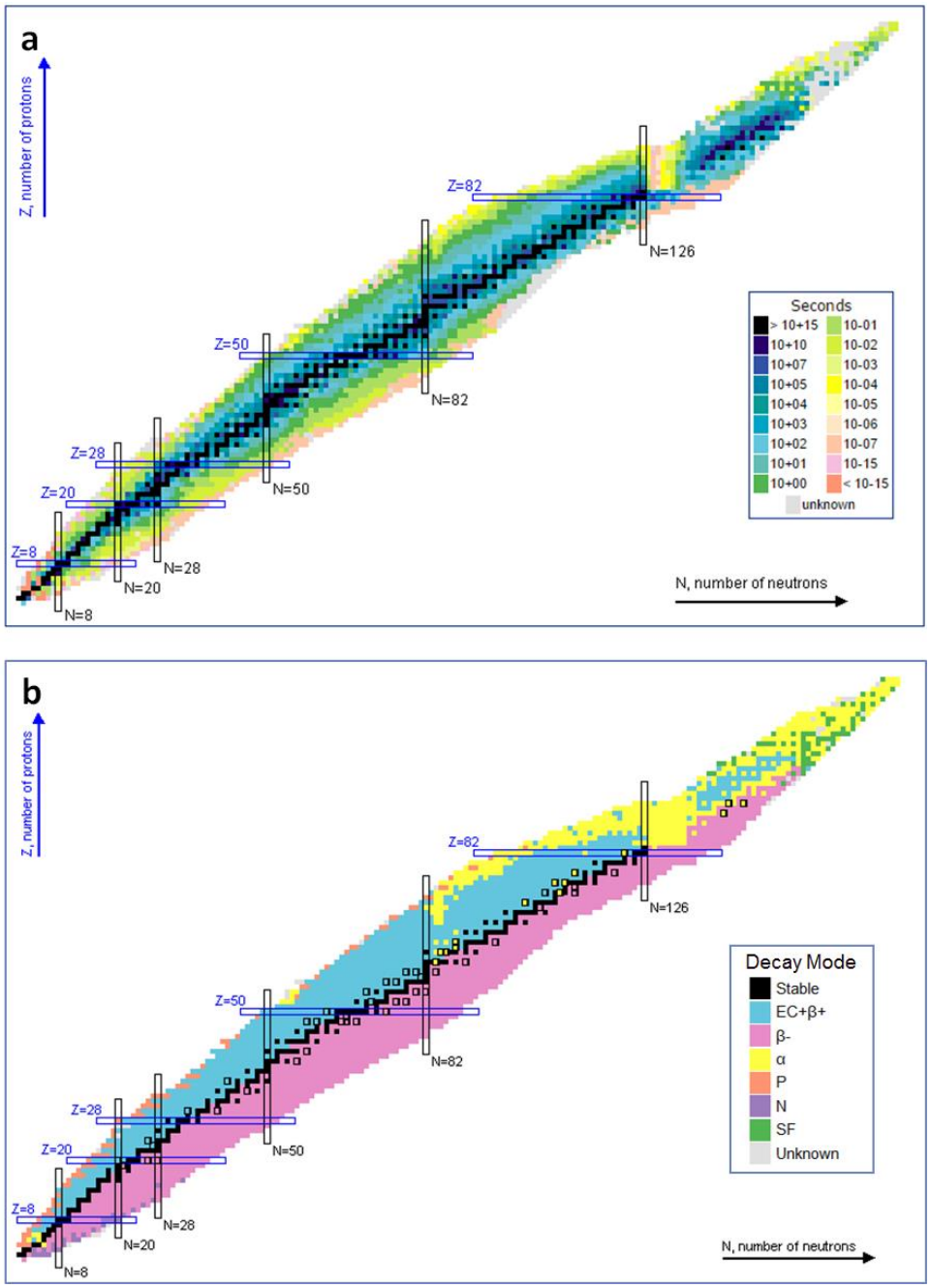


**Figure 7. Segré Diagram Chart of radionuclides**: (a) stability (half-life $t_{1/2}$) and (b) decay modes *(Sonzogni et al. 2013).* Abbreviations: α (alpha decay), $\beta^-$ or $\beta^+$ (beta decay), EC (electron capture), P (proton decay), N (neutron decay), SF (Spontaneous Fission).

## 2. Decay modes

The most common cases of disintegration are those where emission of ionising radiation (***Table 4***) is in the form of high energy rays (i.e., x-rays and gamma-rays) or atomic particles (i.e., alpha, beta or positrons).

**Table 4. Common modes of nuclear decay** *(Averill and Eldredge 2012).*

| Decay Type | Radiation Emitted | Generic Equation | Model |
|---|---|---|---|
| Alpha decay | $^{4}_{2}\alpha$ | $^{A}_{Z}X \longrightarrow {}^{A-4}_{Z-2}X' + {}^{4}_{2}\alpha$ | |
| Beta decay | $^{0}_{-1}\beta$ | $^{A}_{Z}X \longrightarrow {}^{A}_{Z+1}X' + {}^{0}_{-1}\beta$ | 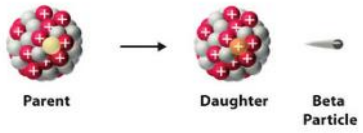  |
| Positron emission | $^{0}_{+1}\beta$ | $^{A}_{Z}X \longrightarrow {}^{A}_{Z-1}X' + {}^{0}_{+1}\beta$ | 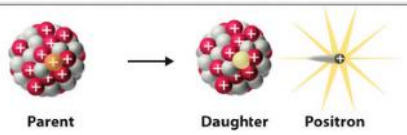  |
| Electron capture | X rays | $^{A}_{Z}X + {}^{0}_{-1}e \longrightarrow {}^{A}_{Z-1}X' + X\ ray$ | 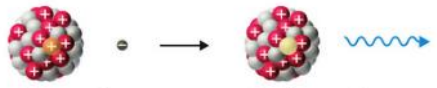  |
| Gamma emission | $^{0}_{0}\gamma$ | $^{A}_{Z}X^{*} \xrightarrow{Relaxation} {}^{A}_{Z}X' + {}^{0}_{0}\gamma$ | |
| Spontaneous fission | Neutrons | $^{A+B+C}_{Z+Y}X \longrightarrow {}^{A}_{Z}X' + {}^{B}_{Y}X' + C\,{}^{1}_{0}n$ | 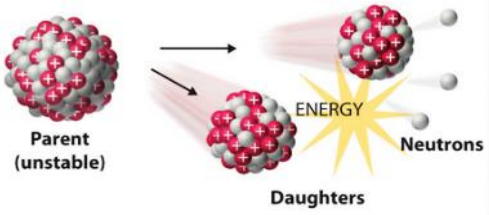  |

Nuclides with high mass number ($A$>$^{209}$Bi) release ***alpha particles (α)*** to reach more stable forms. Such release consists in the emission of two protons and two neutrons (i.e., nucleus of helium atom), resulting in a mass balanced nuclear equation between the parent and daughter atoms (Averill and Eldredge 2012; Nicolet and Erdi-Krausz 2003). ***Beta decay*** occurs when the nucleus is enriched or depleted in neutrons, as it involves the transformation of a neutron into a proton, or vice versa, with the release of negatively charged high-energy electrons from the nucleus ($\beta^-$), or less frequently of positively charged positrons ($\beta^+$), respectively, not changing the atomic mass of the resulting nucleus but increasing/decreasing by one its atomic number (Averill and Eldredge 2012; Nicolet and Erdi-

Krausz 2003). A neutron-poor nucleus can also decay by ***electron capture (EC)***, as it involves the adsorption of an inner shell electron into the atomic nucleus to react with a proton and form a neutron, emitting x-rays (electromagnetic radiation of low energy) when the electron vacant is replaced by a second electron from an outer shell (Averill and Eldredge 2012; Nicolet and Erdi-Krausz 2003). Exceptionally, massive nuclei ($Z \geq 104$) with high neutron-to-proton ratios undergo ***spontaneous fission (SF)***, in which the nucleus breaks into two different elements, releasing large amounts of energy and neutrons (Averill and Eldredge 2012). In any case, many radioisotope decay reactions generate nuclear excited state daughters which return to ground state by emitting photons in the form of ***gamma rays (γ)*** (Averill and Eldredge 2012; Nicolet and Erdi-Krausz 2003).

The physical character and energy of emitted radiation particles and photons determine their interactions with matter (Averill and Eldredge 2012; Nicolet and Erdi-Krausz 2003). Alpha particles exhibit low velocities ($10^7$ m $s^{-1}$) and low penetration power into matter due to their strong interaction linked to the high mass and charge of the alpha particles. Thus, these particles can be stopped by a piece of paper or adsorbed by ~$10^{-2}$ m of air and $10^{-5}$ m or rock (Averill and Eldredge 2012; Nicolet and Erdi-Krausz 2003). However, exposure to internal alpha decay, through ingestion or inhalation of radioactive dust, can cause severe biological damage (Amon and Oberhummer 2007). Beta radiation penetration depends on the initial energy of the particle, whose velocity can reach the speed of light, with a penetration range of ~8 m in air and 1 cm in water for 2 MeV energy (Nicolet and Erdi-Krausz 2003). As they have less mass and charge than alpha particles, they can penetrate paper or skin but can be stopped by a thin sheet of metal such as aluminium (Averill and Eldredge 2012). Contrastingly, gamma radiation is part of the electromagnetic spectrum (radiation energy > 40 keV), travelling at the speed of light, and penetrates deeply into many objects due to its lack of charge and almost no mass (Averill and Eldredge 2012). Therefore, gamma radiation is considered the most dangerous external source of radiation and it can be completely stopped by several cm of lead or special concrete covering (Averill and Eldredge 2012).

These nuclear decays take place at a constant and predictable rate, known as the ***half-life*** time (***$t_{1/2}$***), which is the time required for a radioactive isotope to half the number of original nuclei through a first-order reaction decay (Averill and Eldredge 2012). This means that certain natural radionuclides with very long half-lives are present on Earth since its origin (~$4.5.10^9$ y). Furthermore, it is noteworthy that some radionuclides need several decay events, forming ***decay chains***, to reach the stable nuclear arrangement of ground state. Each step is characterised by its own half-life and decay mode. Such are the cases of $^{238}U$ ($t_{1/2} = 4.47.10^9$ y), $^{235}U$ ($t_{1/2} = 7.04.10^8$ y) and $^{232}Th$ ($t_{1/2} = 1.40.10^{10}$ y) decay series (***Table 5***).

**Table 5. Examples of $^{238}U$, $^{235}U$ and $^{232}Th$ natural decay chains**, showing associated daughter radionuclides and corresponding half-lives. Colours represent particle reactivity (for more information see *Ah and Car 2016*).

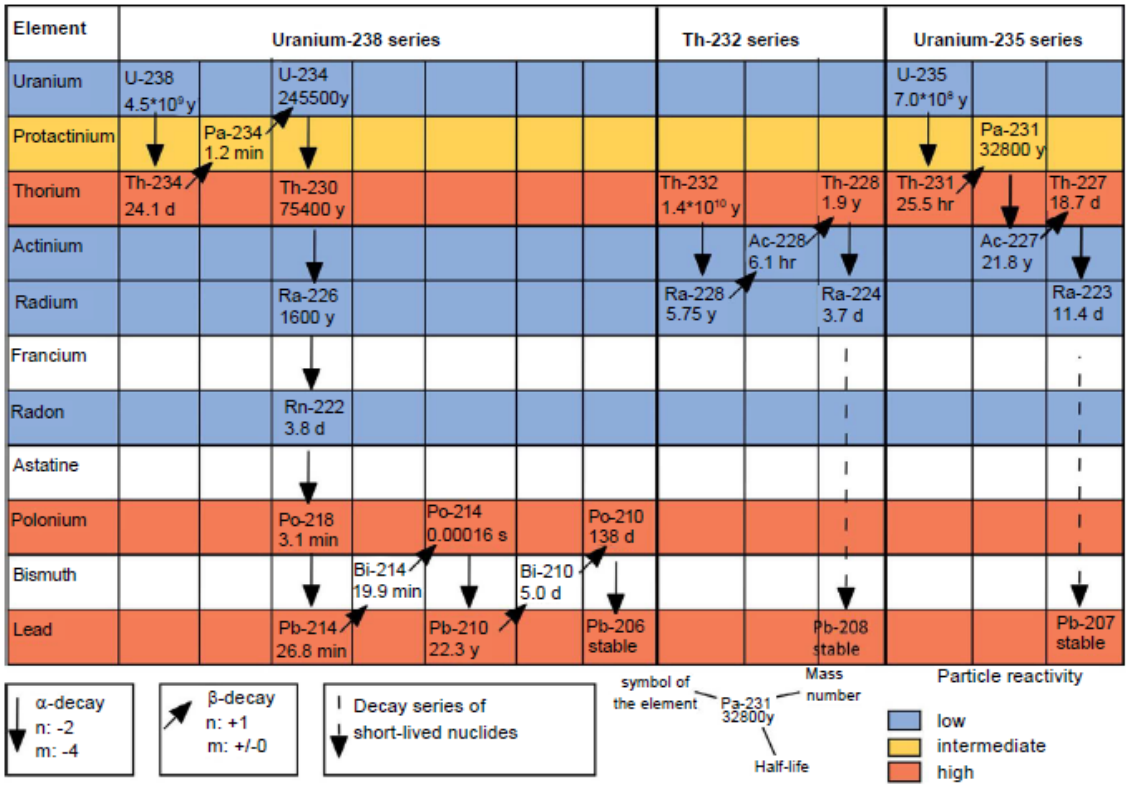


## 3. Energy and radioactivity units

In general, radiation activities in the International System (IS) are accounted as the number of disintegrations per second (Becquerel, Bq). Absorbed doses of exposure to radiation are measured by taking into account not only the energy absorbed (i.e., rad units, J $Kg^{-1}$, or Grays in IS, $10^{-2}$ J $Kg^{-1}$) but also the relative harmfulness of the ionising radiation. This is known as the "equivalent dose" (i.e. rem units) and it is calculated as Q*rad (Q being the biological effectivity or weighting factor: equal to 1 for beta, gamma and X-ray radiation but 20 for alpha particles), usually expressed in Sievert (Sv) in IS (i.e., 100*rem; ICRP 2012).

## 4. Exposure to radiation and biological implications

Natural sources of radiation including rocks/buildings, soils, radon gas production and cosmic radiation cause the greatest exposure for humans to ionising-radiation, accounting for 85% of the annual human radiation dose (WNA 2018). Complementary, up to 14% of public exposure comes from anthropogenic activities such as X-rays and other medical-related treatments, being <1% the exposure coming from past fallouts from nuclear weapons, electricity reactors and coal/geothermal power plants (WNA 2018).

We are all exposed to average doses of ~2.4 mSv $y^{-1}$ from background radiation, varying between 1 – 10 mSv $y^{-1}$, even 50 mSv $y^{-1}$ in certain places, due to intrinsic geological characteristics and/or to altitude (WNA 2018). Importantly, population exposed to high natural doses do not show higher cancer rates or other health problems. Some examples of natural exposures (***Table 6***) can be compared to daily life anthropogenic exposures such as airport security (5 µSv), short flights (5 µSv), long intercontinental flights across the equator (30 µSv, 2-3-fold in higher latitudes), 250h of flight (1 mSv $y^{-1}$), aircrew annual exposure (~5 mSv $y^{-1}$) and nuclear power workers (~50 mSv $y^{-1}$; WNA 2018).

**Table 6. Public exposure to natural radiation** (*WNA 2018*)

| Source of exposure | | Annual effective dose (mSv) | |
|---|---|---|---|
| | | Average | Typical range |
| **Cosmic radiation** | Directly ionising and photon component | 0.28 | |
| | Neutron component | 0.10 | |
| | Cosmogenic radionuclides | 0.01 | |
| | *Total cosmic and cosmogenic* | *0.39* | *0.3–1.0* |
| **External terrestrial radiation** | Outdoors | 0.07 | |
| | Indoors | 0.41 | |
| | *Total external terrestrial radiation* | *0.48* | *0.3-1.0* |
| **Inhalation** | Uranium and thorium series | 0.006 | |
| | Radon (Rn-222) | 1.15 | |
| | Thoron (Rn-220) | 0.1 | |
| | *Total inhalation exposure* | *1.26* | *0.2-10* |
| **Ingestion** | K-40 | 0.17 | |
| | Uranium and thorium series | 0.12 | |
| | *Total ingestion exposure* | *0.29* | *0.2-1.0* |
| **Total** | | **2.4** | **1.0-13** |

The risk of developing cancer above 200 mSv of exposure is well known from high dose cases (comparative examples in ***Table 7***). However, below this value there is a great uncertainty given the incidence of cancer from other factors external to radiation exposure, with no scientific evidence existing for cancer risk or immediate effects at doses < 100 mSv $y^{-1}$ (WNA 2018). Dose rate is equally important to the overall dose as natural mechanisms of the body usually repair cell DNA low-level radiation damage but high-level overwhelms the mechanisms and becomes harmful (WNA 2018).

**Table 7. Comparative whole-body radiation doses and observed effects** *(WNA 2018)*

| Dose | Effects |
|---|---|
| 2.4 mSv $y^{-1}$ | Typical background radiation experienced by everyone (average 1.5 mSv in Australia, 3 mSv in North America). |
| 1.5 to 2.5 mSv $y^{-1}$ | Average dose to Australian uranium miners and US nuclear industry workers, above background and medical. |
| ≤5 mSv $y^{-1}$ | Typical incremental dose for aircrew in middle latitudes. |

| | |
|---|---|
| 9 mSv $y^{-1}$ | Exposure by airline crew flying the New York – Tokyo polar route. |
| 10 mSv $y^{-1}$ | Maximum actual dose to Australian uranium miners. |
| 10 mSv | Effective dose from abdomen & pelvis CT scan. |
| 20 mSv $y^{-1}$ | Current limit (averaged) for nuclear industry employees and uranium miners in most countries. (In Japan: 5 mSv per three months for women) |
| 50 mSv $y^{-1}$ | Former routine limit for nuclear industry employees, now maximum allowable for a single year in most countries (average to be 20 mSv $y^{-1}$ max). It is also the dose rate which arises from natural background levels in several places in Iran, India and Europe. |
| 50 mSv | Allowable short-term dose for emergency workers (IAEA). |
| 100 mSv | Lowest annual level at which increase in cancer risk is evident (UNSCEAR). Above this, the probability of cancer occurrence (rather than the severity) is assumed to increase with dose. No harm has been demonstrated below this dose.<br>Allowable short-term dose for emergency workers taking vital remedial actions (IAEA).<br>Dose from four months on international space station orbiting 350 km up. |
| 130 mSv $y^{-1}$ | Long-term safe level for public after radiological incident, measured 1 m above contaminated ground, calculated from published hourly rate x 0.6. Risk too low to justify any action below this (IAEA). |
| 170 mSv $wk^{-1}$ | 7-day provisionally safe level for public after radiological incident, measured 1 m above contaminated ground (IAEA). |
| 250 mSv | Allowable short-term dose for workers controlling the 2011 Fukushima accident, set as emergency limit elsewhere. |
| 250 mSv $y^{-1}$ | Natural background level at Ramsar in Iran, with no identified health effects (Some exposures reach 700 mSv $y^{-1}$). Maximum allowable annual dose in emergency situations in Japan (NRA). |
| 350 mSv lifetime$^{-1}$ | Criterion for relocating people after Chernobyl accident. |
| 500 mSv | Allowable short-term dose for emergency workers taking life-saving actions (IAEA). |
| 680 mSv $y^{-1}$ | Tolerance dose level allowable to 1955 (assuming gamma, X-ray and beta radiation). |
| 700 mSv $y^{-1}$ | Suggested threshold for maintaining evacuation after nuclear accident.<br>(IAEA has 880 mSv $y^{-1}$ over one month as provisionally safe. |
| 800 mSv $y^{-1}$ | Highest level of natural background radiation recorded, on a Brazilian beach. |
| 1,000 mSv short-term | Assumed to be likely to cause a fatal cancer many years later in about 5 of every 100 persons exposed to it (i.e. if the normal incidence of fatal cancer were 25%, this dose would increase it to 30%)<br>Highest reference level recommended by ICRP for rescue workers in emergency situation. |
| 1,000 mSv short-term | Threshold for causing (temporary) radiation sickness (Acute Radiation Syndrome) such as nausea and decreased white blood cell count, but not death. Above this, severity of illness increases with dose. |
| 5 000 mSv short-term | Would kill about half those receiving it as whole body dose within a month. (However, this is only twice a typical daily therapeutic dose applied to a very small area of the body over 4 to 6 weeks or so to kill malignant cells in cancer treatment.) |
| 10,000 mSv short-term | Fatal within a few weeks. |

Noteworthy, external radiation characterises most of the exposure pathways of radioactive contamination in humans, whether it comes from atmospheric, ground and water bodies or building materials (***Figure 8***). However, during nuclear accidental events there are two other exposure pathways to be taken into account: direct inhalation of radioactive aerosols or gases and ingestion through contaminated foodstuffs and drinkable water (***Figure 8***). Exposure to high radiation levels entails potential long term risks in developing cancers and leukaemia (mostly due to internal radioactive exposure). Nevertheless, significant psychological disturbances on public health (due to lack of radiological/environmental knowledge) are generally the highest and non-negligible impact in the general population after a nuclear power plant accident (Steinhauser et al. 2014).

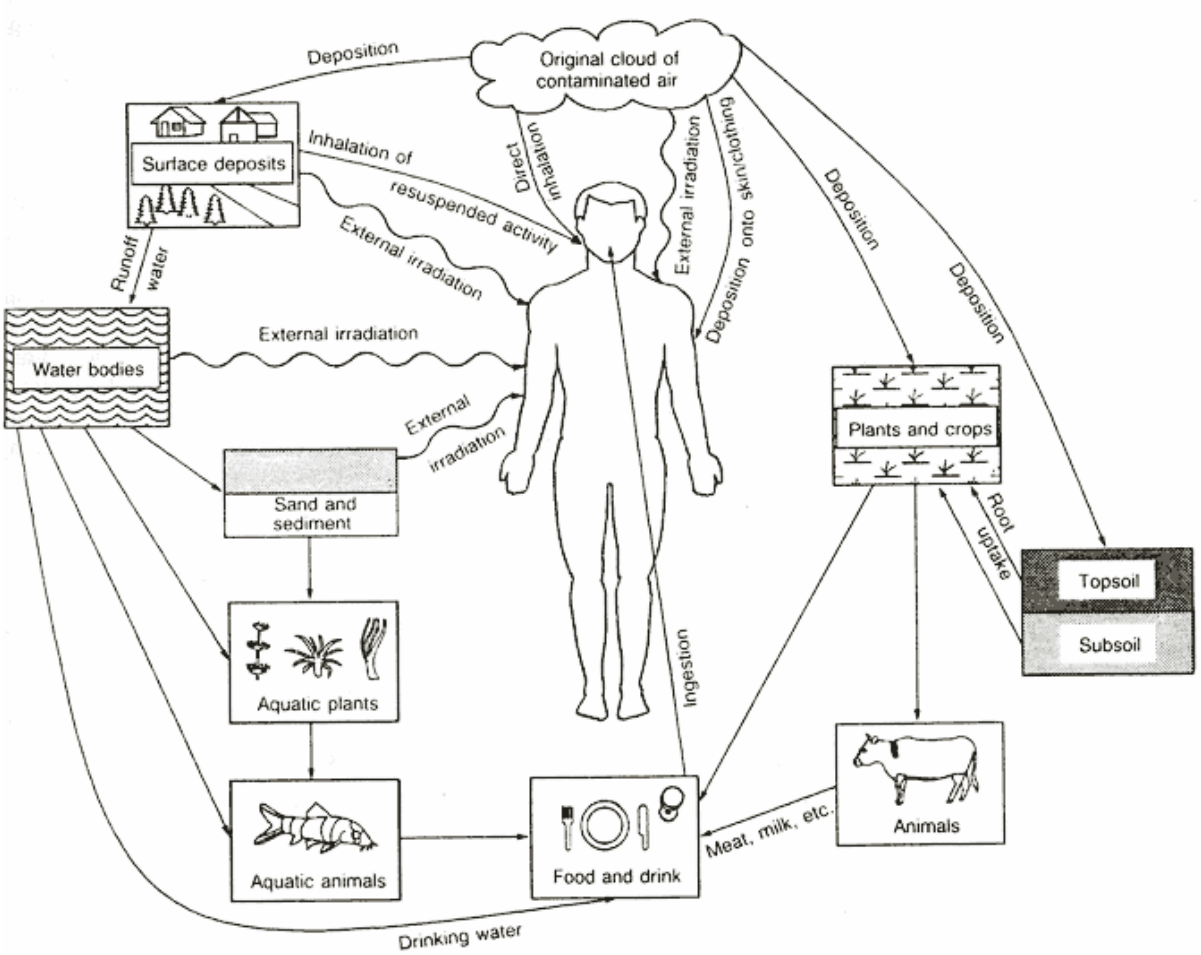


**Figure 8. Main environmental pathways of human radiation exposure** (*IAEA 1991).*

## III. RADIONUCLIDES FROM NUCLEAR POWER PLANTS (NPP)

### 1. Nuclear fission principles and NPP electricity production

The principle of current NPPs relies on fission processes. Fission is induced by bombarding heavy atoms, like U or Pu, with neutrons released from beryllium (excited by previous alpha-emitter atoms) in order to make the nucleus of the heavy atoms more unstable. The newly formed U/Pu excited compound can decay spontaneously into different compounds (e.g., ***Table 5***) or can be subjected to fission, breaking down into lighter atoms of about half the original mass (WNA 2015). The chances of knowing which specific compounds are formed during fission reactions are actually governed by several hundreds of possible combinations (***Figure 9***, WNA 2015). The probability of forming a given nuclide after nuclear fission is referred as "**fission yield**" (Anderson et al. 1941). When the nuclide is formed directly as a product of the moment of fission, its probability is known as the "**independent yield**". However, nuclides can also appear from natural decay of fission products. If this is also taken into account, we refer to the "**cumulative yield**" (independent yield + decay from precursors; Yaffe et al. 1953). Independent fission yields are important for the fundamental understanding of nuclear reactions and short-term practical reactor-operation purposes whereas cumulative yields are relevant for waste storage modelling and control of nuclear reactors.

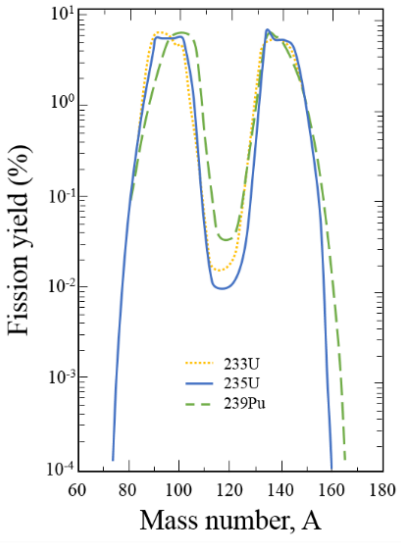


**Figure 9. Smoothed probability distribution of fission products produced from $^{233}$U, $^{235}$U and $^{239}$Pu thermal neutron induced fission** *(Adapted from Seaborg and Loveland 1990).*

Fission processes release energy in the form of kinetic energy, quickly converted into heat as fission fragments travel in the solid fuel. They also release gamma rays and more neutrons, ~2.5 in average, which sustain fission chain reactions within the fuel (WNA 2015). The probability that a neutron is captured within the nucleus of the fuel and the chances that it undergoes fission depends on the velocity of the bombarded neutron (generally better with slow-energy or ***thermal neutrons***) and on the heavy nucleus involved (*i.e.,* fissionable nuclides, generally $^{235}$U and/or $^{239}$Pu; WNA 2015).

***Prompt neutrons*** or neutrons released instantaneously from fissionable or fissile heavy nucleus can also activate fertile isotopes in the fuel to undergo fission (e.g., fertile $^{238}$U → fissile $^{239}$Pu). Differences are: ***fissionable*** (capable of undergoing fission after neutron capture), ***fissile*** (those undergoing fission after low-energy/thermal neutron capture) and ***fertile*** (initially not fissionable but potentially converted to fissile after neutron capture). Otherwise, prompt neutrons are lost through the core walls, especially for those near the sheath with an outwards moving direction, by interacting

with other reactor core materials (e.g., zirconium and steel alloys, acting as moderators) or are lost as resonance capture, which occurs when the neutron has insufficient energy to cause fission. Fast neutrons are generally undesirable for the steady-state of the reactor, thus, generally controlled by moderation. Moderator materials such as graphite or water (light-$^{1}$H or heavy-$^{2}$H) are used to achieve appropriate neutron energies (WNA 2015).

The heat energy released in the fission reactions is used to heat up water pipes, so that water vapour can power the turbines of the electric generator (***Figure 10***). Nuclear power plants control the fission process by control rods within the reactor, which are generally composed of boron (B) and/or cadmium (Cd). Their role is to adsorb the neutrons released in the reactions and limit the number of fission reactions to only those where one neutron is involved per fission step and, thus, controlling the amount of energy generated at a steady level. They can also stop the fission reactions if all the rods are introduced, as they would adsorb all the neutrons. In this case, heat is still produced in the reactor core as a consequence of the radioactive particles released within the de-excitement of transuranic compounds and natural decay of fission products (WNA 2015). The reactor is therefore cooled down so that the heat does not damage the protection structures.

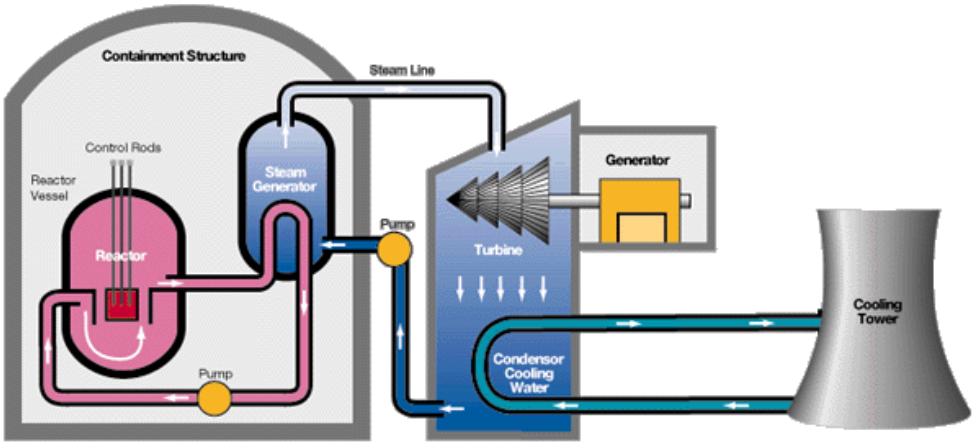


**Figure 10. General scheme of a Pressurised-Water Reactor (PWR) in a NPP** *(Miller 2012).*

Over time, several reactor types and security measures (Generation I, II, III, III+ and lately IV) have been designed and improved to produce electricity with higher efficiency, safety and lower wastes. Some of the most known reactor types are listed here (***Table 8***) being the pressurised water reactors (PWR) the most common reactor used worldwide (94% of NPP; WNA 2015). Details of new generation reactors and trends for future constructions will not be described herein.

**Table 8. Nuclear power plants in commercial operation** *(WNA 2018)*

| Reactor type | Main countries | Number | GWe | Fuel | Coolant | Moderator |
|---|---|---|---|---|---|---|
| Pressurised water reactor (PWR) | US, France, Japan, Russia, China | 292 | 275 | enriched $UO_2$ | water | water |
| Boiling water reactor (BWR) | US, Japan, Sweden | 75 | 73 | enriched $UO_2$ | water | water |
| Pressurised heavy water reactor (PHWR) | Canada, India | 49 | 25 | natural $UO_2$ | heavy water | heavy water |
| Gas-cooled reactor (AGR & Magnox) | UK | 14 | 8 | natural U (metal), enriched $UO_2$ | $CO_2$ | graphite |
| Light water graphite reactor (RBMK & EGP) | Russia | 11 + 4 | 10 | enriched $UO_2$ | water | graphite |
| Fast neutron reactor (FBR) | Russia | 3 | 1.4 | $PuO_2$ and $UO_2$ | liquid sodium | none |
| | **TOTAL** | **448** | **392** | | | |

## 2. Causes of past NPP accidental events

The International Nuclear and Radiological Event Scale (INES, ***Figure 11***) is a tool that rates with a logarithmic scale the safety significance of nuclear and radiological events, including uses and transport of radioactive materials in industrial, medical and nuclear facilities (IAEA 2017). In total, 7 levels are rated for three different categories: people and environment (i.e., degree of radiation doses to humans and environmental dispersion), radiological barriers and control (i.e., degree of unplanned high radiation level release applicable for inside facilities) and defence-in-depth (i.e., degree of unexpected failure of accidental prevention measures with no direct impact on humans and the environment). There are three major NPP accidental events in human history: Three Mile Island (Pennsylvania, 28th March 1979, INES 5), Chernobyl (CNPP, Ukraine, 26th April 1986, INES 7) and Fukushima Daiichi (FDNPP, Japan, 11th March 2011, INES 7). In this study, only INES 7 accidents will be described.

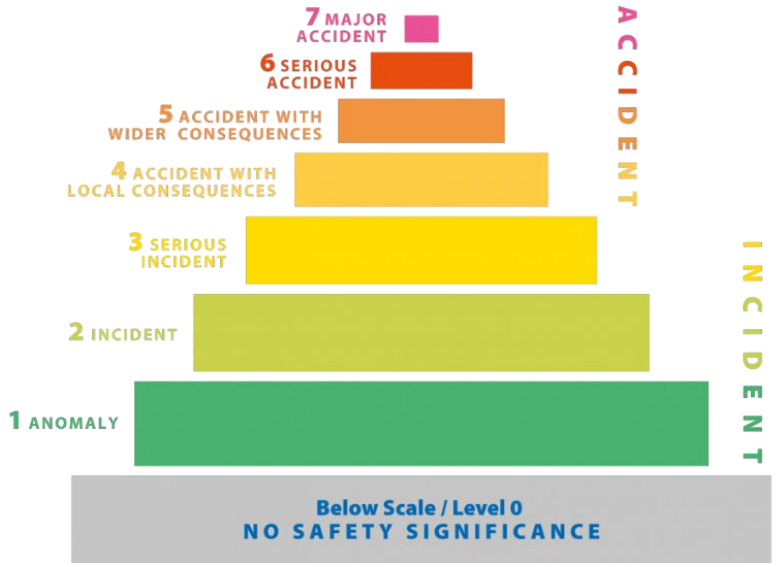


**Figure 11. International Nuclear and Radiological Event Scale, INES** *(IAEA 2017).*

The Chernobyl complex had four nuclear reactors (RBMK-1000 design since 1970, 1977 and 1983) and two more under construction at the time of the accident, with an artificial lake near the river Pripyat for cooling (WNA 2018). They were graphite-moderated boiling light water reactors that used slightly enriched U-oxide fuel (2% $^{235}U$) and water as coolant as well as steam producer to feed the turbines directly (WNA 2018). The accident on 1986 was related to a test of the turbines prior to routine shutdown from maintenance. The idea was to check if the slowing down of the turbines in case of a main loss of the electrical power supply would provide enough electrical power to operate the main core cooling water pumps before relying on the diesel emergency power supply. For this, the automatic emergency core cooling shutdown mechanisms were disabled and, when the reactor was manually shut down, its operating power was below the desirable conditions for the test. The subsequent efforts to recover the power of the reactor were hampered by xenon poisoning (i.e., Xe building up in the fuel rods, reducing fission by absorbing neutrons), thus almost all control rods were completely removed. When the turbine was turned off, feeding water pumps also decreased the cooling supply, favouring heating and steam bubble formation in the cooling water, i.e., reducing the amount of water required to absorb neutrons, burning out the remaining Xe and favouring the fission reaction rate to increase rapidly in the fuel. Such increase in uncontrolled power generation lead to the rupture of fuel elements, ignition of graphite moderators and increased steam formation causing a first steam explosion followed seconds later by others related to $H_2$ build-up due to reaction between the zirconium cladding and steam (WNA 2018). These explosions ejected fuel, moderator and structural materials and left the destroyed core open to the atmosphere. Most of the heavier fallout radioactive fission products and core debris deposited in <100 km from the site whereas light components (fission products and noble gases) where dispersed by the wind (WNA 2018). The release of short-lived fission products resulted in high dose rates in nearby areas and further releases continued for 10 days due to graphite fire (Steinhauser et al. 2014).

The Fukushima Daiichi complex had six nuclear reactors (BWRs, operating since 1971-75) near the coast of Japan, three in working conditions minutes before the earthquake and the other three not operating (WNA 2018). When the earthquake was registered (i.e., magnitude 9.0 in Richter scale in the Pacific Ocean at 163 km from Fukushima NPPs), units 1-3 were automatically shut down and no serious damage was directly made to the reactors by this natural phenomenon. The emergency diesel generators were started up to cool down the reactor as foreseen, based on seawater cooling. However, the tsunami waves generated from the open ocean earthquake caused massive coastline destruction. At the NPPs, the inland waves surpassed the 10 m sea wall protection, submerging and damaging the seawater pumps of both main and auxiliary cooling circuits as well as the diesel generators, electrical switchgears and batteries, leaving the station in blackout (Steinhauser et al. 2014; WNA 2018). This means that the reactor cores were still producing 1.5% of their nominal thermal power from product

decay without cooling nor heat removal. This caused damage and partial meltdown of fuel elements accompanied by bursting of fuel cladding (Steinhauser et al. 2014). This produced steam and high pressure in the reactors, initially released into the dry primary containment through safety valves. However, the drop of the water level produced $H_2$ building up as in CNPP, due to the interaction between the steam and zirconium fuel cladding (WNA 2018). Hydrogen explosions took place, even in unit 4 which only stored spent fuel in water ponds (i.e., standard protocol before being transferred to dry storage). Seawater was also injected in all ponds from units 1-4 to control the developing high heat load but, apparently, the spent fuel in these ponds was not significantly damaged by the explosions nor by the tsunami effect (WNA 2018). Radioactive releases were accounted for both atmospheric (mainly from $H_2$ explosions and controlled venting progressively during one week; Steinhauser et al. 2014) and water compartments (releasing ~10 400 $m^3$ of slightly contaminated water with total activities of 0.15 TBq after 1 month of the accident and continuously during 6 years after the accident; WNA 2018; Song 2018).

## 3. Examples of NPP incidents in France

The Institute of Radioprotection and Nuclear Security (IRSN) in France has a record of historical accidental and incidental events in French NPPs (IRSN 2009). The only accidental event (INES 4) was registered in February 1980 at the Saint-Laurent-des-Eaux (Loir-et-Cher) NPP where a technical failure led to the local ignition of the fuel. The accident seriously damaged the installation but did not entrain important risk outside the facilities. Other incidents (INES 3) occurred in the particle accelerator from Electron Beam System-EBS at Forbach in 1991 and in the aerospace research centre of ONERA at Toulouse in 2008. These incidents were related to serious radiation exposure of interim employees to an industrial accelerator while operating and to exposure of a radioactive source of $^{60}Co$, respectively. Lower incidents (INES 2) have been registered at the plutonium studio (ATPu) at Cadarache in 2006, a medical centre at Dijon in 2007 and at Cruas-Meysse NPP in 2009. The incident with plutonium was related to unsuitable instructions/procedures during overloading of milling processes to reduce powder scrap whereas the one in Dijon was related to irradiation of a technician during radiotherapy treatment of a patient. The incident in Cruas-Meysse NPP consisted on an important loss of cooling systems due to simultaneous failure during the night, compromising the nuclear safety of reactor nº4. The rest of the incidents are generally classified as anomalies (INES 1), and more than several hundred are declared per year. These incidents have several causes which potentially compromise both general human safety (***Figure 12a***) and the environment (***Figure 12b***).

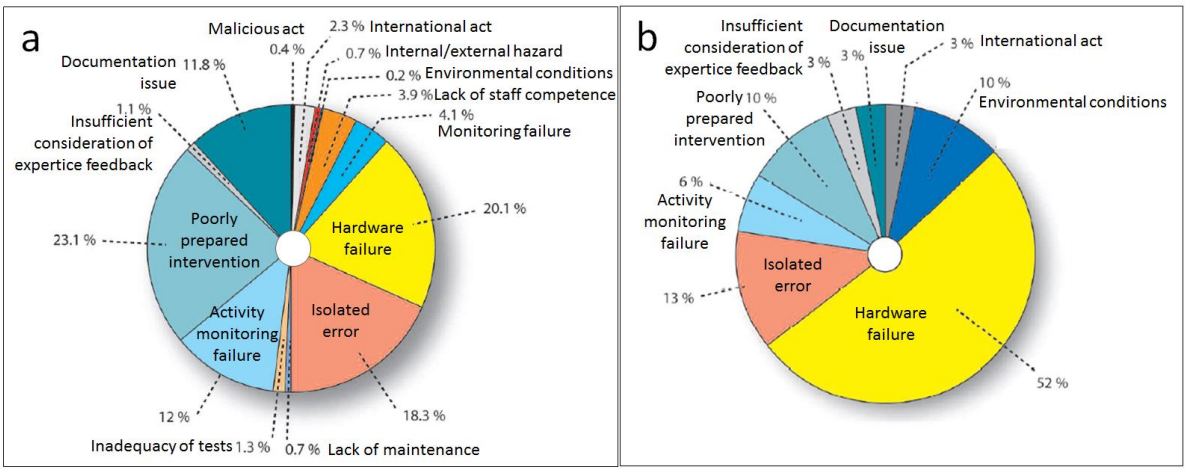


**Figure 12. Summary of breakdown declared incidents in French NPPs in the year 2005** concerning (a) safety and (b) environmental incidents, classified according to main cause. *(ASN Annual Report).*

## 4. Environmental lessons from past NPP accidental events: case of Cs in aquatic systems

It is implied that historical NPP accidents had consequences at the international level and, from the management and nuclear safety point of view, it promoted joint efforts towards the improvement of nuclear safety measures for local NPPs and nuclear installations. For instance, routine riverine sites subjected to NPPs now have long-term surveys to control natural and NPP admissible radioactive level discharges (e.g., French rivers by the IRSN).

It is important to highlight that each accident released different amounts of radionuclides to the environment (Steinhauser et al. 2014), suggesting that there is no standard scenario describing the amount of radionuclides released for predicting potential future accidents and respective environmental discharges and consequences. In any case, several radionuclides are generally followed-up after NPP accidents, or at least quantified at some point after the accidental event mostly in atmospheric samples (***Table 9***), with much lower knowledge and radionuclide diversity for water matrices. The latter remains a current topic of research since the FDNPP accident in 2011 (Buesseler et al. 2017).

In this section, only environmental lessons from accidental events, especially FDNPP in aquatic environments, will be described, particularly centred on Cs transport/dispersion due to its long-term half-life ($^{137}$Cs) and frequency in reported literature. In fact, the successive events leading to the FDNPP accident in March 2011 released important radioactive liquids to the coast and ocean, especially known for radiocaesium (Buesseler et al. 2017). These radiocaesium releases were still observed one year after the accident (Kanda 2013), suggesting that NPP accidental events are not exclusively point sources of contamination.

**Table 9. Examples of activity levels emitted to the atmosphere and ocean after Chernobyl (CNPP) and Fukushima Daiichi (FDNPP) nuclear power plant accidents.** Elements of interest for this work are highlighted (red). *1PBq = $10^{15}$ Bq

| Radionuclide | Half-lives ($T_{1/2}$) | Atmospheric activity (PBq) | | Oceanic activity (PBq)* | |
|---|---|---|---|---|---|
| | | CNPP | FDNPP | CNPP | FDNPP |
| *Noble gases* | | | | | |
| $^{85}$Kr | 10.75 y | 33 [a] | 44 [a] | | |
| $^{133}$Xe | 5.25 d | 6500 [a] | 14000 [a] | | |
| *Volatile* | | | | | |
| $^{3}$H | 12.3 y | 1.4 [a] | N/A | | |
| **$^{129m}$Te** | **33.6 d** | **240 [a]** | **~15 [a]** | | |
| **$^{132}$Te** | **3.20 d** | **~1150 [a]** | **~180 [a]** | | |
| $^{129}$I | 15.7.$10^{6}$ y | 4-4.8.$10^{-5}$ [a] | 5.5.$10^{-5}$ [a] | | |
| $^{131}$I | 8.03 d | ~1760 [a] | 150-160 [a,b] | | ~11 [b] |
| $^{133}$I | 20.8 h | 910 [a] | 146 [a] | | |
| $^{134}$Cs | 2.07 y | ~47 [a] | 11.8 [a] | | 3.5[d] |
| $^{136}$Cs | 13 d | 36 [a] | 2.6 [a] | | |
| $^{137}$Cs | 30.1 y | 85 [a] | 12-36 [a,b] | 16 [b] | 4-27 [b] |
| *Elements with intermediate volatility* | | | | | |
| $^{89}$Sr | 50.5 d | ~115 [a] | ~0.2 [a] | | |
| $^{90}$Sr | 28.9 y | ~10 [a] | ~0.02 [a] | | 0.1-2.2 [b] |
| $^{103}$Ru | 39.2 d | >168 [a] | | | |
| $^{106}$Ru | 372 d | >73 [a] | | | |
| $^{140}$Ba | 12.8 d | 240 [a] | | | |
| *Refractory elements* | | | | | |
| $^{95}$Zr | 64 d | 84 [a] | | | |
| $^{99}$Mo | 66 h | >72 [a] | | | |
| **$^{125}$Sb** | **2.76 y** | **0.23 [a]** | | | |
| $^{141}$Ce | 32.5 d | 84 [a] | | | |
| $^{144}$Ce | 285 d | ~50 [a] | | | |
| $^{154}$Eu | 8.60 y | 0.13 [a] | | | |
| $^{239}$Np | 2.36 d | 400 [a] | | | |
| $^{238}$Pu | 87.7 y | 0.015 [a] | 2-5.$10^{-6}$ [a] | | |
| $^{239}$Pu | 24100 y | 0.013 [a] | | | |
| $^{240}$Pu | 6560 y | 0.018 [a] | | | |
| $^{241}$Pu | 14.3 y | ~2.6 [a] | 1.1.-2.6.$10^{-4}$ [a] | | |
| $^{242}$Pu | 3.76.$10^{5}$ y | 4.$10^{-5}$ [a] | | | |
| $^{241}$Am | 433 y | 0.0024 [a] | | | |
| $^{242}$Cm | 163 d | ~0.4 [a] | | | |
| $^{244}$Cm | 18.1 y | 0.0027 [a] | | | |
| **Total (excluding noble gases)** | | **~5300 [a]** | **~520 (340 – 800)[a]** | | |

[a]Steinhauser et al. 2014; [b]Aliyu et al. 2015; [c]Buesseler et al. 2017; [d]Thakur et al. 2013; N/A: not available or not found

Average release rates of radiocaesium in Fukushima, between the artificial harbour facility of the NPP and coastal waters, were estimated to be 93 GBq $d^{-1}$ in summer 2011 and 8.1 GBq $d^{-1}$ in summer

2012 (Kanda 2013). Dispersion patterns in the open central and western Pacific Ocean using the short-lived $^{134}Cs$ as a proxy of FDNPP signal (compared to past e.g., $^{137}Cs$ background levels of 0.0012 – 0.0015 Bq $L^{-1}$), showed little transport between March and May 2011, and even two years later, towards the islands of Hawaii and Guam, despite that intermediate sites showed $^{134}Cs$ ranging between 0.001 and 0.004 Bq $L^{-1}$ (with 2 to 3-fold increase in background $^{137}Cs$; Kameník et al. 2013). This was explained by the southern boundary of the Kuroshio and its extension currents acting as boundaries for open ocean radioactive dispersion and redirecting it within the North Pacific Gyre and within the Global Ocean conveyor belt (Povinec et al. 2013). Such is the interest on Cs that the Center for Marine and Environmental Radiation (CMER) together with the Woods Hole Oceanographic Institution (WHOI) have recently created a webpage (*http://www.ourradioactiveocean.org/*) to inform about past and current Cs radioactive levels in measured worldwide oceans (from 2011 to nowadays). Activities higher than background levels were also detected in organisms near Japanese coasts (e.g., phytoplankton, macroalgae, mussels) and in migratory species (e.g., fish) in the Atlantic Ocean within the first year after the FDNPP accident (Kanisch and Aust 2013; Baumann et al. 2013; Nakata et al. 2015).

Most of the direct releases of radiocaesium to the water by FDNPP seem to have dispersed along the coastline (i.e., max. 30 km offshore, measured and confirmed by dispersion models; Tsumune et al. 2013) with sporadic open ocean transfer when entering in mesoscale eddies (Choi et al. 2013). Nevertheless, the role of suspended particles is non-negligible, with sinking particles in the subarctic gyre and the subtropical gyre registering FDNPP-derived radiocaesium (0.14 – 0.25 Bq $g^{-1}$) during late March and early April 2011 (Honda et al. 2013). Coastal sediments have been recently regarded as secondary sources of FDNPP-derived radiocaesium due to adsorption of Cs onto sand grains days to weeks after the accident, when waves and tides brought back the dissolved contamination to brackish freshwater-seawater underground mixing areas in the coast, being nowadays released back to the ocean through submarine groundwater discharge even at places far from the site (Sanial et al. 2017). Other continent-ocean interfaces presenting this salinity gradient characteristics are fluvial-estuarine systems, which are also influenced by continental and atmospheric radioactive contamination. In fact, heavy rains six months after the FDNPP (e.g., Typhoon Roke) where shown to increase radioactive Cs dissolved (i.e., from 0.009-0.098 Bq $L^{-1}$ to 0.85 Bq $L^{-1}$) and particulate concentrations (up to 100% of total transported radiocaesium) in rivers from Fukushima Prefecture due to Cs releases from both storage watershed sediments and atmospheric wet deposition (Nagao et al. 2013). Therefore, understanding the radioactive transport and biogeochemical behaviour of other less studied radionuclides in these complex systems require interdisciplinary and comprehensive approaches from multiple environmental compartments. In addition, there is more knowledge about radiocaesium dispersion in aquatic systems than for the rest of the emitted radionuclides (***Table 9***), in particular for antimony (Sb) and tellurium (Te), the elements of interest in this work.

# IV. RADIOACTIVE AND STABLE ISOTOPES OF ANTIMONY AND TELLURIUM

## 1. Radioactive antimony (Sb) and tellurium (Te)

### 1.1. Radionuclides of Sb and Te in NPPs

The presence and concentration of specific radionuclides in the nuclear fuel and reactor core structures depend on the fissionable fuel content and on the fuel burnup, also known as fuel utilisation or the fraction of fuel atoms already spent in fission. For example, higher burnups produce increased fission products and oxygen-to-metal ratios in the fuel (Kleykamp 1985). Nevertheless, even low fuel burnups of 1% produce detectable concentrations of Sb and Te radionuclide fission products (Kleykamp 1985).

The chemical composition of fission products in oxide fuels have different classifications. For instance, Sb falls within the metallic precipitates, forming alloys, e.g., Pd-Sn-Sb-Te ingots (Kleykamp 1985). In fact, activated reactor core structures contain radioactive Sn and Sb due to the presence of Sn in zirconium alloy within core structures, and to Sn activation into radioactive $^{125}$Sb (Iguchi et al. 2006).

However, Te falls within several categories: as metallic precipitates (with U, Pd or Sn), as ceramic precipitates (oxides, e.g., Ba-O-Te or Ba-Cs-Te complexes) and as oxides dissolved in the fuel (like Cs) at low burnups (forming e.g., Pu-O-Te or Ba-Sr-Te-O systems; Kleykamp 1985), depending on the fuel properties and temperatures. In fact, there are registered fuel brands where the fuel cladding is coated with graphite lubricant to minimise pellet or fission product interactions with cladding elements like zirconium (Zr). Such is the case of Te when relatively high centreline temperatures are achieved in the fuel, combining with Cs fission products (e.g., $Cs_2Te$, highly soluble in water) or migrating to form compounds with Pd and Zr at higher oxygen potentials in light-water reactors-LWR (McFarlane 1996). Under accidental conditions, alloying Sn in cladding is put in solution where it can react with Te (SnTe, becoming less water soluble). Thus, at temperatures >1400ºK any segregated Te (elemental, oxide, SnTe or $Cs_2Te$) will become volatile and below this temperature it will dissolve within the coolant or collect within the containment building walls (McFarlane 1996).

This is in accordance with other radionuclide studies after NPP accidental releases classifying Sb as a refractory radionuclide and Te within the volatile species (e.g., ***Table 9***). A refractory element is non-volatile and falls within those elements with boiling points > 1673ºK (Izrael 2002), thus, it is an element that would be expected to be released to the environment in case of accidental events following the fate of the fuel or reactor core structures.

Nevertheless, the VERCORS programme developed by the French Nuclear Protection and Safety Institute (IPSN) in collaboration with EDF, have been performing relevant experiments since 1984 at

the Laboratory of Active Materials (LAMA) facility in the Grenoble centre of CEA (Commissariat à l'Énergie Atomique) to understand the release and behaviour of fission products. That is, they have subjected fuel rods to representative conditions of PWR accidents (i.e., different fuel degradation, partial or total melt down, etc.) at different temperatures and realistic fuel compositions ($UO_2$, MOX, high burn-ups, etc.). Results from several test series concluded that both Sb and Te (as well as Cs) fall within the category of volatile fission products, highly to almost completely released at fuel rod temperatures ~2623ºK (Pontillon et al. 2010).

Furthermore, nuclear fuel reprocessing plants seem to generate liquid low level radioactive waste containing both Te and Sb (Ito et al. 2003). For instance, releases of 1 GBq $y^{-1}$ $^{124}Sb$ and 1000-20000 GBq $y^{-1}$ $^{125}Sb$ have been observed from La Hague, with respective <0.3 mBq $L^{-1}$ and ~1 Bq $kg^{-1}$ activities after 1990's (GRNC 1999). It is also known that nuclear installations (NPP amongst others) are allowed to release in a controlled manner certain radionuclides in their liquid discharges comprising $^{124}Sb$ (IRSN 2013) and $^{125}Sb$, e.g., showing activities of ~0.1 mBq $L^{-1}$ between 2002 and 2012 in the Rhône River (Eyrolle-Boyer et al. 2015), corresponding to 5-10 GBq in 2008 (DEI/SESURE 2010-04, IRSN). Thus, this brief review suggests that the specific forms in which Te and Sb will be released during hypothetical NPP accidents cannot be foreseen, despite their suspected species formed within NPP installations.

### 1.2. Knowledge on Sb and Te radionuclide environmental releases

Little is known about the fate of less studied radionuclide releases after NPP accidents (i.e., CNPP and FDNPP). Furthermore, different NPP accidents display different emission patterns related to the intrinsic accidental characteristics and fuel conditions. In general, the CNPP accident released many refractory elements due to explosions and thermal disintegration (>2700ºK, necessary for the volatilisation of refractory components), emitting 100 km away from the site ~1.5% of the fuel in particulate form. Contrastingly, FDNPP accident was contained enough time to avoid the release of fast-disintegrating isotopes and the reactor did not reach such high temperatures (Steinhauser et al. 2014). Nevertheless, the failure of the cooling systems melted the fuel rods and this is thought to explain the high radioactive indices found in the cooling water. A short summary of radioactive Sb and Te NPP releases into several environmental compartments (mostly focused on aquatic environments) will be briefly described below.

- ***Radioactive Sb***

Out of 42 Sb radionuclides, only three show relevant half-lives rendering Sb radionuclides persistent in environmental compartments: $^{124}Sb$ ($t_{1/2}$ = 60 d), $^{126}Sb$ ($t_{1/2}$ = 12.4 d) and $^{125}Sb$ ($t_{1/2}$ = 2.76

y). Sporadic studies on environmental releases from CNPP mainly focus on $^{125}$Sb, quantifying its activity in different compartments but seldom explaining its speciation nor environmental behaviour. Likewise, there are almost no single studies focusing exclusively on $^{125}$Sb releases, thus adding a difficulty to its bibliographic search and comprehensive environmental understanding. This is related to the relatively low $^{125}$Sb emissions and depositions outside of the CNPP industrial site (i.e. 0.23 PBq on the 6th of May for the 4th reactor; Steinhauser et al. 2014) compared to other emitted radionuclides (***Table 9***).

Nevertheless, $^{125}$Sb was widely dispersed worldwide through atmospheric transport after the CNPP accident, with comparable deposition rates to those of other relevant radionuclides (e.g., Pearson correlation of 0.916 between $^{137}$Cs and $^{125}$Sb in Finnish soils; Lehto et al. 2008). Measurable activities have been found in continental surface samples all over Europe. For example, in Greek grass ($10^5$ Bq kg$^{-1}$) and soils (4.4 Bq kg$^{-1}$; Papastefanou et al. 1988) as well as in Finnish lichen soils (~2000 Bq m$^{-2}$ in 1987, 24% still present in 1990; Lehto et al. 2008) and in the uppermost 3 cm of humus layers (1.4 – 14 Bq kg$^{-1}$ 1999-2000; Ylipieti et al. 2008). Russian territory also contained Sb relicts from CNPP in the first 4 cm of a soil profile 6.5 years after the accident (max. 23.2 ± 3.1 kBq m$^{-2}$) for an estimated original 60 kBq $^{125}$Sb m$^{-2}$ ground deposition compared to 900 kBq $^{134}$Cs m$^{-2}$ and 1600 kBq $^{137}$Cs m$^{-2}$ (Carbol et al. 2003).

Despite the non-direct radioactive discharge of the CNPP accident to aquatic systems, some studies report atmospheric-water interactions and presence of radioactive Sb in aquatic media. A transfer from radioactive debris emitted by CNPP to reactive natural particles in Lake Constance in 1986 showed 300 Bq m$^{-2}$ of $^{125}$Sb sediment loading (Robbins et al. 1992). Contrastingly, $^{125}$Sb deposition from CNPP in the Scheldt Estuary seemed to have no direct impact. Measurements along its salinity and turbidity gradients before and after the accident showed no changes in $^{125}$Sb particle content, attributing the high $^{125}$Sb marine input entering the estuary to the anthropogenic discharges from La Hague and Sellafield (Martin et al. 1994). Furthermore, impacts of $^{125}$Sb in aquatic systems can also be detected in aquatic organisms based on $^{125}$Sb soft tissue content. For instance, marine bivalves and gastropods at Monaco, one month after CNPP accident, contained activities ranging between 0.48 and 4.2 Bq kg$^{-1}$ f.w. in *M. galloprovincialis* and up to 22 Bq kg$^{-1}$ f.w. in *P. lusitanica* (Whitehead et al. 1988). All these studies suggest that atmospheric deposition of radioactive Sb from accidental events is potentially soluble and bioavailable in aquatic systems.

Detectable amounts of $^{125}$Sb also occurred in atmospheric samples and soils after the FDNPP accident (Kojima et al. 2012; Thakur et al. 2013). Furthermore, despite the direct discharge of radionuclides to coastal waters, there are fewer examples of radioactive Sb in aquatic studies than those found for the previous CNPP accident. Only one study in marine bottom sediments near

Fukushima along the coast of Japan reported activities of $^{125}$Sb between 1 and 10 Bq kg$^{-1}$ from May 2011 to February 2012 (Kusakabe et al. 2013).

Long-term studies from continuous $^{125}$Sb discharges from fuel reprocessing plants to the coastal environments use this radionuclide as a radiotracer for the understanding of oceanic hydrodynamic processes. For instance, $^{125}$Sb discharges from the nuclear fuel reprocessing plant of La Hague have been used as a conservative tracer to quantify the contribution of artificial radioactivity from La Hague to the Norwegian Channel and the Barents Sea (e.g., du Bois et al. 1995; Guegueniat et al. 1997; du Bois et al. 1999). Furthermore, studies in the coastal area of La Hague show biotransfer of $^{125}$Sb discharges in macroalgae (i.e., varying concentrations between 1 and 60 Bq kg$^{-1}$ d.w. between 1980-1990; Germain et al. 1990; Masson et al. 1995) and in bivalves/gastropods (i.e., 0.20-2.50 Bq kg$^{-1}$ f.w. and up to 5 Bq kg$^{-1}$ in mussels; Gandon et al. 1998; Germain et al. 1990) with concentrations below detection limits since 2000. These studies suggest that both relatively sporadic (acute, from accidental events) and continuous (chronic, from nuclear facilities) Sb radionuclide releases in aquatic environments are somehow transferred to organisms.

- ***Radioactive Te***

There are more than 30 radionuclides of Te, all showing relatively short half-lives ($t_{1/2}$ < days). The particularity of Te radionuclides is that they present several metastable forms, many of which show longer half-lives than the parent radionuclides: $^{129m}$Te ($t_{1/2}$ = 33.6 d), $^{125m}$Te ($t_{1/2}$ = 57.4 d), $^{127m}$Te ($t_{1/2}$ = 106 d), $^{123m}$Te ($t_{1/2}$ = 119 d). Metastable radionuclides are long-lasting intermediate states (long-lived excited) that some decaying radionuclides present before reaching the daughter radionuclide. Contrastingly, the rest of Te radionuclides present shorter half-lives, finding the highest for $^{132}$Te ($t_{1/2}$ = 3.20 d) and $^{121}$Te ($t_{1/2}$ = 19.2 d). Nevertheless, the most followed Te radionuclides after an accidental NPP event are $^{132}$Te, $^{129}$Te and $^{129m}$Te (e.g., Liu et al. 1990; Hirose et al. 2016). This is likely due to the relatively high fission yield of $^{132}$Te (despite its short half-life) and the fact that $^{129m}$Te decays into $^{129}$Te, explaining its presence in the environment even months after the accidental event. The rest of the aforementioned radionuclides are not followed due to other preferential decay pathways (i.e., not all metastable forms are formed 100% between decaying radionuclide steps) and/or due to low parent radionuclide fission yields. Therefore, despite their relatively longer half-lives, they are less often produced, thus, not followed.

Unlike Sb, Te was released during both CNPP and FDNPP accidents with relevant activities (i.e., 1150 PBq and 180 PBq, respectively, for $^{132}$Te) compared to those of Cs (i.e., between 12 and 85 PBq for $^{137}$Cs) and I (between 150 and 1700 PBq of $^{131}$I, ***Table 9***). Some studies estimate that $^{137}$Cs releases during CNPP accident constituted 33 ± 10% of the core inventory whereas 10-60% of $^{132}$Te was released

during the accident (Guntay et al. 1997). The CNPP-derived Te was observed in European rain water deposition (Santschi et al. 1990) and in airborne samples as far as the United States (i.e., several locations in the western U.S.; Liu et al. 1990). It was also detected in grass from Romania (estimated $^{132}$Te deposition of 344 kBq m$^{-2}$ for May 1986; Cosma 2002) and in seawater and bivalves from the coast of Monaco (i.e., 0.13 – 0.36 Bq L$^{-1}$ on early May 1986, 270 Bq kg$^{-1}$ f.w. in *M. galloprovincialis* and up to 3168 Bq kg$^{-1}$ f.w. in *P. lusitanica*; Whitehead et al. 1988).

Mathematical calculations assessed $^{132}$Te as the third largest radionuclide released from FDNPP accident, after $^{133}$Xe and $^{131}$I (Tagami et al. 2013). Its atmospheric dispersion was worldwide, showing $^{132}$Te activities between March-April 2011 of ~0.02 to 0.3 mBq m$^{-3}$ in Europe (Lozano et al. 2011; Baeza et al. 2012), ranging from 0.01 to 14 mBq m$^{-3}$ in USA and Canada (Thakur et al. 2012) and reaching up to 5400 mBq m$^{-2}$ onsite in Japan (Thakur et al. 2012). Estimations about dose rates from FDNPP deposition in soils suggest that iodine radionuclides ($^{132}$I then $^{131}$I) are the primary contributors to β-ray air dose during the first days after the accidental release. After decaying, dose rates of the next 30 days after the accident are dominated by the $^{129m}$Te/$^{129}$Te radionuclide pair, with $^{134}$Cs and $^{137}$Cs being responsible for the long-term dose (Endo et al. 2014). This is in accordance with the activities observed in rain water from San Francisco Bay during the first 20 days after FDNPP accident, showing highest values for I radionuclides (~1 – 10 Bq L$^{-1}$), then Te (~0.1 – 1 Bq L$^{-1}$) and lowest for Cs (~0.01 – 0.1 Bq L$^{-1}$; Smith et al. 2014).

Despite the higher relevance of radioactive Te compared to Sb, and the direct water discharges from FDNPP to the coastal area, few studies report Te activities from FDNPP in aquatic environments, most of them only mentioning the fact that it has been measured but not specifying its activity values (Kryshev et al. 2012). Nevertheless, it is known that enhanced dissolution of Te fission products from fuel cladding occurs in oxidising conditions when cladding drying out takes place before saltwater intrusion in the reactor (Espegren et al. 2018). An environmental study on marine bottom sediments near Fukushima along the coast of Japan in May 2011 to February 2012 recorded activities of $^{129m}$Te and $^{129}$Te between 10 and 100 Bq kg$^{-1}$ (Kusakabe et al. 2013).

All the above highlight that the importance of Te radionuclides from NPP activities and accidental events is recognised. It has been observed in several environmental compartments, suggesting extensive dispersion and transfer from the NPP into environmentally bioavailable forms. Nevertheless, its environmental behaviour and fate are unknown and need further understanding. Furthermore, environmental releases of Te radionuclides are expected to occur in the future given that some nuclear waste treatment procedures favour Te production from the induced nuclear decay of heavy long-lived actinides in subcritical accelerator driven systems (Maugeri et al. 2014). This further supports the importance of studying the environmental fate of short-lived radionuclides such as Te.

### 1.3. Antimony and tellurium radioactive decay chains

Antimony and Te radionuclides and fission products show natural decays towards more stable elemental forms, like the natural U and Th decay series (***Table 5***). The particularity of these Sb and Te radionuclides is that most radioisotopes belong to the same decay chain (***Figure 13***). In fact, several studies use this well-known decay of Sb radionuclides into Te for scientific purposes, especially in analytical chemistry applications (e.g., specificity of gamma-ray spectra, calibrations of high resolution detectors; Rajput et al. 2012; Egnatuk and Wang 2015) and in specific radionuclide production for nuclear medical theragnostics and other applications (e.g., Uddin et al. 2011). Noteworthy, the most followed-up radionuclides after accidental events (e.g., $^{131}$I, $^{134}$Cs, $^{137}$Cs) are also present in these natural decay series (***Figure 13***).

These decay chains and associated fission yields (***Figure 13***) suggest that Sb radioisotopes are produced in ~8% chance from $^{235}$U fuel and 7% for $^{239}$Pu in <24h from both direct fission and as decaying elements from other fission products, i.e., similar to the ~9 – 12% fission yields for Cs and I isotopes obtained from the same calculations. A small percentage (<0.25%) from other radioisotope decays would still produce Sb isotopes in the following years. The most probable Sb outcomes from nuclear fission reactions are $^{131}$Sb, $^{132}$Sb and $^{133}$Sb, all of which mainly decay to Xe or Cs stable isotopes. From all the possible outcomes, <0.007 % of the cases produce stable Sb isotopes ($^{121}$Sb or $^{123}$Sb), meaning that nearly all the Sb species produced are radioactive.

Similar calculations for Te radionuclides suggest decay and fission yield productions of 24% chance from $^{235}$U fuel and 20% for $^{239}$Pu in <24h, with a small contribution from natural decay of other fission products in the following years. The most probable outcomes are isotopes ranging from $^{130}$Te to $^{135}$Te, eventually decaying into stable Ba, Cs and Xe. In this case, these high isotopic abundances match other studies (i.e., 60% of Te abundances in fuel are from $^{131}$Te, $^{132}$Te, $^{133m}$Te and $^{134}$Te; Alonso and González 1991) and the commonly studied $^{132}$Te after NPP accidental events. From all the possible outcomes, 5-9% of the cases produce stable Te isotopes, meaning that nearly all the Te species produced are radioactive.

These calculations do not take into account specific fuel characteristics. They serve as comparative basis between elements of study but do not represent real accidental conditions. Temporal scales, however, should be somehow representative of their environmental persistence. In any case, these decay series imply that the decay of radioactive Sb and Te emitted to the environment during NPP accidental events involve a change of element over time. This potentially implies a change in the biogeochemical behaviour of the radioactive trace, within the same environmental compartment (e.g., different geochemical behaviours between Sb and Te in aquatic systems), or transfer efficiency/rate

to another compartment involving biological intake or a change in the state of matter (e.g., from radioactive $^{132}$Te to bio-essential, radioactive $^{132}$I or from radioactive $^{133}$I to radioactive gaseous $^{133}$Xe).

Consequently, both decaying timescales and father/daughter elements should be considered in environmental radionuclide dispersion scenarios after hypothetical NPP accidents to better understand how: (i) the chemical speciation and behaviour of radionuclides (particularly Te) will affect the transport and presence of daughter radionuclides (like the biologically hazardous radioactive iodine; McFarlane 1996), and (ii) how environmental timescales (e.g., regional hydrodynamics) and anthropogenic activities (e.g., daily/weekly dredging in estuaries) will coexist in such conditions/events, providing unexpected outcomes. In order to include such radionuclide dispersion scenarios in radioactive risk assessment schemes, information on radioactive dose should also be taken into account.

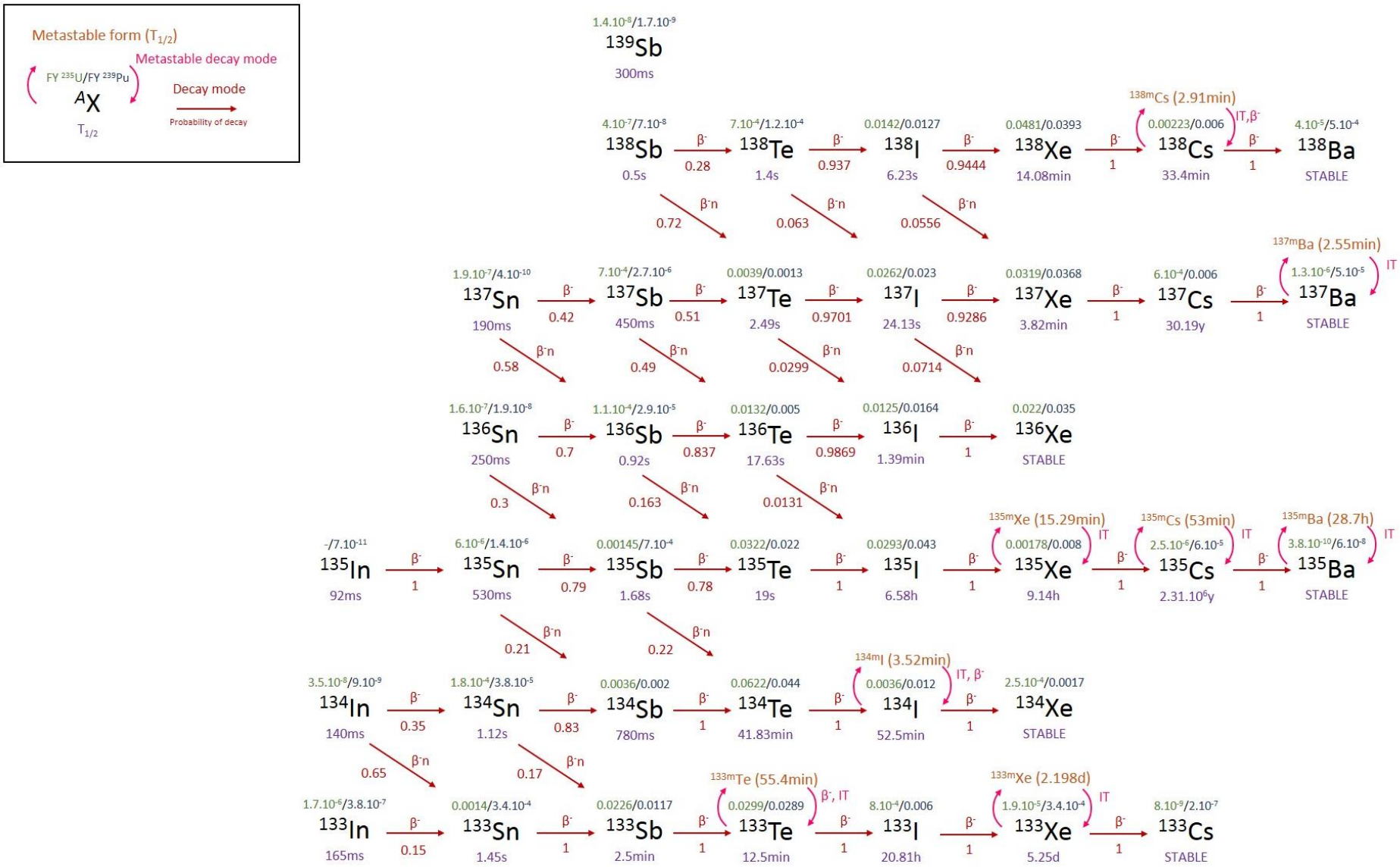
Metastable form ($T_{1/2}$)
Metastable decay mode
FY $^{235}$U/FY $^{239}$Pu
$^{A}$X
$T_{1/2}$
Decay mode
Probability of decay
1.4.10$^{-8}$/1.7.10$^{-9}$
$^{139}$Sb
300ms
$^{138m}$Cs (2.91min)
4.10$^{-7}$/7.10$^{-8}$
$^{138}$Sb
0.5s
0.28
7.10$^{-4}$/1.2.10$^{-4}$
$^{138}$Te
1.4s
0.937
0.0142/0.0127
$^{138}$I
6.23s
0.9444
0.0481/0.0393
$^{138}$Xe
14.08min
1
0.00223/0.006
IT,β$^-$
$^{138}$Cs
33.4min
1
4.10$^{-5}$/5.10$^{-4}$
$^{138}$Ba
STABLE
β$^-$n
0.72
0.063
0.0556
$^{137m}$Ba (2.55min)
1.9.10$^{-7}$/4.10$^{-10}$
$^{137}$Sn
190ms
0.42
7.10$^{-4}$/2.7.10$^{-6}$
$^{137}$Sb
450ms
0.51
0.0039/0.0013
$^{137}$Te
2.49s
0.9701
0.0262/0.023
$^{137}$I
24.13s
0.9286
0.0319/0.0368
$^{137}$Xe
3.82min
1
6.10$^{-4}$/0.006
$^{137}$Cs
30.19y
1
1.3.10$^{-6}$/5.10$^{-5}$
IT
$^{137}$Ba
STABLE
0.58
0.49
0.0299
0.0714
1.6.10$^{-7}$/1.9.10$^{-8}$
$^{136}$Sn
250ms
0.7
1.1.10$^{-4}$/2.9.10$^{-5}$
$^{136}$Sb
0.92s
0.837
0.0132/0.005
$^{136}$Te
17.63s
0.9869
0.0125/0.0164
$^{136}$I
1.39min
1
0.022/0.035
$^{136}$Xe
STABLE
0.3
0.163
0.0131
$^{135m}$Xe (15.29min)
$^{135m}$Cs (53min)
$^{135m}$Ba (28.7h)
-/7.10$^{-11}$
$^{135}$In
92ms
1
6.10$^{-6}$/1.4.10$^{-6}$
$^{135}$Sn
530ms
0.79
0.00145/7.10$^{-4}$
$^{135}$Sb
1.68s
0.78
0.0322/0.022
$^{135}$Te
19s
1
0.0293/0.043
$^{135}$I
6.58h
1
0.00178/0.008
IT
$^{135}$Xe
9.14h
1
2.5.10$^{-6}$/6.10$^{-5}$
IT
$^{135}$Cs
2.31.10$^{6}$y
1
3.8.10$^{-10}$/6.10$^{-8}$
IT
$^{135}$Ba
STABLE
0.21
0.22
$^{134m}$I (3.52min)
3.5.10$^{-8}$/9.10$^{-9}$
$^{134}$In
140ms
0.35
1.8.10$^{-4}$/3.8.10$^{-5}$
$^{134}$Sn
1.12s
0.83
0.0036/0.002
$^{134}$Sb
780ms
1
0.0622/0.044
$^{134}$Te
41.83min
1
0.0036/0.012
IT, β$^-$
$^{134}$I
52.5min
1
2.5.10$^{-4}$/0.0017
$^{134}$Xe
STABLE
0.65
0.17
$^{133m}$Te (55.4min)
$^{133m}$Xe (2.198d)
1.7.10$^{-6}$/3.8.10$^{-7}$
$^{133}$In
165ms
0.15
0.0014/3.4.10$^{-4}$
$^{133}$Sn
1.45s
1
0.0226/0.0117
$^{133}$Sb
2.5min
1
0.0299/0.0289
β$^-$, IT
$^{133}$Te
12.5min
1
8.10$^{-4}$/0.006
$^{133}$I
20.81h
1
1.9.10$^{-5}$/3.4.10$^{-4}$
IT
$^{133}$Xe
5.25d
1
8.10$^{-9}$/2.10$^{-7}$
$^{133}$Cs
STABLE

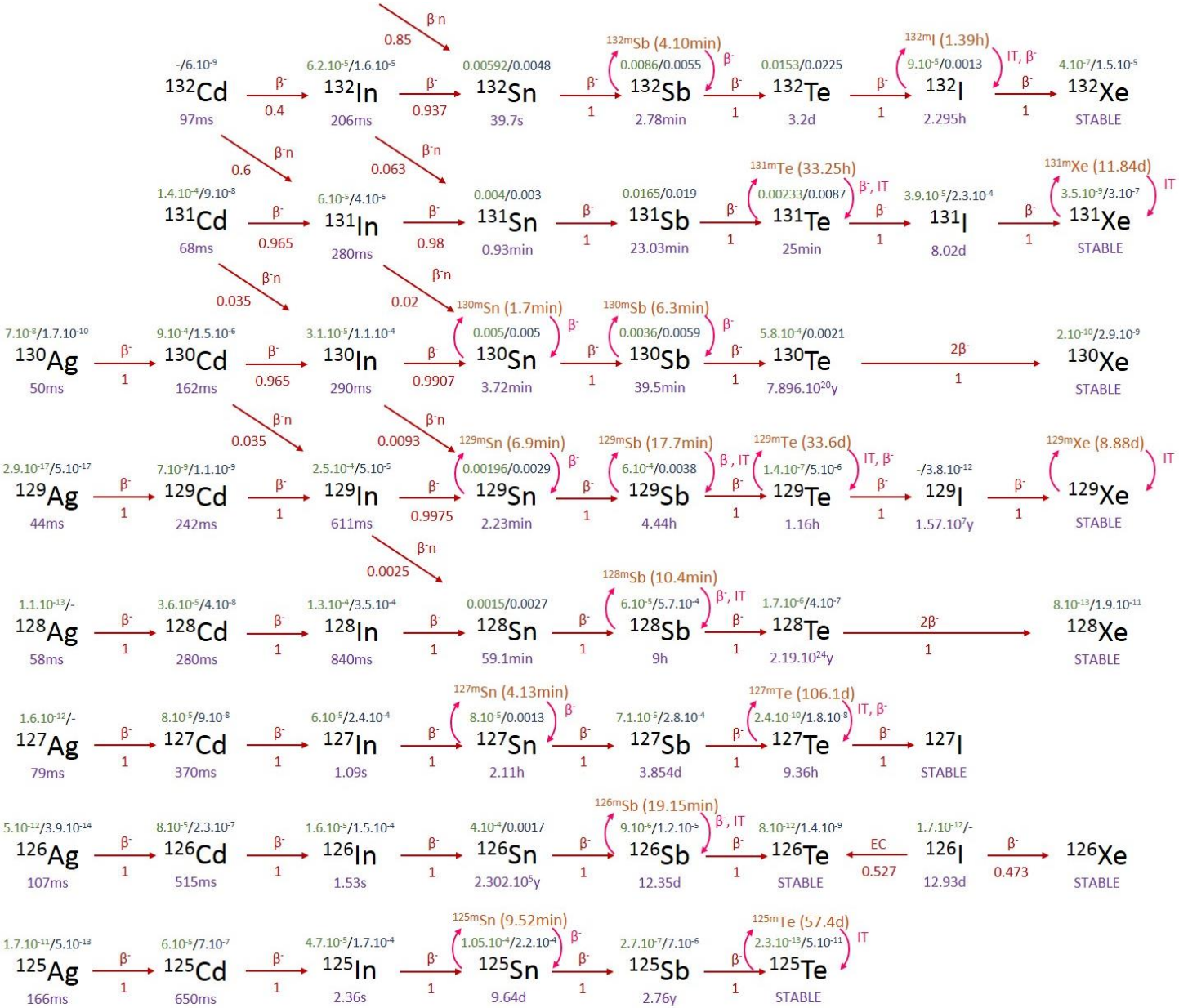
132Cd 97ms
132In 206ms
132Sn 39.7s
132mSb (4.10min)
132Sb 2.78min
132Te 3.2d
132mI (1.39h)
132I 2.295h
132Xe STABLE
131Cd 68ms
131In 280ms
131Sn 0.93min
131Sb 23.03min
131mTe (33.25h)
131Te 25min
131I 8.02d
131mXe (11.84d)
131Xe STABLE
130Ag 50ms
130Cd 162ms
130In 290ms
130mSn (1.7min)
130Sn 3.72min
130mSb (6.3min)
130Sb 39.5min
130Te 7.896.10^20y
130Xe STABLE
129Ag 44ms
129Cd 242ms
129In 611ms
129mSn (6.9min)
129Sn 2.23min
129mSb (17.7min)
129Sb 4.44h
129mTe (33.6d)
129Te 1.16h
129I 1.57.10^7y
129mXe (8.88d)
129Xe STABLE
128Ag 58ms
128Cd 280ms
128In 840ms
128Sn 59.1min
128mSb (10.4min)
128Sb 9h
128Te 2.19.10^24y
128Xe STABLE
127Ag 79ms
127Cd 370ms
127In 1.09s
127mSn (4.13min)
127Sn 2.11h
127Sb 3.854d
127mTe (106.1d)
127Te 9.36h
127I STABLE
126Ag 107ms
126Cd 515ms
126In 1.53s
126Sn 2.302.10^5y
126mSb (19.15min)
126Sb 12.35d
126Te STABLE
126I 12.93d
126Xe STABLE
125Ag 166ms
125Cd 650ms
125In 2.36s
125mSn (9.52min)
125Sn 9.64d
125Sb 2.76y
125mTe (57.4d)
125Te STABLE

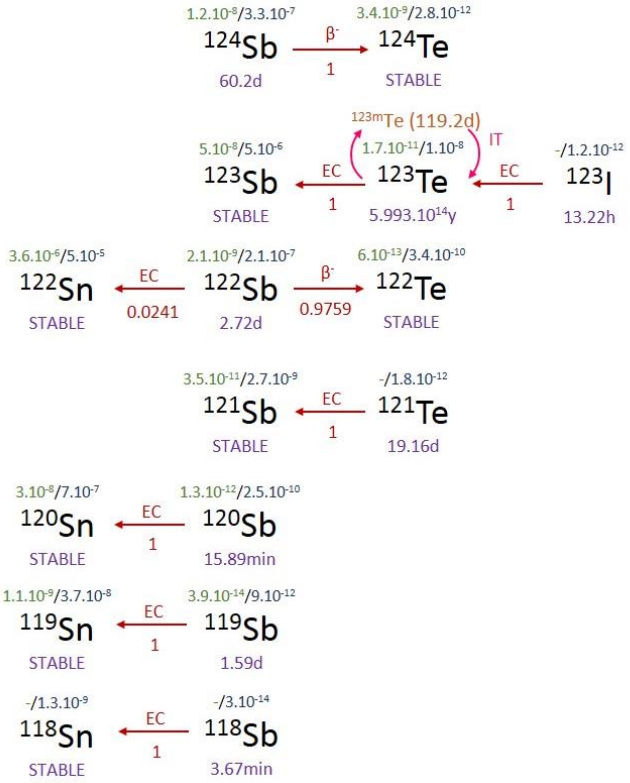


**Figure 13. Decay chains of Sb and Te radionuclides.** Information on corresponding half-lives (below each isotope $^{A}X$), decay modes (electron capture-EC, beta decay-$\beta^-$, isomeric transitions-IT), decay direction (red arrows), decay probability (from 0 to 1) and independent fission yields (FY) for $^{235}U/^{239}Pu$ fuels (above each isotope $^{A}X$) are given. Metastable nuclides (in orange) and respective half-lives are also shown when appropriate, not specifying their probability of being formed. Empty arrows on the right (blue) denote the decay lines containing the most followed-up Sb and Te radionuclides after NPP accidental events. *(The above decay chains have been assembled using available data from Element Collection Inc., and Sonzogni 2013)*.

## 2. Stable antimony (Sb) and tellurium (Te)

This section mainly aims at presenting the current knowledge on environmental biogeochemical behaviour of stable isotopes from the elements of study (Sb and Te) in aquatic systems. It is not intended to be a systematic review, as in fully describing all existing literature (Petticrew 2003), on the elements of study to elucidate their biogeochemical cycles. The idea is rather to provide useful tools concerning background knowledge on Sb and Te cycling in aquatic systems for a better understanding of the results obtained in the following chapters related to estuarine environments.

In general, trace elements show different forms or species in aquatic environments. These range from free ions to complexed species (i.e., forming inorganic ligands, colloids, simple and/or macromolecular organic matter complexes). They can also be adsorbed or incorporated to suspended organic or inorganic particles and interact (i.e., ad/absorb) with living organisms (Filella and Williams 2012). All these forms will determine the environmental behaviour of the trace element within and between compartments (***Figure 14***), that is, its transport, fluxes, reactivity and bioavailability. Elemental sources, environmental concentrations, anthropogenic implications and organism toxicity will be also briefly presented to understand the origin of natural Sb and Te as well as the anthropogenic print in their biogeochemical cycles.

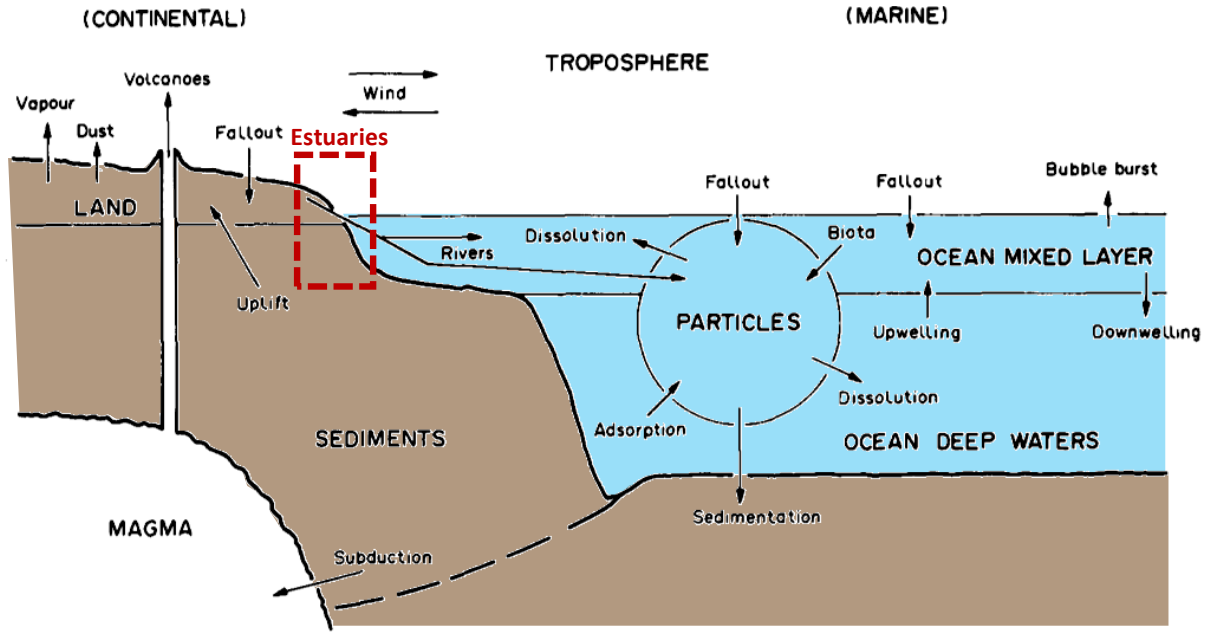


**Figure 14. Schematic example of environmental compartments considered in geochemical cycling models.** Global biogeochemical cycles of trace elements consider several main reservoirs (in capital letters) interacting by fluxes (arrows). Estuaries are highlighted in a red box *(Austin and Millward 1967).*

## 2.1. Sources, applications, chemical properties, concentrations and toxicity of stable Sb

### *2.1.1. Anthropogenic sources and applications*

Natural sources constituting Sb background levels are mainly related to orogenic weathering and transport, e.g., airborne dust, sea-salt spray and soil runoff (Qi et al. 2008; Smichowski 2008). Volcanic eruptions also contribute to natural Sb global emissions, though only between 3 – 5% (Smichowski 2008).

The use of Sb in human civilisation dates back to 4000 b.c. for medicine, veterinary, ornamental and cosmetic purposes (Shortland 2002; Smichowski 2008). It was also used to purify gold (Au) from silver (Ag) and Cu until the 18$^{th}$ century by adding stibnite ($Sb_2S_3$) to the mixture, separating silver sulphide from Au-Sb alloy by decantation during successive melting steps and ultimately separating Au from Sb oxide (Filella et al. 2002a).

Modern applications have broadened Sb uses including it in the manufacturing of semiconductors, lead-acid (LA) batteries, ammunition (as lead-Pb hardener), computer chips, antifriction alloys and PVC cable sheathing (Filella et al. 2002a). In the form of antimony trioxide (ATO-$Sb_2O_3$, forming low soluble $Sb(OH)_3$ in aquatic systems; Herath et al. 2017), Sb is used as pigment in paints, opacifier in ceramics, decolouriser in glassware and flame retardant in plastics, rubber, textiles, and others. A relevant application is also its use as a condensation catalyst (also in the form of ATO) in the manufacture of polyethylene terephthalate (PET; used in drinking bottles, food packaging, etc.), as an additive for vulcanising rubber (as $Sb_2S_5$) and as a component of brake linings (ATO), among other industrial end-products (Cal-Prieto et al. 2000; Filella et al. 2002a; Smichowski 2008; Ferreira et al. 2014). The relative importance of each product (USGS 2018) from primary Sb consumption is: 31% in non-metal products (e.g., glassware and ceramics, as sodium antimonate), 31% in flame retardants (as ATO) and 38% in metal products (e.g., ammunition and LA batteries in automotive vehicles as metallic Sb or antimonial lead; Carlin 2006).

Despite these multiple technical applications, the major sources of Sb contamination are related to coal and fuel combustion (with Sb concentrations between 0.05 – 10 mg $kg^{-1}$; Tian et al. 2014), mining operations, shooting ranges and copper smelters (Filella et al. 2002a; Reimann et al. 2010; Ungureanu et al. 2015), being abrasion from car brake pads, tires, street surfaces and vehicle exhaust emissions the main sources of Sb in urban dust (WHO 2003; Furuta et al. 2005; Harmens et al. 2013).

Atmospheric transport and wet/dry deposition are important dispersion mechanisms given the Sb records in ombrotrophic peat bogs and surface ocean waters (Cutter and Cutter 1995; Shotyk et al. 1996). Peat records from pre-anthropogenic periods suggest worldwide background natural Sb deposition rate fluxes of 0.35 µg $m^{-2}$ $y^{-1}$ (Shotyk et al. 2004). Nowadays, Sb atmospheric levels and

aerosols are mostly dominated by anthropogenic emissions from, e.g., fuel combustion, mining, smelting/refining, brake wear and waste incineration (***Figure 15***) which show short-term, 1-2 weeks, Sb atmospheric residence times (Tian et al. 2014).

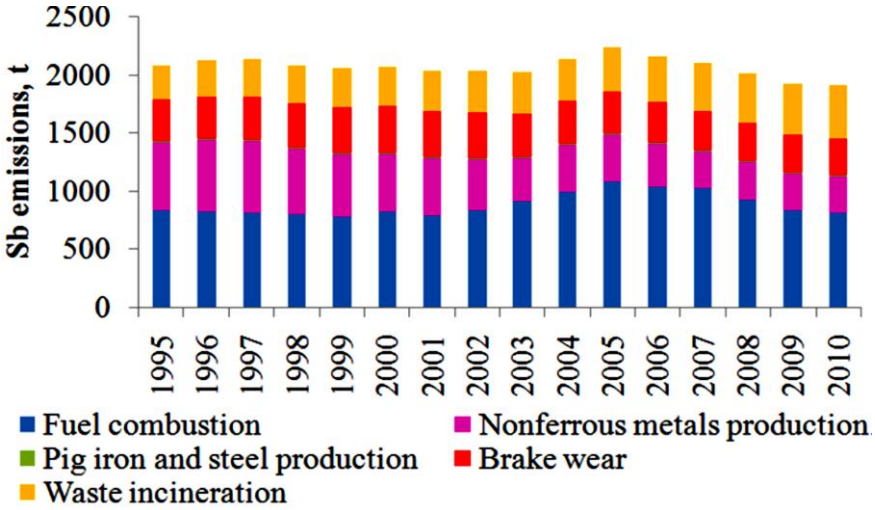


**Figure 15. Atmospheric Sb trends by sectors** *(Tian et al. 2014)*

Anthropogenic emissions have increased natural Sb atmospheric emissions by 100- to 200-fold (Cal-Prieto et al. 2000). This has been evidenced in both ice cores registering Arctic air quality alteration of 50% during the past three decades and in an ombrotrophic peat bog from Switzerland comprising the past 2000 years with enrichment factors of 70 (Shotyk et al. 1996; Krachler et al. 2005).

In fact, world annual production of Sb has increased from 7000 t since the 1900's to 180000 t in 2015 (***Figure 16***), with an increased production rate for the 1990's (Mlynarski 1998). It is currently extracted from Sb ores and world reserves mainly centred in China (> 80% of world output since 1995) and other areas in Bolivia, Mexico, Australia, South Africa and Eastern Countries such as Tajikistan and Russia (Filella et al. 2002a; USGS 2018). It has been estimated that Sb resources can potentially last for 30 years (Butterman and Carlin 2004; Herath et al. 2017). However, market evolution should also be taken into account as Sb has been recently classified as a post-2014 critical element, that is, an element presenting a risk of future supply disruption (Hayes and McCullough 2018).

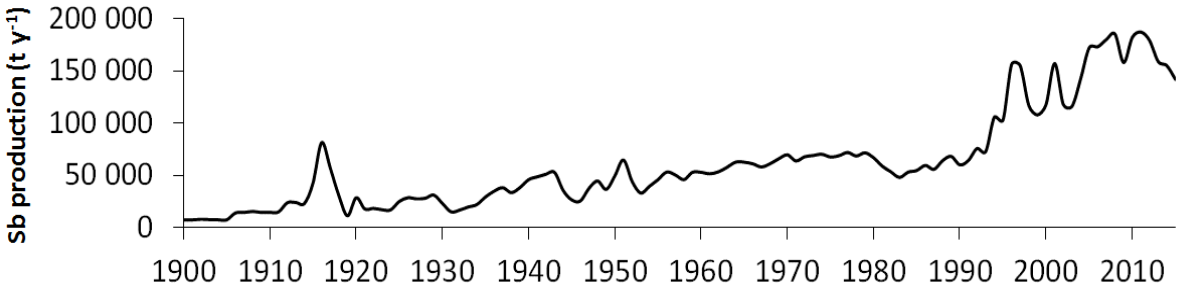


**Figure 16. Worldwide Sb production** between 1900 and 2015 *(Mlynarski 1998).*

Some recycling regulations have been taken with the aim of producing less Sb waste/pollution, optimising natural resources to better satisfy the demand (Carlin 2006). Most of the recycling activities are related to LA batteries showing recycling rates of about 20% for 2000 in the USA. However, future recycling trends are expected to decrease given the new forms of automotive batteries and ammunition, declining the use of Pb (thus, antimonial lead) due to environmental concerns, being replaced by Ca-Pb and tungsten, steel or bismuth-tin alloys, respectively (Butterman and Carlin 2004; Carlin 2006).

### *2.1.2. Environmental speciation and redox dynamics*

- *Chemical speciation*

Antimony (*Z* = 51, *A* = 121.75) is a metalloid belonging to Group 15 of the periodic table together with nitrogen (N), phosphorous (P), arsenic (As) and bismuth (Bi). It has two naturally stable isotopes (i.e. 57.3% $^{121}$Sb and 42.7% $^{123}$Sb; Salminen et al. 2005) and four oxidation states: - III, +III, +V and rarely in elemental form. Metallic Sb is stable in air at room temperature, insoluble in HCl and dissolves in $H_2SO_4$, forming Sb(III)- and Sb(V)-oxides in $HNO_3$ (Biver 2011). In environmental compartments, Sb(III) and Sb(V) are the predominant species (Reimann et al. 2010) being present in both oxic and anoxic conditions in the form of organic and inorganic species (***Figure 17***).

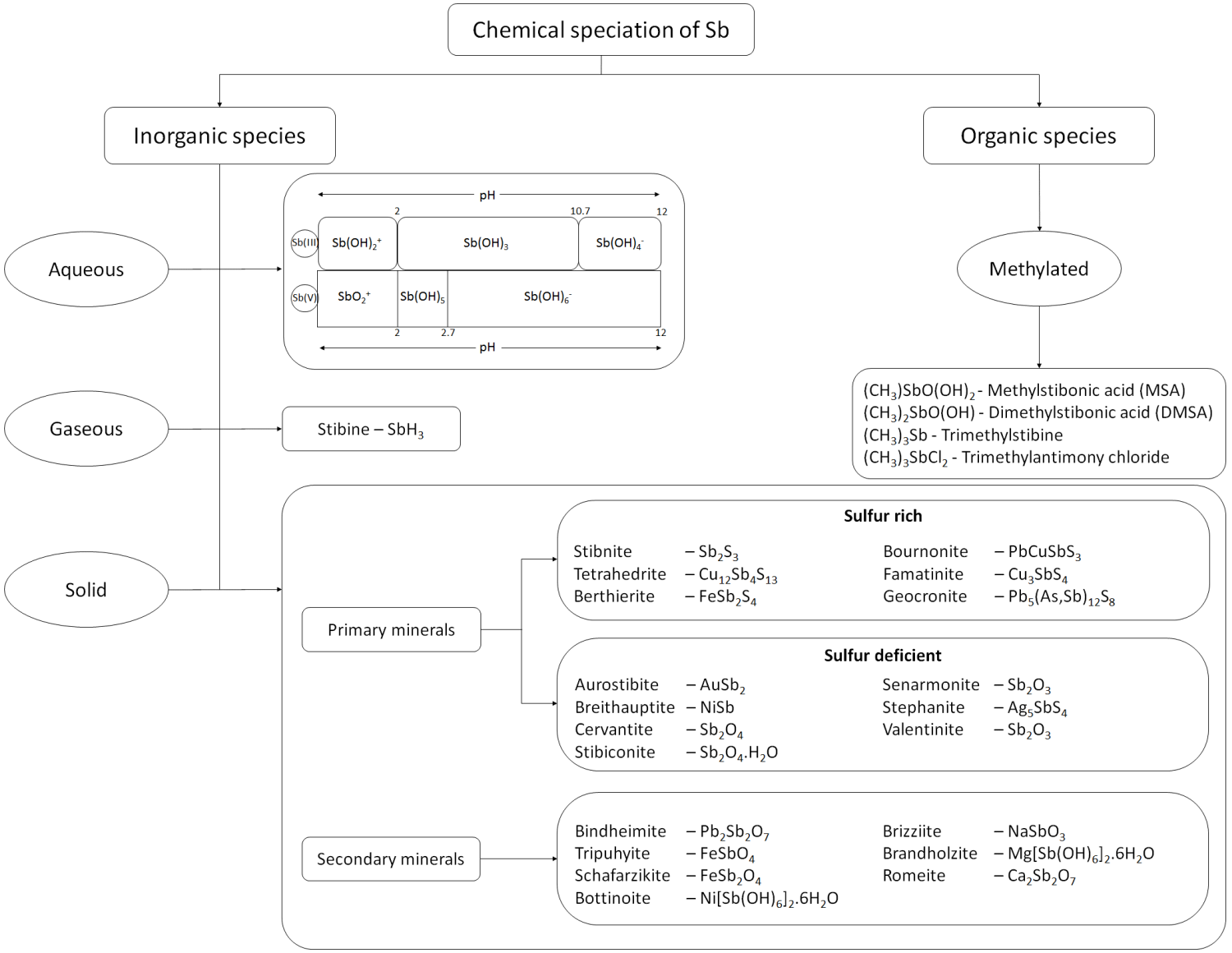


**Figure 17. Common environmental chemical species of Sb.** (*Modified from Herath et al. 2017; for aqueous Sb speciation, personal communication M. Filella*)

- *Volatile species*

The most known inorganic volatile Sb species is hydride stibine ($SbH_3$), a very poisonous gas biologically produced and chemically induced for Sb quantification in analytical hydride generation techniques (Biver 2011). Otherwise, several biomethylated species dominate the organic Sb forms being (mono-)methylstibonic acid (MSA) the most abundant species (Andreae 1983) and trimethylstibine the volatile end-product of successive methylation steps (Wehmeier et al. 2004). They are present in soils, aquatic (i.e., geothermal, freshwater, marine and estuarine waters; Filella et al. 2002a, 2002b; Cutter and Cutter 2006) and biotic systems (Herath et al. 2017). Their production is generally attributed to bacterial, yeast and fungal activities in aerobic and anaerobic environments though the specific biological control and formation mechanisms are still unknown.

It is suspected that Sb has the same cellular uptake pathways as As, i.e., aquaglyceroporin channels allowing $Sb(OH)_3$ intake due to its similarity to glycerol molecules (Mukhopadhyay et al. 2014). Several Sb-glutathione complexes have been observed inside cells, suspected to have relevant roles in biomethylation processes due to the role of glutathione ($C_{10}H_{17}N_3O_6S$) in the detoxification and elimination of toxins, among other functions (Wehmeier et al. 2004). Nevertheless, Sb biomethylation is suggested to be fortuitous rather than a detoxification response, contrary to the case of As (Filella 2010).

- *Inorganic solid mineral phases*

In solid state, Sb is a chalcophile element found at distinct rare ore minerals forming sulphides and oxides such as stibnite ($Sb_2S_3$), valentinite ($Sb_2O_3$), cervantite ($Sb_2O_4$) and kermesite ($Sb_2S_2O$), among others (***Figure 17***). It is found at trace levels within the lattice of ilmenite ($FeTiO_3$) or Mg-olivine and it is commonly present in copper (Cu), silver (Ag) and lead (Pb) ores within recurrent minerals such as galena, sphalerite and pyrite (Filella et al. 2002b; Salminen et al. 2005; Reimann et al. 2010). Secondary minerals (***Figure 17***) are formed by the precipitation of Sb with specific cations forming, for instance, romeite (calcium antimonate) or tripuhyite (iron antimonate). Further details on Sb precipitation are given in section "*Abiotic sequestration processes: sorption and precipitation*".

- *Dissolved free species and the redox paradox*

Antimony generally hydrolyses forming hydroxides and oxo-hydroxide species. The most common dissolved species in aquatic environments are antimonite ($Sb(OH)_3$) and antimonate ($Sb(OH)_6^-$), though pH (***Figure 17***) and redox transformations (***Figure 18***) can show other forms. Several Pourbaix diagrams

have been published to represent different thermodynamic equilibrium conditions for Sb redox and solid/liquid speciation exchanges, many of which based on Sb concentrations far from natural water conditions (Filella et al. 2002b). Those approaching more realistic Sb concentrations (e.g., ~$10^{-8}$ mol $L^{-1}$, including dissolved sulphur species at $10^{-3}$ mol $L^{-1}$) predict soluble $Sb(OH)_3$ in anoxic media (***Figure 18***), with stibnite dominance up to pH 6 and $SbS_2^-$ or $Sb_2S_4^{2-}$ species replacing stibnite at higher pH values (Filella et al. 2002b). In oxic conditions, most Pourbaix diagrams predict relatively high Sb mobility for all pH ranges due to thermodynamic equilibrium favouring stable ionic-forming species of Sb(V) as $Sb(OH)_6^-$ (***Figure 18***; Filella et al. 2002b).

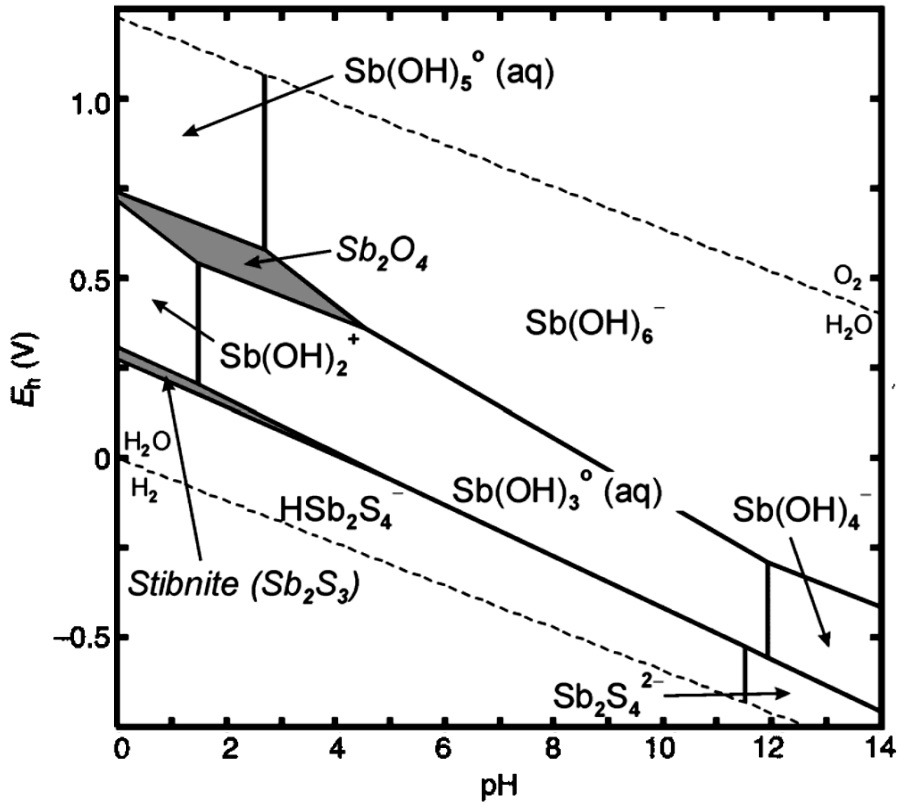


**Figure 18. Eh-pH (Pourbaix) diagram of aqueous speciation of Sb**. Modelling conditions include concentrations of total dissolved Sb of $10^{-9}$ mol $L^{-1}$ at 25ºC, showing with shaded areas the exceeding solubility of Sb relevant solids *(Krupka and Serne 2002).*

Nevertheless, the redox paradox consists on unexpected environmental observations, contradicting predicted Sb species. For instance, there are evidences on Sb(III) presence in environmental oxic conditions ($Sb(OH)_3$), explained by slow kinetics or ligand interactions (Filella et al. 2002a). In fact, the oxidation of Sb(III) to Sb(V) is likely accompanied by a hydrolysis step, making the overall redox process slower than expected (Quentel et al. 2006). Such kinetically-driven reactions explain Sb(III) stability in oxic environments and are actually dependent on the presence of biotic and photochemical redox-inducing molecules in aquatic systems like seawater (Cutter 1992; Cutter and

Cutter 2005). Interactions with organic ligands (e.g., tartaric acid in aquatic systems; Sun et al. 1982) and kinetic resistance to inorganic/abiotic oxidants (Quentel et al. 2006; Cutter and Cutter 2006; Leuz et al. 2006) also explain these observations. For example, the environmental persistence of Sb(III) is variable with spanning kinetics from 125 days (i.e., oxidation and scavenging processes taken into account; Cutter 1992) to few days (< 5 days) when iron and manganese oxides (i.e., oxides, hydroxides and oxyhydroxides) are present, which can be the case in suboxic-oxic interfaces like those found in the Black Sea (Belzile et al. 2001; Filella et al. 2002a).

Thermodynamic estimations favour Sb(III) species in anoxic conditions. However, evidences exist for the non-negligible proportions of Sb(V) in anoxic waters (i.e., ~50 – 60% relevance, Filella et al. 2002a). Hypothesis to this behaviour include (i) Sb(V) remineralisation of sinking detritus from oxic waters, (ii) thiol-complex formation and stabilisation, and/or (iii) water lateral/advection transport of Sb(V) (Filella et al. 2002b and references therein). Nevertheless, recent studies also show rapid removal of Sb(V) in oxic waters and oxic-anoxic interfaces via sorption or precipitation forming secondary mineral phases (***Figure 17***), suggesting that Sb(V) might not be that mobile than expected.

- *Dissolved phase: complexation mechanisms and colloidal interactions*

According to Pearson's classification, explaining the stability of metal complexes and reaction mechanisms of "hard and soft acids and bases (HSAB)", Sb(III) is considered a borderline case (***Figure 19***; Nieboer and Richardson 1980). This implies that it can show class A (ionic bonds, generally seeking oxygen-binding sites) and class B (covalent bonds, generally preferring nitrogen and/or sulphur centres) indistinctly, interacting with both hard (e.g., carboxylates, $-COO^-$) and soft ligands (e.g., thiols, -SH; Biver 2011). This terminology is related to Lewis' definition of hard (i.e., small ionic radii, high positive charge or electronegativity) and soft (i.e., large radii, low charge, intermediate electronegativity) acids (i.e., empty orbitals of valence, electron acceptors) and bases (i.e., filled orbitals with potentially bonding electrons, electron donors, also considered as a proton acceptor as in Brønsted-Lowry bases).

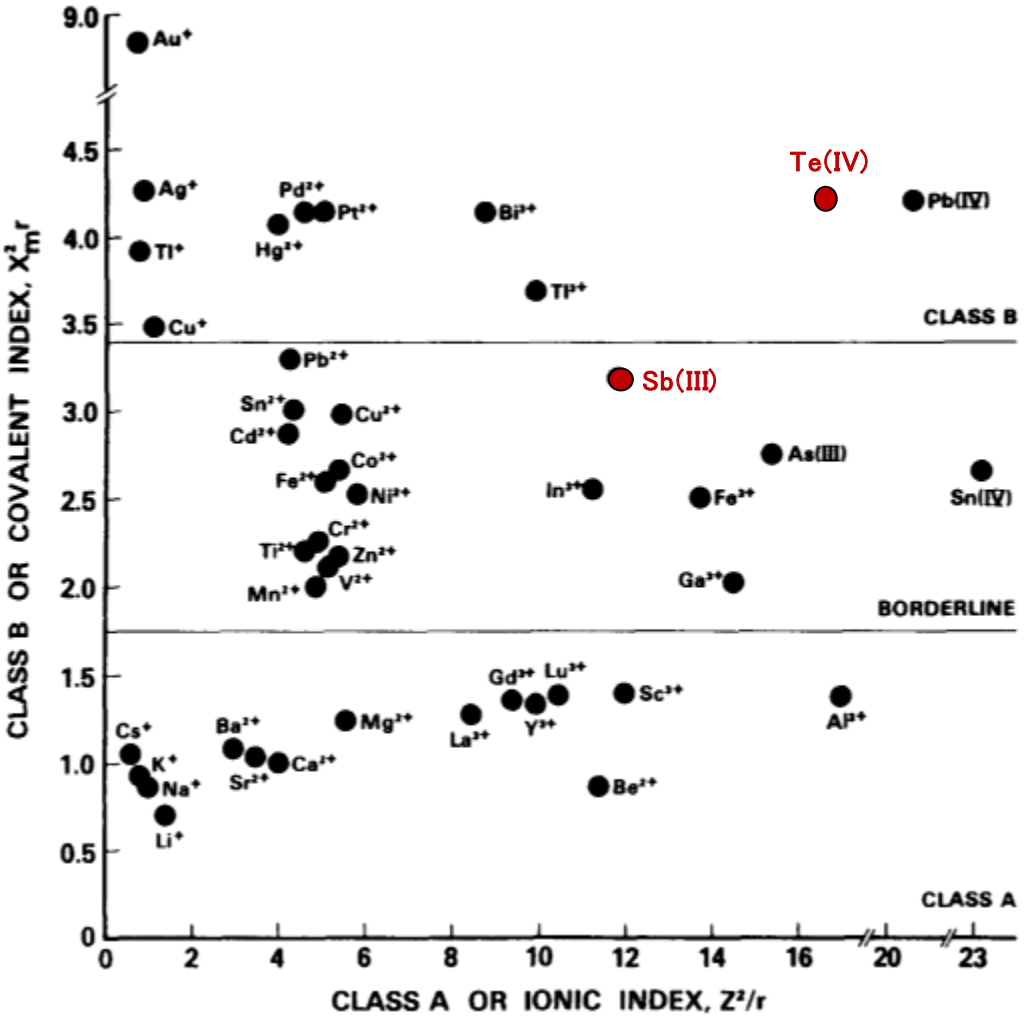


**Figure 19. Separation of metal ions and metalloid ions (As(III) and Sb(III)) into Pearson's modified classification**: class A, borderline and class B. This classification is based on indices where $\chi_m$ is the metal-ion electronegativity (Pauling's units), $r$ is the ionic radius (crystal IR in angstrom units) and $Z$ its formal charge. Specified oxidation states of Pb, As, Sb and Sn imply that simple cations do not exist even in acidic aqueous solutions. Elements of interest for this work have been highlighted (red). Tellurium (IV) has been added to the original image. *(Modified from Nieboer and Richardson 1980)*.

Other mechanisms including Sb complexation to metal-binding ligands (i.e., "electron donors") such as halides, nutrients, and small sized low molecular weight (l.m.w.) ligands like citrates, or macromolecules of high molecular weight (h.m.w.) like humic/fulvic acids, can also favour Sb dissolution and/or stability in dissolved state (***Table 10***).

However, there is little evidence on Sb environmental chlorocomplexation for both Sb(III) and Sb(V) species in seawater, proposing hydroxychloro complexes as the most probable forms (Filella et al. 2002b). Specifically, Sb(III) has been observed to form successive $SbCl_x^{[(x-)+3]+}$ forms and Sb(V) is suspected to have a similar behaviour, though less studied, in strong acidic solutions containing much higher chloride concentrations than those present in seawater (12 mol $L^{-1}$ vs 0.7 mol $L^{-1}$; Filella et al. 2002b).

**Table 10. Class A/B and borderline metal-binding ligands encountered in biological systems** (upper table) **and specific amino acid functional groups** (bottom table). Symbol R represents any alkyl radical (e.g., $CH_3$- ) or aromatic moiety (e.g., phenyl ring). Class A metal ions bind preferentially to ligands in column I, class B to ligands in III and some in II but borderline metals can interact with all types of ligands. *(Nieboer and Richardson 1980).*

LIGANDS ENCOUNTERED IN BIOLOGICAL SYSTEMS

| I. *Ligands preferred by class A metal ions* | II. *Other important ligands* | III. *Ligands preferred by class B metal ions* |
|---|---|---|
| $F^-$, $O^{2-}$, $OH^-$, $H_2O$ | $Cl^-$, $Br^-$, $N_3^-$, $NO_2^-$ | $H^-$, $I^-$, $R^-$, $CN^-$ |
| $CO_3^{2-}$, $SO_4^{2-}$, $ROSO_3^-$, $NO_3^-$ | $SO_3^{2-}$, $NH_3$, $N_2$, $RNH_2$ | CO, $S^{2-}$, $RS^-$, $R_2S$, $R_3As$ |
| $HPO_4^{2-}$, $-O-\overset{\overset{O}{\|}}{\underset{\underset{O^-}{\|}}{P}}-O-$ etc. | $R_2NH$, $R_3N$, $=N-$, $-CO-\tilde{N}-R$ | |
| ROH, $RCO^-$, $-\overset{\overset{O}{\|}}{\underset{\underset{O}{\|}}{C}}-$, ROR | $O_2$, $O_2^-$, $O_2^{2-}$ | |

METAL-ION BINDING SITES IN PROTEINS BASED ON CRYSTALLOGRAPHIC STUDIES

| *Functional groups sought by class A metal ions* | *Functional groups sought by class B metal ions* |
|---|---|
| Carboxylate: $R-\overset{\overset{O}{\|}}{C}-O^-$ | Sulphydryl: —SH |
| Carbonyl: $R-\overset{\overset{O}{\|}}{C}-OR$, $R-NH\overset{\overset{O}{\|}}{C}-R$ | Disulphide: —S—S— |
| Alcohol: $R-\overset{\overset{\|}{}}{\underset{\underset{\|}{}}{C}}-OH$ | Thioether: —SR |
| Phosphate: $R-OPO_3^{2-}$ | Amino: $-NH_2$ |
| Phosphodiester: $R-O-\overset{\overset{O}{\|}}{\underset{\underset{O^-}{\|}}{P}}-O-R$ | Heterocyclic nitrogen: imidazole of histidine, nucleotide bases |

Furthermore, Sb complexation with l.m.w. ligands (i.e., anions such as $CH_3COO^-$ and neutral species such as N-atoms or $NH_2$) has a complex chemistry in both inorganic and biological systems rendering Sb a certain plasticity to environmental conditions. For instance, a borderline metal ion like Sb(III) can bind to, e.g., an amino acid ligand (which has both -$COO^-$ and -$NH_2$ functional groups) in the carboxylate moiety for mildly acid solutions but to the amino group only at sufficiently high pH when the amino group deprotonates (Nieboer and Richardson 1980). Furthermore, this interaction with l.m.w. ligands is also used by phytoplankton organisms as adsorption or defense mechanisms through their exudates in aquatic environments. For instance, Duan et al. (2010) observed Sb interactions with functional groups such as amino (-$NH_2$), mercapto (-SH), methylthio (-S-$CH_3$), hydroxyl (-OH), imidazole (-$C_3N_2$) and carbonyl (-CO-) from several phytoplankton communities in the Bohai Bay absorbing and changing Sb(III) into Sb(V), depending on the phytoplankton species. Interactions with other l.m.w. ligands (e.g., polyaminocarboxylic acids like EDTA or complexants like catechol, tartaric acids, citrate, cysteine, etc.)

exist and are specially used in analytical methods for extraction/enrichment or speciation techniques (Filella et al. 2002b and references therein).

Evidence on Sb complexation to h.m.w. molecules (e.g., formed by aggregates of l.m.w. humic and fulvic acids, carbohydrates, amino acids and fatty acids, highly resistant to microbial degradation; Walter et al. 2007; Reemtsma et al. 2008) is scarce. Most of these studies are related to Sb(III) interactions and oxidation to Sb(V), relying particularly on experimental studies where maximum sorption has been observed in acidic conditions (e.g., pH ~ 4 for Sb(V); Tighe et al. 2005).

Nevertheless, some environmental studies suggest interactions between Sb and natural organic matter (NOM, comprising both l.m.w. and h.m.w. natural ligands) with site-dependent and potentially temporal behaviour (e.g., Sb summer covariation with colloids and particulate matter in Patuxent River estuary; Sigleo and Helz 1981). In freshwater systems, dissolved Sb fractionation shows <10% sorption to h.m.w. ligands (c.a. 0.45 µm - 100 000 Da), ~20% sorption in the smaller colloidal fraction (ca. 100 000 – 1000 Da) and 60 – 80% sorption to the l.m.w. fraction (ca. < 1000 Da) with no correlations between Sb and dissolved organic carbon (DOC; comprising all mentioned fractions; Filella et al. 2002b). Likewise, variable proportions of Sb complexation to organic matter have been registered between 20 – 60% in Belgian coastal waters (Gillain and Brihaye 1985) and over 30% in simulated environmental conditions (Buschmann and Sigg 2004). Nevertheless, NOM can adsorb onto mineral phases like iron oxides, as suggested by Gu et al. (1994) and Zhou et al. (2001), which can bias conclusions regarding NOM-Sb interactions. Thus, attention should be paid when relating poorly-complexed elements like Sb with NOM size fractions (e.g., fulvic acids of 1-2nm) as common results do not imply nor proof binding/sorption interaction (Filella and Williams 2012).

These observations suggest that (Filella and Williams 2012): (i) when applicable, important proportions of NOM complexation can indirectly link Sb fate to NOM remineralisation though, in most cases, (ii) NOM complexation does not play a significant role in Sb environmental fate and, thus, (iii) Sb is mostly found in the dissolved fraction, operationally defined for 0.2 µm filter mesh size (which can include some smaller colloidal matter), defining mesh sizes <0.02 µm as the "truly dissolved fraction" (which includes l.m.w. fraction).

- *Abiotic sequestration processes: sorption and precipitation*

General sorption mechanisms are based on ionic interactions referred as (i) inner-sphere complexes, when there is specific sorption by chemisorption, forming specific bonds between the element of interest and the mineral surface, or (ii) outer-sphere complexes, when non-specific sorption

by electrostatic attraction takes place as the hydration spheres of the mineral prevents a closer approach of the elemental ion.

Antimony can adsorb onto specific mineral phases due to predominantly $H^+$ exchange mechanism with surface structural $-OH_2$ and $–OH^-$ groups at sorption sites (Herath et al. 2017). Most studies have focused on Sb(III) due to its borderline characteristics, favouring mineral interactions, and its concern in Sb toxicity issues compared to Sb(V) species (see section on "*Biological uptake and toxicity*"). Sorption studies generally focus on iron, manganese and aluminum oxide mineral phases, including oxides, hydroxides and oxyhydroxides, which are commonly present in soils and sediments (Wilson et al. 2010; Herath et al. 2017 and references therein). Studies on both experimental solutions and environmental sediments suggest that Sb(III) sorption capacity preferentially decreases as follows: MnOOH > $Al(OH)_3$ > FeOOH, with decreasing sorption as pH increases above 6 despite observed maximum sorption at pH 7-8 for Al and Fe oxides (Thanabalasingam and Pickering 1990; Filella et al. 2002b). It is noteworthy that, concerning environmental mineral abundances in bulk soils/sediments, clay minerals and Al-oxides are more abundant than Fe/Mn oxides unless colloidal forms enhance Fe/Mn oxide stability for a certain period at the freshwater-seawater interface of estuaries (Quentel et al. 2006).

Studies on Sb (III) sorption to Mn oxides have observed all interaction types, from single binding sites (e.g., $Mn(OH)_2$ with $Sb(OH)_5$ in anoxic conditions; Belzile et al. 2001) to both outer-sphere surface complexes (i.e., Sb(V) competition with $Mn^{2+}$ in presence of $SO_3^{2-}$; Liu et al. 2015) and inner-sphere complexes (i.e., interactions with -OH groups in Mn oxide surfaces; Liu et al. 2015). Nevertheless, there is less knowledge on Sb(V) sorption onto Mn oxides (Wilson et al. 2010). A recent study suggests birnessite (δ-$MnO_2$) as a suitable mineral phase for Sb(V) retention in naturally occurring contaminated soils (Essington and Vergeer 2015).

Despite the relative importance of Al-oxides in Sb sorption, there are few studies on clay and Al-oxides and little is known about their interaction mechanisms (Wilson et al. 2010; Herath et al. 2017). Works on sorption experiments with clay minerals such as bentonite (colloidal silt essentially constituted by montmorillonite) have shown fast Sb(III) sorption rates compared to Sb(V), with maximum sorption capacities of 370-555 and 270-500 μg $g^{-1}$, respectively (Xi et al. 2011). These studies also showed anionic competition for Sb(V) sorption with $NO_3^-$, $PO_4^{3-}$ and $SO_4^{2-}$. Likewise, studies of Sb(V) sorption to kaolinite (clay mineral, $Al_2Si_2O_5(OH)_4$) and gibbsite ($Al(OH)_3$) observed a pH-dependence effect with maximum sorption at low pH (i.e., 75% at pH 3.6, decreasing to 20% at pH 9.2 for the former; Xi et al. 2009) explained by Al-oxide protonation. That is, positive surface charges exposed to anionic Sb(V) can bind through electrostatic interactions (Xi et al. 2011) and/or ligand exchange

mechanisms, as observed particularly for As anionic species, in broken clay particle edges (Wilson et al. 2010).

Sorption mechanisms of Sb(III) to Fe oxy(hydr)oxides suggest bidentate corner-sharing inner sphere complexes (e.g., >80% sorption of Sb(III) onto goethite-FeOOH for a wide pH range; Leuz et al. 2006) as well as mono-($SO–Sb(OH)_2$) and binuclear ($(SO)_2–SbOH$) surface complexes onto ferrihydrite from triple layer models (Enders and Jekel 1996). Likewise, experiments have shown inner-sphere complexes of Sb(V) sorption onto Fe oxides such as goethite (pH dependent, max. at pH < 7; Leuz et al. 2006, Scheinost et al. 2006), hematite ($Fe_2O_3$, max. at pH 4; Pierce and Moore 1982; Ambe 1987) and 95% to non-crystalline Fe hydroxides (for pH ranges between 2.5 and 7, max. at pH 4 too; Tighe and Lockwood 2007). However, it seems that Sb(V) sorption onto ferrihydrite is highly suppressed by Sb(III) presence at wide pH ranges between 4 – 10 (Qi and Pichler 2016) and not *vice-versa*. Green rusts, i.e., composites of Fe(II) – Fe(III) double hydroxide layers present in natural sub-oxic soils and sediments (Herath et al. 2017), show high affinities for Sb(V), especially in presence on $SO_4^{2-}$, through two-binding sites (i.e., both edge site inner-sphere and interlayer surface outer-sphere complexes) favouring Sb(V) to Sb(III) reduction in the surface (Mitsunobu et al. 2009). Furthermore, Bolanz et al. (2013) observed that Sb(V) sorption to poorly-crystalline ferrihydrite favoured goethite, feroxyhyte (δ'-FeOOH) and tripuhyite ($FeSbO_4$) formation depending on pH and Sb concentrations.

In addition to sorption, precipitation processes also transfer Sb species from dissolved to particulate phases. For instance, Sb(V) in soils can precipitate in presence of $Ca^{2+}$ (Okkenhaug et al. 2011; Herath et al. 2017) forming calcium antimonite ($Ca[Sb(OH)_6]_2$) or romeite ($Ca_2Sb_2O_7$). Likewise, Sb can precipitate with other metals (Vink 1996; Herath et al. 2017) such as Ni (forming bottinoite, $Ni(H_2O)_6[Sb(OH)_6]_2$), Pb (bindheimite, $Pb_2Sb_2O_7$), Mg (bystroemite, $MgSb_2O_6$), Zn (ordozenite, $ZnSb_2O_6$), Mn (melanostibnite, $Mn(Sb,Fe)O_3$) and Fe (schafarzikite, $FeSb_2O_4$ and tripuhyite, $FeSbO_4$). The latter has a recognised important role as Sb sinks in natural environments reducing, for instance, Sb concentrations in supergene Sb-rich ore deposits (Leverett et al. 2012; Roper et al. 2012). Such precipitations are controlled by respective Sb and complementary elemental site-dependent concentrations, and are generally neglected from Eh-pH diagrams because of lack of thermodynamic data (Vink 1996). Nevertheless, these precipitations seem to be site-specific, thus, generally not acting as controlling processes in Sb environmental mobility given the high solubility of Sb species (Wilson et al. 2010).

- *Biological processes: remineralisation in suboxic environments*

Antimony primary and secondary minerals can further participate in redox processes where they can have relevant roles. Environmental redox conditions are specially observed in soils/sediments presenting, e.g., early diagenesis environments like waterlogged areas or consolidated sediments in river streams. In these cases, redox conditions are achieved due to organic matter deposition from *in situ* biological activities and sediment remineralisation by microorganisms over time (e.g., Tapia and Audry 2013). Such remineralisation implies respiration reactions where organic matter oxidation takes place by using electron acceptors which are chosen in sequential order according to optimal energy consumption criteria (i.e., oxygen is the less energetic terminal but, when consumed, nitrates and Fe/Mn oxides are consumed, releasing reduced species, ***Table 11***).

**Table 11. Examples of redox reactions involved in natural diagenetic systems including Sb species (red)**. Reactions are presented in preferential order concerning energy consumption. *(Modified from Wilson et al. 2010)*

| Reaction | $pe^{0a}$ | $Eh^0$ (V) |
|---|---|---|
| $O_2 + 4H^+ + 4e^- = 2H_2O$ | 20.8 | 1.23 |
| $2NO_3^- + 12H^+ + 10e^- = N_2 + 6H_2O$ | 21.1 | 1.25 |
| $MnO_2 + 4H^+ + 2e^- = Mn^{2+} + 2H_2O$ | 20.4 | 1.21 |
| $Fe(OH)_3$ (amorphous) $+ 3H^+ + e^- = Fe^{2+} + 3H_2O$ | 16.6 | 0.98 |
| α-FeOOH (goethite) $+ 3H^+ + e^- = Fe^{2+} + 2H_2O$ | 13.1 | 0.77 |
| $Sb(OH)_6^- + 3H^+ + 2e^- = Sb(OH)_3 + 3H_2O$ | 12.9 | 0.76 |
| $Sb_2O_5 + 4H^+ + 4e^- = Sb_2O_3$(valentinite) $+ 2H_2O$ | 11.0 | 0.65 |
| $Sb_2O_5 + 6H^+ + 4e^- = 2Sb(OH)_2^+ + H_2O$ | 9.8 | 0.58 |
| $SO_4^{2-} + 10H^+ + 8e^- = H_2S + 4H_2O$ | 5.3 | 0.31 |
| $Sb(OH)_2^+ + 2H^+ + 3e^- = Sb + 2H_2O$ | 3.6 | 0.21 |
| $CO_2 + 8H^+ + 8e^- = CH_4 + 2H_2O$ | 2.9 | 0.17 |
| $Sb_2O_3 + 6H^+ + 6e^- = 2Sb + 3H_2O$ | −2.5 | −0.15 |
| $Sb + 3H^+ + 3e^- = SbH_3$ | −8.6 | −0.51 |

[a] $pe^0 = Eh^0/0.059$ V at 25 °C and $Eh^0$ is the equilibrium redox potential relative to the oxidation of $H_2$(g).

The comparison between classical electron acceptors ($O_2$, $NO_3^-$, Fe/Mn oxides, $SO_4^{2-}$, etc.) and the role of Sb in such early diagenesis suggests Sb(V) reduction to Sb(III) between Fe and sulphate reduction (***Table 11***, Wilson et al. 2010). Moreover, if the remineralisation pursues, reduction of Sb(III) to elemental Sb or stibine can take place at coincident reduction potentials to those of soluble sulphide production, increasing the chances of forming Sb sulphide complexes when respective concentrations are appropriate (Wilson et al. 2010).

- *Real solid samples: bulk samples, solid/liquid partitioning and selective extractions*

It is important to bear in mind that environmental conditions imply bulk (real) soils and sediments, that is, a mixture of several minerals of different compositions and concentrations, contrasting with the generally studied "single-mineral" laboratory experiences. Thus, from the practical and operational view-point, two alternative approaches are used in environmental studies to obtain macroscopic, overall understanding of the biogeochemical behaviour of any trace element in a system.

The first one concerns the solid/liquid distributions or partition coefficients (Kd) defined as the ratio between particulate over dissolved concentrations from environmental samples. For Sb, environmental Kd values are generally low suggesting Sb weak affinities for natural particles in aquatic environments (Filella 2011). This is in accordance with results from many systems showing that total Sb (dissolved + particulate) in stream waters is dominated by an important contribution of the dissolved phase (e.g., Wilson and Webster-Brown 2009 observed 90% of total Sb as dissolved Sb). However, Kd values should be used for intra-study comparisons and not between different systems given the variability of intrinsic conditions: operational dissolved vs particulate fractionation, assumption of C-type isotherm (i.e., constant particulate/dissolved ratio independent of concentrations) and achieved experimental and/or environmental particulate/dissolved equilibrium (Filella 2011).

On the other hand, overall binding interactions of trace elements to solid fractions can be studied from selective extractions (Filella 2011). Selective extractions are leaching methods which are applied on bulk environmental samples to have an overall view of element vs solid interaction by trying to identify the responsible binding/carrier phases. They are popularly used as they have the potential to explain trace element environmental behaviours (e.g., mobility) and elucidate the mechanisms of the processes involved (e.g., ionic exchange). They basically rely on reactants with increasing strength (from water to relatively strong organic complexants and acids) to extract the associated particulate target elements by (i) ion-exchange interactions, or (ii) destruction of the carrier phase (Gleyzes et al. 2002).

Selective extractions can be performed either by sequential procedures (i.e., unique sample subjected to successive reactants and washing steps) or in parallel extractions (i.e., sample aliquots subjected to individual reactants). General studied solid phases comprise: (i) exchangeable/soluble fraction, (ii) reducible (Fe/Mn oxides), (iii) oxidisable (organic matter and sulphurs), and (iv) residual fraction. Sometimes, extractions aim at identifying the specific carrier phases (e.g., crystalline vs amorphous Fe/Mn oxides) and others to mimic environmental conditions (e.g., acid rain leaching, reducing environments, etc.). However, over time different procedures have been suggested and applied, showing that results are method-dependent (Gleyzes et al. 2002; Filella 2011), thus,

concentrations are generally referred to “operationally-defined phases” rather than absolute mineral fractions. Such variations also underscore more disadvantages than advantages to selective extraction methods (***Table 12***), rendering them sometimes unreliable or doubtful. Nevertheless, it is still one of the best macroscopic methods to study trace element binding state in solid phases (precipitated in minerals, complexed with organic ligands, etc.) to estimate their mobility and bioavailability in the environment (Gleyzes et al. 2002).

**Table 12: Advantages and disadvantages of selective extraction methods in sequential vs parallel protocols.**

| | Sequential | Parallel |
|---|---|---|
| **Advantages** | • Final budget is easily achieved (sum of results from selective extractions = total sample concentration) | • No risk of sample loss between fractions [c]<br>• Independent fraction quantification [h]<br>• Less time consuming[a] |
| **Disadvantages** | • Phase overlapping, incomplete dissolution[b,d]<br>• Redistribution into other phases[d]<br>• Contamination risks by successive reactants[g]<br>• Change in speciation along extraction steps[f]<br>• Wash steps can dissolve target elements[e] | • No verification of total budget |
| | ***Method related:***<br>• Low selectivity of reagents (type-, extraction time- and mineral phase-dependent) e.g., possible dissolution of Mn oxides for organic matter fraction with $H_2O_2$ at pH < 5 [d]<br>• Element readsorption/redistribution to other phases [b] e.g., Pb, Cu, Zn even at pH < 3 [d]<br>• No standardised protocol: lack of uniformity in methods, especially for metalloids[d]<br>• Losses occur in filtration of supernatant[e]<br>• Results also depend on extraction kinetics of both phases of interest and target elements[e] | |
| | ***Matrix type related:***<br>• Environmental representativeness: protocols are designed from artificial or spiked sediment/soils[c]<br>• Matrix efficiency: some methods are more efficient for specific soils/sediment types than others (e.g., As extraction is more efficient with orthophosphoric acid in river sediments but ammonium oxalate for soils)[d]<br>• Sample treatment (oven dried vs freeze-dried) can change target element phase distribution[d]<br>• Polluted matrices can show high residual fractions and low reproducibility due to incomplete dissolution in previous extraction steps and aliquot heterogeneity[d] | |
| | ***Quality control related:***<br>• CRM: no certified reference material (CRM) exists for all target elements[d] | |

[a] Baig et al. 2009 ; [b] Müller et al. 2007 ; [c] Audry et al. 2006 ; [d] Gleyzes et al. 2002 ; [e] Wenzel et al. 2001 ; [f] Rosenberg and Ariese 2001 ; [g] Quevauviller 1998 ; [h] Tack et al. 1996

Confusion and reliability in environmental results remain nowadays in the scientific literature due to the indiscriminate use of all protocol types (e.g., Tessier et al. 1979; BCR protocol; Wenzel et al. 2001) for both cationic and anionic extractions (e.g., see reviews in Gleyzes et al. 2002; Filgueiras et al. 2002; Hudson-Edwards et al. 2004; Wilson et al. 2010 and Filella 2011 and references therein). In any

case, Sb-wise, most studies in soils and sediments point out that: (i) Sb is mostly found in the dissolved phase so, when solid, (ii) Sb is mostly found in the residual fraction and, though generally low, (iii) there is a non-negligible presence of Sb in the Fe oxide fraction (Filella 2011).

### *2.1.3. Environmental concentrations and biogeochemical behaviour*

Antimony is considered a trace element in the Earth´s crust, ranking the 63$^{rd}$ position of the most abundant elements (Qi et al. 2008). Crustal concentrations of 0.2 – 1 mg kg$^{-1}$ (Saleh et al. 1998) reach highest abundances in sedimentary rocks (e.g., shales 0.8 – 1.5 mg kg$^{-1}$, clays, fine-grained argillaceous sediments 1.2 – 2.0 mg kg$^{-1}$) and felsic igneous rocks (i.e., up to 7.8 mg kg$^{-1}$; Hall and Pelchat. 1997; Filella et al. 2002a; Salminen et al. 2005). Background soil concentrations range between 0.05 – 8.8 mg kg$^{-1}$ (Wilson et al. 2010), being in general < 1 mg kg$^{-1}$ (Tschan et al. 2009) and presenting the highest concentrations in anthropogenic areas mainly related to mining/smelting activities and shooting ranges (i.e., from 2.5 up to >15 000 mg kg$^{-1}$; Wilson et al. 2010). General enrichment is observed in upper horizons compared to deep horizons (Sterckemann et al. 2004) though at a European scale it is less evident, showing 0.6 mg kg$^{-1}$ median topsoils and 0.47 mg kg$^{-1}$ in subsoils (Salminen et al. 2005).

In non-polluted aquatic systems, Sb dissolved concentrations range between 0.01 – 1.5 µg L$^{-1}$ in groundwater, 1 µg L$^{-1}$ for running freshwater and average 0.2 µg L$^{-1}$ in seawater (Ungureanu et al. 2015). Noteworthy, large scale spatial studies like FOREGS Geochemical Baseline Mapping Programme were conceived after major accidents like that of Chernobyl to provide environmental geochemical baseline concentrations and pollution levels in Europe. In particular, this programme shows expected Sb stream water and sediment median concentrations of 0.07 µg L$^{-1}$ and 0.62 mg kg$^{-1}$, respectively (Salminen et al. 2005).

Nevertheless, the heterogeneous spatial distribution between dissolved and particulate Sb European maps (***Figure 20a,b***) does not show matching patterns. Such distributions can reflect kinetic solid/liquid interactions concerning water/particle residence times and/or biological influence in such natural equilibriums. Moreover, this diversity also suggests a site-dependent influence, despite the potential global atmospheric input, not only from the anthropogenic point of view (i.e., urban influence, industrial activities, etc.) but from orogenic diversity, as suggested by Reimann et al. (2010). In fact, several works have analysed specific river/groundwater sites all over the world, especially during 1980-1990's, showing a great variability on dissolved Sb concentrations with up to 100-fold differences between "pristine" and highly polluted environments (***Figure 21a,b***).

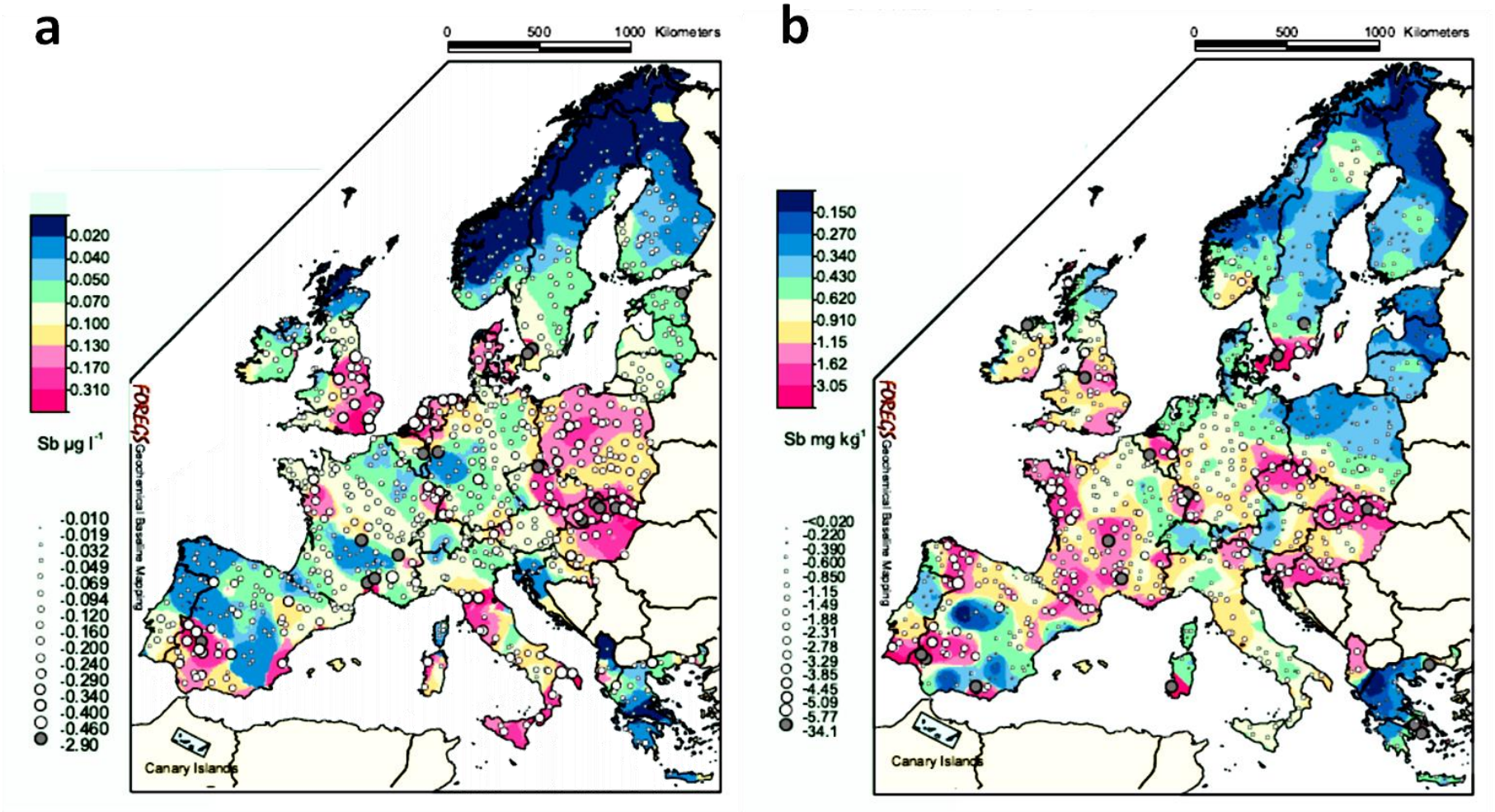


**Figure 20. Antimony dissolved** (µg $L^{-1}$, 0.45 µm filtered, N = 807; a) **and particulate** (mg $kg^{-1}$, <63 µm grain-size, N = 848; b) **concentrations in European streams** sampled between 1998 and 2001 and analysed between 1999 and 2003 *(Salminen et al. 2005).*

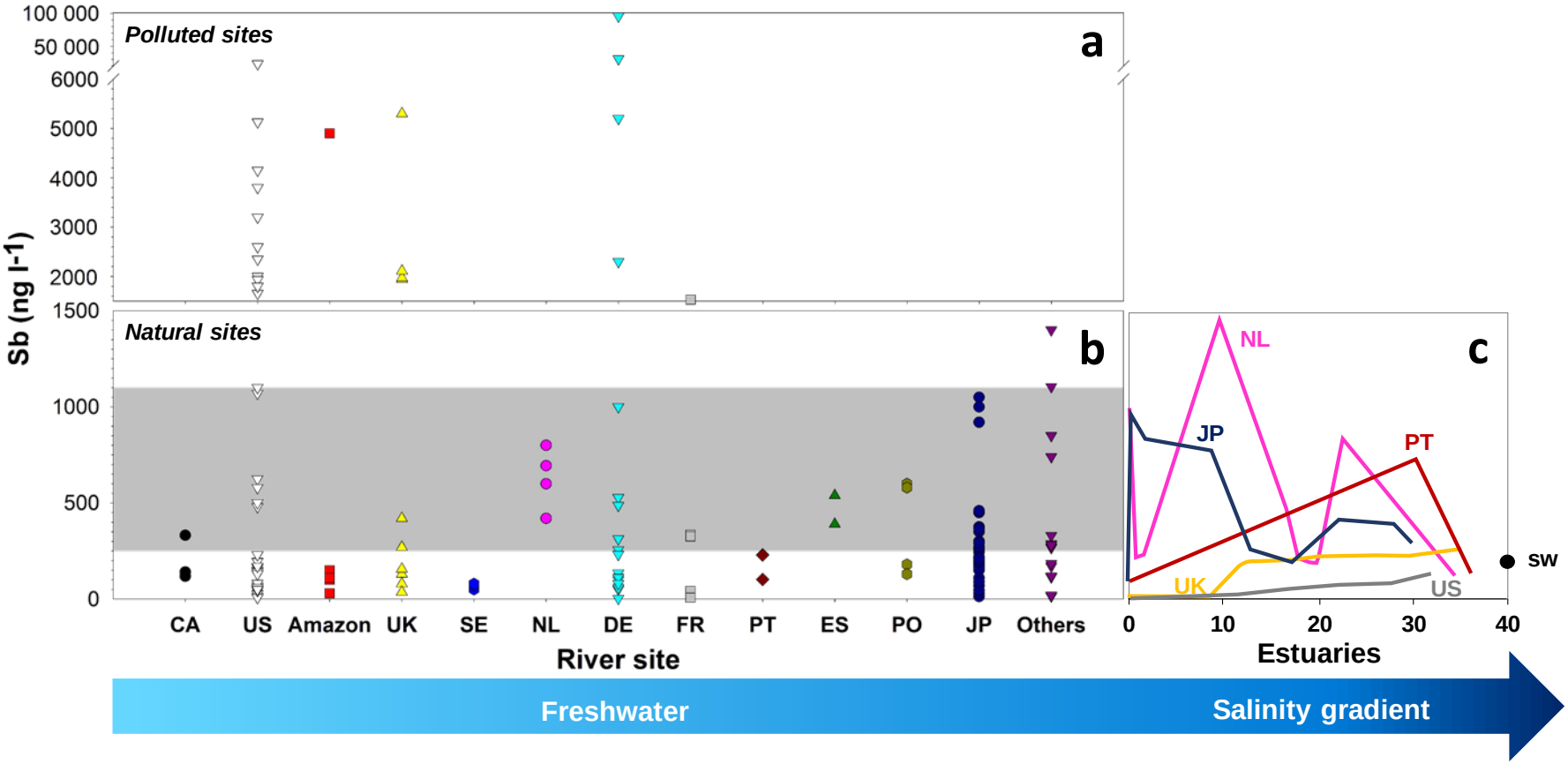


**Figure 21. Worldwide Sb dissolved concentrations** (ng $L^{-1}$) analyzed since 1980's to 2000 for several rivers, groundwater and tap water samples (*data compilation from Filella et al. 2002a*) distributed by countries: Canada (CA), United States (US), Amazon River (Amazon), United Kingdom (UK), Sweden (SE), Netherlands (NL), Germany (DE), France (FR), Portugal (PT), Spain (ES), Poland (PO), Japan (JP) and other Asian countries (Taiwan, Indonesia, etc.). Published worldwide average freshwater concentration ranges (shaded in grey area). Noteworthy the change in scale to distinguish concentrations from highly polluted sites (a) and natural concentrations (b). Most commonly observed dissolved Sb estuarine behaviours along the salinity gradient (c) are also shown for the Tamar Estuary (UK; *van den Berg et al. 1991*), the Tama Estuary (JP; *Byrd 1990*), the Scheldt Estuary (NL; *van der Sloot et al. 1985*), the Tagus Estuary (PT; *Andreae et al. 1983*) and the St. Mary's Estuary (US; *Byrd 1990*). Surface seawater endmember (sw; *Filella et al. 2002a*) is also depicted at a random salinity of S = 40.

Continent-ocean interface environments such as estuarine conditions can decrease (sorption/dilution) or increase (remineralisation/desorption) Sb freshwater dissolved concentrations. Several dissolved Sb patterns explained by different biogeochemical processes have been observed along the salinity and turbidity gradients of some estuaries worldwide (***Figure 21c***). These dissolved Sb concentrations are generally related to 0.45 µm filtered samples, thus, quantifying both colloidal and the "truly dissolved" Sb fractions. There seems to be no unique trend for Sb estuarine behaviour as both conservative (i.e., straight mixing line from freshwater to seawater endmembers due to physical dilution effect) and non-conservative behaviours (i.e., biogeochemical processes causing deviation in Sb concentrations from the theoretical conservative mixing line) have been equally observed in several systems (***Table 13***).

Most conservative behaviours have been observed in relatively small estuaries with shallow depths, occasional high organic matter input and often short residence times (e.g., like the St. Mary's Estuary or the Ochlocknee Bay estuary in the US, ***Table 13***). Importantly, some studies attribute to Sb a conservative behaviour for works performed only at high salinity ranges (e.g., Ren et al. 2016; Wilson and Webster-Brown 2009). This would imply that such studies have actually observed the dilution pattern of dissolved Sb at high salinity from non-conservative systems, which can sometimes be highly influenced by anthropogenic activities (e.g., Tagus Estuary, Portugal, ***Table 13***; Andreae et al. 1983).

Non-conservative behaviours seem to be found in bigger estuaries (depth and size) with higher anthropogenic influence and probably stronger biogeochemical processes due to water mixing and suspended particulate matter (SPM) implications. Noteworthy, most authors explain this behaviour as a combination of both SPM sorption/scavenging effect or Fe/Mn oxide coagulation as colloids (dissolved Sb depletion) and a release during organic matter remineralisation in the maximum turbidity zone (MTZ) or in interstitial waters due to oxygen-depleted conditions (water column Sb addition). Furthermore, some works have linked Sb addition to the nitrogen cycle (inorganic nitrogen referred as the sum of nitrate, $NO_3^-$, nitrite, $NO_2^-$, and ammonia, $NH_4$), as coincident maxima have been observed at two different salinities (i.e., Savannah River estuary, Georgia USA, ***Table 13***; Byrd 1990). This M-shaped pattern along the salinity gradient was also observed in the Geum Estuary (Korea; Byrd 1990), in the Tama Estuary (Tokyo, Japan, explained as an effect from anthropogenic sources; Byrd 1990) and in September 1982 in the Scheldt Estuary (The Netherlands; van der Sloot et al. 1985).

**Table 13. Some examples of Sb behaviour in worldwide estuaries**. Both dissolved ($Sb_d$) trend and particulate ($Sb_p$) descriptions are shown when available from the same study

| Behaviour | System | System characteristics | Dissolved and particulate Sb behaviour | References |
|---|---|---|---|---|
| **Conservative** | Rhine River Estuary (The Netherlands) | Macrotidal<br>A = n.a. [a,i]<br>D = n.a. [b,i]<br>Q = 2 900 $m^3$ $s^{-1}$ [c]<br>$\tau_r$ = 2-3 days [1d]<br>DO ≥ 40% saturation [e] | 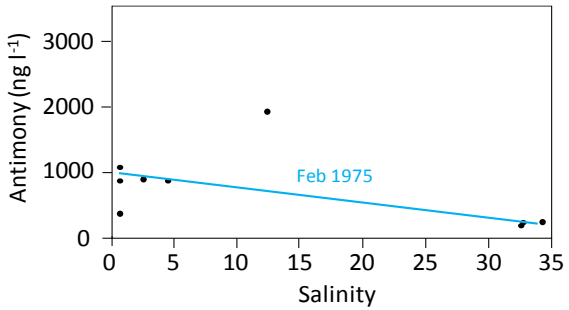 | **van der Sloot et al. 1985**<br>*(Tessier et al. 2002)*[j] |
| | St. Mary's Estuary (Georgia, USA) | Mesotidal<br>A = 64 $km^2$ [a]<br>D = 6.1 m [b]<br>Q = 35 $m^3$ $s^{-1}$ [c]<br>$\tau_r$ = 65 days [2d]<br>DOC > 2.5 mM (30 mg $L^{-1}$) [f] | 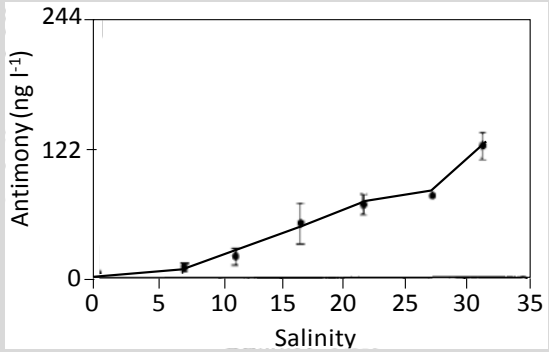 | Alber and Sheldon 1999; **Byrd 1990**<br>*(Dame et al. 2000; NOAA 2012; Pendleton et al. 2004)*[j] |
| | Satilla River estuary (Georgia, USA) | Mesotidal<br>A = n.a. [a,i]<br>D = 4 m [b]<br>Q = 10-1000 $m^3$ $s^{-1}$ (34) [c]<br>$\tau_r$ = 63 days [2d]<br>DOC > 3.3 mM (40 mg $L^{-1}$) [f]<br>Sediment resuspension | 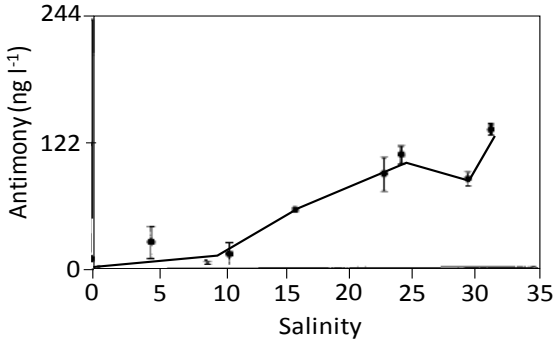 | Alber and Sheldon 1999; **Byrd 1990**; Zheng et al. 2003, 2004<br>*(Alber et al. 2003; Blanton et al. 1999)*[j] |

*(Table 13 Continued)*

| Behaviour | System | System characteristics | Dissolved and particulate Sb behaviour | References |
|---|---|---|---|---|
| **Conservative** | Medway Estuary (Nova Scotia, Canada) | Mesotidal<br>A ≈5 km$^2$ [a]<br>D ≈ 5 m [b]<br>Q = n.a. [i]<br>$\tau_r$ = n.a. [i]<br>DOC > 0.5mM (6 mg L$^{-1}$) [f] | 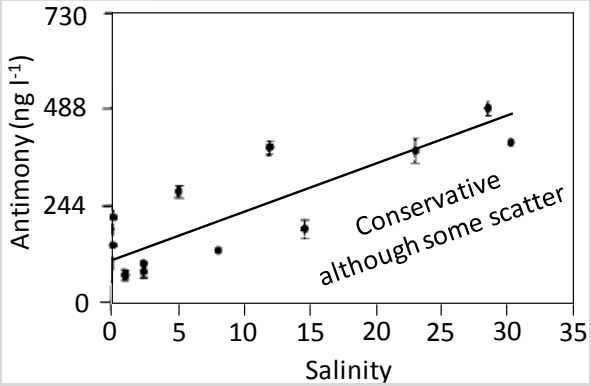 | **Byrd 1990**; |
| | Waikato Estuary (New Zealand) | Mesotidal<br>A = 18 km$^2$ [a]<br>D ≈ 5 m [b]<br>Q = 183-600 m$^3$ s$^{-1}$ [c]<br>$\tau_r$ = < 10 days* [1d]<br>Geothermal-driven system<br>Seasonal dilution patterns | 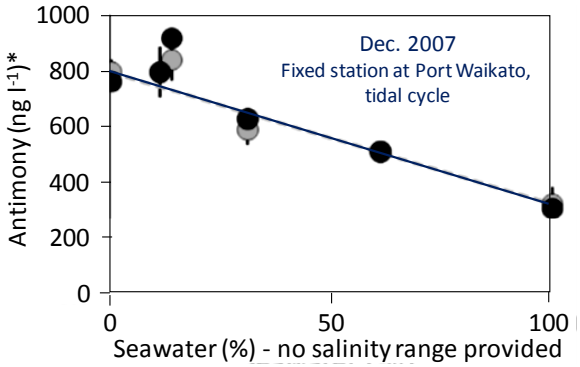 | Jones and Hamilton 2014; **Wilson and Webster-Brown 2009**<br><br>(*concentrations originally in µg kg$^{-1}$) |
| | Ochlockonee Bay estuary (Florida, US) | Microtidal<br>A ≈ 23 km$^2$ [a]<br>D = 7m [b]<br>Q = n.a. [i]<br>$\tau_r$ = n.a. [i] | 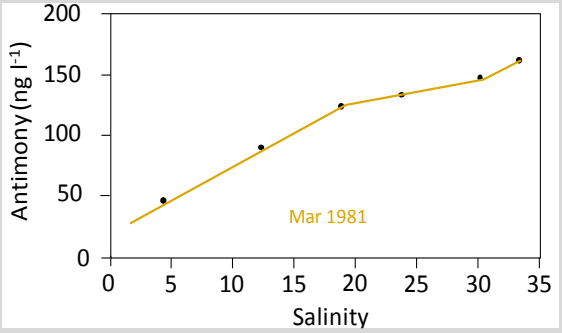 | **Andreae 1983** |

*(Table 13 Continued)*

| Behaviour | System | System characteristics | Dissolved and particulate Sb behaviour | References |
|---|---|---|---|---|
| **Non-conservative** | Tamar River estuary (United Kingdom) | Macrotidal<br>A = n.a. [a,i]<br>D = 30 m [b]<br>Q = 5-38 $m^3$ $s^{-1}$ [c]<br>$\tau_r$ = 1-3 weeks [2d]<br>Defined MTZ (max. 3 g $L^{-1}$) [g]<br>Scavenging at low salinities<br>Interstitial water release (anoxia)<br>Adsorption/desorption reactions | 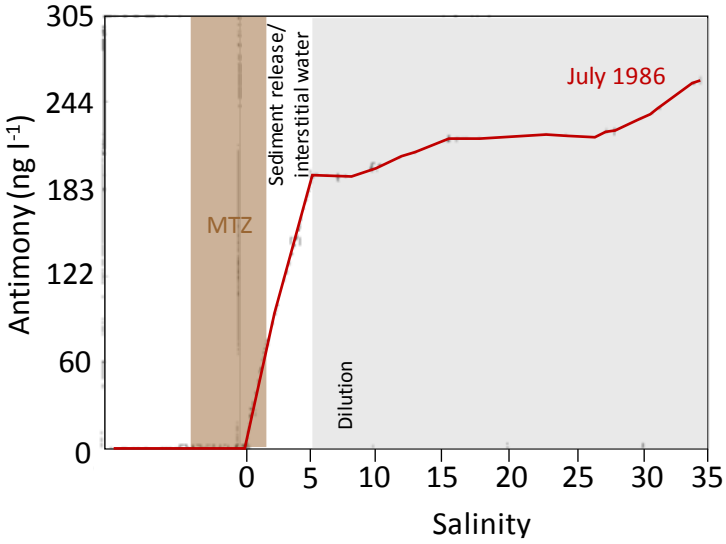 | Bale et al. 2007; Uncles et al. 1983; **van den Berg et al. 1991, 1993**<br><br>*(Tattersall et al. 2003)* [j] |
| | Scheldt Estuary (The Netherlands) | Macrotidal<br>A = 370 $km^2$ [a]<br>D = 15 m [b]<br>Q = 34-253 $m^3$ $s^{-1}$ (107) [c]<br>$\tau_r$ = 2-3 months [1d]<br>MTZ (max. 400 mg $L^{-1}$) [g]<br>OMZ in low salinity [h]<br>Reducing conditions | 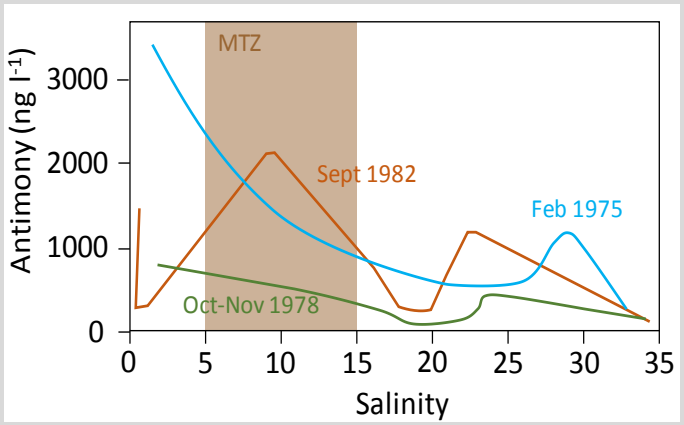 <br>$Sb_p$ decreases from S = 2.5 to S = 35 (influence of low marine $Sb_p$) | BIOCONSULT & NLWKN 2013; **van der Sloot et al. 1985**<br><br>*(Sistermans and Nieuwenhuis 2004; Tessier et al. 2002)* [j] |

*(Table 13 Continued)*

| Behaviour | System | System characteristics | Dissolved and particulate Sb behaviour | References |
|---|---|---|---|---|
| **Non-conservative** | Geum Estuary (Korea) | Macrotidal<br>A ≈ 50 km² [a]<br>D = n.a. [i]<br>Q = n.a. [i]<br>$\tau_r$ = n.a. [i]<br>Extensive mud flats<br>Sediment regeneration or anthropogenic input | 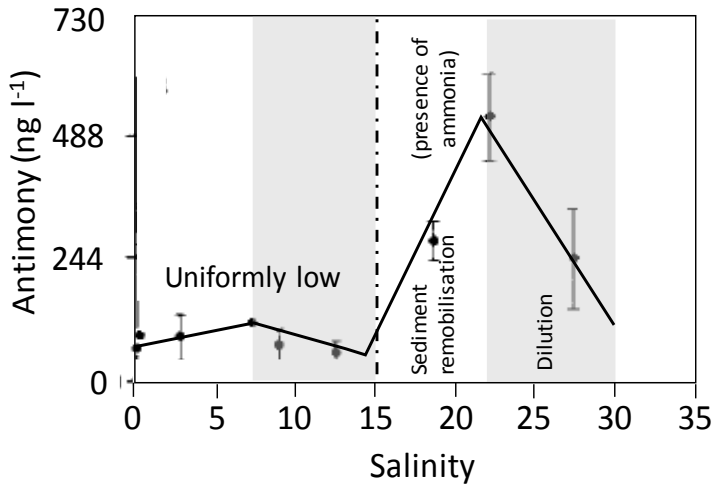 | **Byrd 1990** |
| | Savannah River estuary (Georgia, USA) | Mesotidal<br>A = 121 km² [a]<br>D = 4.6 m [b]<br>Q = 328 m³ s⁻¹ [c]<br>$\tau_r$ ≈ 1 month* [1d]<br>Scavenging at low salinities<br>Reducing conditions<br>Possible link to nitrogen (N) cycle | 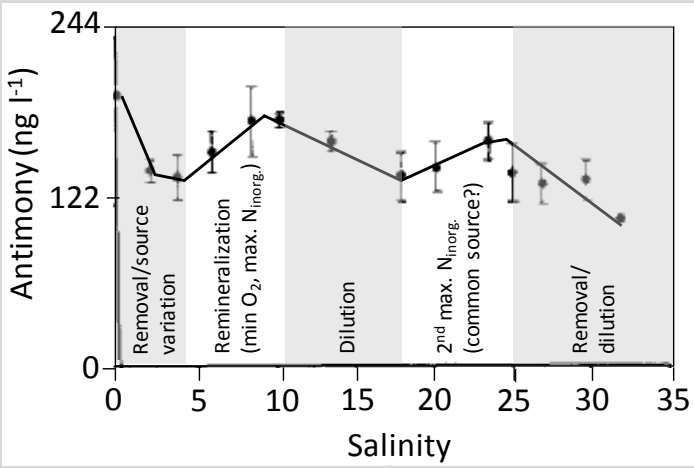 | **Byrd 1990**<br>*(Dame et al. 2000; Reinert and Peterson 2008)* [j] |

*(Table 13 Continued)*

| Behaviour | System | System characteristics | Dissolved and particulate Sb behaviour | References |
|---|---|---|---|---|
| **Non-conservative** | Tama Estuary (Tokyo, Japan) | Mesotidal<br>A = n.a. [i]<br>D = n.a. [i]<br>Q = n.a. [i]<br>$\tau_r$ = n.a. [i]<br>Highly polluted<br>Oxigen consumption and denitrification in sediments | 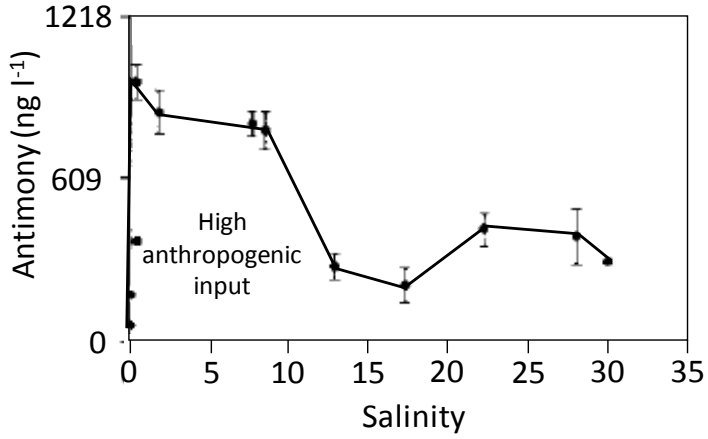 | **Byrd 1990**<br>*(Nishio et al. 1982)* |
| | Tan Shui Estuary (Taiwan) | Mesotidal<br>A = n.a. [a,i]<br>D = 6.5 m [b]<br>Q = 160 $m^3$ $s^{-1}$ [c]<br>$\tau_r$ = 5-9 d [1d]<br>Anthropogenic sources<br>Upstream anoxic estuary | 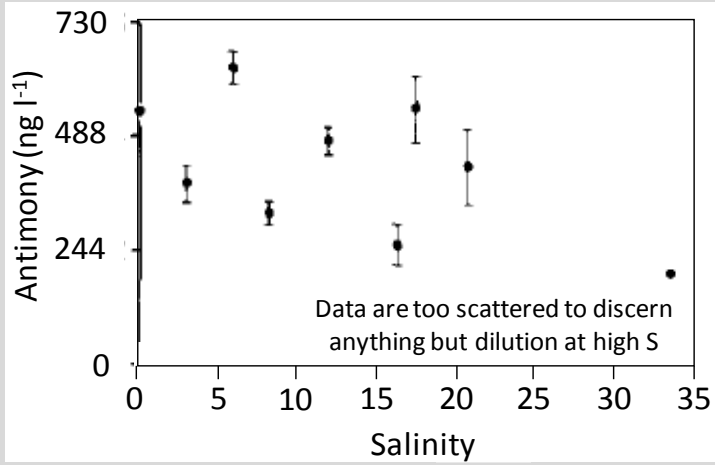 | **Byrd 1990**; Fang and Lin 2002; Liu et al. 2001<br>*(Fan et al. 2006; Liu et al. 2005)* [j] |

*(Table 13 Continued)*

| Behaviour | System | System characteristics | Dissolved and particulate Sb behaviour | References |
|---|---|---|---|---|
| **Non-conservative** | Tagus Estuary (Portugal) | Mesotidal<br>A = 320 km$^2$ [a]<br>D = 10.6 m [b]<br>Q = 300-1000 m$^3$ s$^{-1}$ [c]<br>$\tau_r$ = 10-60 days [1d]<br>Anthropogenic sources | 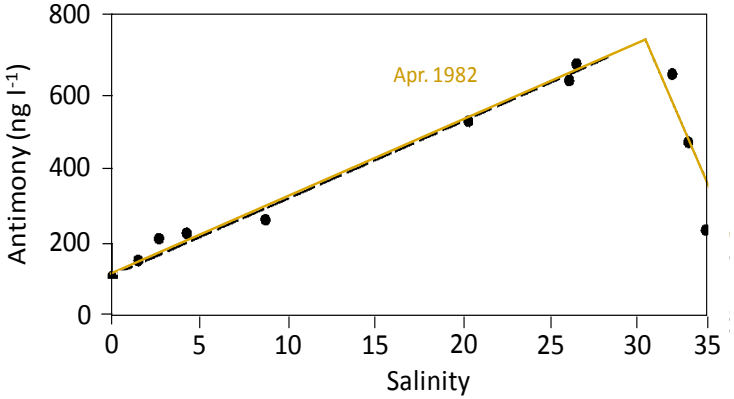 | **Andreae et al. 1983**<br>*(Freire et al. 2006)*[j] |

[a] A = Average estuary surface area
[b] D = Average estuary depth
[c] Q = Seasonal or average discharges. When brackets are also shown, the range corresponds to maximum and minimum discharges and the average is presented in brackets
[d] $\tau_r$ = water residence time in the estuary. *correspond to estimated values, generally considered by dividing stock by fluxes (1). Estimates on flushing time (2) given in the different references are considered equivalent to residence times unless specified otherwise
[e] DO = Dissolved Oxygen
[f] DOC = Dissolved Organic Carbon
[g] MTZ = Maximum Turbidity Zone
[h] OMZ = Oxygen Minimum Zone
[i] n.a. = not available
[j] *References between brackets refer to sources on hydromorphological information (A, D or tidal character) when it is not indicated in the main references (in bold)*

Despite that van der Sloot et al. (1985) did not enter into details to explain the M-shaped Sb pattern of the Scheldt estuary in 1982 (unlike Byrd 1990) it is noteworthy that they detected variable non conservative behaviours along the salinity gradient for the same estuary during three different sampling campaigns (i.e., February 1975, October-November 1978 and September 1982; ***Table 13***). In fact, conservative behaviours are mostly observed during high discharge seasons (December to March) whereas non-conservative behaviours are generally registered during low discharge seasons (observed in ***Table 13*** when published data specified sampling time). This suggests that (i) the same estuary can display different non-conservative patterns of Sb according to hydrological/intrinsic conditions, and (ii) seasonal events within the same estuarine system determine dissolved Sb behaviour. Thus, there is probably no single Sb pattern along the salinity gradient over the year, contrary to other known trace element estuarine reactivity like cadmium (Cd) and silver (Ag), showing the classical bell-shaped desorption/dilution curves (e.g., Dabrin et al. 2009; Lanceleur et al. 2013).

Concerning the seawater endmember, it is noteworthy to highlight the analytical difficulties of working with such complex matrix samples. This not only applies to Sb but to any dissolved trace element. Particularly for Sb, a temporal analysis of published seawater concentrations (Filella et al. 2002a) shows analytical improvements in both accuracy and precision over time, approaching to the established average seawater concentration of 184 ± 45 ng $L^{-1}$ (***Figure 22***).

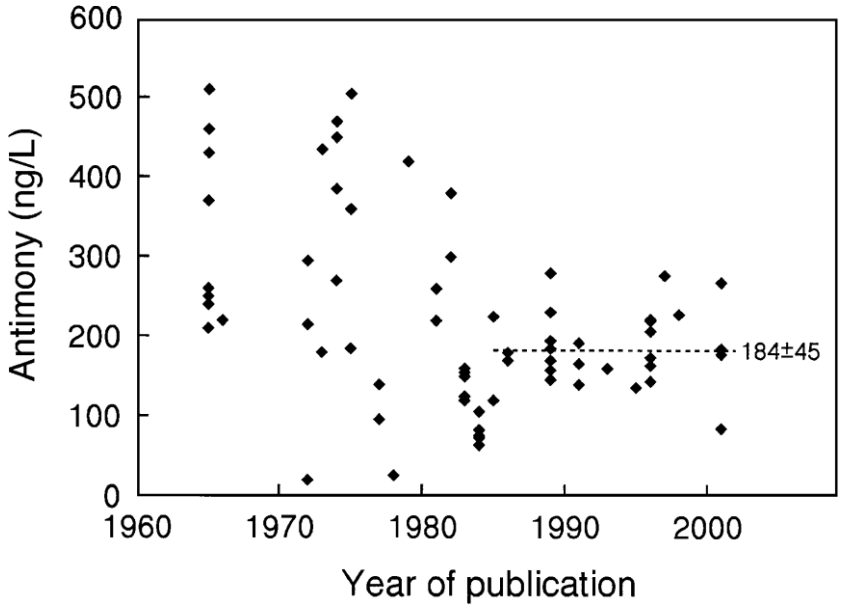


**Figure 22: Surface seawater total dissolved Sb concentrations published between 1960 and 2000**. Average and standard deviation deduced for the last 15 years is also shown *(Filella et al. 2002a).*

Once Sb reaches the ocean, it appears less reactive compared to estuarine processes. Open ocean studies on dissolved Sb suggest both conservative (e.g., in the Atlantic Ocean, Middelburg et al. 1988; in the NW Mediterranean Sea, Takayanagi et al. 1996; in the South Pacific in subtropical/sub-Antarctic

waters, Ellwood and Maher 2002; and in specific seas or basins like Sargasso Sea, Gulf of Mexico, Kau Bay, Filella et al. 2002a and references therein) and mildly scavenged behaviour (e.g., in the eastern and north Atlantic Ocean, Cutter and Cutter 1995, 1998, and subtropical-equatorial Atlantic, Cutter et al. 2001; in the Baltic Sea, Andreae and Froelich 1984; in the SW Mediterranean Sea, Takayanagi et al. 1996). Some authors explain the scavenging behaviour as a result of higher particulate matter supply and longer residence times (e.g., Baltic Sea; Andreae and Froelich 1984; Filella et al. 2002a). Others suggest there can be a misinterpretation in scavenged profiles as Sb can have significant atmospheric input, increasing surface water concentrations (Ren et al. 2016). Cutter and Cutter (2006) tested this hypothesis by sampling in "older" (longer residence time) waters in the Pacific Ocean. They concluded that Sb shows a mildly scavenging behaviour from a good linear correlation coefficient ($r = 0.768$) between Sb and Al (i.e., a known scavenged element).

### *2.1.4. Biological uptake and toxicity*

Antimony is a non-essential element for humans and living organisms (Krachler et al. 2001; Filella et al. 2007). It is involved in metabolic routes and methylation processes but it is potentially toxic at low concentrations (Smichowski 2008; Filella et al. 2009). The relevance of its biological implications depends on its oxidation state, the presence of potential ligands and the solubility of Sb compounds. It has been observed that: (i) elemental Sb is more toxic than its salts, (ii) inorganic Sb species are more toxic than organic ones, and (iii) Sb(III) shows more acute toxicity than Sb(V) species, as it has higher affinity for sulfhydryl groups and red blood cells than the pentavalent form (Krachler et al. 2001; Smichowski 2008).

The historical uses of Sb in medicine have been related to potential bactericide properties in wounds and ulcers. However, its uncontrolled use as internal treatment caused highly toxic effects and was forbidden in France between 1566 and 1666 (Thomson 1926). Smaller doses showed to have laxative, emetic and diaphoretic effects in the form of butter of antimony ($SbCl_3$), glass of antimony (cooling of molten $Sb_2O_3$), tartar emetic ($K_2[Sb_2(C_4H_2O_6].3H_2O$), among others (Biver 2011). Nowadays, pentavalent species and other Sb compounds are used for medical purposes against tropical protozoan diseases such as leishmaniasis, trypanosomasis and bilharziasis (Filella et al. 2002a; WHO 2003). Better tolerated tartar emetic compounds are still used against Platyhelminthes parasites such as *Schistosoma japonicum* (Lauwers et al. 1990). Nevertheless, despite its applications for human welfare, its specific mechanisms of action remain unknown. Trivalent Sb species are suspected to be carcinogenic to humans. However, this subject is still inconclusive as it has only been evidenced in experimental animals (USEPA 1999; WHO 2003) and its genotoxic mechanisms are still unknown (Krachler et al. 2001; Smichowski 2008).

Human exposure routes of concern to Sb are mainly inhalation and ingestion (WHO 2003). Indeed, Sb exposure can cause respiratory problems (e.g., pneumoconiosis), dermatitis, conjunctivitis, cardiotoxicity and gastritis among others (Krachler et al. 2001; WHO 2003; Smichowski 2008). Its residence time in the body is also relevant, as studies on radiolabelled $^{125}Sb$ aerosols have shown average lung retention times in male workers of 850 ± 250 days for non-smokers and 2700 ± 1000 days for smokers (Garg et al. 2003). Average daily inhaled intake is established in 30 ng $m^{-3}$ of air with ~ 15% average adsorption (WHO 2003; Smichowski 2008). In average, it is present at levels < 1 mg $kg^{-1}$ in all human tissues, being more concentrated in lungs, lymph nodes and hair (Filella et al. 2002a). Another exposure pathway contributing to Sb accumulation could be food and feed plants from contaminated soils as well as contamination from food packages, though there is no regulation on marketable Sb maximal levels (Tschan et al. 2009; Pierart et al. 2015). However, edible plants accumulate Sb with potentially adverse phytotoxic (e.g., growth retardation, inhibition of photosynthesis, etc.) and other deleterious effects by decreasing the uptake of some essential elements as well as the synthesis of relevant metabolites (Herath et al. 2017 and references therein).

Nevertheless, antimony bioaccumulation in living organisms is suspected to be low as it is present at very low environmental concentrations (e.g., < 0.008 mg $kg^{-1}$ f.w. in seafood and fish in France and between 0.1 – 0.2 mg $kg^{-1}$ d.w. in freshwater and marine algae), with higher levels in marine food (Filella et al. 2007; Guérin et al. 2011; CFS 2013). Moreover, biomagnification along the food chain has not been specifically evidenced yet. However, according to Pierart et al. (2015), further research is needed to elucidate this and confirm/exclude Sb bioavailability, at least to humans from food sources.

An and Kim (2009) suggest that Sb might be involved in nutritional pathways like that of the nitrogen cycle. This would be somehow in accordance with known phosphate pathways used for As uptake by organisms, the geochemical neighbour of Sb, particularly in marine species (Sanders and Windom 1980). Likewise, Duan et al. (2010) suggest that Sb is involved in the biological cycling of marine phytoplankton due to high correlation factors with nutrients and chlorophyll-a production. Nevertheless, phytoplankton uptake mechanisms are yet unknown (Filella et al. 2007).

## 2.2. Sources, applications, chemical properties, concentrations and toxicity of stable Te

### *2.2.1. Anthropogenic sources and applications*

The first uses of tellurium (Te) for human applications date back to the late 1920's in the treatment of microbial infections such as syphilis and leprosy (De Meio and Henriques 1947; Cunha et al. 2009). Soon after, in the 1930's, Alexander Fleming discovered the antibacterial properties of the oxyanion tellurite ($TeO_3^{2-}$; Fleming 1932; Fleming and Young 1940). Since then, other medical applications have

been developed, mainly related to its highly selective toxicity properties in redox-modulating compounds for cancer treatments and other diseases compromising cellular redox homeostasis (Taylor 1996; Mecklenburg et al. 2009; Jamier et al. 2010). In fact, Te compounds enhance a lethal cocktail of cellular reactive species causing oxidative stress selectively in cells with disturbed redox balance unleashing cellular apoptosis (Jamier et al. 2010).

The main applications of Te are related to its metalloid properties (i.e., photoconductivity, thermoelectricity, non-linear optical responses, high infrared transmittance, catalytic activity, among others; Wang and Guan 2012). It is mainly used as an additive for improving machinability of other materials like steel and iron or modifying physical characteristics of non-ferrous alloys such as aluminium, tin, copper, lead, magnesium, and manganese (USGS 2018). Such application may potentially explain the increasing worldwide production of Te in the early 1950's (***Figure 23***), matching the beginning of the Golden Age (*cf.* second industrial revolution or Post–World War II economic expansion between 1950-1970's; Eichengreen 1945). Likewise, the decrease of Te production from late 1970's to late 1990's could be related to the decreasing use of iron and non-ferrous products (USGS 2018) following several events such as the oil crisis (1973; Vernon 1976), the recession period (1974-1975; Mork and Hall 1980) and the stock market crash (in 1973 and 1987; Mishkin and White 2002). However, other Te applications as a vulcanising agent and accelerator in rubber production (USGS 2018), as a pigment in glass and ceramics (USGS 2018), within batteries (Han et al. 2014) and in thermoelectric materials (e.g. as $Bi_2Te_3$ and PbTe; Chen et al. 2014; Yuan et al. 2014; Zhou et al. 2014) kept on developing at that time.

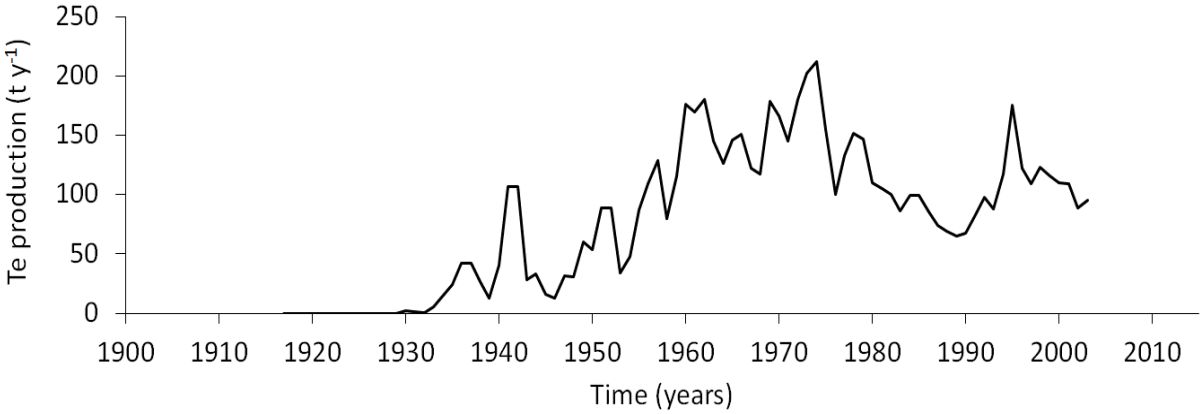


**Figure 23. Worldwide Te production** (t $y^{-1}$) between 1900 and 2015 *(Mlynarski 1998).*

Since the 1990's (***Figure 23***), increased Te applications have also been related to chemical products and its use as a catalyst for synthetic fiber production (USGS 2018). Most importantly, new Te applications have specialised towards photonics, included in rare earth-doped tellurite glasses (Leal et al. 2015; Costa et al. 2016), as CdTe in photovoltaics (Seyedmohammadi et al. 2015) and, as quantum dots for telecommunications, photodetectors and biotechnologies (Turner et al. 2012; Durán-Toro et

al. 2014; Mahdy et al. 2015), among others. Such is the importance of Te in thin-film photovoltaics that current global consumption estimates highlight that 40% of Te applications are related to the solar panel industry, whereas 30% is used in thermo-electric production, 15% for metallurgy purposes, 5% in the rubber industry, and 10% for other end-uses (USGS 2018). In the recent years, applications of Te in nanotechnology account for advances in electronics and medicine (e.g. Baesman et al. 2007).

- *Technology Critical Elements (TCEs)*

Within the European Research Area (ERA), European funded programmes such as COST Actions (European Cooperation in Science and Technology) enable the coordination and development of interdisciplinary science and technology networks, promoting communication and dissemination of nationally funded research activities on innovative and emerging topics. In 2015, the NOTICE COST Action TD1407 (Network on Technology-Critical Elements: From Environmental Processes to Human Health Threats) focused European research on the Technology Critical Elements (TCEs, ***Figure 24***) defined as a group of elements formed by the Platinum Group Elements (PGEs: Ir, Pt, Pd, Rh, Ru, Os), some Rare Earth Elements (REEs: Y, La, Ce, Pr, Nd, Sm, Eu, Gd, Tb, Dy, Ho, Er, Yb, Lu) and other less studied elements (Ga, Ge, **Te**, In, Nb, Ta, Tl; Cobelo-García et al. 2015; Filella and Rodríguez-Murillo 2017).

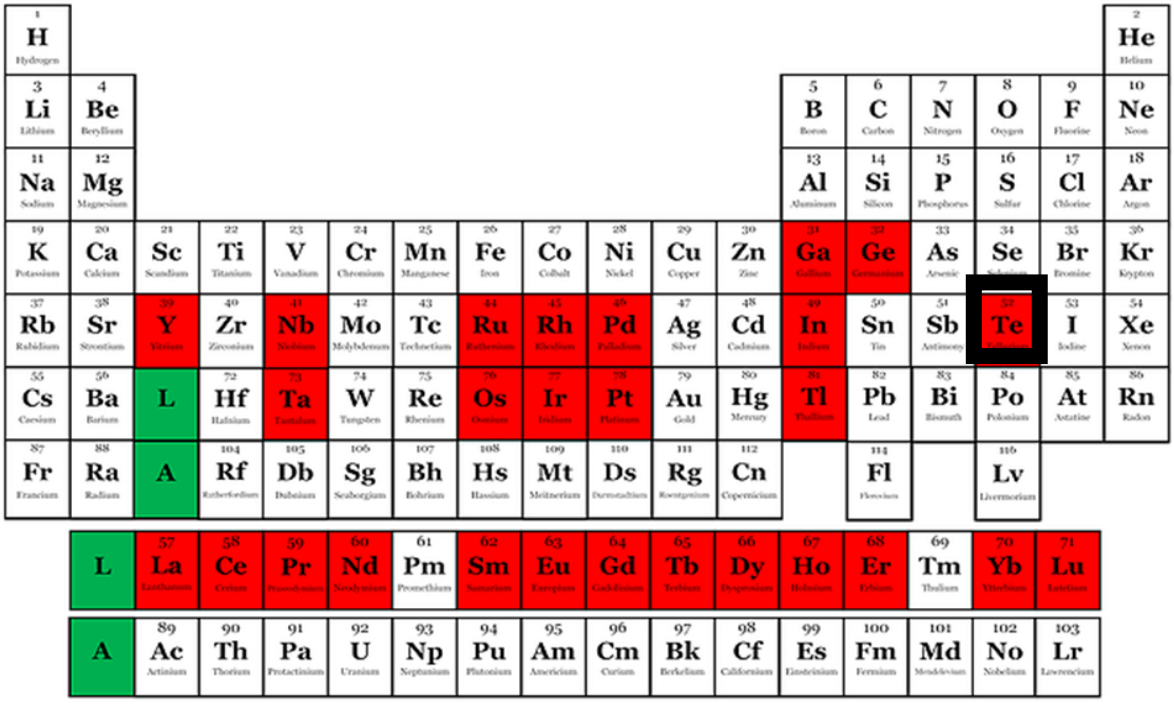


**Figure 24.** Periodic Table highlighting assigned **Technology Critical Elements** (red)**.** Tellurium is denoted by a black square. *(Modified from Cobelo-García et al. 2015).*

The criteria for this classification is the term “criticality” concerning scarcity, as in the case where the future supply of these elements might be compromised. This is due to supply limitations (i.e., concentrations, technological evolution, geopolitical risks, etc.; Filella and Rodríguez-Murillo 2017) compared to the forecasted demand and growth trends, given their specificity in developing technologies (Moss et al. 2011; Cobelo-García et al. 2015). This term, therefore, is dependent on market fluctuations and can be reviewed over time (Hayes and McCullough 2018). In any case, they are elements present in very low environmental concentrations (ultra-trace levels). Therefore, little knowledge exists on their environmental behaviour, cycling and biological impacts (Cobelo-García et al. 2015).

Tellurium is considered a TCE due to the increasing development of green energies, i.e., solar photovoltaics, related to the European goal to reduce greenhouse gas emissions (Biver et al. 2015). In fact, it is expected that photovoltaics will contribute in 13% to the global electricity supply by 2040 (Marwede and Reller 2012). However, the demand of Te is predicted to be three times greater than the supply by 2020-2030 (Moss et al. 2011). This supply is compromised due to the low crustal concentrations of Te, as there are no specific mines devoted to Te extraction and commercialisation purposes (Moss et al. 2011). Only two mining districts can be considered as Te primary ores in the world, contributing to 15% of the annual Te worldwide production: epithermal gold-tellurium vein deposits (Dashuigou and Majiagou in SW China) and epithermal-like mineralisation in the volcanogenic massive sulphide in Kankberg deposit (Skellefte, Sweden; Goldfarb 2014). Thus, Te is mainly obtained as a by-product of copper, silver, lead and gold refining related to the production of the anodic slimes in the electrolytic process, to refining skimmings or from flue dusts and gases generated during smelting (USGS 2018; Schroeder 1967). From these, anodic slimes constitute the main source of Te despite the relatively low, average 30% to 45% recoveries (Ojebuoboh 2008). Significant producers of Te (as by-product from refining activities) are Canada, Belgium, United States, Japan, Peru, Russia, Germany and Finland, being China and Mexico the countries with greatest estimated copper reserves (Moss et al. 2011; USGS 2018).

Research has focused on alternative sources/solutions to alleviate future constraints in Te supply. For instance, oceanographic research studies contemplate seafloor minerals within the new Te resources, as Te may be enriched in ferromanganese nodules (e.g., International Research Project MarineE-tech; Goldfarb 2014). Otherwise, the Department of Energy and the European Union encourage the development of new technologies (e.g. biotechnology) for recycling and recovering Te from mining waste streams (e.g. Ramos-Ruiz et al. 2016) and from main end-use products like thin-film photovoltaic panels (Marwede and Reller 2012). The latter could potentially replace Te photovoltaic demand by 2038 if the efficiency of current photovoltaic systems is substantially improved (Marwede and Reller 2012).

### *2.2.2. Environmental speciation and redox dynamics*

- *Chemical speciation*

Tellurium (*Z* = 52, *A* = 127.6) is a metalloid from the Group 16 of the Periodic Table, together with sulphur (S), oxygen (O) and selenium (Se). It has eight naturally stable isotopes (i.e. 34.08% $^{130}$Te, 31.74% $^{128}$Te, 18.84% $^{126}$Te, 7.07% $^{125}$Te, 4.74% $^{124}$Te, 0.89% $^{123}$Te, 2.55% $^{122}$Te, 0.09% $^{120}$Te) and four oxidation states: -II, 0, +IV and +VI. The reduced forms of Te (-II and 0) can form metal salts and complexes or even bind to organic moieties (Wallschläger and Feldmann 2010). However, most common inorganic forms are mainly found as Te(IV) and Te(VI) (***Figure 25***) in both aqueous and solid forms (Ollivier et al. 2008; Belzile and Chen 2015). The similarity between the oxidation states of Te and those found for Se, related to their proximity in the Periodic Table, is the reason why both Te and Se are generally considered geochemical pairs.

- *Volatile species*

Inorganic Te can form hydride volatile species, mostly known for their applications in analytical quantification techniques (e.g., hydride generation; Zhang and Combs 1996; Hall et al. 1997). Up to seven organic volatile species (***Figure 25***) have been identified for Te including methylated, ethylated and methyl-ethylated complexes (Pinel-Raffaitin et al. 2008). These compounds are produced by bacteria and some fungi in both anaerobic (e.g. compost production; Pinel-Raffaitin et al. 2008) and aerobic conditions developed in sewage and landfill areas (Feldmann and Hirner 1995), in geothermal waters (Hirner et al. 1998), and in sediments of river and harbours (Belzile and Chen 2015).

- *Inorganic solid mineral phases*

Tellurium is a chalcophile element with lithophile tendencies (Salminen et al. 2005) enriched in sulphide and low-temperature supergene minerals. It is mostly found as gold (Au) and silver (Ag) tellurides (i.e., as sylvanite – $AgAuTe_4$ or calaverite and krennerite – $AuTe_2$; with few cases of tellurates and tellurium oxide minerals), in orogenic and epithermal ore systems (Salminen et al. 2005). It is also found in association to platinum group elements (PGE) in Cu-Ni-PGE ore systems (Ames and Farrow 2007; Howell and McDonald 2007).

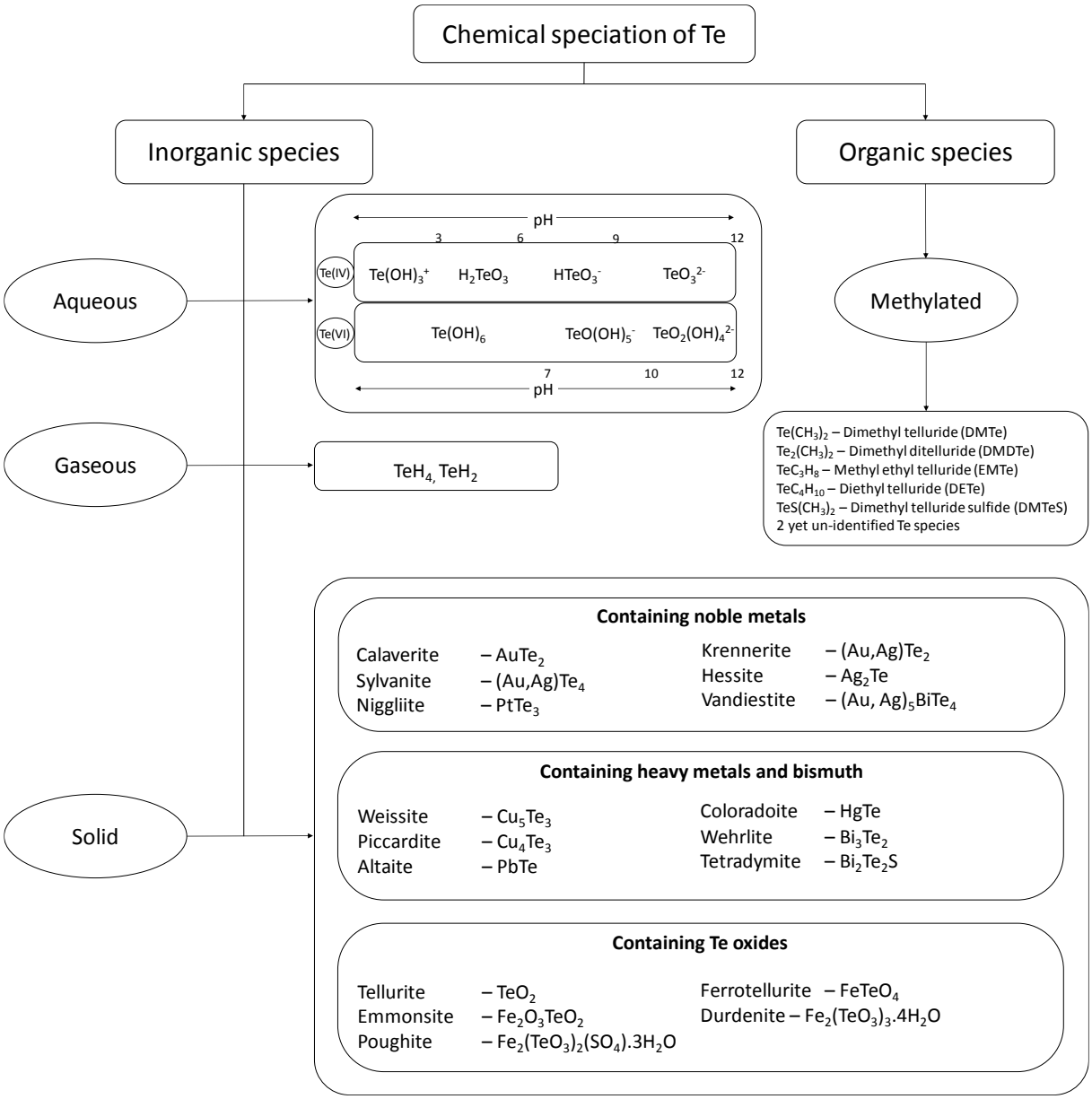


**Figure 25. Common environmental chemical species of Te** *(compilation from Belzile and Chen 2015, Wang 2011 and references therein. Humble Te speciation in aqueous media modified from Brookins 1988, personal communication M. Filella).*

- *Dissolved and particulate speciation*

Thermodynamic calculations suggest that environmental species of dissolved Te commonly show hydroxide ions ($TeO(OH)_3^-$ and $Te(OH)_6$; Casiot et al. 1998; Ba et al. 2010). Several Eh-pH diagrams exist for variable Te concentrations and experimental conditions (e.g., ***Figure 26***). Tellurite forms are not easily oxidised to Te(VI) (Ba et al. 2010). However, there is few information on solid/liquid interactions and Te speciation in solid phases (Harada and Takahashi 2009; Lombi and Holm 2010). One study reports the expected predominance of Te(VI) species in soils exposed to oxidising conditions while Te(IV) dominates under anoxic conditions (Harada and Takahashi 2009). Nevertheless, the two species

may coexist and show similar solid/liquid partitioning in the presence of Fe oxide mineral phases (Harada and Takahashi 2009).

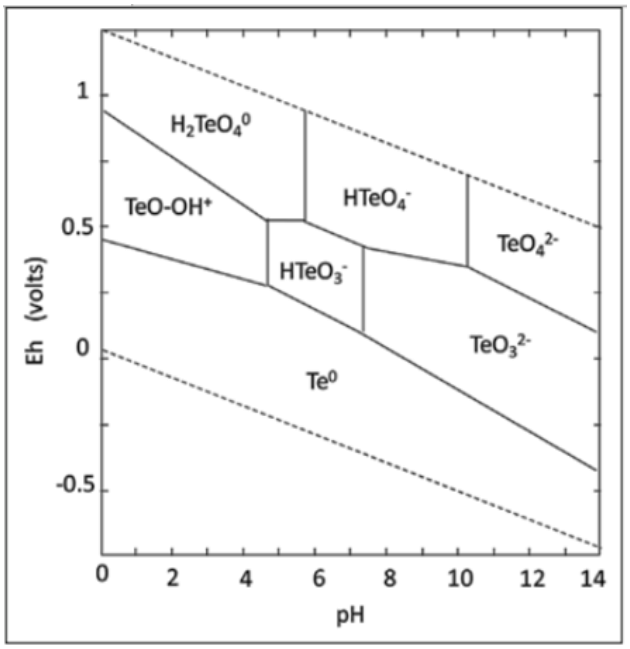


**Figure 26. Eh-pH (Pourbaix) diagram of aqueous speciation of Te**. Modelling conditions include concentrations of total dissolved Te of $10^{-6}$ mol $L^{-1}$ at 25ºC *(Lombi and Holm 2010).*

### *2.2.3. Environmental concentrations and biogeochemical behaviour*

Tellurium has a relatively high abundance in the universe ($9.10^{-7}$%) occupying the 40$^{th}$ position out of 83 described elements (Element Collection Inc. 2007), higher than Sn (48$^{th}$) and Sb (77$^{th}$) and below Se (31$^{st}$). This natural Te source has been used in cosmogenesis studies in order to better understand stellar nucleosynthesis and supernova environments (Audi et al. 2003; Oberli et al. 1998; Fehr et al. 2005), including quantification of Te radionuclides in chondritic and iron meteorite samples (*e.g.,* Goles and Anders 1962; Clark et al. 1967; Smith et al. 1977).

On Earth, Te is a rare element with mean crustal concentrations of about 2-5 µg $kg^{-1}$ (Salminen et al. 2005; Kabata-Pendias 2011; Belzile and Chen 2015) being mostly associated to epithermal ore deposits (McPhail 1995). Lowest concentrations are found in igneous rocks (wide range from 3 to 210 µg $kg^{-1}$; Beaty and Manuel 1973), with average 1-5 µg $kg^{-1}$ in magmatic/ultrabasic rocks, increased content in shales (10 µg $kg^{-1}$; Hall and Pelchat 1997) and highest concentrations in carbonate rocks (1-2 mg $kg^{-1}$ Beaty and Manuel 1973). Generally low Te concentrations are actually comparable to silver (Ag) and gold (Au) abundance in the Earth's crust (i.e. in the order of ~ 80 µg $kg^{-1}$; Salminen et al. 2005), highlighting Te as one of the least abundant elements in the lithosphere (Beaty and Manuel 1973; Belzile and Chen 2015).

Tellurium is present in even lower concentrations in the aquatic systems. It generally presents concentrations ranging between 2 – 25 ng $L^{-1}$ in rain and snow (Belzile and Chen 2015) and, at the European level, the Geochemical Atlas of Europe - FOREGS (***Figure 27a***) reports median concentrations of 2.5 ng $L^{-1}$ in freshwater systems. This Atlas has no available data for particulate Te associated to SPM but reports median concentrations of 30 µg $kg^{-1}$ in European soils (Salminen et al. 2005). Furthermore, published seawater concentrations vary from 0.08 to 910 ng $L^{-1}$ (***Figure 27b,c***). Such wide range reflects (i) the current analytical challenge of Te quantification at low environmental concentrations, often requiring pre-concentration techniques (e.g., hydride generation and voltammetry), and (ii) the lack of available certified reference materials (CRM) to validate such measurements (Biver et al. 2015).

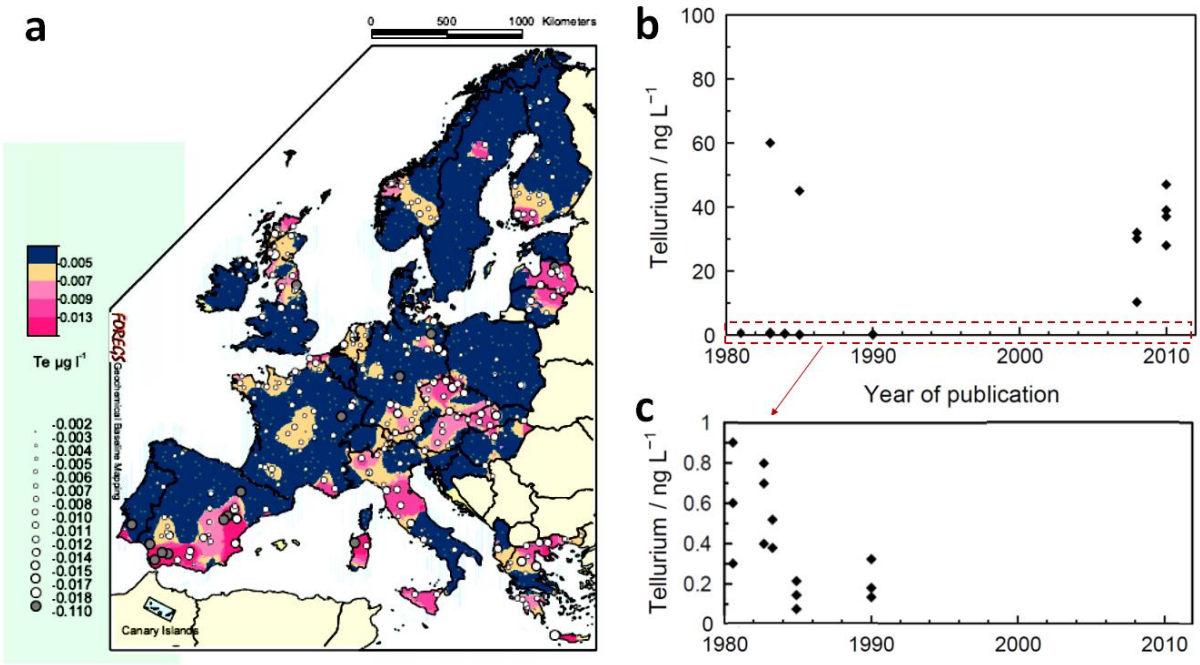


**Figure 27. Environmental concentrations of dissolved Te** in (a) European streams sampled between 1998 and 2001 and analysed between 1999 and 2003 (µg $L^{-1}$, 0.45 µm filtered, N = 807; Salminen et al. 2005), and (b) in surface seawater between 1980 and 2010 (ng $L^{-1}$), with (c) a zoom in box for data <1 ng $L^{-1}$ before 1990 *(Modified from Filella 2013)*.

Analytical difficulties in the quantification of Te imply that few studies exist on the environmental behaviour of Te, particularly for continent-ocean transition systems. To the best of our knowledge, there are only three papers reporting Te behaviour along estuarine turbidity and salinity gradients: two on dissolved Te (van der Sloot et al. 1985; Wu et al. 2014) and one on particulate Te (Duan et al. 2014), indicating contrasting Te behaviours. In fact, van der Sloot et al. (1985) suggest that dissolved Te follows a conservative behaviour along the salinity gradient of the Scheldt Estuary, showing high upstream concentrations (up to 500 ng $L^{-1}$) compared to the seawater endmember (~30 ng $L^{-1}$; ***Figure 28a***). However, Wu et al. (2014) in the Changjiang River Estuary suggest a non-conservative behaviour from increased dissolution of Te(VI) in the high salinity ranges (***Figure 28b***). This trend is supported by

decreasing particulate concentrations from a parallel study in the same system (Duan et al. 2014), despite the delay between the different sampling campaigns (i.e. dissolved concentrations in May 2009, Wu et al. 2014; and particulate concentrations in September 2009, Duan et al. 2014). Thus, further research is required to better understand Te reactivity in these continent-ocean transition systems.

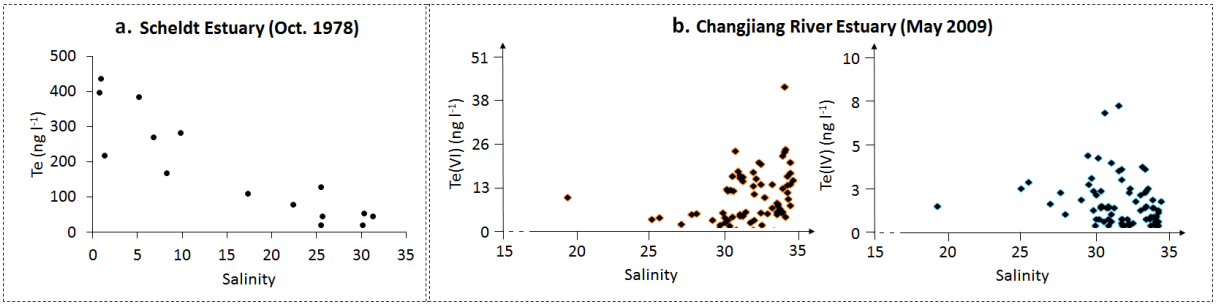


**Figure 28. Dissolved Te reactivity along salinity gradients** of the Scheldt Estuary (total Te; *van der Sloot et al. 1985*) and the Changjiang River Estuary (speciation; *modified from Wu et al. 2014*).

Once in the ocean, Te seems to show a nutrient-type behaviour in continental platform areas, as reported for the Saanich Inlet (Yoon et al. 1990) and the Florida Strait (Andreae 1984). A nutrient-type behaviour could be expected given its assimilation by terrestrial and marine primary producers (Nolan et al. 1991), despite its unknown essential character (Ba et al. 2010). However, this behaviour seems not to be reproducible in all coastal areas, showing unclear patterns for the shallow waters in the East China Sea (Wu et al. 2014). Contrastingly, vertical profiles of Te concentrations in open ocean point towards a general scavenged behaviour, at least for the Atlantic and Pacific Oceans (Lee and Edmond 1985). In any case, Te(VI) seems to be the generally more abundant than Te(IV) in both estuarine and open water systems.

### *2.2.4. Biological uptake and toxicity*

Tellurium is generally considered as a non-essential element for organisms and humans. However, evidences of its assimilation/uptake by organisms as well as its presence in metabolic routes and methylation processes (Nolan et al. 1991; Ba et al. 2010; Baesman et al. 2007) seem to suggest that its essential role in biological compartments might still be overlooked (Chasteen et al. 2009; Ba et al. 2010).

The first biological interaction of Te was registered in the 19$^{th}$ Century in mammals presenting garlic-like breath odour (Gmelin 1824; Hansen 1853; Chasteen et al. 2009). Nowadays, the production and release of organic telluride in mammals is known as a detoxifying response relating sequential reduction and methylation of toxic Te (Chasteen and Bentley 2003).

Tellurium is generally considered a toxic metalloid involved in cell oxidative stress responses (Chasteen and Bentley 2003) with inhibitory effects observed already at 1 μg $L^{-1}$ of Te(IV) in *E. coli* (Turner et al. 1999). Elemental Te(0) is generally considered to be less toxic than its oxyanions, for which Te(IV) is more toxic than Te(VI) (Franke and Moxon 1936; Viñas et al. 2005). Exposure to volatile species such as dimethyltellurium ($(CH_3)_2Te$) and hydrogen telluride ($H_2Te$) seem to induce teratogenic effects relayed to disturbances in the central nervous system (Walbran and Robins 1978; Taylor et al. 1996; Stangherlin et al. 2006). Some human detrimental effects include dementia, intravascular hemolysis, respiratory and cardiac failure (Taylor et al. 1996). Main exposure routes are related to inhalation, skin/external exposure and ingestion, the human body retaining >500 mg of Te in bones, liver, kidney, heart and spleen (Schroeder et al. 1967; Taylor et al. 1996). Reported concentrations in blood and urine are 5 ng $mL^{-1}$ and 50 ng $mL^{-1}$ respectively (Siddick and Newman 1988), with excretion being mostly in the form of tellurides or elemental tellurium (i.e., faecal or urinary; Larner et al. 1996). Reported biological residence times range from 13 days in rats (Taylor et al. 1996) to 145 days in mussels (Whitehead et al. 1988). Tellurium uptake by plants seems to follow similar pathways as Se, presenting highest Te concentrations of ~6 mg $kg^{-1}$ in seleniferous plant species and/or Te-enriched soils (Reimann and de Caritat 2012).

An original detoxifying mechanism of some microorganisms includes the reduction of Te(IV) into elemental Te, forming intracellular black deposits. This production of solid Te is sometimes enhanced in laboratory cultures for commercial purposes, given the recent use of Te nanostructures in technological applications (*e.g.,* Baesman et al. 2007; Bajaj and Winter 2014). Consequently, there has also been a parallel increase in research concerning Te nanoparticle toxicity. However, results seem yet inconclusive as they depend on the tested nanoparticle concentrations, on their configurations (*i.e.,* shapes, sizes, surface chemistry, etc.) and on the organisms which are being affected (Leigh et al. 2012; Monrás et al. 2014; Bruneau et al. 2015). Thus, the direct effects of these Te environmental releases still remain unclear (Tang et al. 2013; Lai et al. 2015).

Contrastingly, certain microorganisms including marine bacteria (Yamada et al. 1997), can present genetic resistance to Te toxic forms. In fact, at least ~10% of the microorganisms present in several environments contain tellurite-resistant genes, with yet unclear purposes (Ollivier et al. 2008). Other bacteria have shown functional proteins constituted by tellurocysteine and telluromethionine (Boles et al. 1995; Budisa et al. 1995). Nevertheless, more research is still required in the field of Te biological implications, uptake mechanisms and cellular interactions (Dong et al. 2007; Babula et al. 2009; Chasteen et al. 2009; Díaz-Vásquez et al. 2014), particularly for organisms in aquatic environments at cellular, individual and ecosystem levels.

## V. CONCLUSION

Given the low frequency of nuclear power plant (NPP) accidental events and the relevance of intrinsic nuclear reactor working conditions at the moment of the accident (i.e., fuel composition, burn-up, etc.), accurate predictions of radionuclide characteristics (quantity, volatile/refractory species, etc.) in future hypothetical NPP accidental releases are still a challenge and quite unknown. Evidences from past accidental events, such as those from Chernobyl and Fukushima Daiichi, suggesting radionuclide dissolution from atmospheric deposition as well as direct discharges of dissolved radionuclides into aquatic systems justify our interest in the presence and potential dispersion of Sb and Te radionuclides in aquatic environments after NPP accidental events.

The present scientific context also highlights current uncertainties concerning (i) the specific radionuclide forms of Sb and Te released after NPP accidents, and (ii) Sb and Te radionuclide behaviour in aquatic environments, particularly in continent-ocean transition systems. In addition, most radionuclides of Sb and Te show short to medium-term half-lives and a clear link through natural decay chains, i.e., being Sb the radioactive parent of Te radionuclides. Therefore, temporal aspects and potential change of element over time in highly dynamic continent-ocean transition systems should be taken into account when developing radionuclide dispersion scenarios.

Environmental studies on stable Sb and Te also highlight the lack of knowledge in the understanding of Sb and Te reactivity and distributions in continent-ocean transition systems. These unknowns are due to (i) few existing case studies, and (ii) the analytical challenges associated to the quantification of low environmental concentrations, especially in complex matrices like seawater, despite ongoing development and improvement of detection limits in analytical instrumentation. Furthermore, studies seldom take into account the temporal variability of biogeochemical processes for a given system, potentially explaining why published observations sometimes show contrasting behaviours. Thus, there is still a lack of comprehensive understanding of the biogeochemical cycles of Sb and Te.

The following chapters will present the approaches performed in this work in order to improve the understanding of the biogeochemical behaviour of Sb and Te in continent-ocean transitions systems, with a focus in two main French systems subjected to NPPs: the Lot-Garonne-Gironde fluvial estuarine system and the Rhône River. This type of study requires important sampling efforts and representative experimental designs, including adapted sample pre-treatment protocols and analytical methods, as will be described in the next chapter.

# CHAPTER 2:

# Materials and methods

# I. INTRODUCTION

The study of the biogeochemical behaviour of Sb and Te in the Lot-Garonne-Gironde fluvial estuarine system and the Rhône River requires both, field campaigns and laboratory experiments. Several field campaigns included in this work comprise: (i) a long-term (2003-2017) monitoring programme at five strategic sites of the Lot-Garonne River system, (ii) sporadic oceanographic campaigns along the salinity and turbidity gradients of the Gironde Estuary during contrasting hydrological conditions, i.e., intermediate (1203 $m^3$ $s^{-1}$, MGTS I), flood (3450 $m^3$ $s^{-1}$, MGTS II), and drought conditions (260 $m^3$ $s^{-1}$, MGTS III and 235 $m^3$ $s^{-1}$, MGTS IV), (iii) a long-term (1984-2017) biomonitoring programme at the estuary mouth, performed by the French National Mussel Watch RNO/ROCCH Programme, and (iv) sporadic sampling of mussels at the Rhône River mouth. The sampling campaigns recovered physical-chemical parameters (water temperature, pH, Eh, etc.) and a set of water and suspended sediment samples to understand both, lithogenic-based and anthropogenic-emitted (inherited) trace element distributions and reactivity. The biological uptake of Sb and Te were studied from soft tissues samples of wild oysters provided by the biomonitoring programme RNO/ROCCH and that of complementary elements (Sn and Se) in Mediterranean mussels.

Laboratory experiments were also performed using water and bulk suspended particle samples collected from the field in both systems (Gironde and Rhône), with the aim of simulating environmentally contrasting salinity and turbidity conditions. These experiments consisted in adsorption kinetics, adsorption isotherms and parallel selective extractions on both, “inherited” (i.e., naturally present trace elements) and “experimental” (i.e., samples isotopically-enriched with spiked stable and radioactive elements). These experimental approaches were chosen in order to (i) better understand adsorption kinetics of simulated anthropogenic releases increasing trace element concentrations in estuarine environments, and (ii) to investigate the similarities and/or potential differences between inherited and spiked solid/liquid partitioning and solid fractionation. These approach will allow to better adjust dispersion scenarios of radionuclide releases in the Gironde Estuary and Rhône River as such events may be considered as cases of anthropogenic discharges into the environment.

This chapter describes how to proceed in each case study, from the sample collection to the data treatment, in order to achieve quality data from field campaigns and laboratory-derived samples before acquiring conclusions and environmental interpretations. Therefore, an introduction of the areas of study and sample collection will be followed by applied sample pre-treatments and analytical quantification methods for Sb and Te. Additional methods for Se quantification in the same environmental samples are also provided given its application in this work as a comparison to Te biogeochemical behaviour. Insights into applied experimental designs are also provided.

# II. AREAS OF STUDY AND SAMPLING SITES

## 1. Areas of study

### 1.1. The Lot-Garonne-Gironde fluvial estuarine system

The principle area of study of this work is the Lot-Garonne-Gironde fluvial estuarine system, located in the southwest of France (***Figure 29***). The Dordogne River and Garonne River are the main contributors of water and suspended particles to the Gironde Estuary, respectively draining major geological formations from the Massif Central and Pyrenean Mountains. The rock composition of the Lot-Garonne-Gironde watershed is described in three geological zones: (i) upstream igneous (i.e., granites and basalts) and metamorphic rocks (i.e., micaschists and gneisses) mainly from the Massif Central, (ii) intermediate Jurassic calcareous sedimentary rocks, and (iii) downstream Tertiary and Quaternary alluvium deposits (BRGM 2014; Audry et al. 2010).

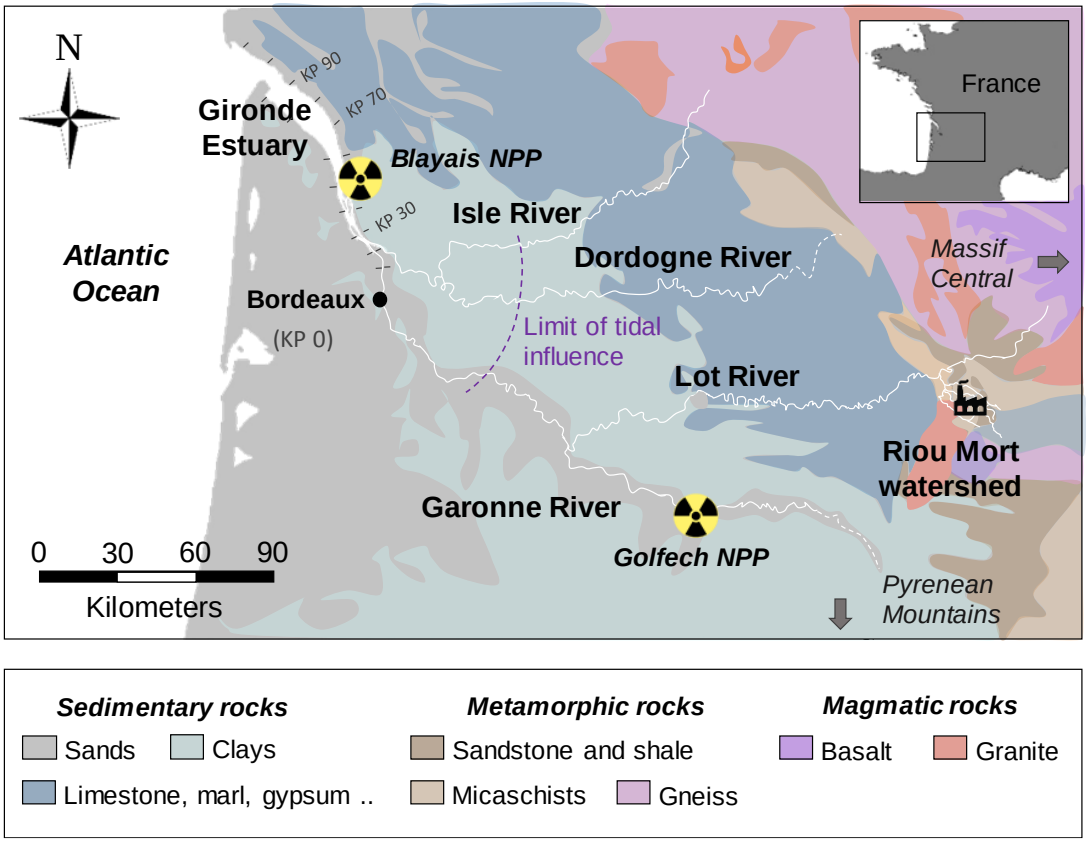


**Figure 29. The Lot-Garonne-Gironde fluvial estuarine system.** Rock composition along the watershed is denoted by the colour code legend (*Adapted from BRGM 2014*). Information on the location of the upstream historical industrial site (industrial icon), the city of Bordeaux (black circle) constituting the kilometric point zero, the assigned estuarine kilometric points (KP) and the two nuclear power plants in the area (Blayais and Golfech) are also shown.

Average freshwater discharges in the last ~60 years have been 586 $m^3$ $s^{-1}$ for the Garonne River (min. 302 $m^3$ $s^{-1}$, max. 880 $m^3$ $s^{-1}$) and 313 $m^3$ $s^{-1}$ for the Dordogne River (min. 119 $m^3$ $s^{-1}$, max.

477 $m^3 s^{-1}$), contributing ~64% and ~31%, respectively, to the total freshwater discharge into the Gironde Estuary (1959 – 2017; DIREN). The general trend of these river discharges through time presents a significant decrease (p-value < 0.001, ***Figure 30***) presenting an increase in the number of drought days per year. This trend is suspected to be related to climate warming, i.e., decreasing the mean annual rainfall as well as the snow reservoirs in the upstream watershed, together with an increase in water-consuming agricultural activities in the area (*e.g.,* maize cropping, stressing water supplies; Jalón-Rojas et al. 2015). Thus, future hydrological conditions in the Lot-Garonne-Gironde fluvial estuarine system may present higher frequency of drought than flood episodes.

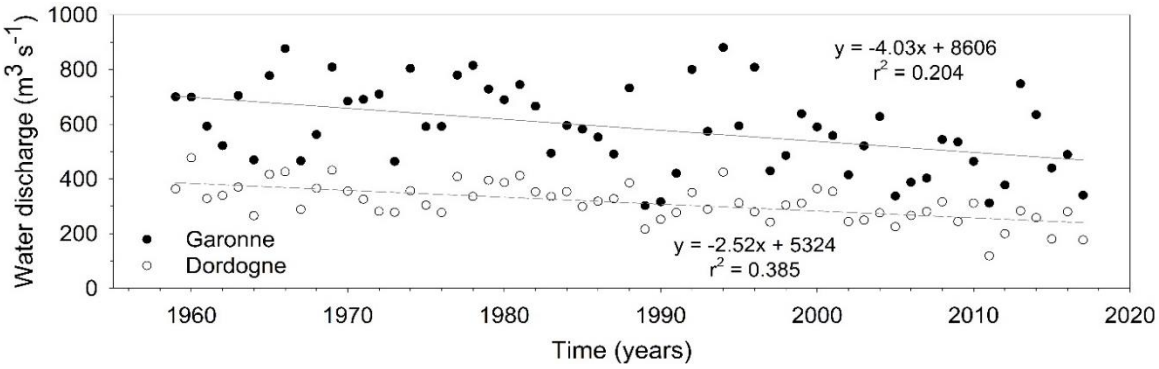


**Figure 30. Water discharge trend (1959-2017) in the Garonne and Dordogne Rivers**. *(Adapted from DIREN)*

### *1.1.1. The Lot River watershed*

The Lot River (***Figure 29***) is a non-negligible affluent of the Garonne River, presenting an original lithogenic composition compared to the main Garonne River watershed. In fact, upstream sites in the Lot River hosts several mineral districts enriched in Zn, Pb, Ag, U, W, Sn, Mo and other metal ores (BRGM 1978, 1983). In addition, the natural geological formation of the Riou Mort River watershed, an important tributary of the Lot River, are mainly composed of (i) Carboniferous (conglomerate and sandstone with intercalation of pelites and coal seams or layers), and (ii) Permian formations (hematite-rich conglomerates, sandstones and mudstones, ***Figure 31***; Coynel et al. 2007*a*).

The Lot River is known for its historical mid-19$^{th}$ century multiple metal contamination (mainly zinc, Zn, and cadmium, Cd) due to several anthropogenic point sources related to 1) open-pit coal mining, 2) Zn ore smelting, and 3) coal-fired power production in the area of Decazeville in the Riou Mort River watershed (Audry et al. 2004a, Blanc et al. 1999, Coynel et al. 2009, Grousset et al. 1999, Lapaquellerie et al. 1995). The contaminating metallurgical (*i.e.,* thermal-extraction) activities ended in 1987, but metal exportation from the industrial area continues due to the drainage and erosion of both landfills containing coal ashes from the former power station and tailings from the ore treatment plant (***Figure 31***). Remediation works have been implemented to treat these point sources, decreasing through time the impact of such multiple metal contamination in the Gironde Estuary (e.g., Dabrin et al. 2009).

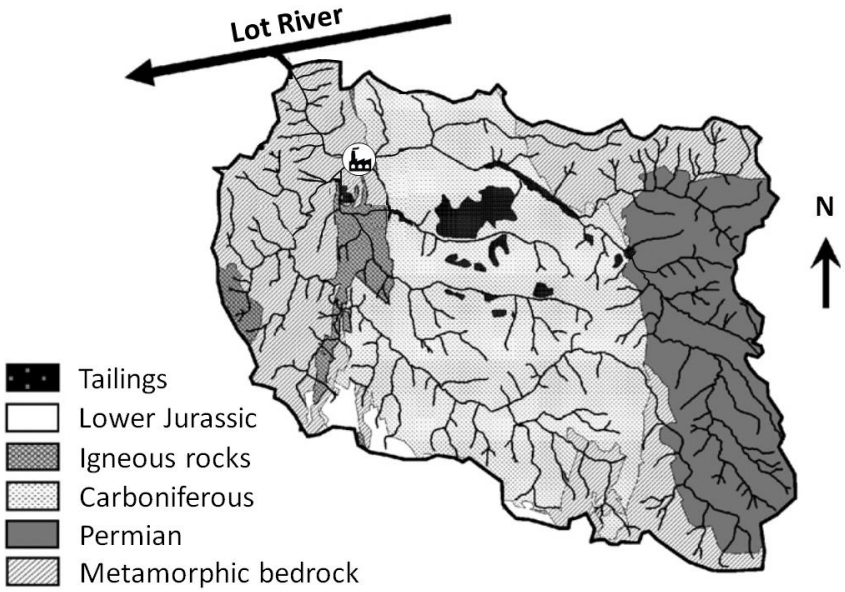


**Figure 31. Natural lithology and presence of anthropogenic tailings in the Riou Mort River watershed.** Location of the historical industrial activities in Decazeville area is also presented *(adapted from Coynel et al. 2007*a).

### *1.1.2. The Gironde Estuary*

- *Estuarine hydrology*

The geographical limit of the Gironde Estuary is located at Bec d'Ambès, where the Garonne and Dordogne rivers join. However, its semidiurnal tidal character (12h 25min) extends the estuarine influence ~100 km upstream from Bec d'Ambès, observing the influence of seawater into the two main river branches: up to the town of La Réole in the Garonne River (70 km upstream from the city of Bordeaux, ***Figure 29***) and up to Pessac-sur-Dordogne in the Dordogne River. Although the amount of seawater entering the Gironde Estuary in every tide is 30-40 times greater than the freshwater discharge (Allen et al. 1977), the volume of freshwater supply into the estuary determines the extension of the horizontal salinity gradient and the strength of the vertical stratification. Thus, the Gironde Estuary is classified as a stratified estuary during high discharge conditions and neap tides, e.g., during winter and spring, and a partially mixed estuary during low river discharges, e.g., in summer and autumn, according to Pritchard's classification (Jouanneau and Latouche 1981).

- *Sediment dynamics*

The combination of two phenomena, (i) the residual circulation developed due to density differences between seawater and freshwater masses (Jouanneau and Latouche 1981), and (ii) the asymmetric tidal wave (Allen et al. 1980) due to the hypersynchronous character of the estuary (convergence > bottom friction; Le Floch 1961), affect estuarine sediment transport. Such conditions

develop a Maximum Turbidity Zone (MTZ) with surface concentrations of Suspended Particulate Matter (SPM) varying from average ~100 mg $L^{-1}$ to ~1000 g $L^{-1}$ (Sottolichio and Castaing 1999). The MTZ presents a characteristic vertical turbidity gradient containing, from top to bottom, turbid water (SPM < 50 g $L^{-1}$), fluid mud (50 g $L^{-1}$ < SPM < 500 g $L^{-1}$) and consolidated sediment (SPM > 500 g $L^{-1}$, ***Figure 32***). The fluid mud is reworked at a tidal scale and is highly eroded during spring tides in wet years (Allen 1972). In any case, this high turbidity gradient triggers the onset of early diagenetic sequences in the fluid mud, playing important roles in trace element estuarine reactivity (Robert et al. 2004).

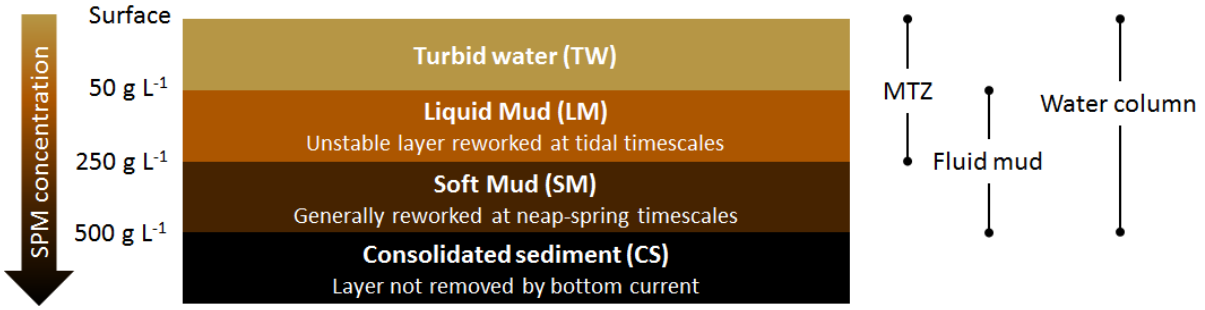


**Figure 32. Vertical turbidity gradient of the maximum turbidity zone (MTZ) in the water column of the Gironde Estuary.** SPM: suspended particulate matter. *(Modified from Audry et al. 2006, after Abril et al. 1999 and Robert et al. 2004).*

The MTZ is mostly found in the low salinity region and migrates seasonally along the estuary due to hydrological influence. The MTZ is capable of entering upstream of the river branches in the summer-autumn period (max. in spring tides; Sottolichio and Castaing 1999) and it can be partly flushed outside of the estuary mouth (usually only 10 – 20 days per year) during specific conditions: continuous, high river discharge during some weeks, during high tidal coefficient (Castaing and Allen 1981). The turbid plume flushing out of the estuary into the coast has two density layers (a surface and a bottom one) which will be subjected to decantation and/or transportation. In fact, the surface plume will drift predominantly north-westwards, with little offshore spreading in winter and spring, and the bottom plume will show a seasonal circulation, spreading southwards in summer and autumn but northwards in winter and spring, depending on coastal hydrodynamics (Froidefond et al. 1998, Jouanneau et al. 1999).

The average residence time of the SPM in the Gironde Estuary has been estimated between 1 and 2 years (Castaing and Jouanneau 1979), explaining why ~4 – 6 million tons of sediments are found in the MTZ compared to the annual supply of ~1.5 – 3 million tons by the Garonne and Dordogne Rivers (Jouanneau 1982). Contrastingly, water residence times are much shorter and present a seasonal character: ~86-day residence times for low discharge conditions and ~18 days during high discharge conditions (Castaing and Jouanneau 1979, Jouanneau and Latouche 1981).

- *Living organisms*

The Gironde Estuary hosts marine, freshwater and characteristic euryhaline organisms ranging from microscopic (e.g., phyto- and zoo-plankton, e.g., Quintin et al. 2012) to macroscopic (e.g., oysters and fish, e.g., Claisse et al. 1992) species. In addition, some of these organisms have essential roles in environmental pollution monitoring studies, acting as bioindicators of integrated trace element concentrations in aquatic environments (Phillips 1977). In fact, the monitoring of wild oysters (*Crassosstrea gigas*, cf. *Magallana gigas*) at the estuary mouth evidenced in the early 1980's the fluvial dispersion and relevant impact of anthropogenic Cd leached from the Lot River (~100 µg $g^{-1}$ dry weight; Claisse et al. 1992). At that time, this Cd contamination in the Gironde Estuary compromised past oyster production in Marennes-Oléron Bay, one of the most important oyster production zones in Europe, due to important Cd bioaccumulation showing Cd concentrations higher than the admissible human consumption levels in oysters (5 µg $g^{-1}$ dry weight; Latouche 1992; Strady et al. 2011). Remediation works in the Riou Mort watershed (***Figure 31***) decreased ever since this coastal contamination. Nevertheless, the biomonitoring of Cd concentrations in soft tissues of wild oysters at the Gironde Estuary mouth witnesses a slow recovery of the admissible human consumption levels for intra-estuarine oyster-farm production (*www.ifremer.fr*), banning today this socio-economic activity within the Gironde Estuary.

### *1.1.3. Nuclear power plants*

Currently operating NPPs in the Garonne-Gironde fluvial estuarine continuum characterise the radioactive context and choice of this system as study area (***Figure 29***). In fact, two NPPs are present in this study area: (i) the Golfech NPP in the upstream Garonne River branch, and (ii) the Blayais NPP in the middle of the Gironde Estuary (***Figure 33***).

**Figure 33. Golfech and Blayais NPPs in the Garonne-Gironde fluvial estuarine system.**

During the past 2 decades, a series of incidents have occurred in both NPPs attributed to levels 1 and 2 of the INES scale (http://france.edf.com/). Furthermore, the Blayais NPP is known for its partial flooding event in December 1999 during a storm. In fact, the Blayais NPP had breakwaters from the

original NPP design but they did not help against the partial flooding of the reactor. This was because the phenomenon in 1999 (i.e., a storm causing high water level and very strong waves in the Gironde Estuary) was an unforeseen event (***Figure 34***) at the time of the original NPP design. Such event lead to the review and reinforcing of protection structures in all French NPPs concerning external floods (e.g., river floods, rainfall, dam bursts, upwelling of the water table, sea swell, etc.; IRSN View-point Report 2007).

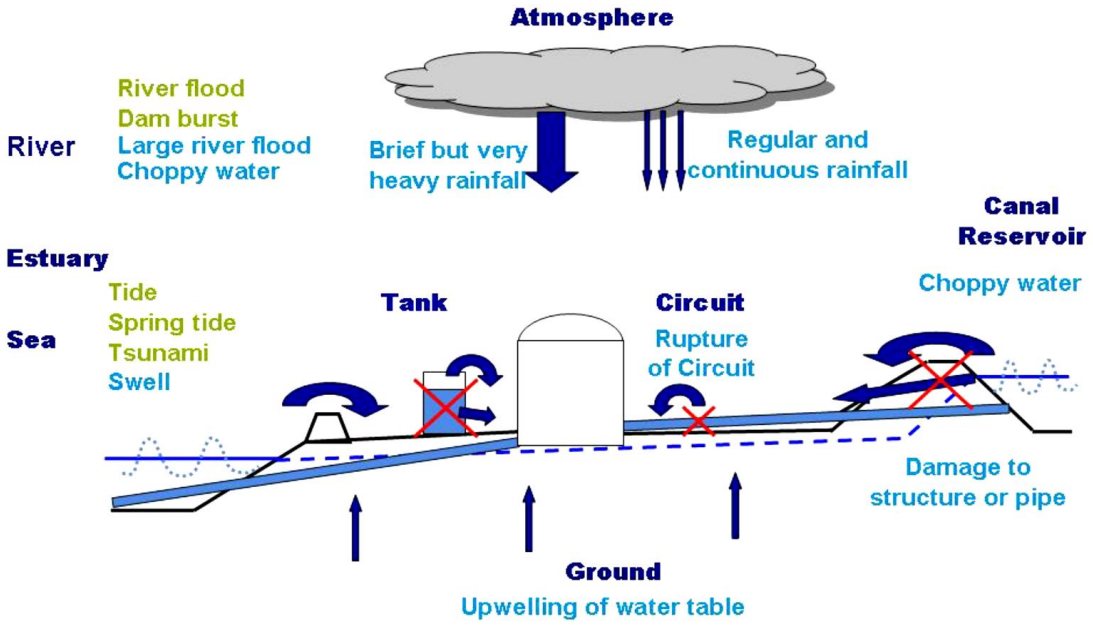


**Figure 34. Sources and associated events causing potential flooding of the Blayais NPP.** Failure of NPP structures (red crosses) and water overflowing into the NPP (arrows) are depicted *(IRSN View-point Report 2007).*

In addition, the Blayais NPP is subjected to a regional ecological monitoring programme, partially performed by the University of Bordeaux with regular oceanographic campaigns (SOGIR: Service d'Observation de la GIRonde). The aim of this programme is to evidence any eventual modifications in the estuarine environment due to the Blayais NPP activities compared to a reference state or baseline corresponding to the ecological status of the Gironde Estuary in the 1970's (Quintin et al. 2012). One of the latest reports concludes that current NPP activities have important dilution effects given the mid-estuarine position of the Blayais NPP, showing no evidence of a significant impact on both physical-chemical (i.e., water temperature, salinity, dissolved oxygen, dissolved organic carbon, chlorophyll and phaeopigments, etc.) and ecological (i.e., zooplankton and benthic macrofauna) monitored parameters.

### 1.2. The Rhône River

The Rhône River, located in the SE of France (***Figure 35***), is the main source of freshwater and SPM to the Mediterranean Sea since the construction of the Aswan Dam in the Nile River (Ollivier et al. 2010). It has a watershed area of 98 800 km$^2$ and an average flow of 1700 m$^3$ s$^{-1}$, overpassing the 3000 m$^3$ s$^{-1}$ during flood events (Ollivier et al. 2010). The Rhône River watershed is characterised by heterogeneous geological formations, i.e., mainly upstream Jurassic and Cretaceous limestones and downstream Quaternary alluvions, with tributaries draining also through several geologically different limestone/marl formations and crystalline, metamorphic and volcanic units (***Figure 35***). Most importantly, it is a watershed subjected to (i) *in situ* precipitation of $CaCO_3$ due to calcite supersaturation, and (ii) relevant SPM load retention due to the influence of >65 dams/hydroelectric reservoirs distributed along its watershed (Ollivier et al. 2010). Near the coast, the Rhône River bifurcates into the "petit Rhône" (<15% flow) and the "Grand Rhône", considered the main Rhône River mouth.

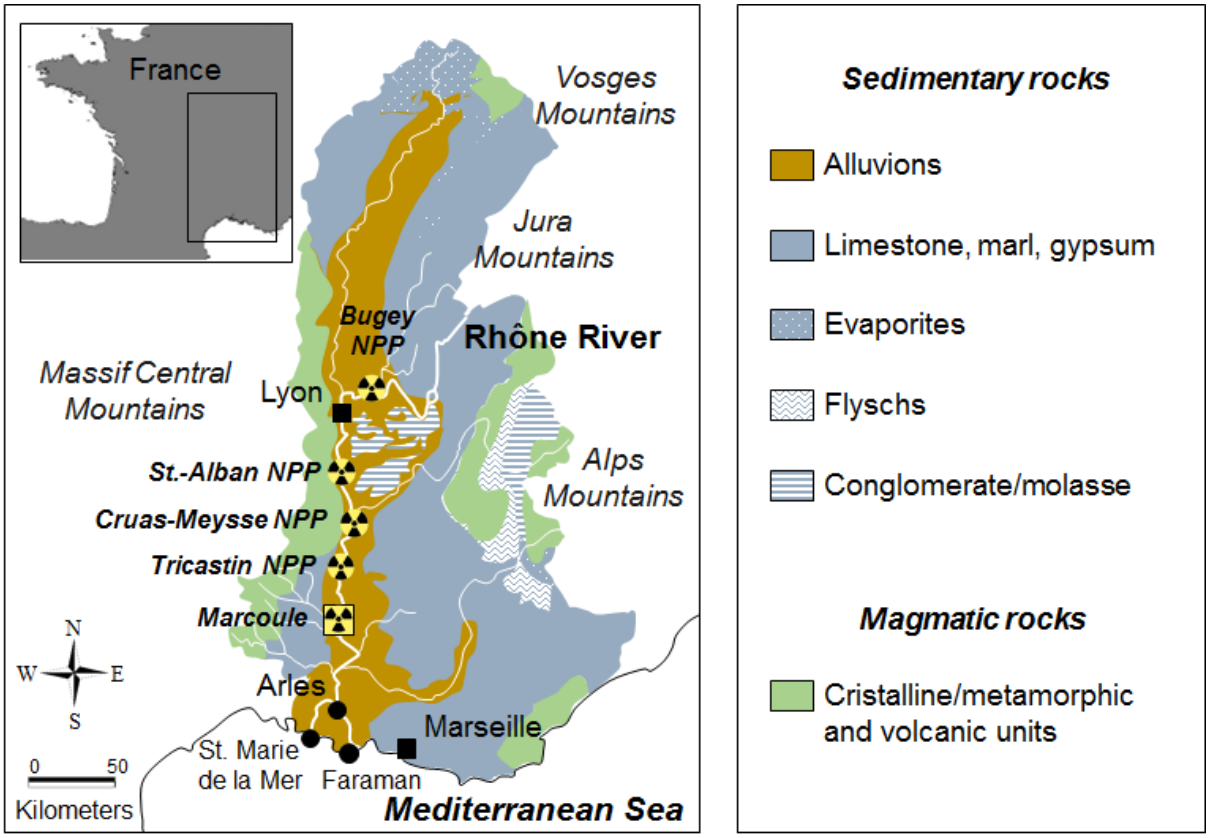


**Figure 35. The Rhône River system.** Major cities (black squares), monitoring sites (black circle) and nuclear facilities (power plants and fuel reprocessing plant) are shown. Rock composition along the watershed is denoted by the colour code legend (*Adapted from Ollivier et al. 2010*).

- *Sediment dynamics*

Once in the coast, a complex intrusion process takes place as the freshwater input flows into the marine waters in the absence of tidal influence. Flocculation and aggregation of particles forms a prodelta (i.e., fine-grained deposits and sand bars; Aloisi and Monaco 1975) with average sediment accumulation rates of 20-50 cm $y^{-1}$, subjected to physical resuspension events (i.e., mainly storms, waves and winds; Marion et al. 2010). The associated suspended plume (e.g., ~30 mg $L^{-1}$ SPM) shows a 1-2 m thickness and seasonal well-defined freshwater-seawater stratification of 10-20 units of difference with surrounding seawater, extending up to 20-30 km offshore (Broche et al. 1998). This plume is transported originally in a southeast direction but soon rotates westwards moving along the Mediterranean coast due to the Coriolis acceleration (Periáñez 2005).

### *1.2.1. Nuclear power plants*

The Rhône River watershed hosts 4 nuclear power plants (***Figure 36***) and one fuel reprocessing plant (***Figure 35***). The IRSN is in charge of the radionuclide monitoring of the Rhône River and, since the opening of the SORA station at Arles in 2002, several efforts have been performed to quantify radionuclide dissolved and particulate fluxes to the Mediterranean Sea. This monitoring includes $^{125}Sb$ measurements, e.g., showing a total activity (dissolved + particulate) ranging from 0.01 to 0.5 mBq $L^{-1}$ in 2008, contributing in 5.8 ± 1.4 GBq of dissolved flux and 0.28 ± 0.15 GBq of particulate flux exportation to the Mediterranean coast (DEI/SESURE 2010-04, IRSN).

**Figure 36. Current NPPs in the Rhône River watershed.**

Despite the triggered general review and reinforcing of protection structures in French NPPs after the flood event at Blayais NPP in 1999, the 2007 report from the IRSN concluded that complementary studies were still required for the Rhône valley NPPs given their complex situation. A flood event occurred in December 2003 causing the loss of cooling water at the Cruas-Meysse and the Tricastin NPPs.

Other phenomena, such as clogging of the steam generator tube support plates, have also been registered in the Rhône valley NPPs, particularly at the Cruas-Meysse NPP in February 2006. The steam generator is in charge of the heat exchange between the 325ºC water heated in the reactor core (primary system) and that in charge of transforming this energy into steam, which will further supply the turbine (***Figure 37***). Such phenomenon risks the rupture of the steam generator due to vibration fatigue cracks, caused by the clogging of water passage ways due to oxide deposits (mainly magnetite) from the corrosion condensers (IRSN View-point Report 2007). Thus, corrective actions (e.g., chemical cleaning) and accurate assessment of other NPPs followed this incident.

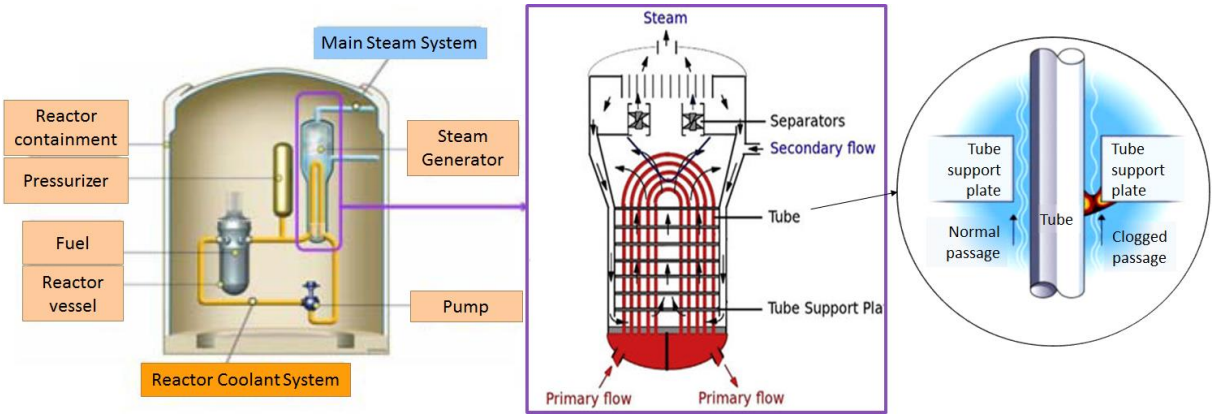


**Figure 37. Diagram of a steam generator of a PWR.** The effect of tube plate clogging is also represented. *(Adapted from IRSN View-point Report 2007 and Yang et al. 2017).*

## 2. Environmental monitoring: fluvial and estuarine sampling sites

- *Fluvial monitoring*

Several sampling sites along the Lot-Garonne-Gironde fluvial estuarine system constitute the setting of water, sediment and biological samples of this work. Upstream long-term monitoring, funded by the Adour-Garonne Water Agency (AEAG), has been performed at the EPOC 5805 (University of Bordeaux) since the early 2000's at five strategic sampling sites (white squares, ***Figure 38***), sampling surface water and sediments from sites located before the confluences of each Lot-Garonne River branches. Long-term records of sediment contamination are also available from core samples obtained

in 2001 (Audry et al. 2004b) due to temporal sediment accumulation at hydroelectric reservoir lakes in Marcenac (registering upstream background conditions) and Cajarc (registering the influence of the historical contamination and subsequent remediation works through time, ***Figure 38***).

- *Estuarine monitoring*

Sporadic oceanographic campaigns along the salinity and turbidity gradients of the Gironde Estuary, also funded by the AEAG, were performed in four hydrological conditions covering flood (3450 $m^3$ $s^{-1}$ in March 2014, MGTS II), intermediate (1203 $m^3$ $s^{-1}$ in March 2015, MGTS I) and drought (260 $m^3$ $s^{-1}$ in October 2015, MGTS III and 235 $m^3$ $s^{-1}$ in June 2017, MGTS IV) water discharges. Out of all experiences, the latter campaign collected samples from the outer most coastal endmember (white crosses, ***Figure 38***). In addition, a parallel sampling campaign in the frame of the European Project SCHeMA (EU FP7-OCEAN 2013.2-Grant Agreement 614002) was performed in the Arcachon Bay (April 2015, ***Figure 38***) and was used in this work as comparative site for trace element behaviour in transition waters from contrasting continent-ocean systems.

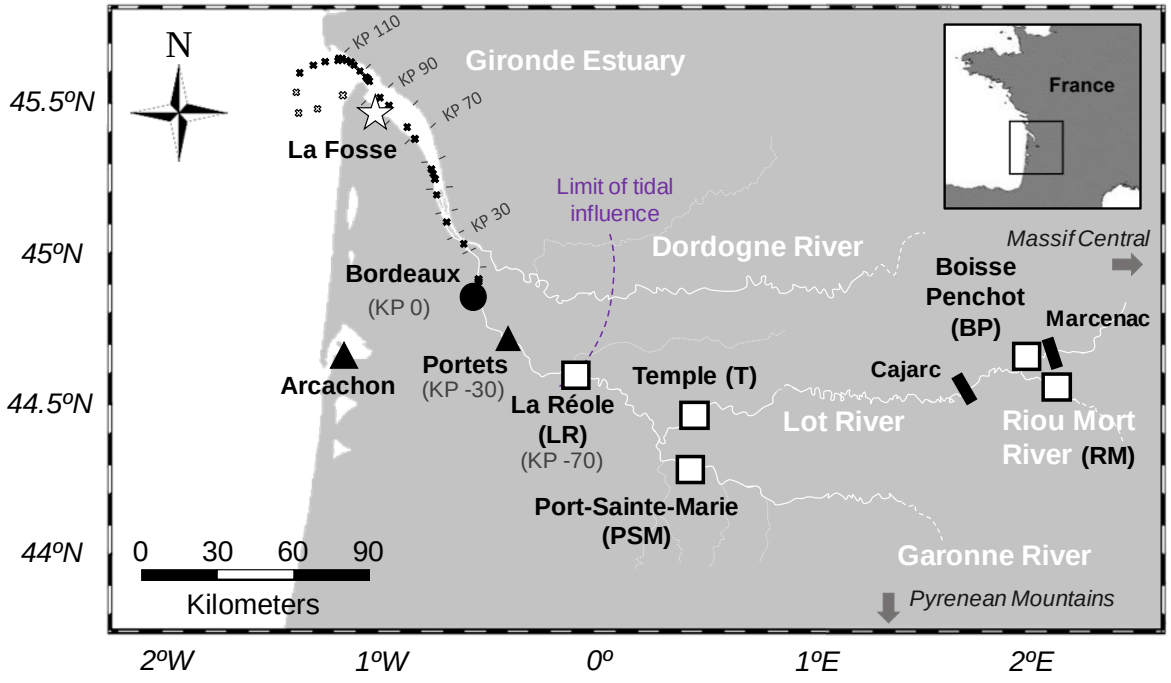


**Figure 38. Sampling sites in the Lot-Garonne-Gironde fluvial estuarine system.** Sampling sites are shown for the long-term monitoring programmes in the (i) upstream Lot-Garonne watershed (white squares), and (ii) estuary mouth (star), as well as for historical sediment records from hydroelectric reservoir lakes in Cajarc and Marcenac (black rectangles), sporadic samplings in Portets and Arcachon (black triangles) and from oceanographic campaigns (white and black crosses).

- *Biomonitoring programmes*

Biomonitoring programmes are generally used to monitor a large variety of chemicals (i.e., inorganic, organic contaminants and radionuclides) and are useful today to explore emerging contaminants like Ag (Lanceleur et al. 2011), Pt (Abdou et al. 2016) and Te (this work) in aquatic systems.

The Mussel Watch Programme RNO/ROCCH conducted by the French Research Institute for the Exploitation of the Sea (Ifremer) since 1979 annually collects samples and stores total soft tissues of wild-growing Japanese oysters (*Crassostrea gigas*, cf. *Magallana gigas*) and mussels (*Mytilus edulis* and *Mytilus galloprovincialis*) from several coastal areas in France (*http://www.ifremer.fr/deltn/pages/rno.htm*). In particular, they collect winter wild oysters from La Fosse site in the Gironde Estuary mouth (***Figure 38***), used in this work.

Another biomonitoring programme in the French Mediterranean coastline is the regional Mediterranean Mussel Watch programme (MMW; Thébault et al. 2008), including the Permanent Observatory of the Radioactivity in the Environment from the Institute of French Nuclear Protection and Safety (IRSN; Calmet et al. 1994). Specifically, biomonitoring of mussels (*Mytilus galloprovincialis*) is performed in order to understand bio-uptake of radionuclides in aquatic environments. In this work, sporadic samples from the monitoring sites at St. Maries de la Mer and Faraman (***Figure 35***) have been analysed as they represent coastal Mediterranean and Rhône influenced sites, respectively (Charmasson et al. 1999). In fact, St. Maries de la Mer is at the mouth of the "petit Rhône" and Faraman is directly located at the main Rhône River mouth ("Grand Rhône", ***Figure 35***).

## 3. Sporadic sampling: collection of specific environmental matrices

- *Lot-Garonne-Gironde fluvial estuarine-system*

Environmental conditions were simulated in the laboratory to study sorption kinetics, sorption isotherms and trace element solid fractionation (selective extractions) in isotopically-labelled experiments. To perform these experiments, sporadic sampling of watershed wet sediments and contrasting water matrices (i.e., freshwater and seawater) were collected in different points of the Garonne-Gironde fluvial estuarine system. Specifically, fresh sediments were collected manually from the river banks of the Garonne River at Portets (~30 km upstream the city of Bordeaux) whereas freshwater was recovered at La Réole and seawater (S = 32) from the Arcachon Bay (***Figure 38***).

- *The Rhône River*

Sporadic sampling of wet SPM from the Rhône River were collected at the SORA station in Arles (~40 km upstream from the mouth, ***Figure 35***). This study comprises several sporadic, mostly winter, sediment samples from 2012-2013 and 2016-2017, treated and analysed for Te and Sb concentrations in order to compare two major French watersheds: the Garonne-Gironde fluvial estuarine system and the Rhône River. In addition, wet SPM from the Rhône River (SORA) was provided in January 2018 for laboratory sorption kinetic experiments.

## III. SAMPLING STRATEGIES

### 1. Labware pre-conditioning, sampled phases and field work approach

- *Labware pre-conditioning*

The collection of environmental samples aiming at the quantification of trace element to ultra-trace element concentrations requires special attention of sample management in order to (i) warrant the sample preservation, and (ii) avoid sample contamination by labware. This is particularly relevant for trace elements already present in labware materials such as Sb in certain plastics. In fact, it has been demonstrated that polyethylene terephthalate (PET) containers used in laboratory procedures release Sb traces, biasing results obtained for analyses of environmental samples (Filella et al. 2009). Other labware like 0.02µm Nucleopore® polycarbonate filters also seem to release Sb traces (Masson et al. 2009, 2011a). This is probably due to the use of Sb as heat stabiliser in plastics like polyvinyl chloride (PVC) or polyvinylpirrolidone (PVP). Therefore, labware materials should be carefully chosen, specially for the collection of water samples, generally easily contaminated.

Despite the choice in the labware composition, all sampling bottles should be previously washed and conditioned before use for sample collection and sample storage to avoid further contamination and sample loss in bottle walls. In this work, all labware used was polypropylene (PP) based and acid-washed in a 10% $HNO_3$ (J.T. Baker). The washing procedure consists in an acid bath during 3 days, followed by rinsing of labware with deionised water and further rising with ultra-pure water (Milli-Q®, 18.2 MΩ Millipore) before leaving it to air-dry in a laminar flow hood. This procedure of acid-washing with $HNO_3$ is in accordance with posterior storage of water samples (acidified 1‰ with $HNO_3$ Ultrex II Ultrapure J.T. Baker) and analyses (diluted in 2% $HNO_3$ Ultrex II Ultrapure J.T. Baker).

- *Operationally defined dissolved and particulate phases*

An environmental sample from aquatic systems presents several compounds of different nature and particle size, ranging from ions and organic compounds to microorganisms and silts or sands. By convention, the “dissolved” and “particulate” phases are generally defined as the filter passing and filter retained materials, respectively, collected after physical separation through 0.45 µm filter mesh sizes (Buffle and Leppard 1995). Nevertheless, this convention does not take into account the fact that there is a natural continuum of multiple nanoparticles and macromolecules belonging to both domains rather than an actual physical boundary specifically defining each phase (***Figure 39***). This intermediate phase is generally referred as the colloidal fraction, composed of several organic (e.g., humic and fulvic acids) and inorganic compounds (Fe/Mn (oxy)hydroxides and silicate phases). The role of the colloidal phase is essential in trace element biogeochemical cycles, determining the transport and

bioavailability of trace elements in aquatic environments (Buffle and Leppard 1995). Therefore, environmental studies discussing about dissolved trace element behaviour and solid/liquid partitioning should address precisely the method used to define the dissolved phase.

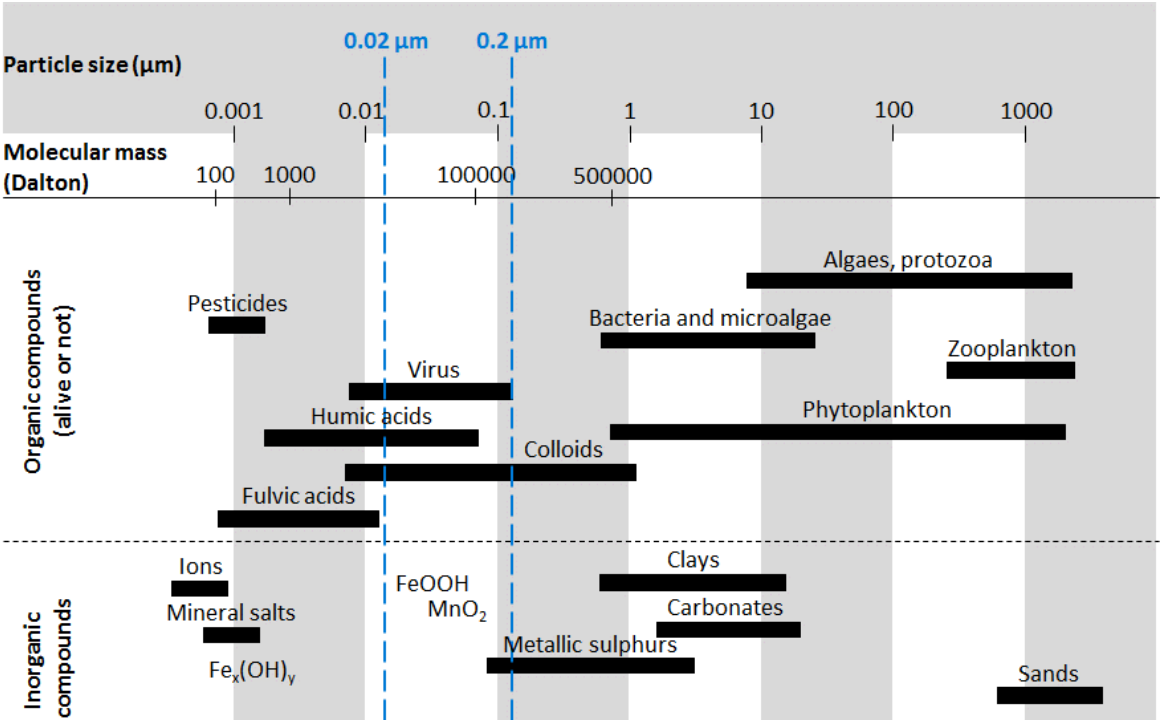


**Figure 39. Size distribution of particles and colloidal compounds in aquatic environmental samples.** *(Adapted from Buffle and Van Leeuwen 1992).*

Several separation techniques have been developed through time allowing to discriminate dissolved and particulate phases more precisely. Some of these techniques include dialyses, centrifugation and ultra-filtrations. In this work, solid/liquid characterisation of trace elements are generally performed with filtration at 0.2 µm and, sporadically, at 0.02 µm in order to discriminate the coarse colloidal phase. This proceeding allows to discriminate three main domains:

- The **"truly" dissolved phase**: <0.02 µm filter passing materials, mainly comprising free ions, Fe hydroxides, fulvic acids and small molecules (e.g., pesticides, etc.).
- The **colloidal phase**: comprised between 0.02 and 0.2 µm, including Fe and Mn (oxy)hydroxides, humic acids, nanoparticles and viruses.
- The **particulate phase**: >0.2 µm, regrouping several microorganisms and mineral phases such as silts or sands. Noteworthy, certain site-dependent sampling schemes require large volumes of water in order to recover enough particulate matter. In such cases, it is not possible to filter such large water quantities with standard 0.2 µm filters, thus, centrifugation techniques are applied.

- *Field work approach*

Environmental sampling in different aquatic systems requires adapted sample collection. In fact, the most obvious difference between freshwater sampling and estuarine sample collection relies on the transport means (***Figure 40***). Fluvial sites can be relatively easily monitored from the river banks. Thus, sampling materials can be set in a van and the five-site sampling campaign in the Lot-Garonne River system can be accomplished in one or two days. The main precautions to take into account are related to the correct sampling strategy in order to obtain representative environmental samples, e.g., avoid remobilisation of river bank deposited sediments or collect water against the river current.

However, estuarine campaigns require a more intense organisation of several months in advance including more human effort (a boat crew), bigger sampling devices and longer sampling campaigns. Oceanographic campaigns in the Gironde Estuary can last from one to two weeks, with sampling strategies organised in two cruises (different scientific groups in each one) and a day off in between. Safety equipment for the staff on-board is also compulsory, comprising safety boots, helmet and life-vest. All the scientific materials must be attached to the boat facilities to avoid accidents due to falling of equipment as a response to potential rough estuarine meteorological and hydrological conditions. Fast sampling is also required in these campaigns as the aim is generally to collect water and sediment samples representative of the salinity and turbidity gradients of the Gironde Estuary, with high salinity resolution. In addition, this sampling is performed in a dynamic system presenting continuous high/low tides, strong/weak tidal coefficients and other estuarine activities (navigation channel, dredging activities, etc.), which have to be taken into account for sample collection feasibility and interpretations of the obtained results.

In any case, sample preservation must be assured between the collection in the field and storage in the laboratory. To assure sample stability, water samples are acidified onsite according to trace element protocol collection and stored in a cooler (river sampling) or fridge (estuarine sampling) from the field to the laboratory.

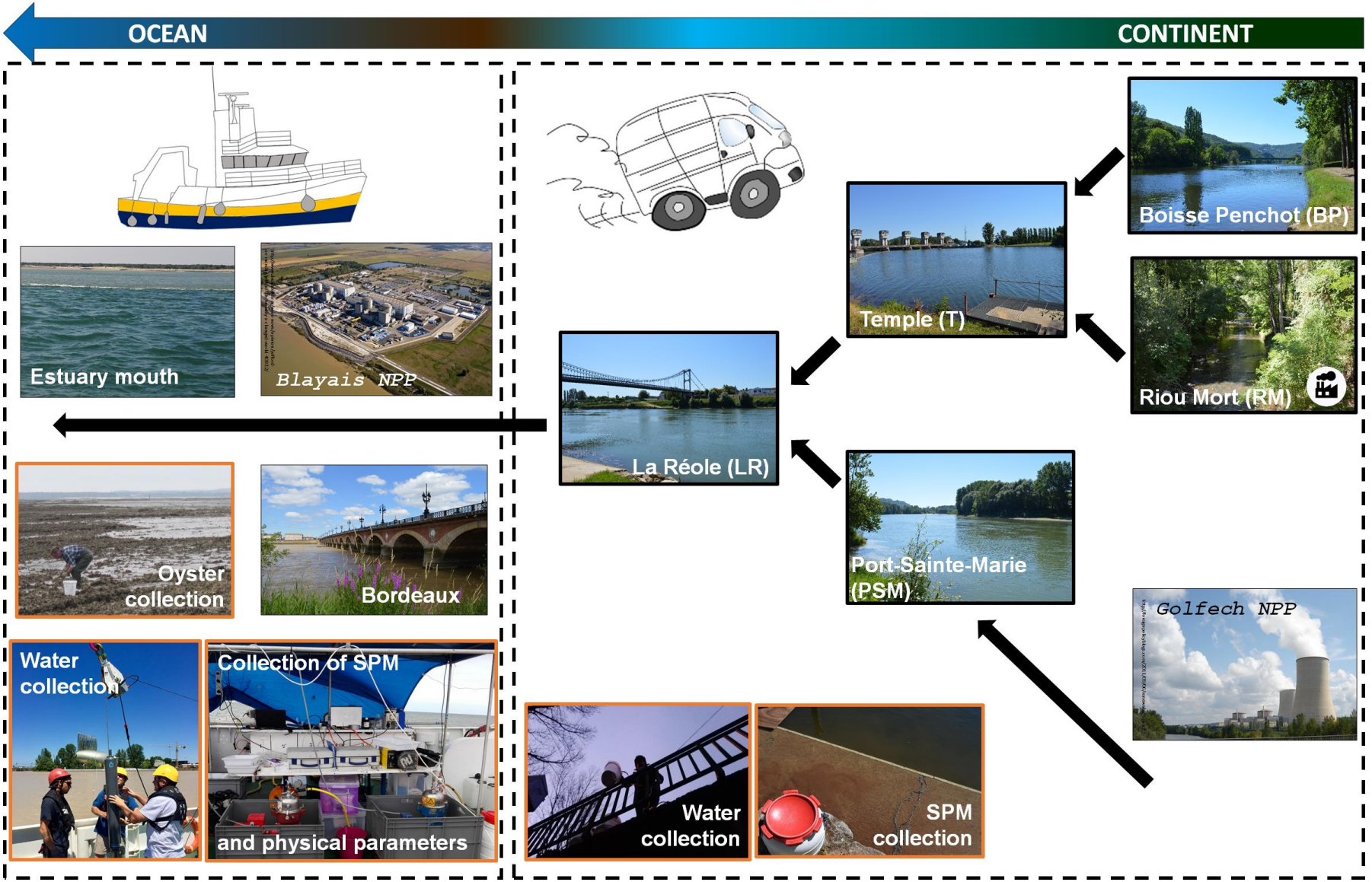


Figure 40. Diagram of sampling sites and sample collection in the Lot-Garonne-Gironde fluvial estuarine system.

## 2. River discharges, SPM concentrations and physical-chemical parameters

Historical records of daily river discharges were obtained from National Hydrographic Bank (DIREN, *http://www.hydro.eaufrance.fr/*), a hydrological online database coordinated by the Service Central d'Hydrométéorologie et d'Appui à la Prévision des Inondations in Toulouse. Quantification of SPM concentrations was performed by filtering precise volumes of water through dry pre-weighed filters (Xilab glass microfiber, 0.7 µm) with filtration units and vacuum pumps (***Figure 41a***). Filters were then dried to constant weight at 50ºC and re-weighed (***Figure 41b***). Physical parameters such as water temperature and conductivity were measured *in situ* (***Figure 41c***) with a TetraCon 96® probe (PROFILINE, WTW) and pH was determined with a Sentix® 41 probe (PROFILINE, WTW), previously calibrated using the manufacturer's specifications and supplied reagents (NIST pH standards).

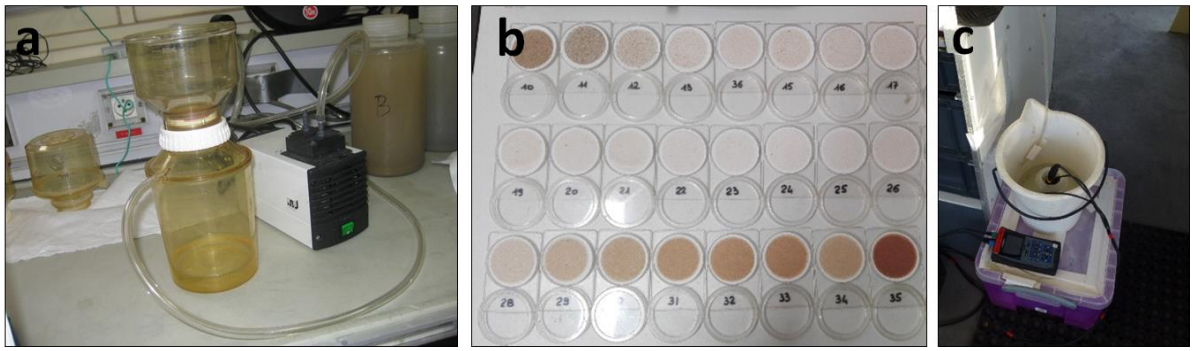


**Figure 41. Materials for measuring SPM concentrations and physical-chemical parameters.** (a) Filtration unit and pump, (b) dried filters showing contrasting SPM loads from different monitoring sites, and (c) *in situ* quantification of physical chemical parameters.

## 3. Collection of water and SPM samples

Sub-surface water was collected in all sampling campaigns with a telescopic arm (~0.3 m depth, 1 m from the river bank, ***Figure 42a***) or a Niskin bottle (on-board at 1 m depth, ***Figure 42b***), using acid-washed polypropylene (PP) bottles, previously rinsed with water from the site. The samples were immediately filtered on-site through 0.2 µm Minisart® cellulose acetate filters into acid-washed polypropylene (PP) bottles (***Figure 42c***), acidified with $HNO_3$ (1/1000 v/v; J.T. Baker ultrapure, 14 M) and stored at 4ºC in the dark pending analysis.

At the same time, SPM samples were collected into 40 L acid-washed polyethylene (PE) drums (***Figure 42a***), previously rinsed with water from the site. Particles were retrieved by centrifugation (Westfalia, 12 000 g; Lapaquellerie et al. 1996), oven-dried (50ºC), ground and homogenised (agate mortar), then stored at room temperature in the dark until analysis.

**Figure 42. Example of (a) fluvial water and SPM collection, (b) water collection in the Gironde Estuary and (c) on board water sampling and storage.**

Sporadic samples for laboratory experiments mainly consisted in wet SPM from the Garonne River and the Rhône River. The former consisted of deposited oxic SPM collected on the river bank with a plastic spatula and stored in plastic bags. All sediment samples from the Rhône River were collected at the SORA station as part of the IRSN systematic sampling of SPM. This SPM collection was performed with a floating telescopic arm at ~50 cm from the water surface and by active, continuous pumping. This means that wet sediment samples were sent to EPOC 5805 (University of Bordeaux), where they were further stored for experimental purposes or pre-treated for analyses.

## 4. Collection of biological samples

The RNO/ROOCH programme (Ifremer) collects on a regular basis two-year old (~8 cm long) wild oysters *Crassostrea gigas* (cf. *Magallana gigas*) during winter (February-March) at La Fosse according to the guidelines for monitoring contaminants in biota (OSPAR commission; *http://www.ospar.org*).

The Mediterranean Mussel Watch programme (IRSN) collects wild mussels (*Mytilus galloprovincialis*) at several Mediterranean coastal sites including St. Maries de la Mer and Faraman. Mussels are selected through a standard grid (for homogeneous size collection purposes) until wet weights of 3–5 kg (corresponding to N > 80 individuals). They are then cleaned from external materials and byssus and pre-treated before analyses.

# IV. EXPERIMENT DESIGNS

## 1. Isotopically-labelled kinetic experiments

### 1.1. Adsorption kinetics and isotherms of stable $^{125}$Te and $^{77}$Se

- *Experimental design*

Isotopically-labelled Te and Se sorption kinetic and isotherm experiments were performed at the EPOC 5805 (University of Bordeaux) within a collaboration with the Institute of Applied Water (AGW) of the Karlsruhe Institute of Technology (KIT, Germany). The aim of this approach was to understand Te and Se geochemical reactivity in simulated estuarine conditions representing the contrasting salinity and turbidity gradients of the Gironde Estuary. This approach was performed with Te and Se spikes given that (i) Se is the assumed geochemical homologue of Te, and (ii) the potential complementary information for understanding Te geochemistry (analytically challenging in complex matrices) compared to the more documented geochemistry of Se.

- *Preparation of mono-isotopic solutions, SPM slurries and water mixtures*

Spike solutions were prepared by dissolution of $^{125}$Te (99.89% purity; Cortecnet, France) and $^{77}$Se (99.20% purity; Cortecnet, France) in HCl (2% Suprapur®, Merck) and $HNO_3$ (2% Suprapur®, Merck), respectively, heated at 70ºC until dissolution on a hotplate.

The conducted sorption experiments simulated four experimental conditions representative of the Gironde Estuary salinity and turbidity gradients: two contrasting water matrices (salinities 0 and 32) and two solid/liquid ratios (100 mg $L^{-1}$ and 1000 mg $L^{-1}$ DW). Freshwater from the Garonne River and seawater from the Arcachon Bay (***Figure 43a***), were filtered with 0.45 µm Teflon filters (FHLC, Merck Millipore Ltd.). Water content in wet sediments from Portets (~30 km upstream from Bordeaux) was evaluated by comparing the masses of precise volumes of wet and dry sediment aliquots (***Figure 43b***).

Isotopically-labelled Te and Se solutions were oxidised with $H_2O_2$ (30 µL 30% J.T. Baker ultrapure) in the different water matrices to favour the oxidation state of $^{125}$Te(VI) and $^{77}$Se(VI), followed by an equilibration period of 24h. Slurries were prepared from the wet sediments and unspiked water matrices and equilibrated during 24h, in order to avoid potential effects of sediment-water interactions during the sorption experiment (***Figure 43c***). Sorption kinetics and isotherms were started when both solutions were mixed in appropriate proportions (***Figure 43d***).

In both kinetics and isotherm experiments, dissolved Te ($Te_d$) and dissolved Se ($Se_d$) were monitored. Particulate concentrations were only determined for isotherm experiments using freshwater slurries with 1000 mg $L^{-1}$ SPM for mass balance calculations. In all cases, the dissolved phase

was separated from the particulate phase by centrifugation (10 min at 4000 rpm; Hettich Rotofix 32A centrifuge) and filtered (0.2 µm Minisart® cellulose acetate) into acid-washed PP 15 mL tubes (***Figure 43e***). These were then acidified with $HNO_3$ (1/1000 v/v, J.T. Baker ultrapure, 14 M) and stored at 4ºC in the dark until analysis.

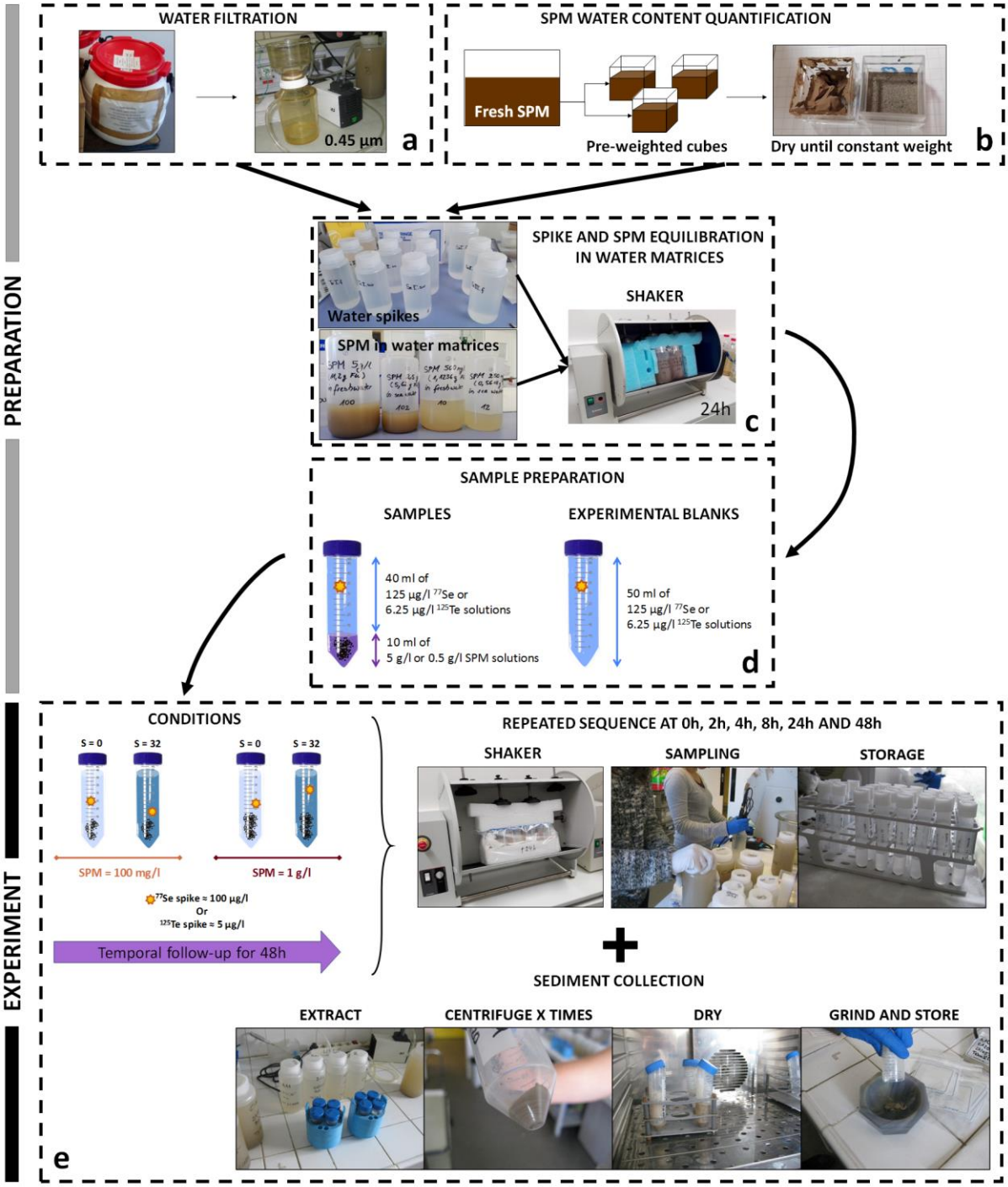


**Figure 43. Summary of preparation steps for Te and Se isotopically-labelled adsorption kinetic and isotherm experiments**. (a-b) Matrix preconditioning, (c) spike equilibration, (d) experimental mixtures, (e) temporal sampling.

- *Adsorption kinetics*

Adsorption kinetics with nominal concentrations of 5 µg $L^{-1}$ of $^{125}$Te(VI) and 100 µg $L^{-1}$ of $^{77}$Se(VI) were performed in acid-washed 50 mL centrifuging polypropylene (PP) tubes with 3 replicates per experimental condition using an automatic overhead shaker (REAX 20 Heidolph Instruments) and sampled at t = 0, 2, 4, 8, 24 and 48h (N=3). Temperature (21.1 ± 0.4 ºC), pH (7.50 ± 0.45) and oxic (104 ± 0.5% saturation) conditions, were kept stable throughout the experiment. In parallel, blank tubes containing only spiked water solutions were used to control $^{125}$Te and $^{77}$Se potential losses onto PP walls over time.

- *Adsorption isotherms*

Adsorption isotherms were performed for two SPM concentrations (100 mg $L^{-1}$ and 1000 mg $L^{-1}$) with initial concentrations of dissolved $^{125}$Te of 0.1, 0.25, 0.5, 1, 2.5, 5 µg $L^{-1}$ and initial concentrations of dissolved $^{77}$Se of 0.5, 5, 10, 25, 50, 75, 100 µg $L^{-1}$ (N=2) and sampled after 48h. Due to analytical constraints, especially at the low concentration ranges, these experiments were only performed in freshwater conditions.

### 1.2. Adsorption/desorption kinetics of $^{75}$Se and $^{113}$Sn radiotracers

- *Experimental design*

Radiotracer sorption and desorption kinetic experiments were performed at the Institute for Nuclear Waste Disposal (INE) of the Karlsruhe Institute of Technology (KIT, Germany). In this case, the aim was to perform adsorption and desorption kinetics of known soluble (e.g., Se) and more strongly particulate (e.g., Sn) trace elements in environmentally representative concentrations (trace) and estuarine-simulated conditions. The choice of these element spikes was a compromise between (i) market availability compared to Te and Sb radionuclides, (ii) geochemical behaviour of Sn and Se potentially representing those of Te and Sb, respectively, and (iii) the application of Sn results in radionuclide dispersion scenarios comprising certain Sn radionuclides as parent of Sb radionuclides. Such experience (***Figure 44***) was conducted with wet SPM from the Garonne and Rhône Rivers in order to compare the results of both continent-ocean transition systems. Opposite to aforementioned kinetic experiments, these radiotracer experiments were performed with Se and Sn radionuclides in the same batch solutions and no automatic shaker was used for safety reasons concerning potential radioactive tube leakage, thus, consequent laboratory contamination.

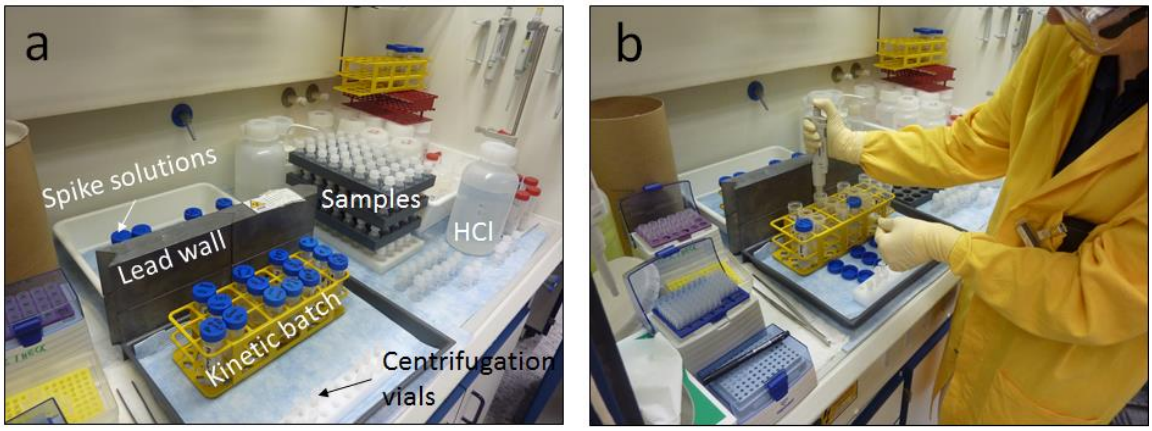


**Figure 44. Fume hood radiotracer experimental conditions.** (a) experimental disposition and (b) sample collection.

- *Preparation of mono-isotopic solutions, SPM slurries and water mixtures*

Radioactive solutions of $^{113}Sn$ (half-life of 115 days, $SnCl_4$ in 6M HCl, >99% purity, Eckert & Ziegler) and $^{75}Se$ (half-life of 120 days, $H_2SeO_3$ in 0.1M HCl, >99% purity, Eckert & Ziegler) were diluted and equilibrated in independent freshwater and seawater matrices for several weeks in order to homogenise/stabilise the radionuclides in each water matrix. The high acidity from $^{113}Sn$ was corrected with NaOH solution (1M, Merck®) and $^{75}Se$ was oxidised to Se(VI) with $H_2O_2$ (30% Merck®). Different experimental slurries (10 mg $L^{-1}$, 100 mg $L^{-1}$ and 1000 mg $L^{-1}$) were prepared in advance in freshwater and seawater matrices for each Garonne and Rhône River SPM (***Figure 45***).

- *Sorption and desorption kinetics*

Joint $^{113}Sn$ (nominal 1000 Bq $mL^{-1}$) and $^{75}Se$ (nominal 100 Bq $mL^{-1}$) sorption kinetics was performed with sample replicates (10 mg $L^{-1}$ N=5, 100 mg $L^{-1}$ N=6 and 1000 mg $L^{-1}$ N=3) and a blank (spiked freshwater and seawater with no SPM) during 48h (i.e., sampling at 0h, 2h, 4h, 6h, 24h and 48h). At the end of the experience, only samples from 100 mg $L^{-1}$ SPM were then desorbed in freshwater (N=3) and seawater (N=3) for 48h (i.e., sampling at 0h, 2h, 4h, 24h and 48h, ***Figure 45***). All batch experiments were performed in acid-washed 50 mL polypropylene (PP) tubes with sporadic manual shaking at room temperature (~28ºC) and neutral pH (7.0-7.2). Initial sample radioactive background levels and potential wall-contribution during desorption experiments was also checked.

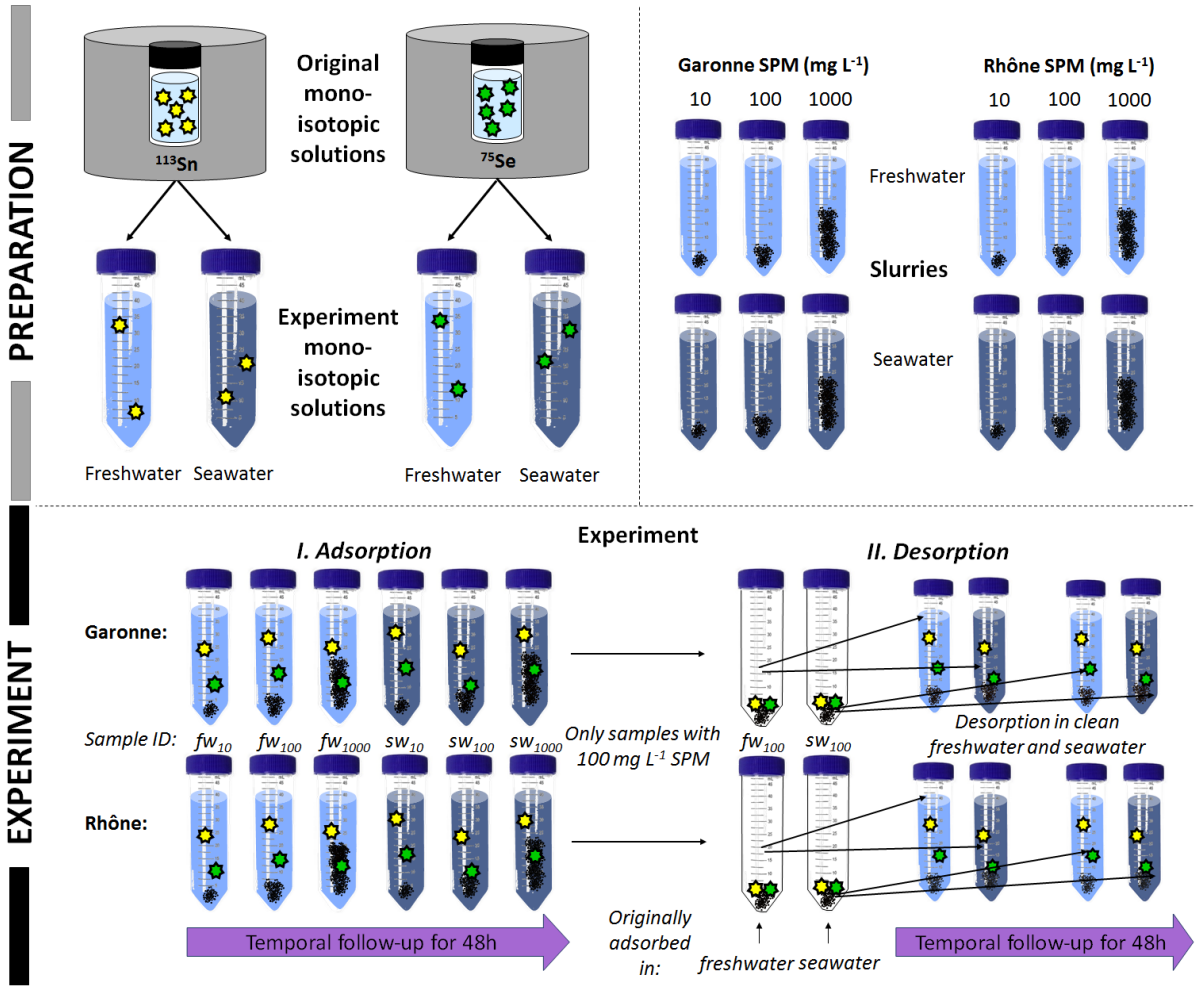


**Figure 45. Experimental design for Se and Sn adsorption kinetics in contrasting estuarine conditions representing the Gironde Estuary and the Rhône River systems.**

- *Solid/liquid separation and sample collection*

Water and SPM matrices during radiotracer experiments could not be physically separated and stored independently due to radioactivity safety measures concerning potential risk of atmospheric contamination and inhalation of radioactive SPM during the drying processes. Therefore, each sampling time consisted in collecting 1.5 mL of homogeneous solution from the PP tubes and centrifuging at 4000-6000 rpm during 20 min for SPM-liquid separation. The dissolved phase was collected by pipetting 1 mL from the supernatant, thus, the rest of the aliquot was disposed away in a unique waste bin. The 1 mL sample was stored in 10 mL light-density polyethylene (LDPE) Kautex™ gamma vials with 9 mL HCl 2% (Merck®, to avoid Sn precipitation in $HNO_3$; Weber 1985) for analysis.

## 2. Adsorption of isotopically-labelled spikes for parallel selective extractions

- *Antimony*

Wet SPM from KP52 was used for isotopically labelled Sb sorption (i.e., $^{123}Sb$) in natural freshwater and seawater matrices from La Réole (at KP-60, tidal influence limit) and from the Gironde Estuary (at S = 22), respectively. Sorption consisted in independent spikes (~2 µg $L^{-1}$) of high purity monoisotopic solution of $^{123}Sb$ (99.43% Oakridge, USA) in freshwater (S = 0), intermediate (S = 11, 50/50 mixture) and estuarine (S = 22) matrices. These spiked matrices were left to equilibrate one night before being exposed during five days to high concentrations of SPM (nominal > 1000 mg $L^{-1}$ DW). All sediment was then recovered by centrifugation (10 min at 4000 rpm; Hettich Rotofix 32A centrifuge), oven-dried (50ºC stove), grinded (in agate mortars) and aliquots (two to three replicates) were used for parallel selective extractions.

- *Tellurium and selenium*

Sorption of monoisotopic spikes of Se and Te were performed in high SPM concentrations (2 - 4 g $L^{-1}$ DW) in freshwater (S = 0) and seawater (S = 32). Spiked slurries were left to equilibrate for 48h (***Figure 46***) with not pre-oxidised solutions of nominal 10 µg $L^{-1}$ of $^{125}Te$ and 100 µg $L^{-1}$ of $^{77}Se$. All sediments were recovered by centrifugation (Hettich Rotofix 32A centrifuge), dried (70ºC stove) and grinded in agate mortars, then aliquoted and extracted with parallel selective extraction protocols.

**Figure 46. Preparation of wet SPM isotopically-labelled spikes for parallel selective extractions.**

# V. SAMPLE PRE-TREATMENT

## 1. Sample drying

### 1.1. Sediments

- *Bulk sediment mineralogy and trace element total digestions*

There are several ways of drying sediment samples. The most commonly applied are air drying, freeze-drying and oven drying, potentially using different temperatures in the latter. Either technique is applicable when drying sediments for analyses of bulk sediment mineralogy, as major sediment minerals (>5% content) do not change their structure during the drying process. Total trace element quantification, however, require precautionary measures in oven-drying techniques as appropriate temperatures should be applied to avoid losing volatile trace elements (e.g., Se volatilises at >70ºC). In this work, most of the sediment samples have been oven-dried at 50ºC for mineralogical analyses and total trace element digestions.

- *Selective extractions*

Sample pre-treatment (freeze-drying vs oven-drying) can affect Fe/Mn oxide mineral crystallisation degree and, thus, apparent major and trace element solid fractionation. In fact, the reducible fraction ("bound to Fe/Mn oxides") can be modified as both freeze-drying and oven-drying (especially the latter at high temperatures, e.g., >100ºC; Gleyzes et al. 2002) can accelerate Fe/Mn oxide crystallisation and promote oxidation of Fe, Mn and S, causing a transfer of certain target element-response from the "bound to Fe and Mn oxide fraction" to the residual fraction (Bordas and Bourg 1998).

In this work, most sediment samples were generally oven-dried at 50ºC and sporadically at <70ºC for parallel selective extractions unless specified differently in specific cases. Such cases require adapted considerations that have been taken into account in the interpretation of results.

### 1.2. Biological materials

Wild oysters collected by the RNO/ROCCH programme are depurated with clean water from the site and dissected for whole soft bodies. Individuals are then pooled (20-60 individuals, depending on size), grinded, freeze-dried and homogenised before storage. This work has benefited from a pool of already, freeze-dried oyster samples from the national bank RNO/ROCCH since 1984 to 2017, in a 2-year interval basis.

Wild mussels from the Mediterranean Mussel Watch programme are opened with a steam oven at 80ºC before freeze-drying and being homogenised as a pool (Thébault et al. 2008). Nevertheless, a further step is applied compared to the standard RNO/ROCCH procedure. In fact, freeze-dried pools are ashed for radionuclide analyses and storage. This work has benefited from direct freeze-dried mussel samples, as well as from ashed samples from the long-term monitoring sample bank.

## 2. Bulk sediment mineralogy preparations

- *Major mineral composition*

Bulk sediment mineralogy preparations and analyses were performed at the Institute of Applied Geosciences (AGW) of the Karlsruhe Institute of Technology (KIT, Germany). Such preparations consisted in introducing and manually pressing the dried sediment samples into appropriate mountings (***Figure 47***).

**Figure 47. Preparations for mineralogical analysis.** Suspended particulate matter from the Garonne-Gironde fluvial estuarine system (light brown) and the Rhône River (dark brown).

- *Clay minerals*

Parallel pre-treatment of dried sediment samples allows to identify clay minerals. This identification of clay minerals was performed with SPM aliquots following a texture identification protocol. Briefly, “unconditioned” SPM samples are put in slurry with an ammonia solution, dispersed in an ultrasound bath for 15 min, gravimetrically separated (1h) and left to dry onto glass platelets for analyses. In parallel, aliquot samples were swollen at 60ºC for 24h in ethylene glycol vapour

atmosphere. In addition, aliquots from the latter pre-treatment were further burned at 550ºC for 3h (muffle oven).

This approach provides information on the weathering degree of sediments in the studied system as specific residual minerals result from the weathering of primary minerals. In fact, such identification is obtained by comparing the diffractograms of all aforementioned pre-treatments according to specific criteria representing the clay mineral properties (***Table 14***).

**Table 14. Criteria for distinguishing clay minerals.** *(Nelson 2014).*

| Primary mineral | Clay mineral | Properties | Texture pre-treatment (spacing on {001} for clay type minerals (Å) | | |
|---|---|---|---|---|---|
| | | | ***Untreated*** | ***Ethylene glycol*** | ***Heated to 550ºC*** |
| Feldspars | Kaolinite | Non-expanding | 7.1 | No change | Destroyed |
| Muscovite and feldspars | Illite | Non-expanding | 10 | No change | Little change |
| Pyroxene, amphibole, and biotite | Chlorite | Non-expanding | 7 | No change | 13.2 |
| Feldspars | Montmorillonite | Expanding clays | 14-15 | 17 | 9.5 |

## 3. Digestions and selective extractions of sediments

- *Total digestions of sediments*

Total trace element concentrations in sediments were determined similarly for particulate Te ($Te_p$) and particulate Sb ($Sb_p$) but differently to that of particulate Se ($Se_p$). Mineralisation of sediment for Te and Sb analysis was achieved using a tri-acid digestion with $HNO_3$ + HCl + HF as described elsewhere (e.g., Schäfer et al. 2002; ***Figure 48***). Briefly, samples of 30 mg were digested in closed PP tubes (DigiTUBEs®, SCP SCIENCE) on a heating block (2h at 110ºC) using 750 µL $HNO_3$ (14 M Suprapur®, Merck), 1.5 mL HCl (10 M Suprapur®, Merck) and 2.5 mL HF (29 M Suprapur®, Fisher). After an evaporation step at 120ºC, re-dissolution of the samples was performed with 250 µL $HNO_3$ (14 M) and heating. After cooling, the samples were brought to 10 mL using Milli-Q water.

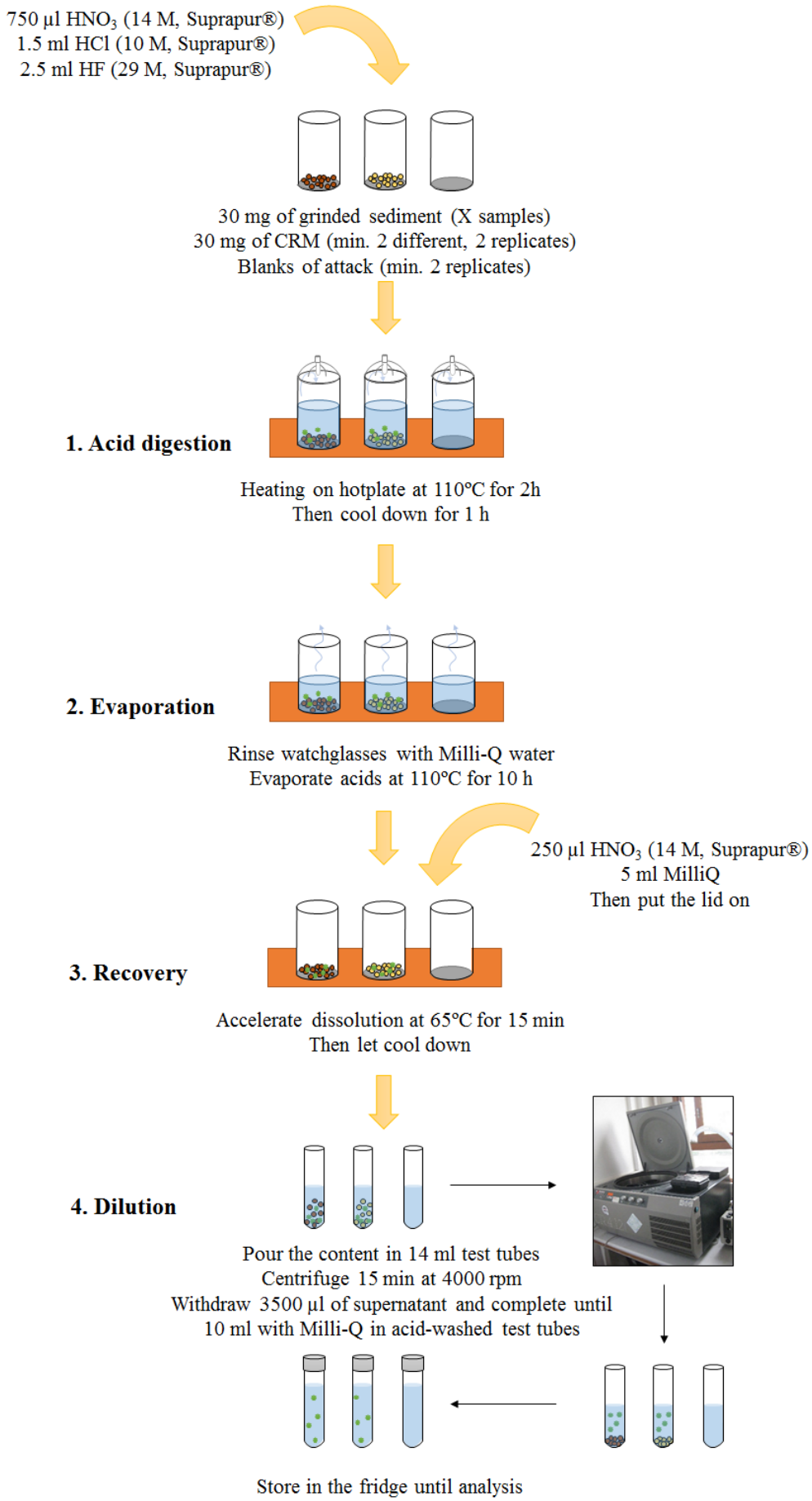


**Figure 48. Hotplate total extraction protocol for sediment digestions**. Described and validated for fluvial sediments and SPM in Schäfer et al. (2002).

For the analysis of $Se_p$ (volatile at > 70ºC, not compatible with the above-described tri-acid digestion) total microwave-assisted sediment digestions (START 1500, MLS GmbH, ***Figure 49***) were performed at the Institute of Applied Geosciences (AGW) of the Karlsruhe Institute of Technology (KIT, Germany). These consisted in the mineralisation of aliquots of 40 - 50 mg of dried and homogenised (agate mortar) sediment (Eiche et al. unpublished). Briefly, 3 mL $HNO_3$ (sub-boiled acid-distilled 65%, p.a. grade, VWR Chemicals), 0.5 mL $H_2O_2$ (30% Rotipuran®, Carl Roth), 0.25 mL HF (40% Suprapur®, Merck KGAA Darmstadt) and 0.5 mL ultrapure Milli-Q water were added. The microwave temperature program was: 18ºC $min^{-1}$ to 75ºC, followed by 7ºC $min^{-1}$ to 110ºC, then 8ºC $min^{-1}$ to 150ºC and 6ºC $min^{-1}$ to 210ºC, with a constant temperature of 210ºC during 10 min before completely cooling down over night. After digestion, samples were transferred into PTFE vessels and evaporated on a hotplate to dryness at 70ºC (no Se evaporation at this temperature), recovered with 270 µl of $HNO_3$ (65% Suprapur), heated at 70ºC for 1h and completed with ultrapure Milli-Q water to a final volume of 6 mL.

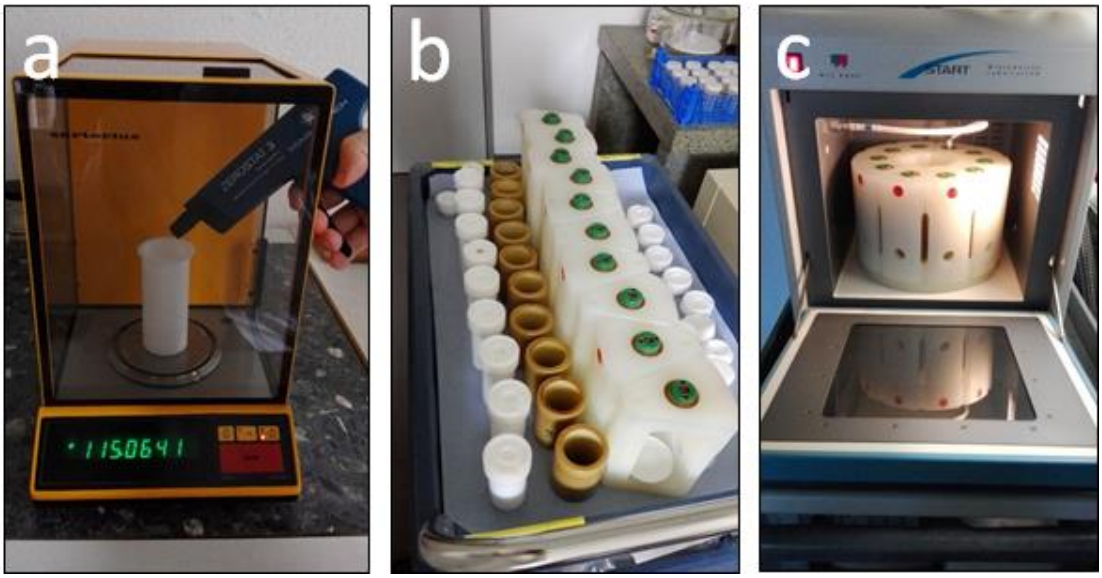


**Figure 49. Required materials for microwave-assisted digestions.** (a) direct sample weighing, (b) teflon vessels and (c) microwave START 1500 (MLS GmbH).

- *Parallel selective extractions*

The targeted operationally defined solid fractions were: F1 – easily exchangeable and/or carbonate fraction (acetate solution extracting carbonates, Mn oxyhydroxides, sulphates and organic matter phases; Bordas and Bourg 1998; Kersten and Förstner 1987), F2 – reducible Fe/Mn oxides (ascorbate solution extracting Mn oxide and amorphous Fe oxide phases; Kostka and Luther 1994), F3 – oxidisable fraction ($H_2O_2$ extraction of organic matter and labile/amorphous sulphide phases; Tessier et al. 1979; Ma et Uren 1995) and F4 – reactive and potentially bioaccessible fraction (HCl 1M acid extraction of amorphous and crystalline Fe and Mn oxides, carbonates, amorphous monosulphurs and phyllosilicate

phases; Huerta-Díaz and Morse 1990; Gasparon and Matschullat 2006). In addition to the latter, acid extraction with $HNO_3$ 1 M was performed on a separate aliquot to discard the $Cl^-$ effect or specific acid effect on F4 obtained from HCl 1 M leaching. The specific extraction protocol is described below (***Figure 50***). All reagents used were of high purity grade unless specified otherwise.

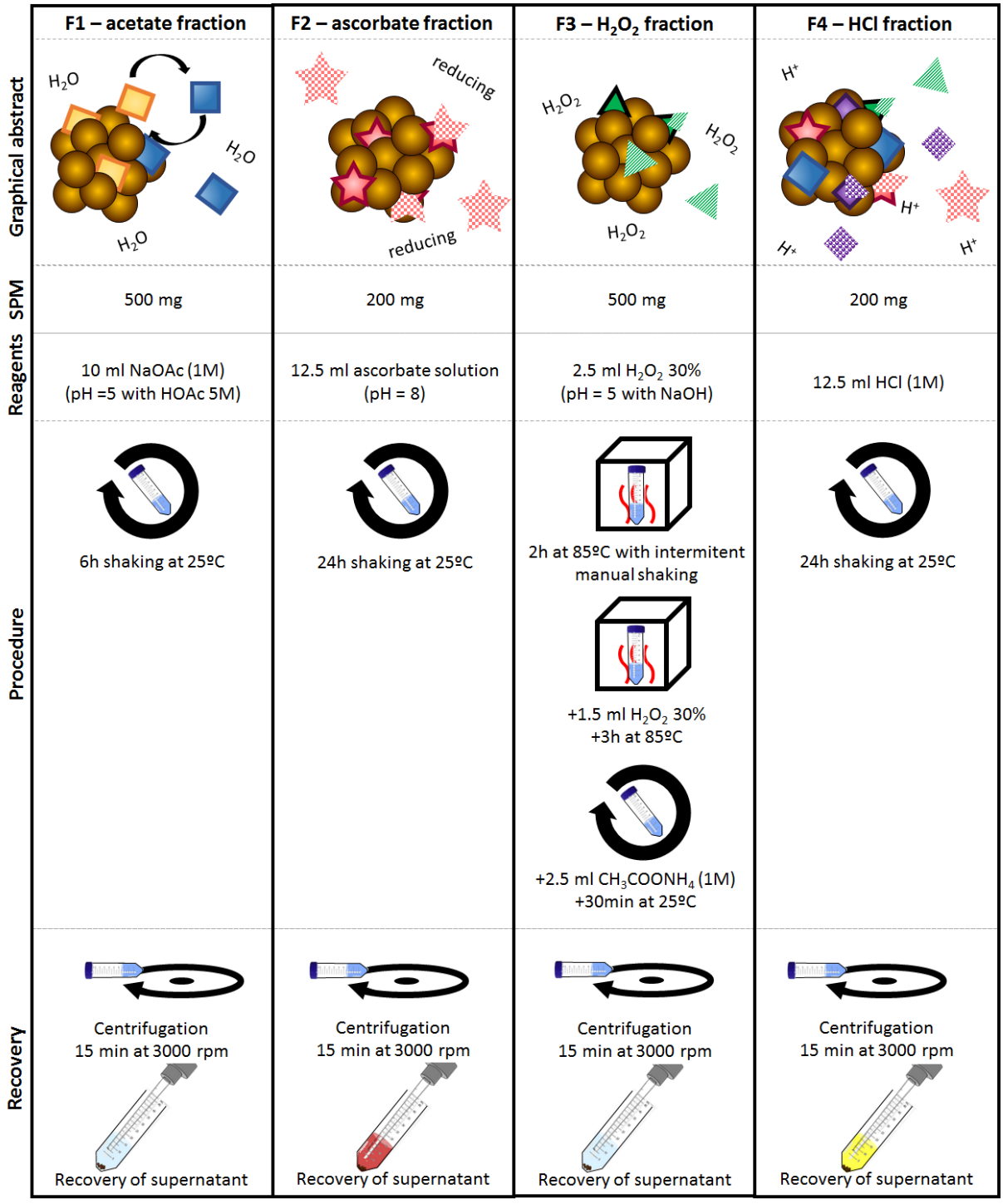


**Figure 50. Protocols of applied parallel selective extractions** *(described in Audry et al. 2006).*

All extractions were performed in acid-washed ($HNO_3$ 10%) PP Falcon 50 mL conical centrifuge tubes (FISHER SCIENTIFIC). Three blanks of each extraction were performed. Currently, no CRM are available for Sb, Te and Se selective fractions. Residual fractions are calculated as the difference between the acid-soluble fraction (F4 or F4N) and the total adsorbed particulate concentration.

Out of all extraction supernatants, only the ascorbate extractions produce a characteristic brown colour (***Figure 51a***) in both Garonne and Rhône River SPM extractions compared to the blanks and the rest of the extractions, giving transparent (acetate and $H_2O_2$ extractions) or yellow (acid extractions, ***Figure 51b***) solutions.

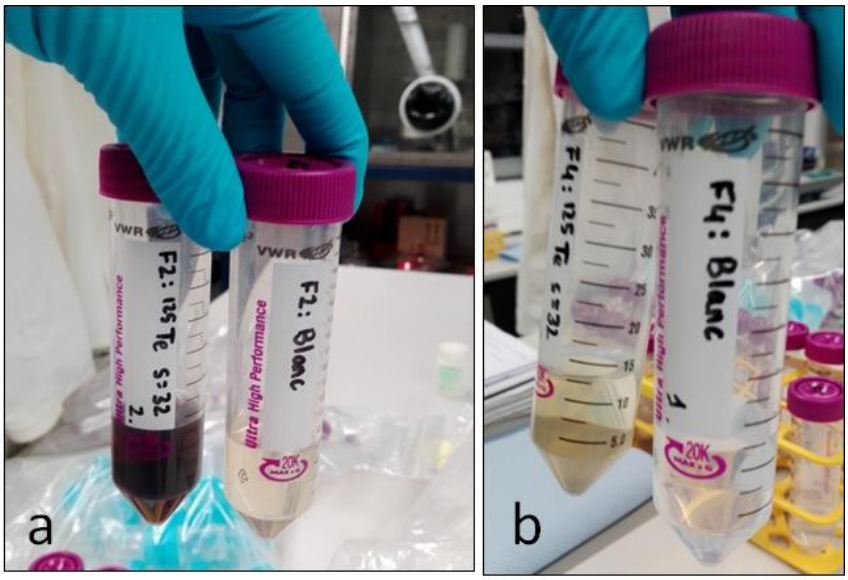


**Figure 51. Example of selective extraction slurries and blanks after (a) ascorbate and (b) HCl extractions.**

## 4. Digestions of biological matrices

Digestions of RNO/ROCCH oyster tissues were performed at the Centre Atlantique (Ifremer, Nantes). Aliquots of ~200 mg of freeze-dried oyster tissues from the RNO/ROCCH sample bank were digested with 4 mL HCl (34-37% Suprapur®, SCP Science) and 2.8 mL $HNO_3$ (67-69% Suprapur®, SCP Science) in a microwave-assisted oven (ETHOS UP, Milestone Srl). The temperature program was set at 9ºC $min^{-1}$ to 180ºC, followed by 30 min at 180ºC before cooling down. These acid digestions were brought to a final 25 mL volume with Milli-Q water (Daskalakis et al. 1997; USEPA 2007). However, due to important interferences on $^{125}Te$, sample aliquots were evaporated at 50-60ºC and recovered in a $HNO_3$ matrix. Therefore, future protocols applied for Te quantification in biological materials should avoid HCl-based methods.

- *Freeze-dried vs ashed mussel samples for trace element quantification*

Mussel individuals (N = 20) from Arriluze (Bilbao coastline, Spain) were collected in February 2016 by collaborators from the University of the Basque Country (UPV/EHU, Spain). Bivalves were opened in the stove (50ºC, 15 - 30 min), dissected and analysed at EPOC 5805 (University of Bordeaux). Samples were freeze-dried (Heto PowerDry LL 3000 at -60ºC) and homogenised (i.e., 10 min at 980 rpm with the Pulverisette Fritsch). Individual samples were pooled afterwards and an aliquot (N = 3) was spared for acid digestions. Other aliquots were subjected to different ashing temperatures (450ºC and 800ºC, N=3) in order to test the validity of biological Se and Te analyses in ashed samples (***Figure 52***), a common proceeding applied for the radionuclide monitoring in biological materials from the Mediterranean Mussel Watch programme, as well as in protocols of other TCE elements such as platinum (Abdou et al. 2019).

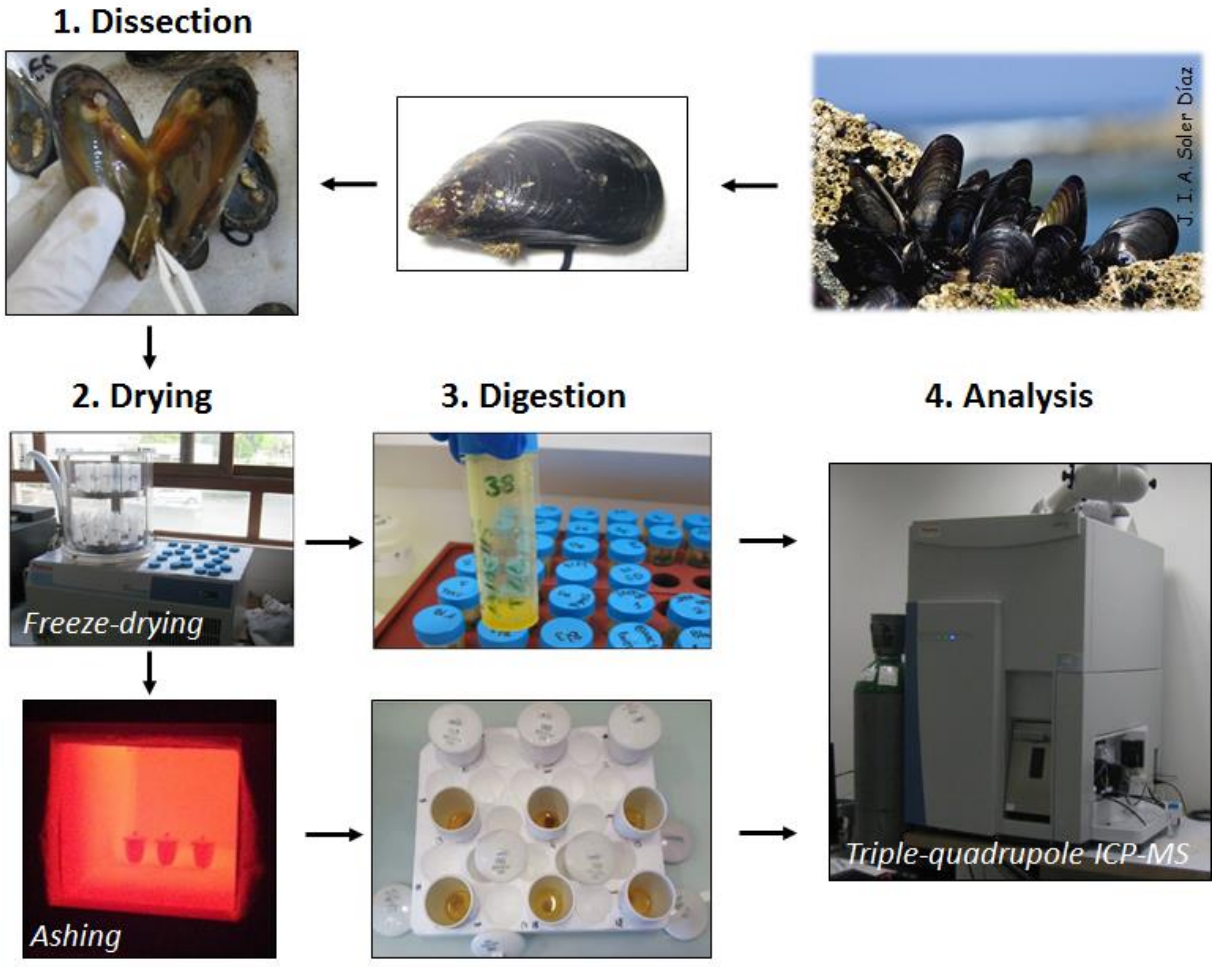


**Figure 52. Scheme of applied mussel sample pre-treatment steps before analysis.**

Acid digestions of freeze-dried samples (~500 mg, N = 3) consisted in closed mineralisation with *aqua regia* (1.4 mL $HNO_3$ 65% Suprapur® 14 M and 2 mL HCl 30% Suprapur® 10 M) in non-acid washed 50 mL PP tubes for 3 h at 90ºC in the hotplate (DigiPREP MS, SCP SCIENCE). Samples were then diluted with 13.6 mL of Milli Q® and stored at 4ºC until analysis (Daskalakis et al. 1997, USEPA 2007). Ashed

samples contained originally ~500 mg of dried tissue which, after ashing at 450ºC (N=3) and 800ºC (N=3) in acid-washed porcelain crucibles (***Figure 52***), were then digested in 3 mL of *aqua regia* for 3h at 110ºC and recovered in final 13 mL Milli-Q water (Abdou et al. 2019). Results showed that the ashing steps caused important trace element losses (highly pronounced for Se and Te) and less evident for Sb (***Table 15***). Therefore, Te and Se cannot be quantified from ashed biological samples.

**Table 15. Biological concentrations (µg $kg^{-1}$) of Te, Sb and Se in wild mussels (*Mytilus galloprovincialis*) from Arriluze (N=20).** Errors correspond to standard deviations (SD). Abbreviations: Limit of Detection (LOD).

| Pre-treatment | Total soft tissue concentrations (µg $kg^{-1}$ d.w.) | | |
|---|---|---|---|
| | Te | Sb | Se |
| *Non-depurated freeze-dried (pool)* | 2.47 ± 0.09 | 82.6 ± 2.6 | 1560 ± 40 |
| *Ashed at 450ºC* | 0.14 ± 0.02 | 69.5 ± 0.3 | 16.5 ± 2.9 |
| *Ashed at 800ºC* | 0.16 ± 0.01 | 74.2 ± 0.6 | < LOD |

# VI. ANALYTICAL METHODS

## 1. Bulk mineralogy

### 1.1. Principle of X-Ray Powder Diffraction (XRD) analyses

Major minerals show specific atomic structures (i.e., disposition of atoms in planes) which act as reflection surfaces of X-rays, diffracting the incident beam. This takes place because the wavelength (λ) of the incident X-ray is smaller than the distance between atom planes (defined by the vector $d_{hkl}$). As mineral crystals contain several atom planes in their structure, all X-ray beams applied to a sediment sample will be diffracted at an angle θ at different distances from the sample surface because the X-ray diffracting from the bottom planes have travelled longer distances than those from the top planes. Thus, a diffraction peak will be produced only when the outgoing X-ray beams from all atom planes are in phase. According to Bragg's law, this happens when the extra distance travelled by the X-ray reaching the bottom plane compared to that above is equal to λ, i.e., equals twice the distance between atom planes times the sinus of the outgoing angle θ (***Figure 53a***).

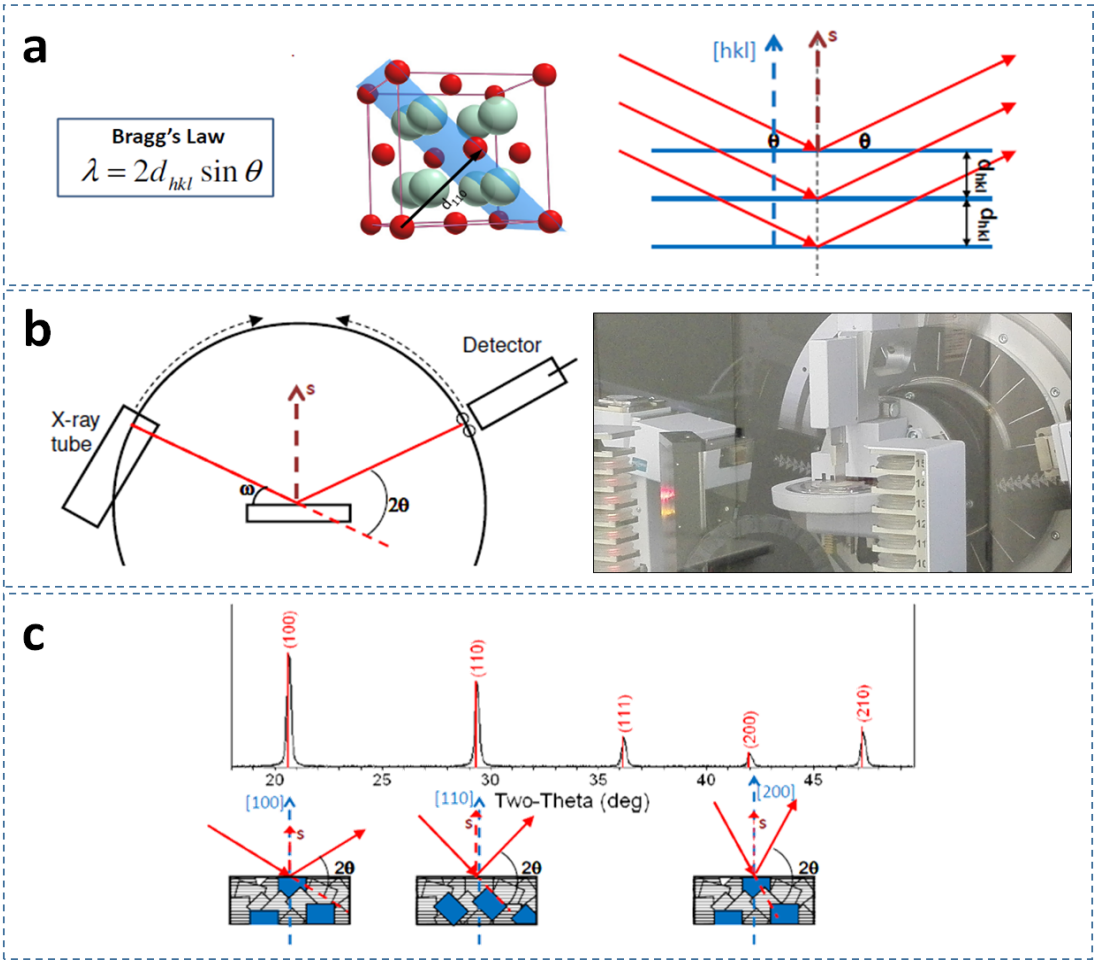


**Figure 53. Principle of X-Ray Powder Diffraction (XRD) measurements.** (a) Bragg's law and simplistic model, (b) XRD Bruker D8 DISCOVER instrument and (c) example of a polycrystalline diffractogram. Abbreviations: normal plane [hkl], diffraction vector *s*, incident angle (ω) and diffraction angle (2θ). *(Speakman, MIT).*

In most cases, λ is fixed, thus, the diffraction peak of a family of planes will produce a response at the specific angle 2θ (***Figure 53b***). The Miller indices (hkl) define the crystallographic direction of the family of parallel planes with a vector [hkl] normal to the atom plane. The vector *s* bisects the angle between the incident and diffracted beam and it is always normal to the surface of the sample. The required wavelength and measurements are performed with an X-Ray Powder Diffraction (XRD) instrument (***Figure 53b***).

Diffracting X-ray will be phase when the crystallographic direction [hkl] of the atom planes is aligned with vector *s*. When this is not applied, diffracting X-ray will be cancelled, blending with the background signal. Thus, polycrystalline samples, such as bulk sediments, will probably present a small percentage of crystallites properly oriented to diffract the applied X-rays. Nevertheless, the XRD measurement assumes that for every set of atomic planes in a sample there is an equal and statistically relevant number of crystallites diffracting the X-ray. Furthermore, the same crystallite can produce more than one diffractogram peak as long as Bragg's law is respected. The vector [hkl] in Bragg's law is used to determine the position of the diffraction peaks in the resulting diffractogram (***Figure 53c***).

- *Major mineral composition and clay mineral analyses*

Major sample mineralogy (> 5 wt.%) was compared among sites from un-oriented oven-dried SPM powder characterised by X-ray diffraction (XRD Bruker D8 DISCOVER from the Institute of Applied Geosciences, AGW-KIT, Germany) using Cu Kα radiation (40 mV/40mA Cu tube X-ray beam). Diffractograms were recorded with an angular range from 2º to 82º 2θ with step width 0.02º and counting time of 0.4 s/step. Diffractograms from clay minerals were recorded at angular range from 2º to 22º 2θ and with the same aforementioned XRD parameters.

Results were contrasted with international peak lists of minerals (Crystallography Open Database QualX and the Crystal Structure Data Base for Minerals WWW-MinCryst) to enable identification of major mineralogical composition. Clay minerals were identified according to the expected diffractogram response after each pre-treatment step (***Table 14***).

## 2. Analyses of stable trace element concentrations

### 2.1. Principle of mass spectroscopy (ICP-MS)

The principle of inductively coupled plasma mass spectrometry (ICP-MS) analysis is based on several steps, including:

- **Nebulisation**: a peristaltic pump drags the liquid sample from the sample tube, through a thin glass tube (micro nebuliser) into a spray chamber. The nebulisation step consists in transforming the liquid sample into a fine aerosol with the help of argon (Ar) gas introduction at the moment of entering the spray chamber. The aerosol is then selected in the spray chamber where the heaviest droplets are discarded before being introduced into the plasma torch.

- **Ionisation**: the plasma torch contains an Ar plasma (6000 – 8000ºK) capable of volatilising, atomising and ionising the elements present in the aerosol, maximising single-charged ions. The degree of ionisation is element-dependent according to the element ionisation energy (***Figure 54a***). This implies that certain elements release more easily electrons of valence than others, depending on how full the electron shells are and the attraction strength from the protons in the atomic nucleus.

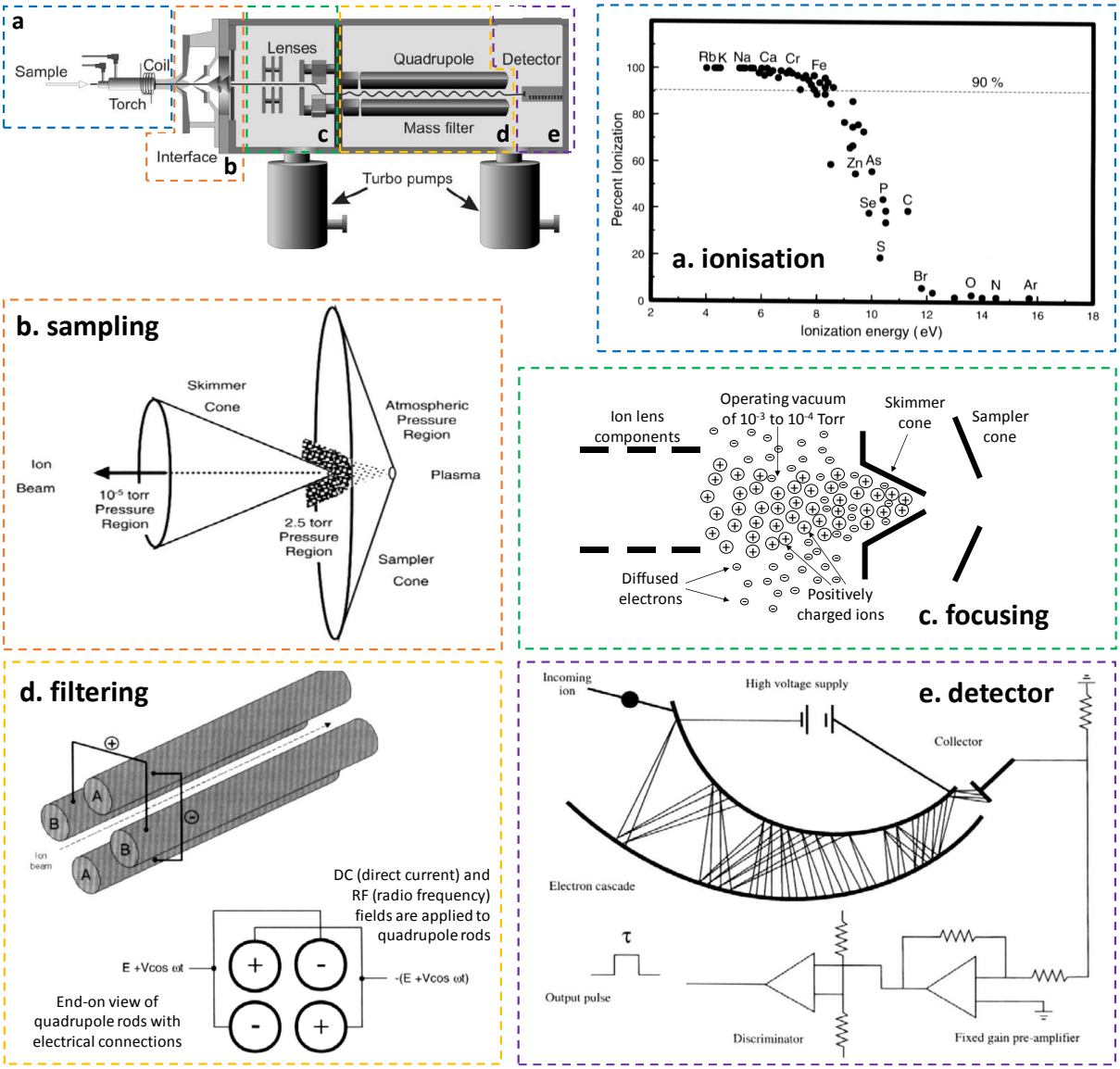


**Figure 54. Principle of single quadrupole ICP-MS technique.** *("An overview of ICP-MS" in dnr.wi.gov)*

These ions then pass to the interface through a sampler cone and a skimmer cone (***Figure 54b***). These cones separate the primary and secondary vacuum differences between the atmospheric pressure in the plasma torch area (760 Torr) and that of $10^{-5}$ Torr after the skimmer cone.

- **Focusing**: in the secondary vacuum zone, some ion lens focus positively charged ions while minimising the transport of unwanted matrix components, particulates, neutral species, photons and electrons by electrostatic attraction (***Figure 54c***). Thus, only positively charged ions are focused to the ion beam to be transported towards the filtering quadrupole.

- **Filtering**: the quadrupole separates ions according to their mass to charge (m/z) ratio, selecting the m/z ratio of the targeted isotope (***Figure 54d***). The most common quadrupole is a mass filter but others applying collision/reaction cell systems, magnetic sector or time-of-flight are also available in the market.

- **Detection**: the selected/targeted ions arriving at the detector produce an ion current which is translated to an electrical signal by electron multipliers (***Figure 54e***), producing a final signal proportional to the number of ions present in the sample. This signal is converted to concentration units by further calculations which require either (i) independent analysis of different dilutions of standard solution ("external calibration"), or (ii) analysis of samples which have been spiked with known quantities of a standard solution ("isotopic dilution").

### 2.2. Single vs triple quadrupole ICP-MS performance

Trace element analyses were mostly performed at the EPOC 5805 (University of Bordeaux) using single or triple quadrupole inductively coupled plasma mass spectrometry (ICP-MS) techniques (***Figure 55***). These techniques are appropriate for this work as they allow to identify and quantify almost simultaneously specific mass to charge (m/z) ions (i.e., isotopic analysis) present in the samples at trace to ultra-trace element concentrations. Both ICP-MS instrumentations are Thermo Fisher Scientific®, with the recent acquisition of the triple quadrupole ICP-MS (iCAP TQ) in August 2017.

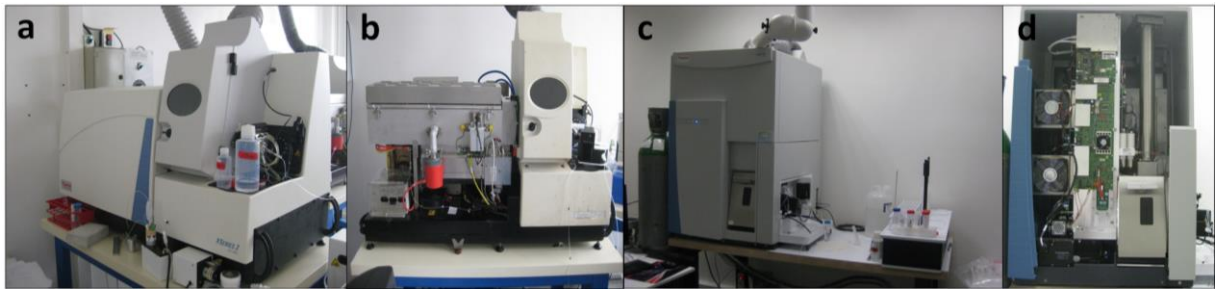


**Figure 55. ICP-MS Thermo Fisher Scientific®.** (a,b) Single quadrupole ICP-MS X-Series 2 and (c,d) triple quadrupole ICP-MS iCAP TQ.

The main advantages of the triple quadrupole ICP-MS over the single quadrupole are that the triple quadrupole instrumentation (i) shows higher sensitivity, and (ii) non-negligible performance when dealing with polyatomic interferences due to intrinsic analysing modes. The choice of the analytical method applied to each environmental sample depends on (i) the target element, (ii) the sample matrix, and (iii) the pre-treatment applied to the sample before analysis. For instance, the single-quadrupole ICP-MS is equipped with a collision cell which allows to remove polyatomic interferences in freshwater matrices. However, it cannot eliminate polyatomic interferences from particle digestions for certain trace elements. In order to better understand this, the main interferences of Sb, Te and Se will be presented followed by the specific instrumental analysing modes applied in this work.

- *Sb, Te and Se interferences*

In mass spectrometry there are two types of mass spectral interferences, that is, two ways in which other substances might match the targeted m/z ratio, contributing in excess to the amount of targeted isotope signal/counts. These interferences can either present isotopes with coincident m/z ratios (i.e., isobaric interferences) or can combine ions that fit with the targeted m/z ratio (i.e., polyatomic interferences). Some examples of these interferences, often challenging due to higher abundances compared to that of targeted elements, are shown for Sb, Te and Se (***Table 16***).

**Table 16. List of interferences in ICP-MS for targeted elements (Sb, Te and Se).** Isotopes that were not used in this work due to low abundance or high interference effects are presented in grey font.

| Isotopes | m/z spectral interferences | |
|---|---|---|
| (abundance) | Isobaric | Polyatomic |
| $^{121}$Sb (57.3%) | | $^{40}$Ar$^{81}$Br, $^{105}$Pd$^{16}$O |
| $^{123}$Sb (42.7%) | $^{123}$Te | $^{107}$Ag$^{16}$O, $^{105}$Pd$^{18}$O |
| $^{124}$Te (4.74%) | $^{124}$Sn | $^{108}$Pd$^{16}$O |
| $^{125}$Te (7.07%) | | $^{89}$Y$^{36}$Ar, $^{85}$Rb$^{40}$Ar, $^{109}$Ag$^{16}$O, $^{107}$Ag$^{18}$O, $^{88}$Sr$^{37}$Cl, $^{90}$Zr$^{35}$Cl |
| $^{126}$Te (18.8%) | $^{126}$Xe | $^{86}$Sr$^{40}$Ar, $^{90}$Zr$^{36}$Ar, $^{86}$Kr$^{40}$Ar, $^{110}$Cd$^{16}$O, $^{110}$Pd$^{16}$O, $^{91}$Zr$^{35}$Cl |
| $^{128}$Te (31.7%) | $^{127}$Xe | $^{88}$Sr$^{40}$Ar, $^{112}$Cd$^{16}$O, $^{112}$Sn$^{16}$O |
| $^{130}$Te (32.1%) | $^{130}$Xe, $^{130}$Ba | $^{90}$Zr$^{40}$Ar, $^{114}$Sn$^{16}$O, $^{114}$Cd$^{16}$O, |
| $^{76}$Se (9.37%) | $^{76}$Ge, $^{152}$Sm$^{++}$ | $^{40}$Ar$^{36}$Ar, $^{39}$K$^{37}$Cl, $^{60}$Ni$^{16}$O, $^{75}$As$^{1}$H |
| $^{77}$Se (7.63%) | $^{154}$Sm$^{++}$, $^{154}$Gd$^{++}$ | $^{40}$Ar$^{37}$Cl |
| $^{78}$Se (23.8%) | $^{78}$Kr, $^{156}$Gd$^{++}$, $^{156}$Dy$^{++}$ | $^{40}$Ar$^{38}$Ar, $^{60}$Ni$^{18}$O |
| $^{80}$Se (49.6%) | $^{80}$Kr, $^{160}$Gd$^{++}$, $^{160}$Dy$^{++}$ | $^{40}$Ar$^{40}$Ar, $^{64}$Zn$^{16}$O, $^{40}$Ar$^{40}$Ca |
| $^{82}$Se (8.73%) | $^{82}$Kr, $^{164}$Dy$^{++}$ | $^{66}$Zn$^{16}$O, $^{81}$Br$^{1}$H |

The present list (***Table 16***) is a general recompilation of potential interferences for Sb, Te and Se isotopic m/z ratios. Some interferences are gas-dependent (e.g., Kr, Xe, ArAr) and mostly common to all analyses unless specific gas bottle series are particularly better purified than others. Other interferences are related to sample matrix and pre-treatment steps performed to environmental samples. The former determines the intensity of the interference by influencing in the abundance of the interfering element. For instance, wild oysters accumulate non-negligible Ag and Cd amounts compared to Te, influencing the quantification of certain Te isotopes. The latter can lead to the formation of specific polyatomic (e.g., chlorine based interferences from HCl-containing digestions), affecting each sample analysis differently.

- *Instrumental analysing modes*

Until recently, isobaric and polyatomic interferences in many cases were mathematically corrected or avoided instrumentally. Mathematical corrections can be applied, for instance, to gas interferences by measuring another isotope from the gas (e.g., $^{131}Xe$) and calculating with the theoretical isotopic abundance the contribution of the specific isobaric interference (e.g., $^{126}Xe$ in $^{126}Te$). Another alternative to this type of gas interference is applying blank corrections to sample signals, that is, to correct the signal of each analysed sample with the signal of at least 10 blank solutions (e.g., 2% $HNO_3$ Ultrex II Ultrapure J.T. Baker). Both methods are valid from the view-point of analytical quality when the final mathematical correction is relatively low (e.g., <20% of the original sample signal).

Instrumental treatment requires regulating instrument settings in order to improve the analytical performance. This is the case of Se quantification in single quadrupole ICP-MS using a collision/reaction cell (CRC-mode, ***Figure 56***). The principle of CRC-mode analysis is a physical separation between polyatomic and the targeted analyte by introducing a gas or gas mixture in a chamber before the quadrupole filtering step (***Figure 54d***). This is based on the assumption that there is a higher probability that the gas particles will collide with the bigger polyatomic interference ions compared to those from the targeted analyte. The collision also implies a reaction process where the polyatomic interference forms a product ion that is later discarded in the quadrupole filtering step.

New generation instruments like the triple quadrupole ICP-MS allow alternative approaches to dealing with mass spectral interferences. Particularly, the Thermo Fisher Scientific® triple quadrupole ICP-MS (iCAP TQ) allows to perform several gas reactions (i.e., He, $H_2$, $O_2$, $NH_4^+$) with different applications. In this work, only the applied reaction modes (He and $O_2$) will be presented.

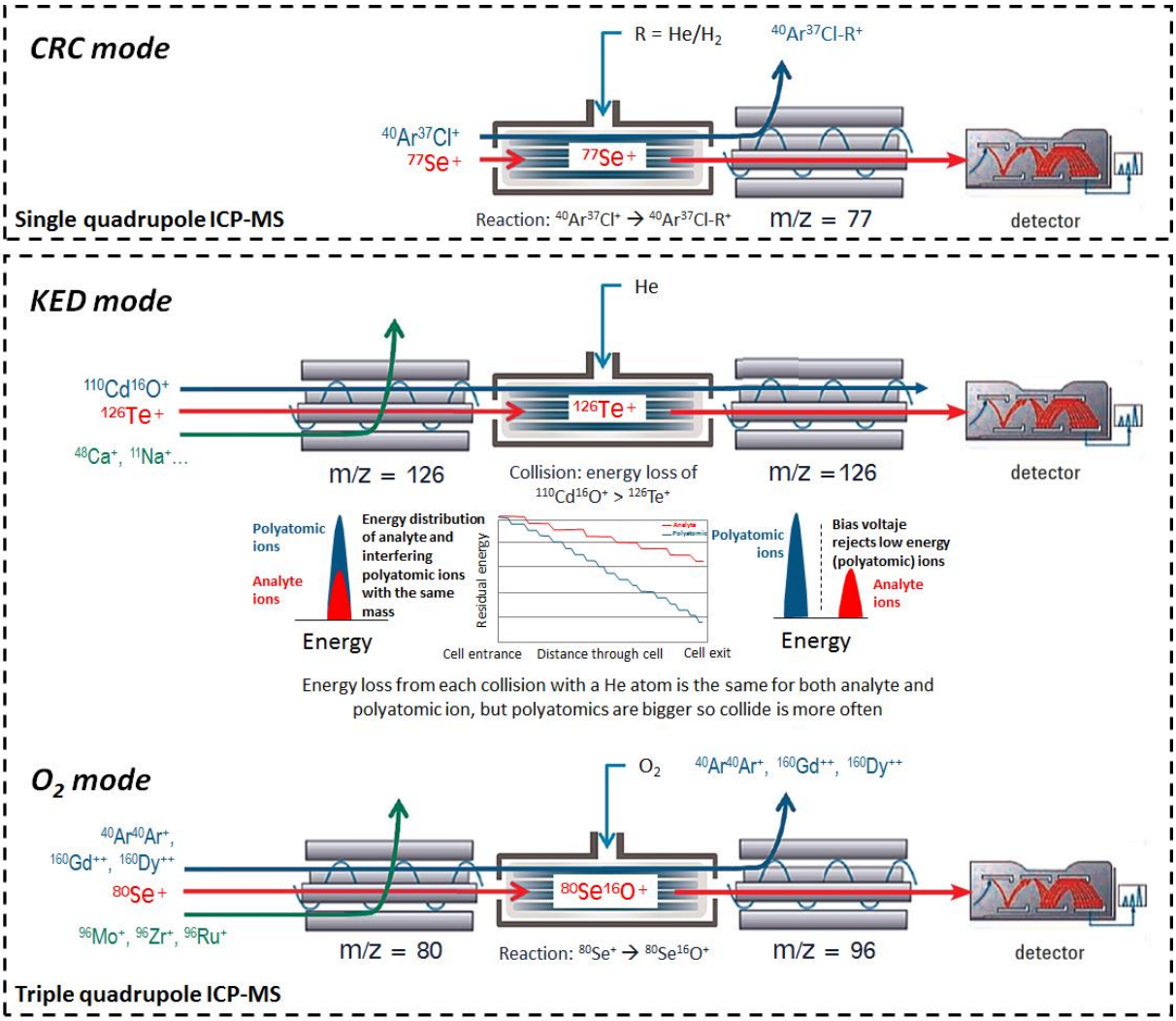


**Figure 56. Analysing modes for single and triple quadrupole ICP-MS.** *(Adapted from Kate Jones www.slideshare.net/KateJones7/142-wahlen).*

In general, the triple quadrupole ICP-MS contains (i) a first quadrupole for m/z filtering, (ii) a collision/reaction cell (i.e., hexapole or quadrupole depending on the construction), and (iii) a last quadrupole for m/z filtering too. The advantage of this evolution in mass spectrometry is that (i) the first quadrupole discards all the non-targeted m/z ratios, (ii) the reaction cell deals with polyatomic and spectral interferences, and (iii) the last quadrupole discards non-targeted m/z by either eliminating the reacted interference or by focusing on a new targeted m/z ratio corresponding to the analyte of interest. There are two ways of dealing with mass spectral interferences (***Figure 56***):

- The **Kinetic Energy Discrimination mode (KED mode)** relies on the addition of He gas in the collision/reaction cell to reduce the ionic energy of the interferences compared to the targeted analyte. This implies that both quadrupoles are set to filter the m/z ratio of the targeted analyte, rejecting the reacted polyatomic ions using a bias voltage step (energy discrimination).

- The **oxygen mode ($O_2$ mode)** consists in adding $O_2$ gas in the collision/reaction cell to react with the targeted analyte in a way that it increases its original m/z ratio to a one exempt of

interferences (mass-shift), present in the collision/reaction given the first m/z quadrupole filter. This implies that the first quadrupole targets the original target analyte m/z ratio and the last one the newly acquired m/z ratio.

## 2.3. Quantification methods

### *2.3.1. External calibration*

- *Environmental samples: water, sediments and oysters*

Most of the analytical approaches in this work apply a quantification method based on external calibration. It is the simplest way of converting the instrumental signal (counts) into a concentration value. External calibration implies that a monoelemental standard solution is diluted several times in an acid matrix (2% $HNO_3$ Ultrex II Ultrapure J.T. Baker) in order to obtain a linear regression curve between the known concentration and the analysed counts. The concentrations of the targeted analyte in the environmental samples must fall within the middle range of concentrations of the calibration curve to assure good analytical precision and adapted detection limits. This approach is performed when little or no matrix effect exists in the environmental samples. This means that there is little differences between the environmental matrix and that of the calibration solutions. In any case, certified reference materials are used for quality control of both calibration curve and any potential pre-treatment steps applied to the samples in order to assure the correct quantification of the targeted analyte.

External calibration was used in this work to quantify dissolved and particulate Sb, Te and Se in environmental freshwater samples, sediments and oyster digestions. In general, Sb was quantified with the single quadrupole ICP-MS whereas Te and Se, presenting more challenging interferences given their relatively low environmental concentrations, were determined with the triple quadrupole ICP-MS.

- *Isotopically-labelled sediments*

Isotopically-labelled sediment samples from laboratory experiments were also analysed with external calibration. However, an additional calculation is needed in the data treatment (***Figure 57***). The idea is that the non-labelled isotope (e.g., $^{121}Sb_{nat}$) provides information on the inherited target element whereas the signal of the labelled isotope (e.g., $^{123}Sb_{ex}$) has to be corrected from the contribution of the natural isotope (e.g., $^{123}Sb_{nat}$). This contribution is calculated from the non-labelled

isotope (e.g., $^{121}Sb_{nat}$) by the natural ratio of isotopic abundances (e.g., $^{121}Sb_{nat}/^{123}Sb_{nat}$). The result corresponds to the spiked concentration and indicates the spiked targeted element.

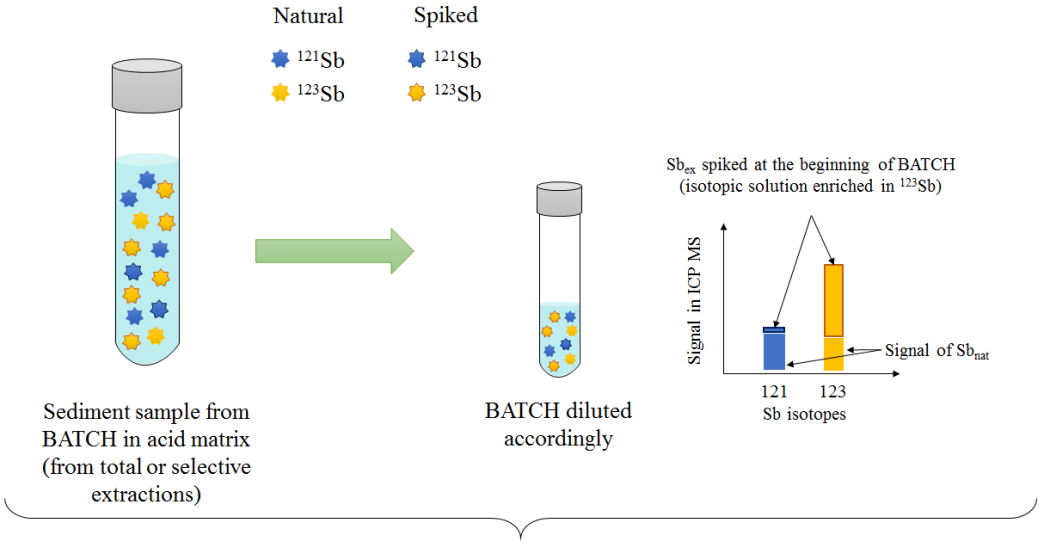


The concentrations within the solutions can be calculated for each isotope with the weighted external calibration curves:

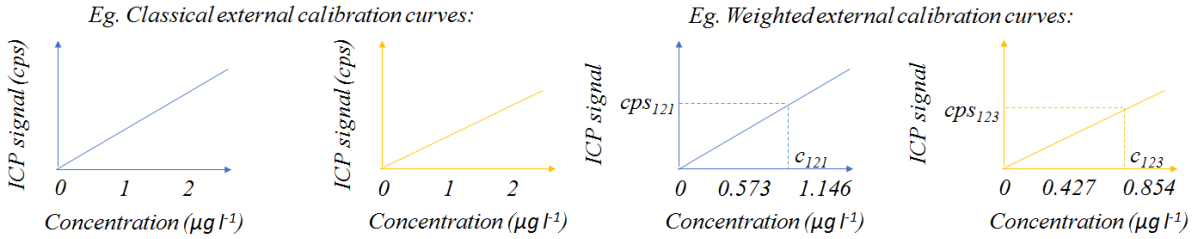


1. $c_{121} = Ab_{121nat} \cdot c_{nat} + Ab_{121\,I123} \cdot c_{I123}$
2. $c_{123} = Ab_{123nat} \cdot c_{nat} + Ab_{123\,I123} \cdot c_{I123}$

Solving the system of 2 equations and 2 unknowns:

$$c_{I123} = \frac{c_{121} \cdot Ab_{123nat} - c_{123} \cdot Ab_{121nat}}{Ab_{121\,I123} \cdot Ab_{123nat} - Ab_{123\,I123} \cdot Ab_{121nat}}$$

$$c_{nat} = \frac{c_{121} \cdot Ab_{123I123} - c_{123} \cdot Ab_{121I123}}{Ab_{123\,I123} \cdot Ab_{121nat} - Ab_{121\,I123} \cdot Ab_{123nat}}$$

Where:

| | |
|---|---|
| $cps_{123}$ | Counts per second (ICP MS signal) for $^{123}Sb$ |
| $cps_{121}$ | Counts per second (ICP MS signal) for $^{121}Sb$ |
| $c_{123}$ | Concentration (µg $l^{-1}$) of total $^{123}Sb$ signal |
| $c_{121}$ | Concentration (µg $l^{-1}$) of total $^{121}Sb$ signal |
| $c_{nat}$ | Concentration (µg $l^{-1}$) of $Sb_{nat}$ |
| $c_{I123}$ | Concentration (µg $l^{-1}$) of $Sb_{ex}$ |

| | |
|---|---|
| $Ab_{121nat}$ | Abundance of $^{121}Sb_{nat}$ = 57.3% |
| $Ab_{123nat}$ | Abundance of $^{123}Sb_{nat}$ = 42.7% |
| $Ab_{121\,I123}$ | Abundance of $^{121}Sb$ in $Sb_{ex}$ = 0.57% |
| $Ab_{123\,I123}$ | Abundance of $^{123}Sb$ in $Sb_{ex}$ = 99.43% |

**Figure 57. Methodology used to determine $Sb_{ex}$ and $Sb_{nat}$ concentrations from BATCH sediment samples.**

### *2.3.2. Isotopic dilution (ID)*

Another analytical approach to quantify target element concentrations in environmental matrices is isotopic dilution (ID). This method is applied when the sample matrix effect is non-negligible compared to the external calibration matrix. Such is the case of seawater samples where there is a high solute concentration, particularly in major seawater ions such as $Cl^-$, $Br^-$, $Na^+$, $K^+$, $Ca^{2+}$, etc. The ID method consists in adding a known quantity of a monoisotopic standard solution to the sample followed by the direct analysis of at least two isotopes of the target element in the sample. This technique is therefore limited to target elements presenting at least two stable isotopes which can be correctly quantified by ICP-MS. Specific calculations for target element quantification (***Figure 58***) are then applied in order to obtain the concentrations of the target element in each sample.

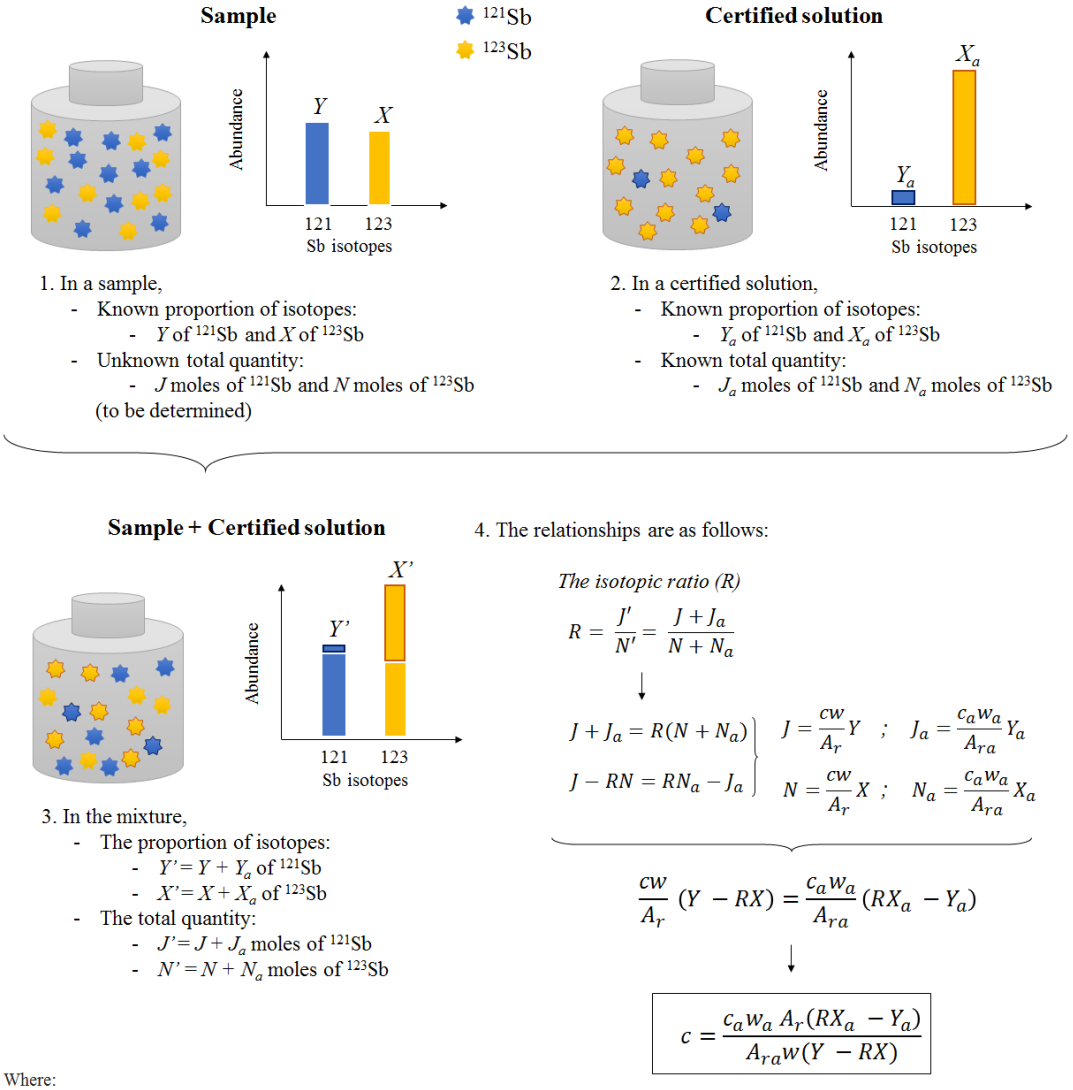


**Figure 58. Principle of isotopic dilution (ID).** (*adapted from Castelle 2008*).

In this work, isotopic dilution was used to quantify dissolved Sb in estuarine brackish samples (from MGTS sampling campaigns and those from the Arcachon Bay) using a monoisotopic solution of $^{123}Sb$ (99.43% purity at 0.2% HCl + 1% $HNO_3$). In addition, sample dilution was performed to obtain isohaline samples (S ~ 1). Gas dilution was also applied with a $PC^3$ Peltier Cooled inlet with ESI cyclonic spray chamber coupled to the single quadrupole ICP-MS (X-Series 2) in order to reduce the amount of solvent entering the ICP-MS. This procedure reduces matrix interferences (i.e. seawater introduction in the ICP-MS), potentially decreasing the ionising strength of the plasma, matrix polyatomic interferences and ideally the clogging of cones due to salt deposition.

This technique could not be applied to quantify dissolved Te and Se in brackish water samples due to:

- Relevant sample dilution effect, required in order to achieve homogeneous and low salinity sample content (S ~ 1), reducing the environmental Te and Se concentrations to very low concentrations (below the ng $L^{-1}$ range for Te). This implies that the sample content approaches the analytical detection limits, compromising the precision of the analytical method.
- Matrix effect implies that elements with already low ionisation energies like Te and Se have even lower probabilities of ionising in the plasma torch because major elements in brackish waters (e.g., $Na^+$, $K^+$, $Ca^{2+}$) are in higher concentrations and ionise more effectively, decreasing the energy available for the target element. Therefore, there is a natural decrease in the instrumental signal for brackish matrices compared to freshwater samples.
- The application of ID to low trace element concentrations requires two complementary points:
    - Low interferences in the two isotopes chosen for analytical quantification. Otherwise, the ID spike should contribute with a signal/concentration high enough to overcome the relevant contribution of the interference. However, in such cases it would be required to:
    - Use a high purity monoisotopic spike. In this way, the addition of the monoisotopic solution would not add impurities to the second isotope measured (as foreseen in ***Figure 58***).

**2.4. Analytical quality control**

Certified reference materials (CRM) used for analytical quality check should be adapted to environmental samples that are being analysed. Currently, there are several CRM for Sb quantification in freshwater (SLRS-4, SLRS-5, TM RAIN-95, TM RAIN-04), sediments (IAEA-433, DC 70311, DC 70317, NIST 8704) and oyster matrices (NIST 1566b). However, there are few CRM available for Te (freshwater NIST 1643f, sediment NCS DC 73307) and Se matrices (e.g., freshwater NIST 1640a, sediment NCS DC

73307, oyster NIST 1566b). Noteworthy, there are no CRM for Sb, Te and Se in seawater matrices nor Te in biological materials. In any case, the CRM used in this work showed correct recoveries of ~90%.

### 2.5. Applied analyses for Sb, Te and Se quantification

A summary of the specific pre-treatment, analytical quantification and corrections applied to the environmental samples and isotopically-labelled samples used in this work is presented (***Figure 59***) as a guide for future analyses on Sb, Te and Se in environmental samples. The specific sample interferences encountered during the work are also described in order to understand how some sample-dependent polyatomic interferences can be overcome.

For instance, both Sb isotopes were always quantified in all environmental samples and $^{77}Se$, $^{78}Se$, $^{80}Se$ and $^{82}Se$ were used to quantify Se. However, only $^{125}Te$ and $^{126}Te$ were used to quantify Te concentrations. Specifically, only $^{126}Te$ could be used to quantify inherited Te in sediment samples as high anomalies/interferences were observed for $^{125}Te$, showing counts that did not follow the natural isotopic abundance. However, $^{125}Te$ was the only isotope available to quantify Te content in freshwater samples, given (i) the very low ng $L^{-1}$ concentration ranges of Te in these samples, and (ii) the high interferences of Xe in the rest of the Te isotopes. Likewise, $^{125}Te$ provided reliable concentrations in biological samples because of high interference effect of $^{110}Cd^{16}O$ in $^{126}Te$. This is understandable given the high bioaccumulation factor of Cd in wild oysters, especially in those from La Fosse in the Gironde Estuary mouth due to the historical anthropogenic Cd contamination (e.g., Claisse et al. 1992, Strady et al. 2011).

Noteworthy, the only way of quantifying Se in sediment and biological matrices was using the $O_2$ mode in triple quadrupole ICP-MS. In fact, this is the most effective method to avoid the strong interference effects of double-charged rare earth elements (REE) which are highly concentrated in these environmental matrices.

Corresponding analytical quality check for each environmental sample analyses is also presented (***Figure 59***). Limits of detection (LOD) of analytical performance are also shown, calculated as three times the standard deviation of 10 blank solutions (2% $HNO_3$ II Ultrapure J.T. Baker).

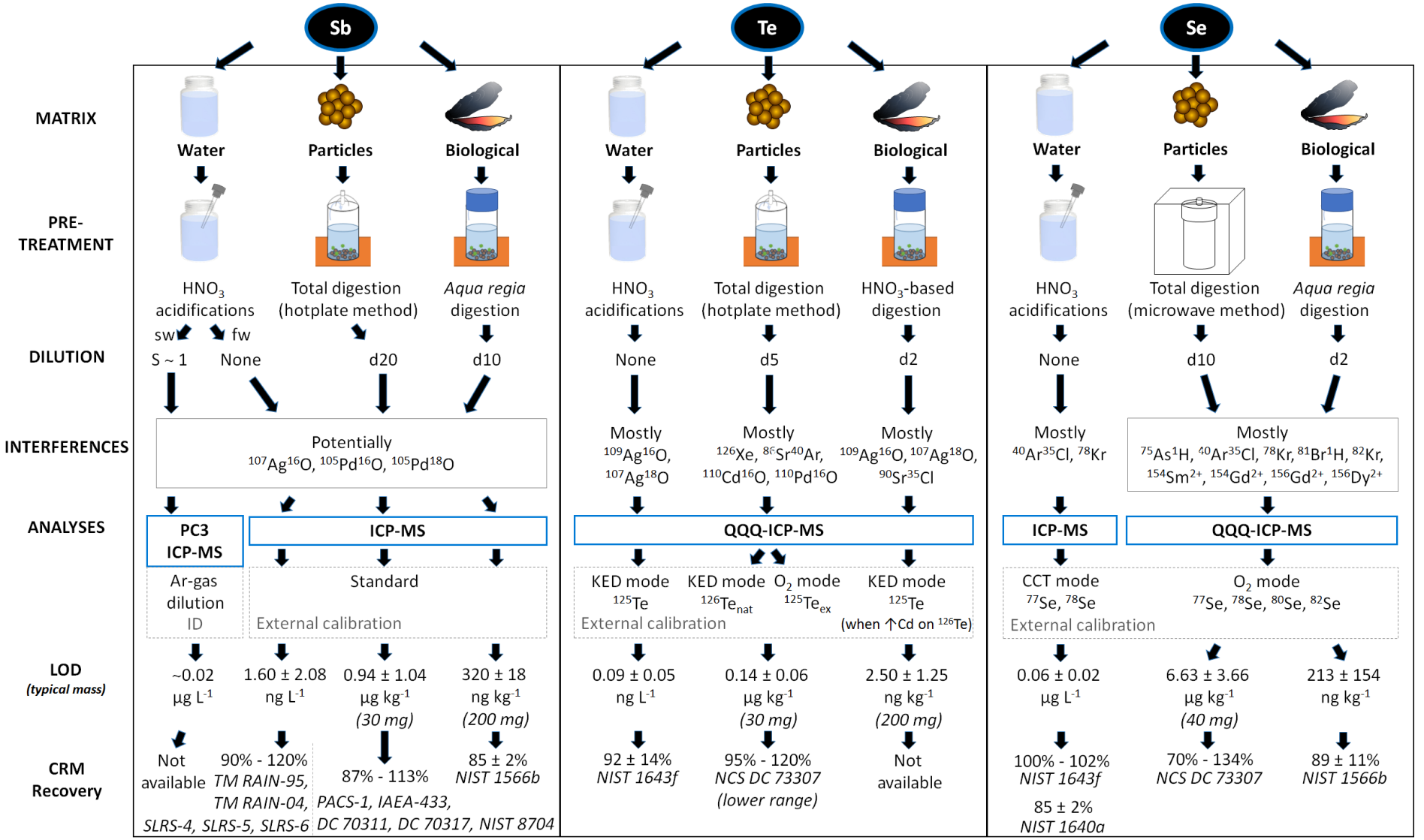


**Figure 59. Analytical scheme to quantify Sb, Te and Se in several environmental samples.** Acronyms: QQQ-ICP-MS (triple-quadrupole ICP-MS), ID (isotopic dilution), CRM (certified reference material), LOD (limit of detection).

## 3. Analyses of radionuclide activities

### 3.1. Principle of gamma-ray spectroscopy

Decaying radionuclides emit specific gamma-radiation when passing from an excited state to a lower energy level. This emission of energy is characteristic for the element, presenting well-defined electromagnetic properties, i.e., orthogonal electric (photons) and magnetic fields within the high frequency and high energy region of the electromagnetic spectrum (i.e., gamma rays, ***Figure 60***).

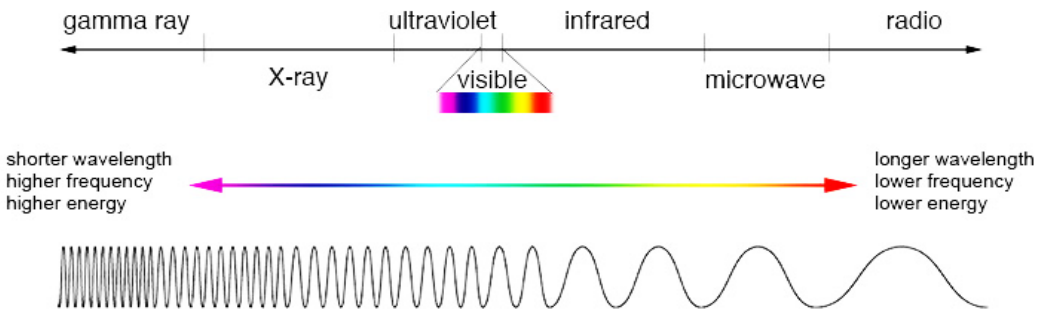


**Figure 60. The electromagnetic spectrum.**

*(From https://imagine.gsfc.nasa.gov/science/toolbox/emspectrum1.html).*

Gamma-rays are emitted through time following the characteristic half-life of the parent nuclei (Knoll 1989) and this emission can be quantified with a gamma-ray counter. Gamma-ray detectors collect information on both photon intensity and energy due to the interacting properties of gamma rays with matter. Gamma-rays interact with matter in several ways (Rizwan 2015) relevant processes are (***Figure 61***):

- **Photoelectric absorption**: when the photon transfers all its energy to an electron in matter. The photoelectron produced is ejected from the atom in the detector carrying the energy from the gamma-ray minus that of the binding energy of the host element. The vacancy in the atom left by the emitted electron is replaced by free electrons from the medium and/or the rearrangement of electrons from other shells in matter, with emission of characteristic X-ray.

- **Compton scattering**: a second possibility for a gamma-ray to interact with an electron in matter is that its energy is only partially transferred to the photoelectron resulting in an energy distribution between the kinetic energy of the ejected electron and the residual energy of the scattered photon.

- **Pair production**: interaction of a gamma-ray (containing energy greater than twice the mass of an electron at rest, 1.022 MeV) with a nucleus of matter releases two subatomic particles: an electron and a positron. The excess energy is converted to kinetic energy shared between the electron and the positron and eventually lost again via ionisation and/or excitation interactions.

The positron finally annihilates, that is, the positron, being the anti-particle of an electron (same mass, different charge) interacts with an electron resulting in their disappearance and replacement by two 0.511 MeV photons. These photons are emitted in opposite directions, falling within the gamma-ray range of the electromagnetic spectrum.

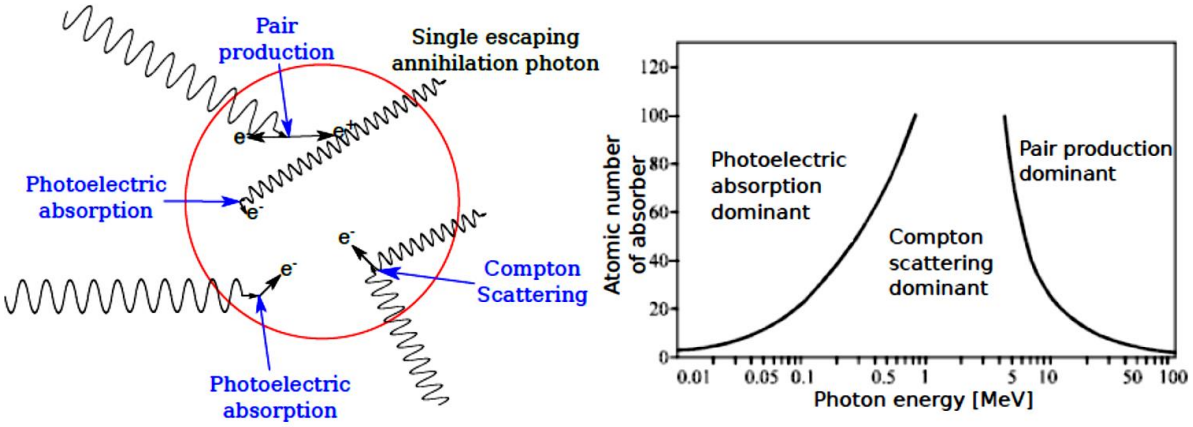


**Figure 61. Diagram of main interactions between gamma-rays and matter** (left): photoelectric absorption, Compton scattering, and pair production. The importance of the three interactions according to the photon energy (from the gamma emission) and the atomic number of the interacting element (constituting the matter in the detector) are shown (right). Lines show cases where there is equal probability of showing boundary interaction properties. *(Rizzi et al. 2010).*

### 3.2. High Purity Germanium detectors

The instrument used in this work is a High Purity Germanium (HPGe) detector. The principle of this technique is based on a Ge crystal as material interacting with the gamma photons. The emitted photons lose their energy within the detector, constituting the basis of the detector signal. In fact, the detector contains semiconductor diodes in P-I-N structure: an Intrinsic or depleted region (I) surrounded by positive (P) and negative (N) electrodes. When the photons interact with the Ge crystal within the depleted region, charge carriers (i.e., holes and electrons) are produced and transported to the electrodes according to the electric field. The produced current is proportional to the energy of the photon (Reguigui 2006). This current is further converted into a voltage pulse and then amplified, showing values, which are proportional to the isotope-dependent gamma energies (KeV).

The HPGe detectors must be operated at liquid $N_2$ temperature (−196ºC) as room temperature results in intolerable instrumental noise and loss of energy resolution. To ensure the low temperature, the detector is kept in a small vacuum container. The cooling of the detector is achieved by connecting a liquid $N_2$ deposit (LN2 Dewar) to the Ge crystal through a copper cable (***Figure 62***).

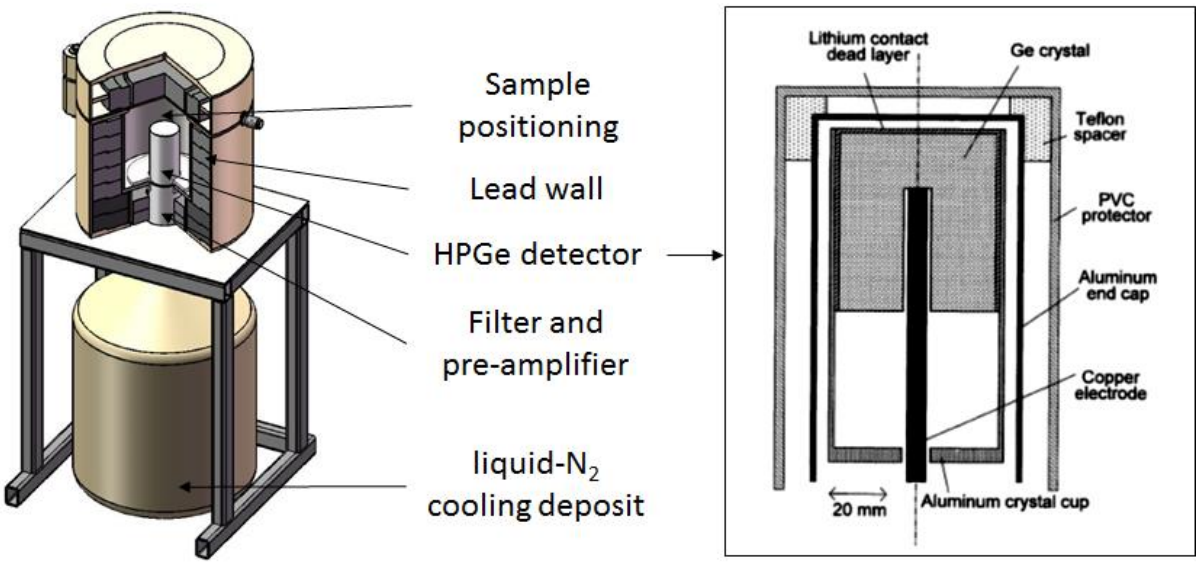


**Figure 62. Diagram of a HPGe detector.** *(www.radek.ru and Saegusa et al. 2000)*

Conversion of instrumental signal to activity values depends (i) on the sample geometry, (ii) on the instrument performance (i.e., counting efficiency and gamma transition efficiency), and (iii) on the target element characteristics (e.g., mass, half-life, etc.). Therefore, the use of standard reference materials for calibration in this system implies (Reguigui 2006):

- Energy calibration, i.e., linear response between the amount of energy transferred to the detector and the height of the electronic signal,
- Peak form and energy resolution, i.e., obtaining good resolution of peaks in the energy/pulse height spectrum, and
- Resolution or efficiency calibration, i.e., verifying that the performance of the instrument results in correct calculated activities from a pulse-height spectrum, ranging within the certified values of a given standard reference material.

Noteworthy, as the element decays over time, the activity of a sample decreases. This means that the activity quantified by gamma-ray spectroscopy is valid for the analysing day (time-dependent). This is particularly relevant for short-lived radionuclides such as $^{113}$Sn (i.e., half-life of 115 days) and $^{75}$Se (i.e., half-life of 120 days). In order to overcome this natural decrease in activity due to radionuclide decay, the activity of the sample must be corrected (re-calculated) for a given day, in accordance with the experimental conditions and requirements for result interpretation.

### 3.3. Quantification of radioactive $^{113}$Sn and $^{75}$Se

The activity of $^{75}$Se was directly measured with the 264.7 keV energy line using a High Purity Germanium detector (HPGe, ORTEC®) by collaborators at the Institute for Nuclear Waste Disposal (INE) of the Karlsruhe Institute of Technology (KIT, Germany). In the same samples, the activity of $^{113}$Sn was measured indirectly from the $^{113}$Sn daughter isotope $^{113m}$In at the 391.7 keV line. The latter is possible once the sample has reached secular equilibrium, that is, the moment when the activity of the daughter isotope ($^{113m}$In) equals that of the parent ($^{113}$Sn). This phenomenon can only occur when the half-life of the daughter radionuclide is much shorter than that of the parent. Secular equilibrium is established through time after several half-lives of the daughter radionuclide, which is for $^{133m}$In within a few hours (half-life = 99.48 min). The gamma detector was calibrated with a certified Multinuclide Standard Solution (2M HCl, Eckert & Ziegler) and showed detection limits of 0.03 Bq mL$^{-1}$.

# VII. DATA TREATMENT

Several mathematical approaches have been applied to the obtained data in each study. The specific treatments have been described in each study according to the environmental or experimental approach. In this section, a brief description of the basic principles applied is presented.

## 1. Statistical approach

### 1.1. Temporal series: trends and seasonal components

There are two types of temporal series: (i) stationary series, i.e., when the average value of the dataset and its variability through time remains constant (e.g., rainfall data), and (ii) non-stationary series, i.e., when the average value and/or the standard deviation varies through time (e.g., Keeling's trend of atmospheric $CO_2$ from the Mauna Loa). Statistical treatment can be applied to temporal datasets when either series comply with the following criteria: (i) the dataset should be complete for the temporal time lapse (e.g., information available for every month in a monthly dataset), (ii) homocedasticity of the dataset should comply through time (homogeneous standard deviations), and (iii) data should not be correlated (i.e., independent sampling between value $t_j$ and $t_{j+1}$, etc.). The latter is verified with a correlation test, discarding the presence of correlation when the resulting correlogram shows values closer to cero than +1 and -1 (Bekkali 2013).

When the dataset complies with all aforementioned criteria, the temporal series can be analysed with classical statistical approaches. These approximations assume that the behaviour of a variable through time (X(t)) is a function of three main components (***Equation 1***):

**Equation 1:**

$$X(t) = f(T(t), S(t), R(t))$$

where,

- **Temporal trend (T(t))**: corresponds to the long-term increasing/decreasing/constant behaviour of the data series (***Figure 63***), generally described by linear regressions. In the case of non-parametric datasets, the statistical significance of the temporal trend is studied with Mann Kendall tests and the slope of such trend is given by Sen's Slope. The latter were used in this work as the environmental datasets of Sb and Te did not show normal distributions.
- **Seasonal variations (S(t))**: corresponding to the cyclic pattern of the dataset (***Figure 63***). The seasonal component can be described by an *additive model* (i.e., X(t) – T(t) = S(t) + R(t), applicable when seasonal fluctuations do not change with changes in trend) or a *multiplicative model* (i.e., X(t) – T(t) = S(t)*R(t), applicable when the magnitude of seasonal fluctuations increases/decreases proportionally to the increase/decrease of the temporal trend). The additive model was considered for statistical treatment of the seasonal component in this work.

Such model allows to calculate the SeAsonal Factor (SAF), quantifying the difference of sampled trace element concentrations to the monthly average in the case where the temporal series showed no trend through time.

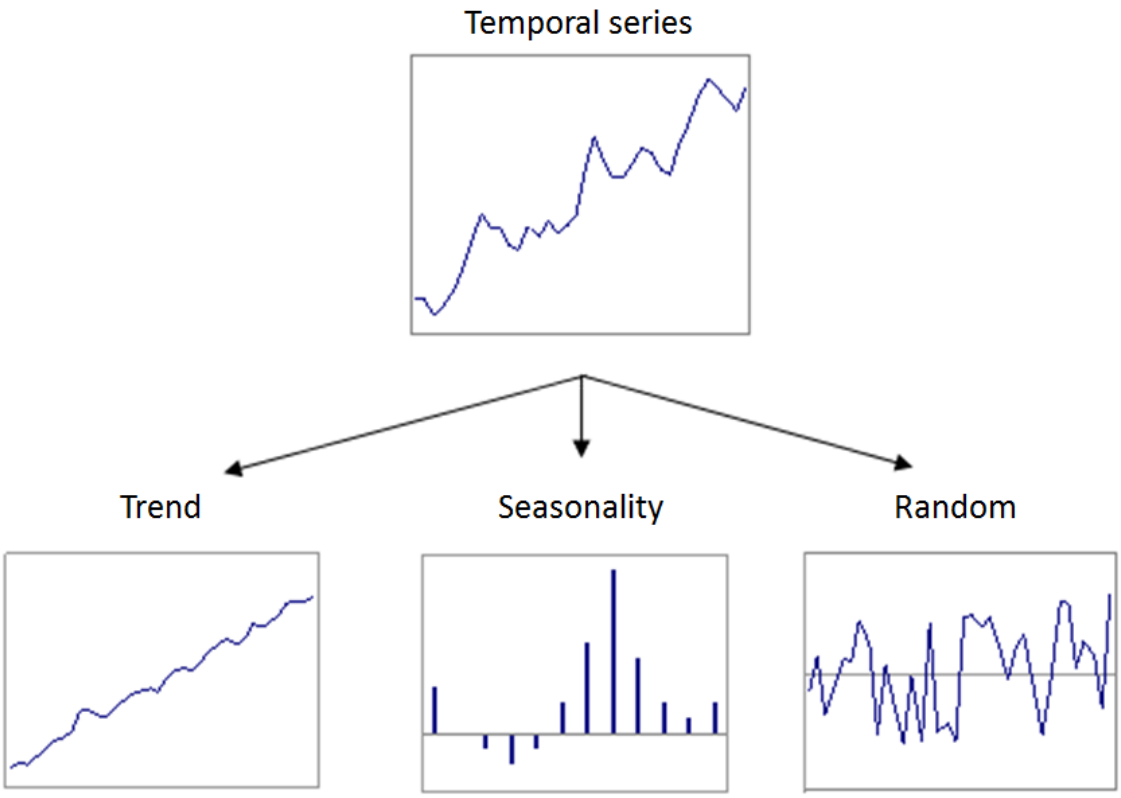


**Figure 63. Graphical representation of mathematical breakdown of temporal series.** *(Modified from Esparza Catalán).*

- **Random component (R(t)):** gathering all the outliers and random points in the dataset (***Figure 63***). It is a component that does not behave systematically or regularly through time, thus, it is unpredictable. Such samples are generally attributed to chance, integrating everything that cannot be explained by the trend T(t) and the seasonal S(t) components (Arellano 2001).

Several statistical programmes allow to perform the aforementioned statistical tests and approaches to quantify each component of the temporal series. In this work, most of the statistical approaches were performed with the SPSS 15.0 software (Statistical Package for the Social Sciences), complemented by the R-CRAN 3.3.1. (Comprehensive R Archive Network) when applicable.

### 1.2. Dissolved and particulate annual fluxes

There are two possible ways of calculating annual fluxes (i.e., water, SPM, trace elements) in aquatic systems according to the sampling frequency: (i) the “reference flux” approach, based on a complete dataset from daily sampling, and (ii) the discharged-weighted approach, based on annual

extrapolations when daily sampling is not possible (Coynel et al. 2004). The former calculation (***Equation 2***) is based on well-known methods for SPM fluxes of rivers (e.g., Meybeck et al. 1993, Walling and Webb 1985):

$$F_{SPM_a} = \sum_{i=1}^{365} (Q_i \cdot SPM_i)$$

**Equation 2:**

where $F_{SPMa}$ is the annual SPM flux (t $y^{-1}$), $Q_i$ the daily ($i$) river discharge ($m^3$ $s^{-1}$) and $SPM_i$ the daily SPM concentrations (mg $L^{-1}$). Note that transformations to comply with the final flux units are not shown in these equations. This equation can be applied to the Lot-Garonne River system due to available information on daily river discharges from the National Hydrographic Databank (DIREN) and daily SPM collection by automated samplers (SIGMA 900P, American Sigma, Colorado) located at strategic sites in the rivers, collecting continuously 1L daily pools every 8 hours (Coynel et al. 2009).

Discharge-weighted SPM flux calculations (***Equation 3***) are based on the idea that a certain sampling frequency along the year is representative of the annual conditions. It is also calculated from known methods (e.g., Meybeck et al. 1994, Meybeck and Ragu 1995, Webb et al. 1997):

$$F'_{SPM_a} = \left(\frac{\sum_{i=1}^{365} Q_i}{365}\right) \cdot \left(\frac{\sum_{i=1}^{n} (Q_i \cdot SPM_i)}{\sum_{i=1}^{n} Q_i}\right)$$

**Equation 3:**

where $F'_{SPMa}$ is the annual discharge-weighted SPM flux (t $y^{-1}$) from a sampling frequency of $n$ days, $Q_i$ the daily ($i$) river discharge ($m^3$ $s^{-1}$) and $SPM_i$ the daily SPM concentrations (mg $L^{-1}$). The first parameter of the equation is generally referred to Q', i.e., the annual water discharge or annual mean of $Q_i$ for $i_{1\rightarrow365}$.

Both SPM annual flux calculations show similar values when the sampling frequency of the discharge-weighted approach is high/representative enough of the annual SPM variability. This has been studied for the Lot-Garonne River system by Coynel et al. (2004), establishing a minimum frequency of three days (i.e., at least 10 samples per month) before obtaining important SPM flux deviations of ± 20% (***Figure 64***).

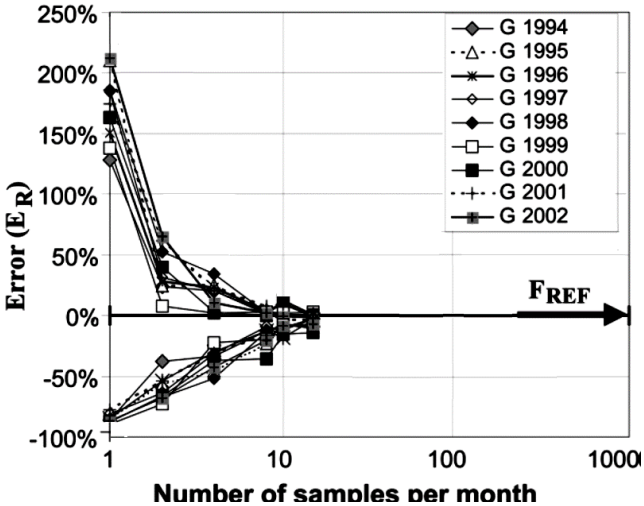


**Figure 64. Maximum error percentages for simulated SPM annual fluxes (1994 to 2002) in the Garonne River (G) as a function of sampling frequency (log scale).** $F_{ref}$ is the annual SPM reference flux calculated from hourly-based sampling frequencies. (*Modified from Coynel et al. 2004).*

Trace element dissolved and particulate annual fluxes can be calculated with aforementioned methods (***Equation 2***, ***Equation 3***) by including information about trace element concentrations. Water and sediment samples are required in order to quantify respective dissolved and particulate concentrations. The automated samplers in the Lot-Garonne River system can be used for high sampling frequency of such parameters. Nevertheless, it is not always possible to set up an automated sampler in every affluent. Thus, the Lot-Garonne River sites are periodically monitored (every ~24 days) at EPOC 5805 (University of Bordeaux) collecting both, *in situ* water/sediment samples for trace element analysis and the bottle samples from the automated samplers.

Calculations for trace element annual fluxes assume (i) constant trace element concentrations between sampling dates for reference flux calculations (***Equation 4***, e.g., Audry et al. 2004a, Lanceleur et al. 2011), or that (ii) the sporadic sampling campaigns are representative of the annual conditions for discharge-weighted calculations (***Equation 5***, e.g., Schäfer et al. 2002, Masson et al. 2011b).

**Equation 4:**

$$F_{X_d} = \sum_{i=1}^{365} Q_i \cdot X_d$$

$$F_{X_p} = \sum_{i=1}^{365} F_{SPMi} \cdot X_p \qquad for \qquad F_{SPMi} = Q_i \cdot SPM_i$$

**Equation 5:**

$$F_{X_d} = Q^{'} \left( \sum_{i}^{n} (Q_i \cdot X_d) \,/ \sum_{i}^{n} Q_i \right)$$

$$F_{X_p} = Q^{'} \left( \sum_{i}^{n} (F_{SPMi} \cdot X_p) \,/ \sum_{i}^{n} Q_i \right) \qquad for \qquad F_{SPMi} = Q_i \cdot SPM_i$$

where $F_{Xd}$ and $F_{Xp}$ are the dissolved and particulate annual fluxes of element *X* (t $y^{-1}$), $Q_i$ the daily (*i*) freshwater discharge ($m^3$ $s^{-1}$), Q' annual water discharge and $F_{SPMi}$ the daily SPM flux (t $y^{-1}$). Note that transformations to comply with the final flux units are not shown in these equations.

Similar values are obtained when both methods are applied for total (dissolved + particulate) annual flux calculations of Sb (2003-2016, ***Figure 65a***) and Te (2014-2017, ***Figure 65b***) from available concentrations in the Lot-Garonne River system (this work). It is possible that trace elements with high particulate affinity (e.g., Te) show more reliable total flux values with the method based on the daily approach (***Equation 4***) given its improved estimation of the particulate flux (***Figure 64***). Nevertheless, more data are needed to confirm this hypothesis. Thus, studies on Sb (relatively soluble) and Te (more particulate) biogeochemical behaviour in the Lot-Garonne River system presented in this work have relied on discharge-weighted annual flux calculations.

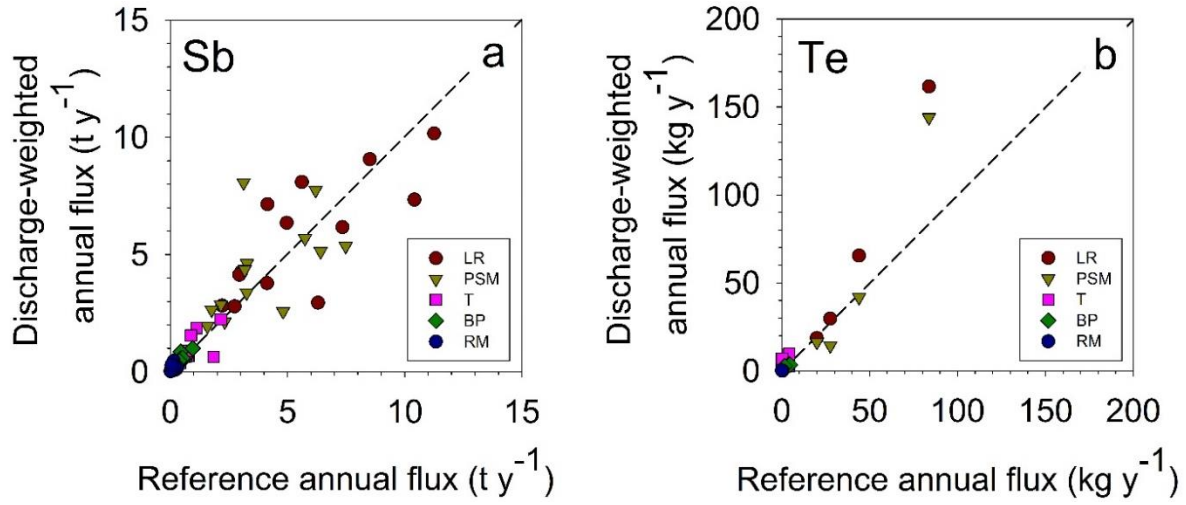


**Figure 65. Total annual fluxes of Sb and Te metalloids in the Lot-Garonne River system.** (a) Sb (2003-2016) and (b) Te (2014-2017).

## 2. Trace element solid/liquid equilibriums

### 2.1. Adsorption isotherms

The exchange of a substance between the dissolved and particulate phases is determined by the physical-chemical properties of the substance and the aquatic media conditions. This exchange has a kinetic component (i.e., fast or slow interaction) and eventually reaches a dynamic equilibrium (i.e., equal sorption and desorption rates) after sufficient contact time, as long as the initial conditions remain unchanged (Foo and Hameed 2010).

Appropriate modelling and thermodynamic considerations provide insights into the adsorption mechanisms (i.e., physisorption vs chemisorption), surface properties and sorption strength of these solid/liquid interactions (Foo and Hameed 2010, and references therein). Physisorption refers to physical adsorption processes governed by van der Waals type interactions (Gaspard 1982). Such interactions comprise energies of the order of $10^{-2}$ eV and are present at both submacroscopic (i.e., colloids) and macroscopic levels (i.e., solid agglomerations). Chemisorption involves interactions where true chemical bonds are formed (i.e., sharing of electrons), comprising energies of the order or greater than 1 eV (Gaspard 1982).

The Langmuir empirical model is the most common two-parameter isotherm employed to describe monolayer chemical saturation onto finite sites with no lateral interactions between adsorbed molecules (no “steric hindrance” or repulsive forces due to overlapping of electron clouds; Langmuir 1918). Thus, elements following Langmuir isotherms reflect homogeneous adsorption, with all sites

presenting equal affinities (***Figure 66a***; Foo and Hameed 2010). The mathematical equation for the Langmuir isotherm (***Equation 6***) is complemented with the dimensionless constant ($R_L$) also known as the separation factor or equilibrium parameter (***Equation 7***) defined by Weber and Chakravorti (1974):

**Equation 6:**
$$X_p = (X_{pmax} \cdot K_L \cdot X_d)/(1 + K_L \cdot X_d)$$

**Equation 7:**
$$R_L = 1/(1 + K_L \cdot X_{d0})$$

where $X_p$ is the concentration of element X in the particulate phase at equilibrium (mg $kg^{-1}$), calculated from the difference in dissolved concentrations between the initial spiked ($X_{d0}$) and the equilibrium ($X_d$) concentrations (µg $L^{-1}$) converted to particulate concentrations with the corresponding SPM ratio, $X_{pmax}$ is the maximum charge of X in the SPM and $K_L$ is the constant of Langmuir (L $\mu g^{-1}$). Values of $R_L$ (***Figure 66b***) indicate the adsorption nature of the isotherm as unfavourable ($R_L$>1), linear ($R_L$=1), favourable (0<$R_L$<1) and irreversible ($R_L$ = 0; Weber and Chakravorti 1974).

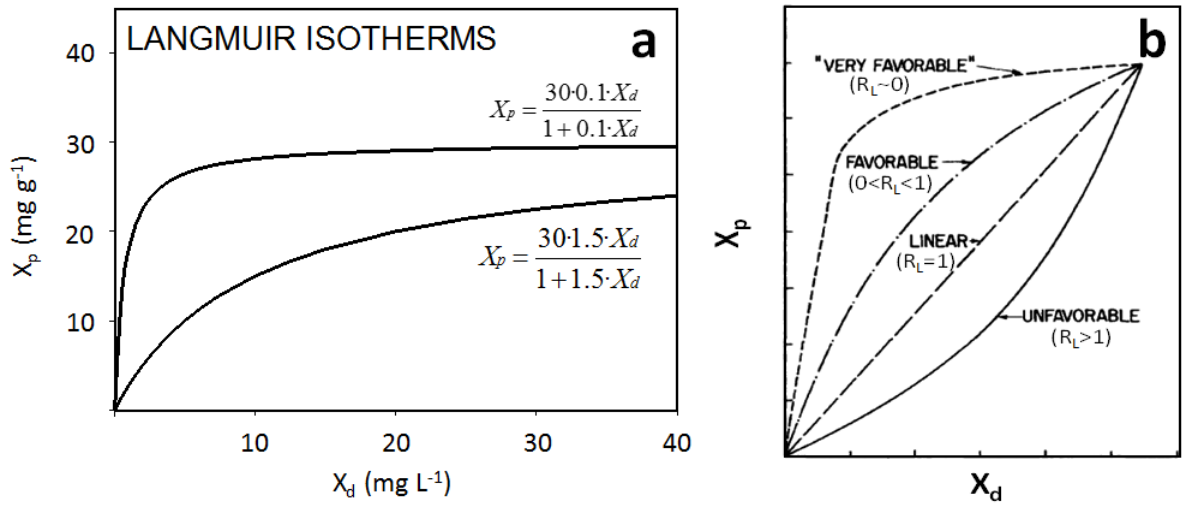


**Figure 66. Examples of Langmuir isotherms.** *Modified from (a) Sorption.ppt (University of Vermont) and (b) Weber and Chakravorti (1974).*

The Freundlich empirical model was the first one to describe heterogeneous (i.e., non-uniform distribution) multilayer adsorption onto a non-homogeneous surface (Freundlich 1907). In this case, stronger binding sites are occupied preferentially, decreasing the adsorption energy exponentially as they fill up (***Figure 67***; Zeldowitsch 1934). The mathematical expression of the Freundlich isotherm (***Equation 8***) represents the adsorption intensity by the $K_F$ constant (i.e., the higher the value the higher the affinity of element X for the particulate phase) and the surface heterogeneity with the *c* value (i.e., the closer to zero the more heterogeneous; Foo and Hameed 2010). When *c* = 1, the relationship between $X_p$ and $X_d$ is linear and $K_F$ equals Kd (i.e., the solid/liquid partition coefficient or distribution coefficient).

**Equation 8:**
$$X_p = K_F \cdot X_d^c$$

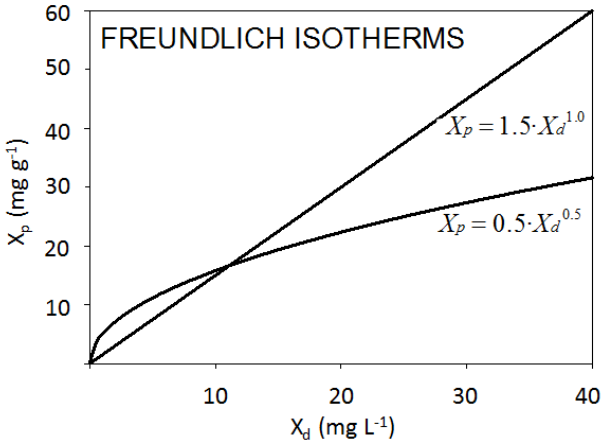


**Figure 67. Example of Freundlich isotherms.** *(Modified from Sorption.ppt, University of Vermont)*

### 2.2. Solid/liquid partition coefficient (Kd)

The partitioning coefficient (Kd) indicates the degree of affinity of an element for the particulate phase, i.e., the higher the Kd, the less easily the element will be transported in the dissolved phase. Such definition relies on two hypotheses (Filella 2011): (1) the operationally-defined distinction between "dissolved" and "particulate" phases, and (2) the existence of a C-type isotherm (i.e., constant ratio between dissolved and particulate concentrations at any trace element concentration), usually applicable for low trace element concentrations (Limousin et al. 2007). Moreover, Kd values generally depend on the abundance and speciation of the element, the time necessary to reach solid/liquid dynamic equilibrium, the particle nature and concentration, the presence of complexing ligands and ligand concentrations, and the biological activity (Ciffroy et al. 2009).

Briefly, Kd (in L kg$^{-1}$) is the particulate ($X_p$, mg kg$^{-1}$) to dissolved ($X_d$, mg L$^{-1}$) concentration ratio of a given element (X, ***Figure 68***). Total element concentrations ($X_T$) can be described as the sum of both $X_d$ and $X_p$. Due to the unit conversion between $X_d$ and $X_p$ involving SPM concentrations, Kd can be related to SPM when $X_p$ is described as a fraction (in percentage) of $X_T$ (***Figure 68***).

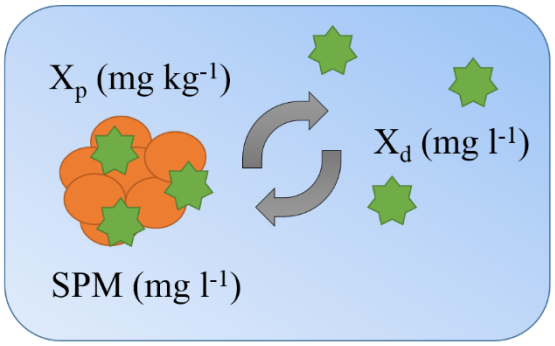


Particle

Metal X

$$K_d = \frac{X_p}{X_d} \qquad (\text{l kg}^{-1})$$

The greater $K_d$ the less soluble X is

$$X_T = X_p(SPM.10^{-6}) + X_d$$

$$\%X_P = \frac{X_p(SPM.10^{-6})}{X_T}$$

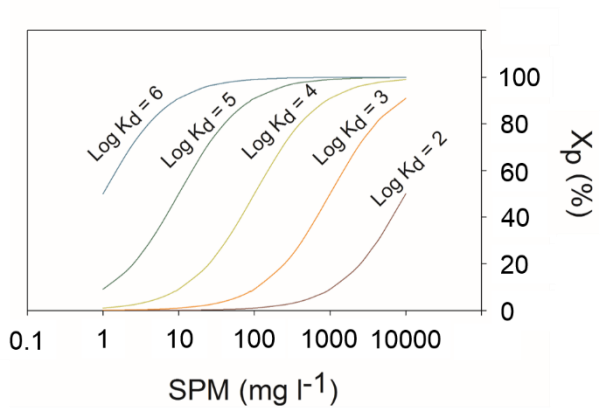


$$\%X_p = \frac{K_d(SPM.10^{-6})}{1 + K_d(SPM.10^{-6})}$$

**Figure 68. Solid/liquid partition coefficient or distribution coefficient (Kd).**

The study of trace element solid/liquid partitioning has three practical approaches (Sung 1995):

- **Field-based**: when Kd is calculated from collected and filtered aquatic environmental samples. This approach assumes that Kd reflects the environmental thermodynamic equilibrium of the target trace element during the sampling conditions.
- **Laboratory-based**: when Kd is calculated from natural samples in laboratory conditions, i.e., resulting from sorption experiments under controlled physical-chemical conditions (temperature, pH, etc.).
- **Controlled-based**: when the study of Kd is based on well-characterized (sometimes synthetic) solid surfaces and solution matrices in order to understand the reaction mechanisms. Nevertheless, this approach seems to be problematic when applying obtained Kd values to environmental conditions.

This work is based on both field-based and laboratory-based Kd values for Sb, Te and Se, generally expressed as $\log_{10}$ Kd. Such approach implies that (i) environmental Kd reflects in a certain way the

inherited solid/liquid distribution of the target element, including both lithogenic- and anthropogenic-based trace elements present in the system, whereas (ii) laboratory approaches rather indicate spiked Kd, simulating the potential solid/liquid distribution of anthropogenic discharges. Both approaches of Kd values provide necessary information for developing dispersion scenarios of Sb and Te radionuclides in aquatic systems.

## 3. Enrichment factors

### 3.1. Geoaccumulation index (I'geo)

Classical calculations of geochemical enrichment factors (EF) for a given element consisted in a simple comparison between the concentration of the element in the sample to that of the same element in the continental crust (e.g., average concentration in the Earth's crust given by the UCC, the Upper Continental Crust, Wedepohl 1995). A modern approach of the EF allowed to include the effect of grain size in trace element concentrations by normalising these to a conservative element (i.e., those almost exclusively influenced by the crustal sources), suggesting that elements showing EF values close to 1 corresponded to natural/crustal sources. This means that EF calculations allowed to compare different sites worldwide given the common reference values (e.g., UCC). Nevertheless, this method did not take into account local variations in geogenic element concentrations, often assigning studied sites as anthropogenically contaminated were, actually, the results were reflecting the naturally enriched geological composition of the area (Reimann and de Caritat 2000).

The geoaccumulation index ($I_{geo}$) was introduced by Müller (1969) to describe the degree of particulate contamination of a sample by normalising the contaminant concentration ($C_s$) by the local geochemical background ($B_s$), further transforming these geochemical data ($log_2$) in order to accommodate the comparison among different sites. Based on this $I_{geo}$, Lee et al. (2008) established a modified $I'_{geo}$ (***Equation 9***) including the potential bias of grain size effect on trace element concentrations at different sites (*s*) with the $M_z$ parameter. This work uses the $I'_{geo}$ given the highly variable transport energy and potential different particle sizes transported in river systems.

**Equation 9:**

$$I'_{geo} = \log_2(C_s/(1.5 \cdot B_s \cdot M_z))$$

where $C_s$ is the concentration of the examined element ($X_i$) at site *s*, 1.5 is a factor to account for background variations in the environment or small anthropogenic influences (Müller 1969), $B_s$ is the geochemical background of $X_i$ and $M_z$ refers to $M_{zC}/M_{zB}$ which is a proxy of the grain size ratio at the studied site ($M_{zC}$) to the reference area ($M_{zB}$). This index classifies soils/sediments into five types: class 1 ($I'_{geo} < 1$, unpolluted to moderately polluted), class 2 ($1 \leq I'_{geo} < 2$, moderately polluted), class 3 (2 ≤

$I'_{geo}$ < 3, moderately to strongly polluted), class 4 (3 ≤ $I'_{geo}$ < 4, strongly polluted), and class 5 ($I'_{geo}$ ≥ 4, strongly to very strongly polluted).

Particulate trace element concentrations are normalised in order to avoid potential grain-size effects as certain trace elements naturally show higher concentrations in smaller particles. This effect is due to the high surface area of exchange, i.e., more available adsorption sites, present in the small particles compared to bigger particles (Loring and Rantala 1992). Normalisation can be performed with several conservative elements, i.e., showing low (e.g., Al, Ti) or no anthropogenic influence (e.g., Sc) depending on the study site (Reimann and de Caritat 2000).

In the Garonne-Gironde fluvial-estuarine system, as in other rivers, thorium (Th) is a conservative lithogenic trace element indicating increasing concentrations with decreasing grain size, *i.e.* an adequate normalising element to correct grain size effects, particularly in silicate-dominated sediments (Krachler and Shotyk 2004; Larrose et al. 2010). Accordingly, we have calculated $I'_{geo}$ (***Equation 10***) using $Th_p$-normalised $X_p$ concentrations as follows:

$$I'_{geo} = \log_2 \left( \frac{\left(\frac{X_p}{Th_p}\right)_s}{1.5 \cdot \left(\frac{X_p}{Th_p}\right)_{ref}} \right)$$

**Equation 10:**

where the reference site for the regional natural geochemical background $(X_p/Th_p)_{ref}$ for studies in the Lot-Garonne-Gironde fluvial estuarine system is generally chosen at Marcenac (***Figure 38***), representative of the upstream Lot River watershed (Coynel et al. 2007a).

### 3.2. Bioaccumulation factor (BAF)

The trace element intake by biota from the dissolved phase into the organism is referred to the *bioavailable fraction* whereas the transfer from the solid phase into solution, rendering the trace elements bioavailable, is referred to the *bioaccessible fraction* (***Figure 69***). In any case, the amount of trace element incorporated by the organism at a given time is lower than the total external concentration. However, organisms can accumulate these trace elements within their tissues through time, concentrating in an integrative way the environmental trace element exposure levels.

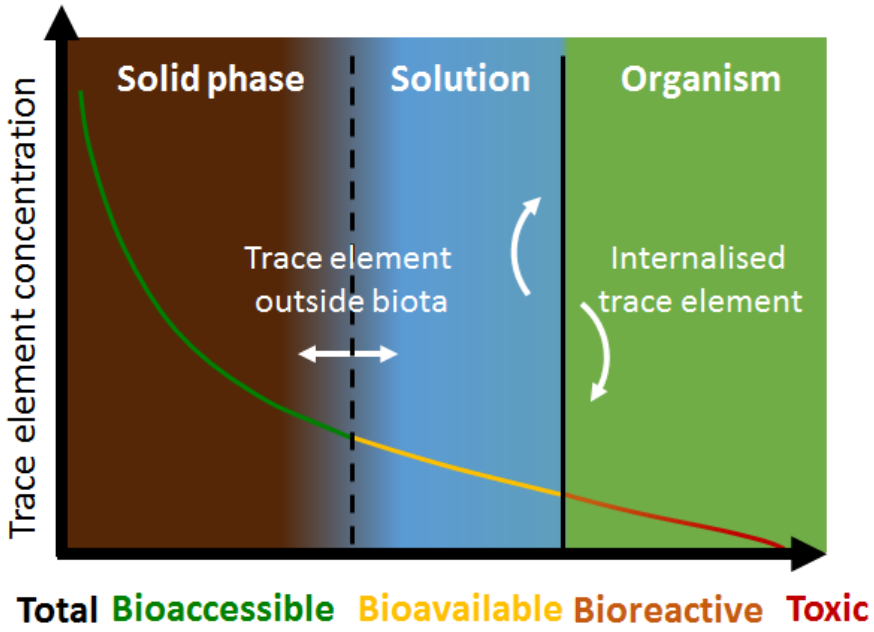


**Figure 69. Terminology of trace element transfer from particles and water into organisms.**

*(Modified from http://rotator.arhel.si/?page_id=5086).*

The bioaccumulation factor (BAF, ***Equation 11***) provides information on trace element biological incorporation and assimilation by an organism through all routes of exposure in natural conditions (i.e., diffusion, ingestion and respiration). It is defined as the ratio between the trace element in the organism's tissue compared to the surrounding concentration at steady state (USEPA 2000, Arnot and Gobas 2006).

**Equation 11:**

$$BAF = \frac{C_B}{C_W}$$

where $C_B$ is the trace element concentration in the organism (in mg $kg^{-1}$) and $C_W$ the dissolved trace element concentration in the water (mg $L^{-1}$), as in this media trace elements potentially show the highest bioavailable compounds compared to the particulate forms (e.g., Lekhi et al. 2008).

## VIII. CONCLUSION

The summary of all the applied methodologies in a single chapter compiles all the know-how acquired during this work and serves as a guideline on how to proceed from the sample uptake to the analysis of Sb, Se and Te in different environmental (i.e., water, sediment and biological samples) and laboratory-derived samples (e.g., isotopically labelled experiments and calculations). The presented descriptions of sampling strategies, sample analyses and data treatment will be integrated in further chapters to better understand the specific methodologies applied accordingly to each type of study. In any case, these methods allow to obtain reliable results for the following environmental interpretations on the biogeochemical behaviour of Sb, Te and Se in the Lot-Garonne-Gironde fluvial estuarine system and the Rhône River.

# CHAPTER 3:

# Biogeochemical behaviour of antimony in the Lot-Garonne-Gironde fluvial estuarine system

# I. INTRODUCTION

The aim of this chapter is to understand the biogeochemical cycle of environmental Sb in the Lot-Garonne-Gironde fluvial estuarine system at high spatial and temporal resolution scales. Combining Sb partition in both freshwater and brackish water with timescales of estuarine hydrological processes and radioactive decay, this chapter provides a qualitative approach to potential estuarine radionuclide dispersion. The present chapter relies on two publications: (i) the long-term monitoring of Sb geochemical behaviour in the freshwater reaches of the Lot-Garonne River system (*Environmental Chemistry*, 2018), and (ii) the second addressing Sb reactivity along the salinity and turbidity gradients of the Gironde Estuary (*Marine Chemistry*, 2016).

The first work analyses result from a long-term monitoring programme performed by the TGM team ("Transferts Géochimiques des Métaux à l'interface continent océan", EPOC 5805, University of Bordeaux), partly funded by the regional Adour-Garonne Water Agency (AEAG). This programme was established to follow-up and understand metal contamination in the Lot-Garonne River system. A 14-year database (2003-2016) of dissolved (<0.2 µm; $Sb_d$) and particulate ($Sb_p$) antimony concentrations has been analysed to understand long-term trends in Sb concentrations and fluxes as well as seasonal patterns at five strategic sampling points within the Lot-Garonne watershed. Additional collection of water samples <0.02 µm filter mesh size during 5 years (2003-2007) of the observation period, allowed to evaluate the relevance of the colloidal fraction in $Sb_d$ transport in this freshwater system. Comparison between upstream geochemical $Sb_p$ background concentrations and site-specific $Sb_p$ concentrations point towards potential anthropogenic Sb sources. Spatial and temporal variations in environmental Sb solid/liquid partitioning (Kd) provide necessary information for developing dispersion scenarios of Sb radionuclides in similar freshwater systems. The assessment of surface-specific Sb fluxes at the watershed scale and the establishment of annual average dissolved and particulate Sb fluxes into the Gironde Estuary complete this work.

The second study covers three estuarine sampling campaigns named MGTS ("Métaux Gironde Transfert et Spéciation"), also performed by the TGM team in 2014/2015. Sampling was performed along the salinity and turbidity gradients of the Gironde Estuary during three contrasting hydrological conditions, i.e., drought, intermediate and flood discharges (MGTS I-III). A comparative study site in the transition waters of the Arcachon Bay (hydrologically independent from the Gironde Estuary) is also presented. The aims of this study are (i) to document and understand Sb reactivity in the highly turbid transition waters of the Gironde Estuary, (ii) to identify the potential influence of water discharges and suspended particulate matter (SPM) hydrodynamics on estuarine Sb reactivity, and (iii) to classify the Gironde Estuary in a global context by comparing the observed Sb behaviour to that registered in other transition systems worldwide. Furthermore, this paper presents estuarine Sb Kd

values and the first preliminary Sb radionuclide dispersion scenarios for potential accidental releases from the Blayais nuclear power plant in the Gironde Estuary during low and high water discharge conditions.

## 1. Biogeochemical behaviour of antimony in the freshwater domain of the Gironde estuary.

*Manuscript published in Environmental Chemistry (2018)*

# Antimony in the Lot-Garonne river system: a 14-year record of solid-liquid partitioning and fluxes

Teba Gil-Díaz, Jörg Schäfer*, Alexandra Coynel, Cécile Bossy, Lionel Dutruch, Gérard Blanc

*Université de Bordeaux, UMR CNRS 5805 EPOC, Allée Geoffroy Saint-Hilaire, 33615 Pessac, France*

* Corresponding author: jorg.schafer@u-bordeaux.fr

## ABSTRACT

Knowledge on the environmental chemistry of antimony (Sb) in aquatic systems is limited and a better understanding of its geochemical behaviour is needed. Based on a fourteen-year survey (2003 – 2016) with monthly measurements of dissolved and particulate Sb at five sites in the Lot-Garonne River system, combined with daily measurements of water discharge and suspended particulate matter, this work characterises Sb behaviour in the upstream major river watershed of the Gironde Estuary. The survey provides a first regional geochemical Sb background in the Garonne River watershed for dissolved (~0.2 µg $L^{-1}$) and Th-normalised particulate Sb ($Sb_p/Th_p$~0.25) concentrations. Observed decreasing temporal trends (<1 ng $L^{-1}$ in dissolved and <0.02 mg $kg^{-1}$ in particulate concentrations per month) at sites representing natural concentrations probably reflect global atmospheric Sb dynamics at the watershed scale. Regular seasonal cycles of solid/liquid partitioning, with high solubility in summer (matching high dissolved and low particulate concentrations), reflect water discharge and suspended particulate matter transport dynamics and possibly seasonal (bio-)geochemical processes. Furthermore, this coefficient decreases from the river to the estuarine reaches (from average $\log_{10} K_d$ 4.3 to minimum 3.7 L $kg^{-1}$) suggesting an increased solubility of Sb in estuarine systems. Flux estimates indicate the relevance of the dissolved fraction in Sb transport (with negligible influence of the colloidal fraction) and a total flux (dissolved + particulate) entering the Gironde Estuary of 5.66 ± 2.96 t $y^{-1}$ (~50% particulate). These results highlight the importance of timescales and environmental parameters for future understanding of Sb biogeochemistry.

***Keywords:*** colloidal fraction, distribution coefficient, Gironde Estuary, temporal series, watershed scale

# 1. INTRODUCTION

Antimony (Sb) is a ubiquitous element in the environment, but its biogeochemical cycle is poorly understood (Filella et al. 2003). Its presence in the environment is both natural, as a component of the Earth's crust (~0.20 – 1.00 mg $kg^{-1}$; Saleh and Wilson 1999), and anthropogenic, mainly related to mining and smelting activities, coal combustion, manufacturing or disposal of glassware, ceramics, plastics, flame retardants, fireworks, and ammunition (USGS 2015; Filella et al. 2002*a*). In aquatic systems, dissolved Sb ($Sb_d$) concentrations are generally ≤ 1 µg $L^{-1}$ in non-polluted freshwater (Filella et al. 2002*a*; Filella et al. 2003) but may reach several hundreds of µg $l^{-1}$ in contaminated areas (He et al. 2012; Resongles et al. 2015). Estimated world average values vary from 0.1 µg $L^{-1}$ (Reimann et al. 2010) to ~1 µg $L^{-1}$ (Filella et al. 2002*a*; Martin and Whitfield 1983) for surface freshwaters and is 0.2 µg $L^{-1}$ for seawater (Filella et al. 2002*a*; Reimann et al. 2010). In sediments, particulate Sb concentrations ($Sb_p$) often range from 0.5 to 2 mg $kg^{-1}$ and rarely exceed 1,000 mg $kg^{-1}$ (Filella et al. 2002*a*; Filella et al. 2003; Wedepohl 1973), being 2.5 mg $kg^{-1}$ the estimated world average in river stream sediments (Martin and Whitfield 1983).

Environmental studies on Sb usually focus on: (i) contaminated environments, *i.e.*, mostly mining areas (*e.g.*, Fu et al. 2016; He et al. 2012), shooting ranges (*e.g.*, Heier et al. 2010), copper smelters or industrial sites (Filella et al. 2002*a*; He et al. 2012), and (ii) the Sb mobility-driving processes from these contaminated areas, related to *e.g.*, underground water transport and speciation (*e.g.*, Fawcett et al. 2015; Hu et al. 2017), effect of redox changes (*e.g.*, Hockmann et al. 2014) and remediation techniques (*e.g.*, Okkenhaug et al. 2016). Thus, few studies concern natural Sb dynamics (Filella et al. 2002*a*; Reimann et al. 2010; Wilson and Webster-Brown 2009). The triggering factor for these studies is the consideration of Sb as a pollutant of priority interest in many European and American regulations (EC 2006; DFG 2012; USEPA 2013) and the expected parallelism to arsenic (As) behaviour (Asaoka et al. 2012; Resongles et al. 2015; Wilson and Webster-Brown 2009). To the best of our knowledge, there are no works on long-term monitoring on $Sb_d$ and $Sb_p$ freshwater concentrations (*i.e.*, system-instant dynamics independent from sediment core-related time series) except for a short (3-year period) study of Ollivier et al. (2011) in the Rhône River. This means that the spatial distribution and behaviour of Sb in environmental studies is usually addressed by more or less frequent sporadic measurements which are generally not followed up over time. Consequently, there is a general lack of knowledge on the temporal dynamics of Sb in surface water, average characteristics, historical or continuous sources/sinks and representativeness of short-term samplings in a given area, complementary to the spatial dimension (Ollivier et al. 2010).

In this study, we present $Sb_d$ and $Sb_p$ concentrations and fluxes at five sites in the Lot-Garonne-Gironde fluvial-estuarine system covering 14 years (2003 - 2016) of observation. The influence of physico-chemical variables such as temperature, pH, conductivity and redox, as well as river discharge (Q) and suspended particulate matter (SPM) concentrations on $Sb_d$ (<0.2 µm), colloidal $Sb_d$ (0.02-0.2

µm) and $Sb_p$ concentrations and partitioning ($K_d$) is addressed to better understand Sb behaviour and transport in one of Europe's main fluvial-estuarine systems at both the annual and seasonal timescales. The main objective of the study is to improve our understanding of the geochemical behaviour, transport and fate of Sb in the freshwater reaches of temperate rivers as a prerequisite for future Sb transport/dispersion models at fluvial continent-ocean interfaces.

## 2. EXPERIMENTAL

### 2.1. Study area

In France, four main river systems (the Rhône River, the Seine, the Loire and the Gironde Estuaries) discharge freshwater and particles into the marine environment. The Gironde fluvial-estuarine system, located in the SW of France (Fig. 1), constitutes the biggest estuary in Europe with a watershed area (A) of approximately 81,000 $km^2$ (Schäfer et al. 2002). The main tributaries of the Gironde Estuary are the Garonne and Dordogne Rivers, respectively contributing ~64% and ~31% to the total freshwater discharge (Q; average ~1000 $m^3 s^{-1}$; DIREN 2015) and ~74% and ~22% to the average SPM flux ($F_{SPM}$; ~1 – 3 Mt $y^{-1}$) into the estuary (Jouanneau and Latouche 1982; Schäfer et al. 2002). In particular, the Garonne River drains a watershed area of ~57,000 $km^2$, with average Q = 19 ± 4.8 $km^3 y^{-1}$ (between 1959 – 2014; DIREN 2015) and average $F_{SPM}$ = 1.38 ± 1.05 Mt $y^{-1}$ (between 1994 – 2012, unpubl. data).

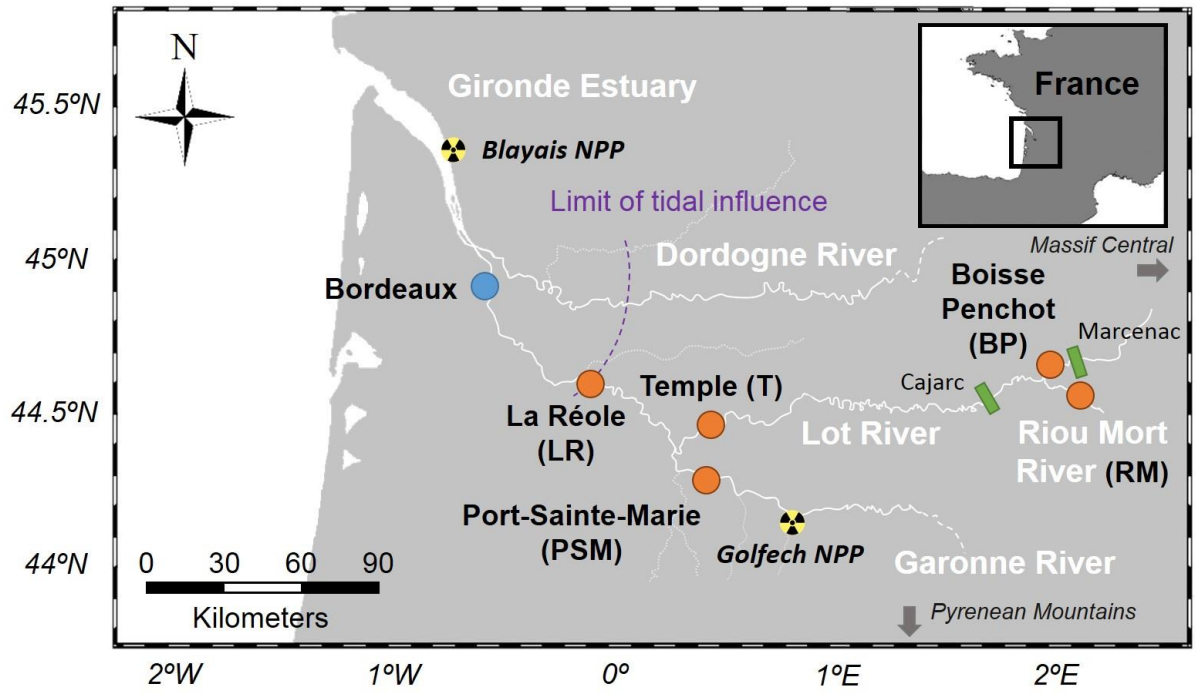


**Figure 1.** Map of the Gironde Estuary and its main river systems (Dordogne and Garonne Rivers). One of the biggest cities in the area (Bordeaux) and the sampling sites along the Garonne River (LR, PSM, T, BP and RM) are shown together with the location of two sediment cores from the watershed (Marcenac and Cajarc reservoir lakes; Coynel et al. 2007*a*) and two nuclear power plants (NPPs) in the area (Golfech and Blayais NPPs).

The Lot-Garonne-Gironde fluvial-estuarine system (Fig. 1) has been affected since the mid-19$^{th}$ century by multiple metal contamination (mainly zinc, Zn, and cadmium, Cd) due to several point sources related to 1) open-pit coal mining, 2) Zn ore smelting and 3) coal-fired power production in the area of Decazeville in the Riou Mort River watershed (a tributary of the Lot-Garonne River system; Audry et al. 2004*b*; Blanc et al. 1999; Coynel et al. 2009; Grousset et al. 1999; Lapaquellerie et al. 1995). The contaminating metallurgical (*i.e.*, thermal-extraction) activities ended in 1987, but metal exportation from the industrial area, including Sb, continues due to the drainage and erosion of both landfills containing coal ashes from the former power station and tailings from the ore treatment plant. Recent emissions still result in high dissolved and particulate Sb concentrations in the river system (*i.e.*, up to 6 µg $L^{-1}$ and 53 mg $kg^{-1}$), especially during intense remobilisation processes such as extreme flood events (Coynel et al. 2007*b*). These flood events, together with lock/floodgate or dam construction works in the Lot River, imply a risk of downstream transport due to resuspension of contaminated sediment, as sediment reservoirs (as observed in the Cajarc sediment core, located downstream the original contamination source of Decazeville, Fig. 1) record historical pollution ($Sb_p$ concentrations > 10 mg $kg^{-1}$; Coynel et al. 2007*a*) in deep sediments corresponding to the 1950-1970 period exported from the Riou Mort watershed.

Natural sources of Sb in the area are ore deposits and former sulphide ore mining areas in the upper reaches of both the Garonne and the Lot River watersheds (BRGM 2014; Masson et al. 2009*b*; Masson et al. 2011). A reservoir sediment core upstream in the area (at Marcenac site, upstream from the Riou Mort confluence, Fig. 1) provide records of background-level undisturbed particulate metal concentrations, suggesting regional Sb background concentrations of 1.63 ± 0.24 mg $kg^{-1}$ (Coynel et al. 2007*a*).

## 2.2. Sampling sites and sampling strategy

The Lot-Garonne-Gironde fluvial-estuarine system has been continuously monitored since 1990 as part of a long-term decontamination monitoring programme, especially for Cd (with complete Sb data since 2003), from the source at the Riou Mort River until the estuarine freshwater reaches (at La Réole, in the Garonne River). Consequently, this study comprises five sampling sites representative of the Lot-Garonne River system (Fig. 1): (1) "Boisse Penchot" (BP) on the Lot River, upstream the confluence with the Riou Mort River (representative of upstream Lot and Massif Central inputs), (2) "Riou Mort River" (RM) at the outlet of the small watershed hosting the identified major anthropogenic point sources, (3) "Temple" (T), a hydroelectric reservoir at the outlet of the Lot River watershed indicative of the Lot River input to the Garonne River, (4) "Port-Sainte-Marie" (PSM) on the Garonne River upstream of the Lot River confluence (*i.e.* representative of inputs from the Garonne watershed including the city of Toulouse and the Pyreneans) and (5) "La Réole" (LR), on the downstream Garonne River, representing the main fluvial entry into the Gironde Estuary). The selection criteria imply that the

sampling sites are representative of each individual sub-watershed contribution to the final downstream flow towards the Gironde Estuary. The average contributions to annual water discharge at La Réole are 69% from PSM, 26% from T, 22% from BP and 0.2% from RM (DIREN 2015). In a natural system, the sum of BP and RM water fluxes should match values registered at T but in this study the water discharge controlled at the reservoir in T could explain the observed difference.

From 2003 to 2016, these sampling sites were periodically monitored (every ~24 days, with additional sampling during floods) to collect data on physico-chemical parameters (water temperature, conductivity, pH and redox potential) and water/sediment samples (N = 242 at LR; N = 231 at PSM; N = 232 at T; N = 219 at BP; N = 243 at RM) for $Sb_d$ and $Sb_p$ analyses. Daily water samples for SPM concentration analysis were performed by hand (1 sample per day) or by automated samplers (SIGMA 900P, American Sigma, Colorado) collecting continuously, every 3 hours, samples for 1L daily pools as described in Coynel et al. (2009).

Water samples for $Sb_d$ analyses were retrieved manually using a telescopic arm (~0.5 m depth, 1 m from the river bank) in acid-cleaned 1 L polypropylene (PP) bottles, previously rinsed 3-times with water from the site. Samples were immediately filtered onsite for $Sb_d$ (0.2 µm Minisart® cellulose acetate; 2003 – 2016 whole period) and for the "truly dissolved" $Sb_{0.02}$ fraction (0.02 µm Anotop 25 Whatman™; only between 2003 – 2007) into acid-washed polypropylene (PP) 30 mL bottles (previously rinsed with an aliquot of the filtrate), acidified with $HNO_3$ (1/1000 v/v; J.T. Baker ultrapure, 14 M) and stored at 4ºC in the dark pending analysis. Suspended particulate matter for $Sb_p$ analyses were collected at 1 m from the river bank and 0.5 m depth into 40 L acid-washed polyethylene (PE) drums (previously rinsed with water from the site) using a PP peristaltic pump and tubing. Particles were retrieved by centrifugation of up to 80 L (Westfalia 12,000 g), then oven-dried (50ºC), homogenised (grinded in agate mortars) and stored at room temperature in the dark until analysis as described elsewhere (Coynel et al. 2009; Schäfer and Blanc 2002).

### 2.3. SPM concentration and physico-chemical parameters

Suspended particulate matter (SPM) concentrations were determined by filtering precise volumes of water through dry pre-weighed filters (Xilab glass microfiber, 0.7 µm), drying the filters to constant weight at 50ºC and re-weighed (Schäfer and Blanc 2002). TetraCon 96® probe (PROFILINE, WTW) was used for *in situ* water temperature and conductivity measurements and a Sentix ® 41 probe (PROFILINE, WTW) for pH, previously calibrated using the manufacturer's specifications and supplied reagents (NIST pH standards). The redox potential of the water (Eh) was measured with a PH-25 CRISON® probe.

## 2.4. Particulate and dissolved Sb analysis

Total sediment digestions for $Sb_p$ and particulate thorium ($Th_p$) were performed with representative subsamples (*i.e.,* 30 mg) in closed PP tubes (DigiTUBEs®, SCP SCIENCE) in a heating block (2 h at 110 ºC) using 1.5 mL HCl (10 M Suprapur®, Merck), 750 µL $HNO_3$ (14 M Suprapur®, Merck) and 2.5 mL HF (29 M Suprapur®, Fisher), as described elsewhere (Schäfer et al. 2002). After evaporation to dryness, re-dissolution with 250 µL $HNO_3$ (14 M) was performed in the heating device and, after cooling, the samples were brought to 10 mL using Milli-Q water.

Concentrations of $Th_p$, $Sb_p$ and $Sb_d$ were quantified by ICP-MS (XSeries 2, THERMO) using external calibration. Other elements such as Cd, Zn, lead (Pb) and As have also been measured but their time series will not be discussed herein, only their relationship to Sb when appropriate, to identify common sources or processes taking place in the Lot-Garonne River system. Parallel digestion and analyses of sediment Certified Reference Materials (CRM: PACS-1 (N=9), IAEA-433 (N=15), NCS DC 70311 (N=28), NCS DC 70317 (N=38), NIST SRM 8704 (N=25); Table S1, Supplementary Data) produced results that differed by less than 4% from the certified ranges with precisions of < 10% R.S.D. Figures of merit for $Sb_d$ analyses were assessed by analysing freshwater CRM (TM RAIN-95 (N=33), TM RAIN-04 (N=84), SLRS-4 (N=159), SLRS-5 (N=165), SLRS-6 (N=20); Table S1, Supplementary Data), suggesting that the obtained results differed by less than 10% from the certified ranges with precision being < 15% R.S.D.

**Table S1.** Record of Certified Reference Materials (CRM) used during the 2003 to 2016 period for validation of particulate (PACS-1, IAEA-433, NCS DC 70311, NCS DC 70317, NIST SRM 8704) and dissolved (TMRAIN-95, TMRAIN-04, SLRS-4, SLRS-5, SLRS-6) Sb analyses.

| Matrix | CRM | Units | Certified | Measured | |
|---|---|---|---|---|---|
| | | | Mean ± SD | Mean ± SD | Replicates |
| Marine sediment | PACS-1 | mg $kg^{-1}$ | 171 ± 14 | 182 ± 19 | N = 9 |
| Marine sediment | IAEA-433 | mg $kg^{-1}$ | 1.96 ± 0.18 | 1.71 ± 0.08 | N = 15 |
| Rock powder | NCS DC 70311 | mg $kg^{-1}$ | 13.8 ± 0.8 | 15.1 ± 1.2 | N = 28 |
| Rock powder | NCS DC 70317 | mg $kg^{-1}$ | 4.44 ± 0.44 | 5.00 ± 0.51 | N = 38 |
| River sediment | NIST SRM 8704 | mg $kg^{-1}$ | 3.07 ± 0.32 | 2.74 ± 0.28 | N = 25 |
| Rain water | TMRAIN-95 | µg $L^{-1}$ | 0.35 ± 0.10 | 0.40 ± 0.03 | N = 33 |
| Rain water | TMRAIN-04 | µg $L^{-1}$ | 0.35 ± 0.07 | 0.32 ± 0.03 | N = 84 |
| River water | SLRS-4 | µg $L^{-1}$ | 0.23 ± 0.04 | 0.28 ±0.03 | N = 159 |
| River water | SLRS-5 | µg $L^{-1}$ | 0.3* | 0.28 ± 0.04 | N = 165 |
| River water | SLRS-6 | µg $L^{-1}$ | 0.34 ± 0.01 | 0.32 ± 0.02 | N = 20 |

*informational value

## 2.5. Modified geoaccumulation index ($I'_{geo}$)

The geoaccumulation index ($I_{geo}$) introduced by Müller (1969) describes the degree of contamination of a sample by normalising ($C_s/B_s$) and transforming ($\log_2$) the geochemical data, which accommodates the comparison among different sites. Based on this $I_{geo}$, Lee et al. (2008) established the modified $I'_{geo}$ (Equation - 1) taking into account the possible grain size effect on trace element concentrations at different sites (*s*). Given the highly variable transport energy and particle sizes transported in river systems, we decided to use this modified $I'_{geo}$:

$$I'_{geo} = \log_2(C_s/(1.5 \cdot B_s \cdot M_z)) \quad (1)$$

where $C_s$ is the concentration of the examined element ($X_i$) at site *s*, 1.5 is a factor to account for background variations in the environment or small anthropogenic influences (Müller 1969), $B_s$ is the geochemical background of $X_i$ and $M_z$ refers to $M_{zC}/M_{zB}$ which is a proxy of the grain size ratio at the studied site ($M_{zC}$) to the reference area ($M_{zB}$). This index classifies soils/sediments into five types: class 1 ($I'_{geo} < 1$, unpolluted to moderately polluted), class 2 ($1 \leq I'_{geo} < 2$, moderately polluted), class 3 ($2 \leq I'_{geo} < 3$, moderately to strongly polluted), class 4 ($3 \leq I'_{geo} < 4$, strongly polluted), and class 5 ($I'_{geo} \geq 4$, strongly to very strongly polluted).

In the Garonne-Gironde fluvial-estuarine system, as in other rivers, Th is a conservative lithogenic trace element indicating increasing concentrations with decreasing grain size, *i.e.* an adequate normalising element to correct grain size effects (Krachler and Shotyk 2004; Larrose et al. 2010). Accordingly, we have calculated $I'_{geo}$ (Equation - 2) using $Th_p$-normalised $Sb_p$ as follows:

$$I'_{geo} = \log_2\left(\frac{\left(\frac{Sb_p}{Th_p}\right)_s}{1.5 \cdot \left(\frac{Sb_p}{Th_p}\right)_{ref}}\right) \quad (2)$$

where the average of $Sb_p/Th_p = 0.18$ observed in the Marcenac core served as reference $(Sb_p/Th_p)_{ref}$ for the regional natural (previous to anthropogenic activity) geochemical background (Coynel et al. 2007*b*).

## 2.6. Distribution coefficient ($K_d$)

Antimony partitioning between dissolved and particulate phases was evaluated using the particle-water distribution coefficient ($K_d$), described in Sung (1995). Briefly, $K_d$ (in L $kg^{-1}$) is calculated by dividing the particulate concentration (mg $kg^{-1}$) by the dissolved (mg $L^{-1}$) concentrations (Equation - 3). The ratio between $Sb_p$ and the total Sb ($Sb_T$, comprising both $Sb_d$ and $Sb_p$, Equation - 4) indicates the fraction of $Sb_p$ (%) (Equation - 5).

$$K_d = Sb_p/Sb_d \quad (3)$$

$$Sb_T = Sb_p \cdot SPM + Sb_d \quad (4)$$

$$Sb_p(\%) = \left(Sb_p \cdot SPM\right)/Sb_T = (K_d \cdot SPM)/(1 + K_d \cdot SPM) \quad (5)$$

where $Sb_p$ is expressed in mg $kg^{-1}$, $Sb_d$ in mg $L^{-1}$, $Sb_T$ in mg $L^{-1}$ and SPM in kg $L^{-1}$. Note that Equation - 5 must be multiplied by 100 to have a percentage.

## 2.7. Annual flux calculations

Historical records on daily river discharges were obtained from the National Hydrographic Databank (DIREN 2015, *http://www.hydro.eaufrance.fr/*). Annual $Sb_d$ (Equation - 6) and $Sb_p$ (Equation - 7) fluxes were calculated for each site by combining these hydrological data with $Sb_d$, $Sb_p$ and SPM concentrations measured every ~24 days, using commonly applied equations (Audry et al. 2004*b*; Masson et al. 2006; Meybeck et al. 1994; Meybeck and Ragu 1995; Webb et al. 1997) for discharged-weighted concentrations as follows:

$$F_{Sb_d} = Q'(\sum_i^n (Q_i \cdot Sb_d) \,/\, \sum_i^n Q_i) \quad (6)$$

$$F_{Sb_p} = Q'(\sum_i^n (F_{SPMi} \cdot Sb_p) \,/\, \sum_i^n Q_i) \qquad for \qquad F_{SPMi} = SPM_i \cdot Q_i \quad (7)$$

where $F_{Sbd}$ and $F_{Sbp}$ are the dissolved and particulate discharge-weighted annual fluxes (t $y^{-1}$), $Q_i$ the daily average water discharge ($m^3$ $s^{-1}$) of the sampled day ($i$), Q' the annual water discharge (annual mean of $Q_i$ for $i_{1\rightarrow365}$) and $F_{SPMi}$ the daily SPM flux (t $y^{-1}$), for an annual database of size $n$ ($n \leq 365$ days). Note that transformations to comply with the final flux units are not indicated in these equations. Annual watershed surface-specific total Sb fluxes (mg $m^{-2}$ $y^{-1}$) were calculated to compare the different sub-watersheds.

## 2.8. Statistical analysis

Data did not satisfy normality (Shapiro-Wilk and Kolmogorov-Smirnov tests) and homoscedastic (Levene's test) conditions, not even after data transformation, due to positively skewed distribution frequencies at all sites. Anomalous data (high Sb concentrations) were identified by the Median Absolute Deviation (MAD; Leys et al. 2013) for a *b* value of 1.4826 and a moderately conservative stringent criterion (median ± 2.5*MAD). The MAD was also used to describe the variability for the median (median ± MAD) as an equivalent of the standard deviation to the mean. Non-parametric ANOVA tests (Kruskal-Wallis and post-hoc Dunn's tests) were performed when comparisons of the median among sites were required.

The $Sb_d$ and $Sb_p$ concentration time series were decomposed applying the additive method (appropriate when the magnitude of the seasonal fluctuations is constant along the temporal trend) in SPSS 15.0 and R-CRAN 3.3.1 to study the trend, seasonality (SeAsonal Factor, SAF) and random (Error, ERR) components of a non-stationary series. The significance of the temporal trends was

evaluated by Mann-Kendall and Sen's Slope non-parametric tests after confirming independence of data over time (*i.e.*, there is no serial correlation in the dataset). The magnitude of the seasonal component was compared among sites with the SAF (which indicates how much the Sb concentrations are above or below the monthly average if the latter had no trend over time). Linear relationships among variables (either concentrations or physical parameters) were verified by Pearson correlations, accepting correlation coefficients of $|r| > 0.5$ for both 95% and 99% confidence.

## 3. RESULTS

### 3.1. Antimony concentrations and distribution frequencies

The 14-year database on $Sb_d$ and $Sb_p$ concentrations showed positively skewed distribution frequencies at all sites (*i.e.*, some sporadic events contribute with anomalously high concentrations, disrupting the normal distribution of the series at each of the sites; *e.g.*, for LR database in Fig. S1a-d, Supplementary data). Anomalous concentrations identified by MAD included $Sb_d$ concentrations > ~0.25-0.30 µg $L^{-1}$ and $Sb_p$ concentrations > ~5-7 mg $kg^{-1}$ for LR, PSM, T and BP (representing 8-15% of the $Sb_d$ or $Sb_p$ datasets per site), and $Sb_d$ > ~2 µg $L^{-1}$ and $Sb_p$ > ~25 mg $kg^{-1}$ for RM (*i.e.*, 21% of $Sb_d$ or $Sb_p$ dataset). When these data were erased from the database (Fig. S1e,f, Supplementary data), bimodal distributions explained the skewed original asymmetry for $Sb_d$ concentrations > ~0.16-0.20 µg $L^{-1}$ and $Sb_p$ concentrations > ~3.5-5 mg $kg^{-1}$ for LR, PSM, T and to a lesser extent BP (*i.e.*, 11-33% and 11-23% of the remaining $Sb_d$ and $Sb_p$ datasets per site, respectively, highest in LR). At the RM site, the respective results were $Sb_d$ > ~1.25 µg $L^{-1}$ and $Sb_p$ > ~17 mg $kg^{-1}$ (*i.e.*, 13-15% of the remaining $Sb_d$ or $Sb_p$ dataset). When comparing high Sb concentrations (anomalous and bimodal cases) among sites over time, certain patterns occur, though not systematically, especially for the first years of the survey (2003 to 2010). That is, ~70% of the high $Sb_d$ concentrations at LR generally matched those at PSM (*i.e.*, upstream Garonne) during all the year, with an additional ~25% contribution to LR $Sb_d$ concentrations from T(+BP) (*i.e.*, Lot River) from late summer to early winter (*i.e.*, June to December). High $Sb_p$ concentrations at LR matched in ~65% of the cases those from T+BP(+RM), throughout most of the year (October to May) with PSM contributing ~ 15% generally during winter-spring (December to April). Such Sb contributions to LR took place during both "average" and high Q and SPM conditions (defining "average" conditions at LR as $Q < 900$ $m^3$ $s^{-1}$ and SPM < 50 mg $L^{-1}$; Fig. S1g,h, Supplementary data). The rest of the anomalies observed at the other sites either showed intra-riverine influences (*e.g.*, site T affected by high Sb from RM or BP or both) that were not observed at LR, or responses to local high Q and SPM conditions (not necessarily observed at LR).

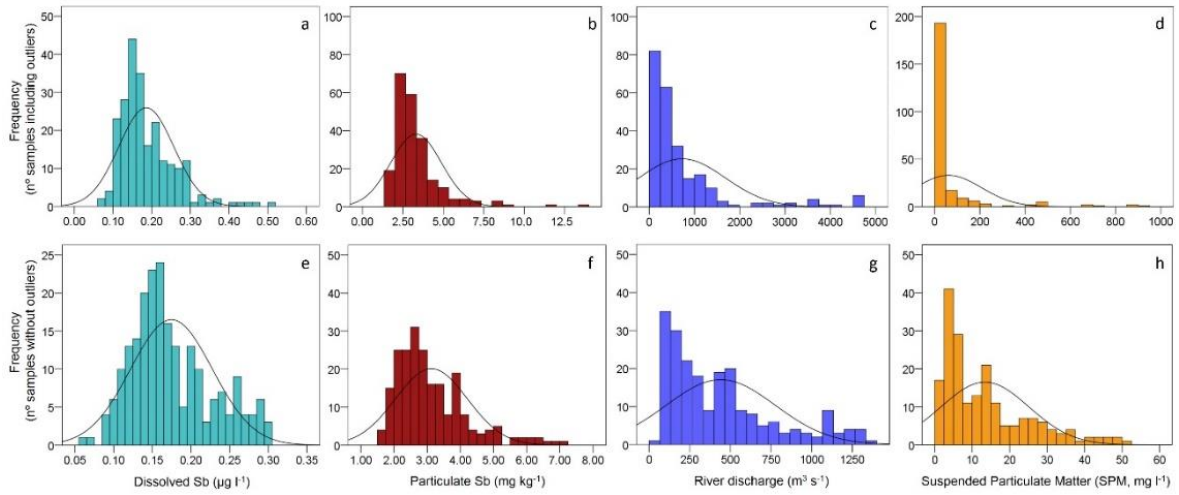


**Figure S1.** Distribution frequency histograms of dissolved Sb (µg $L^{-1}$) and particulate Sb (mg $kg^{-1}$) concentrations, with average daily river discharge ($m^3$ $s^{-1}$) and suspended particulate matter (mg $L^{-1}$), for the whole database at La Réole (from 2003 to 2016): with outliers (a - d) and without outliers (e – h). Corresponding expected Gaussian distributions overlapping each histogram are also shown.

This skewness also implies that the arithmetic mean ± standard deviation (SD) concentrations are not completely representative of the average conditions, thus median ± MAD concentrations are also given (Table 1). In general, the Lot River sites (T and BP) showed significantly ($p < 0.05$) lower $Sb_d$ and higher $Sb_p$ concentrations than the Garonne River sites (LR and PSM). All sites (except for LR and PSM) had significantly different average $Sb_d$. For $Sb_p$ no significant differences ($p < 0.05$; as $Sb_p/Th_p$ ratios) occurred when comparing sites along the same river (*i.e.*, median $Sb_p/Th_p$ ratios are not different between BP and T, nor between LR and PSM). In any case, RM always showed higher concentrations and significant differences with all sites. The observed average physico-chemical parameters are also given in Table 1.

### 3.2. Antimony temporal trends

The 14-year time series showed comparable trends between LR, PSM, T and BP (to a lesser extent for $Sb_d$ at BP; Fig. 2). All data showed maximum values during 2006-2007 and a minimum during 2013-2014 (especially for $Sb_d$). The statistical study of the time series (14 years) indicated significant (p-value < 0.05) increasing (before 2008, except for $Sb_p$ at LR, T and BP due to the high variability) and decreasing (after 2008) trends of the order of ~0.6-1 ng $L^{-1}$ per month for $Sb_d$ and ~0.02 mg $kg^{-1}$ per month for $Sb_p$ for all sites except at the RM site (Fig. 3). where no significant trend occurred for neither $Sb_d$ nor $Sb_p$ temporal series. Moreover, all sites showed regular $Sb_d$ seasonal cycles with highest variations above the average in August/September (SAF of 1.22 µg $L^{-1}$ in RM, ~0.08 µg $L^{-1}$ in LR, PSM and T, and 0.02 µg $L^{-1}$ in BP) and below the average in February/March (SAF roughly 0.55 µg $L^{-1}$ lower than the average in RM, ~0.05 µg $L^{-1}$ in LR, PSM and T, and ~0.03 µg $L^{-1}$ in BP).

**Table 1. Physico-chemical parameters and Sb concentrations.** Mean values ± standard deviations (SD) of physico-chemical parameters, river discharge (Q) and suspended particulate matter (SPM) concentrations from 2003 to 2016 at five sampling sites in the Lot-Garonne river system: La Réole (LR), Port-Sainte-Marie (PSM), Temple (T), Boisse Penchot (BP) and Riou Mort (RM). Dissolved ($Sb_d$) and particulate ($Sb_p$) Sb concentrations (mean ± SD and median ± MAD) are also given, as well as the Th-normalised $Sb_p$ concentrations ($Sb_p/Th_p$ mean ± SD and median), the solid/liquid distribution coefficients ($\log_{10} K_d$) and the $Sb_d$ ("d") and $Sb_p$ ("p") fluxes (mean ± SD) per site. Minimum and maximum values are indicated when applicable.

| Site | Water temp. (°C) | Conduc. (µS cm$^{-1}$) | pH | Eh (mV) | Q (m$^3$ s$^{-1}$) | SPM (mg L$^{-1}$) | $Sb_d$ (µg L$^{-1}$) | | $Sb_p$ (mg kg$^{-1}$) | | $Sb_p/Th_p$ | $\log_{10} K_d$ (L kg$^{-1}$) | $Sb_d$ and $Sb_p$ fluxes (t y$^{-1}$) |
|---|---|---|---|---|---|---|---|---|---|---|---|---|---|
| | Mean ± SD [min. – max.] | | | | Mean ± SD [min. – max.] *Median* | | Mean ± SD [min. – max.] | Median ± MAD | Mean ± SD [min. – max.] | Median ± MAD | Mean ± SD [min. – max.] *Median* | | Mean ± SD |
| **LR** | 15.5 ± 6.8 [4.30 – 29.4] N = 208 | 281 ± 40 [143 – 381] N = 210 | 8.12 ± 0.29 [7.10 – 9.18] N = 206 | 154 ± 53 [42 – 324] N = 196 | 491 ± 475 [54 – 4740] *352* | 30 ± 72 [0 – 942] *11* | 0.19 ± 0.07 [0.06 – 0.51] | 0.16 ± 0.05 | 3.3 ± 1.6 [1.66 – 13.5] | 2.8 ± 0.9 | 0.31 ± 0.16 [0.12 – 1.47] *0.27* | 4.2 ± 0.2 [3.83 – 4.80] *4.24* | d: 2.49 ± 0.66 p: 3.17 ± 2.58 |
| **PSM** | 15.0 ± 6.6 [3.90 – 28.6] N = 191 | 283 ± 52 [58 – 396] N = 194 | 8.13 ± 0.35 [6.73 – 9.90] N = 190 | 154 ± 56 [38 – 293] N = 180 | 336 ± 325 [38 – 4340] *248* | 32 ± 94 [0 – 2320] *10* | 0.20 ± 0.08 [0.08 – 0.63] | 0.18 ± 0.06 | 3.1 ± 1.3 [1.5 – 12.0] | 2.8 ± 0.8 | 0.29 ± 0.12 [0.12 – 0.91] *0.25* | 4.2 ± 0.2 [3.71 – 4.81] *4.20* | d: 1.85 ± 0.43 p: 2.10 ± 1.69 |
| **T** | 15.4 ± 7.1 [3.60 – 31.2] N = 188 | 239 ± 51 [17 – 454] N = 198 | 8.04 ± 0.44 [6.30 – 9.38] N = 192 | 162 ± 60 [9 – 525] N = 183 | 130 ± 132 [11 - 2510] *82* | 14 ± 32 [0 - 1210] *9* | 0.15 ± 0.06 [0.06 – 0.59] | 0.13 ± 0.05 | 4.2 ± 2.0 [0.7 – 15.6] | 4.0 ± 1.3 | 0.47 ± 0.25 [0.13 – 1.90] *0.40* | 4.5 ± 0.2 [3.74 – 5.04] *4.48* | d: 0.51 ± 0.17 p: 0.37 ± 0.39 |
| **BP** | 13.1 ± 6.3 [2.70 – 27.0] N = 185 | 155 ± 116 [15 – 1470] N = 190 | 7.97 ± 0.41 [6.20 – 9.10] N = 185 | 166 ± 69 [1 – 370] N = 178 | 98 ± 103 [3 – 898] *58* | 6 ± 14 [0 – 334] *3* | 0.12 ± 0.06 [0.05 – 0.60] | 0.11 ± 0.04 | 4.7 ± 1.9 [0.7 – 12.6] | 4.3 ± 1.3 | 0.49 ± 0.24 [0.10 – 1.64] *0.42* | 4.6 ± 0.2 [3.84 – 5.30] *4.57* | d: 0.33 ± 0.12 p: 0.12 ± 0.09 |
| **RM** | 14.2 ± 6.1 [6.20 – 27.2] N = 44 | 843 ± 458 [180 – 2190] N = 46 | 8.06 ± 0.31 [7.53-8.90] N = 44 | 150 ± 59 [61– 320] N = 42 | 1 ± 3 [0 - 107] *1* | 74 ± 220 [1 - 5460] *17* | 1.2 ± 1.4 [0.18 – 12.6] | 0.70 ± 0.4 | 13 ± 14 [1.1 – 140] | 9.9 ± 5 | 2.1 ± 4.2 [0.31 – 61.0] *1.40* | 4.1 ± 0.4 [2.96 – 5.09] *4.12* | d: 0.03 ± 0.01 p: 0.13 ±0.19 |

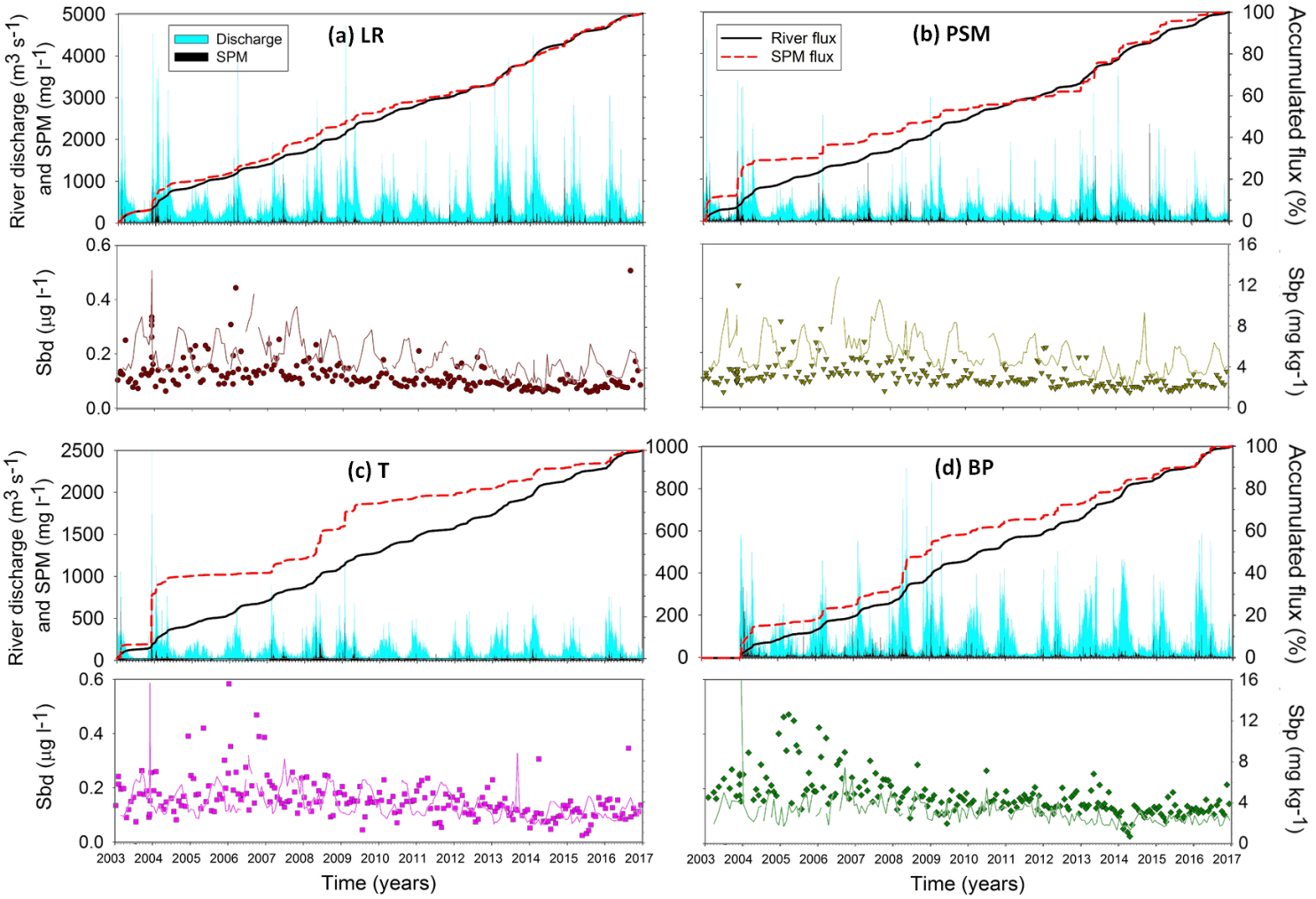


**Figure 2.** Upper panels (a-d): Temporal trends (2003 – 2016) of river discharge (Q, in $m^3\ s^{-1}$, cyan bar chart), suspended particulate matter (SPM, in mg $l^{-1}$, black bar chart) and respective accumulated fluxes (accumulated river flux, solid black lines, and accumulated SPM flux, dashed red lines, both given as percentage). Below (a-d), regular measurements for the same period (2003 – 2016) of $Sb_d$ (µg $l^{-1}$, solid lines) and $Sb_p$ concentrations (mg $kg^{-1}$, filled circles) at four of the sampled sites: La Réole (LR, a), Port-Sainte-Marie (PSM, b), Temple (T, c) and Boisse Penchot (BP, d).

In contrast, $Sb_p$ concentrations showed less explicit seasonal patterns, with a general maximum in winter (January/February) and a minimum in early autumn (August) at all sites except BP. The random component of the time series (ERR) showed similar and stable "noise" patterns over time at all sites, with 20-fold and 5-fold higher scales for RM $Sb_d$ and $Sb_p$ concentrations, respectively. Relatively high ERR variabilities, compared to the rest of the series, occurred at the T and BP sites for $Sb_p$ concentrations before 2007-2008.

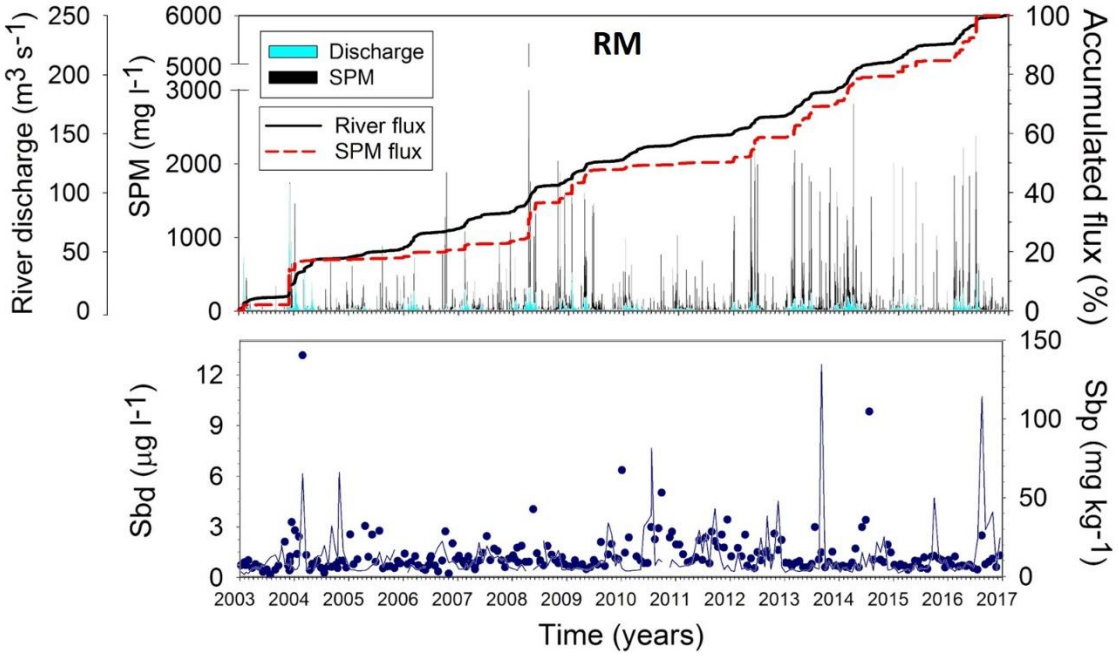


**Figure 3.** Temporal trends (2003 – 2016) of river discharge (Q, in $m^3\ s^{-1}$, cyan bar chart), suspended particulate matter (SPM, in mg $L^{-1}$, black bar chart) and respective accumulated fluxes (accumulated river flux, solid black lines, and accumulated SPM flux, dashed red lines, both given as percentage) in the upper panel. Below, regular measurements for the same period (2003 – 2016) of $Sb_d$ (µg $L^{-1}$, solid lines) and $Sb_p$ concentrations (mg $kg^{-1}$, filled circles) at Riou Mort site (RM).

### 3.3. Relevance of the colloidal fraction

Measurements of both Sb 0.02 µm ($Sb_{d0.02}$) and 0.2 µm ($Sb_{d0.2}$) fractions restricted to the 2003-2007 period suggested a negligible contribution (*i.e.*, standard deviations are within the analytical uncertainty) of colloidal (0.02 – 0.2 µm) fractions to Sb partitioning and transport along the Lot-Garonne River system (Table 2). Data used for calculating $Sb_{d0.02}/Sb_{d0.2}$ ratios (Table 2) was corrected for an average 13 ng $L^{-1}$ potential filter-contamination effect (corresponding to < 10% of $Sb_{d0.02}$ concentration) as observed from 0.02 µm Anotop 25 Whatman™ filters varying between 6 ng $L^{-1}$ and up to 46 ng $L^{-1}$ (assessed from *in situ* blank tests with MilliQ® water). However, such correction might not have been enough in some cases were high $Sb_{d0.02}/Sb_{d0.2} > 1$ have been observed, due to the variable range of potential contamination concentrations and its random influence on samples. Low $Sb_{d0.02}/Sb_{d0.2}$ ratios were not reproducible over time ($Sb_{d0.02}/Sb_{d0.2} < 0.9$ occur min. ~1/10 cases at LR and PSM and max.

~1/4 cases at BP). Moreover, these sporadic observations did not always occur under the same physico-chemical conditions at all sites, despite significant correlations (95% confidence) with Q (r = - 0.909 at LR, r = - 0.774 at PSM, r = -0.657 at BP), temperature (r = 0.788 at LR, r = 0.746 at T, r = 0.596 at BP), dissolved organic carbon (DOC, r = - 0.951 at PSM) and Eh (r = - 0.582 at BP) for $Sb_{d0.02}/Sb_{d0.2}$ ratios < 0.9.

**Table 2. Colloidal antimony fraction.** Mean values ± standard deviations (SD) of $Sb_{d0.02}/Sb_{d0.2}$ ratios during 2003 – 2007 at five sampling sites in the Lot-Garonne river system: La Réole (LR), Port-Sainte-Marie (PSM), Temple (T), Boisse Penchot (BP) and Riou Mort (RM). The frequency of $Sb_{d0.02}/Sb_{d0.2}$ ratios below 0.90 are also shown.

| | **$Sb_{d0.02}/Sb_{d0.2}$** | |
|---|---|---|
| **Site** | **Average ± SD** | **Frequency (<0.9)** |
| **LR** | 0.97 ± 0.11 | N = 8 |
| N = 70 | [0.45 – 1.18] | |
| **PSM** | 0.99 ± 0.08 | N = 8 |
| N = 75 | [073 – 1.20] | |
| **T** | 0.96 ± 0.09 | N = 15 |
| N = 76 | [0.65 – 1.17] | |
| **BP** | 0.95 ± 0.08 | N = 15 |
| N = 61 | [0.80 – 1.12] | |
| **RM** | 0.97 ± 0.09 | N = 10 |
| N = 68 | [0.61 – 1.12] | |

### 3.4. Contamination degree (I'geo)

The $I'_{geo}$ values obtained at the Garonne River sites of LR and PSM were $I'_{geo} < 1$ (class 1: non-polluted; Fig. S2a, Supplementary data) during almost the whole observation period. In contrast, $I'_{geo}$ at the Lot River sites T and BP showed moderate to strong Sb pollution in SPM (class 2 and 3) before 2008, reaching values corresponding to 'unpolluted to moderately polluted' (class 1) in recent years (2013 onwards; Fig. S2b, Supplementary data). At the RM site, $I'_{geo}$ for SPM generally corresponded to 'moderately to strongly polluted' levels (class 3), still reaching 'very strongly polluted' levels (class 5), even in the recent years.

When $I'_{geo}$ values are plotted against $Sb_p/Th_p$ ratios, a single logarithmic equation ($I'_{geo}$ = $1.443Ln(Sb_p/Th_p) + 1.889$) explains the relations of both parameters at all sites due to the common $Sb_p/Th_p$ ratio of reference (*i.e.*, 0.18) used herein. This implies that unpolluted to moderately polluted

conditions are exceeded (*i.e.* $I'_{geo}$ >1) at all sites for $Sb_p/Th_p$ ratios > 0.54, which is generally obtained when $Sb_p$ > 5-6 mg $kg^{-1}$. Such conditions were mostly achieved during 2004-2007 at T and BP, and to a lesser extent at LR and PSM, and still occurred sporadically over time at all sites (especially in 2011-2012), matching the anomalous data obtained at the distribution frequencies (section 3.1).

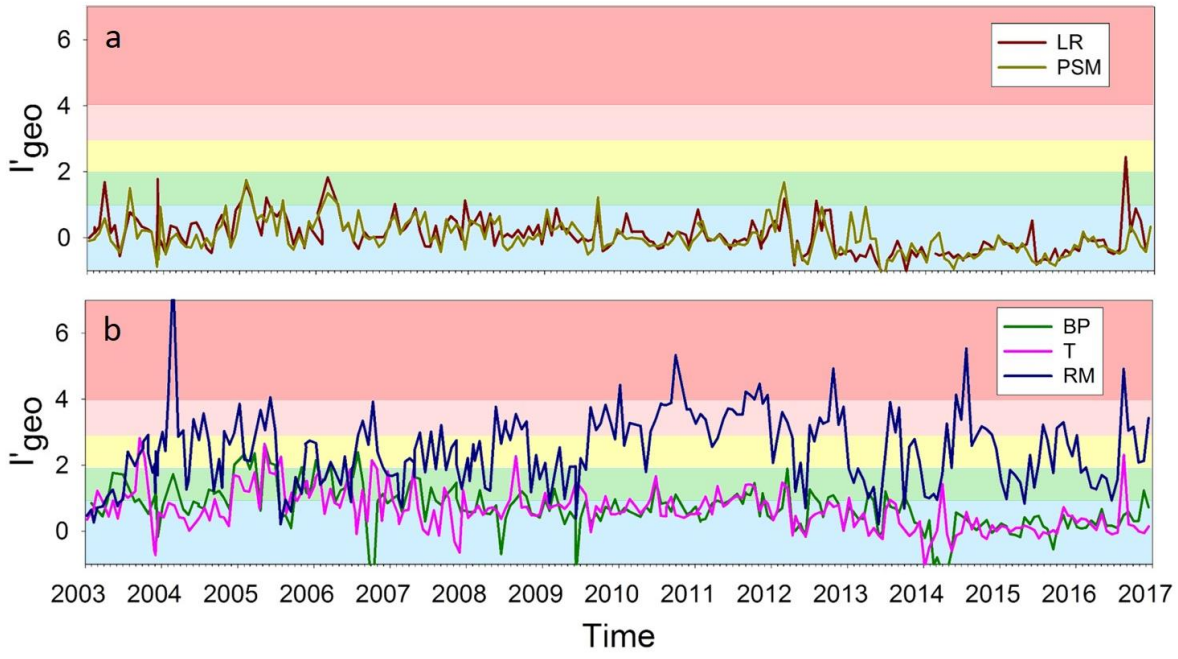


**Figure S2.** Temporal trend of the modified geoaccumulation index ($I'_{geo}$) for the five sampled sites (a: LR and PSM, b: T, BP and RM). Colour code correspond to $I'_{geo}$ classification: class 1 (0–1, unpolluted to moderately polluted, blue), class 2 (1–2, moderately polluted, green), class 3 (2–3, moderately to strongly polluted, yellow), class 4 (3–4, strongly polluted, pink), and class 5 (4–5, strongly to very strongly polluted, red).

### 3.5. Distribution coefficients ($K_d$)

Distribution coefficients at each site ranged from $\log_{10} K_d$ = 3.71 to 5.30 L $kg^{-1}$ (average 4.44 L $kg^{-1}$ for average Eh ~ 160 mV and average pH ~ 8.21; Table 1), *i.e.*, a change by 2 orders of magnitude going along with strong variations in SPM (from 0.10 to 2320 mg $L^{-1}$; *i.e.*, 4 orders of magnitude). The upstream sites (*i.e.*, BP and T) showed a maximum of 80% of total Sb bound to the particulate phase for SPM up to 100 mg $L^{-1}$ (Fig. 4a and b). Higher particulate Sb fractions and SPM concentrations occurred at the LR and PSM sites (*i.e.*, up to 90% of total Sb in the particulate phase for SPM ~ 1000 mg $L^{-1}$ during floods, Fig. 4c and d).

Antimony $K_d$ values in the Lot-Garonne River system also showed clear seasonal variations being low in summer/autumn ($\log_{10} K_d$ ~ 3.9-4.3 L $kg^{-1}$ in July to November; Fig. S3, Supplementary data) and higher during the first four months of the year ($\log_{10} K_d$ ~ 4.3-4.7 L $kg^{-1}$ in January to April) for the sites LR, T and PSM, whereas at BP $K_d$ values were high ($\log_{10} K_d$ ~ 4.4-4.8 L $kg^{-1}$) and relatively stable throughout all the year.

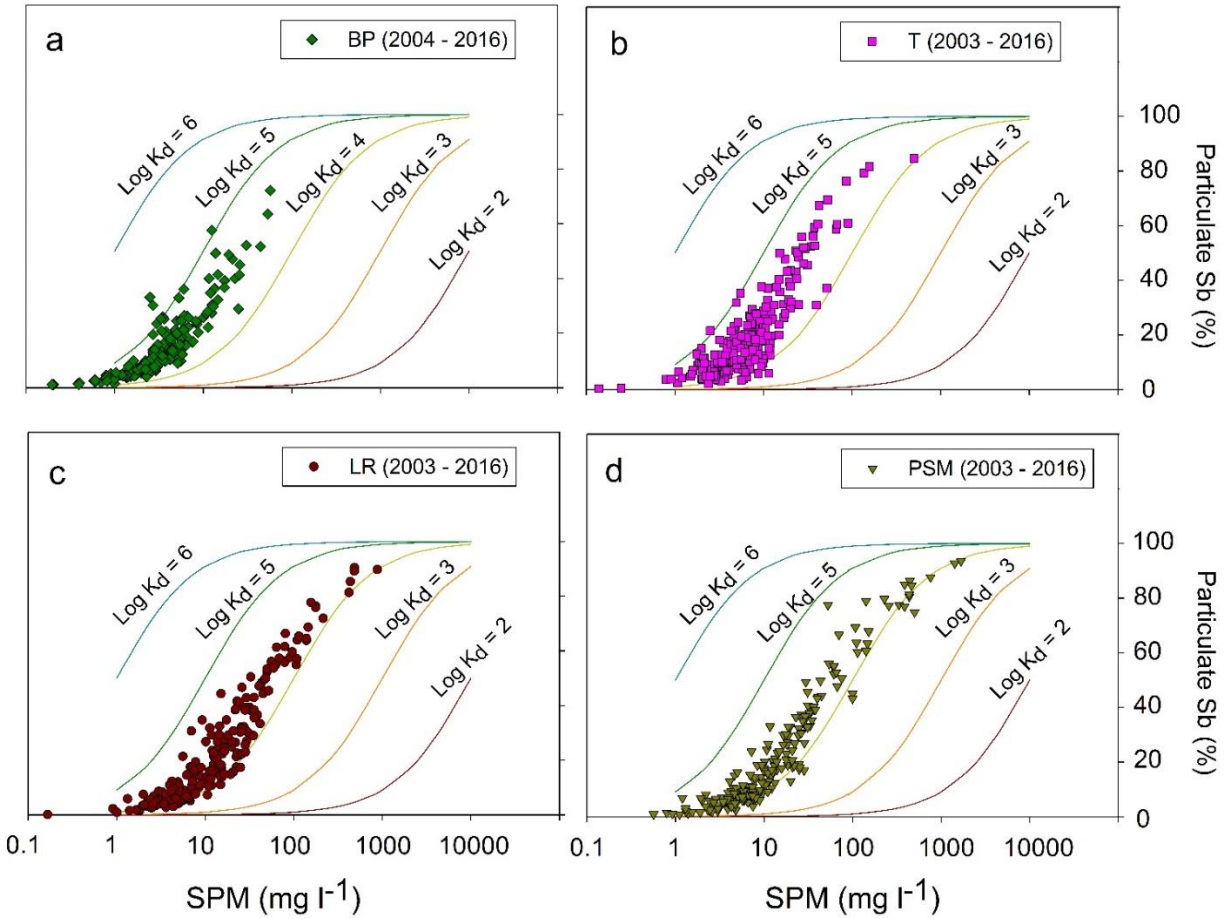


**Figure 4.** Antimony distribution coefficients (log $K_d$) from 2004 to 2016 at Boisse Penchot (BP, a) and from 2003 to 2016 at Temple (T, b), La Réole (LR, c) and Port-Sainte-Marie (PSM, d).

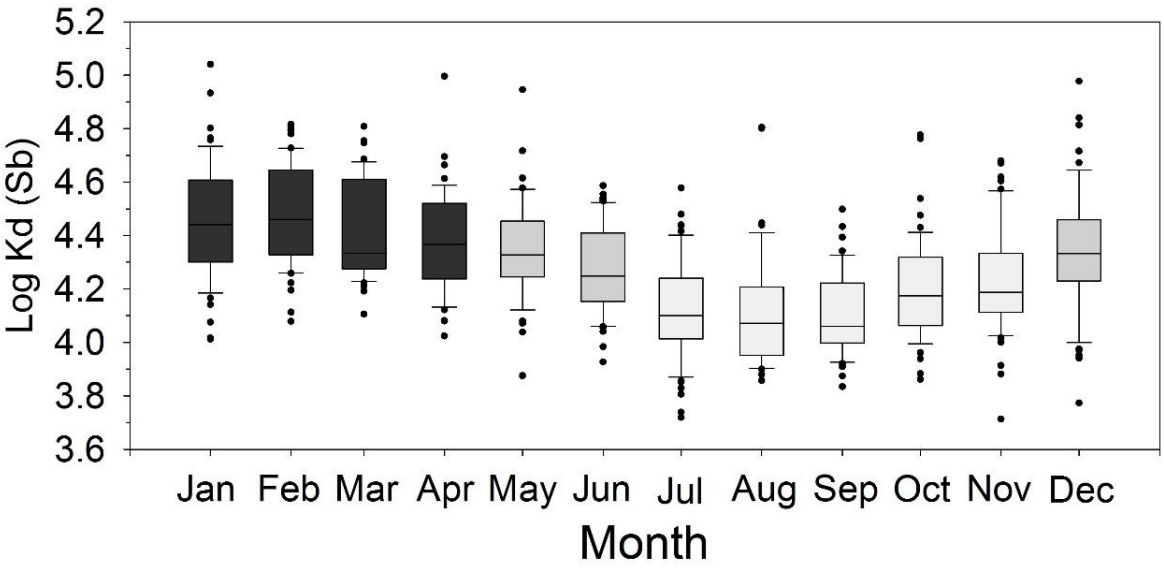


**Figure S3.** Seasonal variation of $\log_{10} K_d$ Sb at La Réole, Temple and Port-Sainte-Marie for 2003-2016.

### 3.6. Annual Sb fluxes

Dissolved and particulate annual Sb fluxes per site (Table 1) do not display any specific trend over time (Fig. S4, Supplementary Data). Average total ($Sb_T$ = $Sb_d$ + $Sb_p$) annual Sb fluxes entering the Gironde Estuary via the Garonne River (*i.e.*, LR site; 2004 to 2016) were 5.66 ± 2.96 t $y^{-1}$ (min. 2.22 t $y^{-1}$, max. 11.3 t $y^{-1}$), with average 48% in particulate form (*i.e.*, 48 ± 19%). The $Sb_T$ fluxes at the other studied sites were: 3.95 ± 1.96 t $y^{-1}$ at PSM (min. 1.58 t $y^{-1}$, max. 7.48 t $y^{-1}$, with 45 ± 20% as $Sb_p$), 0.88 ± 0.54 t $y^{-1}$ at the T site (min. 0.42 t $y^{-1}$, max. 2.16 t $y^{-1}$, 35 ± 14% as $Sb_p$), 0.44 ± 0.19 t $y^{-1}$ at BP (min. 0.21 t $y^{-1}$, max. 1.00 t $y^{-1}$, 25 ± 11 % as $Sb_p$) and 0.16 ± 0.10 t $y^{-1}$ at RM (min. 0.01 t $y^{-1}$, max. 0.29 t $y^{-1}$, 60 ± 25% as $Sb_p$). These average annual fluxes were calculated without taking into account the exceptional fluxes of 2003, as they were influenced by two discrete extreme flood events in February and December 2003 (causing a cumulative precipitation higher than the annual average; Coynel et al. 2007*a*; Ollivier et al. 2010), thus biasing the average ± standard deviation of the long-term records.

## 4. DISCUSSION

### 4.1. Overview on Sb concentrations in the Lot-Garonne River system

The 14-year record from the Garonne and Lot Rivers reveals reproducible differences in annual average $Sb_d$ and $Sb_p$ concentrations between the studied rivers, with relatively higher $Sb_d$ concentrations in the upstream Garonne River (PSM site) but higher $Sb_p$ concentrations in the Lot River (BP and T sites; Table 1). For the four studied sites, spatial differences in average concentrations overlap with long-term changes at both the pluri-annual and the seasonal timescales (for discussion of temporal aspects, see sections 4.3 and 4.4).

Average concentrations for the whole Garonne River watershed, as reflected at the LR site (Table 1) are consistent with independent data on Sb in stream water ($Sb_d$ 0.05 – 0.2 µg $L^{-1}$) and stream sediment ($Sb_p$ 0.91 – 3.05 mg $kg^{-1}$) from 20 sites upstream PSM (Garonne River and tributaries) during spring and winter 1998-1999 (Salminen et al. 2005). The observed $Sb_d$ also fall within the log-normal distribution of $Sb_d$ in rivers (highest frequencies around 1 nM, thus ≈ 0.12 µg $L^{-1}$, with slightly negative skewness) from a variety of drainage basins worldwide (*i.e.*, UK, Germany, Thailand, Taiwan, Korea, Japan, United States and Canada; Asaoka et al. 2012; Byrd 1990; Filella et al. 2002*a*). Furthermore, $Sb_d$ concentrations exported from the Garonne River watershed are below the expected 1 µg $L^{-1}$ for non-polluted freshwater (Filella et al. 2002*a*; Filella et al. 2003), below European River averages (0.25 µg $L^{-1}$; Andreae and Froelich 1984; Filella et al. 2002*a*) and within the range of estimated world river averages (between 0.10 µg $L^{-1}$ and 1.00 µg $L^{-1}$; Filella et al. 2002*a*; Martin and Whitfield 1983). Likewise, $Sb_p$ concentrations in the Garonne River SPM are slightly higher than the average 2.5 mg $kg^{-1}$ for SPM in worldwide rivers (Martin and Whitfield 1983), *i.e.* consistent with the expected level of few mg $kg^{-1}$ (Filella et al. 2002*a*; Filella et al. 2003), although being 5-fold greater than the median $Sb_p$ in

European stream sediments of 0.64 mg $kg^{-1}$ (<0.02 – 34.1 mg $kg^{-1}$; De Vos et al. 2006; Reimann et al. 2010).

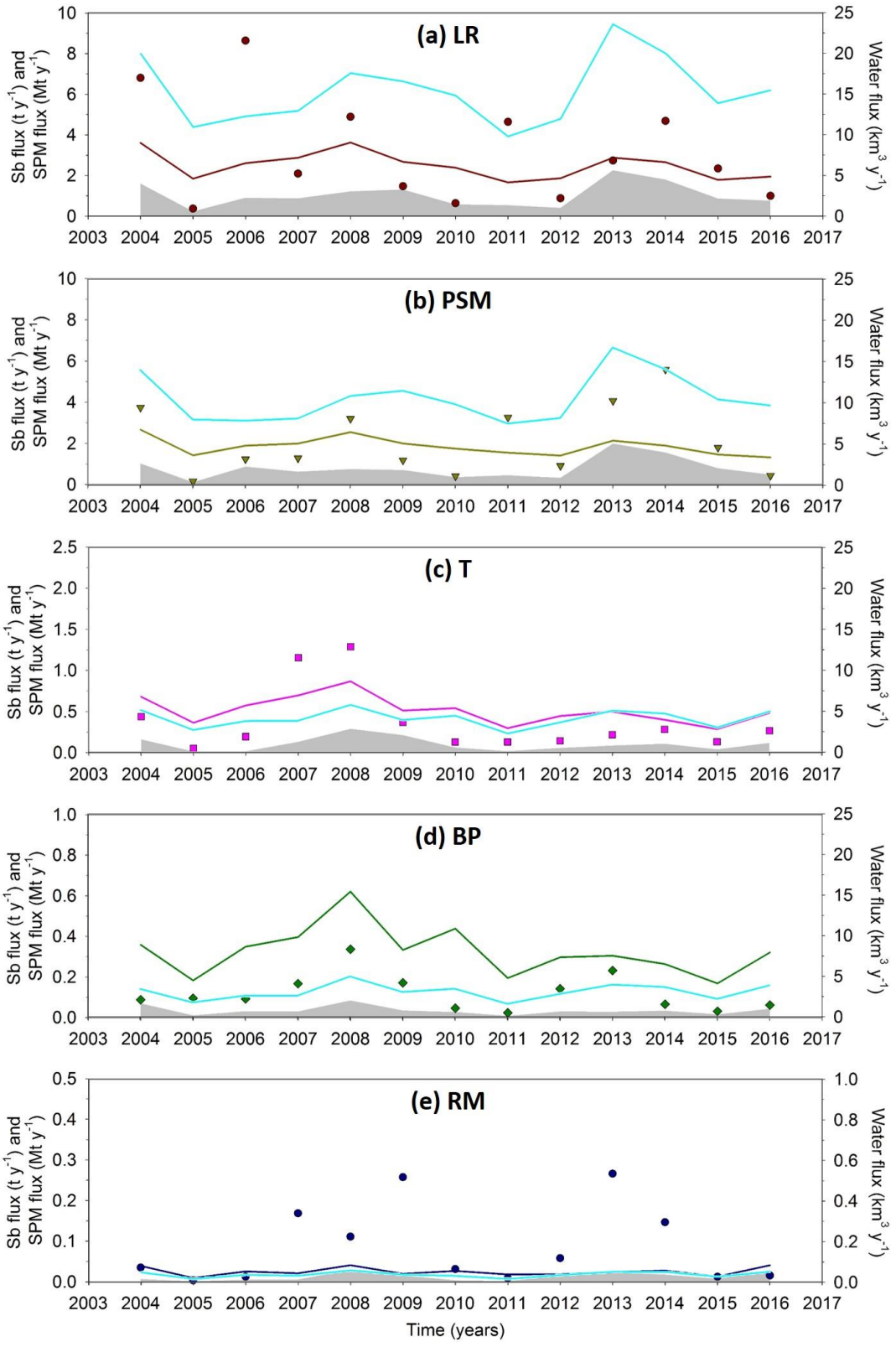


**Figure S4.** Temporal trends (2004 – 2016) of annual water (Q, in $km^3$ $y^{-1}$, cyan solid line) and suspended particulate matter fluxes (SPM, in Mt $y^{-1}$, grey area) with annual $Sb_d$ (t $y^{-1}$, solid lines) and $Sb_p$ discharged-weighted fluxes (t $y^{-1}$, filled circles) at all sampled sites: La Réole (LR, a), Port-Sainte-Marie (PSM, b), Temple (T, c), Boisse Penchot (BP, d) and Riou Mort (RM, e).

The French four major watersheds contribute huge loads of freshwater and SPM to the respective coasts: the Garonne-Gironde fluvial-estuarine system (average Q ~1000 $m^3 s^{-1}$; $F_{SPM}$; ~1 – 3 Mt $y^{-1}$), the Loire (average Q = 750 $m^3 s^{-1}$; $F_{SPM}$ = 0.3 – 1 Mt $y^{-1}$; Cerdan et al. 2012; Ciffroy et al. 2003; DIREN 2015), the Seine (average Q = 430 $m^3 s^{-1}$; $F_{SPM}$ ~ 9 Mt $y^{-1}$; Cerdan et al. 2012; DIREN 2015) and the Rhône Rivers (Q = 1700 $m^3 s^{-1}$; $F_{SPM}$ = 1.2 – 22.7 Mt $y^{-1}$; DIREN 2015; Ollivier et al. 2011). From these, the Lot River (a tributary of the Garonne River) and the Loire River potentially share a common geological upstream source (*i.e.*, the Massif Central). In fact, the Loire River shows comparable $Sb_d$ (average 0.25 ± 0.05 µg $L^{-1}$, N = 184, unpubl. data) and $Sb_p$ concentrations (average 3.2 ± 1.9 mg $kg^{-1}$, N = 133, unpubl. data) at Montjean-sur-Loire (near Nantes) to those observed in this study for the Lot and Garonne River sites (Table 1). Likewise, a monthly sampling campaign in the Seine River between October 2008-2009 (Ayrault et al. 2013) registered average Sb concentrations at Marnay-sur-Seine (*i.e.*, upstream the city of Paris) of 0.11 ± 0.15 µg $L^{-1}$ of $Sb_d$ and 0.36 ± 0.09 mg $kg^{-1}$ of $Sb_p$, whereas at Bougival (*i.e.*, downstream the city of Paris) $Sb_d$ concentrations were 0.21 ± 0.01 µg $L^{-1}$ and 1.22 ± 0.65 mg $kg^{-1}$ for $Sb_p$. Despite this apparent increase in Sb concentrations attributed to the influence of the Paris agglomeration, the range of $Sb_d$ average concentrations in the Seine River are in accordance to those observed in this study. In contrast, the $Sb_p$ concentrations in the Seine River are much lower than those in the Garonne River (*e.g.*, at LR, Table 1), suggesting either urban $Sb_d$ inputs (from the city of Toulouse) and/or lithogenic differences (BRGM 1978, 1983, 1985) between the Seine and Garonne River watersheds, explaining the different $Sb_p$ concentrations.

In the Rhône River, 2-fold higher $Sb_d$ concentrations (average 0.29 ± 0.09 µg $L^{-1}$) and clearly lower $Sb_p$ (1.98 ± 0.88 mg $kg^{-1}$) than those obtained for the Garonne River (this work, LR site) have been reported at Arles (Ollivier et al. 2011). The difference in $Sb_d$ may be due to different wet and dry atmospheric deposition, as atmospheric anthropogenic sources of Sb are non-negligible (Filella et al. 2002*a*; Ollivier et al. 2010), especially in industrial and urban zones (domestic and industrial coal and fuel combustion, abrasion of brake pads, tyres and street surface, etc., contributing up to 100 to 200-fold more Sb than natural emissions; Shotyk and Krachler 2004; Smichowski 2008; WHO 2003). In fact, other works have reported higher Sb concentrations in mosses (indicative of air quality) within the Rhône River watershed (0.13 – 0.25 mg $kg^{-1}$ DW), compared to the Garonne River watershed (0.09 – 0.13 mg $kg^{-1}$ DW; Harmens et al. 2013), and important Sb input to the Rhône River by rain water (contributing to > 80% of total atmospheric input in the Gulf of Lions; Guieu et al. 1993). Additionally, the Rhône River is subjected to multiple urban and industrial sources (*e.g.*, wastewater treatment plants), which can also locally increase $Sb_d$ in rivers by one to two orders of magnitude (Andreae and Froelich 1984; Filella et al. 2002a; Guieu et al. 1993). In domestic wastewaters, Sb is mainly released from plastic and textiles (Tschan et al. 2009), but chemical secondary treatments with ferric compounds can decrease Sb load in wastewater, so that treated domestic wastewaters may have negligible Sb contributions compared to industrial wastewater (Enders and Jekel 1994).

The differences in $Sb_p$ concentrations between the Garonne and Rhône Rivers, especially during floods (high erosion), suggest differences in regional geochemical (lithogenic) $Sb_p$ concentrations. In fact, natural Sb generally show high concentrations in shales (*e.g.*, 0.8 – 2.0 mg $kg^{-1}$; Filella et al. 2002*a*; Hall and Pelchat 1997), clays and argillaceous sediments (> 1 mg $kg^{-1}$; Salminen et al. 2005) and the Rhône River mostly drains limestones, marls, evaporites and quaternary alluviums (Ollivier et al. 2011), whereas the Garonne River mainly flows through sands/clays and limestones (BRGM 2014). In any case, the lithogenic origin of the sediments may also explain why $Sb_p$ in these major French rivers are higher than those in other watersheds more or less affected by industry, urbanisation and agriculture such as, *e.g.*, 0.045 – 0.089 mg $kg^{-1}$ in Sao Paulo Estuary (Silva et al. 2014) or < 1.21 mg $kg^{-1}$ in Daliao River, China (Lin et al. 2012). Therefore, differences in $Sb_p$ concentrations at the regional scale in France could be explained by differences in lithology, and when comparing systems at larger spatial scales, grain-size should also be taken into account, *i.e.*, normalised data (*e.g.*, $Sb_p/Th_p$ ratio) should be used. For instance, higher Sb concentrations have been observed for southern European soils, stream and floodplain sediments as well as stream waters compared to northern European sites (Salminen et al. 2005). Such differences have been related to the last glaciation extent in central Europe, leaving young coarse grained soils in the northern sites and weathered finely grained sediments in the southern areas (thus, grain-size related large scale effect; Reimann et al. 2010). Moreover, Tertiary volcanic activities responsible for the Massif Central formation have been suspected to cause anomalously high $Sb_p$ natural concentrations in topsoils (Reimann et al. 2010). In addition, several Sb-bearing ore deposits exist in the crystalline upstream reaches of the whole Garonne River watershed (*i.e.*, Pyreneans, Massif Central; Fig. 1; BRGM 1978, 1983, 1985). The combination of such conditions may contribute to regional geochemical background.

### 4.2. Assessment of Sb contamination in the Lot-Garonne River system

Out of all sites, RM showed the highest Sb concentrations (Table 1). In fact, maximum Sb values have already been reported for specific sites in the small Riou Mort River watershed ($Sb_p \approx 21$ mg $kg^{-1}$ at the Banel River draining mine tailings and industrial waste; $Sb_p$ up to 53 mg $kg^{-1}$ and $Sb_d \approx 6$ µg $L^{-1}$ in a small stream draining coal ashes from a coal-fired power plant; Coynel et al. 2007*b*). These $Sb_d$ concentrations are lower but similar in magnitude to those in other polluted systems affected specifically by Sb mines (*e.g.*, 13.6 – 113 µg $L^{-1}$ in the Ichinokawa River, Japan (Asaoka et al. 2012) and the average 5.30 µg $L^{-1}$ in the Glenshanna River, Scotland (Filella et al. 2002*a*; Mohammad et al. 1990)) or draining mining and industrial wastes (*e.g.*, 31.0 or 96.0 µg $L^{-1}$ in Bitterfeld and Pfälzer Bergland, Germany; Filella et al. 2002*a*; Ulrich 1998). The Riou Mort watershed has been a historical major Sb source to the Lot River (Audry et al. 2004*b*) as supported by high Sb concentrations (12.8 ± 2.48 mg $kg^{-1}$) in the Cajarc sediments and by correlations (r = 0.83) between Sb and Zn and Cd (for which the industrial origin is well-documented; Audry et al. 2004*b*) in SPM during flood events in the Lot River. These

signals have been attributed to erosion of older, heavily polluted sediments from the historical industrial activities in Decazeville area (Coynel et al. 2007*a*).

The contamination degree of each site and its temporal trend was evaluated with the $I'_{geo}$ index to (i) assess the presence and current relevance of identified Sb anthropogenic sources at RM, as well as to (ii) identify the contamination levels at the other sites and the presence of possible Sb anthropogenic sources. The present work has shown that overall high $Sb_p$ concentrations at the RM site still persist and continue contaminating the Lot River (*i.e.*, no significant temporal trend in Sb concentrations between 2003 – 2016 and no temporal change in Th-normalised $Sb_p$, *i.e.*, $Sb_p/Th_p$ ratio, over time). These observations characterise a moderately to strongly polluted site ($I'_{geo}$ class 3) with episodic peaks ($I'_{geo}$ class 5: very strongly polluted site). Such concentrations could be assigned to anthropogenic sources such as on-going Sb leaching and erosion from the historic ore treatment residues and/or Sb-rich coal ashes (Coynel et al. 2009; Filella et al. 2002*a*; Smichowski 2008) as well as maybe other current activities such as plastic and battery recycling factories or the local wastewater treatment plant (releasing in average 0.6 μg $L^{-1}$ of $Sb_d$, unpubl. data) into the Riou Mort River, which can potentially affect the particulate phase. Such anomalies seem to be spatially restricted (as expected by Reimann et al. 2010) in the Garonne watershed, as few $Sb_p$ concentration anomalies from RM have been found downstream (at T and LR) over time. Nevertheless, it is also possible that the Lot River watershed has a local-specific naturally enhanced $Sb_p$ background due to the erosion of the Lot watershed lithogenic natural composition from (i) Carboniferous (mainly conglomerate and sandstone with intercalation of pelites and coal seams or layers), and (ii) Permian formations (hematite-rich conglomerates, sandstones and mudstones; Coynel et al. 2007*b*). Such formations can locally affect the $Sb_p$ concentrations up to 5 mg $kg^{-1}$ (*i.e.*, site potentially affected by erosion of Permian rocks) and 10 mg $kg^{-1}$ (*i.e.*, sites potentially affected by erosion of Carboniferous rocks and mine tailings and industrial wastes), respectively (Coynel et al. 2007*b*). In any case, such natural concentrations are at least one order of magnitude lower than the highest $Sb_p$ values measured in this study (Table 1). This means that the application of an adapted local $Sb_p$ background for $I'_{geo}$ calculations in the Lot River would decrease the average $I'_{geo}$ trend over time but not to a point that would exclude the anthropogenic contamination for the RM watershed. It is noteworthy that the long-term $I'_{geo}$ record also suggests a pronounced seasonal cycle at the RM site with highest values during summer/autumn. Such seasonal changes could reflect sediment remobilisation and erosion of more or less Sb-rich material from Carboniferous rocks and associated anthropogenic sources and/or sediment dilution-effect due to mixing with Permian rocks (containing lower $Sb_p$ concentrations). This hypothesis needs further investigation.

Furthermore, $I'_{geo}$ values at the Lot River sites T and BP suggest a decrease in SPM contamination after 2008 (from moderately/strongly polluted sites, class 2 and 3, to unpolluted to moderately polluted levels, class 1 in recent years; Fig. S2b, Supplementary data). This observed trend could reflect the erosion of polluted older sediments during floods and/or the effect of lock/floodgate construction works around the site BP and upstream before and during 2007-2008 (Coynel et al. 2007*b*), controlling

downstream SPM discharge since then. The observed higher variability of the random component (ERR) over time at T and BP before 2007-2008 and its stability after 2008 may support this idea. The origin of these $Sb_p$ rich particles could be lithology naturally enriched in Sb (Coynel et al. 2009), upstream ancient mine/ore treatment areas rich in Sb (BRGM 1978, 1983, 1985) and/or the presence of a glassware industry upstream from BP.

In contrast, SPM at the Garonne River sites PSM and LR was non-polluted in Sb ($I'_{geo}$ class 1 Fig. S2a, Supplementary data) during almost the whole observation period, with a slightly decreasing trend over time and sporadic peaks ($I'_{geo}$ class 2) along the year. This suggests particulate Sb point sources from upstream Garonne (either natural sources such as Sb-ores in the Pyrenean Mountains (BRGM 1978, 1983, 1985) or anthropogenic sources from industrial cities such as Toulouse) that occasionally affect the quality of river SPM (class 2).

Despite relatively high lithology-derived $Sb_p$ backgrounds and historical industrial contamination of the Lot-Garonne-Gironde fluvial-estuarine system (mainly affecting the Lot River watershed), $Sb_d$ and $Sb_p$ concentrations at the LR, PSM, T and BP sites are consistently below (particularly after 2008) the EU and USEPA water drinking limits (max. 6 µg $L^{-1}$; Filella et al. 2002*a*; Reimann et al. 2010) and below EU predicted no effect concentration (PNEC) values for sediment (11.2 mg $kg^{-1}$ DW; Reimann et al. 2010), respectively. This is not always the case for $Sb_d$ and $Sb_p$ at the RM site, underlining the role of dilution of point source inputs by uncontaminated material at the larger watershed scale.

### 4.3. Spatial and temporal trends: Lot-Garonne sub-watershed connections

The comparison of $Sb_d$ and $Sb_p$ variations between sites (especially when focussing on isolated events, *i.e.* those causing the positive skewness of the series) may help understanding the relative contributions of sub-watersheds to Sb concentrations and fluxes at LR site (*i.e.* main source of the Gironde Estuary). Data suggests that Sb concentrations and fluxes at the LR site are controlled by inputs (mainly as $Sb_d$) from the upstream Garonne River most of the year, whereas during winter combined Sb input from both the upper Garonne River and the Lot River watersheds (Massif Central Sb-ores) controls exportation into the Gironde Estuary. Although the amount of data supporting this idea is limited to 20-40% of the observations, these results clearly suggest the existing link between sites (spatial influence at a regional scale) within the watershed.

Likewise, temporal trends at each site show both annual and seasonal similarities and influences between sites. In fact, at the annual scale, the high $Sb_p$ variability in the Lot River (T + BP) before 2008 was also observed at LR (Fig. 2), being PSM the only site that actually showed an increasing trend in $Sb_p$ from 2003 to 2008 (*i.e.* +0.01 mg $kg^{-1}$ per month at PSM). The common decreasing trend from 2008 onwards at all sites (LR, PSM, T and BP) suggests a watershed-wide control rather than site-specific control. Similarly, common seasonal patterns at all sites (except BP) depict water discharge-related

influences, implying variable dilution for $Sb_d$ and/or erosion/leaching of different parts of the watershed for $Sb_p$ as a function of discharge, locally overlapped by anthropogenic signals.

At the inter-annual timescale, there is a general increase/decrease pattern (max. around 2006 - 2007 and min. around 2013 – 2014, Fig. 2), in the $Sb_d$ time series at most of the studied sites (except RM, less evident at BP). Monthly discharge-weighted $Sb_d$ concentrations show two peaks in 2007 and 2011, which could be explained by low river discharges, interactions with high $Sb_p$ remobilisation or a maximum in the North Atlantic Oscillation Index in 2011, although no clear signals linking Sb to climatic oscillation indices were observed for the studied time series. In fact, natural processes, and specifically those strongly influenced by climate, govern regional Sb enrichment, concentrations and distribution patterns (Reimann et al. 2010). The hypothesis of major climate oscillation modes (such as El Niño-Southern Oscillation, North Atlantic Oscillation or Antarctic Oscillation, among others) influencing watershed, and specifically water discharge periodicity has already been suggested for SE Europe rivers (Romania, Ukraine, Moldova, etc.) and for the four major river basins in France (the Seine, Loire, Garonne and Rhône Rivers; Briciu and Mihaila 2014; Chevalier et al. 2014). Furthermore, other studies have observed effects of river discharge related to ENSO processes on trace metal behaviour and solubility in transition waters, mainly due to modified sediment transport and biogeochemical processes (*e.g.*, decreased concentrations of labile Cu, Zn, Pb, Cr and Ni in SPM during intense El Niño events in the Patos Lagoon Estuary; Costa et al. 2016). Additionally, concentrations in the troposphere of gases like mercury have been reported to be driven by the Southern Oscillation Index (Slemr et al. 2016). Temporal series of other dissolved trace elements (*e.g.*, As, Cd or Zn, data not shown) in the Lot-Garonne River watershed do not indicate trends similar to that of Sb during the observation period. As Sb can also be transported by the atmosphere (Smichowski 2008), one cannot exclude that climatic oscillations may influence its atmospheric deposition, explaining the observed specific long-term trends at the watershed scale. Furthermore, a long-term survey reports that slightly higher Sb atmospheric emissions have been registered in Europe and worldwide during 2004-2006, followed by a decrease between 2006 and 2010 (Tian et al. 2014). As this survey ended in 2010, no direct comparison is possible with the present work for the period 2010-2015. To the best of our knowledge, there is no evidence in the literature for any direct effect of climatic trends (either through water discharge or atmospheric circulation influences, linked or not to troposphere concentration fluctuations) on Sb concentrations/dynamics in watersheds at decadal timescales, such as those observed here. Therefore, further investigation and longer time series are required to unveil potential relations between climatic events and Sb (trace element) concentrations in watersheds.

### 4.4. Governing processes of seasonal variations in Sb solid/liquid partitioning ($K_d$)

Distribution coefficients at all the studied sites ranged from $\log_{10} K_d$ 3.71 to 5.30 L $kg^{-1}$ (average 4.44 L $kg^{-1}$ for average Eh ~ 160 mV and average pH ~ 8.21; Table 1), which is in accordance with

predictions for river water and sediments at Eh < 200 and pH ~ 7.00 conditions (varying from $\log_{10} K_d$ = 3.3 – 6 L $kg^{-1}$; Asaoka et al. 2012), and falls within the $5^{th}$ – $95^{th}$ percentile range ($\log_{10} K_d$ = 2.7 – 4.7 L $kg^{-1}$, mode of 3.7 L $kg^{-1}$) of the probability density function estimated for river Sb partitioning (Ciffroy et al. 2009). However, Sb $K_d$ values also indicate seasonal patterns (for all studied sites except BP). Seasonal variations in $Sb_d$ and $Sb_p$ concentrations and related $K_d$ values may be due to variations in sources, including rock-weathering, erosion of different watershed areas, or anthropogenic sources such as agriculture (*e.g.*, seasonal cycles in fertiliser application), atmospheric deposition and/or variable dilution by precipitation. In fact, typical seasonal cycles of trace elements in temperate rivers generally reflect hydrological cycles, often going along with lower dissolved element concentrations during floods, due to dilution by rainwater and run-off (Coynel et al. 2007*b*). For some elements (*e.g.*, As), however, seasonal variations in dissolved concentrations have been attributed to both dilution and biogeochemical processes (Masson et al. 2007).

Distribution coefficients ($K_d$) are also known to vary according to different parameters such as: contact or equilibrium time, SPM concentration, particle grain-size and sediment composition (particularly for certain elements like Cs, Co, Mn, I or Ag), redox conditions, water pH and concentration of dissolved complexing ligands or organic components (Ciffroy et al. 2009; Garnier-Laplace et al. 1997). Therefore, $K_d$ is not constant for a given element but rather specific for a given environment (Garnier-Laplace et al. 1997), with a range of temporal variations depending on many factors (*e.g.*, season, hydrology, etc.). For Sb, contact time may increase the $K_d$, whereas the presence of cations, mineral ligands, organic matter, microorganism activity, pH and salinity may decrease it (Garnier-Laplace et al. 1997). The effect of temperature on Sb $K_d$ in aquatic systems, as well as Sb concentrations and all the parameters related to the particulate phase (SPM concentration and composition, *i.e.*, mineral types, organic matter, Fe and Mn oxides, and grain-size) have not been tested before (Garnier-Laplace et al. 1997).

In the Lot-Garonne River watershed, previous works (similar sites as in this study) have reported seasonal cycles of $K_d$ for As, attributing high $As_d$ concentrations and low $K_d$ during summer/autumn to microbial processes for water temperature greater than ~15°C, probably involving reductive dissolution of As-bearing oxy-hydroxides (Masson et al. 2007). In the present study, we observe for the first time a possible influence of water temperature on Sb $K_d$ at the studied sites, being lowest at BP ($r = -0.199$, $p < 0.05$, Fig. 5a) and highest at site T ($r = -0.704$, $p < 0.01$, Fig. 5b). Moreover, an inflexion point at ~13ºC is visible at site T, which is less evident at LR. We suspect that the temperature-related change in As $K_d$ previously observed at LR (Masson et al. 2007) could also exist for Sb, as they are usually compared due to similarities in their geochemical properties (Asaoka et al. 2012; Resongles et al. 2015; Wilson and Webster-Brown 2009). The comparison between As and Sb partitioning throughout the present 14-year study shows a significant correlation between $\log_{10} K_d$ of As and that of Sb at both Lot River sites: BP ($r = 0.521$, $p < 0.01$, Fig. 5c) and, much clearer, at T ($r = 0.743$, $p < 0.01$, Fig. 5d) with a slope of ~1 (where $\log_{10} K_d$ As is correlated to water temperature; $r = -0.793$, $p < 0.01$). These

correlations could be suspected to be mainly supported by similar $As_d$ and $Sb_d$ behaviours as they significantly correlate at BP ($r = 0.384$, $p < 0.01$) and T ($r = 0.703$, $p < 0.01$) and in the Garonne River at PSM ($r = 0.639$, $p<0.01$) and LR ($r = 0.711$, $p<0.01$). All these temperature-controlled parallel $K_d$ shifts support the idea of similar biogeochemical processes controlling As and Sb partitioning consistent with the previously suggested biological As reduction (*i.e.*, from arsenate As(V) to more soluble arsenite As(III); Masson et al. 2007) and the suggested decrease of Sb adsorption on SPM due to bacterial activity (Garnier-Laplace et al. 1997). Furthermore, one cannot exclude that the observed relationship between As and Sb partitioning is partly related to seasonal variations in mineralogical composition, including reactivity of common carrier phases (*e.g.*, iron oxy-hydroxides; Asaoka et al. 2012; Wilson et al. 2010) or parallel adsorption on clays and other mineral phases like ilmenite (Wedepohl 1973). Given that both As and Sb and some of their carrier phases (*e.g.*, Fe and Mn oxy/hydroxides) are redox-sensitive, reductive dissolution could contribute to the seasonal $K_d$ fluctuations (*i.e.*, Eh of down to 9.3 mV have been observed in surface water at site T, Table 1).

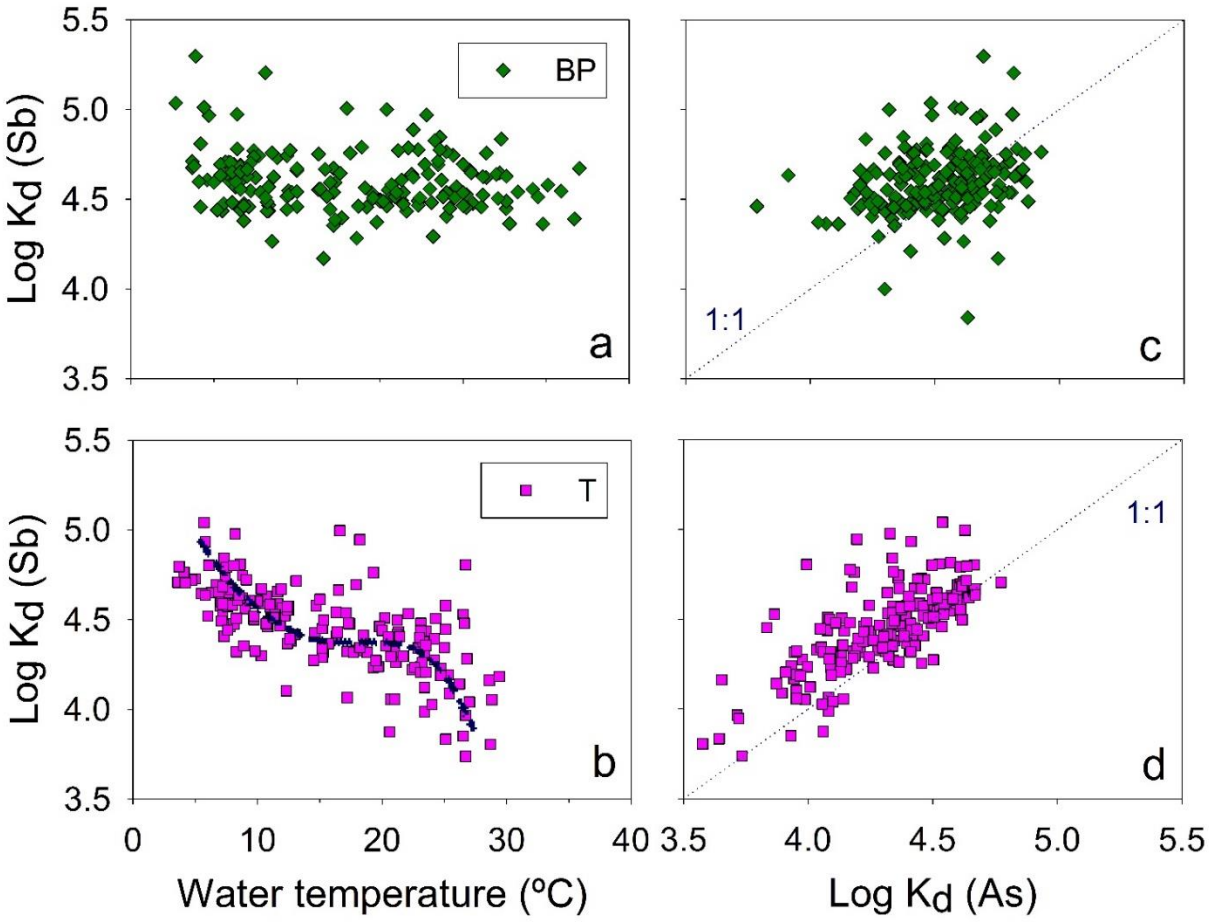


**Figure 5.** Comparison of data obtained at Boisse Penchot (BP, a and c) and Temple (T, b and d): The effect of water temperature on Sb partitioning is shown in a and b, while Sb log $K_d$ is plotted against As log $K_d$ in c and d.

### 4.5. Fluvial Sb input into the Gironde Estuary: estuarine partitioning and gross fluxes

Along the Lot-Garonne-Gironde fluvial-estuarine system, $Sb_p$ concentrations tend to decrease from upstream (*i.e.*, average 4.65 mg $kg^{-1}$ at BP and 3.31 mg $kg^{-1}$ at LR, in this study) to downstream (~1.90 mg $kg^{-1}$ near Bordeaux, Masson et al. 2009*b*, and ~1.20 mg $kg^{-1}$ in the Gironde Estuary mouth; Gil-Díaz et al. 2016). The freshwater $\log_{10} K_d$ range at LR (from 3.83 to 4.80 l $kg^{-1}$) is close to that of the Gironde Estuary (from 3.5 to 4.4 L $kg^{-1}$; Gil-Díaz et al. 2016) although daily comparisons suggest that estuarine $\log_{10} K_d$ are lower by ~0.2 L $kg^{-1}$, reflecting the observed Sb addition in estuarine salinity and turbidity gradients (Gil-Díaz et al. 2016). Similar $\log_{10} K_d$ as in the Gironde Estuary salinity gradient have been observed in the Rhône River (3.4 – 4.2 L $kg^{-1}$; Ollivier et al. 2011) and were attributed to its high chlorine concentrations (~150 – 640 µmol $L^{-1}$) due to the erosion of evaporites along the Saône and Durance Rivers (main tributaries of the Rhône River) and possibly to fertilisers and/or industrial/urban wastewaters (Ollivier et al. 2010).

Masson et al. (2009*b*) estimated from mass balance calculations based on a 17-months survey that both the Garonne and Dordogne Rivers contribute almost similarly (3.3 t $y^{-1}$ and 2.7 t $y^{-1}$, respectively) to the Sb input into the Gironde Estuary. Average annual $Sb_T$ budgets from the present 14-years study suggest that the major part (~70%) of $Sb_T$ entering the Gironde Estuary *via* the Garonne River originates from the part of the watershed upstream from PSM (4.35 ± 2.01 t $y^{-1}$, 52% as $Sb_p$), and that the small RM watershed contributes in average <3% (although during floods RM can contribute up to 4.4 t of $Sb_T$ in a few days; Coynel et al. 2007*a*). Nevertheless, estimated $Sb_T$ fluxes in the Garonne watershed are lower than those found in other systems such as in the Seine River (~ 18 t $y^{-1}$; <5% as $Sb_p$ for 2008-2009; Ayrault et al. 2013) or the Rhône River (*e.g.*, 31 t $y^{-1}$ in 1990, <15% as $Sb_p$, Guieu et al. 1993 and ~ 37 t $y^{-1}$, ~ 60% as $Sb_p$, in 2002, Ollivier et al. 2011) into the coast.

Concerning the relative importance between dissolved or particulate fluxes, the Rhône River shows an $Sb_d$ transport dominance during most hydrological conditions as the cutting Q threshold separating dissolved and particulate flux dominance (*i.e.*, the "water discharge of equivalent fluxes", $Q_e$) for Sb is more than 2-fold greater than the average river discharge (Q = 1700 $m^3 s^{-1}$ vs $Q_e$ = 4100 $m^3 s^{-1}$; Ollivier et al. 2011). This means that in the Rhône River the average Q conditions are generally below the threshold discharge for which the particulate Sb flux becomes dominant (*i.e.* > 50% of total Sb flux), probably due to the numerous dams (N ~ 66) present along the Rhône River and its tributaries, acting as sediment traps (Ollivier et al. 2011). In the Lot-Garonne River system, identified $Q_e$ values (~600 $m^3 s^{-1}$ at LR and PSM, ~200 $m^3 s^{-1}$ at T and ~150 $m^3 s^{-1}$ at BP) are close to average Q for the Garonne (~540 $m^3 s^{-1}$; average for the 1994 – 2015 period; DIREN 2015) and Lot Rivers (~140 $m^3 s^{-1}$; average for the 1993 – 2015 period; DIREN 2015). This suggests a generally balanced contribution of both $Sb_d$ and $Sb_p$ to $Sb_T$ transport at nearly all studied sites (Table 1), reducing the contribution of $Sb_p$ to $Sb_T$ flux to <40% in the Lot River sites (T and BP) as there is $Sb_p$ retention due to sedimentation behind dams and locks.

The observed differences in annual $Sb_T$ fluxes between the sites were assessed by calculating the average surface-specific $Sb_T$ fluxes (*i.e.*, $Sb_T$ flux relative to the watershed area) over the studied period (2003 - 2016). Similar average surface-specific $Sb_T$ fluxes were found at LR (0.15 ± 0.05 mg $m^{-2}$ $y^{-1}$, for A ~ 57,000 $km^2$), PSM (0.12 ± 0.04 mg $m^{-2}$ $y^{-1}$, A ~ 46,300 $km^2$) and T (0.12 ± 0.05 mg $m^{-2}$ $y^{-1}$, A ~ 10,700 $km^2$), but much greater values at RM (1.14 ± 0.63 mg $m^{-2}$ $y^{-1}$, A ~ 155 $km^2$). This homogeneous distribution of surface-specific $Sb_T$ fluxes between the sites LR, PSM and T matches the hypothesis of a watershed-wide Sb control by large scale environmental conditions (*i.e.*, driven by climate oscillation modes or atmospheric deposition). The high surface-specific $Sb_T$ flux at RM may be attributed by the identified anthropogenic point sources in the Riou Mort watershed in contrast to the other studied sub-watersheds where possible anthropogenic Sb contributions probably have minor influence (consistent with the general $I'_{geo}$ < class 2 at these sites). In fact, surface-specific $Sb_T$ fluxes appear low, compared to the annual atmospheric inputs (170 t $y^{-1}$ in 1990 for 18,260 $km^2$) and surface-specific $Sb_T$ fluxes (9.00 ± 5.40 mg $m^{-2}$ $y^{-1}$) estimated for the Rhône coastal area (Guieu et al. 1993).

In any case, this study suggests that Sb fluxes are mostly naturally dominated at a regional scale, in accordance with Reimann et al. (2010), even though at a global scale Sb fluxes (especially those taking place at the crust surface) are anthropogenically influenced to at least 60% (Mittra and Sen 2017)

The present results also suggest that $Sb_d$ transported along the Lot-Garonne River system is probably present as either ions or very small colloids (<0.02 µm), accounting for more than 50% of $Sb_T$ in more than half of the time (Fig. 4). Contrary to the Rhône River, where Sb $\log_{10} K_d$ is negatively correlated to SPM (Ollivier et al. 2011), no clear correlations with SPM ($|r| > 0.5$) exist in the Lot-Garonne River system and $\log_{10} K_d$ varies by one order of magnitude for SPM < 40 mg $L^{-1}$. This observation suggests that, for Sb in the Lot-Garonne River system, there is no distinct "particle concentration effect" which often implies an important colloidal fraction of the studied element (Cobelo-García et al. 2004). This finding is in line with $Sb_{d0.02}/Sb_{d0.2}$ ~ 1 in the Lot-Garonne River system, clearly suggesting that the 0.02-0.2 µm colloidal Sb fraction is negligible in $Sb_d$ transport (Table 2). Furthermore, these results are in accordance with studies of Tanizaki et al. (1985,1992a, 1992b) reporting that < 20% of $Sb_d$ concentrations were associated to colloidal organic carbon (DOC) fractions (between 0.45 µm – 1000 Da) in freshwater systems (Filella et al. 2002*b*). Accordingly, suspicions and evidences of colloidal or amorphous Sb complexes playing important roles in other river watersheds (Filella et al. 2002*b*; Sigleo and Helz 1981) are probably not valid for the Lot-Garonne River system. These findings are relevant for Sb transport modelling at the Gironde Estuary watershed scale, and the general understanding of Sb biogeochemical cycles.

In addition, given the fact that Sb radionuclides (*e.g.*, $^{125}Sb$) enter the aquatic environment by current and accidental releases from nuclear power plants, information on partitioning and transport dynamics at the watershed scale are essential to the development of scenarios predicting Sb radionuclide dispersion in fluvial-estuarine systems. Based on the commonly accepted similar geochemical behaviour (*e.g.*, solubility, speciation, etc.) between stable and radionuclide isotopes of a given element (Gil-Díaz et al.

2016), the Sb dynamics found in this study at the PSM and LR sites are of particular interest for Sb radionuclide transport towards the Gironde Estuary in case of a hypothetical potential accidental release from the Golfech nuclear power plant (located on the Garonne River ~160 km upstream from Bordeaux, Fig. 1).

## ACKNOWLEDGEMENTS

This study is a scientific contribution to the French National Project AMORAD (ANR-11-RSNR-0002) from the National Research Agency, allocated in the framework programme "Investments for the Future" and was partially funded by the ANR Programme TWINRIVERS (ANR-11-IS56-0003) and the FEDER Aquitaine-1999-Z0061. The authors greatly acknowledge support from "l'Agence de l'Eau Adour-Garonne" and are grateful for field work assistance provided by master and PhD students that have contributed along these years to the long-term database and sample bank. The authors thank Dr. M. Filella for fruitful discussions and helpful comments.

## REFERENCES

Andreae MO, Froelich PN (1984). Arsenic, antimony and germanium biogeochemistry in the Baltic Sea. Tellus B: Chemical and Physical Meteorology 36, 101-117

Asaoka S, Takahashi Y, Araki Y, Tanimizu M (2012). Comparison of antimony and arsenic behavior in an Ichinokawa River water-sediment system. Chemical Geology 334, 1-8

Audry S, Blanc G, Schäfer J (2004a). Cadmium transport in the Lot-Garonne River system (France) – temporal variability and model for flux estimation. Science of the Total Environment 319, 197-213

Audry S, Schäfer J, Blanc G, Bossy C, Lavaux G (2004b). Anthropogenic components of heavy metal (Cd, Zn, Cu, Pb) budgets in the Lot-Garonne fluvial system (France). Applied Geochemistry 19, 769-786

Ayrault S, Priadi C, Pape P, Bonté P (2013). Occurrence, Sources and Pathways of Antimony and Silver in an Urban Catchment. In 'Urban Environment' (Eds S Rauch, G Morrison, S Norra, N Schleicher) pp. 425-435. (Springer, Dordrecht)

Blanc G, Lapaquellerie Y, Maillet N, Anschutz P (1999). A cadmium budget for the Lot-Garonne fluvial system (France). Hydrobiologia 410, 331-341

Briciu AE, Mihaila D (2014). Wavelet analysis of some rivers in SE Europe and selected climate indices. Environmental Monitoring and Assessment 186, 6263-6286

Bureau de Recherches Géologiques et Minières (BRGM, 2014) [Internet]. Carrières de France, exploitations actives. [cited 10 December 2015] Available from: http://www.brgm.fr/actualite/brgm-sim-presentent-carte-carrieres-france

Bureau de Recherches Géologiques et Minières (BRGM, 1985). Carte des gîtes minéraux de la France à 1/500000e, feuille de TOULOUSE, Service Géologique National.

Bureau de Recherches Géologiques et Minières (BRGM, 1983). Carte des gîtes minéraux de la France à 1/500000e, feuille de BORDEAUX, Service Géologique National.

Bureau de Recherches Géologiques et Minières (BRGM, 1978). Carte des gîtes minéraux de la France à 1/500000e, feuille de LYON, Service Géologique National.

Byrd JT (1990). Comparative geochemistries of arsenic and antimony in rivers and estuaries. Science of the Total Environment 97, 301-314

Cerdan O, Delmas M, Négrel P, Mouchel JM, Petelet-Giraud E, Salvador-Blanes S, Degan F (2012). Contribution of diffuse hill slope erosion to the sediment export of French rivers. Comptes Rendus Geoscience 344, 636-645

Chevalier L, Laignel B, Massei N, Munier S, Becker M, Turki I, Coynel A, Cazenave A (2014). Hydrological variability of major French rivers over recent decades, assessed from gauging station and GRACE observations. Hydrological Sciences Journal 59, 1844-1855

Ciffroy P, Durrieu G, Garnier JM (2009). Probabilistic distribution coefficients (Kds) in freshwater for radioisotopes of Ag, Am, Ba, Be, Ce, Co, Cs, I, Mn, Pu, Ra, Ru, Sb, Sr and Th — implications for uncertainty analysis of models simulating the transport of radionuclides in rivers. Journal of Environmental Radioactivity 100, 785-794

Ciffroy P, Reyss JL, Siclet F (2003). Determination of the residence time of suspended particles in the turbidity maximum of the Loire estuary by $^{7}$Be analysis. Estuarine, Coastal and Shelf Science 57, 553-568

Cobelo-García A, Prego R, Labandeira A (2004). Land inputs of trace metals, major elements, particulate organic carbon and suspended solids to an industrial coastal bay of the NE Atlantic. Water Research 38, 1753-1764

Costa LDF, Mirlean N, Wasserman JC, Wallner-Kersanach M (2016). Variability of labile metals in estuarine sediments in areas under the influence of antifouling paints, southern Brazil. Environmental Earth Sciences 75, 580. doi:10.1007/s12665-016-5355-5

Coynel A, Blanc G, Marache A, Schäfer J, Dabrin A, Maneux E, Bossy C, Masson M, Lavaux G (2009). Assessment of metal contamination in a small mining- and smelting-affected watershed: high resolution monitoring coupled with spatial analysis by GIS. Journal of Environmental Monitoring 11, 962-976

Coynel A, Schäfer J, Blanc G, Bossy C (2007a). Scenario of particulate trace metal and metalloid transport during a major flood event inferred from transient geochemical signals. Applied Geochemistry 22, 821-836

Coynel A, Schäfer J, Dabrin A, Girardot N, Blanc G (2007b). Groundwater contributions to metal transport in a small river affected by mining and smelting waste. Water Research 41, 3420-3428

De Vos W, Tarvainen T (Chief Eds.), Salminen R, Reeder S, De Vivo B, Demetriades A, Pirc S, Batista MJ, Marsina K, Ottesen RT, O'Connor PJ, Bidovec M, Lima A, Siewers U, Smith B, Taylor H, Shaw R, Salpeteur I, Gregorauskiene V, Halamic J, Slaninka I, Lax K, Gravesen P, Birke M, Breward N, Ander EL, Jordan G, Duris M, Klein P, Locutura J, Bel-lan A, Pasieczna A, Lis J, Mazreku A, Gilucis A, Heitzmann P, Klaver G, Petersell V (2006). Geochemical Atlas of Europe. Part 2 – Interpretation of Geochemical Maps, Additional Tables, Figures, Maps and related publications. Geological Survey of Finland (Espoo, Finland).

Deutsche Forschungsgemeinschaft (DFG, 2012). MAK- und BAT-Werte-Liste (VCH, Weinheim).

Enders R, Jekel R (1994). Entfernung von Antimon(V) und Antimon(III) aus wässrigen Lösungen. Teil I: Mitfällung und Adsorption bei der Flockung mit Eisen(III)-Salzen. [Elimination of Sb(V) and Sb(III) from aqueous solutions. Part I: Coprecipitation and adsorption during flocculation with Fe(III)salts.]. Wasser Abwasser 135, 632-641

European Council (EC, 2006) Directive 2006/11/EC of 15 February 2006 on pollution caused by certain dangerous substances discharged into the aquatic environment of the Community. OJ L64/52

Fawcett SE, Jamieson HE, Nordstrom DK, McCleskey RB (2015). Arsenic and antimony geochemistry of mine wastes, associated waters and sediments at the Giant Mine, Yellowknife, Northwest Territories, Canada. Applied Geochemistry 62, 3-17

Filella M, Belzile N, Chen YW (2002a). Antimony in the environment: a review focused on natural waters I. Occurrence. Earth-Science Reviews 57, 125-176

Filella M, Belzile N, Chen YW (2002b). Antimony in the environment: a review focused on natural waters II. Relevant solution chemistry. Earth-Science Reviews 59, 265-285

Filella M, Belzile N, Chen YW, Elleouet C, May PM, Mavrocordatos D, Nirel P, Porquet A, Quentel F, Silver S (2003). Antimony in aquatic systems. Journal de Physique IV (Proceedings) 107, 475-478

Fu Z, Wu F, Mo C, Deng Q, Meng W, Giesy JP (2016). Comparison of arsenic and antimony biogeochemical behaviour in water, soil and tailings from Xikuangshan, China. Science of the Total Environment 539, 97-104

Garnier-Laplace J, Fournier-Bidoz V, Baudin JP (1997). État des connaissances sur les échanges entre l'eau, les matières en suspension et les sédiments des principaux radionucléides rejetés en eau douce par les centrales nucléaires. Radioprotection 32, 49-71

Gil-Díaz T, Schäfer J, Pougnet F, Abdou M, Dutruch L, Eyrolle-Boyer F, Coynel A, Blanc G (2016). Distribution and geochemical behaviour of antimony in the Gironde Estuary: A first qualitative approach to regional nuclear accident scenarios. Marine Chemistry 185, 65-73

Grousset FE, Jouanneau JM, Castaing P, Lavaux G, Latouche C (1999). A 70 year record of contamination from industrial activity along the Garonne River and its tributaries (SW France). Estuarine, Coastal and Shelf Science 48, 401-414

Guieu C, Zhang J, Thomas AJ, Martin JM, Brun-Cottan JC (1993). Significance of atmospheric fallout on the upper layer water chemistry of the North-Western Mediterranean. Journal of Atmospheric Chemistry 17, 45-60

Hall GEM, Pelchat JC (1997). Analysis of geological materials for bismuth, antimony, selenium and tellurium by continuous flow hydride generation inductively coupled plasma mass spectrometry. Part 1. Mutual hydride interferences. Journal of Analytical Atomic Spectrometry 12, 97-102

Harmens H, Norris D, Mills G (2013). Heavy metals and nitrogen in mosses: spatial patterns in 2010/2011 and long-term temporal trends in Europe. 'NERC/Centre for Ecology and Hydrology', pp. 63 (Bangor, UK)

He M, Wang X, Wu F, Fu Z (2012). Antimony pollution in China. Science of the Total Environment 421, 41-50

Heier LS, Meland S, Ljones M, Salbu B, Stromseng AE (2010). Short-term temporal variations in speciation of Pb, Cu, Zn and Sb in a shooting range runoff stream. Science of the Total Environment 408, 2409-2417

Hockmann K, Lenz M, Tandy S, Nachtegaal M, Janousch M, Schulin R (2014). Release of antimony from contaminated soil induced by redox changes. Journal of Hazardous Materials 275, 215-221

Hu X, He M, Li S, Guo X (2017). The leaching characteristics and changes in the leached layer of antimony-bearing ores from China. Journal of Geochemical Exploration 176: 76-84

Jouanneau JM, Latouche C (1982). Estimation of fluxes to the ocean from mega-tidal estuaries under moderate climates and the problems they present. Hydrobiologia 91, 23-29

Krachler M, Shotyk W (2004). Natural and anthropogenic enrichments of molybdenum, thorium and uranium in a complete peat bog profile, Jura Mountains, Switzerland. Journal of Environmental Monitoring 6, 418-426

Lapaquellerie Y, Jouanneau JM, Maillet N, Latouche C (1995). Pollution en Cd dans les sédiments du Lot (France) et calcul du stock de polluant. Environmental Technology 16, 1145-1154

Larrose A, Coynel A, Schäfer J, Blanc G, Massé L, Maneux E (2010). Assessing the current state of the Gironde Estuary by mapping priority contaminant distribution and risk potential in surface sediment. Applied Geochemistry 25, 1912-1923

Lee M, Bae W, Hung J, Jung HS, Shim H (2008). Seasonal and spatial characteristics of seawater and sediment at Youngil bay, Southeast Coast of Korea. Marine Pollution Bulletin 57, 325-334Leys C, Ley C, Klein O, Bernard P, Licata L (2013). Detecting outliers: Do not use standard deviation around the mean, use absolute deviation around the median. Journal of Experimental Social Psychology 49, 764-766

Lin C, He M, Li Y, Liu S (2012). Content, enrichment, and regional geochemical baseline of antimony in the estuarine sediment of the Daliao river system in China. Chemie der Erde 72, 23-28

Martin JM, Whitfield M (1983). The significance of the river input of chemical elements to the oceans. In 'Trace metals in sea water' (Eds CS Wong, E Boyle, KW Bruland, JD Burton, ED Goldberg) pp. 265-296 (Springer, New York)

Masson M, Blanc G. Schäfer J (2006). Geochemical signals and source contributions to heavy metal (Cd, Zn, Pb, Cu) fluxes to the Gironde Estuary via its major tributaries. Science of the Total Environment 370, 133-146

Masson M, Blanc G, Schäfer J, Parlanti E, Le Coustumer P (2009a). Copper addition by organic matter degradation in the freshwater reaches of a turbid estuary. Science of the Total Environment 409, 1539-1549

Masson M, Lanceleur L, Tercier-Waeber ML, Schäfer J, Hezard T, Larrose A, Bossy C, Blanc G (2011). Distribution and reactivity of oxyanions (Sb, As, V, Mo) in the surface freshwater reaches of the Gironde Estuary (France). Applied Geochemistry 26, 1222-1230

Masson M, Schäfer J, Blanc G, Anschutz P (2007). Seasonal variations and annual fluxes of arsenic in the Garonne, Dordogne and Isle Rivers, France. Science of the Total Environment 373, 196-207

Masson M, Schäfer J, Blanc G, Dabrin A, Castelle S, Lavaux G (2009b). Behavior of arsenic and antimony in the surface freshwater reaches of a highly turbid estuary, the Gironde Estuary, France. Applied Geochemistry 24, 1747-1756

Meybeck M, Pasco A, Ragu A (1994). Etablissement des flux polluants dans les rivières : pourquoi, comment et à quel prix. '4ème Rencontres de l'Agence Régionale pour l'Environnement. In 'Provence-Alpes-Côte d'Azur. Colloque scientifique sur les charges polluantes véhiculées par les fleuves et les rivières en Méditerranée'. Collection 1991–1992–1993

Meybeck M, Ragu A (1995). River Discharges to the Oceans. An Assessment of Suspended Solids, Major Ions, and Nutrients. (UNEP Nairobi)

Mittra A, Sen IS (2017). Anthrobiogeochemical platinum, palladium and rhodium cycles of earth: emerging environmental contamination. Geochimica et Cosmochimica Acta 216, 417-432

Mohammad B, Ure AM, Reglinski J, Littlejohn D (1990). Speciation of antimony in natural waters: the determination of Sb(III) and Sb(V) by continuous flow hydride generation– atomic absorption spectrometry. Chemical Speciation and Bioavailability 3, 117-122

Müller G (1969). Index of geoaccumulation in sediments of the Rhine River. Journal of Geology 2, 108-118

National Hydrographic Databank (DIREN, 2015) [Internet]. Ministère de l'Écologie, du Développement Durable et de l'Énergie. [cited 16 December 2015] Available from: http://www.hydro.eaufrance.fr/

Okkenhaug G, Grasshorn Gebhardt KA, Amstaetter K, Lassen Bue H, Herzel H, Mariussen E, Rossebo Almas A, Cornelissen G, Breedveld GD, Ramussen G, Mulder J (2016). Antimony (Sb) ad lead (Pb)

in contaminated shooting range soils: Sb and Pb mobility and immobilization by iron based sorbents, a field study. Journal of Hazardous Materials 307, 336-343

Ollivier P, Hamelin B, Radakovitch O (2010). Seasonal variations of physical and chemical erosion: A three-year survey of the Rhone River (France). Geochimica et Cosmochimica Acta 74, 907-927

Ollivier P, Radakovitch O, Hamelin B (2011). Major and trace element partition and fluxes in the Rhône River. Chemical Geology 285, 15-31

Reimann C, Matschullat J, Birke M, Salminen R (2010). Antimony in the environment: lessons from geochemical mapping. Applied Geochemistry 25, 175-198

Resongles E, Freydier R, Casiot C, Viers J, Chmeleff J, Elbaz-Poulichet F (2015). Antimony isotopic composition in river waters affected by ancient mining activity. Talanta. 144, 851-861

Saleh MA, Wilson BL (1999). Analysis of metal pollutants in the Houston Ship Channel by inductively coupled plasma/mass spectrometry. Ecotoxicology and Environmental Safety 44, 113-117

Salminen R, Batista MJ, Bidovec M, Demetriades A, De Vivo B, De Vos W, Duris M, Gilucis A, Gregorauskiene V, Halamic J, Heitzmann P, Lima A, Jordan G, Klaver G, Klein P, Lis J, Locutura J, Marsina K, Mazreku A, O'Connor PJ, Olsson SA, Ottesen RT, Petersell V, Plant JA, Reeder S, Salpeteur I, Sandström H, Siewers U, Steenfelt A, Tarvainen T (2005). Geochemical Atlas of Europe. Part 1 – Background Information, Methodology and Maps. Geological Survey of Finland (Espoo, Finland).

Schäfer J, Blanc G (2002). Relationship between ore deposits in river catchments and geochemistry of suspended particulate matter from six rivers in southwest France. Science of the Total Environment 298, 103-118

Schäfer J, Blanc G, Lapaquellerie Y, Maillet N, Maneux E, Etcheber H (2002). Ten-Year-Observation of the Gironde Fluvial System: Fluxes of Suspended Matter, Particulate Organic Carbon and Cadmium. Marine Chemistry 79, 229-242

Shotyk W, Krachler M, Chen B (2004). Antimony in recent, ombrotrophic peat from Switzerland and Scotland: Comparison with natural background values (5,320 to 8,020 $^{14}$C yr BP) and implications for the global atmospheric Sb cycle. Global Biogeochemical Cycles 18, 1

Sigleo AC, Helz GR (1981). Composition of estuarine colloidal material: major and trace elements. Geochimica et Cosmochimica Acta 45, 2501-2509

Silva MM, Leao DJ, Moreira ITA, de Oliveira OMC, Queiroz AFS, Ferreira SLC (2014). Speciation analysis of inorganic antimony in sediment samples from São Paulo Estuary, Bahia State, Brazil. Environmental Science and Pollution Research 22. doi:10.1007/s11356-014-3956-7

Slemr F, Brenninkmeijer CA, Rauthe-Schöch A, Weigelt A, Ebinghaus R, Brunke EG, Martin L, Spain G, O'Doherty S (2016). El Niño-Southern Oscillation influence on tropospheric mercury concentrations. Geophysical Research Letters 43, 1766-1771

Smichowski P (2008). Antimony in the environment as a global pollutant: a review on analytical methodologies for its determination in atmospheric aerosols. Talanta 75, 2-14

Sung W (1995). Some observations on surface partitioning of Cd, Cu and Zn in estuaries. Environmental Science and Technology 29, 1303-1312

Tanizaki Y, Shimokawa T, Nakamura M (1992a). Physicochemical speciation of trace elements in river waters by size fractionation. Environmental Science and Technology 26, 1433-1444

Tanizaki Y, Shimokawa T, Yamazaki M (1992b). Physico-chemical speciation of trace elements in urban streams by size fractionation. Water Research 26, 55-63

Tanizaki Y, Yamazaki M, Nagatsuka S (1985). Physicochemical speciation of trace elements in river water by means of ultrafiltration. Bulletin of the Chemical Society of Japan 58, 2995-3002

Tian H, Zhou J, Zhu C, Zhao D, Gao J, Hao J, He M, Liu K, Wang K, Hua S (2014). A comprehensive global inventory of atmospheric antimony emissions from anthropogenic activities, 1995-2010. Environmental Science and Technology 48, 10235-10241

Tschan M, Robinson BH, Schulin R (2009). Antimony in the soil-plant system – a review. Environmental Chemistry 6, 106-115

Ulrich N (1998). Speciation of antimony(III), antimony(V) and trimethyl stiboxide by ion chromatography with inductively coupled plasma atomic emission spectrometric and mass spectrometric detection. Analytica Chimica Acta 359, 245-253

U.S. Environmental Protection Agency (USEPA, 2013) [Internet]. Priority Pollutant list, in Appendix A, 40 Code of Federal Regulations 423 (U.S. Environmental Protection Agency). [cited 14 January 2016] Available from: http://www.gpo.gov/fdsys/pkg/CFR-2013-title40-vol30/xml/CFR-2013-title40-vol30-part423.xml

U.S. Geological Survey (USGS, 2015) [Internet]. Mineral Commodity Summaries 2015 (U.S. Geological Survey). [cited 11 January 2016] Available from: http://minerals.usgs.gov/minerals/pubs/mcs/2015/mcs2015.pdf.

Wang J, Liu G, Liu Y, Zhou C, Wu Y, Zhang Q (2016). Mobilization of substance around stackable fly ash and the environmental characteristics of groundwater: with particular reference to five elements: B, Ba, Pb, Sb and Zn. Fuel 174, 126-132

Webb BW, Phillips JM, Walling DE, Littlewood IG, Watts C, Leeks GJL (1997). Load estimation methodologies for British river and their relevance to the LOIS RACS (R) program. Science of the Total Environment 194, 379-389

Wedepohl KH (1973). 'Handbook of Geochemistry' (Springer, Berlin)

Wilson SC, Lockwood PV, Ashley PM, Tighe M (2010). The chemistry and behaviour of antimony in the soil environment with comparisons to arsenic: a critical review. Environmental Pollution 158, 1169-1181

Wilson N, Webster-Brown J (2009). The fate of antimony in a major lowland river system, the Waikato River, New Zealand. Applied Geochemistry 24, 2283-2292

World Health Organization (WHO, 2003). Antimony in Drinking-water, Background document for development of WHO Guidelines for Drinking-water Quality. [cited 23 November 2015] Available from: http://www.who.int/water_sanitation_health/dwq/chemicals/antimony.pdf

## 2. Biogeochemical behaviour of antimony in the salinity and turbidity gradient of the Gironde estuary.

*Manuscript published in Marine Chemistry (2016)*

# Distribution and geochemical behaviour of antimony in the Gironde Estuary: A first qualitative approach to regional nuclear accident scenarios

Teba Gil-Díaz [a], Jörg Schäfer [a], Frédérique Pougnet [a], Melina Abdou [a], Lionel Dutruch [a], Frédérique Eyrolle-Boyer [b], Alexandra Coynel [a], Gérard Blanc [a]

[a] *Université de Bordeaux, UMR CNRS 5805 EPOC, Bat 18, Allée Geoffroy Saint-Hilaire, 33615 Pessac, France ;* [b] *Laboratoire d'Etudes Radioécologiques en Milieu Continental et Marin, IRSN/DEI/SESURE/LERCM, Institut de Radioprotection et de Sûreté Nucléaire, IRSN Cadarache BP2, Bat. 153, 13108 Saint Paul lez Durance cedex, France*

## ABSTRACT

Antimony (Sb) is a highly toxic trace element for which environmental biogeochemical cycles are still relatively poorly known, especially in coastal aquatic systems. In addition, Sb is a fission product in nuclear power plants (NPPs), presenting non-negligible decay and consecutive exposition rates over short to mean terms (*i.e.*, $^{125}$Sb isotope: half-life of 2.76 y). Understanding the environmental behaviour and fate of natural stable isotopes and combining this with intrinsic properties of the respective radionuclides (e.g. half-life) is essential to predict the environmental fate and potential dispersion of radioisotopes before accidental NPP events. In the present work, the distribution and geochemical behaviour of stable Sb are determined for the first time in the highly turbid Gironde Estuary. Both dissolved and particulate concentrations along the estuarine salinity and turbidity gradients were quantified during low, intermediate and high freshwater discharges. Results clearly suggest that long residence times within the salinity and turbidity gradients favour the observed non-conservative, additive behaviour of Sb. Distribution coefficients ($\log_{10} K_d \approx 3.5 - 4.4$ L kg$^{-1}$) indicate that in the Maximum Turbidity Zone (MTZ; SPM ~1000 mg L$^{-1}$) ~90% of total Sb occurs in the particulate phase, compared to only ~10% in the less turbid portions of the estuary (SPM ≤ 100 mg L$^{-1}$). We propose a first/broad qualitative approximation (scenarios) to possible behaviour and dispersion of Sb radionuclides in case of accidental release from the Blayais NPP located on the Gironde Estuary. Our results suggest that the hydrological situation and the position of the MTZ during a potential accident can be primordial to residence time and distribution pathways in the estuary. We estimate that (i) high river discharge and a downstream position of the MTZ may favour Sb radionuclide adsorption onto particles, implying long (months to years) residence times in the estuary and a high risk of seasonal upstream transport into the city of Bordeaux, whereas (ii) under low discharge conditions, dissolved Sb species will predominate implying rapid transport and higher dispersion along the coast.

***Keywords:*** antimony, salinity gradient, distribution coefficient, residence time

# 1. INTRODUCTION

The Fukushima Dai-ichi Nuclear Power Plant (FDNPP) event in Japan (11$^{th}$ March 2011) has raised worldwide new questions and doubts concerning nuclear safety and possible accidental impacts on the oceanic environment. The direct and massive contamination of seawater used for urgency reactor cooling and the huge leakages of radioactive seawater were not foreseen as a likely scenario. As a consequence, the French National project AMORAD (ANR-11-RSNR-0002) was initiated in 2013 to unveil means for accurate evaluation of radioactive contamination on humans and environmental compartments at high spatiotemporal resolution (*http://www.irsn.fr*). In France ~75% of the total power supply depend on locally produced nuclear energy in 19 NPPs mostly located in the coastal French Metropolitan territory (WNA 2015). After NPP accidents, the largest inventory among radionuclides released and followed up is mainly dominated by volatile fission products such as noble gases (xenon, Xe, and krypton, Kr), iodine (I) and caesium (Cs) isotopes (Korsakissok et al. 2013; Steinhauser et al. 2014; Thakur et al. 2013; Ueda et al. 2013). However, there are other radioactive elements for which behaviours are unknown although their ranges of action and relevance can be equally important depending on the accidental conditions. In addition, current radionuclide studies are accident-dependent, thus performed after NPP fallout events. This clearly limits our knowledge on their environmental dispersion, persistence and fate to very few case studies, leaving very high uncertainty in dispersion scenarios and risk assessment. Stable isotopes and radionuclides of the same chemical element are commonly accepted to have analogous, or at least have proportional, chemical behaviour (*e.g.*, solubility, speciation, etc.; IAEA Report-422, 2004; Yang et al. 2012). Therefore, studies on stable isotopes improve our understanding of the environmental behaviour of their radioactive analogues, without them being present in the environment.

Antimony (Sb) has a high relative significance among the fission products in NPP with non-negligible radioactivity at relatively medium (< 30 years) exposure terms after the irradiation event (Akatsu et al. 1974; Delacroix et al. 2002). Its isotopes are produced with a probability of ~ 8% from $^{235}$U fuel and ~7% from $^{239}$Pu in less than 24h both by direct fission and by decay of other fission products, which is similar to the fission yields for Cs and I isotopes (9–12%; calculations obtained from information in Sonzogni 2013 and Element Collection Inc. 2007). The isotope with highest half-life ($^{125}$Sb; $T_{1/2}$ = 2.76 y) was emitted by both the Chernobyl (ChNPP, Ukraine 26$^{th}$ April 1986) and the FDNPP accidents (Steinhauser et al. 2014; Thakur et al. 2013). Moreover, $^{125}$Sb was detected in molluscs (Whitehead et al. 1988) and soils (Carbol et al. 2003; Papastefanou et al. 1988) as early as one month and up to 6.5 years after the ChNPP accident, respectively. These measurements reflect the importance of Sb radioisotopes dispersion for direct (through skin contact and/or inhalation) and/or indirect (through food supplies) human exposure.

The study of stable Sb, considered a pollutant of priority interest by the European Community (Directive 2006/11/EC), the German Research Council (DFG 2012) and the U.S. Environmental

Protection Agency (USEPA 2013), was largely neglected until recently (Filella et al. 2002a; Smichowski 2008). Increasing concern on Sb in the last decade has been related to its high contamination levels in certain areas, jeopardising public health. Current studies have focused on Sb determination in atmospheric aerosols (Smichowski 2008), its removal from contaminated waters and wastewaters (Ha et al. 2009; Ungureanu et al. 2015) and its mobility in different soils and crop uptake (Pierart et al. 2015; Wilson et al. 2010; Zhang et al. 2014). Additionally, Sb quantification methods and speciation in a wide range of environmental matrices at trace and ultratrace levels have been reviewed (Ferreira et al. 2014; Nash et al. 2000; Smichowski et al. 1998; Smichowski 2008), confirming its ubiquity in the environment (Asaoka et al. 2012; Filella et al. 2002a; Filella 2011; Silva et al. 2014; Ungureanu et al. 2015; Wilson et al. 2010). Nevertheless, the integration of all this data into a general biogeochemical cycle has not yet been accomplished (Filella et al. 2009) and there is still a lack of knowledge on the chemical processes involved in environmental Sb behaviour, transformation and transport (Filella 2011), especially in advective flow systems (Zhang et al. 2014).

The aim of this study is to characterise the distribution and geochemical behaviour of Sb within the Gironde Estuary in order to evaluate Sb radionuclide behaviour and dispersion within the estuary and the coastal ocean, in case of an accidental release from the Blayais NPP (inside the Gironde Estuary). To achieve this, specific objectives are to (i) provide the first data on Sb dissolved and particulate concentrations and Sb partitioning along the turbidity and salinity gradients of the Gironde Estuary, and (ii) to propose a preliminary qualitative conceptual model (scenarios) for the Gironde estuarine system to predict potential dispersion in case of accidental Sb radionuclide emissions from the Blayais NPP.

## 2. MATERIAL AND METHODS

### 2.1. Study area

The Gironde Estuary is the largest estuary in SW Europe with a total surface area of 635 $km^2$ at high tide and a watershed size of approximately 81,000 $km^2$ (Salomon 2002). The geographical limit of the estuary is at the confluence of the Garonne (average discharge, Q = 594 $m^3 s^{-1}$) and Dordogne (Q = 318 $m^3 s^{-1}$) rivers (Fig. 1). However, the marine influence (*i.e.,* semidiurnal tidal cycle of 12h 25min) extends 180 km upstream from the estuary mouth, defining the limit of the dynamic tide at La Réole on the Garonne River (Kilometric Point: KP -70, Fig. 1). The residual circulation (caused by the salinity-driven vertical gradients) and the hypersynchronous character of the estuary develop a Maximum Turbidity Zone (MTZ) with Suspended Particulate Matter (SPM) concentrations > 1000 mg $L^{-1}$ (Sottolichio and Castaing 1999). The MTZ is mostly found in the low salinity region and migrates up and down the estuary at both seasonal (dependent on river flow) and tidal time scales (Sottolichio and Castaing 1999). This implies that low river discharge conditions (typical of summer seasons) favour the entrance of seawater further upstream in the estuary, causing the MTZ to reach the city of Bordeaux (Sottolichio and Castaing 1999). Drought periods have increased in intensity and duration over the past decades due

to overall decrease in annual average freshwater supply to the Gironde Estuary, favouring the saline intrusion upstream of Bordeaux (Etcheber et al. 2011; Sottolichio et al. 2011). In particular situations (generally 10 - 20 days per year), the MTZ can be partly flushed outside of the estuary when specific conditions are met: continuous and high river discharge during weeks with high tidal coefficient (Castaing and Allen 1981). The SPM has an average residence time in the estuary of 1 - 2 years (Castaing and Jouanneau 1979), whereas the water residence time varies from 86 days in low discharge conditions to ~18 days under high discharge conditions (Castaing and Jouanneau 1979; Jouanneau and Latouche 1981).

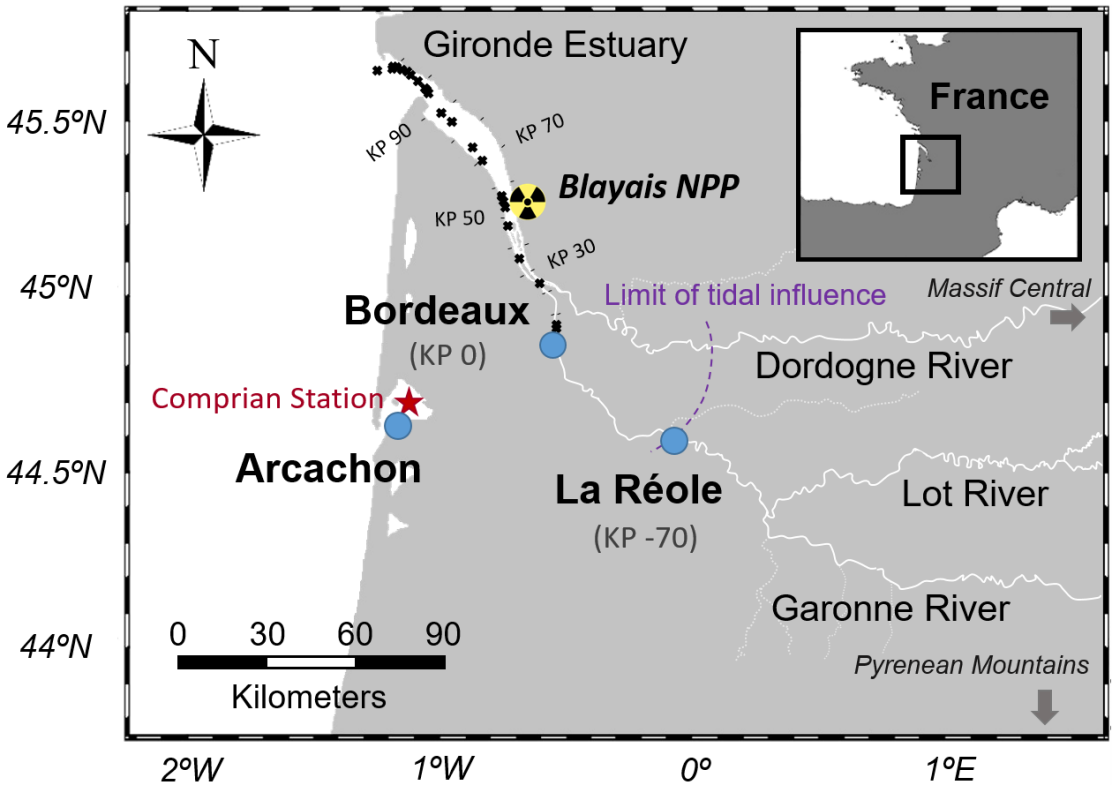


**Figure 1.** Map of the Gironde Estuary. Main cities (circles), river systems (Dordogne, Garonne and Lot rivers) and sampling sites along the Gironde Estuary during three sampling campaigns (crosses, MGTS I – March 2014, MGTS II – March 2015 and MGTS III – October 2015) and at Comprian Station in Arcachon Bay (star) are represented.

Ore deposits and former mining areas in the upper reaches of the Garonne and Dordogne watersheds (Massif Central and the Pyrenean Mountains; Fig. 1) are major sources of many metals and metalloids to the Gironde Estuary, including the oxyanion-forming Sb (BRGM 2014; Masson et al. 2009, 2011). Moreover, anthropogenic point sources of Sb linked to former power station landfills and several industrial tailings (ore treatment, coal mine) have also been identified in the Lot-Garonne River system (Coynel et al. 2007a, 2007b, 2009).

The Gironde Estuary watershed hosts two NPPs. The Golfech NPP is located on the Garonne River ~160 km upstream from Bordeaux and the Blayais NPP directly next to the estuary in the area of Braud-et-Saint-Louis at 48 km NNW of Bordeaux. During the past 2 decades a series of incidents have occurred

in both NPPs, and were attributed to the levels 1 and 2 of the International Nuclear Event Scale (http://france.edf.com/).

## 2.2. Sample collection

Water samples were collected during three longitudinal profiles along the estuarine salinity and turbidity gradients on-board the R/V *Thalia* (IFREMER) in March 2014 (MGTS I, n = 26), March 2015 (MGTS II, n = 23) and October 2015 (MGTS III, n = 26) from Bordeaux to the estuary mouth (Fig. 1) under different discharge conditions: intermediate (Q = 1203 $m^3 s^{-1}$), high (Q = 3450 $m^3 s^{-1}$) and low (Q = 260 $m^3 s^{-1}$), respectively. Water was sampled using Niskin bottles at 1 m depth, immediately filtered onsite through 0.2 µm Minisart® cellulose acetate filters into acid-washed polypropylene (PP) bottles, acidified with $HNO_3$ (2% J.T. Baker Ultrapure, 14 M) and stored at 4ºC in the dark until analysis. Suspended particle samples were collected into 40 L acid-washed polyethylene (PE) drums with a PP peristaltic pump and PP tubing at 1 m depth followed by on-board centrifugation (Westfalia; 12,000 g; Lapaquellerie et al. 1996), dried (50ºC in a drying oven), grinded and homogenised (agate mortar) and stored at room temperature in the dark until analysis.

A fourth sampling campaign was carried out on board the R/V *Planula IV* (CNRS/INSU) in April 2015 in the Arcachon Bay (Comprian Station, Fig. 1). Water samples were collected at 2.5 m depth with high frequency sampling (every hour) during a complete tidal cycle. This bay was chosen for comparison of dissolved and particulate Sb concentrations and partitioning with those in the high salinity-range of the Gironde Estuary. The Arcachon Bay provides relatively similar hydrodynamic characteristics (*i.e.*, meso- to macrotidal bay with semi-diurnal tide cycle and high seawater influence) but drains a totally different watershed and provides very low SPM concentrations, compared to the hyperturbid Gironde Estuary. Water samples were collected into acid-washed PP bottles, thoroughly rinsed with water from the site using an in-house 12V battery powered peristaltic PP pumping, with acid pre-cleaned Tygon tubing previously rinsed with water from the site (~10 minutes). Aliquots for dissolved Sb analysis were collected and processed as aforementioned for the Gironde Estuary. Samples for particulate Sb analyses were recovered by filtration through pre-dried and weighed 0.45 µm Teflon® filters, dried and stored in sealed plastic boxes at room temperature and in the dark until analysis. Previous work comparing SPM recovery by both centrifugation and filtration in fluvial-estuarine systems has shown that both techniques provide similar results (Lapaquellerie et al. 1996).

In all cases, SPM concentrations were determined by filtering precise volumes of water through dry pre-weighed filters (Xilab glass microfiber, 0.7 µm). Filters were then dried to constant weight at 50ºC and re-weighed. Water temperature and conductivity were measured with a TetraCon 96® probe (PROFILINE, WTW) and pH was determined with a Sentix ® 41 probe (PROFILINE, WTW), previously calibrated using the manufacturer's specifications and supplied reagents (NIST pH standards).

### 2.3. Determination of Sb

Dissolved Sb ($Sb_d$) was quantified in diluted samples (to S ~ 1) by ICP-MS (X7 Series, THERMO) equipped with a gas dilution cyclonic spray chamber (PC3 ESI) using isotope dilution with a solution enriched in $^{123}Sb$ (99.43% purity; Oakridge, USA). Analyses of a certified reference material (CRM; TM RAIN-04) produced results that were consistently within the certified range and precision was < 8% (RSD).

Total sediment digestions for particulate Sb ($Sb_p$) quantification were performed on representative subsamples (*i.e.*, 30 mg of dry, powdered and homogenised material) in closed PP reactors (DigiTUBEs®, SCP SCIENCE) on a heating plate (2 h at 110 ºC) using 1.5 mL HCl (10 M Suprapur®, Merck), 750 µL $HNO_3$ (14 M Suprapur®, Merck) and 2.5 mL HF (29 M Suprapur®, Fisher), as described elsewhere (*e.g.*, Schäfer et al. 2002). After evaporation to dryness, re-dissolution of the residues was performed with 250 µL $HNO_3$ (14 M) on a heating plate and, after cooling, brought to 10 mL using Milli-Q water. Particulate Sb and thorium (Th) concentrations were quantified through external calibration using ICP-MS (X7 Series 2, THERMO). The analytical method was quality checked with sediment CRMs (IAEA 433; NIST 2702). Accuracies were 88%, with precision ≤ 4% (RSD).

## 3. RESULTS

### 3.1. Dissolved and particulate Sb

Dissolved Sb concentrations increased with salinity along the Gironde Estuary (Fig. 2a) showing values from the freshwater endmember to S > 27 of: 1.31 ± 0.07 nM (0.16 ± 0.01 µg $L^{-1}$; mean ± standard deviation) to 2.68 ± 0.04 nM (0.33 ± 0.01 µg $L^{-1}$) in low discharge conditions, 0.90 ± 0.08 nM (0.11 ± 0.01 µg $L^{-1}$) to 3.29 ± 0.49 nM (0.40 ± 0.06 µg $L^{-1}$) in intermediate discharge conditions and 0.99 ± 0.08 nM (0.12 ± 0.01 µg $L^{-1}$) to 2.79 ± 0.08 nM (0.34 ± 0.01 µg $L^{-1}$) in high discharge conditions. In any case, concentrations at high salinity ranges fall within the wide range of values expected for North Atlantic coastal waters (~2.46 - 4.11 nM; 0.3 - 0.5 µg $L^{-1}$; Filella et al. 2002b). Average $Sb_d$ concentrations for salinities between 25 and 33 in the Arcachon Bay were 2.05 ± 0.16 nM (0.25 ± 0.02 µg $L^{-1}$), i.e. more similar to measurements for the Atlantic coast off Nantes (1.70 ± 0.06 nM, 0.21 ± 0.01 µg $L^{-1}$, Fig. 2a) and the Loire Estuary mouth (1.81 ± 0.11 nM, 0.22 ± 0.01 µg $L^{-1}$; Takayanagi and Michel 1996).

Particulate Sb in the Gironde Estuary ranged from 9.9 nmol $g^{-1}$ (1.20 mg $kg^{-1}$) to 25 nmol $g^{-1}$ (3.07 mg $kg^{-1}$), showing slightly decreasing trends along the salinity gradient (Fig. 2b) and high variability in the low salinity reaches. Thorium-normalisation ($Sb_p/Th_p$ ratios) produces clearly less variable (*i.e.*, grain-size corrected; Larrose et al. 2010) values, widely independent from SPM concentrations (average 0.16 ± 0.02 for all hydrological conditions; Fig. S1a and b, Supplementary Data). During high discharge, $Sb_p$ concentrations were clearly higher (16.0 ± 0.6 nmol $g^{-1}$; 1.95 ± 0.08 mg $kg^{-1}$) than during

intermediate discharge (12.8 ± 0.6 nmol $g^{-1}$; 1.55 ± 0.07 mg $kg^{-1}$) at S > 5. During low discharge conditions, $Sb_p$ distribution was similar to that in intermediate discharges, yet with a less defined trend along the salinity gradient (Fig. 2b). Average $Sb_p$ concentrations in the Arcachon Bay were 10.9 ± 2.0 nmol $g^{-1}$ (1.32 ± 0.19 mg $kg^{-1}$), showing the same variability when $Sb_p/Th_p$ ratios were calculated (Fig. S1a, Supplementary Data).

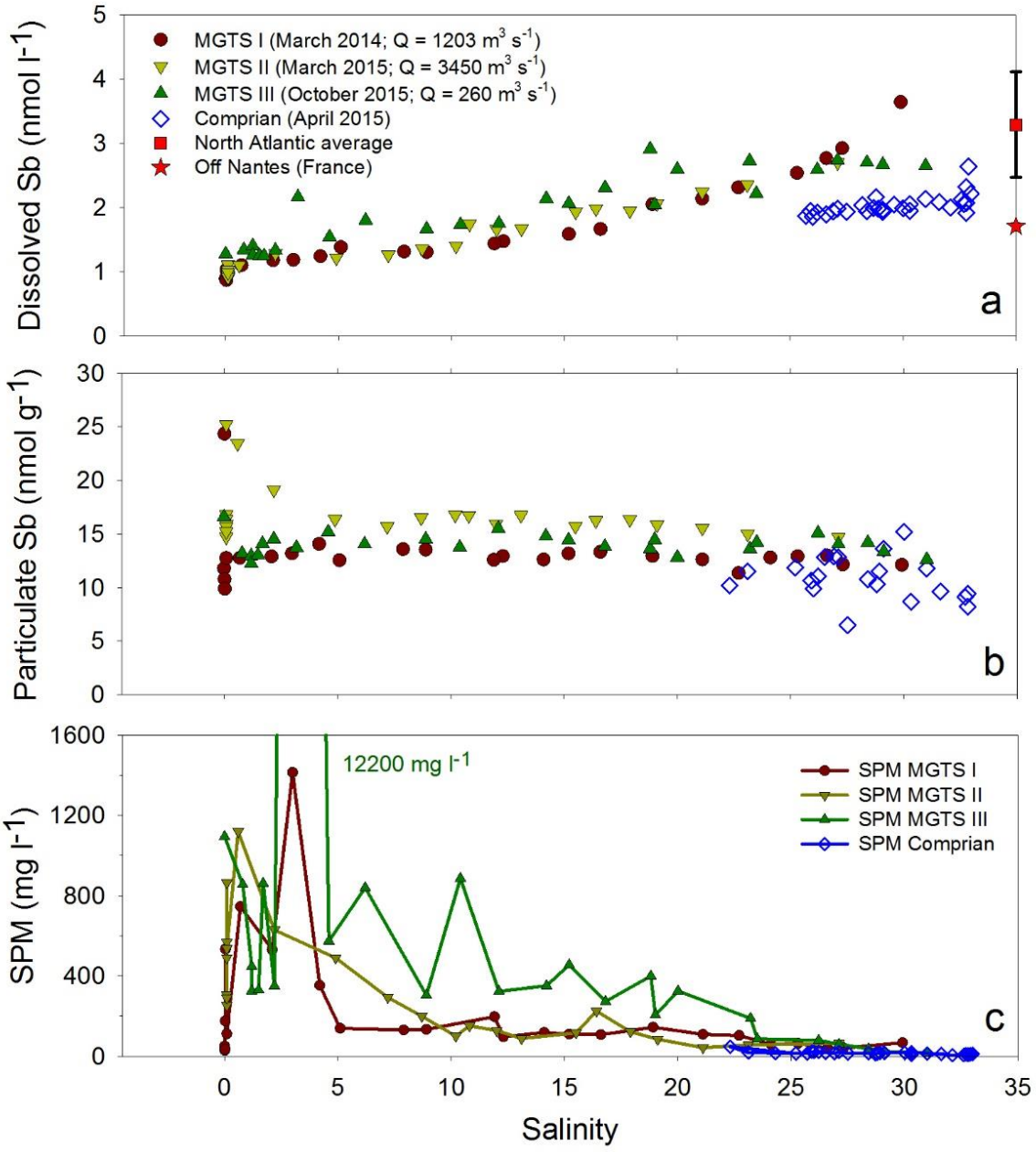


**Figure 2.** Distribution of (a) dissolved Sb (nmol $L^{-1}$), (b) particulate Sb (nmol $g^{-1}$) and (c) SPM (mg $L^{-1}$) concentrations along the salinity gradient during low (MGTS III, October 2015), intermediate (MGTS I, March 2014) and high (MGTS II, March 2015) freshwater discharge conditions in the Gironde Estuary and during a tidal cycle at Comprian Station (Arcachon Bay, April 2015). The average concentration of dissolved Sb in the North Atlantic (from Filella et al. 2002b) and off Nantes (from Takayanagi and Michel 1996) are also shown in (a).

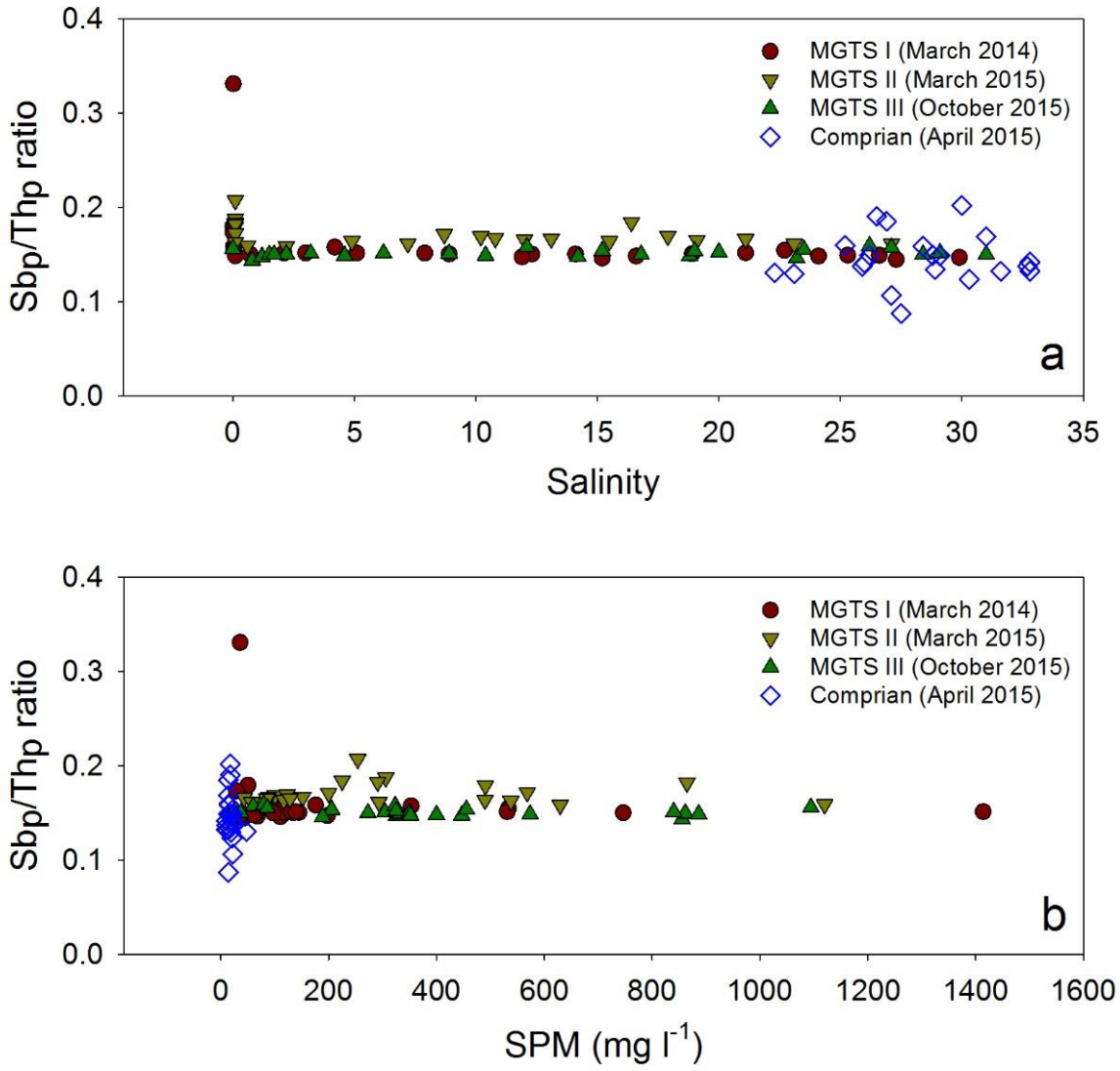


**Figure S1.** Grain-sized corrected $Sb_p$ concentrations ($Sb_p/Th_p$ ratio) is shown along (a) the salinity and (b) the SPM gradient in the Gironde Estuary (MGTS I – intermediate discharge in March 2014, MGTS II – high discharge in March 2015 and MGTS III – low discharge in October 2015) and Arcachon Bay (tiday cycle at Comprian Station, April 2015).

The SPM concentrations along the salinity gradients in the Gironde Estuary were 18 – 12200 mg $L^{-1}$ for low, 29 – 1400 mg $L^{-1}$ for intermediate and 43 – 1100 mg $L^{-1}$ for high discharges, the MTZ occurring in the low salinity ranges (S < 10; Fig. 2c). Arcachon Bay samples showed lower SPM concentrations (5 – 50 mg $L^{-1}$). Average pH and temperatures were 8.21 ± 0.11 and 16.3 ± 0.78ºC for low, 8.16 ± 0.07 and 13.0 ± 0.65ºC for intermediate and 8.07 ± 0.08 and 9.20 ± 0.44ºC for high discharges, respectively (Fig. S2a and b, Supplementary Data) in the Gironde Estuary samples, whereas in the Arcachon Bay samples pH was 7.94 ± 0.08 and temperature was 17.2 ± 1.15ºC.

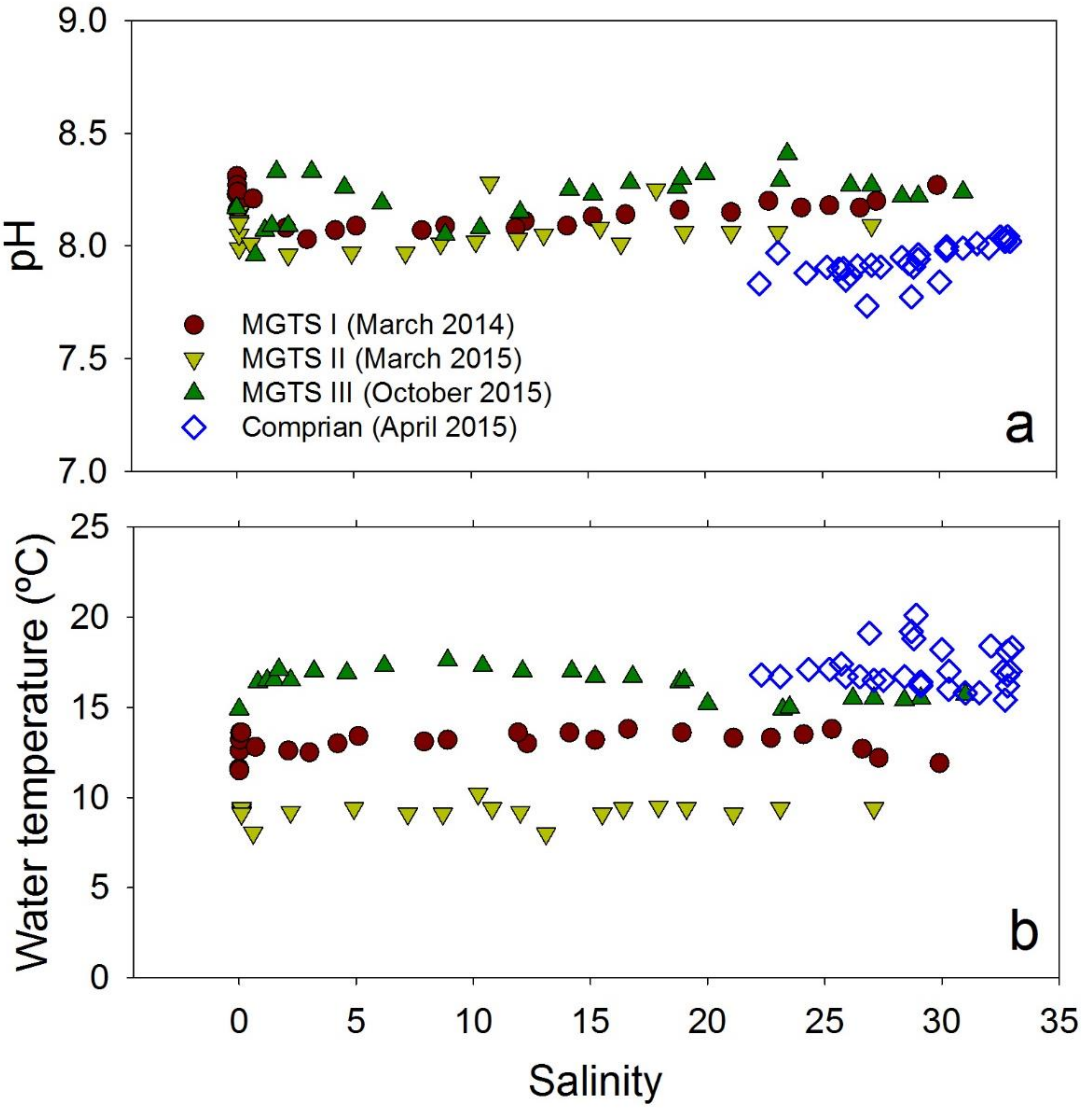


**Figure S2.** (a) pH and (b) water temperature (°C) along the salinity gradient are represented for the Gironde Estuary (MGTS I – intermediate discharge in March 2014, MGTS II – high discharge in March 2015, and MGTS III – low discharge in October 2015) and the Arcachon Bay (tidal cycle at Comprian Station, April 2015).

### 3.2. Distribution coefficient ($K_d$)

Antimony partitioning between the dissolved and particulate phases along the salinity and turbidity gradients was evaluated using the particle-water distribution coefficient ($K_d$) as described in Sung (1995). The $K_d$ (in L $kg^{-1}$) is calculated by dividing the particulate concentration (centrifuged or filter-retained, in mg $kg^{-1}$) by the dissolved (0.2 µm filter-passing, in mg $L^{-1}$) concentrations. The fraction of $Sb_p$ (%) compared to the total Sb ($Sb_t$, which comprises both $Sb_d$ and $Sb_p$) are calculated as follows:

$$K_d = Sb_p/Sb_d$$

$$Sb_t = Sb_p \cdot SPM + Sb_d$$

$$Sb_p(\%) = (Sb_p \cdot SPM)/Sb_t = (K_d \cdot SPM)/(1 + K_d \cdot SPM)$$

where $Sb_p$(%) is the percentage of particulate Sb in the given environment, $Sb_p$ is expressed in mg $kg^{-1}$, $Sb_d$ in mg $L^{-1}$, $Sb_t$ in mg $L^{-1}$ and SPM in kg $L^{-1}$.

Distribution coefficients observed along the Gironde Estuary salinity gradient ($\log_{10} K_d \approx 3.5 – 4.4$ L $kg^{-1}$) decrease with increasing salinity and show highest variability at S = 0 (Fig. 3a). Moreover, $K_d$ indicates that in the MTZ (SPM ≥1000 mg $L^{-1}$) 90-100% of the total Sb is associated with particles, whereas low SPM (≤ 100 mg $L^{-1}$) favour predominance of $Sb_d$, with only ~10% of total Sb in the particulate phase (Fig. 3b). Mean annual $K_d$ values obtained from long-term monitoring at La Réole site, *i.e.* the main fluvial entry of the Gironde Estuary, generally show higher coefficients ($\log_{10} K_d > 4$ L $kg^{-1}$; unpublished data). The comparison between saline and freshwater coefficients suggest that Sb is more soluble within the estuary. Distribution coefficients in the Arcachon Bay follow the trend observed in the Gironde Estuary, with $Sb_p$ contributing less than 20% of total Sb, due to the relatively low SPM concentrations (< 50 mg $L^{-1}$, Fig. 3b).

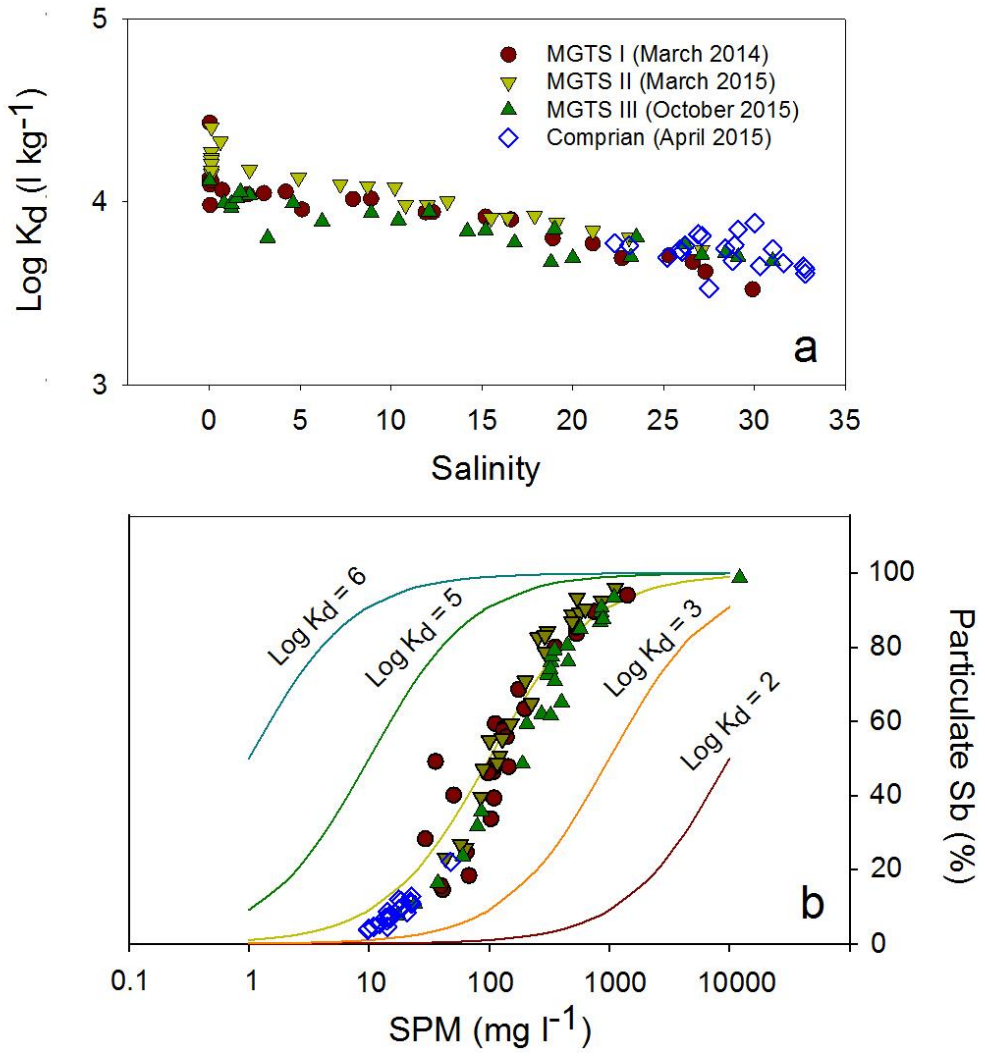


**Figure 3.** Distribution coefficient ($K_d$) for Sb in the Gironde Estuary during low (MGTS III, October 2015), intermediate (MGTS I, March 2014), high (MGTS II, March 2015) freshwater discharge conditions and in the Arcachon Bay (tidal cycle at Comprian Station, April 2015) along (a) the salinity gradient and (b) the SPM concentrations.

# 4. DISCUSSION

## 4.1. Antimony estuarine behaviour and reactivity

Previous studies have shown conservative behaviour of Sb in the freshwater reaches of the Gironde Estuary (between La Réole and Bordeaux; Fig. 1) for different hydrological conditions and SPM concentrations (*i.e.*, 10 – 1000 mg $L^{-1}$; Masson et al. 2009, 2011). Our results complement these findings, strongly suggesting that Sb is non-conservative along the salinity and turbidity gradients of the Gironde Estuary, which is more evident during intermediate and low freshwater discharges (Fig. 2a and b). In addition, the nominal North Atlantic mean $Sb_d$ concentration (NAmc$Sb_d$; 2.46 - 4.11 nM; 0.3 – 0.5 µg $L^{-1}$) is not precise enough to quantify the addition process, deduced from the high $Sb_d$ at S > 25, exceeding NAmc$Sb_d$ and the average $Sb_d$ in the Arcachon Bay. Available average $Sb_d$ concentrations for the NE Atlantic Ocean and, more precisely, for the French coast in the area of Nantes (average 1.76 nM; 0.21 µg $L^{-1}$; Schutz and Turekian 1965; Takayanagi and Michel 1996) clearly support both addition in the Gironde Estuary and apparent conservative behaviour in the Arcachon Bay as a comparative site.

Antimony profiles along salinity gradients have shown both conservative and non-conservative behaviours, presenting different patterns depending on estuary characteristics (Byrd 1990; Filella et al. 2002b, 2003; Wilson and Webster-Brown 2009). Conservative behaviours have been reported for pristine or organic-rich (Dissolved Organic Carbon; DOC > 0.5 mM; 6 mg $L^{-1}$) estuaries (Byrd 1990; van der Sloot et al. 1985; Wilson and Webster-Brown 2009; Table S1, Supplementary Data). Non-conservative behaviours have been related to scavenging, remobilisation processes, remineralisation/redox conditions and anthropogenic sources (Andreae et al. 1983; Byrd 1990; van den Berg et al. 1993; van der Sloot et al. 1985; Table S1, Supplementary Data). The Gironde Estuary shows relatively low DOC concentrations (average 0.15 ± 0.03 mM; 1.8 ± 0.3 mg $L^{-1}$; Huguet et al. 2009). Moreover, the existing data suggest that there are no important anthropogenic Sb sources within the saline reaches of the Gironde Estuary, both for $Sb_p$ (*i.e.*, $Th_p$ normalisation suggests that variations in $Sb_p$ are due to grain-size effects; Fig. S1a, Supplementary Data), and $Sb_d$ as suggested by Tessier et al. (2002) and Masson et al. (2009).

On the other hand, residence times have been proposed to influence Sb seawater scavenging (Filella et al. 2002b). Within low-impacted estuaries, short water residence times (*i.e.*, some days) have shown conservative behaviours in the Rhine River (van der Sloot et al. 1985) and the Waikato Estuary (Wilson and Webster-Brown 2009). Contrastingly, van der Sloot et al. (1985) observed a $Sb_d$ peak in the Scheldt Estuary between S = 20 – 30, with water residence times between 2 – 3 months. These increases in $Sb_d$ were attributed to remineralisation processes in oxygen deficient conditions, as Fe and Mn oxy-hydroxides are major host phases of Sb (Asaoka et al. 2012; Brannon and Patrick 1985; Filella et al. 2002b; Manaka et al. 2007; Wilson et al. 2010). In fact, bottom sediments from the upstream Garonne River have shown high association of Sb to amorphous and crystalline iron oxyhydroxides (Leleyter

and Probst 1999). Thus, Sb release to the dissolved phase is expected to occur when the redox-sensitive carrier phases are reduced, conditions which are favoured by long residence times.

Table S1. Some worldwide estuarine examples of Sb behaviour.

| Behaviour | System | System characteristics | References |
|---|---|---|---|
| Conservative | Rhine River Estuary (The Netherlands) | Macrotidal<br>A = n.a. [a,i]<br>D = n.a. [b,i]<br>Q = 2 900 $m^3 s^{-1}$ [c]<br>$\tau_r$ = 2-3 days [1d]<br>DO ≥ 40% saturation [e] | van der Sloot et al. 1985<br><br>*(Tessier et al. 2002)*[j] |
| | St. Mary's Estuary (Georgia, USA) | Mesotidal<br>A = 64 $km^2$ [a]<br>D = 6.1 m [b]<br>Q = 35 $m^3 s^{-1}$ [c]<br>$\tau_r$ = 65 days [2d]<br>DOC > 2.5 mM (30 mg $L^{-1}$) [f] | Alber and Sheldon 1999; Byrd 1990<br><br>*(Dame et al. 2000; NOAA 2012; Pendleton et al. 2004)*[j] |
| | Satilla River estuary (Georgia, USA) | Mesotidal<br>A = n.a. [a,i]<br>D = 4 m [b]<br>Q = 10-1000 $m^3 s^{-1}$ (34) [c]<br>$\tau_r$ = 63 days [2d]<br>DOC > 3.3 mM (40 mg $L^{-1}$) [f]<br>Sediment resuspension | Alber and Sheldon 1999; Byrd 1990; Zheng et al. 2003, 2004<br><br>*(Alber et al. 2003; Blanton et al. 1999)*[j] |
| | Waikato Estuary (New Zealand) | Mesotidal<br>A = 18 $km^2$ [a]<br>D ≈ 5 m [b]<br>Q = 183-600 $m^3 s^{-1}$ [c]<br>$\tau_r$ = < 10 days* [1d]<br>Geothermal-driven system<br>Seasonal dilution patterns<br>Occasional peaks due to remobilisation events | Jones and Hamilton 2014; Wilson and Webster-Brown 2009 |
| Non-conservative | Tagus Estuary (Portugal) | Mesotidal<br>A = 320 $km^2$ [a]<br>D = 10.6 m [b]<br>Q = 300-1000 $m^3 s^{-1}$ [c]<br>$\tau_r$ = 10-60 days [1d]<br>Anthropogenic sources | Andreae et al. 1983<br><br>*(Freire et al. 2006)*[j] |
| | Scheldt Estuary (The Netherlands) | Macrotidal<br>A = 370 $km^2$ [a]<br>D = 15 m [b]<br>Q = 34-253 $m^3 s^{-1}$ (107) [c]<br>$\tau_r$ = 2-3 months [1d]<br>MTZ (max. 400 mg $L^{-1}$) [g]<br>OMZ in low salinity [h]<br>Reducing conditions<br>Influence of marine $Sb_p$ | BIOCONSULT & NLWKN 2013; van der Sloot et al. 1985<br><br>*(Sistermans and Nieuwenhuis 2004; Tessier et al. 2002)*[j] |

*(Table S1 Continued)*

| Behaviour | System | System characteristics | References |
|---|---|---|---|
| | Savannah River estuary (Georgia, USA) | Mesotidal<br>A = 121 $km^2$ [a]<br>D = 4.6 m [b]<br>Q = 328 $m^3$ $s^{-1}$ [c]<br>$\tau_r \approx$ 1 month* [1d]<br>Scavenging at low salinities<br>Reducing conditions | Byrd 1990<br><br>*(Dame et al. 2000; Reinert and Peterson 2008)*[j] |
| | Tan Shui Estuary (Taiwan) | Mesotidal<br>A = n.a. [a,i]<br>D = 6.5 m [b]<br>Q = 160 $m^3$ $s^{-1}$ [c]<br>$\tau_r$ = 5-9 d [1d]<br>Anthropogenic sources<br>Upstream anoxic estuary | Byrd 1990; Fang and Lin 2002; Liu et al. 2001<br><br>*(Fan et al. 2006; Liu et al. 2005)*[j] |
| | Tamar River estuary (United Kingdom) | Macrotidal<br>A = n.a. [a,i]<br>D = 30 m [b]<br>Q = 5-38 $m^3$ $s^{-1}$ [c]<br>$\tau_r$ = 1-3 weeks [2d]<br>Defined MTZ (max. 3 g $L^{-1}$) [g]<br>Scavenging at low salinities<br>Interstitial water release (anoxia)<br>Adsorption/desorption reactions | Bale et al. 2007; Uncles et al. 1983; van den Berg et al. 1993<br><br>*(Tattersall et al. 2003)*[j] |

[a] A = Average estuary surface area

[b] D = Average estuary depth

[c] Q = Seasonal or average discharges. When brackets are also shown, the range corresponds to maximum and minimum discharges and the average is presented in brackets

[d] $\tau_r$ = water residence time in the estuary. *correspond to estimated values, generally considered by dividing stock by fluxes (1). Estimates on flushing time (2) given in the different references are considered equivalent to residence times unless specified otherwise

[e] DO = Dissolved Oxygen

[f] DOC = Dissolved Organic Carbon

[g] MTZ = Maximum Turbidity Zone

[h] OMZ = Oxygen Minimum Zone

[i] n.a. = not available

[j]*References between brackets refer to sources on hydromorphological information (A, D or tidal character) when it is not indicated in the main references*

Reducing conditions typically occur in interstitial waters, as observed for the Tamar Estuary after sediment remobilisation (van den Berg et al. 1991). However, in hyperturbid estuaries as the Gironde Estuary, suboxic conditions may occur in the water column, related to organic matter bacterial degradation within the MTZ during low river discharges and high temperatures (Goosen et al. 1999; Lanoux et al. 2013) and in the highly turbid "soft mud" layer in the bottom of the MTZ water column (Audry et al. 2006; Robert et al. 2004). Reductive dissolution of Sb is expected to be highest during low freshwater discharge conditions, when higher water temperature and lower pH, compared to the other hydrological conditions, suggest intense respiration processes along the salinity and turbidity gradients (Fig. S2a and b, Supplementary data). The presence of a well-developed "soft mud" layer is much less probable during high discharge situations than during intermediate discharge or even low discharge. The difference in intensity of redox driven Sb release may contribute to the observed differences in Sb addition for the different hydrological situations, although the addition in the high salinity range does not coincide with the MTZ (Fig. 2a and c). Mid-estuary (mid-salinities) releases of Sb have also been related to adsorption-desorption reactions (Filella et al. 2002b; van den Berg 1993). The dissolution of $Sb_p$ with increasing salinity in Mediterranean estuaries has been suspected to result from both desorption from the FeOOH fraction (dependent of salinity and SPM concentrations) and/or redox processes related to Fe and Sb speciation (Migon and Mori 1999; Ritchie et al. 2013). In fact, several combinations of ionic strength and pH conditions have shown to affect differently the sorption behaviour of Sb species onto different mineral phases, implying both changes on the particle surface electrostatic potential (binding sites) and ionic interactions/competitions (Wilson et al. 2010 and references therein).

The processes behind all these observations could induce the differences observed in the Gironde Estuary. The measured oxic conditions at the sampling depths (though not indicative of lack of reducing conditions at deeper depths) together with the suspected slow interaction/kinetics in the area (Masson et al. 2009) and the lack of *a priori* anthropogenic sources suggest that Sb behaviour in the Gironde Estuary is related to residence times: high (short water residence times) and intermediate/low river discharges (longer residence times).

Normalisation to $Th_p$ is often used to correct grain size induced effects on particulate metal concentrations as it is a conservative lithogenic element and its concentration increases with smaller grain size (Krachler and Shotyk 2004; Loring and Rantala 1992, Larrose et al. 2010). In this study, the comparison between $Sb_p$ concentrations and $Sb_p/Th_p$ ratios along the Gironde Estuary suggests minor influence of grain size effects in the freshwater/low salinity reaches ($S < 5$), especially under high discharge conditions.

Variable $Sb_p$ concentrations and $Sb_p/Th_p$ ratios in freshwater endmember samples observed for the different hydrological conditions probably reflect variable mixing proportions between particles freshly derived from the watershed and particles having undergone longer periods of estuarine mixing. In fact, the freshwater samples in MGTS I and II were retrieved during ebb and in MGTS III during tidal flood. The commonly observed freshwater $Sb_p/Th_p$ ratios at La Réole site (average 0.19 ± 0.09 during 2013-

2014, N = 33, unpublished) explain the variability observed at low salinities (Fig. S1a, Supplementary data). The $Sb_p/Th_p$ ratio along the estuary (0.16 ± 0.02) is slightly below this freshwater average suggesting that estuarine particles get depleted in $Sb_p$ over time. Accordingly, estuarine differences for S > 5 in average $Sb_p$ concentrations between campaigns can be explained by a combination of (i) grain-size effects, (ii) particle renewal due to erosion and fluvial transport from the watershed, and (iii) shorter average particle residence times during high discharges, limiting Sb dissolution during particle transport towards the ocean.

Following the same reasoning, the waters in the Arcachon Bay were considered representative of short residence times at the measured tidal time scale. Thus, the low $Sb_d$ concentrations found at high salinities support the addition hypothesis for the Gironde Estuary. The variability observed in $Sb_p$ (*i.e.,* 14%) is consistent with observations during a tidal cycle in the Wadden Sea (*i.e.,* 15%), influenced by oceanic sediment (less concentrated in Sb) and low SPM concentrations (11 – 46 mg $L^{-1}$; van der Sloot et al. 1985).

### 4.2. Qualitative scenarios for accidental Sb radionuclide releases

Based on the obtained results, two different preliminary scenarios for an accidental release of Sb radionuclides from the NPP of Blayais are proposed, corresponding to the most contrasting hydrological situations in the Gironde Estuary. There is little information on the forms of accidentally released Sb (*i.e.,* dissolved or associated to fuel particles) and different accidents display different emission patterns. If Sb was released in particulate forms, dissolution/desorption kinetics should be taken into account to develop contamination scenarios, as desorption rates for natural compounds in seawater vary among natural marine aerosol particles (40% in 24h; Crecelius 1980), urban particles (27% in 2h; Austin and Millward 1986) and polluted North Sea coastal aerosols (83% in 100h; Kersten et al. 1991). However, the water masses in the central part of the hyperturbid Gironde Estuary generally show clearly lower salinities than seawater and very high SPM concentrations, especially in the presence of the MTZ. Such conditions are expected to limit Sb release from particles and favour adsorption of dissolved Sb onto particles, the latter being of major importance in case of dissolved Sb radionuclide release. This suggests that radioactive $Sb_p$ in the estuary will be controlled by the complex interplay of particulate dynamics (MTZ) and the geochemical gradients (salinity, redox), as described in the scenarios below.

The proposed simplified scenarios focus on dissolved Sb radionuclide releases as a first approach to foresee the range of possible dispersion patterns according to the hydrodynamic and biogeochemical conditions within the estuary. The distribution between dissolved and particulate phases appears as the major control parameter, determining the physical transport (spatial scale) and the residence time (temporal scale) of the radionuclides in the different areas of the estuarine system. We cannot exclude that interactions between anthropogenic Sb or radionuclides released to the dissolved phase and estuarine particles could be different from the observed distributions between the particulate and the

dissolved fractions (*i.e.*, specific of reactive, exchangeable sediment fractions). Similarities between distribution coefficients for stable and radioactive Sb have not been proven, as it is the case for other elements such as Cs or Sr (Ciceri et al. 1988). Furthermore, the Kd values in this study are derived from total $Sb_p$ concentrations (instead of exchangeable or reactive Sb fractions), including the non-reactive fraction fixed in the mineral lattice. Accordingly, these scenarios may somewhat overestimate the role of particles in the fate of dissolved Sb radionuclide release (due to supposed lower $K_d$ values for reactive Sb fractions). Despite these limitations, the observed estuarine $K_d$ values fall within the 5th – 95th percentile range of freshwater radioactive Sb $K_d$ ($\log_{10} K_d = 2.7 – 4.7$ L $kg^{-1}$) estimated by Ciffroy et al. (2009). Therefore, the following scenarios are based on (i) total $K_d$, and (ii) the assumption of similar partitioning behaviour of both radioactive and stable Sb.

**Scenario 1 – accident during high river discharge conditions:** During high freshwater discharges salinity levels near the Blayais NPP (KP 52) are relatively low and the MTZ is displaced towards the centre/mouth of the Gironde Estuary (Sottolichio and Castaing 1999). Such conditions favour low SPM in front of the NPP, limiting adsorption of radioactive $Sb_d$ releases, so that the majority (up to 90%) would remain in the dissolved phase (Fig. 3b). Within the receiving water masses, the radionuclides would undergo fast transport (within a few days) to the downstream estuary (*i.e.*, short residence times due to high freshwater discharge), where efficient adsorption onto the MTZ could occur (up to ~ 90% of the total Sb exchange if SPM $\geq$ 1000 mg $L^{-1}$). The resulting radioactive SPM can either be rapidly exported to the coastal ocean (only if the appropriate conditions are met) or remain in the estuary for months to years (average particle residence time 1-2 years, Fig. 4a). Particle release to the coastal ocean poses a radioactive contamination risk to both wildlife along the coast and humans due to seafood production, such as commercial oyster farming in the Marennes Oléron area (north of the Gironde Estuary mouth), fishery, beach-near housing and other activities. The recycled particles in the estuary are expected to migrate upstream during low river discharges and reach the city of Bordeaux, especially when drought situations last for weeks to months (Fig. 4b). Antimony radionuclides will most probably be associated to the Fe/Mn oxides of the SPM, thus their mobility will be sensitive to redox processes over time. When the MTZ is located upstream the estuary near Bordeaux, as typically occurring during the summer drought, high water temperatures and urban wastewater releases into a quasi-stagnant water body oscillating in the fluvial estuary enhance redox gradients (*i.e.*, dissolved $O_2$ depletion; Lanoux et al. 2013) in the water column. Hypoxic conditions induce the risk of reductive dissolution of both Mn/Fe hydroxides and $Sb_p$ in the bottom of the MTZ (Audry et al. 2006; Robert et al. 2004) resulting in increased radioactive Sb mobility, including the possibility of repeated reduction-oxidation and related dissolution-adsorption cycles. Anoxic conditions at a few mm or cm below the sediment water interface (*e.g.*, Schäfer et al. 2010) and frequent erosion/sedimentation cycles (Audry et al. 2007) limit the probability of radionuclide burial in the estuarine sediments. Therefore, this scenario implies high probability of relevant particulate radionuclide persistence and mobility inside the estuary with a

relatively high exposure risk for the Bordeaux population. At the interannual timescale, only radioactive decay (production of other chemical radioelements or stable isotopes) and/or exportation to the coastal ocean under favourable hydrodynamic conditions would limit Sb radionuclide persistence in the estuary.

**Scenario 2 – accident during low river discharge conditions (drought):** Low freshwater discharges favour saline intrusion, resulting in increased salinity along the estuary and the migration of the MTZ into the fluvial estuary, reaching the Bordeaux urban agglomeration. Accordingly, accidentally released $Sb_d$ radionuclides from the Blayais NPP will mostly remain in the dissolved phase (up to 90%; Fig. 3b) due to low SPM concentrations. Despite longer water residence times during drought periods (compared to high discharge periods), this dissolved phase will be transported towards the coastal ocean relatively fast (*i.e.*, within some weeks) without entering the MTZ, and will be diluted by coastal seawaters (Fig. 4c). The remaining (down to ~10%; Fig. 3b) minor particulate fraction will probably remain in the estuary for a longer time and join the MTZ in the following months (Fig. 4d). This implies that clearly less Sb radionuclides will be introduced into the MTZ than in Scenario 1. Accordingly, the Scenario 2 describes the minimum persistence of radioactive contamination in the Gironde Estuary, including the Bordeaux agglomeration. However, this scenario also suggests maximum coastal dispersal, affecting resources such as fisheries, seafood production, wildlife and tourism. The strong predominance of radioactive $Sb_d$ forms in seawater (high salinity and low SPM) may imply bioavailability and accumulation in the marine food chain, either by direct or trophic exposure after assimilation by phytoplankton. Therefore, even for maximum dispersion and dilution scenarios, one cannot discard human health risk linked to internal and indirect exposure by seafood consumption.

In all cases, radioactive isotopes (associated to dissolved or particulate phases) will release radiation ($\gamma$ and $\beta^-$) from days to years after a potential accident, especially medium half-live radionuclides like $^{125}Sb$. Furthermore, radionuclides will decay into other radioactive or stable daughter elements (*e.g.*, Xe, Cs, Ba, I, Te and Sn) which may show different (radio-)chemical behaviours/affinities and follow new hydrodynamic and biogeochemical controls. Thus, further research is necessary to develop scenarios accounting for their respective behaviour and fate in estuarine gradients.

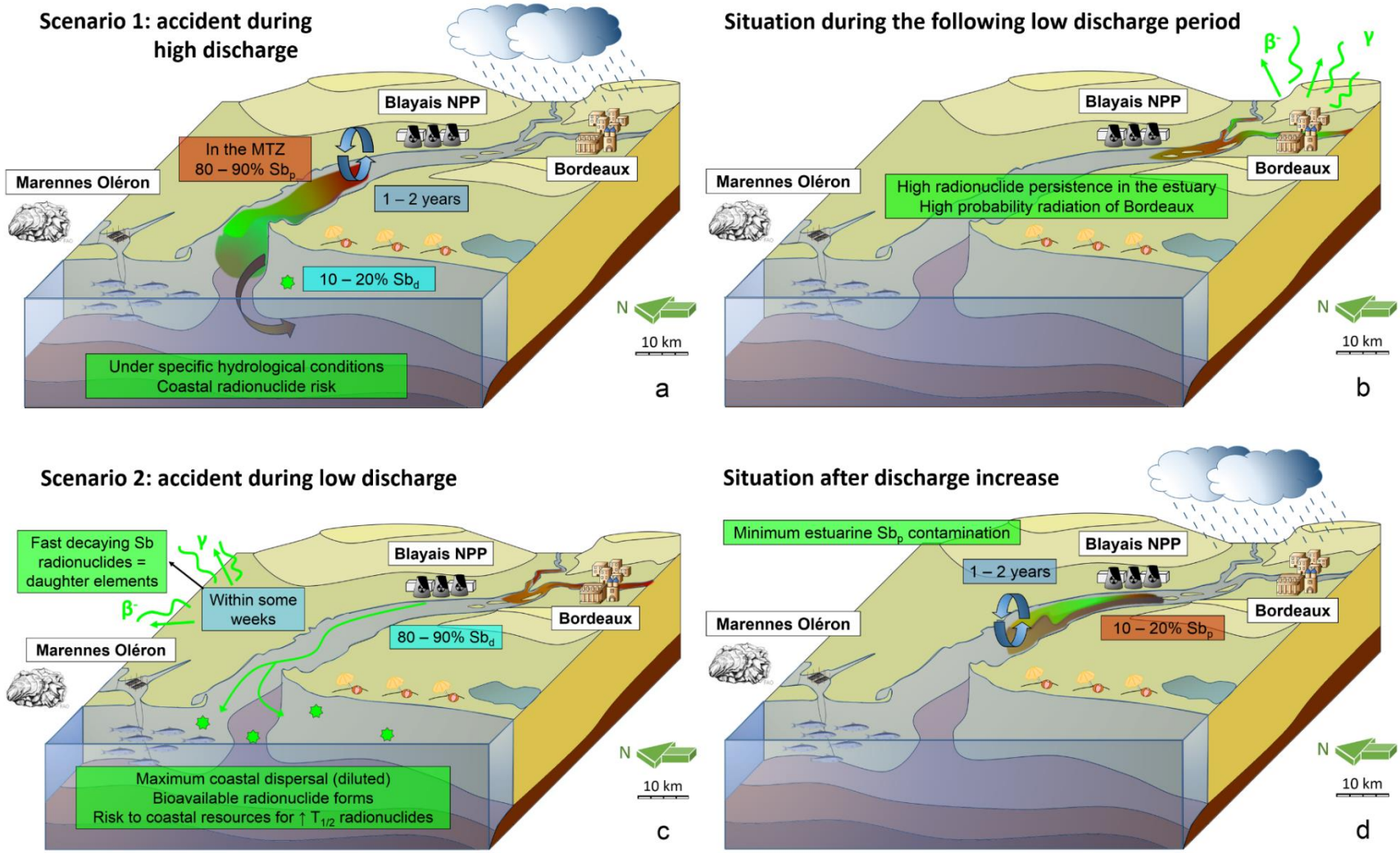


**Figure 4.** Proposed scenarios for an accidental release of dissolved Sb radionuclides from the Blayais NPP in (a) high discharge conditions favouring estuarine retention in the estuary and possible coastal expulsion of the MTZ, (b) low discharge conditions favouring upstream migration of the MTZ, (c) low discharge conditions favouring maximum coastal dispersion in dissolved forms and (d) intermediate to high discharge conditions favouring low radioactivity in the estuary associated to particulate phases.

## 5. CONCLUSIONS

This study contributes to the knowledge on Sb geochemical behaviour in a natural environment such as highly dynamic estuarine gradients. We present for the first time data on dissolved and particulate Sb concentrations and partitioning in the Gironde Estuary, the largest estuary in southwest Europe and main source of transition waters to the Bay of Biscay. The investigation of stable isotope behaviour is a valid approach to predict the behaviour of radioactive homologues in accidental NPP scenarios.

- Residence time seems to be a driving factor of Sb behaviour in the Gironde Estuary.
- Antimony in the Gironde Estuary shows a non-conservative behaviour, more evident in low and intermediate discharge conditions. This contrasts with observations in the freshwater reaches (Masson et al. 2009), suggesting high Sb reactivity in the salinity, turbidity and redox gradients, more pronounced under drought conditions. Further studies of Sb reactivity in reducing conditions are needed to validate the suspected enhanced Sb solubility and release from the particulate phase.
- Partitioning of Sb depends on salinity and turbidity gradients, with salinity increasing solubility, whereas high SPM concentrations favour adsorption of Sb.
- A first qualitative approach to dispersion scenarios for possible accidental $Sb_d$ radionuclide releases from the Blayais NPP suggests that high river discharge conditions during the accident can favour Sb adsorption on the particulate phase. This implies either rapid partial expulsion to the coastal ocean or persistence of Sb medium-lived (< 30 years) radioisotopes within the estuary and upstream transport to the Bordeaux city area during the following dry season.
- During low discharge conditions, radionuclides are more likely to remain in dissolution and will follow water dynamics, *i.e.* directly move to the coastal ocean, without the MTZ acting as a "barrier". This scenario implies a lower radiation risk for the Bordeaux agglomeration, but a higher dispersion along the coast possibly affecting coastal ecosystems.
- Further studies are necessary to (i) increase the spatio-temporal resolution of the proposed scenarios, and (ii) include the dynamics of daughter products.

## ACKNOWLEDGEMENTS

This study contributes to the Project AMORAD (ANR-11-RSNR-0002) from the National Research Agency, allocated in the framework programme "Investments for the Future" and has benefited from support by the ANR Programme Adapt'Eau (ANR-11-CEPL-008), the European Community and the Region Aquitaine (FEDER Aquitaine-1999-Z0061). The authors greatly acknowledge support from "l'Agence de l'Eau Adour-Garonne" and the European Project SCHEMA (EU FP7-OCEAN 2013.2-Grant Agreement 614002). We are also grateful to C. Bossy, A. Husson, H. Derriennic, L. Gorse, M. Tercier-Waeber and M. Coll-Crespi for field work assistance, and to the crew of the French Oceanographic R/V *Thalia* (sampling campaigns MGTS I doi 10.17600/14008300; MGTS II doi 10.17600/15009300; MGTS III doi 10.17600/15010600) and R/V *Planula IV*.

**REFERENCES**

Akatsu, E., Tomizawa, T., Aratono, Y., 1974. Separation of antimony-125 in fission products. J. Nucl. Sci. Technol. 11(12), 571-574.

Alber, M. and Sheldon, J. E., 1999. Trends in salinities and flushing times of Georgia estuaries. Proceedings of the 1999 Georgia Water Resources Conference, held March 30-31, at the University of Georgia. Kathryn J. Hatcher, editor, Institute of Ecology, The University of Georgia, Athens, Georgia

Alber, M., Alexander, C., Blanton, J., Chalmers, A., Gates, K. (2003) [Document]. The Satilla River estuarine system: the current state of knowledge. [cited 17 September 2015] Available from: http://www.gcrc.uga.edu/pdfs/satilla_sok.pdf

Andreae, M.O., Byrd, J.T., Froelich, P.N. Jr. (1983). Arsenic, antimony, germanium and tin in the Tejo Estuary, Portugal: modelling a polluted estuary. Environmental Science and Technology, 17, 731-737.

Asaoka, S., Takahashi, Y., Araki, Y., Tanimizu, M., 2012. Comparison of antimony and arsenic behavior in an Ichinokawa River water-sediment system. Chem. Geol. 334, 1-8.

Audry, S., Blanc, G., Schäfer, J., 2006. Solid state partitioning of trace metals in suspended particulate matter from a river system affected by smelting-waste drainage. Sci. Total Environ. 363, 216-236.

Audry, S., Blanc, G., Schäfer, J., Robert, S., 2007. Effect of estuarine sediment resuspension on early diagenesis, sulfide oxidation and dissolved molybdenum and uranium distribution in the Gironde estuary, France. Chem. Geol. 238, 149-167.

Austin, L.S. and Millward, G.E., 1986. Atmosphere–coastal ocean fluxes of particulate arsenic and antimony. Cont. Shelf. Res. 6, 459-474.

Bale, A.J., Uncles, R.J., Villena-Lincoln, A., Widdows, J., 2007. An assessment of the potential impact of dredging activity on the Tamar Estuary over the last century: bathymetric and hydrodynamic changes. Hydrobiologia. 588: 83-95.

BIOCONSULT & NLWKN (2013): Comparative Analysis of Sediment Management Strategies in the Estuaries of Humber, Scheldt, Elbe and Weser – Study in the Framework of the Interreg IVB Project TIDE. 76 pages. Bremen, Oldenburg.

Blanton, J.O., Alexander, C.R., Alber, M., Kineke, G., 1999. The mobilization and deposition of mud deposits in a coastal plain estuary. Limnologica. 29, 293-300.

Brannon, J.M. and Patrick Jr., W.H., 1985. Fixation and mobilization of antimony in sediments. Environ. Pollut. 9B, 107-126.

Bureau de Recherches Géologiques et Minières (BRGM). Carrières de France, exploitations

Actives, 2014. [Internet]. [cited 13 July 2015]. Available from: http://www.brgm.fr/actualite/brgm-sim-presentent-carte-carrieres-france

Byrd, J.T., 1990. Comparative geochemistries of arsenic and antimony in rivers and estuaries. Sci. Total Environ., 97/98, 301-314.

Carbol, P., Solatie, D., Erdmann, N., Nylén, T., Betti, M., 2003. Deposition and distribution of Chernobyl fallout fission products and actinides in a Russian soil profile. J. Environ. Radioactivity, 68, 27-46.

Castaing, P. and Jouanneau, J.M., 1979. Temps de résidence des eaux et des suspensions dans l'estuaire de la Gironde. J. Rech. Oceanogr. IV, 41-52.

Castaing, P. and Allen, G.P., 1981. Mechanisms controlling seaward escape of suspended sediment from the Gironde: a macrotidal estuary in France. Mar. Geol. 40, 101-118.

Ciceri, G., Traversi, A.L., Martinotti, W., Queirazza, G., 1988. Radionuclide partitioning between water and suspended matter: comparison of different methodologies. Stud. Environ. Sci. 34, 353-375.

Ciffroy, P., Durrieu, G., Garnier, J.-M. 2009. Probabilistic distribution coefficients (Kds) in freshwater for radioisotopes of Ag, Am, Ba, Be, Ce, Co, Cs, I, Mn, Pu, Ra, Ru, Sb, Sr and Th – implications for uncertainty analysis of models simulating the transport of radionuclides in rivers. J. Environ. Radioactiv. 100, 785-794.

Council Regulation (EC) 2006/11/EC of 15 February 2006 on pollution caused by certain dangerous substances discharged into the aquatic environment of the Community [2006] OJ L64/52.

Coynel, A., Schäfer, J., Dabrin, A., Girardot, N., Blanc, G., 2007a. Groundwater contributions to metal transport in a small river affected by mining and smelting waste. Water. Res. 41, 3420-3428.

Coynel, A., Schäfer, J., Blanc, G., Bossy, C., 2007b. Scenario of particulate trace metal and metalloid transport during a major flood event inferred from transient geochemical signals. Appl. Geochem. 22, 821-836.

Coynel, A., Blanc, G., Marache, A., Schäfer, J., Dabrin, A., Maneux, E., Bossy, C., Masson, M., Lavaux, G., 2009. Assessment of metal contamination in a small mining- and smelting-affected watershed: high resolution monitoring coupled with spatial analysis by GIS. J. Environ. Monitor. 11, 962-976.

Crecelius, E.A., 1980. The solubility of coal fly ash and marine aerosols in seawater. Mar. Chem. 8, 245-250.

Dame, R., Alber, M., Allen, D., Mallin, M., Montague, C., Lewitus, A., Chalmers, A., Gardner, R., Gilman, C., Kjerfve, B., Pinckney, J., Smith, N., 2000. Estuaries of the South Atlantic coast of North America: their geographical signatures. Estuaries. 23(6), 793-819.

Delacroix, D., Guerre, J.P., Leblanc, P., Hickman, C., 2002. Radionuclide and radiation protection data handbook 2002. Radiation Protection Dosimetry, 98(1). Kent, England. Nuclear Technology Publishing.

DFG (Deutsche Forschungsgemeinschaft), 2012. MAK- und BAT-Werte-Liste. VCH, Weinheim.

Element Collection Inc.: Gray, T., Mann, N., Whitby, M. (2007). [Internet] Periodic Table of Isotopes. [cited 10 March 2015]. Available from: http://periodictable.com/Isotopes/051.123/index.p.full.html

Etcheber, H., Schmidt, S., Sottolichio, A., Maneux, E., Chabaux, G., Escalier, J.-M., Wennekes, H., Derriennic, H., Schmeltz, M., Quéméner, L., Repecaud, M., Woerther, P., Castaing, P., 2011. Monitoring water quality in estuarine environments: lessons from the MAGEST monitoring program in the Gironde fluvial-estuarine system. Hydrol. Earth. Syst. Sci. 15, 831-840.

Fan, L.F., Shieh, W.Y., Wu, W.F., Chen, C.-P., 2006. Distribution of nitrogenous nutrients and denitrifiers strains in estuarine sediment profiles of the Tanshui River, northern Taiwan. Estuar. Coast. Shelf. S. 69, 543-553.

Fang, T.-H. and Lin, C.-L., 2002. Dissolved and particulate trace metals and their partitioning in a hypoxic estuary: the Tanshui Estuary in Northern Taiwan. Estuaries. 25(4A), 598-607.

Ferreira, S.L.C., dos Santos, W.N.L., dos Santos, I.F., Junior, M.M.S., Silva, L.O.B., Barbosa, U.A., de Santana, F.A., de S. Queiroz, A.F., 2014. Strategies of sample preparation for speciation analysis of inorganic antimony using hydride generation atomic spectrometry. Microchem. J. 114, 22-31.

Filella, M., Belzile, N., Chen, Y.-W., 2002a. Antimony in the environment: a review focused on natural waters II. Relevant solution chemistry. Earth-Sci. Rev. 59, 265-285.

Filella, M., Belzile, N., Chen, Y.-W., 2002b. Antimony in the environment: a review focused on natural waters I. Occurrence. Earth-Sci. Rev. 57, 125-176.

Filella, M., Belzile, N., Chen, Y.-W., Elleouet, C., May, P.M., Mavrocordatos, D., Nirel, P., Porquet, A., Quentel, F., Silver, S., 2003. Antimony in aquatic systems. J. Phys. IV. 107, 475-478.

Filella, M., Williams, P., Belzile, N., 2009. Antimony in the environment: knowns and unknowns. Environ. Chem. 6, 95-105.

Filella, M., 2011. Antimony interactions with heterogeneous complexants in waters, sediments and soils: A review of data obtained in bulk samples. Earth-Sci. Rev. 107, 325-341.

Freire, P., Taborda, R., Andrade, C. (2006). [Internet] Caracterização das praias estuarinas do Tejo. Actas do 8º Congresso da Água. Figueira da Foz: Associação Portuguesa dos Recursos Hídricos, 12p. [cited 17 September 2015] Available from: http://www.deltanet-project.eu/tagus

Goosen, N. K., Kromkamp, J., Peene, J., Van Rijswijk, P., Van Breugel, P., 1999. Bacterial and phytoplankton production in the maximum turbidity zone of three European estuaries: the Elbe, Westerschelde and Gironde. J. Marine Syst. 22, 151-171.

Ha, N.T.H., Sakakibar, M., Sano, S., 2009. Phytoremediation of Sb, As, Cu, and Zn from contaminated water by the aquatic macrophyte Eleocharis acicularis. Clean-Soil. Air. Water. 37, 720-725.

Huguet, A., Vacher, L., Relexans, S., Saubusse, S., Froidefond, J.M., Parlanti, E., 2009. Properties of fluorescent dissolved organic matter in the Gironde Estuary. Org. Geochem. 40, 706-719.

International Atomic Energy Agency (IAEA), 2004. Sediment distribution coefficients and concentration factors for biota in the marine environment. Vienna, p. 103 (Technical reports series, ISSN 0074–1914; no. 422)

Jones, H.F.E. and Hamilton, D.P. (2014). [Internet] Assessment of the Waikato River estuary and delta for whitebait habitat management: field survey, GIS modelling and hydrodynamic modelling. [cited 18 September 2015] Available from: http://www.waikatoregion.govt.nz/PageFiles/29308/TR201435.pdf

Jouanneau, J.M. and Latouche, C., 1981. The Gironde Estuary. In: Contributions to Sedimentology, Vol. 10. Stuttgart, pp. 1-115.

Kersten, M., Kriews, M., Forstner, U., 1991. Partitioning of trace metals released from marine aerosols in coastal seawater. Mar. Chem. 36, 165-182.

Korsakissok, I., Mathieu, A., Didier, D., 2013. Atmospheric dispersion and ground deposition induced by the Fukushima nuclear power plant accident: a local-scale simulation and sensitivity study. Atmos. Environ. 70, 267-279.

Krachler, M. and Shotyk, W., 2004. Natural and anthropogenic enrichments of molybdenum, thorium and uranium in a complete peat bog profile, Jura Mountains, Switzerland. J. Environ. Monitor. 6(5), 418-426.

Lanoux, A., Etcheber, H., Schmidt, S., Sottolichio, A., Chabaud, G., Richard, M., Abril, G., 2013. Factors contributing to hypoxia in a highly turbid, macrotidal estuary (the Gironde, France). Environ. Sci.: Processes. Impacts. 15, 585-595.

Lapaquellerie Y, Maillet N, Jouanneau J-M, Coakley JP, Latouche C., 1996. Flux de matières en suspension et de cadmium dans le Lot. Hydroécol. Appl. 8, 173-191.

Larrose, A., Coynel, A., Schäfer, J., Blanc, G., Massé, L., Maneux, E., 2010. Assessing the current state of the Gironde Estuary by mapping priority contaminant distribution and risk potential in surface sediment. Appl. Geochem. 25, 1912-1923.

Leleyter, L. and Probst, J.-L., 1999. A new sequential extraction procedure for the speciation of particulate trace elements in river sediments. Int. J. Environ. An. Ch. 73(2), 109-128.

Liu, W.-C., Hsu, M.-H., Kuo, A.Y., 2001. Investigation of long-term transport in Tanshui River estuary, Taiwan. J. Waterw. Port. C-ASCE. 61-71.

Liu, W.-C., Hsu, M.-H., Kuo, A.Y., Kuo, J.-T., 2001. The influence of river discharge on salinity intrusion in the Tanshui Estuary, Taiwan. J. Coastal. Res. 17(3), 544-552.

Loring, D.H. and Rantala, R.T.T., 1992. Manual for the geochemical analyses of marine sediments and suspended particulate matter. Earth-Sci. Rev. 32(4), 235-283.

Manaka, M., Yanase, N., Sato, T., Fukushi, K., 2007. Natural attenuation of antimony in mine drainage water. Geochem. J. 41, 17-27.

Masson, M., Schäfer, J., Blanc, G., Dabrin, A., Castelle, S., Lavaux, G., 2009. Behavior of arsenic and antimony in the surface freshwater reaches of a highly turbid estuary, the Gironde Estuary, France. Appl. Geochem. 24, 1747-1756.

Masson, M., Lanceleur, L., Tercier-Waeber, M.-L., Schäfer, J., Hezard, T., Larrose, A., Bossy, C., Blanc, G., 2011. Distribution and reactivity of oxyanions (Sb, As, V, Mo) in the surface freshwater reaches of the Gironde Estuary (France). Appl. Geochem. 26, 1222-1230.

Migon, C. and Mori, C., 1999. Arsenic and antimony release from sediments in a Mediterranean estuary. Hydrobiologia. 392, 81-88.

Nash, M.J., Maskall, J.E., Hill, S.J., 2000. Methodologies for determination of antimony in terrestrial environmental samples. J. Environ. Monitor. 2, 97-109.

National Oceanic and Atmospheric Administration (NOAA, 2012). [Internet]. [cited 21 September 2015] Available from: http://estuarinebathymetry.noaa.gov/bathy_htmls/S170.html

Papastefanou, C., Manolopoulou, M., Charalambous, S., 1988. Silver-110 m and 125Sb in cherbobyl fallout. Sci. Total Environ. 72, 81-85.

Pendleton, E. A., Thieler, E.R., Williams, S. J. (2004). [Internet] Coastal vulnerability assessment of Cumberland Island National Seashore (CUIS) to sea-level rise. U.S. Geological Survey Open-File Report 2004-1196. [cited 17 September 2015] Available from: http://pubs.usgs.gov/of/2004/1196/images/pdf/CUIS.pdf

Pierart, A., Shahid, M., Séjalon-Delmas, N., Dumat, C., 2015. Antimony bioavailability: knowledge and research perspectives for sustainable agricultures. J. Hazard. Mater. 289, 219-234.

Reinert, T.R. and Peterson, J.T., 2008. Modelling the effects of potential salinity shifts on the recovery of striped bass in the Savannah River estuary, Georgia-South Carolina, United States. Environ. Manage. 41, 753-765.

Ritchie, V.J., Ilgen, A.G., Mueller, S.H., Trainor, T.P., Goldfarb, R.J., 2013. Mobility and chemical fate of antimony and arsenic in historic mining environments of the Kantishna Hills district, Denali National Park and Preserve, Alaska. Chem. Geol. 335, 172-188.

Robert, S., Blanc, G., Schäfer, J., Lavaux, G., Abril, G., 2004. Metal mobilization in the Gironde Estuary (France): the role of the soft mud layer in the maximum turbidity zone. Mar. Chem. 87, 1-13.

Salomon, J.-N., 2002. L'inondation dans la basse vallée de la Garonne et l'estuaire de la Gironde lors de la "tempête du siècle" (27-28 décembre 1999). Géomorph. Relief. Process. Environ. 8, 127-134.

Schäfer, J., Blanc, G., Lapaquellerie, Y., Maillet, N., Maneux, E., Etcheber, H., 2002. Ten-year observation of the Gironde tributary fluvial system: fluxes of suspended matter, particulate organic carbon and cadmium. Mar. Chem. 79, 229-242.

Schäfer, J., Castelle, S., Blanc, G., Dabrin, A., Masson, M., Lanceleur, L., Bossy, C., 2010. Mercury methylation in the sediments of a macrotidal estuary (Gironde Estuary, south-west France). Estuar. Coast. Shelf. S. 90, 80-92.

Schutz, D.F., Turekian, K.K., 1965. The investigation of the geographical and vertical distribution of several trace elements in sea water using neutron activation analysis. Geochim. Cosmochim. Acta. 29, 259-313.

Silva, M.M., Leao, D.J., Moreira, I.T.A., de Oliveira, O.M.C., Queiroz, A.F.S., Ferreira, S.L.C., 2014. Speciation analysis of inorganic antimony in sediment samples from São Paulo Estuary, Bahia State, Brazil. Environ. Sci. Pollut. R. 25.

Sistermans, P. and Nieuwenhuis, O. (2004). [Internet] Western Scheldt Estuary (The Netherlands). EUROSION Case Study. [cited 21 September 2015] Available from: http://copranet.projects.eucc-d.de/files/000142_EUROSION_Western_Scheldt.pdf

Smichowski, P., Madrid, Y., Cámara, C., 1998. Analytical methods for antimony speciation in waters at trace and ultratrace levels. A review. Fresen. J. Anal. Chem. 360, 623-629.

Smichowski, P., 2008. Antimony in the environment as a global pollutant: a review on analytical methodologies for its determination in atmospheric aerosols. Talanta. 75, 2-14.

Sonzogni, A.A. (2013). [Internet] Chart of Nuclides NuDat 2.6 - National Nuclear Data Center. Brookhaven National Laboratory. [cited 10 March 2015] Available from: http://www.nndc.bnl.gov/nudat2/reCenter.jsp?z=51&n=68

Sottolichio, A. and Castaing, P. (1999). A synthesis on seasonal dynamics of highly-concentrated structures in the Gironde estuary. C. R. Acad. Sci. Paris, Sciences de la Terre et des Planètes. 329, 795-800.

Sottolichio, A., Hurther, D., Gratiot, N., Bretel, P., 2011. Acoustic turbulence measurements of near-bed suspended sediment dynamics in highly turbid waters of a macrotidal estuary. Cont. Shelf. Res. 31, S36-S49.

Steinhauser, G., Brandl, A., Johnson, T.E., 2014. Comparison of the Chernobyl and Fukushima nuclear accidents: A review of the environmental impacts. Sci. Total Environ. 470–471, 800-817.

Sung, W., 1995. Some observations on surface partitioning of Cd, Cu and Zn in estuaries. Environ. Sci. Technol. 29, 1303-1312.

Takayanagi, K. and Michel, P., 1996. Semi-automated determination of dissolved antimony in seawater and sediment pore water. Bunseki. Kagaku. 45, 1115-1120.

Tattersall, G.R., Elliott, A.J., Lynn, N.M., 2003. Suspended sediment concentrations in the Tamar estuary. Estuar. Coast. Shelf. S. 57, 679-688.

Tessier, E., Amouroux, D., Abril, G., Lemaire, E., Donard, O.F.X., 2002. Formation and volatilisation of alkyl-iodides and –selenides in macrotidal estuaries. Biogeochemistry. 59, 183-206.

Thakur, P., Ballard, S., Nelson, R., 2013. An overview of Fukushima radionuclides measured in the northern hemisphere. Sci. Total Environ. 458-460, 577-613.

Ueda, S., Hasegawa, H., Kakiuchi, H., Akata, N., Ohtsuka, Y., Hisamatsu, S., 2013. Fluvial discharges of radiocaesium from watersheds contaminated by the Fukushima Dai-ichi nuclear power plant accident, Japan. J. Environ. Radioactiv. 118, 96-104.

Uncles, R.J., Bale, A.J., Howland, R.J.M., Morris, A.W., Elliott, R.C.A., 1983. Salinity of surface water in a partially-mixed estuary and its dispersion at low run-off. Oceanol. Acta. 6(3), 289-296.

Ungureanu, G., Santos, S., Boaventura, R., Botelho, C., 2015. Arsenic and antimony in water and wastewater: overview of removal techniques with special reference to latest advances in adsorption. J. Environ. Manage. 151, 326-342.

U.S. Environmental Protection Agency (2013). [Internet] Priority Pollutant list. In: Appendix A, 40 Code of Federal Regulations 423. [cited 18 July 2015] Available from: http://www.gpo.gov/fdsys/pkg/CFR-2013-title40-vol30/xml/CFR-2013-title40-vol30-part423.xml

van den Berg, C.M.G., Khan, S.H., Daly, P.J., Riley, J.P., Turner, D.R., 1991. An electrochemical study of Ni, Sb, Se, Sn, U and V in the Estuary of Tamar. Estuar. Coast. Shelf. S. 33, 309-322.

van den Berg, C.M.G., 1993. Complex formation and the chemistry of selected trace elements in estuaries. Estuaries. 16, 512-520.

van der Sloot, H.A., Hoede, D., Wijkstra, J., Duinker, J.C., Nolting, R.F., 1985. Anionic species of V, As, Se, Mo, Sb, Te and W in the Scheldt and Rhine Estuaries and the Southern Bight (North Sea). Estuar. Coast. Shelf. S. 21, 633-651.

Whitehead, N.E., Ballestra, S., Holm, E., Huynh-Ngoc, L., 1988. Chernobyl radionuclides in shellfish. J. Environ. Radioactiv. 7, 107-121.

Wilson, S.C., Lockwood, P.V., Ashley, P.M., Tighe, M., 2010. The chemistry and behaviour of antimony in the soil environment with comparisons to arsenic: a critical review. Environ. Pollut. 158, 1169-1181.

Wilson, N. and Webster-Brown, J., 2009. The fate of antimony in a major lowland river system, the Waikato River, New Zealand. Appl. Geochem. 24, 2283-2292.

World Nuclear Association (WNA, 2015). [Internet]. [cited 10 February 2015] Available from: http://www.world-nuclear.org/Information-Library/

Yang, G. S., Zheng, J., Tagami, K., Uchida, S. (2012): Direct determination of tellurium in soil and plant samples by sector-field inductively coupled plasma mass spectrometry for the study of soil-plant transfer of radioactive tellurium following the Fukushima Daiichi nuclear power plant accident.

In Environmental monitoring and dose estimation of residents after accident of TEPCO's Fukushima Daiichi nuclear power stations. Edited by S. Takahashi, H. Yamana, T. Takahashi, K. Takamiya, S. Fukutani, N. Sato and M. Nakatani. Research Reactor Institute, Kyoto University, Japan. pp. 174-178, ISSN 978-4-9906815-0-0.

Zhang, H., Li, L., Zhou, S., 2014. Kinetic modelling of antimony(V) adsorption-desorption and transport in soils. Chemosphere. 111, 434-440.

Zheng, L., Chen, C., Alber, M., Liu, H., 2003. A modelling study of the Satilla River Estuary, Georgia II: suspended sediment. Estuaries. 25(3), 670-679.

Zheng, L., Chen, C., Zhang, F.Y., 2004. Development of water quality model in Satilla River estuary, Georgia. Ecol. Model. 178: 457-482.

## II. CONCLUSION

The main outcomes of the presented studies on the environmental biogeochemical behaviour of Sb in the Lot-Garonne-Gironde fluvial estuarine system are:

- The particulate Sb ($Sb_p$) concentrations in suspended particulate matter (SPM) from the Lot-Garonne River system are relatively high (from ~3 mg $kg^{-1}$ to ~10 mg $kg^{-1}$) compared to $Sb_p$ concentrations reported for other major French rivers (~1 mg $kg^{-1}$ in the Seine River and ~3 mg $kg^{-1}$ in the Loire River). This finding may be attributed to the intrinsic lithogenic composition of the SW France and locally to the influence of past mining and metallurgy activities on $Sb_p$ in the upstream Lot River watershed sites.
- Dissolved Sb concentrations ($Sb_d$, ~0.16 µg $L^{-1}$) showed similar temporal trends at all watershed sites, matching recent Sb anthropogenic emissions at the global scale. These observations suggest the non-negligible influence from atmospheric Sb deposition on $Sb_d$ concentrations in the Lot-Garonne River system. At the seasonal scale, $Sb_d$ showed summer/winter variations as previously observed for arsenic (As), the geochemical pair of Sb, in this same watershed. This seasonality is potentially related to water discharge effects (e.g., low $Sb_d$ concentrations during high water discharges) and/or biotic/abiotic reductive dissolution of Sb from particulate carrier phases (e.g., enhanced microbial $Sb_p$ dissolution in summer, increasing $Sb_d$ concentrations). In any case, $Sb_d$ concentrations have low particle concentration effect (PCE) as the contribution of the colloidal fraction to the dissolved fraction (operationally defined as <0.2 µm filter-passing $Sb_d$) seems to be low. This finding implies a generally low influence of the colloidal fraction on dissolved Sb transport at the watershed scale throughout the year.
- The proximity of the average annual water discharge (Q) to the theoretical value of water discharge of equivalent fluxes ($Q_e$) suggests a general 50:50 contribution of dissolved and particulate Sb fluxes to the total Sb transport in the Lot-Garonne River watershed. Total flux estimations suggest that central/upstream Garonne River Sb inputs are the dominating (~70%) source of Sb entering into the Gironde Estuary.
- Antimony solid/liquid partitioning (Kd) within the estuarine reaches suggests that ~90% of total Sb concentrations is bound to particles in high suspended particulate matter concentrations (~1000 mg $L^{-1}$) such as those encountered in the maximum turbidity zone (MTZ). The slight decrease in Sb Kd along the salinity and turbidity gradients reflects Sb addition to the water column within the Gironde Estuary, potentially depending on the geochemical conditions related to water and SPM residence times.
- Preliminary dispersion scenarios for hypothetic accidental nuclear power plant releases of Sb radionuclides into the Gironde Estuary are based on (i) the assumption that stable and

radioactive Sb isotopes have similar environmental behaviour, and (ii) Sb partitioning as determined from natural Sb Kd values. Contrary to commonly expected dilution and rapid expulsion of intra-estuarine point source dissolved contaminant releases due to short water residence times during high discharge conditions, an accidental release during high discharge conditions would favour efficient Sb radionuclide adsorption and retention within the downstream positioned estuarine MTZ. Such scavenging would result in a long residence time (~1-2 years) and upstream transport of Sb radionuclides towards the Bordeaux agglomeration during the seasonal MTZ migration in the following drought season. Contrastingly, an accidental release under drought conditions, when the MTZ position is upstream from the point source, would result in a higher presence of $Sb_d$ radionuclides in the Gironde Estuary. The dispersion of $Sb_d$ radionuclides would be then controlled by water residence times (up to ~86 days) implying continuous expulsion to the coastal ocean. The biological implications of wildlife exposure to this potentially more bioavailable fraction are unknown.

# CHAPTER 4:

# Particulate carrier phases of Sb, a fractionation approach

# I. INTRODUCTION

Sediments and soils are relatively complex mixtures of different mineral phases and organic matter. The distribution of particulate elements such as contaminants, radionuclides and/or geochemical tracers among these potential carrier phases controls their reactivity, mobility and potential bioaccessibility. The latter are often assessed by approaches called 'operationally-defined speciation', 'solid state partitioning' or 'fractionation', based on selective extraction schemes simulating the potential release of particulate elements from their respective carrier phases under different environmental conditions (e.g., Gleyzes et al. 2002; Hudson-Edwards et al. 2004).

Fractionation studies on trace elements face strong analytical challenges given: (i) the complexity and multicomponent character of environmental matrices such as bulk sediment mineralogy, (ii) the low (sometimes ultra-trace) concentration levels of the target element, and (iii) the limited selectivity of existing methods. Thorough identification and evaluation of potential problems and biases caused by analytical artefacts is a prerequisite to obtain realistic, environmentally meaningful results. There is a huge number of published protocols resulting from revisited methods and adaptations to specific solid matrices, constituting the "kitchen recipes" of selective extractions. The first part of the chapter gives a brief description of current knowledge on selective extraction protocols and their mechanisms of action.

The second part of the chapter addresses analytical challenges and methodological limitations related to the determination of Sb carrier phases in sediments as well as their consequences on the interpretation of fractionation results. This work aims at (i) evaluating the different extraction performances and potential artefacts by comparing Sb fractions extracted by the most known protocols for Fe/Mn oxides and acid-soluble phases in SPM from the Garonne and Rhône Rivers, and (ii) identifying general carrier phases for both inherited and spiked Sb in Garonne River sediments, contributing to the development of preliminary radionuclide dispersion scenarios.

## 1. Selective extraction methods

### 1.1. Origin and evolution of most known selective extraction methods

Early published methods on selective extraction schemes were related to phosphorous fractionation, given its role as second most limiting nutrient (after nitrates) for terrestrial primary production (Lajtha et al. 1999). In fact, most of the selective extraction protocols at that time, comprising calcium phosphate, aluminum phosphate and iron phosphate extractions (Dean 1938; Chang and Jackson 1957), aimed at understanding the potential availability/mobility of phosphorous species in specific soil fractions. These selective extraction methods were mostly based on ion exchange mechanisms and were soon applied to other compounds also present in the soils in order to understand processes such as compound bioavailability and plant uptake influences (Jackson 1958).

The interest in soil fractionation was translocated over time towards the identification of solid mineral phases allowing to distinguish residual from non-residual fractions in marine sediments (Goldberg and Arrhenius 1958). First approaches focused on Fe oxide fractions, given their importance as efficient scavengers of several metals (Jenne 1968). These methods used different reagents with different purposes changing from the ion exchange approach of the phosphorous fractionation to mineral phase dissolution techniques. The latter were mainly characterised by: (i) dithionite-based solutions for dissolution of total Fe oxides (Mehra and Jackson 1960), (ii) oxalate solutions for amorphous and crystalline Fe oxides (Schwertmann 1964), and (iii) hydroxylamine solutions for amorphous and crystalline Fe oxides phases (dissolving variable degrees of crystallinity according to extraction conditions; Chester and Hugues 1967). Results from these Fe extractions were applied to associated trace elements of concern such as Ni, Co, Cu, Cd and Cr to assess their mobility and potential bioaccessibility compared to total concentrations in bulk solid samples. The first studies on trace element fractionation in sediments, focused on sediments presenting diagenetic processes in semi-enclosed seas and nearshore sediments (e.g., Presley et al. 1972; Gupta and Chen 1975).

The development of a consolidated selective extraction protocol distinguishing several mineral target fractions in river sediments hosting Cd, Co, Cu, Ni, Pb and Zn with a sequential procedure was proposed by Tessier et al. (1979). The whole sequential extraction scheme comprised five fractions representing fractions supposed to be mobilised under contrasting environmental conditions: (i) exchangeable elements, (ii) those bound to carbonates, (iii) those bound to Fe/Mn oxides, (iv) those bound to organic matter, and (v) the rest in the non-extractable residual fraction. Their work has ever since remained as a reference in selective extraction studies, and over time has been modified and adjusted to other target fractions and elements. Modifications from the original protocol in Tessier et al. (1979) concerning reagents, extraction times/conditions and solid/liquid proportions, to improve extract efficiency/selectivity or adjust the method to specific samples and target elements, have

constituted the "selective extraction kitchen" of the past years (e.g., Filella 2011 and references therein). Such developments have shown method-dependent results (Gleyzes et al. 2002; Filella 2011), thus, generally referring to "operationally-defined carrier phases" rather than specific mineral fractions.

In an attempt to standardise the numerous protocols and the interpretations of their results, the Community Bureau of Reference (BCR) has released a four-step sequential protocol for sediments and soils in 1987, based on Tessier et al. (1979) and comprising acid extractable, reducible, oxidisable and residual fractions (Ure et al. 1993). Likewise, the BCR has provided certified reference materials (CRM: sediment CRM 601, CRM 701 and soil CRM 483) to quality check the selective extractions for "classical" target trace elements (Cd, Cr, Cu, Ni, Pb and Zn). However, this did not solve the confusion among protocols as modifications of the BCR protocol and the related evaluations were further published (e.g., Quevauviller et al. 1993; Davidson et al. 1998). In fact, further works continued applying both Tessier's and the BCR's protocol, highlighting sometimes the differences in efficiency of the former over the latter in highly polluted sediments (López-Sánchez et al. 1993) or *vice versa*, e.g., in sewage-sludges (Alborés et al. 2000). Thus, neither methods achieved to make results comparable among studies in order to understand and reliably compare trace element solid fractionations among sites and environmental compartments.

Furthermore, element speciation (and solid fractionation) is sample-dependent as soils, sediments and sludges can present different trace element mobility (Davidson et al. 1998). Even different isotopes of the same element can be leached in different proportions during the same extraction modifying the natural isotopic ratios (Pérez-Moreno et al. 2018). This implies that the use of CRM provided by the BCR, even if correctly extracted by applying the BCR protocol (Sutherland 2010), may not be reliable for quality control if the natural sample in question has other mineral composition and element speciation.

In any case, most known protocols were originally designed for cationic target elements (some examples in ***Table 17***). Accordingly, these methods have shown relevant methodological artefacts in extractions of anion species, e.g., underestimating the organic-associated elements (As and Mo) or showing oxyanion re-adsorption onto incompletely dissolved Al/Fe hydroxides (affecting As and Mo but not Sb or Se; Groenenberg et al. 2017), particularly problematic for interpretations of As mobility, given its high toxicity (Gleyzes et al. 2002). Therefore, some authors have produced anion-adapted protocols (***Table 17***), based on the original phosphorous extraction methods from Chang and Jackson (1957) to address As mobility, given the parallelism between phosphate ($H_2PO_4^-$) and As(V) species ($H_2AsO_4^-$; Zangi and Filella 2012).

**Table 17: Summary of most commonly used reagents and identified artefacts/remarks in cation- and anion-adapted (mostly sequential) selective extractions**

| FRACTION | CATION-BASED METHOD | | ANION-BASED METHOD | |
|---|---|---|---|---|
| | REAGENTS | ARTEFACTS/REMARKS | REAGENTS | ARTEFACTS/REMARKS |
| **Exchangeable** (weakly sorbed species) | *Name:* **$MgCl_2$** [T]<br>*pH:* pH 7 [a]<br>*Action:* $Mg^{2+}$ strong ion exchange, $Cl^-$ weak complexing ability [a]<br>*Use:* general good correlation with plant uptake [a,Env] | • Not recommended for Cd (overestimation due to chlorocomplexation) [a]<br>• Can attack carbonate fraction (2-3%), avoided by decreasing extraction time [a]<br>• Decrease in pH during extraction can lead to partial dissolution of carbonates and Mn oxides [a] | *Name:* **$MgCl_2$** [e] or **$(NH_4)SO_4$** [h] or **$NaNO_3$** [c]<br>*pH:* pH 7 [a]<br>*Action:* ion-exchange [c]<br>*Use:* exchangeable or ionically bound outer-sphere complexes [c,h] | - |
| | *Name:* **$NH_4OAc$** (ammonium acetate)<br>*pH:* pH 7 [a]<br>*Action:* $NH^{4+}$ ion exchange, acetate metal complexation, more stable (reducing re-adsorption/precipitation) than $Cl^-$ [a]<br>*Use:* general good correlation with plant uptake [a] | • Can attack organic matter (OM) [a] | *Name:* **$NaH_2PO_4$** [e] or **$NH_4H_2PO_4$** [h] or **$KH_2PO_4$** [c]<br>*pH:* ~5 [e]<br>*Action:* $PO_4^{3-}$ ion exchange [c]<br>*Use:* specifically bound or inner-sphere complexes though not selective as kinetic plateaus are not always obtained [c,h] | • Can remove As adsorbed to Fe and Mn phases [c] |
| **Reducible** (Fe/Mn oxides) | *Name:* **$NH_2OH$** (hydroxylamine) with **HCl, $HNO_3$** [BCR] or **HOAc** [T]<br>*pH:* generally <3 [a]<br>*Action:* reducing agent ($E^o$=-1.87V), HCl/HOAc to avoid readsorption through complexation [a] | • Mn oxide dissolution is fast, degrees of Fe oxide dissolution can be achieved with the recipe [a]<br>• Observed Pb desorption in $NH_2OH.HCl$ from Mn oxides and re-adsorption onto Fe oxides (overestimation of Pb in following step) [j]<br>• weakly adsorbed metals (like Ca) can be easily desorbed due to pH decrease without implying Fe oxide dissolution [j] | *Name:* **$NH_4C_2O_4/H_2C_2O_4$** (oxalate/oxalic acid) [d,e,h]<br>*pH:* pH buffer (<4.2) [a]<br>*Action:* low reducing ($E^o$= -0.38V) AND high Fe complexing agent (promote ligand dissolution at -OH groups) [a]<br>*Use:* specific for amorphous or low crystalline Fe oxides after Mn | • UV-catalytic extraction. In absence of light Fe(III) hydroxides are not reduced [a]:<br>1. Inner-sphere oxalate-Fe(III) complex (enhanced if ascorbic acid is included, to form more labile Fe(II)-O bond complex)<br>2. Detachment kinetically driven by oxalate concentration and oxide type<br>• decreased Fe extraction when no buffer action at pH > 4.2 [a] |

<table>
<tr><td rowspan="4">Reducible<br>(Fe/Mn oxides)</td><td>Use: Mn oxides and can differentiate between degrees of crystalline Fe oxides [a,Env]</td><td>• NOT appropriate for metalloids like As, Se or Sb because of re-adsorption onto crystalline Fe oxides, e.g., goethite, especially with $HNO_3$ [a,c,h]</td><td>oxide leaching step [a] when ascorbate is added it is no longer specific (dissolves crystalline Fe oxides) and it is considered to be strong (similar to CDB) [c,Env]</td><td>• Hydrous Al oxides are also extracted (very stable) [a]<br>• Cases of attacked crystalline Fe oxides (maghemite, lepidocrocite and goethite) [a]<br>• Oxalate-Fe(II) complex in solution can enhance/catalyse Fe(III) reduction, thus no longer specific extraction: “oxalate fraction” thus overestimates amorphous Fe(III) oxides and underestimates crystalline Fe(III) oxides [a,l]<br>• Can precipitate Ca and Pb oxalate salts (Ca and Pb underestimation) [a]<br>• $NH_4C_2O_4/H_2C_2O_4$ is inadequate for Sb, better $NH_4C_2O_4/H_2C_2O_4$/ascorbate with no change in speciation [f]</td></tr>
<tr><td>Name: $Na_2S_2O_4$ (sodium dithionite) or $Na_2S_2O_4/NaHCO_3$ (CDB, citrate dithionite buffered)<br>pH: needs buffer (e.g., citrate $NaHCO_3$) to stabilise pH ~7-8<br>Action: strong reducing agent (oxidation potential $E^o$= -1.12V), dissolves Mn oxides and even well crystallised Fe oxides [a]<br>Use: in pedology and for total Fe fractionation (amorphous and crystalline phases) [a,l]</td><td>• Needs strong ligand to avoid FeS precipitation [a]<br>• oxalate solution seems better to extract amorphous Al [a]<br>• Zn contamination from impurities in commercial dithionite salts [a]<br>• Trace metal underestimation due to precipitation with sulphide and sulphate formations [a]<br>• Citric and oxalic acids are considered strong organic complexants [i]</td><td>Name: NaOH [g]<br>pH: pH ~ 10 [g]<br>Action: surface bound fractions [h]<br>Use: Fe and Al oxides [a]</td><td>• Can dissolve OM and Pb-arsenate [c]</td></tr>
<tr><td colspan="2">Name: $C_6H_8O_6$/ $Na_3C_6H_5O_7.2H_2O$/ $NaCHO_3$: ascorbate solution (ascorbic acid/citrate/ carbonate) [b]<br>pH: pH 8 [b]<br>Action: ascorbic acid reducing conditions (decreasing $E^o$ with increasing pH), citrate alkalinising and complexing ability, carbonate pH buffer [b]<br>Use: Mn oxides and reactive Fe oxides (amorphous) [b,l]</td><td colspan="2">• Ascorbic acid (Vitamin C) has two oxidation stages/molecules at ordinary temperatures (25-37ºC) in aqueous solutions:<br>1. the first one occurs at pH<4 and is reversible (+0.15 < $E^o$ < +0.24 V)<br>2. the second one, achieved at pH>4, is irreversible (-0.05 < $E^o$ < +0.02 V) unless pH changes to >7.5 breaking into l-threonic acid and oxalic acid [k]</td></tr>
</table>

***(Table 17 Continued)***

| FRACTION | CATION-BASED METHOD | | ANION-BASED METHOD | |
|---|---|---|---|---|
| | REAGENTS | ARTEFACTS/REMARKS | REAGENTS | ARTEFACTS/REMARKS |
| **Oxidisable** (organic matter and sulphurs) | *Name:* **$H_2O_2$/$NH_4OAc$** [T,BCR] (hydrogen peroxide/ammonium acetate)<br>*pH:* pH 2 [BCR] (with dilute $HNO_3$) [T] – 5 [b]<br>*Action:* $H_2O_2$ oxidising agent, $NH_4OAc$ soft complexant [a]<br>*Use:* trace metals associated to complex particulate organic material like humic substances, carbohydrates, proteins, fats, waxes, and resins [a] | • Major by-product is oxalic acid (from OM destruction) which can dissolve Fe oxides and cause precipitation of soluble oxalates (this effect is totally destroyed with further $H_2O_2$) [a]<br>• $H_2O_2$ has reducing ability at pH < 5, reducing Mn oxides [a]<br>• This extraction excludes pyrite [m] | Unspecified differently | • **Se overestimation due to oxidation of Se(IV) → Se (VI) from other mineral phases** [a] |
| | *Name:* **NaClO** (sodium hypochlorite)<br>*pH:* pH ~ 8 [a]<br>*Action:* oxidising agent [a]<br>*Use:* in alkaline conditions minimises amorphous and clay mineral attack [a] | • Can oxidise Mn oxides and dissolve carbonates [a] | | |
| **Acid soluble** | *Name:* **NaOAc/HOAc** [BCR]* (acetate/acetic acid)<br>*pH:* generally, pH 5 [a]<br>*Action:* NaOAc (buffer), HOAc for carrier phase dissolution [a]<br>*Use:* "mild acid", efficient for carbonate extraction [h] | • High fraction of total Mn frequently obtained (not from partial Mn oxides attack but from e.g., dolomite from $Mn^{2+}$ substitution of $Mg^{2+}$ or $Ca^{2+}$) [a]<br>• Potential dissolution of FeS and $PbSO_4$ (Pb overestimation) and precipitation with sulphide ions (underestimation for others) [a] | *Name:* **HOAc** (acetic acid)<br>*pH:* 2 [a]<br>*Action:* e.g., weakly extracted As [c]<br>*Use:* "mild acid" [c, Env] | |

| | | | | |
|---|---|---|---|---|
| **Acid soluble** (carbonate + specifically sorbed sites in clay surface + OM + Fe/Mn oxyhydroxides) | | • Incomplete $CaCO_3$ dissolution for high carbonate samples (e.g., 16%), overestimates following step in [T], is variable among carbonate species (e.g., Pb, Mn, Zn) and frequent pH adjustment along extraction is recommended [a] | | |
| | ***General gastric-simulating extractions and/or both cation/anion used acid soluble solutions*** | | | |
| | *Name:* **HCl** [e]<br>*pH:* <1<br>*Action:* competitive $H^+$ desorption and partial dissolution, with $Cl^-$ complexation (e.g., Fe-Cl) [e]<br>*Use:* Co-precipitated target elements with acid volatile sulphide (AVS), carbonates, Mn oxides, very amorphous Fe oxyhydroxides [e] ; with higher molarity even crystalline Fe oxides, clay minerals and Al oxides [i]. In any case, mostly extracting Fe(II) (potentially less Fe(III) than oxalate buffer) if no hydroxylamine is added for total Fe (Fe(II) + Fe(III)) extraction [l] | • Enhanced dissolution due to clorocomplexation e.g., Cd | *Name:* **$HNO_3$** [e]<br>*pH:* <1<br>*Action:* competitive $H^+$ desorption and partial dissolution and oxidation (e.g., crystalline sulphides in a sequential procedure) [e]<br>*Use:* As co-precipitated with pyrite and amorphous sulphide [e] | - |

***(Table 17 Continued)***

| FRACTION | CATION-BASED METHOD | | ANION-BASED METHOD | |
|---|---|---|---|---|
| | REAGENTS | ARTEFACTS/REMARKS | REAGENTS | ARTEFACTS/REMARKS |
| **Residual** (refractory crystalline lattice)l | *Name:* **$HNO_3$/HCl/HF/$HClO_4$** (different acid mixtures) [a]<br>*pH:* acid<br>*Action:* carrier phase dissolution by strong acids [a]<br>*Use:* for total metal budget concentration:<br>[BCR] - Sediment residue from step 3 is digested in *aqua regia* ($HNO_3$/HCl, considered a pseudo-total extraction)<br>[T] *– sediment from step 4 is extracted with* HF-$HClO_4$ mixture | • The sum of 4 steps = original pseudo total *aqua regia* of sediment [BCR] | Unspecified differently | - |

Source references: [a] Gleyzes et al. 2002 ; [b] Audry et al. 2006 ; [c] Hudson-Edwards et al. 2004 ; [d] Montperrus et al. 2002 ; [e] Keon et al. 2001 ; [f] Leuz 2006 ; [g] Chang and Jackson 1957 ; [h] Wenzel et al. 2001 ; [i] Filella 2011 ; [j] Tipping et al. 1985 ; [k] Borsook et al. 1937 ; [l] Kostka and Luther 1994; [m] Audry et al. 2010; [n] Groenenberg et al. 2017

[T] Part of the protocol in Tessier et al. (1979)

[BCR] Part of the BCR protocol; described in Sutherland 2010

[Env] Described in each paper to have applications for environmental interpretations

* Multiple applications: reagent classified as “acid soluble” extractions for HOAc in [BCR], as “exchangeable fraction” for NaOAc/HOAc in [b] and for NaOAc at pH 8 in [T] but as “carbonate bound fraction” for NaOAc/HOAc at pH 5 in [T]

Noteworthy, anion-adapted protocols (Wenzel et al. 2001) generally use oxalate reagents for extraction of elements associated with the Fe/Mn oxide carrier phases. The origin of the use of oxalate reagent is a general (non-anion based) soil extraction procedure from Zeien and Brümmer (1989), used as an alternative to avoid Zn contamination from dithionite reagents, targeting the crystalline Fe oxide carrier phase (Shuman 1982). Compared to hydroxylamine extractions, oxalate seems more appropriate in anion-based studies (see artefacts listed in ***Table 17***) as the former showed potential underestimation due to As sorption onto goethite (crystalline Fe oxide), whereas oxalate ions compete more efficiently for phosphate sites on goethite (Wenzel et al. 2001). Furthermore, oxalate extractions can achieve complete crystalline Fe oxide dissolution in certain cases (e.g., when using oxalate with ascorbate solutions).

The final aim of the selective extraction is: (i) to efficiently/selectively extract target trace elements in operationally-defined phases, or (ii) to obtain information on trace element mobility in environmental conditions. This is why Kostka and Luther (1994) recommend to differentiate between reactive Fe oxides (i.e., extracted with ascorbate solution at pH 8; ***Table 17***) and crystalline Fe oxides extracted with oxalate-based solutions. They defined reactive Fe oxides as those that readily react with sulphides, to form iron sulphides and pyrite, and organic acids, reliably representing environmental processes such as mineral conversion in early diagenesis.

Nevertheless, for some unknown reason, the above considerations have not been taken into account in many selective extractions later-on and the confusion and reliability in environmental results still remain nowadays in the scientific literature due to the indiscriminate use of all protocol types (e.g., Tessier et al. 1979; BCR protocol; Wenzel et al. 2001) for both cationic and anionic extractions (e.g., see reviews in Gleyzes et al. 2002; Filgueiras et al. 2002; Hudson-Edwards et al. 2004; Wilson et al. 2010, and Filella 2011 and references therein).

### 1.2. Important known modes of action of reducible (Fe/Mn oxide) fraction methods

The Fe oxide/hydroxide fraction is generally targeted given: (i) its relevant sorption role for many target elements, determining their reactivity/mobility (Jenne 1968), and (ii) the diverse response of Fe minerals (amorphous vs crystalline) to reagents/extraction conditions. Amorphous Fe minerals include ferrihydrite ($Fe(OH)_3$) and lepidocrocite (α-FeOOH), whereas crystalline structures occur in goethite (α-FeOOH), hematite (α-$Fe_2O_3$), and magnetite ($Fe_3O_4$).

The reducible fraction comprises the general dissolution of Fe and Mn oxides. This operationally defined fraction will be assigned as “F2” contrasting with acid-soluble operationally defined fractions (“F4”) which, by definition, should include F2 carrier phases. The different extraction power of each reagent solution can be understood from their known modes of action (***Figure 70***), generally showing

decreasing dissolution of Fe and Mn oxides in the following order: acid extractions (***Figure 70a***), oxalate-based solutions (***Figure 70b,c,d***), hydroxylamine-based solutions (not shown in ***Figure 70***) and ascorbate-based solutions (***Figure 70e***). Noteworthy, out of all the aforementioned solutions, only the purely ascorbate-based extraction does not present acid conditions (***Table 17***).

Iron extraction by F2 reducible solutions (i.e., oxalate-, hydroxylamine- or ascorbate-based) not only depends on the Fe oxide content in SPM but on the Fe oxide "quality" concerning both crystalline degree and Fe(II) vs Fe(III) presence, that is, the individual mineral type (Stumm and Sulzberger 1992). Kostka and Luther (1994) compared extraction efficiencies between oxalate and ascorbate solutions applied to marine bulk SPM. They observed that the presence of Fe(II) minerals enhanced oxalate extracting power on final Fe dissolution, concluding that the oxalate solution extraction is a non-effective measure of amorphous Fe minerals (i.e., overestimating amorphous Fe(III) minerals and underestimating crystalline Fe(III) minerals). Generally, the crystalline Fe(III) (hydr)oxide lattice exchanges its $O^{2-}$ or $OH^{-}$ ligands for oxalate ligands forming inner-sphere bidentate mononuclear surface complexes as Fe(III)-$C_2O_4^{2-}$ (Stumm and Sulzberger 1992). The complex can be released into solution (destroying the first mineral lattice layer): (i) in a non-reducing reaction, thermodynamically possible but kinetically constrained (***Figure 70d***), or (ii) by a photochemically driven reaction (***Figure 70c***), reducing mineral Fe(III) to Fe(II) according to the oxalate concentrations and the Fe oxide type, consuming oxalate in the process (i.e., converted into $CO_2$ and radical $CO_2^{-\cdot}$) and releasing aqueous Fe(II) (Stumm and Sulzberger 1992; Gleyzes et al. 2002). However, there is a third mechanism of oxalate performance explaining the observations in Kostka and Luther (1994). In the presence of Fe(II) species dissolved from Fe(II) containing mineral oxides (e.g., magnetite, $Fe^{2+}Fe^{3+}{}_2O_4$), silicates (e.g., chlorite) or even sulphides (e.g., pyrite-$FeS_2$ or FeS; Kostka and Luther 1994; Poulton and Canfield 2005), oxalate forms Fe(II)-dissolved oxalate complexes (***Figure 70b***) which catalyse the reduction and dissolution of crystalline Fe(III) oxides like hematite (Sulzberger et al. 1989) and goethite (Kostka and Luther 1994). The formation of Fe(II)-oxalate complexes and association to crystalline Fe(III) (hydr)oxide lattice constitute an organic bridge between the Fe(III) mineral and the Fe(II)-oxalate complex allowing an electron transfer independent from photochemical considerations. This process reduces mineral Fe(III) faster than oxalate alone (***Figure 70d***) and in the solution remain the oxidised Fe(III)-$C_2O_4^{2-}$ complex and aqueous Fe(II) from the mineral lattice through rehydration (labile Fe(II)-O bond; Stumm and Sulzberger 1992). The remaining mineral surface is finally reconverted to its original configuration i.e. consists of a newly exposed Fe(III) (hydr)oxide lattice layer (Stumm and Sulzberger 1992). Consequently, although magnetite is a crystalline Fe oxide mineral, its relevant role in oxalate solutions suggests that it should be included within reactive Fe minerals (Kostka and Luther 1994).

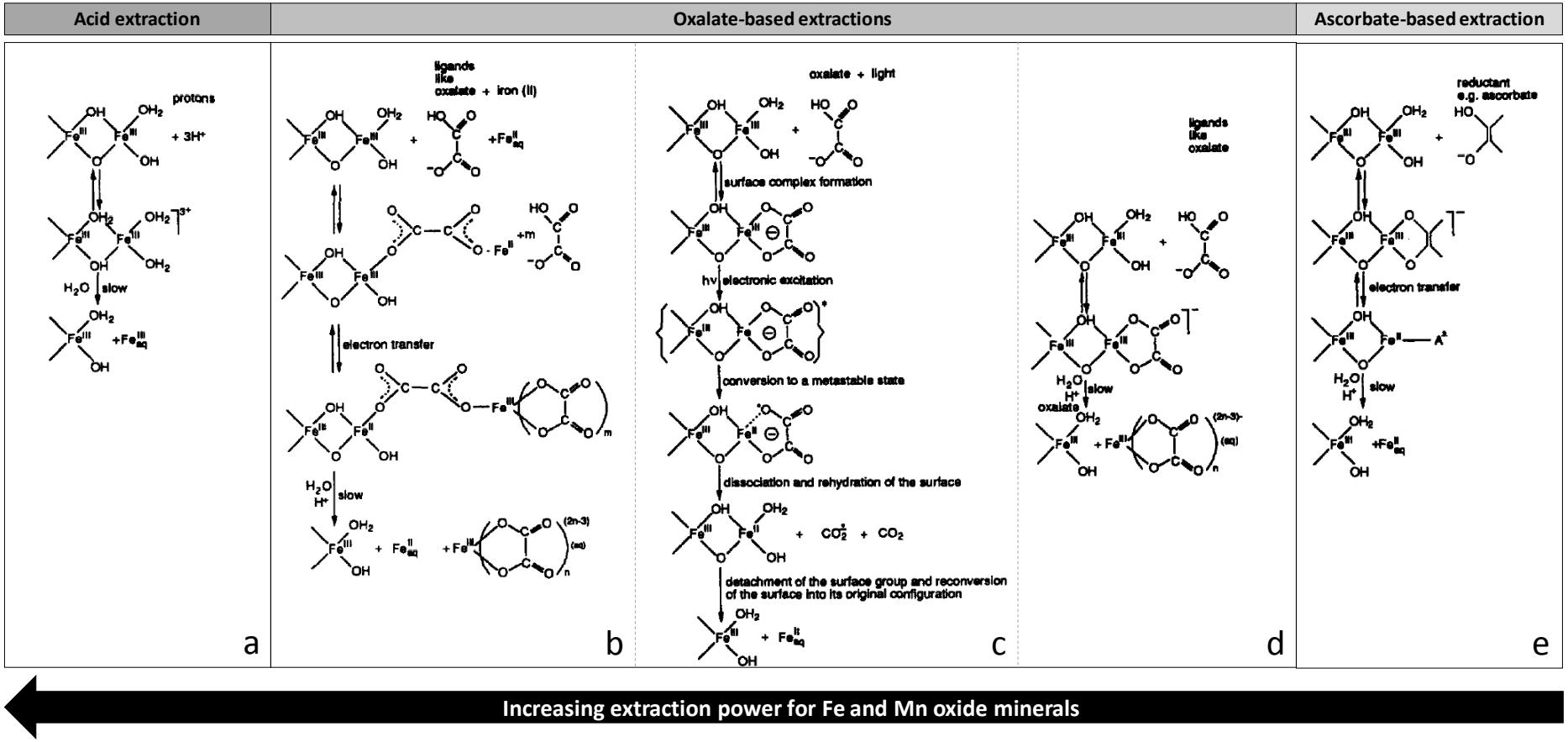


**Figure 70. Known modes of action of acid-based (a), oxalate-based (b,c,d) and ascorbate-based solutions (e) in selective extractions.** The oxalate solution shows different responses if the extraction is performed in the presence of Fe(II) minerals (b), with light (c) or in the dark (d). *(Adapted from Stumm and Sulzberger 1992).*

Hydroxylamine-based solutions generally show stronger reducing power (Eº-1.87V) than oxalate buffer solutions (Eº-0.38V; Kotrly and Sucha 1985; Gleyzes et al. 2002). In general, hydroxylamine solutions are known for extracting amorphous Fe (hydr)oxides and different degrees of crystalline Fe (hydr)oxides according to the specific extraction recipe (Gleyzes et al. 2002; Henkel et al. 2016). Specifically, the hydroxylamine-acetic acid (HA) method from Chester and Hughes (1967) has been reported to extract several phases due to its double action related to its reducing and complexing properties. Phases extracted due to the reducing mode of action of the hydroxylamine are (i) easily reducible Fe hydroxides and oxyhydroxides (i.e., ferrihydrite, lepidocrocite), and (ii) partially other reducible Fe oxides (e.g., magnetite and goethite; Poulton and Canfield 2005). The choice of the complexing agent, in this case HOAc (generally used in the protocol from Tessier et al. 1979 for the carbonate fraction) may affect solution pH resulting in dissolution of (iii) highly reactive Fe phases like carbonate Fe (e.g., siderite, $FeCO_3$).

During the ascorbate-based extractions, the mono-anion ascorbate forms an inner-sphere (bidentate mononuclear) complex on Fe(III) (hydr)oxide surfaces, reducing Fe(III) to the easily detachable Fe(II) form (i.e., Fe(II)-O bond) releasing aqueous Fe(II) and an oxidised ascorbate radical (***Figure 70e***; Stumm and Sulzberger 1992). Noteworthy, two ascorbate radicals can react to form a dehydroascorbate (DHAA) molecule and a renewed mono-anionic ascorbate, readily reducing another Fe(III) from the mineral lattice surface (Stumm and Sulzberger 1992; Fennema 1996). More precisely, Borsook et al. (1937) described two oxidation states for ascorbic acid (vitamin C) dependent on pH: (i) DHAA formed at pH < 4, which can reversibly become ascorbic acid again (experimental $+0.15 < Eº < +0.24$ V), and (ii) the 2,3-diketo-*l*-gulonic acid (DKG) irreversibly formed at pH > 4 (experimental $-0.05 < Eº < +0.02$ V) and stable unless pH increases > 7.5, breaking into *l*-threonic acid ($C_4H_8O_5$) and oxalic acid. However, anoxic conditions favour other degradation products of the latter (e.g., xylosone or furonic acid, ***Figure 71***), potentially causing the characteristic brownish colour of the ascorbate extraction solution (Hayashi et al. 1983; Fennema 1996).

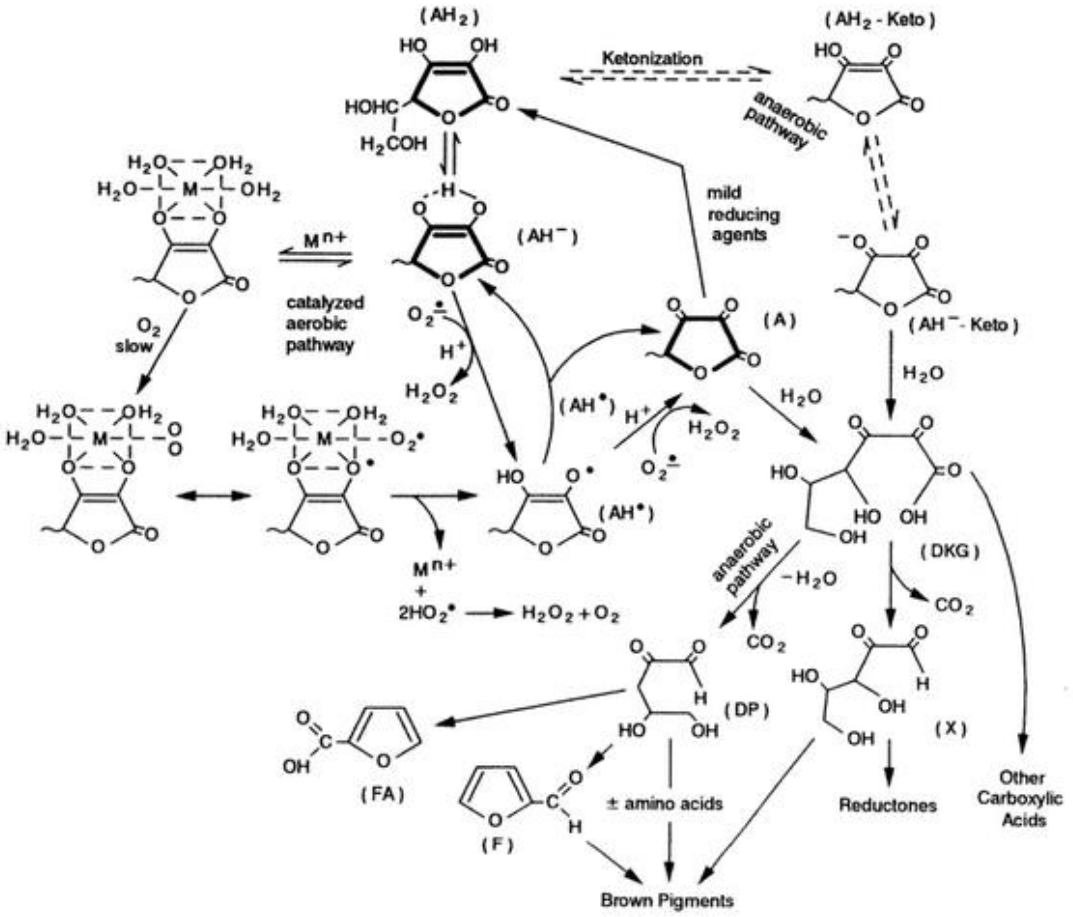


**Figure 71. Overview of mechanisms of oxidative and anaerobic degradation of ascorbic acid.** Structures with bold lines represent primary sources of vitamin C. Abbreviations: fully protonated ascorbic acid ($AH_2$), ascorbate monoanion ($AH^-$), semidehydroascorbate radical ($AH^•$), dehydroascorbic acid (A), 2-furonic acid (FA), 2-furaldehyde (F), 2,3-diketo-*l*-gulonic acid (DKG), 3-deoxypentosone (DP), xylosone (X), metal catalyst ($M^{n+}$), perhydroxyl radical ($HO_2$). *(Fennema 1996).*

### 1.3. Parallel selective extractions and total digestions: overview of bulk sediment carrier phases

The parallel selective extractions schemes selected in the present work and applied to bulk sediments include the following five main fractions (protocols described in *Chapter 2/Materials and Methods*):

- ***F1 – acetate fraction ("easily exchangeable/carbonate fraction")***

The commonly applied reagents targeting either the easily exchangeable fraction (e.g., $MgCl_2$) or the carbonate fraction (e.g., $NH_4OAc$) are not selective enough to differentiate independently each of these operationally-defined fractions. Furthermore, such reagents may also attack additional non-targeted phases, such as Mn oxyhydroxydes, sulphates and organic matter (Bordas and Bourg 1998, Kersten and Förstner 1987). Although the original protocol of Tessier et al. (1979) aimed at the

selective dissolution of carbonate carrier phases with an NaOAc 1M/HOAc extraction at pH ~ 5, described for sediments with low carbonate content ($CaCO_3$ < 16%), this protocol can be adapted for sediments with higher carbonate contents (55% < $CaCO_3$ < 88%) by controlling the pH throughout the extraction procedure (Orsini and Bermond 1993). Therefore, this work refers to the F1-fraction as the fraction extracted by NaOAc 1M/HOAc extraction under controlled pH, as suggested by Orsini and Bermond (1993). Results will be classified and interpreted as belonging to the "acetate fraction" rather than referring to specific carrier phases involved in the extractions.

- ***F2 – ascorbate fraction ("amorphous Fe/Mn oxides")***

The aim is to extract trace elements carried by amorphous Fe and Mn oxides, as they are the ones involved in environmental early diagenetic processes in greater measure than the crystalline phases (e.g., goethite – α-FeOOH or hematite – $Fe_2O_3$), generally of detrital origin (Canfield 1989). Thus, this study is based on the original protocol defined by Kostka and Luther (1994) concerning ascorbate extractions ($C_6H_8O_6/C_6H_5Na_3O_7.2H_2O/CHNaO_3$) at pH ~ 8.

- ***F3 – $H_2O_2$ fraction ("organic matter and monosulphurs")***

The organic matter present in bulk sediments can contain associated trace elements (i.e., through incorporation or complexation) with more or less important roles in environmental systems (Santschi et al. 1997). The organic fraction is composed of biomolecules (carbohydrates, proteins, etc.) and different polymers (e.g., humic and fulvic acids), thus, different oxidising reagents can be used to dissolved such carrier phases. The most commonly applied are $H_2O_2$ (Tessier et al. 1979) and NaClO (Shuman 1983). However, NaClO can show low selectivity, partly dissolving amorphous/mineral clays, Mn oxides (Pickering 1986) and carbonates (Gommy 1997). Therefore, this work focuses on the $H_2O_2$ extraction using $NH_4OAc$ as complexing agent (Tessier et al. 1979). The original protocol in Tessier et al. (1979) performed this extraction in acid media ($HNO_3$, pH ~ 2). Given that selective extractions in this work are conducted in parallel, an acidification of such $H_2O_2$ fraction could compromise the solubilisation of other carrier phases, thus, this extraction was performed at pH ~ 5, as validated by Ma and Uren (1995).

- ***F4 – acid-soluble fraction ("carbonates, Fe/Mn oxides, phyllosilicates,...")***

The so-called acid-soluble fractions combine the dissolution of several carrier phases comprising hydrous aluminosilicates and sulphides in addition to amorphous and crystalline Fe/Mn oxides and carbonates (Huerta-Díaz and Morse 1990; Gasparon and Matschullat 2006). Consequently, acid-

soluble fractions include ascorbate-fractions and other labile carrier phases in contrary to the so-called residual fraction (= not acid-soluble), which is considered as widely "inert" in the surficial biogeochemical processes, i.e. the associated trace elements are not bioaccessible. Accordingly, the acid-soluble fraction can be a proxy for the potentially bioaccessible fraction of trace elements from bulk sediment, especially for organisms presenting similar acid digestion systems. As such, the acid-soluble fraction may provide relevant information about the potential ecological risk of trace element intake by biota (Bryan and Langston 1992, Langston 1999). In this work, acid-soluble fractions are generally studied with 1M HCl extractions, and occasionaly with parallel 1M $HNO_3$ extractions, considered to be an appropriate compromise between extraction efficiency and representativity of ecotoxicity data (Luoma and Bryan 1981, 1982; Ying et al. 1992; Snape et al. 2004).

- ***Residual – (total concentration - F4)***

The residual fraction constitutes all the mineral phases which are not extracted in the acid-soluble fraction, given that the latter dissolves the maximum number of reactive carrier phases compared to the aforementioned fractions (from F1 to F4). In this work, the residual fraction is calculated as the difference between total trace element concentrations in sediments (i.e., determined from total sediment digestions, protocols described in *Chapter 2/Materials and Methods*) and that obtained after acid-soluble extraction (F4).

## 2. Parallel selective extractions on particulate antimony.

*Manuscript to be submitted to Applied Geochemistry*

# Fractionation of inherited and spiked antimony (Sb) in fluvial/estuarine bulk sediments: unexpected anomalies in parallel selective extraction protocols

Teba Gil-Díaz[1], Jörg Schäfer*[1], Montserrat Filella[2], Lionel Dutruch[1], Cécile Bossy[1]

[1]*Université de Bordeaux, UMR CNRS 5805 EPOC, Allée Geoffroy Saint-Hilaire, 33615 Pessac, France;* [2]*Department F.-A. Forel, University of Geneva, Boulevard Carl-Vogt 66, CH-1205 Geneva, Switzerland*

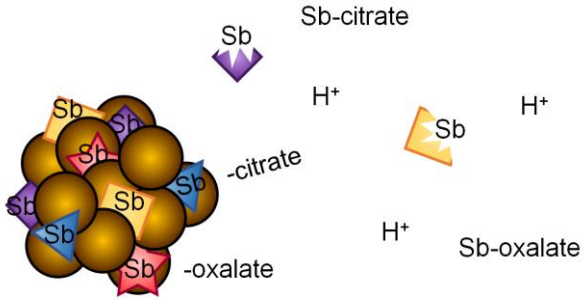


## ABSTRACT

Selective extractions are widely used in sediment, soil and sludge samples to assess trace element carrier phases, mobility and potential bioaccessibility. Commonly used selective parallel extractions were applied to natural and isotopically-labelled bulk sediments from the Gironde fluvial-estuarine system and the Rhône River (France) to determine the solid phase fractionation of antimony (Sb), a priority contaminant in EU and US regulations and an important radionuclide in decay series occurring in the environment after nuclear power plant accidents. Antimony fractions obtained from several, parallel selective extraction solutions targeting Fe/Mn oxides (i.e., hydroxylamine-, oxalate- and ascorbate-based, herein assigned as "F2") and acid-soluble operationally defined phases (HCl- and $HNO_3$-based, herein assigned as "F4") were compared (i) between each other's, and (ii) with those of other trace elements (Co, Cu, Ni, Pb, Zn, Th and U) in the same extractions. The solid fractionation of inherited Sb and spiked Sb was studied by applying a complete set of parallel selective extractions to isotopically-labelled sediments of the Gironde Estuary. Results suggest protocol-related and sediment-dependent anomalies in Sb selective extractions, compared to results expected from the operationally-defined extraction scheme and obtained for other trace elements. In fact, Sb fractions extracted with oxalate- and ascorbate-based solutions were greater than acid-soluble fractions (1M HCl and 1M $HNO_3$) in the Garonne/Gironde fluvial estuarine sediments. A similar anomaly occurred for oxalate-based extractions of Sb in Rhône River sediments. These observations suggest that reducing conditions and the presence of strongly complexing organic ligands in the environment may mobilise respectively 2-fold and ~5-fold more Sb from natural bulk sediment and from sediments spiked with isotopically-

labelled Sb than the acid-soluble fraction, usually used to assess the reactive, potentially bioaccessible fractions. The underestimation of the reactive, potentially bioaccessible fractions of Sb may bias the environmental interpretation of Sb solid fractionation and must be taken into account when assessing stable Sb cycles and Sb radionuclide dispersion scenarios in continent-ocean transition systems.

***Keywords:*** antimony, selective extractions, suspended particulate matter, isotopic labelled sediments

## 1. INTRODUCTION

Solid phases (e.g., suspended matter, sediments, soils) play a fundamental role in the biogeochemical cycles of potentially toxic trace elements (metals and metalloids). Suspended particle dynamics control the transport and/or long-term retention of trace elements along river courses and in coastal/estuarine areas. Sediment quality guidelines and regulations are based on total particulate concentrations but trace element mobility/solubility and bioaccessibility actually depend on particle composition. Accordingly, the interactions of trace elements and specific geochemical carrier phases may control trace element solid/liquid partitioning and reactivity, affecting the degree of exposure of biota to certain contaminants. Solid carrier phases include carbonates, sulphides, organic matter, iron and manganese oxides, clays, among other fractions (Jenne 1968; Kheboian and Bauer 1987) which react differently to trace element concentrations/species and environmental conditions (Kersten and Förstner 1987). In fact, trace elements might show different environmental behaviours, widely independent from their total concentrations in the solid (Agemian and Chau 1976). Reliable assessment of trace element contamination in sediments requires to correctly evaluate the mobility/solubility and bioavailability of particulate trace elements under different physico-chemical conditions (Luoma and Bryan 1981).

Different methods, often referred to as "selective extraction techniques", "speciation schemes" or "fractionation analysis" according to IUPAC (Gleyzes et al. 2002), have been developed to determine trace element solid fractionation. The Fe oxide/hydroxide fraction is generally targeted given: (i) its relevant sorption role for many target elements, determining their reactivity/mobility (Jenne 1968), and (ii) the diverse response of Fe minerals (amorphous vs crystalline) to reagents/extraction conditions. Amorphous Fe minerals include ferrihydrite ($Fe(OH)_3$) and lepidocrocite (α-FeOOH), whereas crystalline structures occur in goethite (α-FeOOH), hematite (α-$Fe_2O_3$), and magnetite ($Fe_3O_4$).

Environmental studies addressing the Fe oxide fraction by using classical schemes such as those defined by Tessier et al. (1979) and by the Community Bureau of Reference (BCR; Ure et al. 1993) rely on hydroxylamine acid solutions, that dissolve Fe oxides of variable degrees of crystallinity according to the extraction conditions. These extractions can be complemented with stronger reagents like dithionite or oxalate and ascorbate solutions, which may strongly or completely dissolve crystalline Fe fractions (Mehra and Jackson 1960; Leuz 2006; Henkel et al. 2016). Kostka and Luther (1994) defined the "reactive/mobile Fe oxide fraction" extracted by an ascorbate solution at pH 8 as environmentally

applicable extraction for amorphous Fe oxides. This fraction includes Fe oxides that readily react with sulphides to form iron sulphides and pyrite as well as with organic acids, which is expected to reliably represent environmental processes such as Fe mineral reconversions in early diagenesis (Froelich et al. 1979). However, extraction with an ascorbate solution at pH 8 is not a widespread method (e.g., Reyes and Torrent 1997; Rutten and de Lange 2002) and the response of redox-sensitive species to such extraction under reducing conditions is unknown. In fact, the indiscriminate application of these methods targeting Fe/Mn oxides to extract trace elements other than the originally designated ones, seems unwise, as extraction conditions can also affect the element speciation/behaviour during the extraction (Müller et al. 2007). For example, the incomplete dissolution of crystalline Fe oxides during hydroxylamine extractions can cause As sorption onto goethite, underestimating the extraction of As anionic species in contrast to oxalate solutions (pH ~ 3; i.e., "anion-adapted" protocol; Wenzel et al. 2001). This could also be the case for other redox-sensitive elements such as Sb, for which little is known about its behaviour during selective extractions.

The aim of this study is to determine environmentally representative solid phase fractionation of Sb in natural bulk sediments from the Gironde Estuary and the Rhône River, i.e., sediments not associated to highly contaminated areas. Given the unknown response of Sb to selective extracting conditions, this work first compares Sb parallel extractions with different reagents targeting (i) the Fe/Mn oxide fraction (hydroxylamine, oxalate and ascorbate solutions, designated as "F2" solutions), and (ii) the bioaccessible fraction (1M HCl and 1M $HNO_3$ solutions, designated as "F4" solutions). The behaviour of Sb during these extractions is compared with that of "classical" trace (Co, Cu, Ni, Pb, U, Zn) and major elements (Fe and Mn). Finally, the application of a conventional parallel selective extraction scheme to bulk SPM from the Garonne River, previously spiked with isotopically-labelled Sb, aims at evaluating the solid fractionation of both natural and inherited Sb under contrasting salinity and turbidity conditions.

## 2. MATERIAL AND METHODS

### 2.1. Study areas

Sampling sites are located in two study areas at the continent-ocean interfaces of the Gironde fluvial-estuarine system (SW France) and the Rhône River (SE France). In total, three sediment samples were collected (Fig. 1): (i) suspended particulate matter (SPM) at the Kilometric Point 52 (PK52) in the Gironde Estuary, (ii) deposited river bank sediments at Portets (PK-30) along the Garonne River, i.e., the main tributary to the Gironde Estuary, and (iii) SPM collected with a sediment trap (TAS) at the SORA station (Station Observatoire du Rhône à Arles) in the Rhône River. Detailed descriptions of sampling techniques and materials are given in Gil-Diaz et al. (2016) for the Gironde SPM and Masson et al. (2018) for the Rhône. Wet sediments were kept in the fridge and aliquots were freeze-dried (PK52 and TAS) or oven-dried at 70ºC (PK-30), homogenised and further divided into subsamples for parallel selective extractions with F2 and F4 protocol solutions.

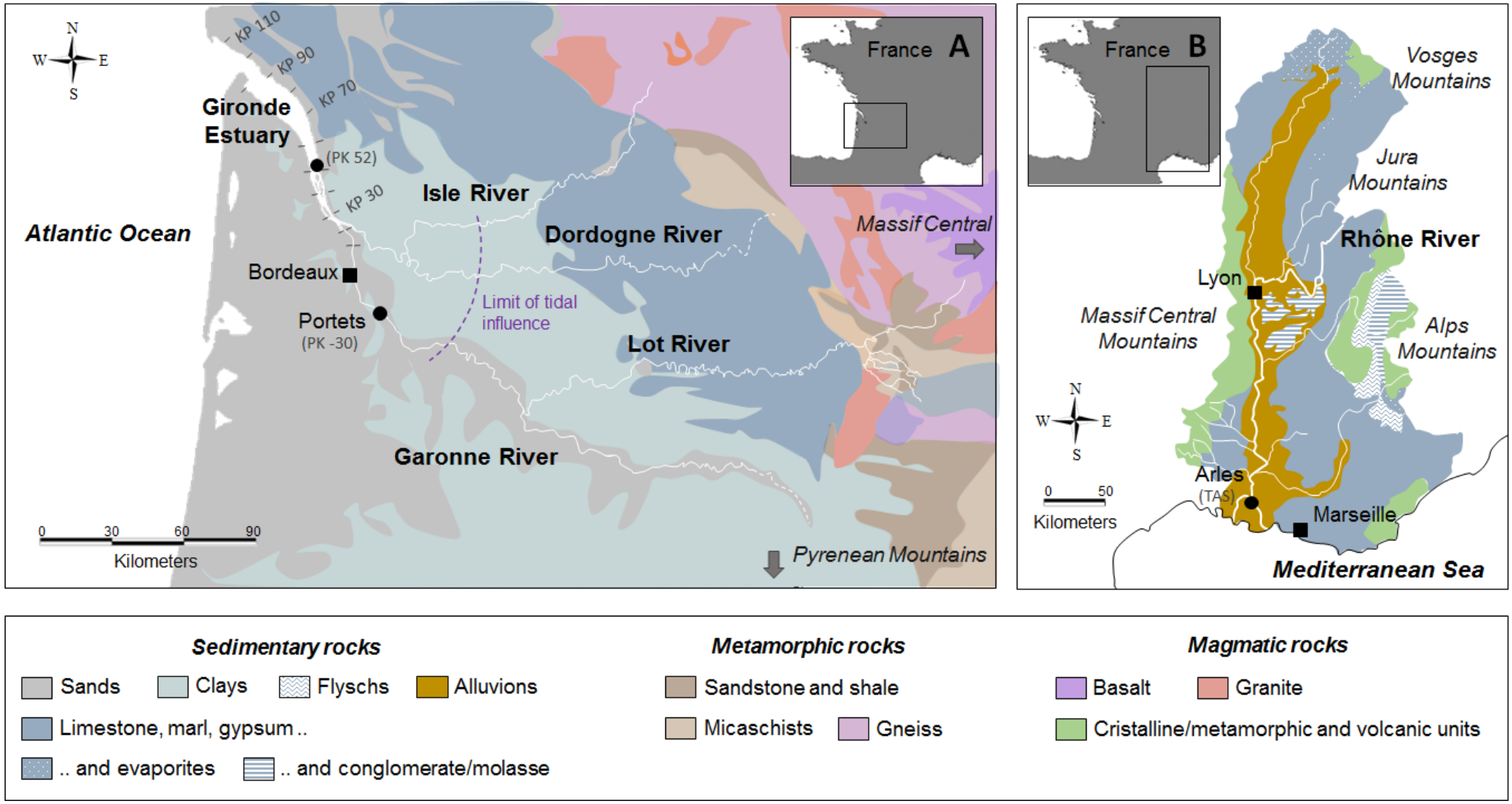


**Fig. 1.** Map of the Lot-Garonne-Gironde fluvial-estuarine system (A) and the Rhône River (B). Main cities (squares), sampling sites (circles), rivers and Kilometric Points (KP or PK) are shown. Rock composition along the watershed are denoted by the colour code legend: (A) adapted from BRGM (2014) and (B) simplified from Ollivier et al. (2010).

## 2.2. Preparation of isotopically-labelled ($^{123}$Sb) sediments

Wet SPM from PK52 was used for batch sorption experiments using isotopically-labelled Sb. For this, filtered (0.45 µm Teflon filters, FHLC, Merck Millipore Ltd.) aliquots (1L) of natural freshwater (S = 0) from La Réole (at PK-60, tidal influence limit) and brackish water from the Gironde Estuary (S = 22) and a 50/50 mixture of both matrices (S = 11) were spiked with high purity monoisotopic solution of $^{123}$Sb (99.43% Oakridge, USA) to nominal concentrations of 2 µg $L^{-1}$. The spiked matrices were left to equilibrate overnight, before being exposed during five days to high concentrations of SPM (nominal >1000 mg $L^{-1}$ dry weight, DW) in a tumbling shaker. The sediments were then recovered by centrifugation (10 min at 4000 rpm; Hettich Rotofix 32A centrifuge), oven-dried (50ºC stove), grinded in agate mortars and aliquots of each condition prepared for parallel selective extractions comprising several fractions (i.e., F1 to F4, see below).

## 2.3. Parallel selective extractions comparing F2 and F4 solutions

Three types of selective extraction solutions targeting Fe/Mn oxide minerals (F2 solutions, Table 1) were applied to natural sediment aliquots of PK52, PK-30 and TAS for parallel extractions. The first solution contains hydroxylamine ($NH_2OH$, ACS ThermoFisher® Acros Organics) using acetic acid as complexing agent (HOAc, PlasmaPURE SCP SCIENCE®; Chester and Hughes 1967, Tessier et al. 1979). The second extraction follows the known oxyanion-adapted protocol (Wenzel et al. 2001, based on Shuman 1982) consisting of an oxalate buffer extraction with oxalic acid ($C_2H_2O_4$, analytical grade, Fisher Scientific®) and ammonium oxalate as complexing agent ($(NH_4)_2C_2O_4$, R.P. NORMAPUR®). The third extraction uses ascorbic acid as reducing agent ($C_6H_8O_6$, ACS ThermoFisher® Acros Organics), sodium citrate as complexing agent ($Na_3C_6H_5O_7$, Merck®) and sodium bicarbonate ($NaHCO_3$, J.T. Baker) to buffer the pH of the reaction (Kostka and Luther 1994, based on Ferdelman 1988). In addition, operationally-defined potentially bioaccessible fractions (F4 solutions, Table 1) were determined by parallel extractions with either HCl (1M, Suprapur®) or $HNO_3$ (1M, Suprapur®).

All extractions were performed in acid-washed ($HNO_3$ 10%) PP Falcon 50 mL conical centrifuge tubes (FISHER SCIENTIFIC) previously rinsed with MilliQ water, dried under a laminar flow hood and stored in double-sealed plastic bags pending the experimental use. Natural sediments were extracted with three replicates in each selective extraction, run together with three blanks of each extraction to verify potential reagent contaminations.

### 2.4. Conventional parallel selective extraction scheme (F1 to F4)

Solid fractionation of the isotopically-labelled PK52 was studied with four parallel fractions:

- (F1) easily exchangeable and carbonate fraction, i.e., carbonates, Mn oxyhydroxides, sulphates and organic matter phases (Kersten and Förstner 1987; Bordas and Bourg 1998) with an acetate solution (1:20 w/v ratio for 1M NaOAc, J.T. Baker) at pH ~ 5 adjusted with 5M HOAc (PlasmaPURE SCP SCIENCE®) during 6h with permanent shaking at 25ºC (Tessier et al. 1979),
- (F2) reactive Fe/Mn oxides fraction as extracted by the above-described ascorbate solution (Kostka and Luther 1994),
- (F3) oxidisable fraction, attributed to organic matter and labile/amorphous sulphide phases (Tessier et al. 1979), extracted with $H_2O_2$ (30%, J.T. Baker) in a tumbling shaker during 5h at 85ºC, adding $NH_4OAc$ (Merck®) as complexing agent during the last 30min of shaking (Ma and Uren 1995) with a final 1:40 w/v ratio
- (F4) potentially bioaccessible fraction as assessed through the 1M HCl extraction.

As in the previous experience, these extractions were performed in acid-washed ($HNO_3$ 10%) PP Falcon 50 mL conical centrifuge tubes (FISHER SCIENTIFIC). Isotopically-labelled sediment was extracted with only one replicate per condition due to mass limitations, run together with three blanks of each extraction.

### 2.5. Total element digestion

Total element concentrations were quantified from tri-acid total digestions as described in Schäfer et al. (2002). Briefly, 30 mg of dried and homogenised sediments were digested on a heating plate (2 h at 110 °C) with 1.5 mL HCl (10 M Suprapur®, Merck), 750 µL $HNO_3$ (14 M Suprapur®, Merck) and 2.5 mL HF (29 M Suprapur®, Fisher) in closed PP reactors (DigiTUBEs®, SCP SCIENCE). An evaporation step was then followed by re-dissolution of the residues with 250 µL $HNO_3$ (14 M), finally brought to 10 mL using Milli-Q® water. Parallel total digestions (N=2) of CRMs (river sediment NIST 8704, stream sediment DC 73384 and marine sediment NIST 2702) were performed for quality monitoring purposes.

The residual fraction in this work was calculated as the difference between the total element concentration (tri-acid digestion) and that obtained in the acid-soluble fraction (1M HCl acid-soluble fraction, F4).

**Table 1.** Reagents and methods used for reactive Mn/Fe oxide and bioaccessible (acid-soluble) extractions.

| **PROTOCOLS** | **Reducible Fe/Mn oxide fraction (F2 solutions)** | | | **Bioaccessible acid-soluble fraction (F4 solutions)** | |
|---|---|---|---|---|---|
| **Reagent** | Hydroxylamine + HOAc (HA) | Oxalate buffer (Ox) | Ascorbate solution (Asc) | HCl | $HNO_3$ |
| **Solid/liquid ratio (w/v)** | 1:100 (50 mg in 5 mL) | 1:100 (400 mg in 40mL) | 1:50 (200 mg in 12.5 mL) | 1:50 (200 mg in 12.5 mL) | 1:50 (200 mg in 12.5 mL) |
| **Solutions** | 1M $NH_2OH.HCl$ 25% v/v HOAc[a] | 0.2M $(NH_4)_2C_2O_4$ 0.2M $C_2H_2O_4$ pH < 3[b] | 12.5 g $Na_3C_6H_5O_7$ 12.5 g $NaHCO_3$ Deaerating with $N_2$ 5 g $C_6H_8O_6$ pH = 8[c] | 1M HCl | 1M $HNO_3$ |
| **Extracting conditions** | 48 h shaking at 25ºC | 4 h shaking in the dark at 25ºC | 24 h shaking at 25ºC | 24h shaking at 25ºC | 24h shaking at 25ºC |
| **Target phases** | Mn oxides and amorphous Fe oxides (e.g., ferrihydrite, lepidocrocite), including highly reactive Fe phases like carbonate Fe (e.g., siderite $FeCO_3$) due to HOAc[e] and potentially short-range ordered to highly crystalline phases according to the sediment characteristics[f] | All Mn oxides (e.g., associated to organic matter) and short-range ordered[g] to highly crystalline Fe oxides like magnetite[e,h] especially in presence of Fe(II)-bearing minerals[i] | Amorphous Mn and Fe oxides[c]. Citrate solution in excess avoids precipitation of Fe(II) oxy(hydr)oxides[j] | Amorphous and crystalline (incompletely) Fe/Mn oxyhydroxides, Fe(II)-bearing minerals, organic matter, carbonates, amorphous sulphides and hydrous aluminosilicates[c,k,l] (except goethite and hematite[m])<br><br>1M HCl has sufficient buffering capacity to dissolve carbonates and has a limited impact on the residual clays or sulphides[n]<br><br>$HNO_3$ favours pyrite ($FeS_2$) dissolution[k] | |

[a] Chester and Hughes 1967; [b] Shuman 1982; [c] Kostka and Luther 1994; [e] Poulton and Canfield 2005; [f] Tack et al. 2006; [g] Miller et al. 1986; Wilcke et al. 1998; [h] Suda et al. 2013; [i] Stumm and Sulzberger 1992; [j] Henkel et al. 2016; [k] Huerta-Díaz and Morse 1990; [l] Gasparon and Matschullat 2006; [m] Raiswell et al. 1994; [n] Billings and Ragland 1968

### 2.6. Quantification of Fe, Mn, Sb and other trace elements

All trace elements (Sb, Co, Cu, Ni, Pb, U and Zn) were analysed by ICP-MS (X7 Series, THERMO®) using external calibration. Extracted Fe and Mn contents were analysed by ICP-OES (700 Series, Agilent®) with external calibration only for sediments from the Gironde Estuary. All calibrations were performed with mono-elemental solutions (SPEX CertiPrep®) and analytical performances were quality checked with certified reference waters (CRM: TMRAIN-04, TMRAIN 23.4, SLRS-6, SRM 1640a; NIST 1643-f) for ICP-MS and ICP-OES measurements, producing accuracies between 81% and 119% with precisions of 1% to ~20% (details in Supplementary data, Table S1).

Given the lack of adapted CRM for multi-element selective extractions, the resulting dissolutions from selective extractions could not be quality checked. Nevertheless, trace element concentrations in extracted dissolutions were generally > 10-fold higher than the respective analytical limits of detection (LODs; for average minimum values see Supplementary data, Table S1), except for some extractions from TAS sediment, probably due to relatively low total concentrations compared to sediments from the Gironde Estuary. Iron and Mn concentrations in extracted dissolutions were always 12 to 1000 times higher than LOD (Supplementary data, Table S1), except for TAS samples. Quality data from CRMs (river sediment NIST 8704, stream sediment DC 73384 and marine sediment NIST 2702) total extractions showed Sb recoveries of 85% ± 12%.

In all extractions of isotopically-labelled sediments, both inherited ($Sb_{nat}$) and spiked ($Sb_{ex}$) concentrations were determined as follows:

$$\mathrm{Sb_{ex}} = \frac{^{121}\mathrm{Sb} \cdot \mathrm{Ab_{123nat}} - {}^{123}\mathrm{Sb} \cdot \mathrm{Ab_{121nat}}}{\mathrm{Ab_{121ex}} \cdot \mathrm{Ab_{123nat}} - \mathrm{Ab_{123ex}} \cdot \mathrm{Ab_{121nat}}}$$

$$\mathrm{Sb_{nat}} = \frac{^{121}\mathrm{Sb} \cdot \mathrm{Ab_{123ex}} - {}^{123}\mathrm{Sb} \cdot \mathrm{Ab_{121ex}}}{\mathrm{Ab_{123ex}} \cdot \mathrm{Ab_{121nat}} - \mathrm{Ab_{121ex}} \cdot \mathrm{Ab_{123nat}}}$$

where all $Sb_{ex}$ and $Sb_{nat}$ correspond to spike and natural Sb concentrations, respectively, $^{121}Sb$ and $^{123}Sb$ are the concentrations of the respective isotopes as determined by abundance-weighted external calibration curves, i.e., external calibration curves recalculated to represent independent $^{121}$Sb and $^{123}$Sb concentrations, and *Ab* corresponds to the natural (nat) or spiked (ex) isotopic abundances: $Ab_{121nat}$ = 0.573; $Ab_{123nat}$ = 0.427; $Ab_{121ex}$ = 0.0057; $Ab_{123ex}$ = 0.9943.

**Table S1.** Analytical performance of dissolved (all in µg $L^{-1}$ except * in ng $L^{-1}$; mean ± standard deviations, SD) certified reference materials (CRM: rain water TMRAIN-04, TMRAIN 23.4; river water SLRS-6, NIST 1643-f; spring water SRM 1640a), maximum limits of detection (LOD = 3·SD(blanks)) and minimum sample fold above LOD for all extraction solutions performed.

| Element | TMRAIN-04 | | TMRAIN 23.4 | | SLRS-6 | | *SRM 1640a* / NIST 1643-f | | LOD | Factor >LOD |
|---|---|---|---|---|---|---|---|---|---|---|
| | Certified | Measured | Certified | Measured | Certified | Measured | Certified | Measured | | |
| Co | 0.25 ± 0.06 | 0.26 ± 0.02 | 7.08 ± 0.55 | 6.49 ± 0.14 | 53 ± 12* | 56.6 ± 9.1* | 25.1 ± 0.2 | 21.8 ± 0.8 | 0.05 | 10 |
| Cu | 7.03 ± 0.80 | 6.81 ± 0.75 | 8.52 ± 0.83 | 8.00 ± 0.14 | 23.9 ± 1.80 | 23.1 ± 0.9 | 21.7 ± 0.7 | 18.7 ± 1.1 | 0.18 | 5 |
| Fe | 24.7 ± 4.1 | 25.1 ± 0.7 | 14.7 ± 2.4 | 12.8 ± 0.2 | 84.3 ± 3.6 | 77.5 ± 1.2 | *36.8 ± 1.8* | *35.4 ± 1.6* | 0.75 | 400 |
| Mn | 6.70 ± 0.66 | 6.70 ± 0.31 | 8.78 ± 0.63 | 8.52 ± 0.19 | 2.12 ± 0.10 | 1.93 ± 0.05 | *40.4 ± 0.4* | *39.5 ± 1.8* | 0.39 | 1000 |
| Ni | 0.91 ± 0.12 | 0.89 ± 0.08 | 4.96 ± 0.62 | 5.61 ± 0.22 | 0.62 ± 0.02 | 0.67 ± 0.04 | 59.8 ± 1.4 | 52.0 ± 2.8 | 0.29 | 10 |
| Pb | 0.35 ± 0.07 | 0.34 ± 0.01 | 2.98 ± 0.27 | 2.56 ± 0.03 | 0.17 ± 0.03 | 0.16 ± 0.02 | 18.5 ± 0.08 | 15.8 ± 0.1 | 24.3* | 10 |
| Sb | 0.35 ± 0.07 | 0.34 ± 0.01 | 3.26 ± 0.32 | 2.91 ± 0.03 | 0.34 ± 0.01 | 0.31 ± 0.01 | 55.5 ± 0.4 | 49.5 ± 0.9 | 5.13* | 10 |
| Th | - | - | - | - | - | - | - | - | 23.8* | 5 |
| U | 0.29 ± 0.03 | 0.24 ± 0.01 | 5.00 ± 0.39 | 4.06 ± 0.01 | 69.8 ± 3.4* | 57.5 ± 1.8* | - | - | 7.23* | 20 |
| Zn | 8.47 ± 2.11 | 10.1 ± 0.1 | - | - | 1.76 ± 0.12 | 1.95 ± 0.43 | 74.4 ± 1.7 | 83.3 ± 3.4 | 0.50 | 10 |
| Replicates | N = 8 (ICP-MS)<br>N = 8 (ICP-OES) | | N = 4 (ICP-MS)<br>N = 5 (ICP-OES) | | N = 7 (ICP-MS)<br>N = 3 (ICP-OES) | | N = 3 (ICP-MS)<br>N = 7 (ICP-OES) | | - | - |

# 3. RESULTS

## 3.1. Fractionation (F2 and F4 extractions) of Fe, Mn and trace elements in sediments from the Gironde and Rhône River systems

Sediments from the Garonne/Gironde fluvial estuarine system (PK52 and PK-30) showed systematically higher Fe, Mn and trace element concentrations in all selective extractions and total digestions compared to the Rhône River sediments (TAS, Fig. 2). This difference on extraction pattern between watersheds was also observed for Al content and is probably due to differences in mineral composition and/or grain size distribution. Sediments of the Gironde Estuary show characteristic particulate organic carbon (POC) contents ranging from 0.05 to 1.5% (Etcheber et al. 2007; Coynel et al. 2016) and grain sizes of mainly silts and some sands (i.e., grain size diameter ranging from 7 to 480 µm; Coynel et al. 2016) whereas the Rhône River sediments show variable POC contents from 1.5 to 3.5% for silts (10-15µm).

Selective extractions targeting Fe/Mn oxides extracted similar amounts of Fe and Mn from Gironde Estuary sediments when using either hydroxylamine or oxalate buffer solutions (Fig. 2). The extracted Fe and Mn fractions were always consistent with, or smaller than, those obtained from the acid extractions (1M HCl and 1M $HNO_3$, Fig. 2), accounting for ~35% of total Fe content and ~90% of total Mn in the Garonne/Gironde sediments (PK52, PK-30). However, the ascorbate solution always showed lower Fe and Mn extractions, equivalent to ~3% and ~15% of total Fe and Mn concentrations, respectively.

Similar to the fractionation pattern of Fe and Mn obtained for F2 and F4 extractions, highest trace element fractions occurred in F4 solutions, with concentrations in hydroxylamine and oxalate solutions similar or slightly lower than those in acid-soluble fractions (Fig. 2). Again, the lowest extraction efficiencies were obtained with the ascorbate solution for all studied trace elements (Co, Cu, Ni, Pb, Zn and U), except Pb in the oxalate extraction (Fig. 2).

In contrast, the applied parallel selective extractions showed unexpected results for Sb extractions, with Sb concentrations in the reducible (F2) fractions using oxalate and ascorbate clearly greater than those in the acid-soluble fractions (F4; Fig. 2). In fact, Sb was more efficiently extracted with oxalate (~12% of total Sb in PK52, ~40% in TAS) and ascorbate solutions (~6% of total Sb in PK52, ~10% in TAS) than with hydroxylamine (~1.5% of total Sb in PK52, ~7% in TAS) and 1M acids (~2% of total Sb in PK52, ~10% in TAS). Thus, the detected anomaly is reproducible among sediments from both study areas, and more pronounced in the Garonne/Gironde fluvial estuarine system than in the Rhône River.

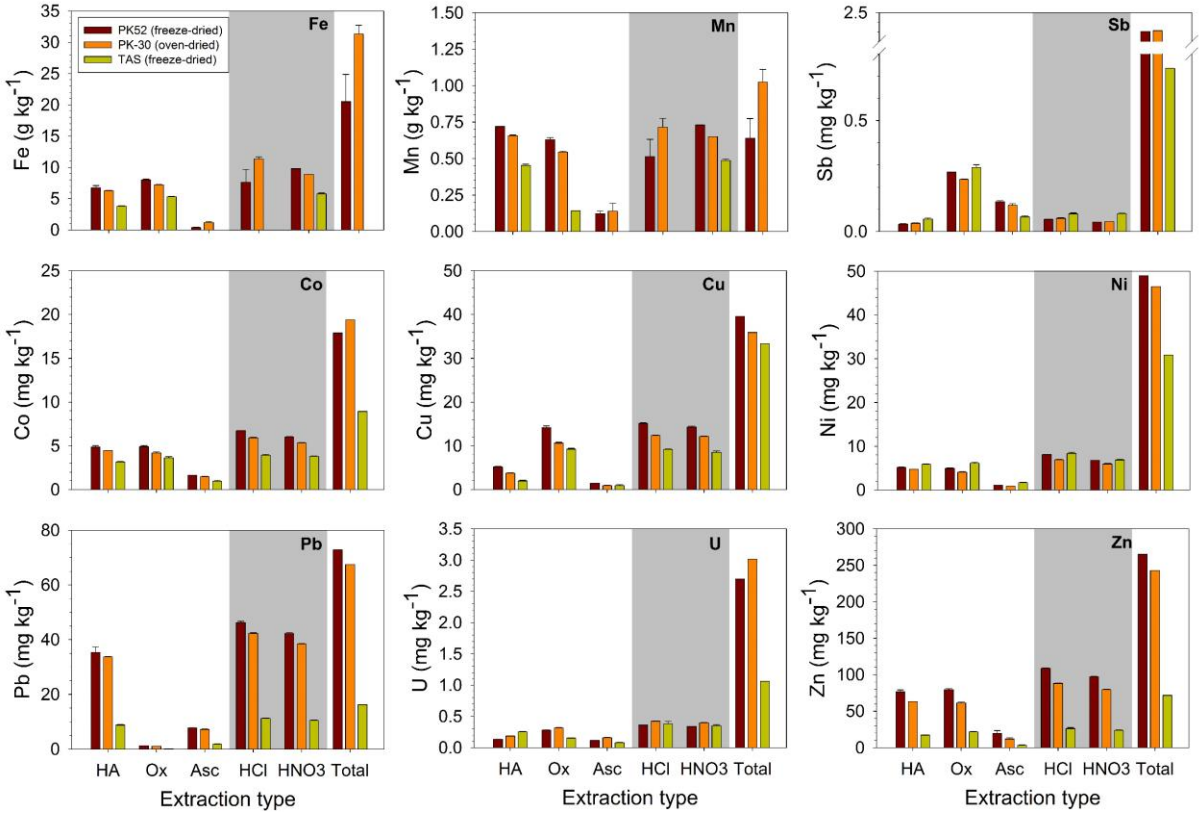


**Fig. 2.** Selectively extracted and total concentrations (N=3) of Fe, Mn, Co, Cu, Ni, Pb, Sb, U and Zn in sediments from PK-30 (oven-dried SPM from Portets, Gironde Estuary), PK52 (freeze-dried SPM, Gironde Estuary) and TAS (freeze-dried SPM from Arles, Rhône River). F2 solutions: HA: hydroxylamine+HOAc, Ox: oxalate buffer and Asc: ascorbate solution. F4 solutions (in grey area): 1M HCl and 1M $HNO_3$.

### 3.2. Fractionation of natural and spiked Sb adsorbed to SPM in contrasting estuarine conditions

Results from the complete selective extraction scheme (F1 to F4) showed similar fractionation patterns for spiked Sb ($Sb_{ex}$) compared to that of inherited/natural Sb ($Sb_{nat}$), independent from salinity (Fig. 3). However, the extracted fractions of $Sb_{ex}$ were consistently and clearly higher than those of $Sb_{nat}$, with the mobility of $Sb_{ex}$ in the different fractions being between 2-fold (F4) and 10-fold (F1) greater than that of $Sb_{nat}$. The highest extracted Sb concentrations occurred in the F2-Asc fraction (i.e., reducible Fe/Mn oxides, equivalent to ~55% of total sorbed $Sb_{ex}$ and 10% of total $Sb_{nat}$), followed by the F1-acetate fraction (i.e., easily exchangeable and/or carbonate fraction, equivalent to ~22% of total $Sb_{ex}$ and 2% of total $Sb_{nat}$). These fractions were higher than the acid-soluble fraction (F4, equivalent to ~12% of total $Sb_{ex}$ and 5% of total $Sb_{nat}$). The lowest Sb fractions were obtained within the F3-$H_2O_2$ fraction (i.e., oxidisable phases, ~5% of total $Sb_{ex}$ and 1% of total $Sb_{nat}$).

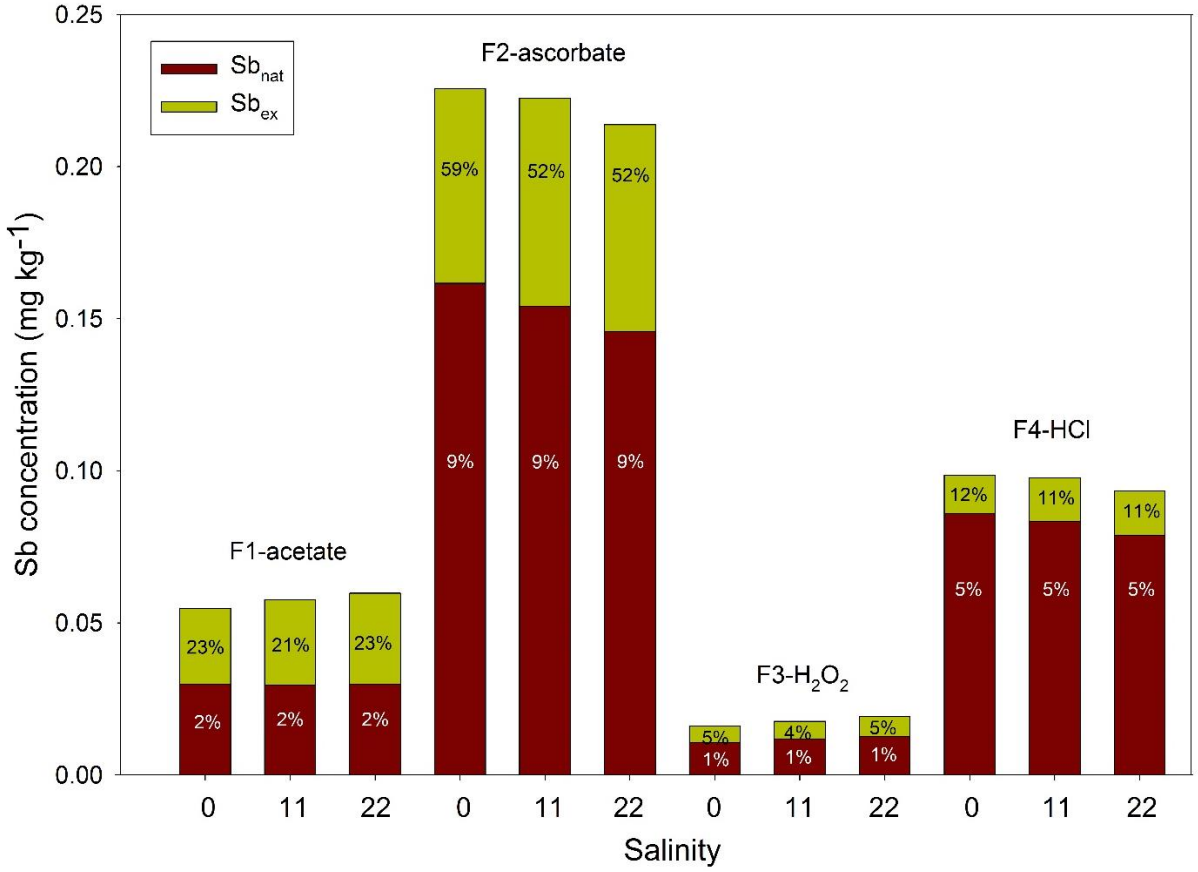


**Fig. 3.** Parallel selective extractions of Sb (N = 3) from sediments isotopically-labelled sediments, prepared by 5-days incubations of SPM = 1000 mg $L^{-1}$ in three salinity matrices (S=0, S=11 and S=22). Absolute concentrations (mg $kg^{-1}$) of $Sb_{nat}$ and $Sb_{ex}$ and fractions (% of total $Sb_{nat}$ and % of total $Sb_{ex}$) are given. F1: acetate extracted fraction ("easily exchangeable and/or carbonate fraction"), F2: ascorbate extracted fraction ("amorphous Fe/Mn oxides and citrate-complexed Sb"), F3: $H_2O_2$-soluble fraction ("oxidisable fraction"), F4: 1M HCl-soluble fraction ("potentially bioaccessible").

# 4. DISCUSSION

## 4.1. The F2 fractions obtained from oxalate, hydroxylamine and ascorbate-based reagents

The extraction efficiency of the different reagents commonly applied to assess the F2 fraction, attributed to Fe/Mn oxydes and hydroxides, depends not only on the abundance of Fe and Mn phases present but also on their quality in terms of crystallinity degree and Fe(II) vs Fe(III) presence (Stumm and Sulzberger 1992). The results for Fe and Mn obtained in the present work are widely consistent with a previous comparison of extraction efficiencies of the oxalate- and ascorbate-based extractions applied to marine sediments (Kostka and Luther 1994). These authors mentioned that the oxalate extraction might be too strong, due to the presence of Fe(II) minerals enhancing the oxalate extracting power from other mineral phases such as sulphides, silicates and crystalline Fe oxides (e.g. hematite), which leads to an overestimation of amorphous Fe(III) minerals and underestimating crystalline Fe(III) minerals. To the best of our knowledge, this is the first study directly comparing the parallel extraction efficiencies

of oxalate- and ascorbate-based reagents to those of hydroxylamine-based extractions from estuarine and river sediments. The fact that hydroxylamine extracted similar proportions of Fe and Mn as oxalate solutions may suggest that the acid pH of these reagents also contributes to Fe and Mn release from mineral phases other than the targeted amorphous or partially crystalline phases. In fact, the ascorbate solution is the only non-acidic F2 extraction reagent (pH=8). This observation is consistent with Kostka and Luther (1994) highlighting the selectivity and efficiency of the ascorbate solution, dissolving Fe(II) and Fe(III) amorphous (hydr)oxides but not magnetite, or other crystalline Fe phases (at least at pH > 6; Zinder et al. 1986; Reyes and Torrent 1997), not even other Fe-bearing mineral phases like chlorite (Kostka and Luther 1994).

High Mn extraction efficiencies (~90% Mn extraction out of total Mn) obtained with the oxalate and hydroxylamine extractions (Fig. 2), being similar to Mn in the acid-soluble fractions (1M HCl and 1M $HNO_3$), are consistent with the acid character of the extraction and the effect of HOAc on carbonates. In fact, Mn is highly present in both oxide and carbonate fractions (Presley et al. 1972). Therefore, the relatively low Mn concentrations in ascorbate extractions of sediments from all studied sites compared to hydroxylamine and oxalate solutions suggest specific solubilisation of poorly crystalline Mn oxides by ascorbate.

Given the similar values obtained from hydroxylamine and oxalate extractions, the present results suggest that, in parallel extractions, both BCR/Tessier et al. 1979 (cation-adapted) and Wenzel et al. 2001 (anion-adapted) protocols are applicable to evaluate Co, Ni, Zn and U fractions bound to amorphous and some crystalline Fe/Mn oxides in sediments from the Garonne/Gironde and Rhône River systems. The lower Pb extraction efficiency of the oxalate solution may be attributed to Pb-oxalate salt formation (Gleyzes et al. 2002), potentially leading to a 5-fold underestimated Pb fraction in amorphous and partly crystalline oxides, compared to ascorbate extraction. General lower trace element extractions in oven-dried (PK-30) sediments compared to freeze-dried (PK52) sediments are attributed to pre-treatment conditions favouring a transfer of trace element extractions from the reactive fraction to the residual fraction due to crystallisation of Fe/Mn (hydr)oxides (Bordas and Bourg 1998; Gleyzes et al. 2002).

### 4.2. The anomalous fractionation of Sb in F2 and F4 extractions

Classical extraction schemes imply that the acid-soluble fraction (F4; 1M HCl) comprises the fractions extracted by F2 reagents (reduction of amorphous and partly crystalline oxides/hydroxides; Huerta-Díaz and Morse 1990; Gasparon and Matschullat 2006; Snape et al. 2004). The comparison of the results obtained from three different F2 and two different F4 extractions applied to three different sediments confirms this paradigm for Fe and Mn, i.e. the main oxide/hydroxide-forming metals, as well as for a number of trace elements, such as Co, Ni, Zn and U.

The observed behaviour of Sb in the same extractions shows that the F4 fraction of Sb cannot entirely comprise the F2 fraction, which can be considered as "anomalous" because it strongly differs from the commonly accepted relative extraction efficiencies of the different reagents. This anomaly is observed in the ascorbate and the oxalate extractions of Gironde Estuary sediments and the oxalate extraction of Rhône River sediments, although the latter corresponds to the "anion-adapted" F2 protocol proposed for As, the geochemical pair of Sb (Wenzel et al 2001).

The inverse relationship between the F2 and F4 fractions of Sb may relate to (i) enhanced Sb solubilisation from non-target carrier phases by oxalate/ascorbate solutions, and/or (ii) Sb losses due to precipitation and/or sorption onto remaining solid phases such as incompletely dissolved crystalline Fe oxides during F4 acid extractions.

Precipitation of Sb in acidic conditions appears unlikely given the low extracted concentrations, probably far from solubility limits (max. ~0.2 mg $kg^{-1}$ for Sb in PK52, equivalent to ~3 µg $L^{-1}$ during the extraction). For example, Sb(III) precipitation as $Sb_2O_3$ at pH = 3 would require relatively high concentrations (e.g., >63 µM, ~7.6 mg $L^{-1}$; Leuz 2006). However, given the recommendations to stabilise Sb in highly concentrated standard solutions in dilute $HNO_3$ by adding HF or organic ligands (e.g., tartrate or citrate/oxalate; *www.inorganicventures.com*), and the fact that insoluble Sb(V) salts may form in acid conditions (i.e., $NaSbO_3$, $KSbO_3$ or $Mg^{2+}$/$Ca^{2+}$-related; Pauling 1933; Blandamer et al. 1974), Sb precipitation cannot be fully excluded.

However, the following observations do not support it: (i) similar Sb concentrations in both HCl and $HNO_3$ extractions (differences in oxidising power and complexing properties), (ii) the relatively short storage time (few days), and (iii) the fact that the acid-extracted Sb fraction (F4) is always slightly greater than the hydroxylamine-extracted fraction (F2) for all sediments studied. The latter observation corresponds to the expected relation between F2 and F4 and implies very incomplete Sb removal by precipitation. Furthermore, the ascorbate-extracted Sb fraction (at pH= 8) in Rhône River sediments is similar to the acid-soluble fraction, which again would point to incomplete Sb precipitation in both 1M HCl and $HNO_3$.

Enhanced Sb solubilisation from non-target carrier phases by oxalate/ascorbate solutions is consistent with observations showing that independent Sb(III) and Sb(V) adsorbed to standard/synthetic goethite were extracted in oxalate buffer solution with 73% extraction of total Sb(III) and 36% of total Sb(V) from an undissolved/unaffected goethite mineral (Leuz 2006). Accordingly, the oxalate-based so-called anion-adapted protocols (Wenzel et al. 2001) would produce higher extractions for Sb in oxalate solutions than the hydroxylamine-based standard BCR procedure and that from Tessier et al. (1979). Leuz (2006) concluded that oxalate buffer solutions are not adequate for Sb selective extractions from amorphous and crystalline operationally defined phases because the oxalate itself directly interacts and desorbs Sb from unreacted mineral phases.

White and Rose (1953) observed that both oxalic and citric acids were good complexing agents of Sb for extraction purposes. The presence of citrate as a complexing agent in the ascorbate reagent may enhance its extraction efficiency compared to the inorganic hydroxylamine extraction, implying a citrate-ligand complexing effect on Sb from non-attacked mineral phases. In fact, citrate is used as a complexing agent for Sb speciation in analytical chemistry (e.g., HPLC-ICP-MS and in hydride generation; Zheng et al. 2001; Potin-Gautier et al. 2005). The citrate-effect would be due to complexation, rather than changes in Sb redox state, as citrate does not induce redox Sb(V) and Sb(III) species transformations (Mohammad et al. 1990; Potin-Gautier et al. 2005). The use of citrate in selective extractions is pertinent because citrate is present and active in several environmental compartments: involved in cellular metabolic pathways (e.g., in oysters and fish; Cooper et al. 2002; Ivanina et al. 2011), as part of the estuarine dissolved organic matter from terrestrial plant exudates (Mucha et al. 2010), in $H_2S$-producing bacteria in estuarine sediments (Jyothsna et al. 2013) and affecting trace element behaviour by complexation (Francis et al. 1992). Although Sb complexation by citrate would be more efficient under acidic conditions, as observed for many other organic ligands (Stumm and Sulzberger 1992, Filella and May 2005), even at pH=8 (ascorbate extraction) one cannot exclude enhanced Sb solubility and mobilisation from other mineral phases due to the presence of citrate. However, one would expect that this additional Sb extracted derives from binding sites on carrier phases that also are extracted by 1M acids. As such, organic complexation may partly explain the differences observed for the three F2 solutions tested, but not the higher apparent extraction efficiency of ascorbate and oxalate extractions compared to that of the 1M acid extractions.

Previous work on Sb fractioning by oxalate and/or ascorbate (F2) and dilute HCl (F4) extractions have not identified such inconsistencies because of limited sensibility in Sb detection (Prieto 1998) and/or because these extractions were performed sequentially (Manaka et al. 2007), which masks selectivity biases. To the best of our knowledge, there is to date no published work on Sb fractionation using parallel F2 and F4 extractions which might provide additional information. Therefore, more experimental work is necessary to completely understand the apparent artefacts when applying commonly accepted extraction protocols, including the anion-adapted oxalate extraction.

### 4.3. Solid fractionation of natural and anthropogenically added Sb

Sediment contamination by the anthropogenic release of dissolved Sb into the Gironde Estuary was mimicked by exposing fresh PK52 SPM (~1g $L^{-1}$ SPM) to isotopically-labelled $^{123}Sb$ in three salinity conditions (0, 11 and 22). The amount of isotopically-labelled Sb spiked to the sediments of the Gironde Estuary was ~5% of the total Sb available in the solution, whatever the salinity. Assessment of solid fractionation of both inherited and spiked Sb by a complete parallel selective extraction scheme (F1 to F4) showed that the studied SPM can efficiently adsorb anthropogenic Sb in addition to their inherited Sb load. In the present work, the fractionation results obtained from parallel extractions suggest that the

ascorbate-extracted and the acid-soluble fractions are the most important reactive fractions for inherited Sb. However, the isotopically-labelled Sb had the highest recoveries in the ascorbate-extracted (F2: ~52%) and acetate-extracted (F1: ~21%) fractions (Fig. 3). This observation suggests that anthropogenic Sb readily adsorbs to the most reactive carrier phases.

Both, inherited and spiked (isotopically-labelled) Sb were present in all fractions, including the residual fraction (i.e. not extracted by 1M HCl), representing 90% of the spiked Sb. This result was rather surprising, as one would expect the spiked Sb to adsorb onto reactive carrier phases and not to the so-called residual fraction. This observation supports the above discussed hypothesis of an incomplete Sb extraction and/or recovery (Sb losses by acid precipitation) by conventional protocols targeting the acid-soluble fractions and even the oxalate-extracted F2 fraction, as supported by previously reported incomplete recoveries of spiked Sb (Brannon and Patrick 1985). The inherited Sb in SPM from the Gironde Estuary were mostly (~95%) in the residual fraction, which is consistent with the majority of published Sb fractionation results (Filella 2011). However, given the above considerations, one cannot exclude that the acid-soluble fraction may strongly underestimate the potentially reactive Sb in natural sediments. These findings imply that the existing estimates of the potentially bioaccessible Sb fractions in sediments may be biased and that there is a need for a deeper understanding of the (i) interactions between Sb and the respective potential carrier phases, and (ii) efficiencies of selective extraction techniques in view of future ecological risk assessment of Sb contamination by both, stable isotopes and Sb radionuclides.

## 5. CONCLUSIONS

Selective extraction F2 protocols using organic ligands (i.e. citrate and oxalate) tend to overestimate the Sb fraction associated to the target operationally defined carrier phases (i.e. non-selective extraction of Sb without destruction of the carrier phases).

The fractions of both, inherited and spiked Sb extracted by F2 protocols using organic ligands are greater than the acid-soluble F4 fractions, which is not consistent with the extraction efficiencies for target carrier phases as commonly observed for other trace elements. This anomaly also occurs for the so-called anion-adapted protocol developed for As, the geochemical pair of Sb, and only becomes visible in parallel extraction approaches. Sequential methods are probably subjected to the same artefact, but do not allow identifying it.

Low recoveries of both inherited and spiked Sb in the acid-soluble fractions suggest Sb losses, implying the risk of systematic underestimation of the potentially bioaccessible fraction, when applying traditional extraction schemes. This may have consequences on the mobility- and ecological risk assessment of anthropogenically released Sb (stable isotopes and radionuclides) into aquatic environments.

Further research on mechanisms involved in the selective dissolution of Sb is a prerequisite for the development of (i) a specific extraction scheme reliably simulating environmental Sb carrier phases and behaviour, and (ii) future understanding of the consequences of anthropogenic Sb inputs into the environment. The application of commonly accepted extraction schemes to "new" elements, such as emerging trace element contaminants, for which the protocols were not developed, adapted and tested, implies the risk of producing biased results and interpretations.

## ACKNOWLEDGEMENTS

This study was funded by the French National Project AMORAD (ANR-11-RSNR-0002) from the National Research Agency, allocated in the framework programme "Investments for the Future" and the FEDER Aquitaine-1999-Z0061. The authors acknowledge Franck Gîner from the IRSN at Cadarache for providing wet sediments from the SORA station in the Rhône River as well as Linda Makni, Jean-Baptiste Kucharski, Aude Charrier, Pierre-Yves Gourvès and Clément Pereto for the laboratory assistance provided, contributing to the different results of this work.

## REFERENCES

Agemian, H., Chau, A. S. Y. (1976). Evaluation of extraction techniques for the determination of metals in aquatic sediments. Analyst, 101(1207), 761-767.

Blandamer, M. J., Burgess, J., Peacock, R. D. (1974). Solubility of sodium hexahydroxoantimonate in water and in mixed aqueous solvents. Journal of the Chemical Society, Dalton Transactions, (10), 1084-1086.

Bordas, F., Bourg, A. C. (1998). A critical evaluation of sample pretreatment for storage of contaminated sediments to be investigated for the potential mobility of their heavy metal load. Water, Air, and Soil Pollution, 103(1-4), 137-149.

Brannon, J. M., Patrick Jr, W. H. (1985). Fixation and mobilization of antimony in sediments. Environmental Pollution Series B, Chemical and Physical, 9(2), 107-126.

Bureau de Recherches Géologiques et Minières (BRGM). Carrières de France, exploitations actives (2014). <http://www.brgm.fr/actualite/brgm-sim-presentent-carte-carrieres-france> Last accessed on the 13/07/2015.

Chester, R., Hughes, M. J. (1967). A chemical technique for the separation of ferro-manganese minerals, carbonate minerals and adsorbed trace elements from pelagic sediments. Chemical geology, 2, 249-262.

Coynel, A., Gorse, L., Curti, C., Schafer, J., Grosbois, C., Morelli, G., Ducassou, E., Blanc, G., Maillet, G.M., Mojtahid, M. (2016). Spatial distribution of trace elements in the surface sediments of a major European estuary (Loire Estuary, France): Source identification and evaluation of anthropogenic contribution. Journal of Sea Research, 118, 77-91.

Etcheber, H., Taillez, A., Abril, G., Garnier, J., Servais, P., Moatar, F., Commarieu, M. V. (2007). Particulate organic carbon in the estuarine turbidity maxima of the Gironde, Loire and Seine estuaries: origin and lability. Hydrobiologia, 588(1), 245-259.

Ferdelman, T. G. (1988). The distribution of sulfur, iron, manganese, copper and uranium in a salt marsh sediment core as determined by a sequential extraction method (Doctoral dissertation, University of Delaware).

Filella, M. (2011). Antimony interactions with heterogeneous complexants in waters, sediments and soils: a review of data obtained in bulk samples. Earth-science reviews, 107(3-4), 325-341.

Filella, M., May, P. M. (2005). Critical appraisal of available thermodynamic data for the complexation of antimony (III) and antimony (V) by low molecular mass organic ligands. Journal of Environmental Monitoring, 7(12), 1226-1237.

Francis, A. J., Dodge, C. J., Gillow, J. B. (1992). Biodegradation of metal citrate complexes and implications for toxic-metal mobility. Nature, 356(6365), 140.

Froelich, P., Klinkhammer, G. P., Bender, M. L., Luedtke, N. A., Heath, G. R., Cullen, D., Dauphin, P., Hammond, D., Hartman, B., Maynard, V. (1979). Early oxidation of organic matter in pelagic sediments of the eastern equatorial Atlantic: suboxic diagenesis. Geochimica et cosmochimica acta, 43(7), 1075-1090.

Gasparon, M., Matschullat, J. (2006). Trace metals in Antarctic ecosystems: results from the Larsemann Hills, East Antarctica. Applied Geochemistry, 21(9), 1593-1612.

Gleyzes, C., Tellier, S., Astruc, M. (2002). Fractionation studies of trace elements in contaminated soils and sediments: a review of sequential extraction procedures. TrAC Trends in Analytical Chemistry, 21(6-7), 451-467.

Henkel, S., Kasten, S., Poulton, S. W., Staubwasser, M. (2016). Determination of the stable iron isotopic composition of sequentially leached iron phases in marine sediments. Chemical Geology, 421, 93-102.

Huerta-Díaz, M. A., Morse, J. W. (1990). A quantitative method for determination of trace metal concentrations in sedimentary pyrite. Marine Chemistry, 29, 119-144.

Jenne, E. A. (1968). Controls on Mn, Fe, Co, Ni, Cu, and Zn concentrations in soils and water: the significant role of hydrous Mn and Fe oxides.

Jyothsna, T. S., Rahul, K., Ramaprasad, E. V. V., Sasikala, C., Ramana, C. V. (2013). Arcobacter anaerophilus sp. nov., isolated from an estuarine sediment and emended description of the genus Arcobacter. International journal of systematic and evolutionary microbiology, 63(12), 4619-4625.

Kersten, M., Förstner, U. (1987). Cadmium associations in freshwater and marine sediment. Cadmium in the Aquatic Environment, 51-88.

Kheboian, C., Bauer, C. F. (1987). Accuracy of selective extraction procedures for metal speciation in model aquatic sediments. Analytical chemistry, 59(10), 1417-1423.

Kostka, J. E., Luther III, G. W. (1994). Partitioning and speciation of solid phase iron in saltmarsh sediments. Geochimica et Cosmochimica Acta, 58(7), 1701-1710.

Leuz, A. K. (2006). Redox reactions of antimony in the aquatic and terrestrial environment (Doctoral dissertation, ETH Zurich).

Luoma, S. N., Bryan, G. W. (1981). A statistical assessment of the form of trace metals in oxidized estuarine sediments employing chemical extractants. Science of the Total Environment, 17(2), 165-196.

Ma, Y., Uren, N.C., (1995). Application of a new fractionation scheme for heavy metals in soils. Comm. Soil Sci. Plant Anal., 26: 3291-3303.

Masson, M., Angot, H., Le Bescond, C., Launay, M., Dabrin, A., Miège, C., Le Coz, J., Coquery, M. (2018). Sampling of suspended particulate matter using particle traps in the Rhône River: Relevance and representativeness for the monitoring of contaminants. Science of The Total Environment, 637, 538-549.

Mehra, O. P., Jackson, M. L. (1960). Iron oxide removal from soils and clays by a dithionite–citrate system buffered with sodium bicarbonate. In Clays and clay minerals: proceedings of the Seventh National Conference (pp. 317-327).

Mohammad, B., Ure, A. M., Reglinski, J., Littlejohn, D. (1990). Speciation of antimony in natural waters: the determination of Sb (III) and Sb (V) by continuous flow hydride generation-atomic absorption spectrometry. Chemical Speciation & Bioavailability, 2(3), 117-122.

Mucha, A. P., Almeida, C. M. R., Bordalo, A. A., Vasconcelos, M. T. S. (2010). LMWOA (low molecular weight organic acid) exudation by salt marsh plants: natural variation and response to Cu contamination. Estuarine, Coastal and Shelf Science, 88(1), 63-70.

Ollivier, P., Hamelin, B., Radakovitch, O. (2010). Seasonal variations of physical and chemical erosion: A three-year survey of the Rhone River (France). Geochimica et Cosmochimica Acta 74, 907-927

Pauling, L. (1933). The formulas of antimonic acid and the antimonates. Journal of the American Chemical Society, 55(5), 1895-1900.

Potin-Gautier, M., Pannier, F., Quiroz, W., Pinochet, H., De Gregori, I. (2005). Antimony speciation analysis in sediment reference materials using high-performance liquid chromatography coupled to hydride generation atomic fluorescence spectrometry. Analytica Chimica Acta, 553(1-2), 214-222.

Poulton, S. W., Canfield, D. E. (2005). Development of a sequential extraction procedure for iron: implications for iron partitioning in continentally derived particulates. Chemical Geology, 214(3-4), 209-221.

Presley, B. J., Kolodny, Y., Nissenbaum, A., Kaplan, I. R. (1972). Early diagenesis in a reducing fjord, Saanich Inlet, British Columbia—II. Trace element distribution in interstitial water and sediment. Geochimica et Cosmochimica Acta, 36(10), 1073-1090.

Raiswell, R., Canfield, D.E. and Berner, R.A., (1994). A comparison of iron extraction methods for the determination of degree of pyritization and the recognition of iron-limited pyrite formation. Chem. Geol., 111: 101-110.

Reyes, I., Torrent, J. (1997). Citrate-ascorbate as a highly selective extractant for poorly crystalline iron oxides. Soil Science Society of America Journal, 61(6), 1647-1654.

Rutten, A., de Lange, G. J. (2002). A novel selective extraction of barite, and its application to eastern Mediterranean sediments. Earth and Planetary Science Letters, 198(1-2), 11-24.

Schäfer J, Blanc G, Lapaquellerie Y, Maillet N, Maneux E, Etcheber H (2002). Ten-Year-Observation of the Gironde Fluvial System: Fluxes of Suspended Matter, Particulate Organic Carbon and Cadmium. Marine Chemistry, 79, 229-242.

Shuman, L. M. (1982). Separating Soil Iron-and Manganese-Oxide Fractions for Microelement Analysis 1. Soil Science Society of America Journal, 46(5), 1099-1102.

Ure, A. M., Quevauviller, P., Muntau, H., Griepink, B. (1993). Speciation of heavy metals in soils and sediments. An account of the improvement and harmonization of extraction techniques undertaken under the auspices of the BCR of the Commission of the European Communities. International journal of environmental analytical chemistry, 51(1-4), 135-151.

Wenzel, W. W., Kirchbaumer, N., Prohaska, T., Stingeder, G., Lombi, E., Adriano, D. C. (2001). Arsenic fractionation in soils using an improved sequential extraction procedure. Analytica chimica acta, 436(2), 309-323.

White, C. E., Rose, H. J. (1953). Separation of antimony by solvent extraction. Analytical Chemistry, 25(2), 351-353

Zheng, J., Iijima, A., Furuta, N. (2001). Complexation effect of antimony compounds with citric acid and its application to the speciation of antimony (III) and antimony (V) using HPLC-ICP-MS. Journal of Analytical Atomic Spectrometry, 16(8), 812-818.

Zinder, B., Furrer, G., Stumm, W. (1986). The coordination chemistry of weathering: II. Dissolution of Fe (III) oxides. Geochimica et Cosmochimica Acta, 50(9), 1861-1869.

## II. CONCLUSION

The presented studies on Sb solid fractionation by applying a battery of commonly used extraction protocols to different river and estuarine sediments have revealed unknown artefacts in the selective extraction of Sb from operationally-defined mineral phases:

- An It is commonly admitted that the acid-soluble (F4) fraction comprises the target phases and associated elements extracted by the F2 fractions using ascorbate/citrate-, hydroxylamine- or oxalate-based reagents. In contrast to more commonly studied trace elements (Cu, Ni, Pb and Zn), Sb showed greater extraction efficiencies of F2 compared to F4 fractions, especially for F2 reagents containing organic complexants.
- This apparently element-specific anomaly is protocol-dependent and, to a lesser extent, sediment-dependent. In fact, it occurred in bulk sediments from the Garonne/Gironde fluvial-estuarine system, when using ascorbate and oxalate buffer solutions and only for oxalate buffer solutions in sediments from the Rhône River.
- The so-called anion-adapted oxalate-based F2 extraction initially developed for fractionation analyses of As, the geochemical pair of Sb, overestimates the Sb fraction bound to amorphous and crystalline Fe/Mn oxides.
- In contrast, the results point toward a systematic underestimation of the acid-soluble fraction as observed from incomplete recoveries of both, inherited and spiked Sb. Although the precise mechanism involved in such Sb "losses" under acidic conditions remains unknown, their existence clearly suggests that the application of acid-extractions to assess the potentially bioaccessible Sb fraction in sediments may produce biased results and interpretations.
- Anthropogenically released Sb tends to adsorb onto the most reactive fractions of fluvial/estuarine sediments, namely the F2-ascorbate-extracted fraction assigned to the reactive Fe/Mn oxides (~50% of the total adsorbed spiked Sb) and easily exchangeable/carbonate fractions (F1-acetate) accounting for ~20%. These reactive fractions may be easily mobilised from the sediments due to changing redox conditions or ionic competition.
- Further research on mechanisms involved in the selective dissolution of Sb is a prerequisite for the development of (i) a specific extraction scheme reliably simulating environmental Sb carrier phases and behaviour, and (ii) future understanding of the consequences of anthropogenic Sb inputs into the environment. The application of commonly accepted extraction schemes to "new" elements, such as emerging trace element contaminants, for which the protocols were

not developed, adapted and tested, implies the risk of producing biased results and interpretations

# CHAPTER 5:

# Biogeochemical behaviour of tellurium in the Lot-Garonne-Gironde fluvial estuarine system

# I. INTRODUCTION

There are few environmental studies on Te biogeochemical behaviour, especially in continent-ocean transition systems. The three published works on Te in estuarine systems have focused separately on either dissolved Te species or particulate concentrations for sporadic field campaigns, without presenting the general reactivity of total Te (dissolved + particulate). Therefore, the aim of this chapter is to understand spatial and temporal aspects of the biogeochemical behaviour of Te in complex continent-ocean transition systems such as the Lot-Garonne-Gironde River continuum. Two distinct studies are presented in this chapter:

The first work shows Te reactivity in the Lot-Garonne-Gironde fluvial-estuarine system from a four-year record (2014-2017) of dissolved ($Te_d$) and particulate ($Te_p$) Te concentrations at five strategic sampling points within the watershed. This allows to determine Te seasonal dynamics, watershed interconnectivity and preliminary annual gross fluxes into the Gironde Estuary. Furthermore, this follow-up is complemented with particulate concentrations from estuarine sampling campaigns covering a wide range of hydrological conditions, from drought to flood (MGTS I-IV). This allows insights into Te reactivity along the salinity and turbidity gradients of the Gironde Estuary as well as presenting coastal ocean endmember values for dissolved and particulate Te. A long-term record of Te concentrations in wild oysters at the estuary mouth (1984-2017) is also analysed to have an idea of Te impact in economically relevant organisms and to unveil potential historical and/or recent bioaccumulation of anthropogenic contaminants.

The second work contains original information on Te solid/liquid sorption kinetics, isotherms and solid fractionation in contact with SPM of the estuarine system and a comparison with Se- behaviour, the commonly presumed chemical homologue of Te. The objective of this study is to (i) understand Te solid/liquid distribution kinetics in the salinity and turbidity gradients of the Gironde Estuary, (ii) determine inherited and spiked Te distribution among the different operationally-defined carrier phases, (iii) detect methodological artefacts in the parallel selective extraction procedure, similar to that of Sb in the ascorbate fraction, and (iv) compare these results for Te and Se to evaluate their commonly presumed similarity in environmental behaviour and fate. Based on these results this chapter presents the first tentative simulation of anthropogenic dissolved Te (and Se) releases into the Gironde Estuary as a first step towards scenarios of Te (and Se) radionuclides dispersion in geochemical gradients at the continent-ocean interface.

## 1. Biogeochemical behaviour of tellurium in the freshwater domain of the Gironde watershed.

*Manuscript submitted for publication in Environmental Chemistry*

# Tellurium behaviour in a major European fluvial-estuarine system (Gironde, France): fluxes, solid/liquid partitioning, and bioaccumulation in wild oysters

Teba Gil-Díaz[a], Jörg Schäfer[a]*, Lionel Dutruch[a], Cécile Bossy[a], Frédérique Pougnet[a], Melina Abdou[a], Antoine Lerat-Hardy[a], Clément Pereto[a], Hervé Derriennic[a], Nicolas Briant[b], Teddy Sireau[b], Joël Knoery[b], Gérard Blanc[a]

[a] *Université de Bordeaux, UMR CNRS 5805 EPOC, Allée Geoffroy Saint-Hilaire, 33615 Pessac, France;* [b] *IFREMER - RBE/BE/Laboratoire de Biogéochimie des Contaminants Métalliques, BP 21105, Nantes F-44311, France*

*corresponding author: jorg.schafer@u-bordeaux.fr

## HIGHLIGHTS

- Little is known on the environmental behaviour of Te in transition waters
- Te concentrations show seasonal patterns within geological background levels
- Dominant fraction of estuarine Te is particulate and depends on hydrological residence times
- Quantified Te uptake in wild oysters shows no distinct long-term trend
- Results suggest no dominant current anthropogenic sources of Te in the Gironde estuarine system

## ENVIRONMENTAL CONTEXT

Tellurium (Te) is an element used in current technological applications like solar electric power generation panels and its radionuclides may be released during nuclear power plant accidents, but its environmental behaviour is yet poorly known. We investigate recent Te dissolved and particulate distributions and transport from the river watershed to the Gironde Estuary mouth, where a historical (>30 years) record provides insight into Te accumulation in wild oysters over time. These results constitute the first comprehensive study on natural Te behaviour in a major fluvial-estuarine continuum, necessary for predictive modelling of Te radioactive risk assessment.

## ABSTRACT

Tellurium (Te) is a Technology Critical Element (TCE) with largely unknown environmental behaviour, especially in continent-ocean interface systems. This is due to the lack of studies in aquatic environments and to analytical challenges limiting the determination of its naturally low (ultra-trace) environmental levels. We performed a comprehensive study of Te in the Lot-Garonne-Gironde fluvial-estuarine system to better understand seasonal variations, solid/liquid partitioning (Kd), gross fluxes, estuarine dynamics, and transfer to wild oysters at the estuary mouth. A temporal record (2014-2017) of dissolved ($Te_d$) and particulate ($Te_p$) Te concentrations at five sites in the Lot-Garonne River system shows little differences between sites, with average ~1 ng $L^{-1}$ and ~50 µg $kg^{-1}$ respective concentrations. Watershed $Te_d$ and $Te_p$ follow parallel seasonal patterns, resulting in constant partitioning ($log_{10}$ Kd ~ 4.75 L $kg^{-1}$), with constant annual gross dissolved fluxes (~ 15.0 kg $y^{-1}$) and variable gross particulate fluxes (from 6.50 to 140 kg $y^{-1}$) entering the Gironde Estuary. Estuarine reactivity in contrasting hydrological conditions (from flood to drought) suggest that grain-size effects and/or estuarine hydrological residence times strongly affect $Te_p$ behaviour. Historical records (1984-2017) of Te in wild oysters at the estuary mouth vary from 1.33 to 2.89 µg $kg^{-1}$ dry weight (d.w.), without any clear long-term trend. This study provides rare knowledge on Te environmental dynamics in aquatic systems, suggesting that although no current anthropogenic sources were identified in the economically developed Lot-Garonne-Gironde fluvial estuarine system there is a non-negligible bioaccumulation in wild oysters at the estuary mouth.

**Keywords:** *Technology Critical Element, Lot River, Garonne River, Gironde Estuary, RNO/ROCCH*

## 1. INTRODUCTION

Tellurium (Te) is a chalcophile metalloid with numerous applications in medicine and other fields due to its thermoelectric, catalytic and photonic properties (Wang and Guan 2012). Worldwide Te applications rank as follows (USGS 2018): (i) 15% as additive for improving machinability of steel and iron, or for modifying physical characteristics of non-ferrous alloys like aluminium, tin, copper, lead, magnesium, and manganese, (ii) 30% in thermoelectric materials (e.g. as $Bi_2Te_3$ and PbTe; Chen et al. 2014; Zhou et al. 2014), and (iii) 40% in photonics (e.g., as rare earth-doped tellurite glasses, as CdTe in photovoltaics or as quantum dots for telecommunications, photodetectors and biotechnologies; Leal et al. 2015; Turner et al. 2012; Mahdy et al. 2015).

The use of Te in the thin-film solar panel industry classifies Te within the Technology Critical Elements (TCE), as its low lithological, crustal abundances (average ~2 µg $kg^{-1}$; Salminen et al. 2005; Kabata-Pendias 2011) and the fact that it is extracted as a by-product from copper and lead refineries (USGS 2018) imply the risk of Te shortcuts in view of future socioeconomic demands (Cobelo-García

et al. 2015). Increasing and diverse uses can potentially release Te to the environment as an emerging contaminant (despite little environmental evidence; Biver and Filella 2016; Filella and Rodríguez-Murillo 2017). Nevertheless, Te is listed among the European water pollution priority substances (Directive 2006/11/EC) due to its potential high toxicity for both organisms and humans (Schroeder et al. 1967).

Little is known about Te cycling and its biogeochemical behaviour in environmental compartments, especially in aquatic environments (Belzile and Chen 2015). This is mainly related to analytical challenges as dissolved concentrations are within the ng $L^{-1}$ range (e.g., median of 2.5 ng $L^{-1}$ and maximum values of ~110 ng $L^{-1}$ in European streams; Salminen et al. 2005). However, there is little information on Te behaviour in freshwater suspended sediments, let alone temporal trends or seasonality. Furthermore, seawater Te concentrations are poorly constrained as published concentrations until now range between 0.08 and 910 ng $L^{-1}$, apparently independent from the pre-concentration and pre-reduction steps needed according to the analytical method, with no published data <1 ng $L^{-1}$ since 1990 (Filella 2013; Biver et al. 2015). This contrasts with its known high-particulate affinity (Whitehead et al. 1988; Wu et al. 2014) with particulate Te concentrations ranging between <5 – 880 µg $kg^{-1}$ in marine sediments (Belzile and Chen 2015). In fact, open ocean vertical profiles support that Te behaves as a scavenged element (Lee and Edmonds 1985, Yoon et al. 1990, Wu et al. 2014). However, little is known about estuarine environments, as there are only three case studies on dissolved Te (van der Sloot et al. 1985; Wu et al. 2014) and particulate Te (Duan et al. 2014a) reactivity along salinity gradients. Although there is no proof of Te being a biologically essential element (Chasteen et al. 2009; Ba et al. 2010), it seems to be assimilated by plants (e.g. Yang et al. 2014) and aquatic organisms, showing average ~12 µg $kg^{-1}$ fresh weight (f.w.) in oysters and 2-3 µg $kg^{-1}$ f.w. in shellfish from French markets and food consumption surveys (Guérin et al. 2011; Millour et al. 2012).

The aim of this study is to provide a comprehensive view of Te biogeochemical behaviour in transition waters of the Lot-Garonne-Gironde fluvial-estuarine system. For this, a recent 4-year record (2014-2017) on dissolved and suspended particulate Te monitoring at five selected sampling points along the Lot-Garonne watershed was performed to assess Te dynamics (i.e., seasonal behaviour, solid/liquid partitioning, enrichment factors and gross fluxes). In addition, sampling campaigns (2014-2017) along the salinity and turbidity gradients of the Gironde Estuary aim at providing insights into estuarine Te reactivity in different hydrological conditions (from low to high discharge conditions). Finally, Te accumulation in wild oysters of the estuary mouth (La Fosse) from the French National Mussel Watch Programme (RNO/ROCCH) are studied to evaluate potential Te transfer to seafood.

# 2. EXPERIMENTAL

## 2.1. Area of study

### 2.1.1. The Lot-Garonne-Gironde fluvial estuarine system

The Lot River watershed is known for historical metal pollution (Cd, Pb, Cu, Hg) from former mining and Zn-Cu smelting activities (1842 to 1987), and due to accidental events and long-term lixiviation of open-air waste disposals/tailings from the area of Decazeville (Audry et al. 2004). This historical multi-metal pollution and ongoing decontamination due to remediation works have produced contrasting geochemical signals in the hydroelectric lake sediments along the Lot River (e.g., Ag, Cd, Cu, Zn, Pb, Hg; Audry et al. 2004; Lanceleur et al. 2011a,b) upstream (geochemical background; Marcenac site) and downstream (Cajarc site) of the confluence of the Lot River and the Riou Mort River, draining the former industrial area (Figure 1). The accompanying long-term decontamination monitoring programme at five sites along the Riou Mort-Lot-Garonne River continuum to the estuarine freshwater reaches (La Réole site; Figure 1) has enabled several long-term studies on biogeochemical dynamics of trace elements at the watershed scale (e.g., Ag, Sb, Gd; Lanceleur et al. 2011a; Gil-Díaz et al. 2018; Lerat-Hardy et al. 2019). The different sites are: (1) "Boisse Penchot" (BP) on the upstream Lot River, (2) "Riou Mort" (RM) at the outlet of the Riou Mort River watershed hosting the identified industrial point sources, (3) "Temple" (T), at the outlet of the Lot River watershed, (4) "Port-Sainte-Marie" (PSM) on the upstream Garonne River (*i.e.* representative of influences from the city of Toulouse and the Pyrenean mountains) and (5) "La Réole" (LR), on the downstream Garonne River, at the upper limit of tidal influence, i.e., the main fluvial input to the Gironde Estuary.

The Gironde Estuary constitutes an important continent-ocean interface system, being one of the largest estuaries in Europe, located on the Atlantic Coast in the SW of France (Figure 1). The Gironde Estuary drains the Garonne and the Dordogne River watersheds with a total area of approximately 81 000 $km^2$ (Salomon 2002; Schäfer et al. 2002) hosting important urban/industrial hot-spots (mainly the cities of Bordeaux and Toulouse), extensive vineyard surfaces (up to 12% of the Aquitaine territorial surface in 2011; *www.gironde-tourisme.fr*), natural and timber forests (up to 50% of the territory in 2011; *www.gironde-tourisme.fr*) and sporadic, scattered solar electrical power installations, especially along the Garonne River (*http://www.solarenergymaps.com/Europe.html#.WQdnc9w6_IU*).

The estuary receives an average freshwater discharge (Q) of ~1000 $m^3 s^{-1}$ (~64% from the Garonne River; DIREN) and features a semi-diurnal tide (cycles of 12 h 25 min) which extends 180 km upstream from the estuary mouth (up to La Réole). Average water residence times vary from 86 days in low discharge conditions to ~18 days in high discharge (Castaing and Jouanneau 1979; Jouanneau and Latouche 1981). Suspended Particulate Matter (SPM) has an average residence time of 1-2 years, forming a strong Maximum Turbidity Zone (MTZ of > 1000 mg $L^{-1}$; Castaing and Jouanneau 1979; Sottolichio and Castaing 1999). This MTZ migrates seasonally due to variations in freshwater discharge and marine intrusion, showing an upstream position in dry/low-discharge seasons (partly upstream the

city of Bordeaux) and a downstream position (near KP 50; Figure 1) in wet/high-discharge seasons (Sottolichio and Castaing 1999). Coastal expulsion of the MTZ needs continuous high river discharge over a long period, displacing the MTZ towards the estuarine mouth, and a strong tidal coefficient (> 85, spring tides), so that ebb conditions can drag the MTZ seawards (Allen et al. 1980; Castaing and Allen 1981; Doxaran et al. 2009).

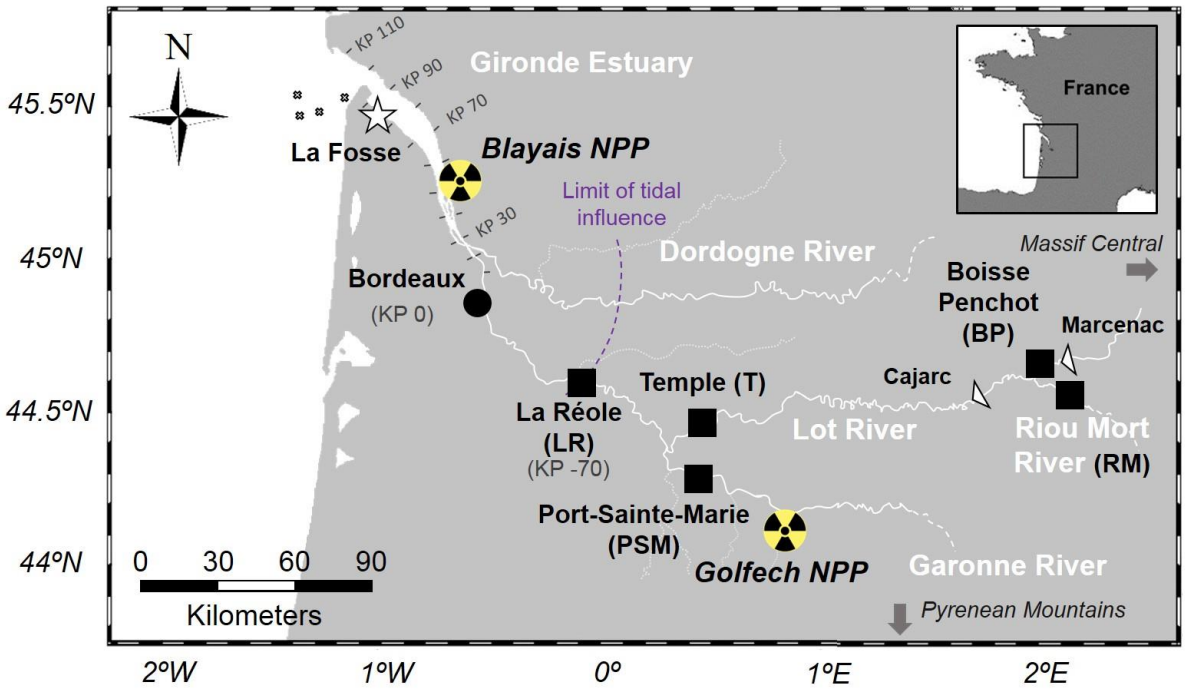


**Figure 1.** Location of sampling sites in the Lot-Garonne-Gironde fluvial estuarine system: upstream sediment cores at Cajarc and Marcenac water reservoirs in the Lot River (triangles), 4-year monitoring sites at RM, BP, T, PSM and LR (squares), coastal ocean sampling points (MGTS IV, empty crosses) and oyster sampling site (La Fosse, RNO/ROCCH, star). Locations of nuclear power plants (NPP) are also shown.

The Gironde Estuary mouth hosts wild oysters with the La Fosse site (Figure 1) being part of the National Network for the Observation of Marine Environment Quality (RNO/ROCCH; i.e. the French Mussel-Watch; *http://www.ifremer.fr/deltn/pages/rno.htm*). This programme has sampled, analysed and stored total soft tissues of wild-growing Japanese oysters (*Crassostrea gigas*, cf. *Magallana gigas*) and mussels (*Mytilus edulis* and *Mytilus galloprovincialis*) since 1979 initially reflecting the historical metal (Cd) contamination derived from the Lot River (*http://www.ifremer.fr/deltn/pages/rno.htm*). As a result, proper oyster production in the estuary has been banned and metals exported from the Gironde Estuary to the coastal ocean can reach the Marennes-Oléron Bay, one of the most important oyster production zones in Europe (Latouche 1992).

## 2.2. Sampling strategies

### 2.2.1. Water and particles

Water and SPM samples were collected manually using similar protocols for both watershed monitoring sites (~monthly frequency from 2014 to 2017: N = 64 at LR, N = 62 at PSM, N = 62 at T, N = 63 at BP, N = 62 at RM) and estuarine longitudinal sampling campaigns named MGTS for "Métaux Gironde Transfert et Spéciation" (N = 26 for MGTS I in March 2014, N = 23 for MGTS II in March 2015, N = 26 for MGTS III in October 2015 and N = 20 for MGTS IV in June 2017). The latter were performed along the estuarine salinity gradient from Bordeaux to the estuary mouth on board the R/V *Thalia* (IFREMER) during four different hydrological situations covering a wide range of freshwater discharges ($Q_{MGTS\ I}$ = 1203 $m^3\ s^{-1}$; $Q_{MGTS\ II}$ = 3450 $m^3\ s^{-1}$; $Q_{MGTS\ III}$ = 206 $m^3\ s^{-1}$, Gil-Díaz et al. 2016, $Q_{MGTS\ IV}$ = 235 $m^3\ s^{-1}$).

Sub-surface water was sampled with a telescopic arm (~0.3 m depth, 1 m from the river bank) or a Niskin bottle (on-board at 1 m depth), using acid-washed polypropylene (PP) bottles, previously rinsed with water from the site. The samples were immediately filtered on-site through 0.2 µm Minisart® cellulose acetate filters into acid-washed polypropylene (PP) bottles, acidified with $HNO_3$ (1/1000 v/v; J.T. Baker ultrapure, 14 M) and stored at 4ºC in the dark pending analysis. At the same time, SPM samples were collected into 40 L acid-washed polyethylene (PE) drums, previously rinsed with water from the site. Particles were retrieved by centrifugation (Westfalia; 12 000 g; Lapaquellerie et al. 1996), oven-dried (50 °C), ground and homogenised (agate mortar), then stored at room temperature in the dark until analysis.

### 2.2.2. Biological material (wild oysters)

The RNO/ROOCH programme (IFREMER) collects on a regular basis two-year old (~8 cm long) wild oysters *Crassostrea gigas* (cf. *Magallana gigas*) during winter (February-March) at the La Fosse (Figure 1) according to the guidelines for monitoring contaminants in biota (OSPAR commission; *http://www.ospar.org*). After depuration with particle-free water from the site, whole soft bodies are dissected, pooled (20-60 individuals, depending on size), ground, freeze-dried and homogenised, and stored in the National Mussel watch sample bank pending Te analyses. For this study, oyster samples were extracted from the sample bank covering the period from 1984 to 2017 (N = 18), with 2-year intervals.

### 2.2.3. SPM concentrations and physico-chemical parameters

Precise volumes of water were filtered *in situ* through dry pre-weighed filters (Xilab glass microfiber, 0.7 µm) for quantification of SPM concentrations. Filters were then dried to constant weight at 50ºC and re-weighed. Physical-chemical parameters such as water temperature and conductivity (TetraCon 96® probe, PROFILINE, WTW), pH (Sentix ® 41 probe, PROFILINE, WTW) and redox potential of the water (Eh, PH-25 CRISON® probe) were measured *in situ*.

## 2.3. Sample treatment and Te quantification

### 2.3.1. Dissolved Te ($Te_d$)

Only freshwater samples were analysed for $Te_d$ in this study due analytical limitations in seawater samples (matrix effects and low expected concentrations). Freshwater was directly analysed by external calibration with triple quadrupole ICP-MS (iCAP-TQ, THERMO®) in Kinetic Energy Discrimination KED-mode (He). Only m/z $^{125}Te$ was used for total dissolved Te ($Te_d$) quantification due to important $^{126}Xe$ (16 – 80%), $^{110}Cd^{16}O$ (~50% in Riou Mort samples), $^{110}Pd^{16}O$ (5-25%) and $^{86}Sr^{40}Ar$ (10-40%) and variable interferences on $^{126}Te$ (Filella and Rodushkin 2018). Polyatomic interferences on $^{125}Te$ were < 0.1% (i.e., $^{109}Ag^{16}O$ and $^{107}Ag^{18}O$, none observed for $^{89}Y^{36}Ar$; Filella and Rodushkin 2018). Detection limits (LOD) were 0.09 ± 0.05 ng $L^{-1}$ (N = 14 analyses of 10 blanks of 2% $HNO_3$ J.T. Baker ultrapure) and recoveries from freshwater Certified Reference Materials (CRM NIST 1643f, N = 76) were 92 ± 14%.

### 2.3.2. Particulate Te ($Te_p$)

Representative aliquots of SPM (i.e., ~30 mg) were digested in acid-cleaned closed PP tubes (DigiTUBEs®, SCP SCIENCE) in a Teflon®-coated heating block (2 h at 110ºC; SCP Science) with 1.5 mL HCl (10M Suprapur®, Merck), 750 µL $HNO_3$ (14 M Suprapur®, Merck) and 2.5 mL HF (29 M Suprapur®, Fisher), as described elsewhere (Schäfer et al. 2002; Gil-Díaz et al. 2018). After evaporation to dryness and re-dissolution of the residue with 250 µL $HNO_3$ (14 M) in the heating block, the samples were completed to 10 mL using Milli-Q water.

Concentrations of particulate Te ($Te_p$) were quantified by triple quadrupole ICP-MS (iCAP-TQ, THERMO®) in KED-mode (He) using external calibration. In this case, $^{125}Te$ m/z was highly interfered compared to $^{126}Te$, not related to $^{90}Zr^{35}Cl$ (<1%), $^{88}Sr^{37}Cl$ (<1%), $^{109}Ag^{16}O$ (<1%), $^{89}Y^{36}Ar$ (<1%) nor $^{85}Rb^{40}Ar$ (low blanks), potentially suggesting non-negligible roles of other not yet identified polyatomic interferences (e.g., $^{39}K$ $^{86}Sr$, $^{56}Fe^{69}Ga$ and others) doubling $^{125}Te$ signal compared to the expected $^{125}Te/^{126}Te$ natural ratio. Therefore, natural Te was quantified from $^{126}Te$ correcting for $^{126}Xe$ (generally <12%), $^{86}Sr^{40}Ar$ (generally <7%), $^{110}Cd^{16}O$ (generally <6%) and $^{110}Pd^{16}O$ (generally <2%) interferences

estimated from independent respective monoelemental solutions and analytical blanks (2% $HNO_3$). Quality monitoring was performed using two CRM: freshwater NIST 1643f (for ICP-MS calibration performance, N=29) and stream sediment NCS DC 73307 (for digestion performance, N=36). Results show good recoveries of 96 ± 3% in NIST 1643f and values consistently within the range of certified concentrations for stream sediment NCS DC 73307 (i.e., between 25.3 – 32.5 µg $kg^{-1}$ for a certified value of 41 ± 15 µg $kg^{-1}$), and a limit of detection (LOD) of 0.42 ± 0.17 ng $L^{-1}$ (N=80). Complementary, thorium (Th) was also measured for grain-size correction purposes (i.e., recoveries of 90% in marine sediment NIST SRM 2702, N=12, and 85% for NIST® RM 8704 N=36).

### 2.3.3. Te in biological material

Aliquots of ~200 mg of freeze-dried oyster tissues from the RNO/ROCCH sample bank were digested with 4 mL HCl (34-37% Suprapur®, SCP Science) and 2.8 mL $HNO_3$ (67-69% Suprapur®, SCP Science) in a microwave-assisted oven (ETHOS UP, Milestone Srl). The temperature programme was set at 9ºC $min^{-1}$ to 180ºC, followed by 30 min at 180ºC before cooling down. These acid digestions were brought to a final 25 mL volume with Milli-Q water (Daskalakis et al. 1997; USEPA 2007). However, due to important interferences on $^{125}Te$ (~30% for AgO and ~60% for $^{90}Sr^{35}Cl$) and $^{126}Te$ (2% for $^{126}Xe$, 1-4% for $^{110}Pd^{16}O$, 1-11% for $^{86}Sr^{40}Ar$ and most importantly ~80% for $^{110}Cd^{16}O$, high Cd concentrations in oysters due to historical pollution in the Gironde Estuary), sample aliquots were evaporated at 50-60ºC and recovered in $HNO_3$ matrix. After this treatment, only $^{125}Te$ was used to quantify Te content in oyster tissues, taking into account the interferences of $^{90}Sr^{35}Cl$ (now <4%) and AgO (~30-40%) corresponding to 12-21% variability in Te quantification.

Like with $Te_p$, biological Te was determined by triple quadrupole ICP-MS (iCAP-TQ, THERMO®) in KED-mode (He) using external calibration. In all cases, digestion blanks (N=3 per digestion batch) were used to control any contamination from the digestion processes (< 1 ng $L^{-1}$ for LOD of 0.02 ng $L^{-1}$, N=10). As there is no CRM for Te in biological materials, only reproducibility was monitored using a CRM used for complementary elements like Sb, Sn and Se (NIST Oyster Tissue 1566b) showing ~15% relative standard deviations (RSD) in microwave assisted digestions (3.20 ± 0.52 µg $kg^{-1}$, N=11).

### 2.4. Modified geoaccumulation index ($I'_{geo}$)

The modified geoaccumulation index ($I'_{geo}$, Equation 1) introduced by Lee et al. (2008), based on the original index by Müller (1969), describes the degree of contamination of a sample and the potential grain size effect ($M_z$) on trace element concentrations at different sites (*s*) by normalising the concentration ($C_s$) of the examined element (Xi) at site *s* to the geochemical background ($B_s$) of Xi ($C_s/B_s$). Given the highly variable transport energy and hence particle sizes transported in river systems, we decided to use this modified $I'_{geo}$:

$$I'_{geo} = \log_2(C_s/(1.5 \cdot B_s \cdot M_z)) \quad (1)$$

where 1.5 is a factor to account for background variations in the environment or small anthropogenic influences (Müller 1969) and $M_z$ refers to $M_{zC}/M_{zB}$ which is a proxy of the grain size ratio at the studied site ($M_{zC}$) compared to the reference area ($M_{zB}$). This $I'_{geo}$ index classifies soils/sediments into five categories: class 1 ($I'_{geo} < 1$, unpolluted to moderately polluted), class 2 ($1 \leq I'_{geo} < 2$, moderately polluted), class 3 ($2 \leq I'_{geo} < 3$, moderately to strongly polluted), class 4 ($3 \leq I'_{geo} < 4$, strongly polluted), and class 5 ($I'_{geo} \geq 4$, strongly to very strongly polluted).

In the Garonne-Gironde fluvial-estuarine system, Th is used as an adequate normalising element to correct grain size effects (Krachler and Shotyk 2004; Larrose et al. 2010). Accordingly, we have calculated $I'_{geo}$ (Equation - 2) using $Th_p$-normalised $Te_p$.

$$I'_{geo} = \log_2\left(\frac{\left(\frac{Te_p}{Th_p}\right)_s}{1.5 \cdot \left(\frac{Te_p}{Th_p}\right)_{ref}}\right) \quad (2)$$

where the average of $Te_p/Th_p = 4.2.10^{-3}$ present in the Marcenac core (Gil-Díaz et al. unpublished) is used as reference $(Te_p/Th_p)_{ref}$ for the regional natural geochemical background.

### 2.5. Distribution coefficient (Kd)

Tellurium partitioning between dissolved and particulate concentrations can be described by the particle-water distribution coefficient (Kd; Sung 1995). Briefly, Kd (in L $kg^{-1}$) is the particulate (mg $kg^{-1}$) to dissolved (mg $L^{-1}$) concentration ratio (Equation 3). Total Te ($Te_T$, Equation 4) can be described as the sum of both $Te_d$ and $Te_p$. Both equations can be combined to describe the relationship between the particulate fraction of Te (%) and Kd (Equation - 5).

$$K_d = Te_p/Te_d \quad (3)$$

$$Te_T = Te_p \cdot SPM + Te_d \quad (4)$$

$$Te_p(\%) = (Te_p \cdot SPM)/Te_T = (K_d \cdot SPM)/(1 + K_d \cdot SPM) \quad (5)$$

where $Te_p$ is expressed in mg $kg^{-1}$, $Te_d$ in mg $L^{-1}$, $Te_T$ in mg $L^{-1}$ and SPM in kg $L^{-1}$. Such experimental Kd can be used to estimate the dissolved Te environmental concentrations if equilibrium conditions are assumed (Filella 2011).

### 2.6. Annual Te fluxes

Annual fluxes of $Te_d$ (Equation 6) and $Te_p$ (Equation 7) were calculated by combining daily river discharges from the National Hydrographic Databank (DIREN) with measured $Te_d$, $Te_p$ and SPM

concentrations (~24-day frequency) using commonly applied equations (e.g., Meybeck et al. 1994; Meybeck and Ragu 1995; Webb et al. 1997) for discharged-weighted concentrations.

$$F_{Te_d} = Q'(\sum_i^n (Q_i \cdot Te_d) / \sum_i^n Q_i) \quad (6)$$

$$F_{Te_p} = Q'(\sum_i^n (F_{SPMi} \cdot Te_p) / \sum_i^n Q_i) \quad \text{for} \quad F_{SPMi} = SPM_i \cdot Q_i \quad (7)$$

where $F_{Ted}$ and $F_{Tep}$ are the dissolved and particulate discharge-weighted annual fluxes (kg $y^{-1}$), $Q_i$ the daily average water discharge ($m^3$ $s^{-1}$) of the sampled day (i), Q' the annual water discharge (annual mean of $Q_i$ for $i_{1\rightarrow365}$) and $F_{SPMi}$ the daily SPM flux (t $y^{-1}$), for an annual database of size n ($n \leq 365$ days). Necessary unit transformations are not indicated in these equations. In addition, surface-specific annual total Te fluxes (g $m^{-2}$ $y^{-1}$; i.e. normalised by the watershed area) can also be calculated to better compare and normalise fluxes between different sub-watersheds.

### 2.7. Bioaccumulation factors (BAF)

The bioaccumulation factor (BAF, Equation 8) provides information on contaminant absorption in the organism by all routes of exposure in natural conditions. It is defined as the ratio between the contaminant in the organism's tissue compared to the surrounding concentration at steady state (USEPA 2000, Arnot and Gobas 2006).

$$BAF = \frac{C_B}{C_W} \quad (8)$$

where $C_B$ is the chemical concentration (Te) in the organism (in mg $kg^{-1}$) and $C_W$ the dissolved chemical concentration ($Te_d$) in the water (mg $L^{-1}$), as in this form it shows potentially the highest bioavailability between dissolved and particulate forms (e.g., Lekhi et al. 2008).

## 3. RESULTS

### 3.1. Recent Te dynamics in the Lot-Garonne River watershed: concentrations, distribution coefficients (Kd), contamination degrees ($I'_{geo}$) and annual fluxes

The four-year survey (2014-2017) on Te in the Lot-Garonne River watershed showed similar average $Te_p$ and $Te_d$ concentrations for all sites (i.e., ~50 µg $kg^{-1}$ and ~0.9 ng $L^{-1}$ at La Réole, Port-Sainte-Marie, Temple and Boisse Penchot, Table 1). Out of all sites, only Riou Mort presented average ~1.25-fold higher $Te_p$ concentrations (Table 1), not taking into account the anomaly in March 2017 (Figure 2e), corresponding to respectively 0.005 and 0.010 Th-normalised ratios. The temporal variations in both $Te_p$ and $Te_p/Th_p$ showed similar seasonal patterns without any clear inter-annual trend (Figure 2a-e) and were opposite to those observed for water discharge or SPM transport at all sites (Figure 2e).

**Table 1.** Overview on physical-chemical parameters (water temperature, conductivity, pH and redox potential (Eh)), river discharge (Q), suspended particulate matter (SPM) concentrations, dissolved ($Te_d$) and particulate ($Te_p$) Te concentrations as well as thorium-normalised $Te_p$ concentrations ($Te_p/Th_p$), solid/liquid distribution coefficients ($log_{10}$ Kd) and $Te_d$ ("d") and $Te_p$ ("p") fluxes from 2014 to 2017 at five sampling sites in the Lot-Garonne River system: La Réole (LR), Port-Sainte-Marie (PSM), Temple (T), Boisse Penchot (BP) and Riou Mort (RM). Generally, mean values ± standard deviations (SD), with minimum and maximum (in brackets) and median values are given per site.

| **Site** | **Water temp. (°C)** | **Conduct. (µS cm$^{-1}$)** | **pH** | **Eh (mV)** | **Q (m$^3$ s$^{-1}$)** | **SPM (mg L$^{-1}$)** | **$Te_d$ (ng L$^{-1}$)** | **$Te_p$ (µg kg$^{-1}$)** | **$Te_p/Th_p$** | **$log_{10}$ $K_d$ (L kg$^{-1}$)** | **$Te_d$ and $Te_p$ fluxes (kg y$^{-1}$)** |
|---|---|---|---|---|---|---|---|---|---|---|---|
| | **Mean ± SD [min. – max.]** ***Median*** | **Mean ± SD [min. – max.]** ***Median*** | **Mean ± SD [min. – max.]** ***Median*** | **Mean ± SD [min. – max.]** ***Median*** | **Mean ± SD [min. – max.]** ***Median*** | **Mean ± SD [min. – max.]** ***Median*** | **Mean ± SD [min. – max.]** ***Median*** | **Mean ± SD [min. – max.]** ***Median*** | **Mean ± SD [min. – max.]** ***Median*** | **Mean ± SD [min. – max.]** ***Median*** | **Mean ± SD [min. – max.]** |
| **LR** | 15.4 ± 6.5<br>[5.3 – 28.1]<br>*15.0* | 288 ± 23<br>[238 – 346]<br>*286* | 8.27 ± 0.27<br>[7.73 – 9.40]<br>*8.23* | 130 ± 43<br>[43 – 247]<br>*126* | 476 ± 465<br>[79 – 4500]<br>*321* | 32 ± 92<br>[0 – 2180]<br>*13* | 1.04 ± 0.32<br>[0.56 – 2.02]<br>*0.98* | 48.2 ± 7.5<br>[32.0 – 65.0]<br>*47.7* | 0.0048 ± 0.0010<br>[0.0030 – 0.0081]<br>*0.0047* | 4.68 ± 0.13<br>[4.32 – 4.96]<br>*4.68* | d: 15.0 ± 4.4<br>[12.1 – 21.5]<br>p: 53.9 ± 60.7<br>[6.7 – 140] |
| **PSM** | 15.1 ± 6.3<br>[5.7 – 26.5]<br>*14.7* | 291 ± 32<br>[222 – 374]<br>*289* | 8.24 ± 0.21<br>[7.41 – 8.72]<br>8.26 | 138 ± 41<br>[52 – 264]<br>*134* | 333 ± 312<br>[58 – 3720]<br>*246* | 28 ± 86<br>[0 – 2320]<br>*10* | 1.00 ± 0.47<br>[0.33 – 2.66]<br>*0.91* | 49.9 ± 8.1<br>[34.9 – 69.7]<br>*49.2* | 0.0048 ± 0.0010<br>[0.0027 – 0.0079]<br>*0.0047* | 4.74 ± 0.18<br>[4.27 – 5.16]<br>*4.73* | d: 8.05 ± 3.44<br>[5.09 – 13.0]<br>p: 46.0 ± 58.2<br>[7.6 – 131] |
| **T** | 16.1 ± 6.9<br>[5.8 – 28.7]<br>*16.4* | 256 ± 47<br>[148 – 454]<br>*251* | 8.13 ± 0.39<br>[7.16 – 9.31]<br>*8.09* | 143 ± 49<br>[44 – 297]<br>*140* | 120 ± 124<br>[11 - 762]<br>*68* | 12 ± 12<br>[0 - 143]<br>*8* | 0.89 ± 0.17<br>[0.46 – 1.33]<br>*0.87* | 49.8 ± 10.9<br>[22.6 – 76.8]<br>*50.4* | 0.0055 ± 0.0019<br>[0.0035 – 0.0120]<br>*0.0048* | 4.74 ± 0.13<br>[4.28 – 5.01]<br>*4.76* | d: 3.00 ± 1.19<br>[1.72 – 4.02]<br>p: 2.77 ± 2.18<br>[0.43 – 5.63] |
| **BP** | 13.4 ± 6.1<br>[5.4 – 27.0]<br>*12.6* | 174 ± 170<br>[93 – 1470]<br>*149* | 8.15 ± 0.33<br>[7.51 – 8.94]<br>*8.14* | 146 ± 48<br>[30 - 286]<br>*140* | 95 ± 100<br>[9 – 590]<br>*52* | 5 ± 9<br>[0 – 146]<br>*3* | 0.81 ± 0.28<br>[0.26 – 1.52]<br>*0.80* | 51.7 ± 13.1<br>[31.0 – 93.0]<br>*48.3* | 0.0053 ± 0.0016<br>[0.0032 – 0.0091]<br>*0.0048* | 4.82 ± 0.16<br>[4.47 – 5.23]<br>*4.83* | d: 2.14 ± 0.65<br>[1.51 – 2.74]<br>p: 0.91 ± 0.35<br>[0.45 – 1.20] |
| **RM** | 14.4 ± 5.8<br>[4.7 – 27.2]<br>*14.2* | 904 ± 423<br>[276 - 2150]<br>*827* | 8.18 ± 0.30<br>[7.58 – 8.96]<br>*8.13* | 151 ± 41<br>[61 – 237]<br>*143* | 1 ± 2<br>[0 - 31]<br>*1* | 72 ± 220<br>[0 - 2810]<br>*13* | 1.01 ± 0.23<br>[0.50 – 1.51]<br>*1.00* | 67.5 ± 37.0<br>[20.3 – 204]<br>*60.1* | 0.0107 ± 0.0051<br>[0.0025 – 0.0365]<br>*0.0100* | 4.81 ± 0.25<br>[4.28 – 5.69]<br>*4.81* | d: 0.04 ± 0.02<br>[0.02 – 0.06]<br>p: 0.13 ±0.11<br>[0.03 – 0.28] |

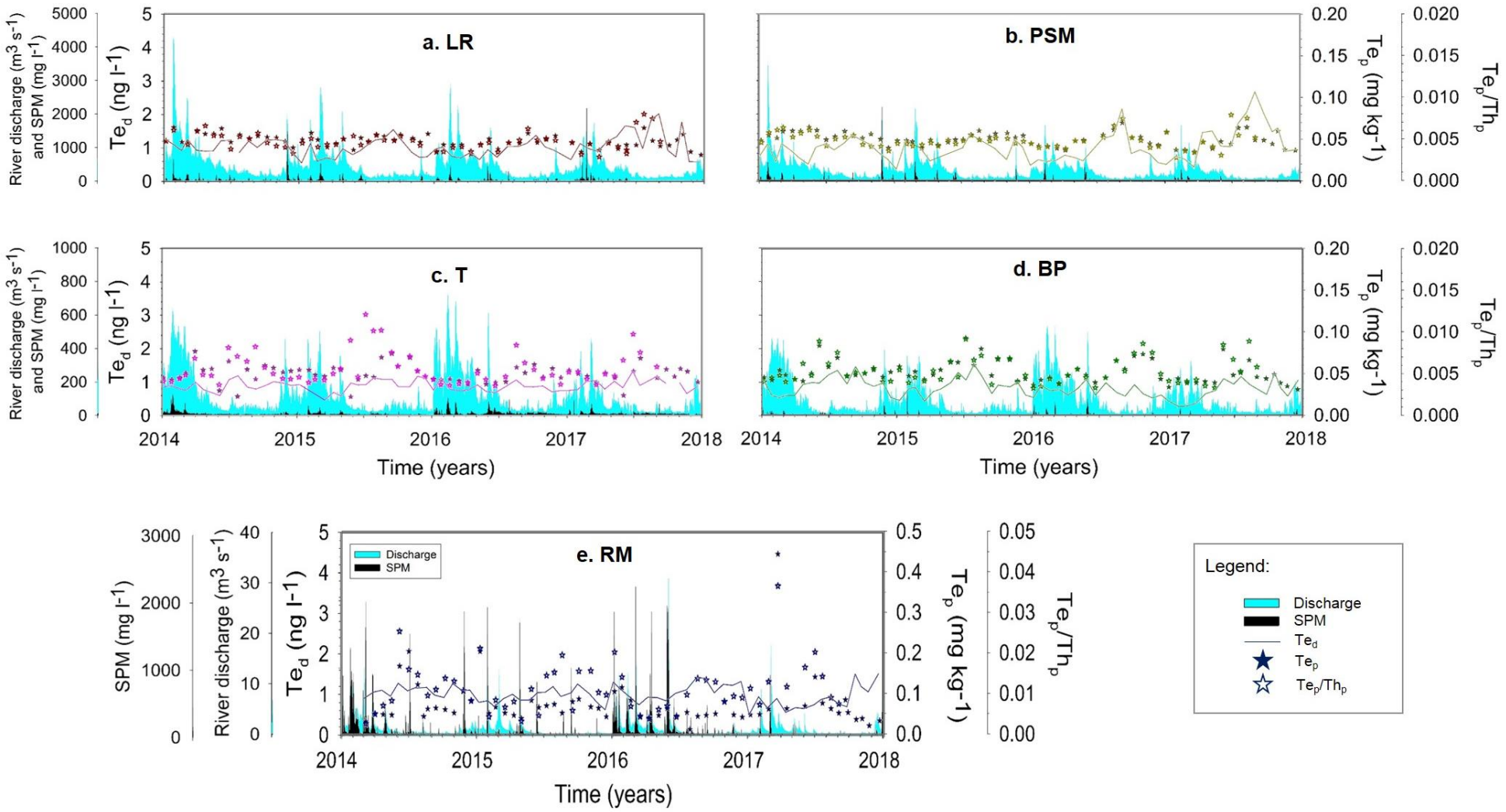


**Figure 2.** Four-year follow-up (2014-2017) of particulate Te ($Te_p$, filled stars) and dissolved Te ($Te_d$, lines) in the Lot-Garonne fluvial system: La Réole (LR, a), Port-Sainte-Marie (PSM, b), Temple (T, c), Boisse Penchot (BP, d) and Riou Mort (RM, e). Thorium-normalised particulate Te concentrations ($Te_p/Th_p$, empty stars), daily water discharges (cyan bar charts) and suspended particulate matter concentrations (SPM, black bar charts) are also shown.

Dissolved Te concentrations displayed variations that were mostly parallel to those of the particulate phase especially at La Réole (Figure 2a), Port-Sainte-Marie (Figure 2b), Boisse Penchot (Figure 2d) and Riou Mort (Figure 2e). Due to these co-variations between dissolved and particulate concentrations, $\log_{10}$ Kd values were almost constant (4.7-4.8 L $kg^{-1}$) at all sites, without seasonal variations (Table 1).

Contamination degrees of watershed SPM in $Te_p$ showed class 1 $I'_{geo}$ (i.e., $I'_{geo} < 1$, unpolluted to moderately polluted) at all studied sites except for sporadic class 2 $I'_{geo}$ values (i.e., $1 \leq I'_{geo} < 2$, moderately polluted for Te) at Riou Mort. When the $I'_{geo}$ is plotted against $Te_p/Th_p$ ratios, a unique logarithmic equation ($I'_{geo} = 1.443 \cdot \ln(Te_p/Th_p) + 7.313$) points out that SPM in the Lot-Garonne-Gironde fluvial-estuarine system exceed class 1 conditions at $Te_p/Th_p$ ratios > 0.013. These conditions are only present in sporadic Riou Mort SPM (Figure 2e) and in deep sediments from the historical core in the hydroelectric reservoir lake of Cajarc (Gil-Díaz et al., unpublished).

Annual Te total fluxes (sum of dissolved and particulate) varied among sites and increased from the upstream sites (i.e., ~3 kg $y^{-1}$ at Boisse Penchot and ~ 0.2 kg $y^{-1}$ Riou Mort) to the most downstream sites (~69 kg $y^{-1}$ at La Réole and ~54 kg $y^{-1}$ at Port-Sainte-Marie, Table 1). Nevertheless, the data suggest high annual variability among sites, especially related with particulate fluxes, dissolved fluxes being relatively constant over the sampled years.

### 3.2. Particulate Te distribution in the Gironde fluvio-estuarine system

Within the estuarine salinity and turbidity gradients, $Te_p$ varied from 24.7 µg $kg^{-1}$ to 49.3 µg $kg^{-1}$ for all sampling campaigns, with Th-normalised data ranging from 0.002 to 0.005 (Figure 3a,b,c,d). In low discharge conditions $Te_p$ (40.0 ± 4.6 µg $kg^{-1}$ in MGTS III and 35.7 ± 6.1 µg $kg^{-1}$ in MGTS IV; Figure 3c,d) and high discharge conditions (40.1 ± 3.4 µg $kg^{-1}$ in MGTS II, Figure 3b) show lower averages than intermediate discharge conditions (41.0 ± 6.6 µg $kg^{-1}$ in MGTS I, Figure 3a).

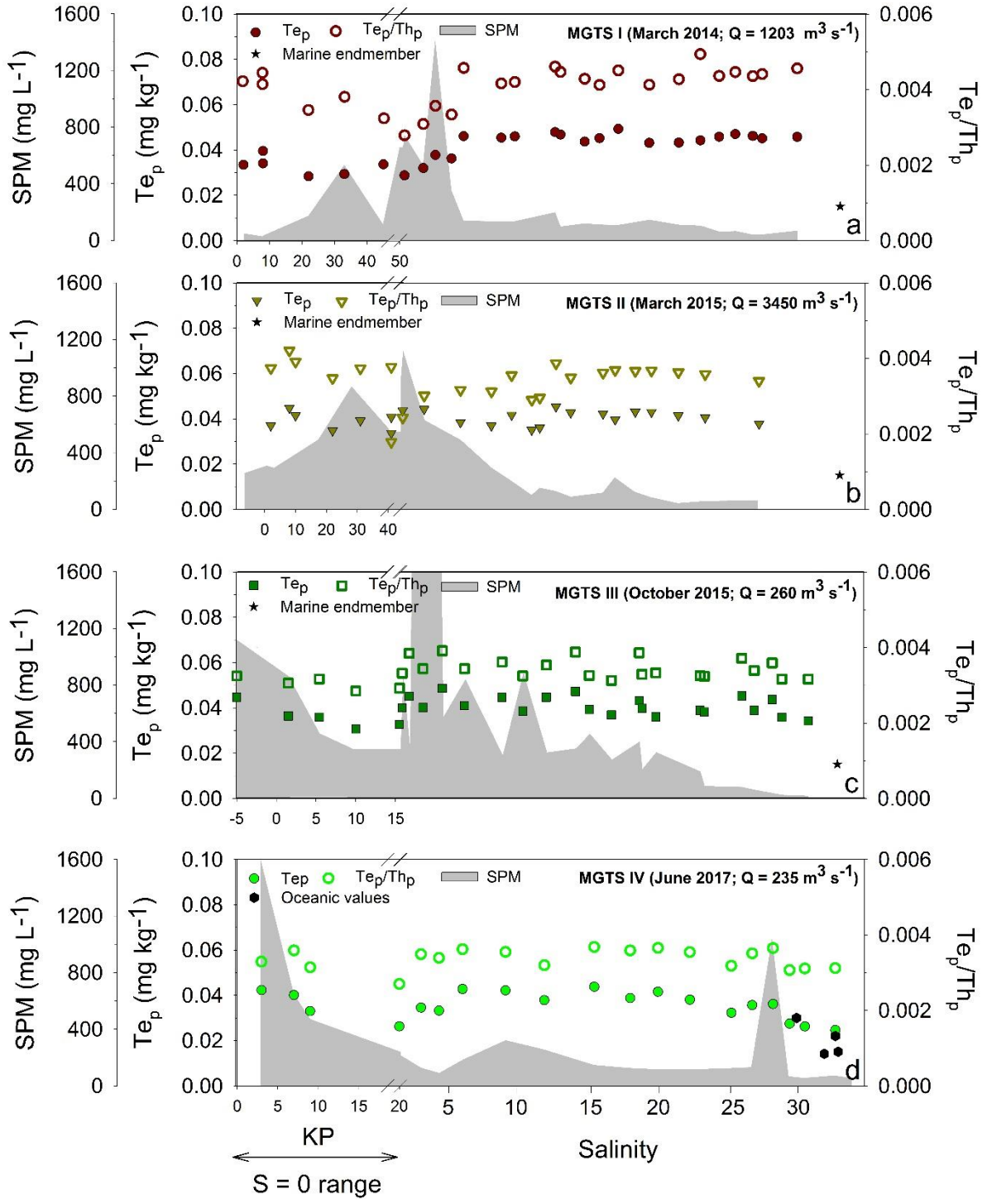


**Figure 3.** Tellurium distribution along the salinity and turbidity gradients of the Gironde Estuary during four sampling campaigns (MGTS): (a) intermediate discharge (MGTS I), (b) high discharge (MGTS II), and two low discharge conditions (c, MGTS III) and (d, MGTS IV). Values in the S=0 salinity range are expressed in kilometric points (KP) for spatial resolution. Suspended particulate matter (SPM) concentrations (shaded grey), particulate Te concentrations ($Te_p$, filled symbols), thorium-normalised particulate Te concentrations ($Te_p/Th_p$, empty symbols), and the marine endmember $Te_p$ (stars).

### 3.3. Tellurium concentrations in whole tissue of wild oysters

The Te concentrations in wild oysters from the La Fosse site ranged between 1.33 and 2.89 µg $kg^{-1}$ dry weight (d.w.), with no particular trend at the long-term (1984-2017, Figure 4). Other oxyanion-forming elements like selenium (Se) and antimony (Sb) were also determined in this temporal series. Comparisons between Te and Sb in wild oysters of La Fosse showed parallel temporal variations (data not shown).

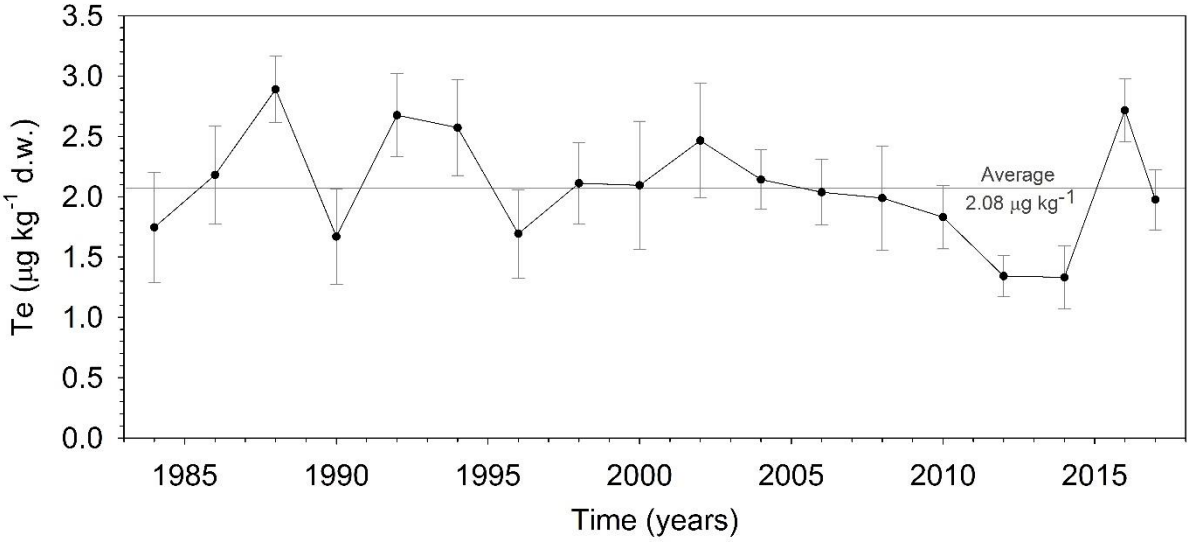


**Figure 4.** Long-term record (1984-2017) of Te in soft tissue from pools of winter (February/March) wild oysters *Crassostrea gigas* from the French National Mussel Watch Programme RNO/ROCCH at La Fosse site.

## 4. DISCUSSION

### 4.1. Tellurium concentrations at the watershed scale

Dissolved Te concentrations in the Lot-Garonne River system show medians between 0.8 – 1 ng $L^{-1}$ (Table 1). Such concentrations correspond to the lower range of expected Te freshwater ranges in Europe (median 2.5 ng $L^{-1}$, < 5 ng $L^{-1}$ in SW France; Salminen et al. 2005) but are clearly higher than reported concentrations in the Orinoco River (0.28 ng $L^{-1}$; Yoon et al. 1990) and the Mississippi River (0.53 ng $L^{-1}$; Yoon et al. 1990). However, higher concentrations in freshwater have been recently reported for the Haraz and the Tajan Rivers in Iran (respectively 29 ng $L^{-1}$ and 36 ng $L^{-1}$; Najafi et al. 2010).

Particulate Te concentrations in most studied sites presented $Te_p$ ~50 µg $kg^{-1}$ and $Te_p/Th_p$ ratios of 0.005. These concentrations are within published $Te_p$ ranges in river and ocean SPM such as in the Arno River and the Venice Lagoon (i.e., 5 – 93 µg $kg^{-1}$; Barghigiani et al. 1995), the East China Sea (i.e., 20 – 96 µg $kg^{-1}$; Duan et al. 2014b) and the Pacific Ocean (i.e., 20 – 880 µg $kg^{-1}$; Yoon et al. 1990). This concentration range is also in accordance with other French watersheds like that of the Rhône River

where concentrations of 21.5 to 87.0 µg $kg^{-1}$ have been observed in irregularly collected samples (mostly during the winter season) from 2012-2013 and 2016-2017 at Arles (Gil-Díaz et al. unpublished).

The upstream Lot River watershed hosts mineral districts enriched in Zn, Pb, Ag, U, W, Sn, Mo and Bi ores (BRGM 1978, 1983) where Te can also be associated (*www.mindat.org*) due to its highly chalcophile characteristics. Tellurium may be enriched in sulphides and low-temperature supergene minerals (mainly as Pb-bearing minerals, but also in sylvanite, $AgAuTe_4$, calaverite/krennerite, $AuTe_2$and others; *www.mindat.org*). This may explain why slightly higher $Te_p$ concentrations occurred in SPM from the Riou Mort site (~60 µg $kg^{-1}$ median concentrations, i.e., median 0.010 $Te_p/Th_p$ ratios) although these levels remain below the critical class 1 $I'_{geo}$ criteria.

Sporadic high $Te_p$ concentrations in the Riou Mort (up to ~240 or 400 µg $kg^{-1}$, class 2 $I'_{geo}$, Figure 2e) suggest other processes related to remobilisation of historical sediments and smelter waste. In fact, the site of Decazeville in the Riou Mort watershed is known for its historical metallurgical activities mainly related to Zn smelting (firstly obtained by thermic-reduction until 1922 and since then by electrolysis until its closure in 1987; Audry et al. 2004). Tellurium is mainly produced as a by-product from refining of non-ferrous metals such as Cu, Ag, Pb and Au (i.e., from anodic slime resulting in the electrolytic process or from refining skimmings or flue dusts and gases generated during smelting; Schroeder 1967; USGS 2018; Filella and Rodríguez-Murillo 2017), as well as in dusts from blast furnace refining of lead (Řezanka and Sigler 2008). In any case, $Te_p$ sporadic releases in the Riou Mort area appear relatively low compared to other anthropogenically-influenced sites showing $Te_p$ concentrations of the order of few to several mg $kg^{-1}$ such as ~0.18-1 mg $kg^{-1}$ in sediments from the old town of Venice, (Barghigiani et al. 1995) up to ~75 mg $kg^{-1}$ locally in harbour sediment from Baltimore (Dolor et al. 2009).

Flood events can favour high erosion rates and mobilisation of particulate trace elements from the Riou Mort watershed (topsoils and waste heaps), as already observed for Cd, Sb and Zn (Coynel et al. 2007). Nevertheless, the highest $Te_p$ concentrations in the Riou Mort (and in all studied sites) occurred recurrently/systematically during low water and SPM discharges (Figure 2). This suggests (i) a common and seasonal biogeochemical behaviour of Te at the watershed scale, and (ii) no particular evidence of increasing recent anthropogenic releases. The absence of environmental anomalies due to high concentrations of Te in this early stage of massive industrial applications is consistent with predictions based on bibliographic research (Filella and Rodríguez-Murillo 2017) and experimental leaching of solar panels (Biver and Filella 2016), although one cannot exclude that longer time series in the future may reveal such anomalies.

### 4.2. Seasonal patterns in Te concentrations and fluxes

The four-year record in the river sampling sites shows parallel seasonal behaviour of $Te_d$ and $Te_p$ over time. Matching peaks of concentration variations in upstream sites (Boisse Penchot and Port-Sainte-Marie) and downstream sites (especially at Temple in 2015-2016 and La Réole in 2017, respectively) may reflect either a general reason at the watershed scale or the transfer of a given concentration pulse along the river continuum (from upstream to downstream), more or less attenuated by dilution effects. Noteworthy, the seasonal component of the four-year series can be estimated using the SeAsonal Factor (SAF) of non-stationary series (Gil-Díaz et al. 2018), quantifying the difference of $Te_p$ or $Te_d$ from the average concentration. Given the temporal limitation of the available data, the present SAF values may only serve as indicative first approaches to Te seasonality in the Lot-Garonne fluvial system. The obtained SAF values suggest that for the most upstream sites in each sub-watershed, namely Boisse Penchot (upstream Lot River) and Port-Sainte-Marie (upstream Garonne River), $Te_p$ concentrations show differences from average values with an amplitude of ±10 µg $kg^{-1}$ (equivalent to ~ ±20%), with minimum values in March and maximum values in August. The more downstream sites show similar trends with some delay in May (minimum) and September (maximum), and lower amplitudes (~10%).

This apparent seasonal pattern is less defined for $Te_d$ concentrations but minimum (in March) and maximum (July-August) values occur synchronously at all sites and are in phase with the $Te_p$ variations of the upstream sites. Interestingly, the Lot River sites show symmetrical $Te_d$ SAF amplitudes of ±0.17 ng $L^{-1}$ (i.e., ±20%) at Temple and ±0.36 ng $L^{-1}$ (i.e., ±45%) at Boisse Penchot, whereas the Garonne River sites show asymmetric differences from average values with respective maxima of +0.40 ng $L^{-1}$ (+40%) and minima of -0.12 ng $L^{-1}$ (-12% at La Réole) to -0.35 ng $L^{-1}$ (-35% at Port-Sainte-Marie).

Such parallel, seasonal behaviour of both dissolved and particular phases is uncommon as generally particulate concentrations do not show such obvious changes as dissolved concentrations. In fact, clear seasonal patterns in the dissolved phase, with low winter concentrations and high summer values, also occur in the Lot-Garonne River system for Sb (Gil-Díaz et al. 2018), arsenic-As (Masson et al. 2007), molybdenum-Mo, vanadium-V (Coynel et al. unpublished) and caesium-Cs (Gil-Díaz et al. unpublished), but not in the particulate concentrations. Similar variation patterns also occur for Te, As, Mo, Se and V dissolved concentrations in alkaline stream waters of the Mediterranean region (Salminen et al. 2005). Like V, Sb, As and Mo, Te is an oxyanion considered to be soluble at pH 7, forming hydroxide species (i.e. $TeO_2(OH)^-$ and $Te(OH)_6$; Filella and Rodríguez-Murillo 2017). Seasonal variations in dissolved V and Mo in the Mississippi River (Shiller 1997) were mainly explained by weathering rate from source silicate rocks (Shiller and Mao 2000) and secondarily by *in situ* redox pumping (Moore 1994) and oxygen depletion conditions in bottom waters and sediments (Shiller and Mao 1999). Likewise, previous studies in the Lot-Garonne watershed have explained dissolved As seasonal variations by reduction of As(V) to more soluble As(III) and/or As-bearing mineral dissolution

by microorganisms at water temperatures >15ºC (Masson et al. 2007), being less intense for Sb (Gil-Díaz et al. 2018).

Despite the shared seasonal behaviour, all these oxyanions seem to have different properties or expected behaviours, making it difficult to attribute their common variations to a single mechanism. In fact, reducing processes causing As reduction and increasing its solubility should reduce V(V) species (more mobile) to V(IV) species, which are actually subtracted from the dissolved phase by sorption to SPM (Shiller and Mao 1999, 2000). Likewise, dissolution of Fe/Mn oxyhydroxides (abiotic or biologically-mediated) could increase dissolved As, Sb, Mo and V concentrations due to common mineral sources and high affinity for these mineral phases (Salminen et al. 2005). Other biogeochemical parameters measured in the water column (i.e., dissolved organic carbon – DOC, particulate organic carbon – POC and chlorophyll-a – Chl-a) do not match the seasonal behaviour observed in the aforementioned oxyanions and differ in concentrations between sampling sites, suggesting that processes related to primary production as a potential release mechanism can be ruled out.

However, the fact that all these elements show potentially common mineral sources in the watershed (Salminen et al. 2005), and that Cs also shows the same aforementioned seasonal variability suggests that Te watershed behaviour may be related to chemical weathering processes with increased rate in late-summer. In fact, Cs is a cation with only one oxidation state (+1), typically found in granites from K-substitutions in K-feldspars and micas as well as within fluorine deposits (*www.mindat.org*). Its seasonal pattern is most evident at Boisse Penchot and Riou Mort, showing 4-fold higher $Cs_p$ concentrations than the Garonne River sites (Gil-Díaz et al. unpublished). This points to Cs release by weathering of rocks and minerals at the European level (FOREGS database; Salminen et al. 2005), and is consistent with strong Cs enrichments in Hercynian leucogranite intrusions and Cs-rich fluorine mineral ores in the Massif Central (BRGM 1978, 1983). Furthermore, stream concentrations of Cs are typically geology-dominated, decreasing rapidly due to its strong binding affinity to clays (Salminen et al. 2005). Accordingly, efficient sorption of Te to Fe-oxides like ferrihydrite (Hayes et al. 2011) and clay minerals (Hayes et al. 2012) in SPM appears as likely, given its suspected high particulate affinity (Whitehead et al. 1988; Wu et al. 2014). Furthermore, Te(IV) and Te(VI) seem to equally adsorb to Fe(III) hydroxides and Te(IV) to illite mineral phases in soils affected by abandoned mine areas (Harada and Takahashi 2009, Qin et al. 2017), thus a change in their redox speciation would not imply different redox-related seasonal sorption behaviours. Accordingly, the above considerations and the constant Kd along the different seasons, suggest rapid equilibration of Te between the dissolved and the particulate phases, after the supposed $Te_d$ release due to intensification of weathering processes during summer.

Annual $Te_d$ fluxes are relatively constant at each site over the 4-year period. In contrast, $Te_p$ fluxes show higher variability and mostly reflected general SPM transport at the watershed scale. Surface-specific total (dissolved + particulate) Te fluxes are similar for most sites with $1.21 \pm 1.14$ g $m^{-2}$ $y^{-1}$ at La Réole, $1.17 \pm 1.32$ g $m^{-2}$ $y^{-1}$ at Port-Sainte-Marie and $1.11 \pm 0.67$ g $m^{-2}$ $y^{-1}$ at Riou Mort. The Temple site shows two-fold lower surface-specific total Te fluxes of $0.54 \pm 0.30$ g $m^{-2}$ $y^{-1}$. This observation may

suggest that Te fluxes at Temple have their main origins in the upstream watershed (Boisse Penchot and Riou Mort), and that rocks (i.e., limestones and marls) and soils in the central/lower part of the Lot River watershed are poor in mobile/soluble Te forms. Given that (i) the upstream Garonne River watershed (upstream of Port-Sainte-Marie) constitutes 81% of the total Garonne River watershed area (integrated at La Réole), and (ii) both sites have comparable surface-specific total Te fluxes we can suggest that most of the Te arriving to the Gironde Estuary comes from the Garonne River watershed upstream from Port-Sainte-Marie.

### 4.3. Tellurium solid/liquid partitioning

In general, partitioning coefficients (Kd) indicate element affinity for the particulate phase, i.e., the higher the Kd, the less easily the element will be transported in the dissolved phase. Such definition relies on two hypotheses (Filella 2011): (1) the operationally-defined distinction between "dissolved" and "particulate" phases and (2) the existence of a C-type isotherm (i.e., the ratio between dissolved and particulate concentrations is the same at any concentration, which usually occurs for low concentrations; Limousin et al. 2007). Moreover, its value generally depends on the abundance and speciation of the element, the equilibrium time of the interaction, particle nature and concentration, complexing ligand concentrations and biological activity (Ciffroy et al. 2009).

In contrast to existing studies on Te in fluvial-estuarine systems (van der Sloot et al. 1985; Wu et al. 2014; Duan et al. 2014a), this is the first paper presenting natural Kd values for Te ($\log_{10}$ Kd ~4.7-4.8 L $kg^{-1}$, Table 1). Furthermore, these freshwater Kd values are in accordance with experimentally determined Te partition coefficients for higher SPM concentrations (i.e., $\log_{10}$ Kd ~4.9 L $kg^{-1}$ in 100 mg $L^{-1}$ SPM and $\log_{10}$ Kd ~5.3 L $kg^{-1}$ in 1000 mg $L^{-1}$ SPM). The latter were obtained from sorption batch experiments at constant temperature (21.1 ± 0.4 ºC) with dissolved concentrations of up to 5 µg $L^{-1}$, variable SPM concentrations (i.e., 100 mg $L^{-1}$ and 1000 mg $L^{-1}$ SPM) and equilibration times of 48 h. The experimental conditions included a 0.2 µm-defined dissolved phase (i.e., thus, including potential colloidal fractions) and oxidised Te species, i.e., Te(VI) from $H_2O_2$ pre-experimental treatment (Gil-Díaz et al. unpublished/*Chapter 5*). These results suggest that both inherited and spiked Te compounds have similar solid/liquid partitioning in turbidity ranges as potentially occurring in natural aquatic systems (Figure 5). This information is important for oceanographic and radiological models, where Kd values are not always determined in the environment, thus assuming similarities with experimental Kd (IAEA 2004).

Furthermore, the aforementioned batch sorption experiments in seawater suggest that $\log_{10}$ Kd values are similar to those in freshwater (Figure 5). Therefore, natural or experimental Kd values can provide an estimate of natural $Te_d$ concentrations from measured $Te_p$, even in complex matrices like those along the salinity and turbidity gradients in the Gironde Estuary. These Kd values can be applied to environmental $Te_p$ concentrations assuming a C-type isotherm for both 100 mg $L^{-1}$ and 1000 mg $L^{-1}$

SPM given that experimental isotherms clearly showed that the environmental Te concentrations fall within the linear range of the general Langmuir isotherm (Gil-Díaz et al. unpublished/*Chapter 5*).

Based on this approach, the estimated $Te_d$ for the high-salinity range in the Gironde Estuary and covering a wide range of turbidity (taking the average $log_{10}$ Kd of 4.96 L $kg^{-1}$ for both 100 and 1000 mg $L^{-1}$ in the Gironde Estuary) ranged from 0.27 to 0.52 ng $L^{-1}$ for S>20 for all sampled hydrological conditions. Such concentrations are consistent with a cluster of typical values reported for oceanic and coastal waters published before 1990's (< 1 ng $L^{-1}$; Filella 2013; Biver et al. 2015). However, clearly higher $Te_d$ seawater concentrations have been recently reported for the East China Sea coastal waters (1 – 9 ng $L^{-1}$; Wu et al. 2014), in seawater near the Chinese cities of Zhuhai and Dalian (10 – 32 ng $L^{-1}$; Huang and Hu 2008) and in the Caspian Sea (28 ng $L^{-1}$; Najafi et al. 2010). Further work is necessary to explain these concentration differences.

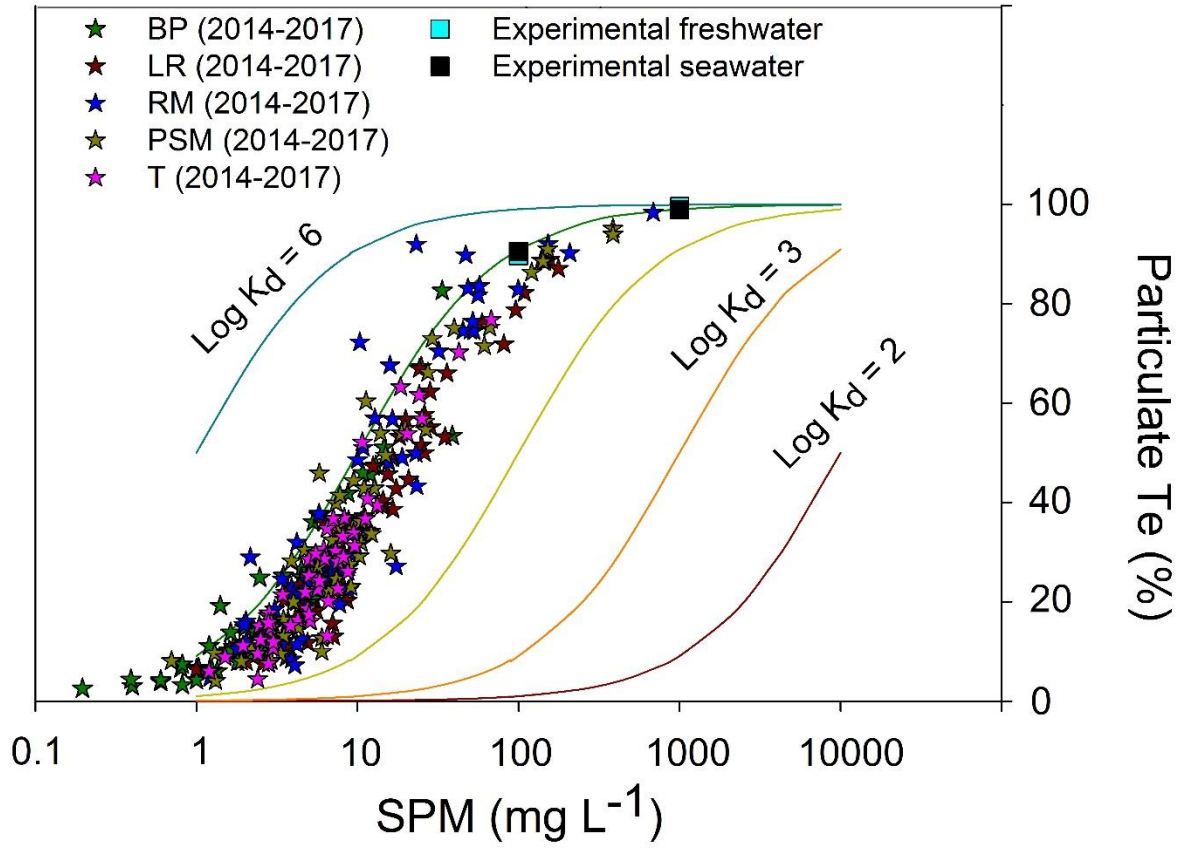


**Figure 5.** Solid/liquid partitioning (Kd) of Te vs suspended particulate matter (SPM) concentrations at five sites in the Lot-Garonne River system (stars): La Réole (LR), Port-Sainte-Marie (PSM), Temple (T), Boisse Penchot (BP) and Riou Mort (RM). Estimated Kd values at equilibrium after 48h sorption batch experiments in freshwater and seawater conditions for 100 mg $L^{-1}$ and 1000 mg $L^{-1}$ SPM (Gil-Díaz et al. unpublished/*Chapter 5*) are also shown.

### 4.4. Tellurium estuarine reactivity

Compared to typical river values, the freshwater reaches of the estuary show an initial ~30% decrease in $Te_p$, especially during low discharge conditions (i.e., long residence times of water and SPM within the estuary), in the presence of high SPM (Figure 3 c,d). A less intense decrease occurs for intermediate discharge conditions (Figure 3a), whereas during flood conditions $Te_p$ are constant throughout the salinity gradient (MGTS II; Figure 3b). In the MTZ, both $Te_p$ and $Th_p$ vary similarly, decreasing $Th_p$ suggesting the presence of coarser particles (e.g. Larrose et al. 2010). These observations suggest that $Te_p$ depend on variations in particle size, consistent with the observed efficient equilibration between the dissolved and the particulate phases. In the absence of a potential mixing endmember strongly characterised by Te-depleted particles, the minimum $Te_p/Th_p$ ratios in the MTZ during low- to intermediate discharge were probably influenced by dissolution/mobilisation processes driven by intense mineralisation of particulate organic matter in this part of the estuary (Abril et al. 1999; Etcheber et al. 2007). In fact, intense organic matter mineralisation in the upstream part of the MTZ could locally release $Te_d$, which would then be re-adsorbed in other mineral phases such as Fe/Mn oxides and clays (Duan et al. 2014b). This process would suggest a potential exchange of Te carrier phases within the MTZ. In the downstream part of the MTZ and over the main part of the salinity range, $Te_p$ nearly doubles to ~40 µg $kg^{-1}$ with $Te_p/Th_p$ increasing to ~0.0034 (Figure 3). These increases may be attributed to equilibration between the dissolved and particulate phases, implying re-adsorption of dissolved Te onto the particles in the MTZ. This observation is in accordance with the constant experimental Kd values (Figure 5) in contrasting salinities (i.e., S=0 and S=32) and SPM variations (i.e., over two orders of magnitude). In fact, $Te_d$ varies from 10% of total Te in ~100 mg $L^{-1}$ SPM to <1% in ~1000 mg $L^{-1}$ SPM. The observed non-conservative behaviour in the Gironde Estuary is consistent with that in the Changjiang Estuary turbidity gradient (i.e., $20 \leq SPM \leq 100$ mg $L^{-1}$), reporting no correlation between $Te_d$ concentrations and salinity (S>25; Wu et al. 2014).

The simultaneous decreases of $Te_p$ and $Th_p$ in the high salinity range of the estuary mouth under low discharge conditions (Figure 3c,d) probably reflect the increasing presence of marine organic matter as supported by increasing POC values (from 1.20% to 1.66% in drought conditions, and 1.50% to 2.00% in intermediate conditions; data not shown). In fact, sediment characteristics (i.e., grain-size and total organic carbon content) are expected to largely control Te distribution in coastal environments (Duan et al. 2014b).

### 4.5. Tellurium historical record in wild oysters

Long-term records (1984-2017) of Te in wild oysters at the Gironde Estuary mouth show stable values with no specific trend. These levels are similar to those in shellfish from other French coastal areas (2-3 µg $kg^{-1}$; Guerin et al. 2011) and from wild oysters from the Arcachon Bay (1.18 ± 0.52 µg $kg^{-1}$ in 2014, N=20; Gil-Díaz et al. unpublished). Nevertheless, higher concentrations have been

observed in wild oysters from the Bilbao Estuary (3.48 ± 1.39 µg $kg^{-1}$ in 2014, N=20; Gil-Díaz et al. unpublished), an estuary currently highly populated and known for its past metal pollution due to historical industrial activities (Belzunce et al. 2001; Borja et al. 2006). These observations, together with the observed high particulate affinity of Te, could suggest that current anthropogenic Te discharges to fluvial systems could be buffered in highly turbid continent-ocean transition systems such as the Gironde Estuary, decreasing the uptake of Te as an emerging contaminant in coastal organisms. Therefore, the potential influence of current Te anthropogenic releases could be studied in biomonitoring organisms, like wild oysters, from continent-ocean systems presenting lower SPM content.

The absence of anomalous Te concentrations in the Gironde Estuary oysters and the fact that there is no clear temporal trend is the opposite of what occurs for other anthropogenically released metals in these oysters (e.g. Cd, Ag, Pt; Lanceleur et al. 2011b; Abdou et al. 2016). This observation may suggest that potential emerging Te sources in the watershed have not caused measurable Te accumulation in the Gironde oysters either due to relatively low emissions or limited bioconcentration. Based on estimated $Te_d$ of 0.46 ng $L^{-1}$ in the estuary mouth (15<S<25), estimated BAFs for Te in oysters range from 2900 to 6300, i.e. are similar in magnitude to those of Se (3600 – 8200, for dissolved Se concentrations of ~0.31 µg $L^{-1}$). These BAF in the Gironde oysters are similar in magnitude as those determined for Pt (~$10^3$; Abdou et al. 2016) and much lower than known BAFs for Cd and Ag (~$10^6$; Lanceleur et al. 2011b). Nevertheless, research on Te and Se organotropism in wild oysters from the Gironde Estuary mouth (pool of N=5 in 2014) point out different biological roles between both metalloids as Te and Se in the digestive gland account for ~50% of the total soft tissue content, whereas in the gills Se accounts for ~30% and Te for ~14% (Gil-Díaz et al. unpublished). Therefore, one may assume a mixed Te uptake in filter feeders combining direct and trophic pathways.

Despite the yet unknown biological role of Te (Chasteen et al. 2009) studies in other aquatic environments have observed interactions between Te contents in seawater and organisms. In fact, historical records of $Te_p$ in a sediment core from the East China Sea (i.e., enrichment factors-EF ~2 at ~20 cm depth corresponding to 1989) are thought to be explained by frequent phytoplankton development from red tides during the late 1980's, enriching the sediment with both Te and Se (Duan et al. 2014b). Likewise, marine phytoplankton and crustaceans interact directly with $Te_d$ radiotracers (i.e., concentrations of ~ 1 µg $L^{-1}$), with instantaneous Te precipitation in elemental form within phytoplankton cultures but no apparent direct trophic transfer/bioaccumulation (Nolan et al. 1991). This ability of microorganisms to produce elemental Te is used in the nanotechnology industry for Te applications, yet for concentrations much higher than environmental levels (mg $L^{-1}$ range; Baesman et al. 2007). After biological uptake, Te shows intracellular reactivity, as it can damage cells and be biomethylated (Řezanka and Sigler 2008; Chasteen et al. 2009). All these observations suggest that one cannot exclude physiological effects of Te in oysters and other seafood, albeit at much higher environmental levels than currently encountered. Further research is necessary to (i) clarify and evaluate the respective importance of both uptake pathways, and (ii) understand the fate and effects of Te in

organisms, particularly in comparison with Se, a known essential micronutrient and geochemical peer of Te (Řezanka and Sigler 2008; Zeng 2009).

## ACKNOWLEDGEMENTS

This study is a scientific contribution to the French National Project AMORAD (ANR-11-RSNR-0002) from the National Research Agency, allocated in the framework programme "Investments for the Future" and was partially funded by the ANR Programme TWINRIVERS (ANR-11-IS56-0003) and the FEDER Aquitaine-1999-Z0061. The authors greatly acknowledge support from "l'Agence de l'Eau Adour-Garonne", the European Project SCHEMA (EU FP7-OCEAN 2013.2-Grant Agreement 614002) and the RNO/ROCCH tissue bank, with Anne GROUHEL as current manager of the ROCCH. We are also grateful to the crew of the French Oceanographic R/V Thalia (sampling campaigns MGTS I doi 10.17600/14008300; MGTS II doi 10.17600/15009300; MGTS III doi 10.17600/15010600 and MGTS IV).

## REFERENCES

Abdou, M., Schäfer, J., Cobelo-García, A., Neira, P., Petit, J. C., Auger, D., Chiffoleau, J.-F., Blanc, G. (2016). Past and present platinum contamination of a major European fluvial–estuarine system: Insights from river sediments and estuarine oysters. Marine Chemistry, 185, 104-110.

Abril, G., Etcheber, H., Le Hir, P., Bassoullet, P., Boutier, B., Frankignoulle, M. (1999). Oxic/anoxic oscillations and organic carbon mineralization in an estuarine maximum turbidity zone (The Gironde, France). Limnology and Oceanography, 44(5), 1304-1315.

Allen, G. P., Salomon, J. C., Bassoullet, P., Du Penhoat, Y., De Grandpre, C. (1980). Effects of tides on mixing and suspended sediment transport in macrotidal estuaries. Sedimentary Geology, 26(1-3), 69-90.

Arnot, J.A., Gobas, F.A.P.C. (2006). A review of bioconcentration factor (BAF) and bioaccumulation factor (BAF) assessments for organic chemicals in aquatic organisms. Environmental Reviews, 14: 257-297

Audry, S., Schäfer, J., Blanc, G., Jouanneau, J. M. (2004). Fifty-year sedimentary record of heavy metal pollution (Cd, Zn, Cu, Pb) in the Lot River reservoirs (France). Environmental Pollution, 132(3), 413-426.

Ba, L. A., Döring, M., Jamier, V., Jacob, C. (2010). Tellurium: an element with great biological potency and potential. Organic and Biomolecular Chemistry, 8(19), 4203-4216.

Baesman, S. M., Bullen, T. D., Dewald, J., Zhang, D., Curran, S., Islam, F. S., Beveridge, T.J., Oremland, R. S. (2007). Formation of tellurium nanocrystals during anaerobic growth of bacteria that use Te oxyanions as respiratory electron acceptors. Applied and Environmental Microbiology, 73(7), 2135-2143.

Barghigiani, C., D'Ulivo, A., Lampugnani, L., Pellegrini, G., Romboli, L., Zamboni, R. (1995, May). Distribution of As, Sb, Se, Te and Hg in some sediments of the Venice Lagoon. In International Conference on Chemistry and the Mediterranean Sea. Taranto, Italy (p. 139).

Belzile, N., Chen, Y. W. (2015). Tellurium in the environment: A critical review focused on natural waters, soils, sediments and airborne particles. Applied Geochemistry, 63, 83-92.

Belzunce, M. J., Solaun, O., Franco, J., Valencia, V., Borja, Á. (2001). Accumulation of organic matter, heavy metals and organic compounds in surface sediments along the Nervión Estuary (Northern Spain). Marine Pollution Bulletin, 42(12), 1407-1411.

Biver, M., Quentel, F., Filella, M. (2015). Direct determination of tellurium and its redox speciation at the low nanogram level in natural waters by catalytic cathodic stripping voltammetry. Talanta, 144, 1007-1013.

Biver, M., Filella, M. (2016). Bulk dissolution rates of cadmium and bismuth tellurides as a function of pH, temperature and dissolved oxygen. Environmental Science and Technology, 50(9), 4675-4681

Borja, Á., Muxika, I., Franco, J. (2006). Long-term recovery of soft-bottom benthos following urban and industrial sewage treatment in the Nervión estuary (southern Bay of Biscay). Marine Ecology Progress Series, 313, 43-55.

Bureau de Recherches Géologiques et Minières (BRGM) (1978). Carte des gîtes minéraux de la France à 1/500000e, feuille de LYON, Service Géologique National.

Bureau de Recherches Géologiques et Minières (BRGM) (1983). Carte des gîtes minéraux de la France à 1/500000e, feuille de BORDEAUX, Service Géologique National.

Castaing, P., Allen, G. P. (1981). Mechanisms controlling seaward escape of suspended sediment from the Gironde: a macrotidal estuary in France. Marine Geology, 40(1-2), 101-118.

Castaing, P., Jouanneau, J. M. (1979). Temps de résidence des eaux et des suspensions dans l'estuaire de la Gironde. Journal Recherche Océanographie IV, 41-52.

Chasteen, T. G., Fuentes, D. E., Tantaleán, J. C., Vásquez, C. C. (2009). Tellurite: history, oxidative stress, and molecular mechanisms of resistance. FEMS Microbiology Reviews, 33(4), 820-832.

Chen, Z., Xu, G. D., Chen, S., Zhang, J. H., Wang, M. M. (2014). Hydrothermal synthesized nanostructure Bi–Sb–Te thermoelectric materials. Journal of Alloys and Compounds, 588, 384-387.

Ciffroy, P., Durrieu, G., Garnier, J. M. (2009). Probabilistic distribution coefficients (Kds) in freshwater for radioisotopes of Ag, Am, Ba, Be, Ce, Co, Cs, I, Mn, Pu, Ra, Ru, Sb, Sr and Th–implications for uncertainty analysis of models simulating the transport of radionuclides in rivers. Journal of Environmental Radioactivity, 100(9), 785-794.

Cobelo-García, A., Filella, M., Croot, P., Frazzoli, C., Du Laing, G., Ospina-Alvarez, N., Rauch, S., Salaun, P., Schäfer, J., Zimmermann, S. (2015). COST action TD1407: network on technology-critical elements (NOTICE)—from environmental processes to human health threats. Environmental Science and Pollution Research, 22(19), 15188-15194.

Coynel, A., Schäfer, J., Blanc, G., Bossy, C. (2007). Scenario of particulate trace metal and metalloid transport during a major flood event inferred from transient geochemical signals. Applied Geochemistry, 22(4), 821-836.

Council Regulation (EC) 2006/11/EC of 15 February 2006 on pollution caused by certain dangerous substances discharged into the aquatic environment of the Community [2006] OJ L64/52

Daskalakis, K.D., O'Connor, T.P., Crecelius, E.A. (1997). Evaluation of digestion procedures for determining silver in mussels and oysters. Environmental Science and Technology, 31, 2303-2306

DIREN - National Hydrographic Databank [internet]. Ministère de l'Écologie, du Développement Durable et de l'Énergie, 2015 [cited 16 December 2015]. Available from: http://www.hydro.eaufrance.fr/

Dolor, M. K., Helz, G. R., McDonough, W. F. (2009). Sediment profiles of less commonly determined elements measured by Laser Ablation ICP-MS. Marine Pollution Bulletin, 59(4-7), 182-192.

Doxaran, D., Froidefond, J. M., Castaing, P., Babin, M. (2009). Dynamics of the turbidity maximum zone in a macrotidal estuary (the Gironde, France): Observations from field and MODIS satellite data. Estuarine, Coastal and Shelf Science, 81(3), 321-332.

Duan, L. Q., Song, J. M., Yuan, H. M., Li, X. G., Li, N., Ma, J. K. (2014a). Distribution, chemical speciation and source of trace elements in surface sediments of the Changjiang Estuary. Environmental Earth Sciences, 72(8), 3193-3204.

Duan, L. Q., Song, J. M., Yuan, H. M., Li, X. G., Li, N., Ma, J. (2014b). Selenium and tellurium fractionation, enrichment, sources and chronological reconstruction in the East China Sea. Estuarine, Coastal and Shelf Science, 143, 48-57.

Etcheber, H., Taillez, A., Abril, G., Garnier, J., Servais, P., Moatar, F., Commarieu, M. V. (2007). Particulate organic carbon in the estuarine turbidity maxima of the Gironde, Loire and Seine estuaries: origin and lability. Hydrobiologia, 588(1), 245-259.

Filella, M. (2011). Antimony interactions with heterogeneous complexants in waters, sediments and soils: a review of data obtained in bulk samples. Earth-Science Reviews, 107(3-4), 325-341.

Filella, M. (2013). Food for thought: a critical overview of current practical and conceptual challenges in trace element analysis in natural waters. Water 5, 1152 – 1171

Filella, M., Rodríguez-Murillo, J. C. (2017). Less-studied TCE: are their environmental concentrations increasing due to their use in new technologies? Chemosphere, 182, 605-616.

Filella, M., Rodushkin, I. (2018). A concise guide for the determination of less-studied technology-critical elements (Nb, Ta, Ga, In, Ge, Te) by inductively coupled plasma mass spectrometry in environmental samples. Spectrochimica Acta Part B: Atomic Spectroscopy, 141, 80-84.

Gil-Díaz, T., Schäfer, J., Pougnet, F., Abdou, M., Dutruch, L., Eyrolle-Boyer, F., Coynel, A., Blanc, G. (2016). Distribution and geochemical behaviour of antimony in the Gironde estuary: A first qualitative approach to regional nuclear accident scenarios. Marine Chemistry, 185, 65-73.

Gil-Díaz, T., Schäfer, J., Coynel, A., Bossy, C., Dutruch, L., Blanc, G (2018). Antimony in the Lot–Garonne river system: a 14-year record of solid–liquid partitioning and fluxes. Environmental Chemistry. DOI:10.1071/EN17188

Guérin, T., Chekri, R., Vastel, C., Sirot, V., Volatier, J. L., Leblanc, J. C., Noël, L. (2011). Determination of 20 trace elements in fish and other seafood from the French market. Food Chemistry, 127(3), 934-942.

Hayes, S., Foster, A. L., Balistrieri, L. S. (2011, December). Examining tellurium geochemistry using laboratory-based sorption studies and spectroscopic investigation of natural samples. In AGU Fall Meeting Abstracts.

Hayes, S. M., Foster, A., Balistrieri, L. (2012, November). Tellurium speciation in surficial weathering environments. In 2012 GSA Annual Meeting in Charlotte.

Huang, C., Hu, B. (2008). Speciation of inorganic tellurium from seawater by ICP-MS following magnetic SPE separation and preconcentration. Journal of Separation Science, 31, 760-767

IAEA, I. (2004). Sediment distribution coefficients and concentration factors for biota in the marine environment. International Atomic Energy Agency: Vienna, Austria.

Jouanneau, J.M., Latouche, C., 1981. The Gironde Estuary. Contributions to Sedimentology. vol. 10, pp. 1–115 (Stuttgart)

Kabata-Pendias, A. (2011). Trace Elements in Soils and Plants. CRC Press, Taylor and Francis Group.

Krachler, M., Shotyk, W. (2004). Natural and anthropogenic enrichments of molybdenum, thorium and uranium in a complete peat bog profile, Jura Mountains, Switzerland. Journal of Environmental Monitoring 6, 418–426.

Lanceleur, L., Schäfer, J., Bossy, C., Coynel, A., Larrose, A., Masson, M., Blanc, G. (2011a). Silver fluxes to the Gironde Estuary–Eleven years (1999–2009) of monitoring at the watershed scale. Applied Geochemistry, 26(5), 797-808.

Lanceleur, L., Schäfer, J., Chiffoleau, J. F., Blanc, G., Auger, D., Renault, S., Baudrimont, M., Audry, S. (2011b). Long-term records of cadmium and silver contamination in sediments and oysters from the Gironde fluvial–estuarine continuum–Evidence of changing silver sources. Chemosphere, 85(8), 1299-1305.

Lapaquellerie, Y., Maillet, N., Jouanneau, J.-M., Coakley, J.P., Latouche, C., 1996. Flux de matières en suspension et de cadmium dans le Lot. Hydroécologie Appliquée, 8, 173–191.

Larrose, A., Coynel, A., Schäfer, J., Blanc, G., Massé, L., Maneux, E. (2010). Assessing the current state of the Gironde Estuary by mapping priority contaminant distribution and risk potential in surface sediment. Applied Geochemistry, 25(12), 1912-1923.

Latouche, C. (1992). La pollution par le cadmium des huîtres sauvages de l'Estuaire de la Gironde. Origine. Mécanismes responsables de la fixation du cadmium. Ichtyophysiol Acta, 15, 139-152.

Leal, J. J., Narro-García, R., Desirena, H., Marconi, J. D., Rodríguez, E., Linganna, K., De la Rosa, E. (2015). Spectroscopic properties of tellurite glasses co-doped with $Er^{3+}$ and $Yb^{3+}$. Journal of Luminescence, 162, 72-80.

Lee, D. S., Edmond, J. M. (1985). Tellurium species in seawater. Nature, 313(6005), 782.

Lee, M., Bae, W., Chung, J., Jung, H. S., Shim, H. (2008). Seasonal and spatial characteristics of seawater and sediment at Youngil bay, Southeast Coast of Korea. Marine Pollution Bulletin, 57(6-12), 325-334.

Lekhi, P., Cassis, D., Pearce, C. M., Ebell, N., Maldonado, M. T., Orians, K. J. (2008). Role of dissolved and particulate cadmium in the accumulation of cadmium in cultured oysters (*Crassostrea gigas*). Science of the Total Environment, 393(2-3), 309-325.

Lerat-Hardy, A., Coynel, A., Dutruch, L., Pereto, C., Bossy, C., Gil-Díaz, T., Capdeville, M.J., Blanc, G., Schäfer, J. (2019). Rare Earth Element fluxes over 15 years into a major European Estuary (Garonne-Gironde, SW France): Hospital effluents as a chance of increasing gadolinium anomalies. Science of the Total Environment, 656, 409–420.

Limousin, G., Gaudet, J. P., Charlet, L., Szenknect, S., Barthes, V., Krimissa, M. (2007). Sorption isotherms: a review on physical bases, modeling and measurement. Applied Geochemistry, 22(2), 249-275.

Mahdy, M. A., Mahdy, I. A., El Zawawi, I. K. (2015). Characterization of Pb24Te76 quantum dot thin film synthesized by inert gas condensation. Spectrochimica Acta Part A: Molecular and Biomolecular Spectroscopy, 134, 302-309.

Masson, M., Schäfer, J., Blanc, G., Anschutz, P. (2007). Seasonal variations and annual fluxes of arsenic in the Garonne, Dordogne and Isle Rivers, France. Science of the Total Environment, 373(1), 196-207.

Meybeck, M., Ragu, A. (1995). river Discharges to the Oceans. An Assessment of Suspended Solids, Major Ions, and Nutrients (UNEP: Nairobi)

Meybeck, M., Pasco, A., & Ragu, A. (1994). Etablissement des flux polluants dans les rivières : pourquoi, comment et à quel prix. 4eme Rencontres de l'Agence Régionale pour l'environnement. In Provence-Alpes-Côte d'Azur. Colloque scientifique sur les charges polluantes véhiculées par les fleuves et les rivières en Méditerranée.

Millour, S., Noël, L., Chekri, R., Vastel, C., Kadar, A., Sirot, V., Leblanc, J.-C., Guérin, T. (2012). Strontium, silver, tin, iron, tellurium, gallium, germanium, barium and vanadium levels in foodstuffs from the Second French Total Diet Study. Journal of Food Composition and Analysis, 25(2), 108-129.

Moore, J. N. (1994). Contaminant mobilization resulting from redox pumping in a metal-contaminated river-reservoir system. Advances in Chemistry.

Müller G (1969). Index of geoaccumulation in sediments of the Rhine river. The Journal of Geology, 2, 108–118.

Najafi, N.M., Tavakoli, H., Alizadeh, R., Seidi, S. (2010). Speciation and determination of ultra-trace amounts of inorganic tellurium in environmental water samples by dispersive liquid-liquid microextraction and electrothermal atomic absorption spectrometry. Analytica Chimica Acta, 670, 18-23.

Nolan, C., Whitehead, N., Teyssie, J. L. (1991). Tellurium—speciation in seawater and accumulation by marine phytoplankton and crustaceans. Journal of Environmental Radioactivity, 13(3), 217-233.

Qin, H.-B, Takeichi, Y., Nitani, H., Terada, Y., Takahashi, Y. (2017). Tellurium distribution and speciation in contaminated soils from abandoned mine tailings: comparison with selenium. Environmental Science and Technology, 51(11), 6027-6035.

Řezanka, T., Sigler, K. (2008). Biologically active compounds of semi-metals. In Studies in natural products chemistry (Vol. 35, pp. 835-921). Elsevier.

Salminen, R., Batista, M.J., Bidovec, M., Demetriades, A., De Vivo, B., De Vos, W., Duris, M., Gilucis, A., et al. (2005). Geochemical Atlas of Europe (FOREGS). Part 1 – Background Information, Methodology and Maps.

Salomon, J. N. (2002). L'inondation dans la basse vallée de la Garonne et l'estuaire de la Gironde lors de la géomorphologie : relief, processus, environnement, 8(2), 127-134.

Schäfer, J., Blanc, G., Lapaquellerie, Y., Maillet, N., Maneux, E., Etcheber, H., (2002). Ten-Year-Observation of the Gironde Fluvial System: Fluxes of Suspended Matter, Particulate Organic Carbon and Cadmium. Marine Chemistry, 79, 229.

Schroeder, H. A., Buckman, J., Balassa, J. J. (1967). Abnormal trace elements in man: tellurium. Journal of Clinical Epidemiology, 20(3), 147-161.

Shiller, A. M. (1997). Dissolved trace elements in the Mississippi River: seasonal, interannual, and decadal variability. Geochimica et Cosmochimica Acta, 61(20), 4321-4330.

Shiller, A. M., Mao, L. (1999). Dissolved vanadium on the Louisiana Shelf: effect of oxygen depletion. Continental Shelf Research, 19(8), 1007-1020.

Shiller, A. M., Mao, L. (2000). Dissolved vanadium in rivers: effects of silicate weathering. Chemical Geology, 165(1-2), 13-22.

Sottolichio, A., Castaing, P. (1999). A synthesis on seasonal dynamics of highly-concentrated structures in the Gironde estuary. Comptes Rendus de l'Académie des Sciences-Series IIA-Earth and Planetary Science, 329(11), 795-800.

Sung, W. (1995). Some observations on surface partitioning of Cd, Cu and Zn in estuaries. Environmental Science and Technology, 29, 1303.

Turner, R. J., Borghese, R., Zannoni, D. (2012). Microbial processing of tellurium as a tool in biotechnology. Biotechnology Advances, 30(5), 954-963.

U.S. Environmental Protection Agency (2000). Methods for measuring the toxicity and bioaccumulation of sediment-associated contaminants with freshwater invertebrates. Second edition. EPA 600/R-99/064

U.S. Environmental Protection Agency (Revised in 2007). Determination of Trace Metals By SW-846. Method 6020A. Inductively Coupled Plasma-Mass Spectrometry. EPA, Connecticut

USGS (2018) [Internet]. U.S. Geological Survey, Mineral Commodity Summaries, Tellurium. [cited 01 August 2018]. Available from: https://minerals.usgs.gov/minerals/pubs/commodity/selenium/

van der Sloot, H. A., Hoede, D., Wijkstra, J., Duinker, J. C., Nolting, R. F. (1985). Anionic species of V, As, Se, Mo, Sb, Te and W in the Scheldt and Rhine estuaries and the Southern Bight (North Sea). Estuarine, Coastal and Shelf Science, 21(5), 633-651.

Wang, X., Guan, W. (2012). Large-scale synthesis of flower-like Te nanocrystals with uniform branches by a surfactant-assisted method. Nanoscience Methods, 1(1), 86-92.

Webb, B.W., Phillips, J.M., Walling, D.E., Littlewood, I.G., Watts, C., Leeks, G.J.L. (1997). Load estimation methodologies for British river and their relevance to the LOIS RACS (R) program. The Science of the Total Environment 194–195, 379–389.

Whitehead, N. E., Ballestra, S., Holm, E., Huynh-Ngoc, L. (1988). Chernobyl radionuclides in shellfish. Journal of Environmental Radioactivity, 7(2), 107-121.

Wu, X., Song, J., Li, X. (2014). Occurrence and distribution of dissolved tellurium in Changjiang River estuary. Chinese Journal of Oceanology and Limnology, 32(2), 444-454.

Yang, G., Zheng, J., Tagami, K., Uchida, S. (2014). Soil-to-crop transfer factors of tellurium. Chemosphere, 111, 554-559

Yoon, B. M., Shim, S. C., Pyun, H. C., Lee, D. S. (1990). Hydride generation atomic absorption determination of tellurium species in environmental samples with in situ concentration in a graphite furnace. Analytical Sciences, 6(4), 561-566.

Zeng, H. (2009). Selenium as an essential micronutrient: roles in cell cycle and apoptosis. Molecules, 14(3), 1263-1278.

Zhou, Y., Li, L., Tan, Q., Li, J. F. (2014). Thermoelectric properties of Pb-doped bismuth telluride thin films deposited by magnetron sputtering. Journal of Alloys and Compounds, 590, 362-367.

## 2. Biogeochemical behaviour of tellurium in the salinity and turbidity gradient of the Gironde estuary.

*Publication: to be submitted to Applied Geochemistry*

# Tellurium and selenium sorption kinetics and solid fractionation under contrasting estuarine salinity and turbidity conditions

Teba Gil-Díaz[a], Jörg Schäfer[a]*, Virginia Keller[b], Elisabeth Eiche[b], Lionel Dutruch[a], Claudia Möβner[b], Markus Lenz[c], Frédérique Eyrolle-Boyer[d]

[a]*Université de Bordeaux, UMR CNRS 5805 EPOC, NB18, Allée Geoffroy Saint-Hilaire, 33615 Pessac, France;* [b]*Institute of Mineralogy and Geochemistry, Karlsruhe Institute of Technology (KIT), Adenauerring 20b, 76131 Karlsruhe, Germany;* [c]*Institute for Ecopreneurship, University of Applied Sciences and Arts Northwestern Switzerland (FHNW), School of Life Sciences, Gründenstrasse 40, 4132 Muttenz, Switzerland;* [d]*Institut de Radioprotection et de Sûreté Nucléaire (IRSN), PRP-ENV, SESURE/LERCM, SERIS/LM2E, L2BT, STEME/LMRE, BP 3, 13115, Saint Paul Lez Durance, France*

*corresponding author: jorg.schafer@u-bordeaux.fr

## HIGHLIGHTS

- Aquatic biogeochemistry of Te is widely unknown, generally compared to that of Se
- Te and Se adsorption kinetics and solid fractionation are simulated for estuarine gradients
- >90% of Te adsorbed to particles, independent from salinity, whereas Se adsorbed <30%
- Selective extractions showed differences between inherited and spiked Te and Se carrier phases
- Spiked Te and Se sorption experiments are used for radionuclide dispersion scenarios

## ABSTRACT

Tellurium (Te) is a Technology Critical Element (TCE) and a relevant product of nuclear fission. It has an unknown environmental biogeochemical cycle, mostly related to current analytical challenges in measuring its ultra-trace dissolved concentrations in complex environmental matrices. It is therefore generally compared to its geochemical pair selenium (Se), which shows a narrow range between diet essentiality and toxicity properties. Batch experiments using isotopically-labelled Te and Se were performed with fresh suspended particulate matter (SPM) from the fluvial part of the Gironde Estuary, simulating both estuarine salinity (S=0 vs S=32) and turbidity (100 mg $L^{-1}$ vs 1000 mg $L^{-1}$) gradients to understand the importance of the particulate phase in Te reactivity under estuarine conditions and verify the resemblance to Se behaviour. These experiments addressed sorption kinetics, sorption isotherms and fractionation from selective extractions of final equilibrated SPM. Results show a strong, salinity-

independent affinity of Te for the particulate phase ($log_{10}$ Kd ~ 4.9 L $kg^{-1}$), following a Langmuir-type isotherm. Contrastingly, Se adsorbs clearly less to estuarine SPM ($log_{10}$ Kd ~ 2.5 L $kg^{-1}$), following a Freundlich-type isotherm. Selective extractions highlight differences between Te and Se distributions among operationally defined fractions, suggesting higher mobility of particulate Se. Based on these results the paper presents a first dispersion scenario on the environmental fate of radioactive Te from hypothetical nuclear power plant accidental releases in coastal aquatic systems such as the Garonne-Gironde fluvial-estuarine system.

*Keywords:* tellurium, selenium, technology critical elements, sorption kinetics, isotherms, selective extractions, distribution coefficient (Kd)

## 1. INTRODUCTION

Radioactive tellurium (Te) is produced during nuclear fission reactions in non-negligible quantities. All Te radionuclides have a 13-16% probability of being produced from $^{239}$Pu- and $^{235}$U-based fuels compared to ~11% for Cs and ~10% for I radionuclides (unpublished data calculated from Element Collection Inc. and Sonzogni 2013). There is little information on the specific Te species released from nuclear power plant (NPP) accidents, potentially presenting both (i) volatile/intermediate (Morewitz 1981), and (ii) refractory character (e.g., forming metal/oxide compounds; Kleykamp 1985; Izrael 2002 and references therein). Though different NPP accidents display different emission patterns, Te radionuclides were released into the environment during both April-1986 Chernobyl (CNPP) and March-2011 Fukushima Daiichi (FDNPP) accidental events (Steinhauser et al. 2014). In these cases, short-term half-life Te radionuclides (e.g., $^{132}$Te half-life of 3.2 days) produced important atmospheric radioactive emissions ($^{132}$Te: ~1150 PBq at CNPP and ~180 PBq at FDNPP) comparable to $^{137}$Cs and $^{131}$I, the most monitored radionuclides after NPP accidental events (~85 PBq and ~1700 PBq at CNPP, ~37 PBq and ~160 PBq at FDNPP, respectively; Steinhauser et al. 2014). Emitted Te radionuclides were still detected in the atmosphere one month after the FDNPP accident reflecting their non-negligible environmental persistence and potential worldwide atmospheric dispersion (Baeza et al. 2012; Ishikawa et al. 2014; Leppänen et al. 2013). In fact, radioactive Te has been detected in FDNPP fallouts (Saegusa et al. 2013) and in seawater from Monaco, after CNPP (May 1986), yet with relatively low $^{129}$Te activities in the dissolved (0.13 Bq $L^{-1}$) and particulate (1.18 mBq $L^{-1}$) phases (Whitehead et al. 1988). The latter study further suggested for the first time the moderate particle-reactive behaviour of radioactive Te and its potential intake by marine bivalves (i.e., up to 340 Bq $kg^{-1}$ DW in mussel soft tissues; Whitehead et al. 1988).

On the other hand, radioactive selenium (Se) is a widely known fission product of nuclear reactions. It can be released to the environment during several steps of the nuclear fuel cycle comprising NPP wastewaters and spent nuclear fuel, with recent research focusing specifically on $^{79}$Se mobility (half-life of ~$10^5$ y) from waste storage and nuclear waste disposal areas (Aguerre and Frechou 2006; Asai et al.

2011; Hamed et al. 2017). Selenium is considered a highly soluble, mobile and biologically essential and toxic trace element with a more comprehensive biogeochemical cycle (e.g., Tan et al. 2016; Winkel 2016) than that of Te. Due to their potential chemical similarity, the environmental behaviour of Te is generally compared to that of Se (Belzile and Chen 2015).

Given the worldwide dispersion of past NPP accidental releases in both aquatic and atmospheric compartments, the development of management plans for hypothetical future accidental NPP events requires knowledge on radionuclide behaviour including adsorption kinetics under environmentally-representative conditions. Worldwide, many NPPs are located on fluvial-estuarine systems, for which little is known on Te (Wu et al. 2014; Duan et al. 2014; Biver et al. 2015) and Se (Measures and Burton 1978; Cutter 1989; Bizsel et al. 2017) environmental dispersion and biogeochemical behaviour.

This study aims at determining Te and Se reactivity in estuarine salinity and turbidity gradients through isotopically-labelled sorption experiments (kinetics and isotherms) using bulk sediments and natural water matrices. Parallel selective extractions of particles previously exposed to isotopically-labelled Te and Se address solid fractionation for both, inherited and spiked concentrations. The results will be discussed with respect to natural timescales of environmental conditions (i.e., semi-diurnal tidal variations, seasonal migration of the estuarine maximum turbidity zone, etc.) as occurring in the fluvial-estuarine system of the Gironde Estuary (SW France hosting two NPPs: the Blayais NPP and the Golfech NPP, Gil-Diaz et al. 2018) to better understand and predict the environmental fate and potential dispersion of fast-living Te vs long-living Se radionuclides in case of a hypothetical accidental NPP event.

## 2. MATERIAL AND METHODS

### 2.1. Experimental design

The conducted sorption experiments simulated four experimental conditions representative of the Gironde Estuary salinity and turbidity gradients: two contrasting water matrices (salinities 0 and 32) and two solid/liquid ratios (100 mg $L^{-1}$ and 1000 mg $L^{-1}$ DW). Freshwater from the Garonne River and seawater from the Arcachon Bay, were filtered with 0.45 µm Teflon filters (FHLC, Merck Millipore Ltd.). Freshwater sediments were sampled at Portets (~30 km upstream from Bordeaux) on the Garonne River and the water content was evaluated by comparing the masses of precise volumes of wet and dry sediment aliquots.

Spike solutions were prepared by dissolution of $^{125}$Te (99.89% purity; Cortecnet, France) and $^{77}$Se (99.20% purity; Cortecnet, France) in HCl (2% Suprapur®, Merck) and $HNO_3$ (2% Suprapur®, Merck), respectively, heated at 70ºC until dissolution. Isotopically-labelled Te and Se solutions were oxidised with $H_2O_2$ (30 µL 30% J.T. Baker ultrapure) in the different water matrices to favour the oxidation state of $^{125}$Te(VI) and $^{77}$Se(VI), followed by an equilibration period of 24h. Slurries were prepared from the

fresh sediments and unspiked water matrices and equilibrated during 24h, to avoid potential effects of sediment-water interactions during the sorption experiment.

Sorption kinetics with nominal concentrations of 5 µg $L^{-1}$ of $^{125}$Te(VI) and 100 µg $L^{-1}$ of $^{77}$Se(VI) were performed in acid-washed 50 mL centrifuging polypropylene (PP) tubes with 3 replicates per experimental condition using an automatic overhead shaker (REAX 20 Heidolph Instruments) and sampled at t = 0, 2, 4, 8, 24 and 48h (N=3). Temperature (21.1 ± 0.4 ºC), pH (7.50 ± 0.45) and oxic (104 ± 0.5% saturation) conditions, were kept stable throughout the experiment. In parallel, blank tubes containing only spiked water solutions were used to control $^{125}$Te and $^{77}$Se potential losses onto PP walls over time.

Adsorption isotherms were performed for two SPM concentrations (100 mg $L^{-1}$ and 1000 mg $L^{-1}$) with initial concentrations of dissolved $^{125}$Te of 0.1, 0.25, 0.5, 1, 2.5, 5 µg $L^{-1}$ and initial concentrations of dissolved $^{77}$Se of 0.5, 5, 10, 25, 50, 75, 100 µg $L^{-1}$ (N=2) and sampled after 48h. Due to analytical constraints, especially at the low concentration ranges, these experiments were only performed in freshwater conditions.

In both kinetics and isotherm experiments, dissolved Te ($Te_d$) and dissolved Se ($Se_d$) were monitored. Particulate concentrations were only determined for isotherm experiments using freshwater slurries with 1000 mg $L^{-1}$ SPM for mass balance calculations. In all cases, the dissolved phase was separated from the particulate phase by centrifugation (10 min at 4000 rpm; Hettich Rotofix 32A centrifuge) and filtered (0.2 µm Minisart® cellulose acetate) into acid-washed PP 15 mL tubes. These were then acidified with $HNO_3$ (1/1000 v/v; J.T. Baker ultrapure, 14 M) and stored at 4ºC in the dark until analysis.

### 2.2. Parallel selective extractions and total digestions

High SPM concentrations (2 - 4 g $L^{-1}$ DW) in freshwater (S = 0) and seawater (S = 32) were left to equilibrate for 48h in not pre-oxidised solutions of nominal 10 µg $L^{-1}$ of $^{125}$Te and 100 µg $L^{-1}$ of $^{77}$Se. All sediments were recovered by centrifugation (Hettich Rotofix 32A centrifuge), dried (70ºC stove) and grinded in agate mortars, then aliquoted and extracted with parallel selective extractions (two replicates per extraction mode; Table 1). The targeted operationally defined solid fractions were: F1 – easily exchangeable and/or carbonate fraction (acetate solution extracting carbonates, Mn oxyhydroxides, sulphates and organic matter phases; Bordas and Bourg 1998; Kersten and Förstner 1987), F2 – reducible Fe/Mn oxides (ascorbate solution extracting Mn oxide and amorphous Fe oxide phases; Kostka and Luther 1994), F3 – oxidisable fraction ($H_2O_2$ extraction of organic matter and labile/amorphous sulphide phases; Tessier et al. 1979; Ma et Uren 1995) and F4 – reactive and potentially bioaccessible fraction (HCl 1M acid extraction of amorphous and crystalline Fe and Mn oxides, carbonates, amorphous monosulphurs and phyllosilicate phases; Huerta-Díaz and Morse 1990; Gasparon and Matschullat 2006). In addition to the latter, acid extraction with $HNO_3$ 1 M was performed

on a separate aliquot to discard the Cl effect or specific acid effect on F4 obtained from HCl 1 M leaching. All reagents used were of high purity grade except $H_2O_2$ (p.a. grade). High natural Te contamination of ~35 µg $L^{-1}$ was observed in the extraction blanks of F3 potentially from the $H_2O_2$ solution or the added ammonium acetate. This contamination is suspected to have been adsorbed into other than $H_2O_2$-extracted solid fractions (given the Te behaviour, see results), thus not affecting the natural Te identified in F3 fraction. All extractions were performed in acid-washed ($HNO_3$ 10%) PP Falcon 50 mL conical centrifuge tubes (FISHER SCIENTIFIC). Three blanks of each extraction were performed. Currently, no CRM are available for Te and Se selective fractions. Residual fractions are calculated as the difference between the acid-soluble fraction (F4 or F4N) and the total adsorbed particulate concentration.

**Table 1:** Parallel selective extractions as described in Audry et al. (2006).

| Sediment fraction | Sample weight (mg) | Reagents | Procedure |
|---|---|---|---|
| F1 – Acetate extraction<br>(easily exchangeable and/or carbonate fraction = carbonates + Mn oxyhydroxides + sulphates + organic matter) | 500 | 10 mL of sodium acetate (NaOAc, 1 M) + pH adjustment with acetic acid (HOAc, 5 M) during extraction | 6 h shaking at 25ºC |
| F2 – Ascorbate extraction<br>(reducible Fe/Mn oxides = Mn oxides and amorphous Fe oxides) | 200 | 12.5 mL ascorbate solution (pH = 8) | 24 h shaking at 25ºC |
| F3 – $H_2O_2$ extraction<br>(oxidisable fraction = organic matter and labile/amorphous sulphides) | 500 | 2.5 mL $H_2O_2$ 30% (at pH 5 with NaOH) + 1.5 mL $H_2O_2$ 30% + 2.5 mL ammonium acetate (1 M) | 2 h + 3 h at 85ºC + 30 min shaking at 25ºC |
| F4 – HCl extraction or $HNO_3$ extraction (acid soluble)<br>(reactive and potentially bioaccessible = amorphous and crystalline Fe/Mn oxides + carbonate fractions + amorphous monosulphurs + phyllosilicates) | 200 | 12.5 mL HCl or $HNO_3$ (Suprapur®, 1 M) | 24 h shaking at 25ºC |

Total sediment concentrations were determined differently for particulate Te ($Te_p$) and particulate Se ($Se_p$). Mineralisation of sediment for Te analysis was achieved using a tri-acid digestion with $HNO_3$ + HCl + HF as described elsewhere (e.g., Schäfer et al. 2002). Briefly, samples of 30 mg were digested in closed PP tubes (DigiTUBEs®, SCP SCIENCE) on a heating block (2 h at 110 ºC) using 750 µL $HNO_3$ (14 M Suprapur®, Merck), 1.5 mL HCl (10 M Suprapur®, Merck) and 2.5 mL HF (29 M Suprapur®, Fisher). After an evaporation step at 120ºC, re-dissolution of the samples was performed with 250 µL $HNO_3$ (14 M) and heating. After cooling, the samples were brought to 10 mL using Milli-Q water.

For the analysis of $Se_p$ (volatile at > 70ºC, not compatible with the above-described tri-acid digestion) total microwave-assisted digestions (START 1500, MLS GmbH) were performed with aliquots of 40 - 50 mg of dried (50ºC drying oven) and homogenised (agate mortar) sediment (Eiche et al. unpublished). Briefly, 3 mL $HNO_3$ (sub-boiled acid-distilled 65%, p.a. grade, VWR Chemicals), 0.5 mL $H_2O_2$ (30% Rotipuran®, Carl Roth), 0.25 mL HF (40% Suprapur®, Merck KGAA Darmstadt) and 0.5 mL ultrapure Milli-Q water were added. The temperature program was: 18ºC $min^{-1}$ to 75ºC, followed by 7ºC $min^{-1}$ to 110ºC, then 8ºC $min^{-1}$ to 150ºC and 6ºC $min^{-1}$ to 210ºC, with a constant temperature of 210ºC during 10 min before completely cooling down over night. After digestion, samples were transferred into PTFE vessels and evaporated on a hotplate to dryness at 70ºC (no Se evaporation at this temperature), recovered with 270 µL of $HNO_3$ (65% Suprapur), heated at 70ºC for 1h and made up with ultrapure Milli-Q water to a final volume of 6 mL.

### 2.3. Tellurium quantification

Dissolved Te in samples from freshwater kinetics and isotherms experiments were directly analysed by ICP-MS (XSeries 2, Thermo Fisher Scientific) using external calibration. Seawater matrices were diluted in 2% $HNO_3$ (J.T. Baker ultrapure, 14 M) and quantified with external calibration in an adapted salty matrix. In all cases, recoveries were between 85 – 91% for NIST 1643f CRM (N=4) with a limit of detection (LOD) of 0.01 µg $L^{-1}$ (N=10). Given this LOD, the spiked concentrations and the dilution effect, it is assumed that pre-existing natural $^{125}Te$ in the kinetics and isotherm samples is negligible in the water matrices as its expected concentrations are in the range of 1 ng $L^{-1}$ (Filella 2013; Belzile and Chen 2015). The latter is corroborated by upstream freshwater analyses (Gil-Díaz et al. unpublished/*Chapter 5*) and confirmed in these experimental samples by natural $^{126}Te$ concentrations below LOD.

Digestates of particles from the isotherm experiments using 1000 mg $L^{-1}$ SPM in freshwater were quantified with an QQQ-ICP-MS (Agilent 8800, at the FHNW, Basel, Switzerland) using external calibration, $^{103}Rh$ as internal standard and oxygen-shift mode collision gas for $^{125}Te$ ($^{125}Te + {}^{16}O \rightarrow {}^{141}TeO$). A certified reference material (NCS 73307) was used for quality checkup of the total digestions showing mean ± SD recovery values of 94 ± 17% (N=3).

Particulate Te in total digestions and selective extractions were quantified by QQQ-ICP-MS (iCAP-TQ, THERMO®) using external calibration. Given the very low natural $Te_p$ concentrations (~0.04 mg $kg^{-1}$), natural Te was quantified from $^{126}Te$ measured in KED-mode (He), correcting for $^{86}Sr^{40}Ar$, $^{110}Cd^{16}O$ and $^{110}Pd^{16}O$ interferences (Filella and Rodushkin 2018) with respective monoelemental solutions (influencing < 0.1%) and $^{126}Xe$ from analytical blanks (2% $HNO_3$). Spiked $^{125}Te$ was determined by mass-shift $O_2$-mode (iCAP-TQ, THERMO®), better correcting for sporadic polyatomic interferences such as ~10% $^{85}Rb^{40}Ar$, ~5-10% $^{89}Y^{36}Ar$ and ~0.1% $^{107}Ag^{18}O$ (Filella and Rodushkin 2018), or ~0.1-10% $^{88}Sr^{37}Cl$ (unpublished). Certified reference materials were used for instrumental

quality check-up (freshwater NIST 1643f) and total digestions (stream sediment NCS 73307). Recoveries were 95 ± 5% (N=5) in the KED-mode, 89 ± 10% (N=5) in the $O_2$-mode for NIST 1643f and 99 ± 14% (N=4) in the KED-mode and 70 ± 19% (N=4) in the $O_2$-mode for NCS 73307. Natural Te was quantified from both Te-spiked SPM and Se-spiked SPM (i.e., no influence from potential $^{125}$Te spike effect). In selective extractions, natural Te concentrations ranged from 5-fold (in F2 extractions) to 200-fold (in F4 extractions) above LOD (0.1 ng $L^{-1}$, N=10).

### 2.4. Selenium quantification

Dissolved Se concentrations from sorption kinetics and isotherms were quantified by ICP-MS (XSeries 2, Thermo Fisher Scientific, KIT, Germany) using external calibration, CRC-mode (He:$H_2$ mixture at 92%: 8% to minimise $^{40}Ar^{37}Cl$ interferences) and $^{103}Rh/^{115}In$ as internal standards. Analytical quality control was followed with certified drinking water (CRM-TMDW) and freshwater (NIST 1643f) standards showing recoveries ranging between 98 – 106% for the former (N=16) and 100-102% for the latter (N=16), with a LOD of 0.06 µg $L^{-1}$ (N=10). Natural $Se_d$ concentrations were estimated to be 0.14 ± 0.03 µg $L^{-1}$ in freshwater (N=32) and ~0.31 µg $L^{-1}$ for seawater (unpublished).

Total $^{77}$Se digestions from the 1000 mg $L^{-1}$ SPM isotherm experiment were quantified by QQQ-ICP-MS (Agilent 8800, FHNW, Basel, Switzerland) using external calibration, $^{103}$Rh as internal standard and oxygen-shift mode collision gas for $^{77}$Se ($^{77}Se + {}^{16}O \rightarrow {}^{93}SeO$) to avoid doubly charged Rare Earth Element (REE) interferences (mainly $^{154}Sm^{++}$, $^{154}Gd^{++}$). The CRM NCS 73307 showed recoveries of total digestions ranging from 70 to 134% (N=3).

Analyses of Se in selective extractions, namely particulate $Se_{nat}$ and $Se_{ex}$ were quantified with the $O_2$-mode of the QQQ-ICP-MS (iCAP-TQ, THERMO®) using external calibration, eliminating the known polyatomic interferences (e.g., $^{40}Ar^{37}Cl$, $^{154}Sm^{++}$ and $^{154}Gd^{++}$ in $^{77}$Se, $^{78}$Kr, $^{156}Gd^{++}$ and $^{156}Dy^{++}$ in $^{78}$Se, $^{81}Br^{1}H$ and $^{82}$Kr in $^{82}$Se) on both natural ($^{78}$Se, $^{80}$Se, $^{82}$Se) and spike ($^{77}$Se) isotopes. Particulate $Se_{nat}$ was quantified from both Te-spiked and Se-spiked slurries. Analytical quality check showed recoveries of 95 ± 3% for NIST 1643f and 85 ± 2% for NIST 1640a. Total adsorbed Se was calculated from the difference between spiked and final $Se_d$ after 48h.

### 2.5. Distribution coefficient (Kd)

Tellurium and Se partitioning between dissolved and particulate concentrations can be evaluated from the kinetic experiments at equilibrium by using the particle-water distribution coefficient (Kd), described in Sung (1995). Briefly, Kd (in L $kg^{-1}$) is the particulate (mg $kg^{-1}$) to dissolved (mg $L^{-1}$) concentration ratio (Equation 1). The relative contribution of the particulate concentration ($X_p$) of a

given element X to the total (dissolved + particulate) concentration of the same element ($X_T$, Equation 2) is expressed as the fraction of $X_p$ ($F_p$, expressed in percentage, Equation 3).

$$K_d = X_p / X_d \quad (1)$$

$$X_T = X_p \cdot SPM + X_d \quad (2)$$

$$F_p(\%) = (X_p \cdot SPM)/X_T = (K_d \cdot SPM)/(1 + K_d \cdot SPM) \quad (3)$$

where $X_p$ is expressed in mg $kg^{-1}$, $X_d$ in mg $L^{-1}$, $X_T$ in mg $L^{-1}$ and SPM in kg $L^{-1}$. This Kd should also match the slope of the isotherm experiments.

### 2.6. Adsorption isotherm models

The exchange of a substance between the dissolved and particulate phases reaches a dynamic equilibrium (i.e., equal sorption and desorption rates) after sufficient contact time (Foo and Hameed 2010). Appropriate modelling and thermodynamic considerations provide insights into the adsorption mechanisms (i.e., physisorption vs chemisorption), surface properties and sorption strength (Foo and Hameed 2010, and references therein).

The Langmuir empirical model is the most common two-parameter isotherm employed to describe monolayer chemical saturation onto finite sites with no lateral interactions between adsorbed molecules (no "steric hindrance"; Langmuir 1918). Thus, elements following Langmuir isotherms reflect homogeneous adsorption, with all sites presenting equal affinities (Foo and Hameed 2010). The mathematical equation for the Langmuir isotherm (Equation 4) is complemented with the dimensionless constant ($R_L$) also known as the separation factor or equilibrium parameter (Equation 5) defined by Weber and Chakravorti (1974):

$$X_p = (X_{pmax} \cdot K_L \cdot X_d)/(1 + K_L \cdot X_d) \quad (4)$$

$$R_L = 1/(1 + K_L \cdot X_{d0}) \quad (5)$$

where $X_p$ is the concentration of element X in the particulate phase at equilibrium (mg $kg^{-1}$), calculated from the difference in dissolved concentrations between the initial spiked ($X_{d0}$) and the equilibrium ($X_d$) concentrations (µg $L^{-1}$, converted to particulate concentrations with the corresponding SPM ratio), $X_{pmax}$ is the maximum charge of X in the SPM and $K_L$ is the constant of Langmuir (L $\mu g^{-1}$). Values of $R_L$ indicate the adsorption nature of the isotherm as unfavourable ($R_L>1$), linear ($R_L=1$), favourable ($0<R_L<1$) and irreversible ($R_L = 0$; Weber and Chakravorti 1974).

The Freundlich empirical model was the first one to describe heterogeneous (i.e., non-uniform distribution) multilayer adsorption on a non-homogeneous surface (Freundlich 1907). In this case, stronger binding sites are occupied preferentially, decreasing the adsorption energy exponentially as

they fill up (Zeldowitsch 1934). The mathematical expression of the Freundlich isotherm (Equation 6) represents the adsorption intensity by the $K_F$ constant (i.e., the higher the value the higher the affinity for the particulate phase) and the surface heterogeneity with the c value (i.e., the closer to zero the more heterogeneous; Foo and Hameed 2010). When c = 1, the relationship between $X_p$ and $X_d$ is linear and $K_F$ = Kd (distribution coefficient).

$$X_p = K_F \cdot X_d^c \quad (6)$$

## 3. RESULTS

### 3.1. Tellurium sorption kinetics and isotherms

Sorption kinetics of dissolved Te ($Te_{ex}$) is rapid (> 40% in less than 3 min., Figure 1a) independent from salinity, but highly dependent on the solid/liquid ratios, showing ~90% sorption in 1000 mg $L^{-1}$ SPM within 3 min. Equilibrium between the dissolved and particulate phases was achieved at ≥ 48h in 100 mg $L^{-1}$ SPM and in < 5h for 1000 mg $L^{-1}$ SPM. Experimental blanks (i.e., no SPM) showed no measurable $Te_{ex}$ loss or adsorption onto tube walls throughout the whole experiment duration. Estimated particulate concentrations were used to calculate partitioning coefficients for $Te_{ex}$ at 48h of adsorption time, showing $\log_{10}$ Kd values in freshwater of 4.94 ± 0.02 L $kg^{-1}$ for 100 mg $L^{-1}$ and 5.31 ± 0.01 l $kg^{-1}$ for 1000 mg $L^{-1}$, whereas in seawater Kd values were 4.98 ± 0.02 L $kg^{-1}$ for 100 mg $L^{-1}$ and 4.96 ± 0.09 L $kg^{-1}$ for 1000 mg $L^{-1}$.

Sorption isotherms showed non-linear correlations at low SPM concentrations (100 mg $L^{-1}$, Figure 1b) following a Langmuir isotherm. Langmuir parameters were $K_L$ = 3.91 L $\mu g^{-1}$ and b = 50.7 mg $kg^{-1}$ with a separation factor of "favourable" to "very favourable" due to $R_L$ variations between 0.72 and 0.05. Nevertheless, higher SPM content of 1000 mg $L^{-1}$ showed a linear behaviour representative of a Freundlich isotherm (Figure 1c) with relatively low heterogeneity (c = 1). The value of ~0.02 mg $kg^{-1}$ at the intercept represented the natural Te in the SPM, thus, included in the $Te_p$ concentrations. Calculated $Te_p$ concentrations were in accordance with directly analysed $Te_p$ (< 15% difference, within analytical error) from 1000 mg $L^{-1}$ experimental isotherm sediments.

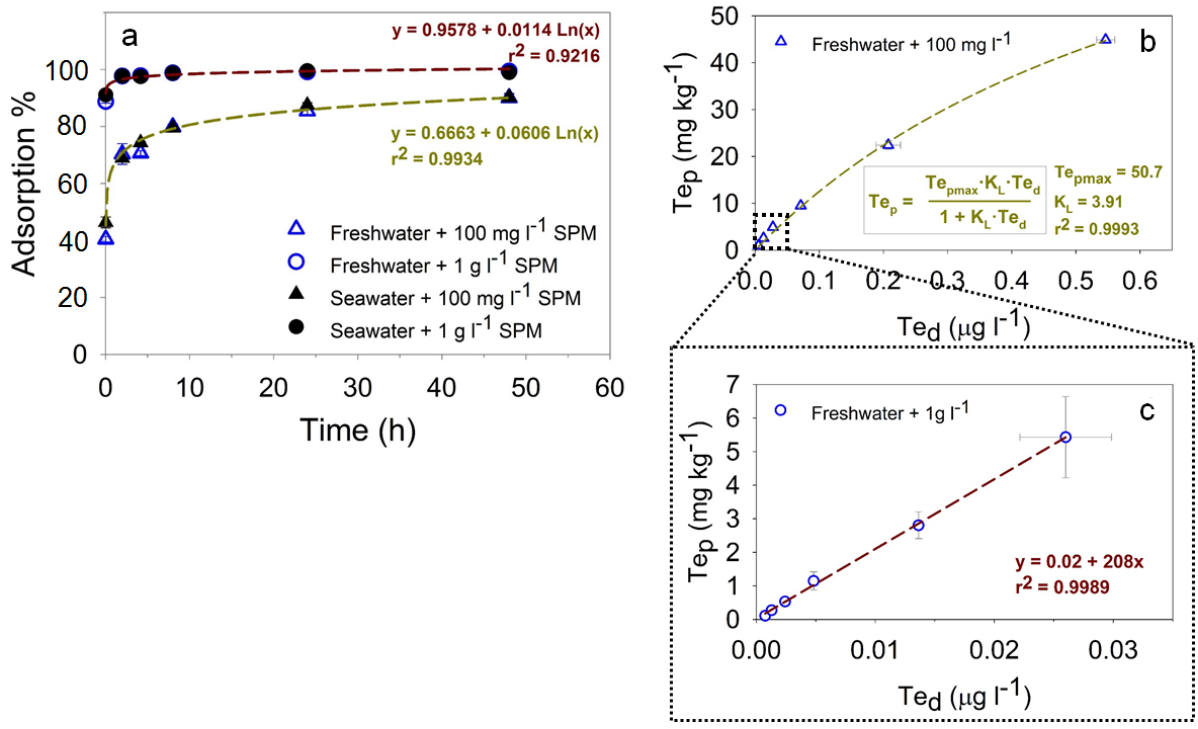


**Figure 1.** Tellurium sorption kinetics (N=3) in freshwater (empty symbols) and seawater (filled symbols) matrices for 100 mg $L^{-1}$ (triangles) and 1000 mg $L^{-1}$ (circles) SPM content (a). Adsorption percentages are calculated as the difference between initial spiking concentration and $Te_d$ at each sampling time. Tellurium isotherms (N=2, after 48h equilibration) for freshwater sorption in 100 mg $L^{-1}$ (b) and 1000 mg $L^{-1}$ SPM content (c) are also shown. Curves and equations correspond to respective fitting regressions. Error bars correspond to standard deviations (SD).

### 3.2. Selenium sorption kinetics and isotherms

Selenium sorption kinetics ($Se_{ex}$, Figure 2a) was less rapid than that of $Te_{ex}$ (Figure 1a), showing < l0% sorption after 3 min of exposure. There seems to be an effect of both salinity (i.e., higher sorption in seawater) and SPM concentration (i.e., higher sorption in 1000 mg $L^{-1}$), reaching solid/liquid equilibrium in < 24h for 1000 mg $L^{-1}$ with max. 25% sorption. Precise sorption kinetics and equilibrium time for 100 mg $L^{-1}$ (max. 5% sorption) were uncertain as all $Se_d$ values were close to the experimental blank concentrations with a 4% variability shown by the standard deviation. Experimental blanks showed no measurable $^{77}Se$ loss or adsorption onto tube walls along the experiment. Estimated $\log_{10}$ Kd values at 48h were: 2.51 ± 0.08 L $kg^{-1}$ for 100 mg $L^{-1}$ and 2.42 ± 0.04 L $kg^{-1}$ for 1000 mg $L^{-1}$ in freshwater, whereas in seawater they were 2.87 ± 0.10 L $kg^{-1}$ for 100 mg $L^{-1}$ and 2.57 ± 0.04 L $kg^{-1}$ for 1000 mg $L^{-1}$.

Sorption isotherms for both SPM conditions (100 mg $L^{-1}$ and 1000 mg $L^{-1}$) showed similar concentrations and linear correlations, representative of a Freundlich isotherm (Figure 2b). The value at the intercept of ~0.26 mg $kg^{-1}$ represented natural Se included in the $Se_p$ values. Calculated $Se_p$

concentrations tended to be ~30% higher than those directly measured for 1000 mg $L^{-1}$ SPM isotherm samples.

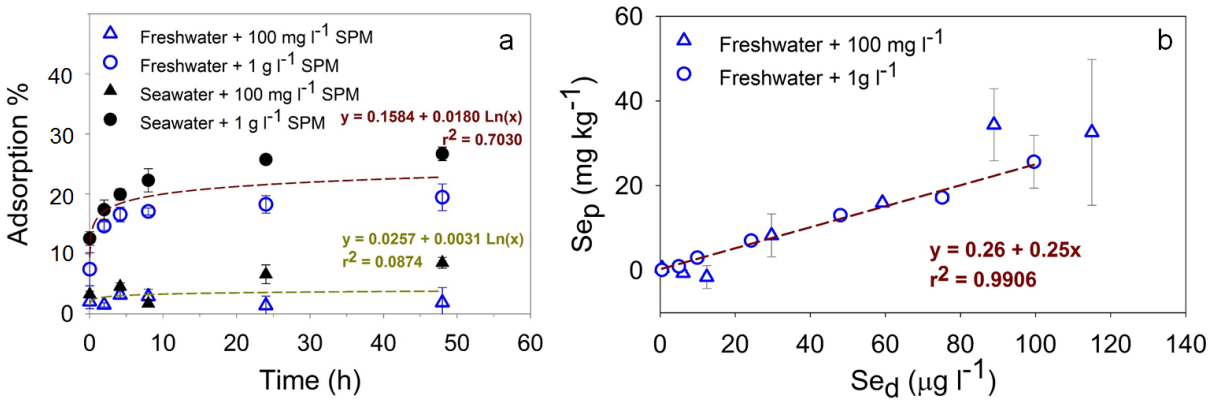


**Figure 2.** Selenium sorption kinetics (N=3) in freshwater (empty symbols) and seawater (filled symbols) matrices for 100 mg $L^{-1}$ and 1000 mg $L^{-1}$ SPM content (a) as well as its freshwater sorption isotherms (N=2, after 48h equilibration) in 100 mg $L^{-1}$ (triangles) and 1000 mg $L^{-1}$ (circles) SPM content (b). Adsorption percentages are calculated as the difference between initial spiking concentration and $Se_d$ at each sampling time. Curves and equations correspond to respective fitting regressions. Error bars correspond to standard deviations (SD).

### 3.3. Selective extractions

Selective extractions from both freshwater (S=0) and seawater (S=32) experiments of independent $^{125}Te$ and $^{77}Se$ spikes showed differences between spiked and inherited concentrations as well as distinct fractionation patterns for both elements (Figure 3). Relative contributions of each extracted fraction to total (natural or spiked) Te concentrations were estimated using concentrations of natural Te of 0.05 mg $kg^{-1}$ and $Te_{ex}$ of 2.68 mg $kg^{-1}$ in S=0 and 3.20 mg $kg^{-1}$ in S=32. Similarly, the natural Se concentration of 0.37-0.53 mg $kg^{-1}$ was compared to the average $Se_{ex}$ of 25.7 mg $kg^{-1}$ in both, freshwater and seawater.

The acid-soluble fractions showed the highest natural Te contribution (~50% in F4 and ~30% in F4N, Figure 3a) for freshwater experiments and were 10-20% lower in seawater experiments. Average natural Te contribution was 14% in the $H_2O_2$ fraction (F3, associated to organic matter), <2% in both, the easily exchangeable or carbonate fractions (F1) and the amorphous Mn/Fe oxide fraction (F2; Figure 3a). In contrast, $Te_{ex}$ sorbed preferentially (average ~60%) to the acid-soluble mineral phases (comprising amorphous and crystalline Fe and Mn oxides, carbonates, amorphous monosulphurs (e.g., acid volatile sulphides and FeS) and phyllosilicate phases; F4-F4N), implying a ~40% retention in the residual fraction. Up to 10% of $Te_{ex}$ was sorbed in the F1-acetate (easily exchangeable or carbonates fraction) and F2-ascorbate (Mn/Fe oxides) extracted fractions, obtaining a lower, <0.2% extraction with the oxidisable fraction (F3-$H_2O_2$ organic matter and labile/amorphous sulphide phases). In any case, low differences (~5%) were observed between freshwater-adsorbed and seawater-adsorbed $Te_{ex}$ except for acid-soluble fractions where this difference varied from 10 to 30%.

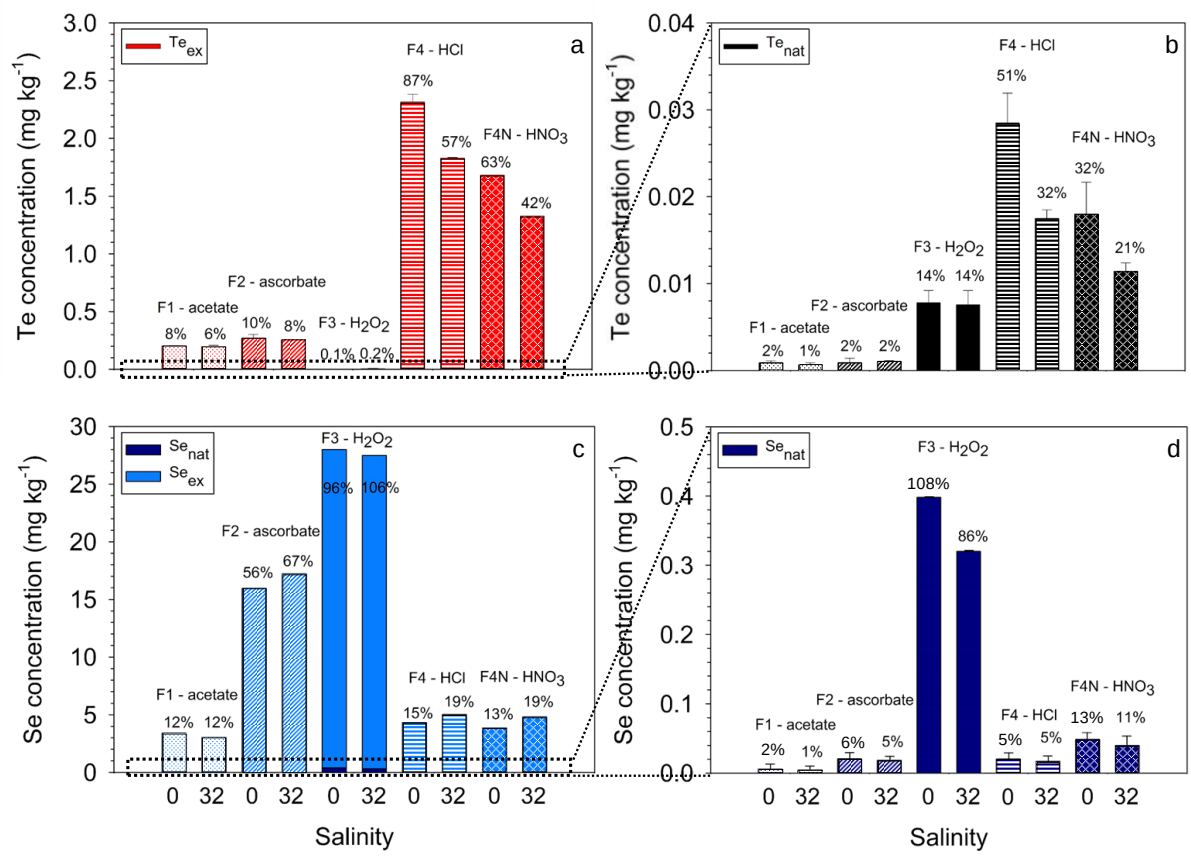


**Figure 3.** Distribution of natural Te ($Te_{nat}$, N=3, a), spiked Te ($Te_{ex}$, N=3, b), natural Se ($Se_{nat}$, N=3, c) and spiked Se ($Te_{ex}$, N=1, d) in selective extractions after sorption in freshwater (S=0) and seawater (S=32) conditions. Targeted parallel operationally-defined solid-phase fractions were: F1 – easily exchangeable and/or carbonate fraction (acetate extraction), F2 – reducible Fe/Mn oxides (ascorbate extraction), F3 – oxidisable fraction ($H_2O_2$ extraction) and F4 – reactive and potentially bioaccessible fraction (HCl 1 M extraction as F4 and $HNO_3$ 1M extraction as F4N). Percentages represent the extracted concentration in each fraction compared to total particulate concentration. Error bars correspond to standard deviations (SD).

Selective extractions for $Se_{nat}$ showed highest contributions (up to ~80%) in the F3-$H_2O_2$ fraction (targeting organic matter and labile/amorphous sulphide phases) of SPM exposed to contrasting salinities (Figure 3b). Acid-soluble fractions obtained from 1M HCl showed 2-fold lower $Se_{nat}$ extractions than 1M $HNO_3$. Ascorbate solutions extracted concentrations of $Se_{nat}$ similar to that of HCl-extracted aliquots, and the lowest $Se_{nat}$ fractions occurred in acetate extractions (~1%, Figure 3b). Spiked concentrations were also highly extracted in the F3-$H_2O_2$ fraction, representing 95-105% of total sorbed $Se_{ex}$. Noteworthy, the second most important fraction was the F2-ascorbate fraction, extracting ~60% of $Se_{ex}$, presumably from amorphous Mn/Fe oxide mineral phases. This amount of $Se_{ex}$ extracted was higher than that in the acid-soluble fractions F4 and F4N, both extracting ~20% of $Se_{ex}$. Only 12% of $Se_{ex}$ was leached in the easily exchangeable/carbonate fraction (F1-acetate extraction). Differences between freshwater-adsorbed and seawater-adsorbed $Se_{ex}$ were <10%.

# 4. DISCUSSION

## 4.1. Tellurium reactivity and solid fractionation in estuarine salinity and turbidity gradients

Results from sorption isotherms suggest a relatively high Te affinity for the particulate phases, as previously reported for Te radionuclides (Whitehead et al. 1988) and natural Te in the Changjiang Estuary (Wu et al. 2014). The observed $\log_{10}$ Kd values for experimentally adsorbed Te are similar to typical values in the Garonne-Gironde fluvial-estuarine system (Gil-Díaz et al. unpublished/*Chapter 5*; data not shown) ranging from 4.9 to 5.3 L $kg^{-1}$. These values are up to one order of magnitude greater than those of natural As (3.5 – 4.8 L $kg^{-1}$) and Sb (3.8 – 4.8 L $kg^{-1}$; Gil-Díaz et al. 2018) suggesting that the solubility/mobility of both natural and experimentally adsorbed Te is lower than that of natural As and Sb. Experimentally adsorbed Se showed even lower partitioning (2.4 – 2.9 L $kg^{-1}$, this study) with ~2 orders of magnitude lower than those of Te, suggesting that Se and Te solubility in environmental matrices may be very different.

Tellurium partitioning may also be compared to that of Cs, given (i) their potential common sources from weathering/remobilisation processes in the watershed (Gil-Díaz et al. unpublished), and (ii) their non-negligible radioactivity after accidental events (Steinhauser et al. 2014), making them relevant for radionuclide dispersion models. While the observed Te partitioning suggests relatively constant $\log_{10}$ Kd of ~ 4.9 L $kg^{-1}$, the reported Cs $\log_{10}$ Kd values range from < 4.7 L $kg^{-1}$ in river systems (Ciffroy et al. 2009) to typical values of $\log_{10}$ Kd 5.1 to 6.8 L $kg^{-1}$ in the Garonne-Gironde fluvial system (Gil-Díaz et al. unpublished). Furthermore, Te $\log_{10}$ Kd values are similar for both freshwater and seawater matrices with a maximum decrease of only -0.3 L $kg^{-1}$ in the seawater, similar decreases to that observed for Sb in the Gironde Estuary (i.e., -0.2 L $kg^{-1}$; Gil-Díaz et al. 2018). In contrast, the difference in Cs $\log_{10}$ Kd between freshwater and seawater is -1.4 L $kg^{-1}$ under experimental conditions (Oughton et al. 1997). Therefore, one would expect only little desorption of Te along estuarine salinity gradients, compared to Cs mobilisation. This major difference in estuarine geochemical behaviour represents important information for the development of continent-ocean transition models anticipating potential Te and Cs radionuclide dispersion after accidental NPP releases.

The sorption of Te dissolved onto the particulate phase fits a Langmuir (chemisorption-driven) behavior for both the low SPM ratio (~100 mg $L^{-1}$; Figure 1b) and the high SPM condition (1000 mg $L^{-1}$; Figure 1c), suggesting monolayer adsorption of Te at equal bonding energy sites until saturation, which would be achieved at ~50 mg $kg^{-1}$ for Garonne River SPM. This saturation concentration combined with kinetics results suggest that, in the maximum turbidity zone (MTZ) of the Gironde Estuary (SPM ≥ 1000 mg $L^{-1}$; Sottolichio and Castaing 1999), a hypothetic $Te_d$ concentration of 50 µg $L^{-1}$ could be retained to ~90% within <3 min and nearly all $Te_d$ (98%) would adsorb to the SPM in less than 2 h (Figure 1a). Such a high $Te_d$ concentration in the Gironde Estuary would imply Te addition in the order of 200 tons, which is unlikely, especially in the case of potential NPP accidents. However, relatively low masses of released radionuclides may produce high radiation. For example, a maximum

of 68 000 000 Bq $m^{-3}$ of $^{137}Cs$ (equivalent to ~20 ng $L^{-1}$) has been detected in early April in surface waters adjacent to the FDNPP, decreasing to 10 000 Bq $m^{-3}$ (equivalent to ~3 pg $L^{-1}$) in early 2012 (Buesseler et al. 2017). Therefore, assuming that the amounts of Te released would be similar in magnitude (or lower) than those of $^{137}Cs$, nearly all $Te_d$ radionuclides potentially released/produced in the Gironde Estuary would be highly retained in the particulate phase, even in seawater conditions. The latter is in accordance with the scavenged behaviour of Te observed in open ocean profiles of the Pacific and Atlantic Oceans, the East China Sea and the Angola and Panama Basins (Lee and Edmond 1985; Yoon et al. 1990; Wu et al. 2014).

The acid-soluble fraction (attributed to the sum of amorphous and crystalline Fe and Mn oxides, carbonates, amorphous monosulphurs and phyllosilicate phases) is commonly considered to represent the fraction potentially bioaccessible to organisms (ANZECC and ARMCANZ 2000). Based on this idea, the extractions suggest that ~30% of natural Te in the SPM and ~60% of the experimentally added $Te_{ex}$ retained in the particulate phase would be potentially bioaccessible. Interestingly, this observation also suggests that ~40% of the experimentally adsorbed $Te_{ex}$ could not be recovered by 1M acid extraction, i.e. would be bound to the so-called residual fraction, typically attributed to minerals that are considered as relatively insoluble under respective conditions (Gupta and Chen 1975). However, Te adsorption to different mineral fractions would not be consistent with the observed fit between the experimental adsorption isotherm and the Langmuir model, unless different fractions showed relatively similar surface properties regarding Te sorption. Differences in Te dissolution between 1M HCl (F4) and 1M $HNO_3$-based (F4N) extractions (~20% higher in HCl, Figure 3) observed for both naturally and experimentally-adsorbed Te, suggest that HCl may have stronger extraction efficiency than $HNO_3$, although previous work has reported similar stability and solubility in both HCl and $HNO_3$ solutions (Inorganic Ventures 2016).

Furthermore, these results appear to be in opposition with the higher Te adsorption observed in SPM in seawater conditions compared to that in freshwater (3.20 vs 2.70 mg $kg^{-1}$, respectively). In fact, the relatively low acid-soluble extractions obtained from SPM exposed to seawater compared to freshwater conditions suggest that Te binds somehow strongly in seawater conditions (i.e., not related to easily exchangeable binding sites). This observation is in accordance with the observed negative correlation between the labile fraction of $Te_p$ and the salinity gradient in the Changjiang Estuary (Duan et al. 2014) as well as with the potential precipitation of Te in presence of insoluble silver chlorides (Inorganic Ventures 2016). Nevertheless, further research is required to verify these hypotheses and the specific binding modes of Te to amorphous and crystalline Fe and Mn oxides, amorphous monosulphurs and phyllosilicate phases.

Low extraction of natural Te from the exchangeable/carbonate (<10% in F1), the amorphous Fe/Mn oxide fraction (<10% in F2) and the organic matter fraction (~14% in F3) are consistent with natural Te extractions in marine SPM from the East China Sea (Duan et al. 2014). In fact, Duan et al. (2014) observed 13% and 11% Te in the exchangeable and carbonates fraction (i.e., from an acetate-solution

extraction), 11% in the Fe–Mn oxides (i.e., from a hydroxylamine-based solution) and 15% in the organic matter fraction (i.e., from $H_2O_2$-solution extraction), leaving ~50% in the so-called "residual" fraction. Similarly, the residual fraction (accounted as the difference between total Te and that in F4) of the Garonne River SPM carried ~50% of the natural Te.

For the experimentally adsorbed $Te_{ex}$ simulating potential anthropogenic Te release into the natural environment the results suggest that up to ~99% would be fixed onto SPM within few hours, depending on SPM concentrations. After sediment deposition in the estuarine banks and bed during tidal slacks, the onset of early diagenetic processes might potentially release (i) up to 10% of $Te_{ex}$ due to reductive dissolution of reactive Fe and Mn oxyhydroxides as simulated by ascorbate extractions (F2), and (ii) less than 1% of $Te_{ex}$ adsorbed to organic matter ($H_2O_2$ extraction, F3). The relatively low F3 fraction obtained for $Te_{ex}$ compared to that of natural Te (14%) may suggest that Te physisorption or chemisorption onto particulate organic matter may be smaller than Te fixation by active incorporation (absorption).

The observed results are applicable to Te(VI) sorption behavior, which is assumed to be representative of environmental conditions as Te(VI) is the most abundant species found in aquatic systems (Lee and Edmond 1985; Yoon et al. 1990), representing up to 5-fold the abundance of Te(IV) in the Changjiang Estuary (Wu et al. 2014). The precise Te species released to the environment after a NPP accident are unknown, potentially varying between events depending on the specific accident conditions. In fact, the presence and concentration of radionuclide species in the nuclear fuel depend on several factors including fuel composition and fuel burnup (Kleykamp 1985). Nevertheless, both Te(IV) and Te(VI) equally adsorb to Fe(III) hydroxides and Te(IV) to illite mineral phases (Harada and Takahashi 2009, Qin et al. 2017). Thus, this work may serve as a preliminary approach to radionuclide Te dispersion fate scenarios in the Gironde Estuary.

In a scenario of Te radionuclide dispersion after hypothetical NPP accidental events the above considerations suggest a dominant role of the estuarine SPM in Te retention and dispersion independent from the hydrological situation. Both, relatively low (~100 mg $L^{-1}$) and high (>1000 mg $L^{-1}$) SPM concentrations would result in almost total sequestration of Te due to adsorption of Te radionuclides on suspended particles. Long particle residence times in the Gironde Estuary (1-2 years, Castaing and Jouanneau 1979), clearly greater than half-lives of most Te radionuclides (e.g., 3.2 days for $^{132}$Te to ~3 months for $^{127m}$Te) would imply that the maximum decay would take place inside the estuary, except for specific hydrodynamic conditions allowing for massive particle expulsion to the coastal ocean (few days per year; Allen et al. 1980; Castaing and Allen 1981). The main decay products are radioactive or stable iodine daughter nuclides (e.g. $^{129}$I with $1.57.10^7$ y half-life) which will then likely be mobilised to the water column (or pore waters) due to their relatively high solubility.

### 4.2. Selenium reactivity and solid fractionation in estuarine salinity and turbidity gradients

The experimentally determined sorption of Se in SPM from the Garonne River is considerably lower than that of Te, in accordance with the mobile character of Se in aquatic systems (Fernández-Martínez and Charlet 2009). The corresponding Kd values ($log_{10}$ Kd from 2.4 to 2.9 L $kg^{-1}$) are in the low Kd range of values reported for natural (stable and radioactive) Se in estuarine/coastal systems such as the San Francisco Estuary ($log_{10}$ Kd of 2.0 – 4.5 L $kg^{-1}$ for 100 mg $L^{-1}$ SPM; Benoit et al. 2010) and 19 Japanese coastal regions ($log_{10}$ Kd of 2.6 – 3.9 L $kg^{-1}$; Takata et al. 2016). In fact, Kd values are generally site-dependent as SPM mineralogy can strongly control elemental solid/liquid partitioning and Se Kd values have been observed to depend on grain size and organic matter (Takata et al. 2016). Sediments of the Gironde Estuary show characteristic particulate organic carbon (POC) contents ranging from 0.05 to 1.5% (Etcheber et al. 2007; Coynel et al. 2016) and grain sizes of mainly silts and some sands (7 - 480 µm; Coynel et al. 2016).

Marine and estuarine environments generally present higher abundances of Se(VI) over Se(IV) (Cutter 1978; Cutter and Bruland 1984; Guan and Martin 1991). The observed Se(VI) adsorption kinetics fit a pseudo-second order reaction, suggesting that the main process involving Se(VI) removal from the solution are physicochemical interactions (physisorption) with rate-limiting chemisorption surfaces (Robati 2013). This sorption pattern is in accordance with bidentate outer-sphere and monodentate inner-sphere complexes reported for selenate adsorbed on ferric-Fe(III) (hydr-)oxides and clay minerals like kaolinite (Su and Suarez 2000; Peak and Sparks 2002; Nothstein 2016), despite the higher affinity of selenite (Se(IV)) inner-sphere complexes to these mineral phases (Hamdy and Gissel-Nielsen 1977; Hayes et al. 1987).

Such interactions are relatively weak reflecting the selective extractions results (Figure 3b), as more than half of the acid-soluble fraction (F4) is contributed by exchangeable Se forms (F1). This distribution of Se between several mineral phases is also in line with the heterogeneous sorption sites identified from Se(VI) Freundlich isotherms. Such weak interactions could be subjected to ionic strength competition, decreasing Se(VI) sorption onto SPM (Su and Suarez 2000). However, the observed differences in Se sorption between freshwater- and seawater-exposed SPM fall within the analytical error.

Co-existing Se(IV) and Se(VI) forms may partly explain differences in parallel selective extractions of $Se_{nat}$ and $Se_{ex}$. In fact, the selective extraction using oxidising reagents (i.e. the F3-$H_2O_2$ and the F4N-$HNO_3$ fractions; Figure 3c,d) generally show a high mobilisation of Se, probably due to the oxidation of Se(IV) to the more mobile Se(VI). Strong oxidants like $H_2O_2$, used to chemically oxidise the organic matter, as well as $HNO_3$ compared to HCl, can oxidise Se(IV) from carrier phases other than the target phase (Gruebel et al. 1988). Thus, although high Se content in the organic matter fraction would fit the nutrient type behaviour of Se in marine environments (e.g., Cutter and Bruland 1984, Cutter and Cutter 1995), the fact that the amount of Se extracted by $H_2O_2$ (F3) close to 100% could also include Se

extracted from other phases by oxidation (Figure 3), implying non-selectivity of the fractionation for Se.

In general, it is commonly accepted that the 1M acid-soluble fraction includes mineral phases extracted in the ascorbate fraction, thus trace element concentrations in F4 should be equal to or greater than in F2 fractions (Huerta-Díaz and Morse 1990; Kostka and Luther 1994; Gasparon and Matschullat 2006). The similar $Se_{nat}$ concentrations in both F4-HCl and F2-ascorbate fractions (Figure 3d) are in accordance with this statement, potentially suggesting that most (if not all) of the natural Se in the F4-HCl fraction was extracted from the amorphous Fe/Mn oxide carrier phases (F2-ascorbate fraction). In contrast, $Se_{ex}$ was greater in the F2-ascorbate fraction than in the acid soluble fractions (F4 and F4N, Figure 3c). Interestingly, this effect of inversed extraction efficiency of parallel selective extractions (F2 vs F4) also occurred for both inherited and spiked Sb in the same SPM from the Garonne River (Gil-Díaz et al. unpublished/*Chapter 4*). Thus, these results suggest an anomaly (compared to more commonly analysed elements such as Cd, Cu, Zn, Pb, etc.) for F2-ascorbate extractions of metalloids like Se and Sb, but not Te. This effect could be potentially due to strong organic complexation of Se and Sb by the citrate present in the ascorbate solution, thus extracting higher metalloid concentrations, independently from the dissolution of the targeted mineral carrier phase (Gil-Díaz et al. unpublished/*Chapter 4*). These observations suggest that reducing conditions and the presence of strong organic ligands, as occurring in sub-oxic early diagenetic conditions (Froelich et al. 1979), potentially enhance $Se_{ex}$ solubility, compared to $Se_{nat}$.

Combining the above findings, one would assume that, after a potential accidental release from NPPs in the Gironde Estuary, the majority of dissolved radioactive Se may be rapidly expulsed to the coastal ocean and <30% retention in the particulate phase of the MTZ. Given the similarities between sorption isotherms and Kd at 100 mg $L^{-1}$ and 1000 mg $L^{-1}$ SPM concentrations, dissolved Se probably is dominant for a wide range of SPM concentrations and dissolved radioactive Se releases. Moreover, reducing, suboxic conditions as existing in the MTZ water column (Robert et al. 2004) may further increase Se mobility due to leaching from particles subjected to early diagenetic processes.

Noteworthy, this expected dominance of dissolved Se radionuclides could enhance radioactivity transfer to the biological compartment, given the nutrient behaviour of Se (Tan et al. 2016). In fact, aquatic microorganisms naturally methylate Se as a part of their detoxifying mechanisms (Cooke and Bruland 1987). In the presence of Se radionuclides bio-methylation processes might produce radioactive volatile Se (e.g., $^{75}Se$, $^{79}Se$ and $^{82}Se$) species which must be taken into account for accidental dispersion scenarios. Such Se methylation is a seasonal process (i.e., low in winter and quantifiable in summer) with estimated average fluxes of the order of $10^5$ g $y^{-1}$ for the Gironde Estuary (Amouroux and Donard 1997). Such methylation is species-dependent and can potentially show non-negligible atmospheric dispersion (Luxem et al. 2015).

Thus, accidental releases of dissolved Se radionuclides such as $^{75}Se$ (~119 d half-life), $^{79}Se$ (~$10^5$ y half-life) and $^{82}Se$ (~$10^{19}$ y half-life) are expected to follow the dynamics of the estuarine water column (e.g. estuarine water residence times of 18 to 86 days), implying (i) continuous exportation of dissolved radioactive Se to the coast during winter/high discharge conditions, (ii) bio-availability to primary producers and the related food chain, and (iii) potential seasonal production of radioactive methylated species exported to the atmosphere.

## 5. CONCLUSION

Batch experiments with bulk SPM and natural freshwater/seawater matrices simulating contrasting estuarine turbidity and salinity gradients showed different sorption kinetics, particulate affinity and solid fractionation distribution for Te and Se. Experimental results strongly suggest that the fluvial-estuarine geochemical cycles of Te and Se are not comparable in terms of reactivity, solubility and bioavailability. Further knowledge on Te speciation and sorption mechanisms is required in environmental studies.

The solid fractionation results suggest that anthropogenic releases of dissolved Te and Se to the aquatic environment do not fully mimic inherited element distribution among SPM mineral phases. The observed differences imply that (i) spiked $Te_p$ is potentially more bioavailable than the $Te_p$ already naturally present, and that (ii) Te might be fixed in the organic matter fraction mainly through biological active pathways. Comparison of Se solid partitioning with results of selective extractions commonly applied to other trace elements point out to two anomalies: (i) enhanced dissolution of Se species in oxidising conditions probably due to oxidation of Se(IV) to the more soluble Se(VI) and subsequent mobilisation from other solid carrier phases (non-selectivity), and (ii) potential extraction by dissolved organic complexants in addition to release from reducible mineral phases. These findings clearly show that the use of commonly applied extraction schemes to other than originally tested target elements may produce artefacts that need thorough evaluation and must be taken into account for environmental interpretations.

Preliminary dispersion scenarios of hypothetical releases of Te and Se radionuclides into the Garonne-Gironde fluvial-estuarine system suggest high potential adsorption of Te radionuclides onto estuarine SPM in all hydrological conditions (flood and drought) implying long estuarine residence times (up to several years), and the risk of seasonal upstream movement when a hypothetic accident happens in a period when the MTZ is down estuary. In contrast, Se radionuclides would preferentially remain in the dissolved phase continuously exported to the coastal ocean within several weeks, implying a risk of transfer to primary producers and the related food chain including seafood.

## ACKNOWLEDGEMENTS

This study is a scientific contribution to the French National Project AMORAD (ANR-11-RSNR-0002) from the National Research Agency, allocated in the framework programme "Investments for the Future". The authors gratefully acknowledge the financial assistance of the FEDER Aquitaine-1999-Z0061 and the German Academic Exchange Service DAAD.

## REFERENCES

Aguerre, S., Frechou, C. (2006). Development of a radiochemical separation for selenium with the aim of measuring its isotope 79 in low and intermediate nuclear wastes by ICP-MS. Talanta, 69(3), 565-571.

Allen, G. P., Salomon, J. C., Bassoullet, P., Du Penhoat, Y., De Grandpre, C. (1980). Effects of tides on mixing and suspended sediment transport in macrotidal estuaries. Sedimentary Geology, 26(1-3), 69-90.

Amouroux, D., Donard, O. F. (1997). Evasion of selenium to the atmosphere via biomethylation processes in the Gironde estuary, France. Marine Chemistry, 58(1-2), 173-188.

ANZECC and ARMCANZ, 2000. Australian and New Zealand guidelines for fresh water and marine water quality. Australian and New Zealand Environment and Conservation Council/Agriculture and Resource Management Council of Australia and New Zealand, Canberra

Audry, S., Blanc, G., Schäfer, J. (2006). Solid state partitioning of trace metals in suspended particulate matter from a river system affected by smelting-waste drainage. Science of the Total Environment, 363(1-3), 216-236.

Asai, S., Hanzawa, Y., Okumura, K., Shinohara, N., Inagawa, J., Hotoku, S., Suzuki, K., Kaneko, S. (2011). Determination of 79Se and 135Cs in spent nuclear fuel for inventory estimation of high-level radioactive wastes. Journal of Nuclear Science and Technology, 48(5), 851-854.

Baeza, A., Corbacho, J. A., Rodríguez, A., Galván, J., García-Tenorio, R., Manjón, G., Mantero, J., Vioque, I., Arnold, D., Grossi, C., Serrano, I., Vallés, I., Vargas, A. (2012). Influence of the Fukushima Dai-ichi nuclear accident on Spanish environmental radioactivity levels. Journal of Environmental Radioactivity, 114, 138-145.

Belzile, N., Chen, Y. W. (2015). Tellurium in the environment: A critical review focused on natural waters, soils, sediments and airborne particles. Applied Geochemistry, 63, 83-92.

Benoit, M. D., Kudela, R. M., Flegal, A. R. (2010). Modeled trace element concentrations and partitioning in the San Francisco estuary, based on suspended solids concentration. Environmental Science and Technology, 44(15), 5956-5963.

Biver, M., Quentel, F., Filella, M. (2015). Direct determination of tellurium and its redox speciation at the low nanogram level in natural waters by catalytic cathodic stripping voltammetry. Talanta, 144, 1007-1013.

Bizsel, N., Ardelan, M. V., Bizsel, K. C., Suzal, A., Demirdag, A., Sarıca, D. Y., Steinnes, E. (2017). Distribution of selenium in the plume of the Gediz River, Izmir Bay, Aegean Sea. Journal of Marine Research, 75(2), 81-98.

Bordas, F., Bourg, A. C. (1998). A critical evaluation of sample pretreatment for storage of contaminated sediments to be investigated for the potential mobility of their heavy metal load. Water, Air, and Soil Pollution, 103(1-4), 137-149.

Buesseler, K., Dai, M., Aoyama, M., Benitez-Nelson, C., Charmasson, S., Higley, K., Maderich, V., Masqué, P., Morris, P.J., Oughton, D., Smith, J. N. (2017). Fukushima Daiichi–derived radionuclides in the ocean: transport, fate, and impacts. Annual Review of Marine Science, 9, 173-203.

Castaing, P., Allen, G. P. (1981). Mechanisms controlling seaward escape of suspended sediment from the Gironde: a macrotidal estuary in France. Marine Geology, 40(1-2), 101-118.

Castaing, P., Jouanneau, J. M. (1979). Temps de résidence des eaux et des suspensions dans l'estuaire de la Gironde. Journal Recherche Océanographie IV, 41-52.

Ciffroy, P., Durrieu, G., Garnier, J. M. (2009). Probabilistic distribution coefficients (Kds) in freshwater for radioisotopes of Ag, Am, Ba, Be, Ce, Co, Cs, I, Mn, Pu, Ra, Ru, Sb, Sr and Th–implications for uncertainty analysis of models simulating the transport of radionuclides in rivers. Journal of Environmental Radioactivity, 100(9), 785-794.

Cooke, T. D., Bruland, K. W. (1987). Aquatic chemistry of selenium: evidence of biomethylation. Environmental Science and Technology, 21(12), 1214-1219.

Coynel, A., Gorse, L., Curti, C., Schafer, J., Grosbois, C., Morelli, G., Ducassou, E., Blanc, G., Maillet, G.M., Mojtahid, M. (2016). Spatial distribution of trace elements in the surface sediments of a major European estuary (Loire Estuary, France): Source identification and evaluation of anthropogenic contribution. Journal of Sea Research, 118, 77-91.

Cutter, G. A. (1978). Species determination of selenium in natural waters. Analytica Chimica Acta, 98(1), 59-66.

Cutter, G. A. (1989). The estuarine behaviour of selenium in San Francisco Bay. Estuarine, Coastal and Shelf Science, 28(1), 13-34.

Cutter, G. A., Bruland, K. W. (1984). The marine biogeochemistry of selenium: A re-evaluation. Limnology and Oceanography, 29(6), 1179-1192.

Cutter, G. A., Cutter, L. S. (1995). Behavior of dissolved antimony, arsenic, and selenium in the Atlantic Ocean. Marine Chemistry, 49(4), 295-306.

Duan, L. Q., Song, J. M., Yuan, H. M., Li, X. G., Li, N., Ma, J. K. (2014). Distribution, chemical speciation and source of trace elements in surface sediments of the Changjiang Estuary. Environmental Earth Sciences, 72(8), 3193-3204.

Element Collection Inc.: Gray, T., Mann, N., Whitby, M. (2007). Periodic Table of Isotopes. < http://periodictable.com/Isotopes/051.123/index.p.full.html> Last accessed on the 10/03/2015

Etcheber, H., Taillez, A., Abril, G., Garnier, J., Servais, P., Moatar, F., Commarieu, M. V. (2007). Particulate organic carbon in the estuarine turbidity maxima of the Gironde, Loire and Seine estuaries: origin and lability. Hydrobiologia, 588(1), 245-259.

Fernández-Martínez, A., Charlet, L. (2009). Selenium environmental cycling and bioavailability: a structural chemist point of view. Reviews in Environmental Science and Bio/Technology, 8(1), 81-110.

Filella, M. (2013). Food for thought: a critical overview of current practical and conceptual challenges in trace element analysis in natural waters. Water, 5(3), 1152-1171.

Filella, M., Rodushkin, I. (2018). A concise guide for the determination of less-studied technology-critical elements (Nb, Ta, Ga, In, Ge, Te) by inductively coupled plasma mass spectrometry in environmental samples. Spectrochimica Acta Part B: Atomic Spectroscopy, 141, 80-84.

Foo, K. Y., Hameed, B. H. (2010). Insights into the modeling of adsorption isotherm systems. Chemical Engineering Journal, 156(1), 2-10.

Freundlich, H. (1907). Über die adsorption in lösungen. Zeitschrift für physikalische Chemie, 57(1), 385-470. [Over the adsorption in solution, Journal of Physical Chemistry, 57 (1907), 385–471.]

Froelich, P., Klinkhammer, G. P., Bender, M. L., Luedtke, N. A., Heath, G. R., Cullen, D., Dauphin, P., Hammond, D., Hartman, B., Maynard, V. (1979). Early oxidation of organic matter in pelagic sediments of the eastern equatorial Atlantic: suboxic diagenesis. Geochimica et Cosmochimica Acta, 43(7), 1075-1090.

Gasparon, M., Matschullat, J. (2006). Trace metals in Antarctic ecosystems: results from the Larsemann Hills, East Antarctica. Applied Geochemistry, 21(9), 1593-1612.

Gil-Díaz, T., Schäfer, J., Coynel, A., Bossy, C., Dutruch, L., Blanc, G. (2018). Antimony in the Lot–Garonne river system: a 14-year record of solid–liquid partitioning and fluxes. Environmental Chemistry. DOI: 10.1071/EN17188

Gruebel, K. A., Leckie, J. O., Davis, J. A. (1988). The feasibility of using sequential extraction techniques for arsenic and selenium in soils and sediments. Soil Science Society of America Journal, 52(2), 390-397.

Guan, D. M., Martin, J. M. (1991). Selenium distribution in the Rhone delta and the Gulf of Lions. Marine Chemistry, 36(1-4), 303-316

Gupta, S. K., Chen, K. Y. (1975). Partitioning of trace metals in selective chemical fractions of nearshore sediments. Environmental Letters, 10(2), 129-158.

Hamed, M. M., Holiel, M., El-Aryan, Y. F. (2017). Removal of selenium and iodine radionuclides from waste solutions using synthetic inorganic ion exchanger. Journal of Molecular Liquids, 242, 722-731.

Hamdy, A. A., Gissel-Nielsen, G. (1977). Fixation of selenium by clay minerals and iron oxides. Zeitschrift für Pflanzenernährung und Bodenkunde, 140(1), 63-70.

Hayes, K. F., Roe, A. L., Brown, G. E., Hodgson, K. O., Leckie, J. O., Parks, G. A. (1987). In situ X-ray absorption study of surface complexes: Selenium oxyanions on α-FeOOH. Science, 238(4828), 783-786.

Huerta-Diaz, M. A., Morse, J. W. (1990). A quantitative method for determination of trace metal concentrations in sedimentary pyrite. Marine Chemistry, 29, 119-144.

Inorganic Ventures (2016). <www.inorganicventures.com> Last accessed on the 28/07/2018

Ishikawa, T. (2014). A brief review of dose estimation studies conducted after the Fukushima Daiichi Nuclear Power Plant accident. Radiation Emergency Medicine, 3, 21-27.

Izrael, Y.A. (2002). Radioactive fallout after nuclear explosions and accidents. Elsevier, Saint Louis.

Kersten, M., Förstner, U. (1987). Cadmium associations in freshwater and marine sediment. Cadmium in the Aquatic Environment, 51-88.

Kleykamp, H. (1985). The chemical state of the fission products in oxide fuels. Journal of Nuclear Materials, 131(2-3), 221-246.

Kostka, J. E., Luther III, G. W. (1994). Partitioning and speciation of solid phase iron in saltmarsh sediments. Geochimica et Cosmochimica Acta, 58(7), 1701-1710.

Langmuir, I. (1918). The adsorption of gases on plane surfaces of glass, mica and platinum. Journal of the American Chemical Society, 40(9), 1361-1403.

Leppänen, A. P., Mattila, A., Kettunen, M., Kontro, R. (2013). Artificial radionuclides in surface air in Finland following the Fukushima Dai-ichi nuclear power plant accident. Journal of Environmental Radioactivity, 126, 273-283.

Lee, D. S., Edmond, J. M. (1985). Tellurium species in seawater. Nature, 313(6005), 782.

Luxem, K. E., Vriens, B., Wagner, B., Behra, R., Winkel, L. H. (2015, April). Selenium uptake and volatilization by marine algae. In EGU General Assembly Conference Abstracts (Vol. 17).

Ma, Y., Uren, N.C., 1995. Application of a new fractionation scheme for heavy metals in soils. Communications in Soil Science and Plant Analysis, 26, 3291-3303.

Measures, C. I., Burton, J. D. (1978). Behaviour and speciation of dissolved selenium in estuarine waters. Nature, 273(5660), 293.

Morewitz, H. A. (1981). Fission product and aerosol behavior following degraded core accidents. Nuclear Technology, 53(2), 120-134.

Nothstein, A. K. (2016). Selenium Transfer between Kaolinite or Goethite Surfaces, Nutrient Solution and Oryza Sativa (Vol. 41). KIT Scientific Publishing.

Oughton, D. H., Børretzen, P., Salbu, B., Tronstad, E. (1997). Mobilisation of 137Cs and 90Sr from sediments: potential sources to arctic waters. Science of the Total Environment, 202(1-3), 155-165.

Peak, D., Sparks, D. L. (2002). Mechanisms of selenate adsorption on iron oxides and hydroxides. Environmental Science and Technology, 36(7), 1460-1466.

Qin, H.-B, Takeichi, Y., Nitani, H., Terada, Y., Takahashi, Y. (2017). Tellurium distribution and speciation in contaminated soils from abandoned mine tailings: comparison with selenium. Environmental Science and Technology, 51(11), 6027-6035.

Robati, D. (2013). Pseudo-second-order kinetic equations for modeling adsorption systems for removal of lead ions using multi-walled carbon nanotube. Journal of Nanostructure in Chemistry, 3(1), 55.

Robert, S., Blanc, G., Schäfer, J., Lavaux, G., Abril, G. (2004). Metal mobilization in the Gironde Estuary (France): the role of the soft mud layer in the maximum turbidity zone. Marine Chemistry, 87(1-2), 1-13.

Saegusa, J., Kikuta, Y., Akino, H. (2013). Observation of gamma-rays from fallout collected at Ibaraki, Japan, during the Fukushima nuclear accident. Applied Radiation and Isotopes, 77, 56-60.

Schäfer J, Blanc G (2002). Relationship between ore deposits in river catchments and geochemistry of suspended particulate matter from six rivers in southwest France. Science of the Total Environment, 298, 103-118

Sonzogni, A.A. (2013). Chart of Nuclides NuDat 2.6 - National Nuclear Data Center. Brookhaven National Laboratory. <http://www.nndc.bnl.gov/nudat2/reCenter.jsp?z=51&n=68> Last accessed on the 10/03/15.

Sottolichio, A., Castaing, P. (1999). A synthesis on seasonal dynamics of highly-concentrated structures in the Gironde estuary. Comptes Rendus de l'Académie des Sciences-Series IIA-Earth and Planetary Science, 329(11), 795-800.

Steinhauser, G., Brandl, A., Johnson, T.E. (2014). Comparison of the Chernobyl and Fukushima nuclear accidents: A review of the environmental impacts. Science of the Total Environment, 470-471, 800-817

Su, C., Suarez, D. L. (2000). Selenate and selenite sorption on iron oxides an infrared and electrophoretic study. Soil Science Society of America Journal, 64(1), 101-111.

Sung, W. (1995). Some observations on surface partitioning of Cd, Cu and Zn in estuaries. Environmental Science and Technology, 29, 1303

Tan, L. C., Nancharaiah, Y. V., van Hullebusch, E. D., Lens, P. N. (2016). Selenium: environmental significance, pollution, and biological treatment technologies. Biotechnology Advances, 34(5), 886-907.

Takata, H., Aono, T., Tagami, K., Uchida, S. (2016). A new approach to evaluate factors controlling elemental sediment–seawater distribution coefficients (Kd) in coastal regions, Japan. Science of the Total Environment, 543, 315-325.

Tessier, A., Campbell, P. G., Bisson, M. (1979). Sequential extraction procedure for the speciation of particulate trace metals. Analytical Chemistry, 51(7), 844-851.

Weber, T. W., Chakravorti, R. K. (1974). Pore and solid diffusion models for fixed-bed adsorbers. AIChE Journal, 20(2), 228-238.

Whitehead, N. E., Ballestra, S., Holm, E., Huynh-Ngoc, L. (1988). Chernobyl radionuclides in shellfish. Journal of Environmental Radioactivity, 7(2), 107-121.

Winkel, L. H. (2016). The global biogeochemical cycle of selenium: Sources, fluxes and the influence of climate. In Global Advances in Selenium Research from Theory to Application: Proceedings of the 4th International Conference on Selenium in the Environment and Human Health (pp. 3-4). CRC Press/Balkema.

Wu, X., Song, J., Li, X. (2014). Occurrence and distribution of dissolved tellurium in Changjiang River estuary. Chinese journal of oceanology and limnology, 32(2), 444-454.

Yoon, B. M., Shim, S. C., Pyun, H. C., Lee, D. S. (1990). Hydride generation atomic absorption determination of tellurium species in environmental samples with in situ concentration in a graphite furnace. Analytical Sciences, 6(4), 561-566.

Zeldowitsch, J. (1934). Adsorption site energy distribution. Acta Physicochimica URSS, 1, 961-973.

## II. CONCLUSION

This is the first comprehensive environmental study on Te in a fluvial-estuarine system at a high spatial and temporal resolution, with insights into both inherited and spiked Te solid fractionation. The main outcomes of the presented studies are:

- Dissolved and particulate Te concentrations in the Lot-Garonne River system are similar among studied sites showing respective average values of ~1 ng $L^{-1}$ and ~50 µg $kg^{-1}$. These concentrations were close to geological background levels, suggesting that current freshwater Te dynamics are mostly dominated by natural processes, even in the historically contaminated Lot River sites.

- Furthermore, the parallel variation of dissolved and particulate Te concentrations (both showing high concentrations in summer and low concentrations in winter) in the Lot-Garonne River system represent an uncommon seasonal behaviour compared to other trace elements, including those forming oxyanions (e.g. As, Mo, Sb and V). This behaviour may be potentially related to watershed rock weathering and fast Te adsorption onto SPM.

- This is the first study determining environmental solid/liquid partitioning of Te ($log_{10}$ Kd ~4.75 L $kg^{-1}$), being rather constant at all sampling sites and throughout the seasons. This freshwater $log_{10}$Kd value matches the experimentally determined Te $log_{10}$Kd in seawater, suggesting that for estuarine conditions, dissolved Te (extremely difficult to measure due to complex matrix and ultra-trace concentrations) can be estimated from natural particulate Te concentrations and the general $log_{10}$Kd.

- Under estuarine conditions, the huge majority of Te would be expected to be in the particulate phase with ~90% being adsorbed for average turbidity (SPM ~100 mg $L^{-1}$) reaching up to almost 99% of total Te in the MTZ (SPM ~1000 mg $L^{-1}$). This is in accordance with the expected decrease in dissolved Te from the freshwater reaches (~1 ng $L^{-1}$) towards the seawater endmember (estimated at ~0.3-0.5 ng $L^{-1}$) due to adsorption in the SPM of the Gironde Estuary.

- The high affinity of Te for the particulate phase reflected in Te sorption kinetic experiments for contrasting salinity and turbidity conditions is representative of those in the Gironde Estuary. In fact, more than 90% of spiked Te was rapidly adsorbed in the presence of 1000 mg $L^{-1}$ SPM, reaching equilibrium between the dissolved and particulate phase in less than 5h. These observations suggest that anthropogenic releases of dissolved Te would most likely result in high adsorption, linking the fate of anthropogenic Te to the estuarine SPM dynamics (e.g., long residence times, upstream migration in drought conditions, etc.).

- Solid fractionation experiments suggest that both inherited and spiked Te are mostly associated to the acid-soluble fraction, that is, associated to operationally-defined amorphous and crystalline Fe and Mn oxides, carbonates, amorphous monosulphurs and phyllosilicate phases. Noteworthy, inherited Te is present in the organic matter fraction contrasting to spiked Te, for which the $H_2O_2$ fraction was poor. These findings suggest that spiked Te may be mainly directly incorporated into the organic matter by active biological pathways and not by physical-chemical sorption. Furthermore, Te does not show the ascorbate anomaly observed in other elements like Sb or Se, supporting different geochemical behaviour of Te compared to its commonly assumed geochemical pair Se.

- Long-term records of Te in wild oysters at the estuary mouth show average concentrations in soft tissues of 2.08 µg $kg^{-1}$ d.w. with no clear trend over the past 33 years. These results contrast with other known anthropogenic trace elements affecting these oyster samples (Cd, Ag and Pt), for which historical contaminations have been related to past industrial activities in the upstream Lot River and successively emerging anthropogenic releases. Efficient fixation of Te in the particulate phase, especially in turbid water bodies, could probably out-compete bio-uptake from the dissolved phase.

- Comparison with other sites along the Atlantic coast (i.e., Comprian in the Arcachon Bay, France, and Arriluze in the Basque Country, Spain) suggests that Te concentrations in wild oysters may be higher in areas subjected to direct urban runoff and low turbidity. Accordingly, one cannot exclude that current anthropogenic activities release Te into aquatic systems, where it may enter the marine food chain, but in highly turbid areas such as the Gironde Estuary the presence of SPM may totally scavenge potentially bioavailable dissolved Te. This suggests that studies aiming at monitoring any potential contamination and bio-transfer of Te as a TCE and emerging contaminant in coastal systems should focus on environments with relatively low SPM concentrations.

# CHAPTER 6:

# Trace element reactivity of Sn and Se in contrasting fluvial-estuarine systems – a comparative approach between the Gironde Estuary and the Rhône River

# I. INTRODUCTION

This chapter focuses on the comparison of the fate of radionuclides potentially released from nuclear power plants in both the Gironde and the Rhône fluvial estuarine systems. The chapter is structured as follows:

The first part documents outcomes of an experimental approach using radiotracers to study sorption and desorption kinetics of radionuclides at environmentally representative trace element concentrations in contrasting estuarine conditions. For this, we exposed sediments from the Gironde Estuary and from the Rhône River to dissolved selected radiotracers of tin (Sn) and selenium (Se), which were directly available on the market. Selenium and Sn radionuclides are commonly present in spent nuclear fuel from fission reactions forming high-level radioactive waste (HLW). Current concern lies on their potential environmental release, mobility and bioavailability, given their long-term environmental persistence (half-lives) and potential biological roles. These Sn and Se radiotracers were assumed to show adsorption kinetics close to those of the highly particle-active Te (Sn) and the more soluble Sb (Se).

Adsorption and desorption kinetics of Sn and Se radiotracers are studied, simulating contrasting salinity conditions and SPM concentrations (S=0, S=32; SPM = 10 mg $L^{-1}$, 100 mg $L^{-1}$ and 1000 mg $L^{-1}$), representative of the Gironde Estuary and the Rhône River systems. The desorption approach simulates the reversible sorption dynamics as they may occur in coastal systems (e.g. after particle expulsion to the coastal ocean). Laboratory-Kd values obtained for Sn and Se radiotracers are compared to field-Kd values for Sn and Se and to laboratory-Kds of stable Se (*Chapter 5*), to better understand how the way of Kd determination may influence radionuclide dispersion scenarios. This work is complemented with analyses of major mineral composition of the applied bulk sediments in order to better interpret the results.

The second part of this chapter addresses the biological transfer of Sn and Se to wild oysters from the Gironde Estuary and to mussels from the Rhône River. These results are complemented with preliminary insights into Sn and Se organotropism in wild oysters in order to contrast intra-estuarine Sn and Se reactivity to environmental biotransfer of Sn and Se. Results on Cs bioaccumulation in these samples are also provided, adding perspectives to the study of multi-element radionuclide dispersion scenarios in continent-ocean transition systems.

## 1. Reactivity of tin and selenium radionuclides with particles from the Gironde and Rhône fluvial-estuarine systems in simulated contrasting estuarine conditions.

*Publication: to be submitted to Journal of Environmental Radioactivity*

# Tin-113 and Selenium-75 radiotracer adsorption and desorption kinetics in contrasting estuarine salinity and turbidity conditions

Teba Gil-Díaz[a], Frank Heberling[b*], Elisabeth Eiche[c], Markus Fuss[b], Melanie Böttle[b], Virginia Keller[c], Jörg Schäfer[a]

*[a]Université de Bordeaux, UMR CNRS 5805 EPOC, Allée Geoffroy Saint-Hilaire, 33615 Pessac, France; [b] Institute for Nuclear Waste Disposal (INE), Karlsruhe Institute of Technology (KIT), Hermann von Helmholtz Platz 1, 76344 Eggenstein-Leopoldshafen, Germany; [c]Institute of Mineralogy and Geochemistry (AGW), Karlsruhe Institute of Technology (KIT), Adenauerring 20b, 76131 Karlsruhe, Germany*

*Corresponding author: frank.heberling@kit.edu

## ABSTRACT

Batch experiments were performed to study adsorption and desorption kinetics of $^{75}$Se and $^{113}$Sn radiotracers at environmentally representative concentrations of ~0.3 ng $L^{-1}$ and ~3 ng $L^{-1}$, respectively. The radiotracers were incubated with wet bulk sediments from the Gironde Estuary and the Rhône River, combining freshwater and coastal seawater salinity (S=0, S=32) and three different Suspended Particulate Matter (SPM) concentrations (10 mg $L^{-1}$, 100 mg $L^{-1}$, 1000 mg $L^{-1}$) to simulate six hydrologically contrasting situations for each particle type. Results showed no measurable adsorption for $^{75}$Se under the experimental conditions, whereas >85% of $^{113}$Sn rapidly adsorbed onto the particles during the first hours of exposure. Adsorption efficiency increased with increasing SPM concentrations and tended to be greater for the Rhône River sediments, potentially reflecting the abundance of carbonate or Fe/Mn oxide mineral phases. Desorption of spiked sediments exposed to filtered, unspiked freshwater and seawater only occurred for $^{113}$Sn (~10% of the previously adsorbed $^{113}$Sn) in the Garonne River sediments. This study suggests that, in the hypothetical case of accidental radionuclide releases, soluble radionuclides like Se will remain in the dissolved phase, follow water mass hydrodynamics and may be potentially highly bioavailable to biota. In contrast, the fate and transport of highly particle-active radionuclides such as Sn will be linked to those of sediments. Long particle residence times such as those in the Gironde Estuary, combined with little desorption in the coastal area imply the risk of radionuclide transport during the seasonal upstream migration of the Maximum Turbidity Zone (MTZ) during the following drought season, implying the risk of radionuclide transport towards the city of Bordeaux. In the Rhône system, one would expect rapid expulsion of radionuclides with dilution of Se in the west Mediterranean coast and temporal storage of particle-active radionuclides in the pro-delta followed by subsequent westward dispersion on the shelf. Information on reactivity of radionuclides is

non-negligible for improving the precision of current approaches aiming at modelling environmental radionuclide dispersion scenarios in continent-ocean transition systems.

***Keywords:*** tin, selenium, radiotracers, kinetics, partition coefficient (Kd), Gironde Estuary, Rhône River

## 1. INTRODUCTION

Selenium (Se) and tin (Sn) radionuclides are commonly present in spent nuclear fuel from fission reactions forming high-level radioactive waste (HLW), generally stored in geological repositories (Asai et al. 2011, 2013). Environmental releases of Se and Sn radionuclides can either occur from the leakage of radioactive wastes or directly from potential nuclear power plant accidental events (Morewitz 1981; Abe et al. 2014). Current concern lies on their potential environmental release, mobility and bioavailability, given their long-term environmental persistence (half-lives of $2.9.10^5$ y for $^{79}$Se and $2.3.10^5$ y for $^{126}$Sn) and potential environmental mobility and biological roles.

In fact, stable Se is a micronutrient and plays fundamental roles in major metabolic pathways including hormone metabolism, antioxidant defence, and Hg-triggered detoxifying mechanisms, especially in aquatic organisms (Cuvin-Aralar and Furness 1991; Zeng 2009). Stable Sn is required in very small quantities for organism welfare (Eichenberger 1986). Accordingly, organisms exposed to Se and Sn radionuclides can also show non-negligible uptake levels of radioactive Se and Sn at different levels of the trophic chain (Konovalenko et al. 2014). To date, little is known about the environmental behaviour and dispersion of Se and Sn radionuclides in aquatic environments, particularly in continent-ocean transition systems with highly dynamic salinity and turbidity gradients.

The aim of this study is to understand the water-particle distribution of inorganic Se and Sn in contrasting salinity and turbidity conditions as observed in the Gironde Estuary (hosting 2 NPPs) and the Rhône River (hosting 4 NPPs and one nuclear fuel reprocessing facility). The obtained results are then integrated in qualitative simple radionuclide dispersion scenarios anticipating potential accidental releases.

## 2. MATERIALS AND METHODS

### 2.1. Areas of study

The Gironde Estuary is a major continent-ocean transition system in Europe with an estuarine surface area of 635 $km^2$ at high tide and an associated watershed of 81,000 $km^2$ (Fig. 1a). It is geographically delimited by the confluence of two main rivers: the Garonne River (freshwater discharges from 302 $m^3$ $s^{-1}$ to 880 $m^3$ $s^{-1}$) and the Dordogne River (discharges from 119 $m^3$ $s^{-1}$ to 477 $m^3$ $s^{-1}$; 1959 – 2017, DIREN). The semidiurnal tidal cycle of 12h 25min extends the marine influence to the limit of the

dynamic tide at La Réole on the Garonne River (Fig. 1a). Average annual solid discharges of 2 – 4 Mt enter the Gironde Estuary (Castaing 1981; Schäfer et al. 2002). Average Suspended Particulate Matter (SPM) concentrations are ~100 mg $L^{-1}$ and the strong tidal hydrodynamics develop a Maximum Turbidity Zone (MTZ) of up to 6 Mt of SPM with SPM concentrations of >1000 mg $L^{-1}$ (Castaing 1981; Sottolichio and Castaing 1999). This MTZ is subjected to seasonal migrations between the estuary mouth and the fluvial estuary, upstream the city of Bordeaux (Sottolichio and Castaing 1999). Massive expulsion of the MTZ to the coastal area only occurs for specific hydrological conditions (i.e., high water discharge during several weeks and high tidal coefficient; Castaing and Allen 1981; Doxaran et al. 2009). Coastal dispersion through the estuarine plume shows two density layers (surface vs bottom), which can settle off the Gironde Estuary mouth and/or be transported north-westwards or southwards according to the seasonal coastal currents (Froidefond et al. 1998; Jouanneau et al. 1999). In the Gironde Estuary, water residence times vary from ~18 days during high discharge conditions to 86 days in low discharge conditions, whereas average residence time of SPM is 1-2 years (Castaing and Jouanneau 1979; Jouanneau and Latouche 1981).

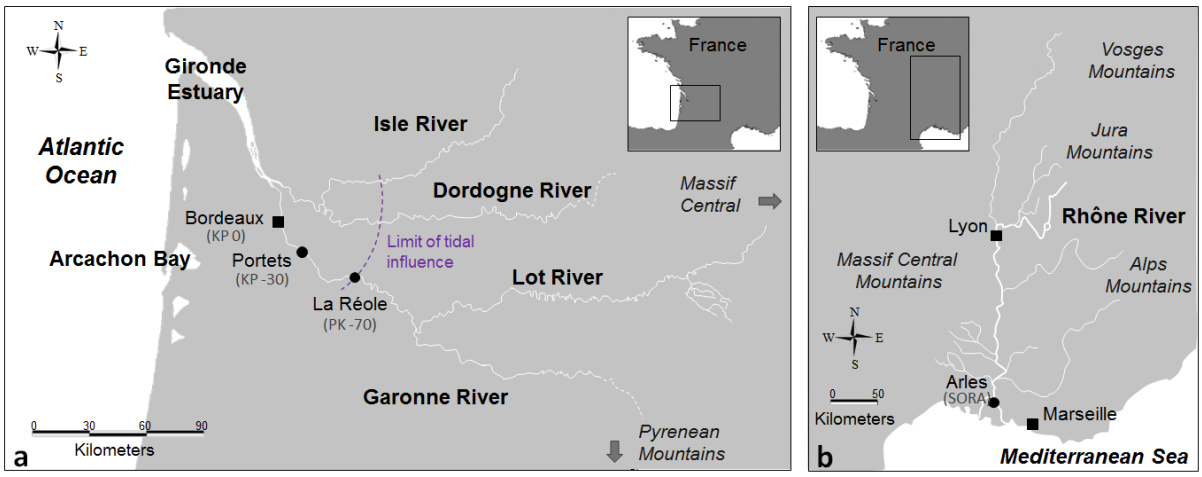


**Fig. 1.** Map of (a) the Lot-Garonne-Gironde fluvial-estuarine system and (b) the Rhône River. Main cities (squares), sampling sites (circles), rivers and kilometric points (PK) are also shown.

The Rhône River is one of the largest rivers in Europe (i.e., 816 km long, Fig. 1b) and since 1968 (i.e., construction of the Aswan dam in the River Nile; Ollivier et al. 2010) the main fluvial system contributing freshwater to the Mediterranean Sea. Its watershed of 98,800 $km^2$ provides an average freshwater discharge of 1700 $m^3$ $s^{-1}$ (i.e., at Beaucaire, 60.5 km from the river mouth) and the contained nutrients support 20-70% of the coastal primary production of the west Mediterranean Sea (Lefevre et al. 1997; Ludwig et al. 2009). Annual solid discharges vary from 2 – 20 Mt (average 4.6 Mt $y^{-1}$), of which 70% during flood events (Pont 1997; Pont et al. 2002; Marion et al. 2010). Nevertheless, the average SPM concentrations range 10-50 mg $L^{-1}$ (Periáñez 2005) and particle transport in general is highly influenced by 66 dams constructed along its course (Ollivier et al. 2010). At 50 km from the river mouth, the river splits into two branches, forming "le Grand Rhône" (52 km long, draining 85% of the water discharge during floods) and "le Petit Rhône" (60 km long; Ollivier et al. 2010). At the shore, a

complex intrusion process takes place as the freshwater flows into the marine waters in the absence of tidal influence. Flocculation and aggregation of particles form a prodelta (i.e., fine-grained deposits and sand bars; Aloisi and Monaco 1975) with average sediment accumulation velocities of 20-50 cm $y^{-1}$, subjected to physical resuspension events (i.e., mainly by storms, waves and winds; Marion et al. 2010). The associated suspended plume (e.g., ~30 mg $L^{-1}$ SPM) shows a 1-2 m thickness and seasonal, well-defined freshwater-seawater stratification of 10-20 units of difference with surrounding seawater, extending up to 20-30 km offshore (Broche et al. 1998). This plume is initially oriented in a southeast direction but soon rotates westwards moving along the Mediterranean coast due to Coriolis acceleration (Periáñez 2005).

### 2.2. Sample collection

Freshwater from the Garonne River and seawater from the Arcachon Bay, were filtered through 0.45 µm Teflon filters (FHLC, Merck Millipore Ltd.) and stored at 4ºC. Wet sediments from the Garonne River banks were collected manually during low-tide at Portets, ~30km upstream from Bordeaux (Fig.1a). Wet sediments from the Rhône River were collected at the SORA station (Station Observatoire du Rhône en Arles, ~40 km upstream le Grand Rhône) by the IRSN (Institut de Radioprotection et de Sûreté Nucléaire, Cadarache) with active, continuous pumping from a floating arm at ~50 cm below the water surface (Masson et al. 2018). Water content of wet sediments was evaluated, before preparing the experimental slurries, by comparing the masses of precise volumes of wet and dry sediment aliquots.

### 2.3. Sediment characterisation

Major sample mineralogy (>5 wt.%) of sediments from sites was determined from un-oriented oven-dried (50°C) sediment powder characterised by X-Ray Diffraction (XRD Bruker D8 DISCOVER, AGW-KIT, Germany) using Cu Kα radiation (40 mV/40mA Cu tube X-ray beam). Diffractograms were recorded with an angular range from 2º to 82º 2θ with step width 0.02º and counting time of 0.4 s/step. Results were compared to international peak lists of minerals (Crystallography Open Database QualX and the Crystal Structure Data Base for Minerals WWW-MinCryst) to identify major mineralogical composition. Further identification of clay minerals was performed from sediment aliquots following a texture identification protocol and obtaining diffractograms at angular range from 2º to 22º 2θ (Eiche et al. unpublished). Briefly, "unconditioned" sediment samples were put in slurry with an ammonia solution, dispersed in an ultrasound bath for 15 min, gravimetrically separated (1h) and left to dry onto glass platelets for analyses. In parallel, aliquot samples were swollen at 60ºC for 24h in ethylene glycol vapour atmosphere and, sample aliquots from the latter were further burned at 550ºC for 3h (muffle oven).

## 2.4. Experimental design

Radionuclide solutions of $^{113}Sn$ ($SnCl_4$ in 6M HCl, >99% purity, Eckert & Ziegler) and $^{75}Se$ ($H_2SeO_3$ in 0.1M HCl, >99% purity, Eckert & Ziegler) were diluted, independently, in freshwater and seawater matrices several weeks before the experiments in order to homogenise/stabilise the radionuclides. The high acidity from $^{113}Sn$ was corrected with NaOH solution (1M, Merck®) and $^{75}Se$ was oxidised to Se(VI) with $H_2O_2$ (30% Merck®). Batch experiment slurries were prepared by mixing wet bulk sediments from the Gironde Estuary and the Rhône River with filtered water from the Garonne River (S=0) and the Arcachon Bay (S=32), simulating three different SPM concentrations: 10 mg $L^{-1}$, 100 mg $L^{-1}$, and 1000 mg $L^{-1}$. The number of sample replicates was N=5 for 10 mg $L^{-1}$, N=6 for 100 mg $L^{-1}$ and N=3 for 1000 mg $L^{-1}$.

Adsorption kinetics started when the standard solutions of $^{113}Sn$ (nominal 1000 Bq $mL^{-1}$, equivalent to ~3 ng $L^{-1}$) and $^{75}Se$ (nominal 100 Bq $mL^{-1}$, equivalent to ~0.3 ng $L^{-1}$) were added, together, into the slurries of 30 mL. Aliquots were sampled at 0h, 2h, 4h, 6h, 24h and 48h. Experimental blanks, i.e., spiked freshwater and seawater with no sediments, were also followed over time to verify adsorption onto reactor walls. Desorption experiments were performed with the slurry samples containing 100 mg $L^{-1}$ of sediments, after centrifugation and emptying the initial water content. Out of the 6 replicates, three were desorbed in unspiked freshwater and the other three in unspiked seawater for 48h, sampling at 0h, 2h, 4h, 24h and 48h. This means that sediments that were previously exposed to $^{75}Se/^{113}Sn$ adsorption in freshwater conditions were desorbed in clean freshwater (N=3) and seawater (N=3). The similar treatment was applied to samples previously exposed to $^{75}Se/^{113}Sn$ in seawater. The potential contribution of radionuclide desorption from the tube walls during the desorption experiments was also checked under the same experimental conditions from the blank tubes.

Batch experiments were performed in acid-washed 50 mL polypropylene (PP) tubes with sporadic manual shaking at room temperature (~28ºC) and neutral pH (7.0-7.2). Sampling consisted of collecting 1.5 mL of homogeneous samples at each sampling time, followed by centrifugation at 4000-6000 rpm during 20 min for SPM-liquid separation. Supernatant water was then recovered with a 1 mL pipette and stored in 10 mL light-density polyethylene (LDPE) Kautex™ gamma vials with 9 mL HCl 2% (Merck®, to avoid Sn precipitation in $HNO_3$; Weber 1985) for analysis.

## 2.5. Radiotracer gamma analyses

Both $^{75}Se$ and $^{113}Sn$ activities were analysed in the initial matrices (experimental background levels) and in the experimental batch kinetic samples using a High Purity Germanium detector (HPGe, ORTEC®, INE-KIT, Germany). The activity of $^{75}Se$ was directly measured with the 264.7 keV energy line, whereas that of $^{113}Sn$ was measured indirectly from its daughter isotope, $^{113m}In$, at the 391.7 keV line. The gamma detector was calibrated with a certified Multinuclide Standard Solution (2M HCl, Eckert & Ziegler) and showed detection limits of 0.03 Bq $mL^{-1}$. All gamma results were mathematically

corrected to a unique date to overcome the decrease in signal related to radionuclide decaying (i.e., half-lives of 120 d for $^{75}$Se and 115 d for $^{113}$Sn).

## 3. RESULTS

### 3.1. Bulk sediment mineralogy

Diffractograms have been normalised to quartz signal to compare both sediment types (Fig. 2). Results showed the presence of both feldspar minerals (mainly anorthite and orthoclase) and a wide variety of phyllosilicates (i.e., kaolinite, chlorite, illite, montmorillonite/smectite, muscovite and vermiculite). Clay minerals such as kaolinite, illite, micas (biotite/muscovite), chlorite, smectites (montmorillonite) and vermiculite were readily observed in the texturised preparations (Supplementary materials, Fig. S1). Kaolinite and chlorite signals were present in both sediments (seldom overlapping), whereas the montmorillonite/smectite content is clearly higher in the Gironde system (i.e., the proportion of swelling montmorillonite with ethylene glycol treatment in the Rhône River sediment is negligible). Interestingly, some oxides are also identified in the XRD patterns (i.e., spinel group minerals, Fig. 2), from which Fe and Mn oxi(hydr)oxides (with variable crystalline degrees) seem to be relatively more abundant in the Garonne/Gironde system.

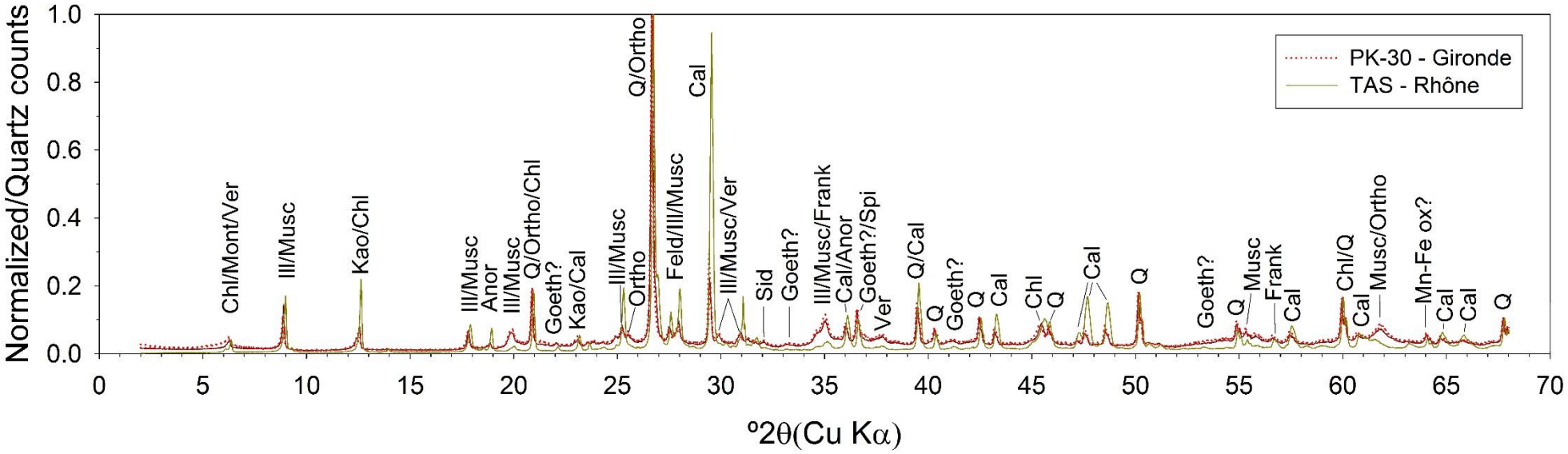


**Fig. 2.** XRD patterns from bulk samples in the Gironde Estuary (PK-30) and Rhône River (TAS). Abbreviations: **Anor** = Anorthite (tectosilicate, $CaAl_2Si_2O_8$); **Cal** = Calcite (carbonate, $CaCO_3$); **Chl** = Chlorite (Fe(II) containing silicate, $(Fe,Mg,Al)_6(Si,Al)_4O_{10}(OH)_8$); **Feld** = Feldspar (tectosilicate, $(K,Na)AlSi_3O_8$ – $CaAl_2Si_2O_8$); **Frank** = Franklinite (oxide from spinel group, $ZnFe_2O_4$); **Goeth** = Goethite (oxide, α-FeOOH); **Ill** = Illite (phyllosilicate, $(K,H_3O)(Al,Mg,Fe)_2(Si,Al)_4O_{10}[(OH)_2,(H_2O)]$); **Kao** = Kaolinite (phyllosilicate, $Al_2Si_2O_5(OH)_4$); **Mont** = Montmorillonite (phyllosilicate $(½Ca,Na,)(Al,Mg,Fe)_4(Si,Al)_8O_{20}(OH)_4{\cdot}nH_2O$); **Musc** = Muscovite (phyllosilicate, $KAl_2(AlSi_3O_{10})(OH,F)_2$); **Ortho** = Orthoclase (tectosilicate, $KAlSi_3O_8$); **Q** = Quartz ($SiO_2$); **Sid** = Siderite (carbonate, $FeCO_3$); **Spi** = Spinel (oxide); **Ver** = Vermiculite (phyllosilicate, $(Mg,Ca)_{0,7}(Mg,Fe,Al)_6(Al,Si)_8O_{22}(OH)_4{\cdot}8H_2O$); **Mn-Fe ox** = less crystalline manganese and iron oxides.

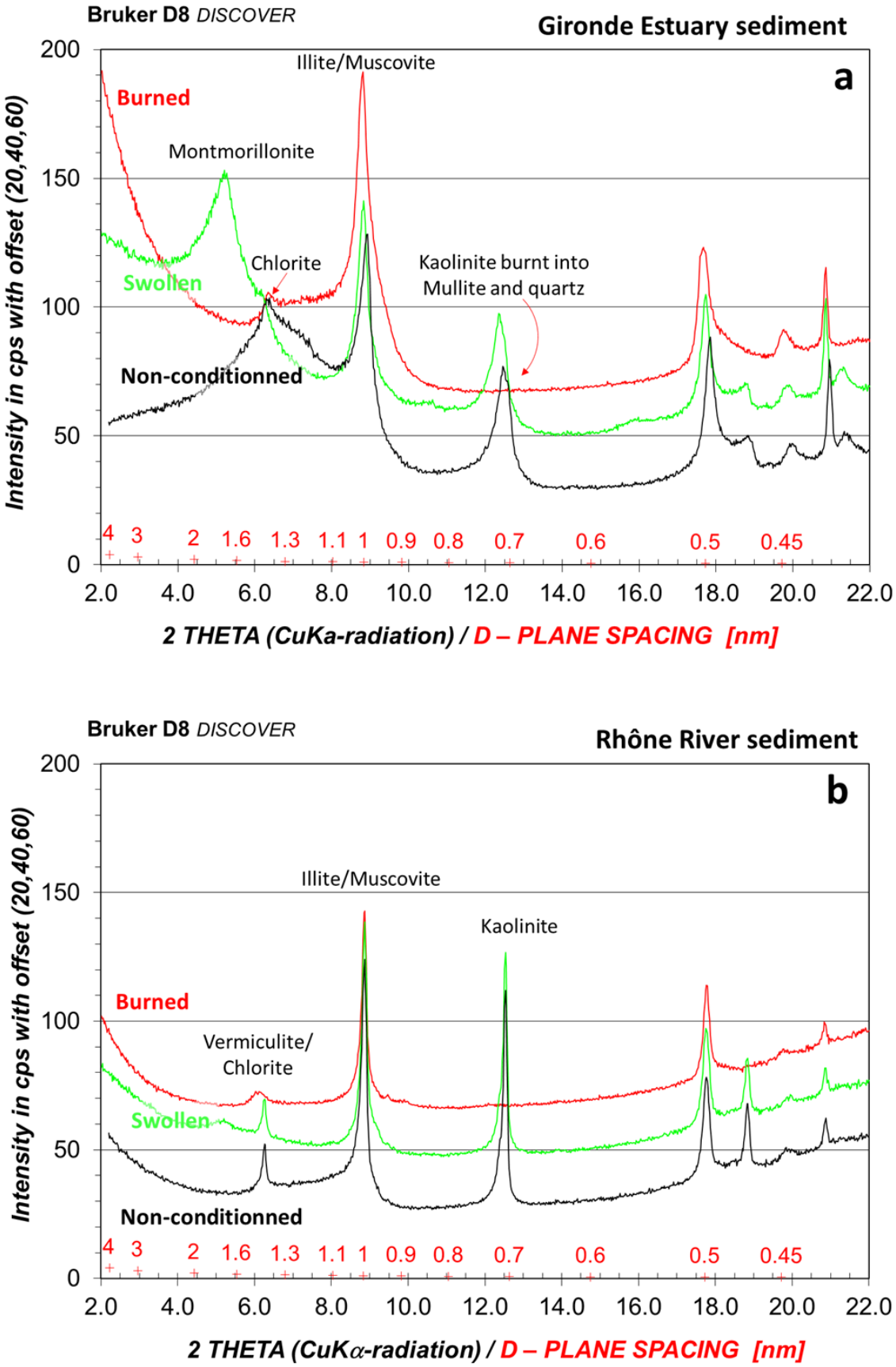


**Fig. S1.** Clay mineral diffractograms of (a) the Gironde Estuary and (b) the Rhône River sediments.

### 3.2. Adsorption kinetics

Natural radioactive background present in the Gironde Estuary and Rhône River sediment slurries contributed with activities of 0.30 Bq $mL^{-1}$ to the $^{113}Sn$ signals, but had no relevant impact on $^{75}Se$ activities. Experimental blanks suggest stable $^{75}Se$ concentrations along both, sorption and desorption experiments for all water matrices (Fig. 3a). However, blanks of $^{113}Sn$ showed 50-90% loss of Sn during the first 6h of the experiment, more important in freshwater than seawater matrices (Fig. 3b).

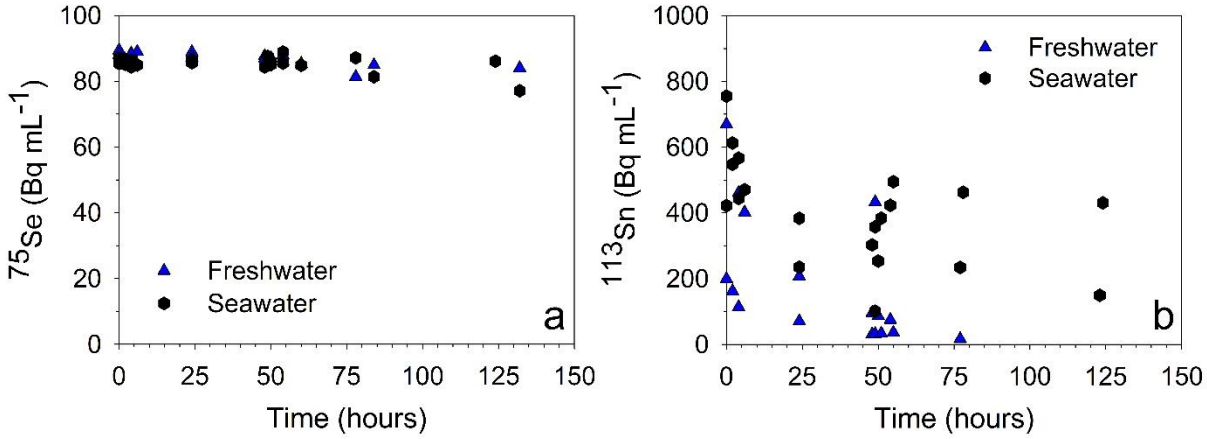


**Fig. 3.** Temporal distribution of (a) $^{75}Se$ and (b) $^{113}Sn$ experimental blank activities in freshwater (blue triangles) and seawater (blank hexagons) during sequential adsorption and desorption slurry kinetic experiments (~125h in total). Nominal spike concentrations were 100 Bq $mL^{-1}$ for $^{75}Se$ and 1000 Bq $mL^{-1}$ for $^{113}Sn$.

Results from the 48h Se kinetic adsorptions showed rather similar $^{75}Se$ activities in sample slurries and average blanks (Table 1). The resulting estimated Se adsorptions for both Gironde and Rhône sediment types were ± 5%, falling within the analytical error of the analyses. Estimated solid/liquid partitioning (Kd) for the 1000 mg $L^{-1}$ sediment conditions showed $\log_{10}$ Kd values <2 L $kg^{-1}$ for both freshwater and seawater matrices in Gironde and Rhône sediment types (Table 1).

Adsorption of $^{113}Sn$ in all sediment concentrations was fast, as average activities from the first 4-6h of the adsorption kinetics compared to average blank activities showed >85% adsorption for both sediments (Table 2). Adsorption percentages were calculated from dissolved $^{113}Sn$ activities obtained in each experimental slurry compared to 50% of the average activities found in the blanks (Table 2) in order to correct for the ~50% Sn loss attributed to precipitation in the first 6h of the experiment. The latter assumes that experimental conditions causing Sn precipitation are comparable between slurries and blanks. Estimated solid/liquid partitioning showed freshwater $\log_{10}$ Kd values ranging from 5.09 to 6.57 L $kg^{-1}$ and seawater $\log_{10}$ Kd values ranging from 4.6 to 6.2 L $kg^{-1}$ for both studied sediments.

**Table 1.** Average activities from the 48h kinetic experiments of $^{75}Se$ sorption in sediment slurries (10 mg $L^{-1}$, 100 mg $L^{-1}$, 1000 mg $L^{-1}$) with the Gironde Estuary and Rhône River sediments in freshwater and seawater matrices. Maximum solid/liquid partitioning (Kd) for 1000 mg $L^{-1}$ conditions are also shown.

| *Activities (Bq mL$^{-1}$)* | | **Gironde Estuary sediments** | | | **Rhône River sediments** | | |
|---|---|---|---|---|---|---|---|
| **Batch conditions:** | | **Average** | **SD** | **Adsorption** | **Average** | **SD** | **Adsorption** |
| Freshwater $^{75}Se$ | Blank | *88* | *2* | - | *88* | *1* | - |
| | 10 mg $L^{-1}$ | *87* | *2* | 2% | *90* | *1* | -2% |
| | 100 mg $L^{-1}$ | *87* | *0* | 2% | *91* | *2* | -4% |
| | 1000 mg $L^{-1}$ | *84* | *1* | 5% | *89* | *1* | -1% |
| | ***Max. $Log_{10}$ Kd*** | ***1.93*** | - | - | ***0.95*** | - | - |
| Seawater $^{75}Se$ | Blank | *86* | *1* | - | *85* | *1* | - |
| | 10 mg $L^{-1}$ | *87* | *2* | -1% | *87* | *0* | -2% |
| | 100 mg $L^{-1}$ | *86* | *0* | 0% | *87* | *0* | -3% |
| | 1000 mg $L^{-1}$ | *83* | *1* | 4% | *85* | *1* | 0% |
| | ***Max. $Log_{10}$ Kd*** | ***1.79*** | - | - | ***1.20*** | - | - |

**Table 2.** Average activities from the first 4-6h kinetic experiments of $^{113}Sn$ sorption in sediment slurries (10 mg $L^{-1}$, 100 mg $L^{-1}$, 1000 mg $L^{-1}$) with both sediments in freshwater and seawater matrices.

| *Activities (Bq mL$^{-1}$)* | | **Gironde Estuary sediments** | | | **Rhône River sediments** | | |
|---|---|---|---|---|---|---|---|
| **Batch conditions:** | | **Average** | **SD** | **Adsorption** | **Average** | **SD** | **Adsorption** |
| Freshwater $^{113}Sn$ | Blank | *511* | *115* | - | *157* | *43* | - |
| | 10 mg $L^{-1}$ | *7* | *1* | 97% | *13* | *9* | 83% |
| | 100 mg $L^{-1}$ | *19* | *11* | 93% | *3* | *0* | 97% |
| | 1000 mg $L^{-1}$ | *2* | *0* | 99% | *1* | *0* | 99% |
| Seawater $^{113}Sn$ | Blank | *601* | *103* | - | *471* | *55* | - |
| | 10 mg $L^{-1}$ | *43* | *15* | 86% | *15* | *7* | 94% |
| | 100 mg $L^{-1}$ | *24* | *6* | 92% | *12* | *9* | 95% |
| | 1000 mg $L^{-1}$ | *3* | *2* | 99% | *5* | *4* | 98% |

### 3.3. Desorption kinetics

Desorption tests of $^{113}Sn$ from blank tube walls in clean freshwater and seawater showed activities of ~60 Bq $mL^{-1}$, corresponding to <20% of the observed losses. Considering that the rest of the $^{113}Sn$ losses may be related to definitive Sn losses (either adsorption to container walls or precipitation), results from adsorption kinetics of $^{113}Sn$ obtained during the first 4-6 hours in all slurries were averaged and these average values were used for Kd estimates. Desorption experiments from the slurries could contain

leftover spiked water from the previous adsorption experiments, estimated to be <10% of $^{113}$Sn activities and <50% of $^{75}$Se activities measured during the desorption kinetics experiment.

Results show that $^{75}$Se desorption is sediment-dependent rather than salinity-dependent (Fig. 4a,b). In fact, desorption of $^{75}$Se from the Gironde Estuary sediments in all adsorption/desorption exposure conditions was almost constant i.e. very quick at the beginning of the experiment, corresponding to ~1.5 Bq mL$^{-1}$ (i.e., corresponding to <2% of the spiked $^{75}$Se, Fig. 4a,b). The Rhône River sediments showed lower $^{75}$Se desorption than Gironde Estuary sediments, with activities close to the expected contribution of the spiked solution from the previous adsorption conditions, left behind in the experiment tube and diluted with the clean water during desorption ("estimated residual"). However, the trend to increasing activities during the first 24h of desorption suggests slower desorption of $^{75}$Se from Rhône River sediments previously spiked in freshwater (Fig. 4a). Desorption of $^{75}$Se adsorbed during seawater exposure to the Rhône River sediments and desorbed in freshwater conditions showed two-fold greater recoveries (~2 Bq mL$^{-1}$, i.e., <2% of the spiked $^{75}$Se) than that of the same sediment in seawater conditions (Fig. 4b).

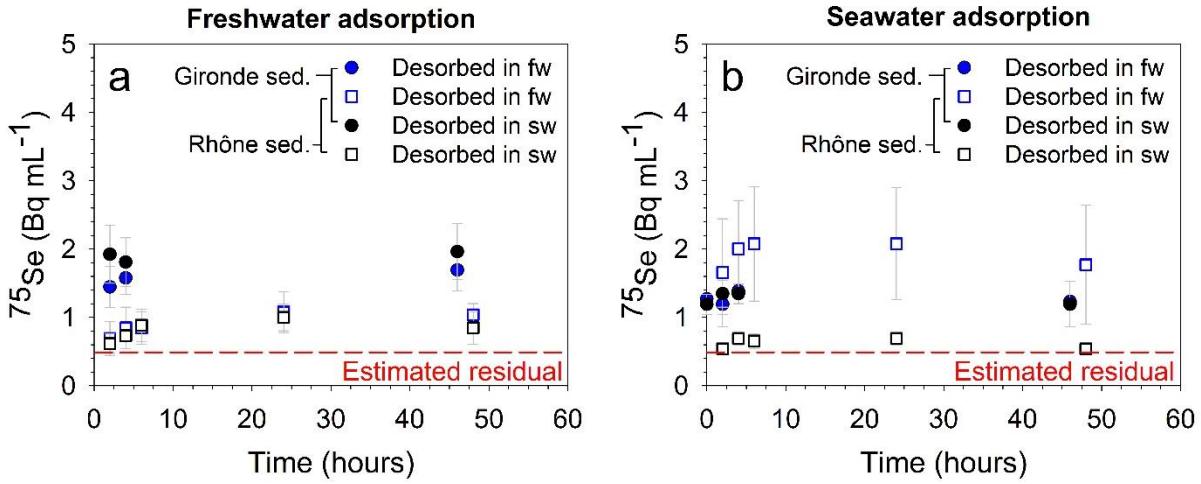


**Fig 4.** Desorption kinetics of $^{75}$Se in freshwater (blue) and seawater (black) conditions from Gironde Estuary (filled circles) and Rhône River (empty squares) sediments in (a) freshwater and (b) seawater conditions. Error bars correspond to standard deviations between replicates (N=3). The estimated contribution by left-over solution from previous adsorption experiment, potentially influencing $^{75}$Se activities during desorption (red dotted line), is also shown.

Desorption of $^{113}$Sn was both sediment-dependent and salinity-independent (Fig. 5). Except for some anomalous data, potentially related to Sn desorption from tube walls (Fig. 5a,c), $^{113}$Sn desorption from the Garonne River sediments was 5-10 Bq mL$^{-1}$, corresponding to 8-13% of the spiked $^{113}$Sn. Almost 10-fold lower $^{113}$Sn desorption was obtained from the Rhône sediments (Fig. 5b,d), desorbing <1% of the originally spiked $^{113}$Sn.

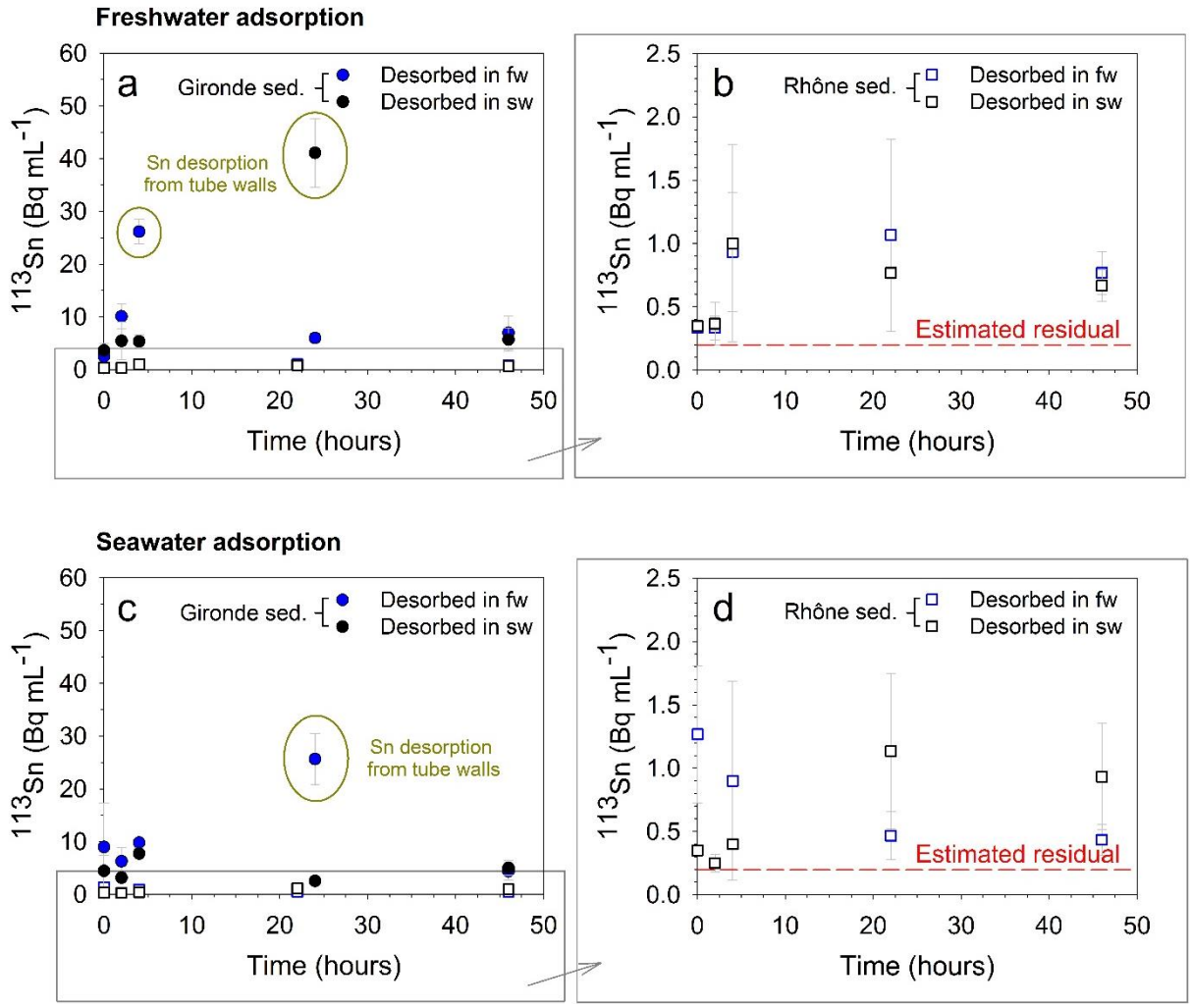


**Fig 5.** Desorption kinetics of $^{113}$Sn in freshwater (blue) and seawater (black) conditions from Gironde Estuary (filled circles) and Rhône River (empty squares) sediments in (a,b) freshwater and (c,d) seawater conditions. Error bars correspond to standard deviations between replicates (N=3). The estimated contribution from left-over solution from previous adsorption spiked water, potentially influencing $^{113}$Sn activities during desorption (red dotted line), is also shown.

## 4. DISCUSSION

### 4.1. Selenium estuarine reactivity

Radiotracer sorption kinetics of Se at ultra-trace levels (~0.3 ng L$^{-1}$) showed negligible adsorption, with estimated $\log_{10}$ Kd values <2 L kg$^{-1}$ for both the Gironde Estuary and Rhône River sediments. A similar study on Se adsorption kinetics performed with stable $^{77}$Se(VI) for the same Gironde Estuary sediments (i.e., 100 and 1000 mg L$^{-1}$) and contrasting water matrices at nominal concentrations of 100 µg L$^{-1}$ of Se showed $\log_{10}$ Kds of ~2.5 L kg$^{-1}$ in freshwater and of 2.6-2.8 L kg$^{-1}$ in seawater adsorptions (Gil-Díaz et al. unpublished/*Chapter 5*). These observations suggest that, in environmental conditions representative of the Gironde Estuary, $10^6$-fold variations in concentrations of dissolved Se induce changes of less than one order of magnitude in the $\log_{10}$ Kd values. Accordingly, Se may adsorb to sites

of low sorption energy even in the presence of very high dissolved Se concentrations. In fact, Se is a relatively soluble element in environmental compartments and can show an unreactive character in estuarine salinity and turbidity gradients (Seyler and Martin 1991). Total dissolved Se concentrations along estuarine salinity gradients mostly range from 0.04-2.00 μg $L^{-1}$ and show linear distributions, negatively-related with salinity (e.g., Measures and Burton 1978; van der Sloot et al. 1985; Cutter 1989; van den Berg et al. 1991; Seyler and Martin 1991; van den Berg 1993). Few studies report its non-conservative, generally seasonal, behaviour in estuarine systems, greatly related to biological activities (i.e., low-salinity or mid-estuarine maximum, e.g., Cutter 1989; Yao et al. 2006; Chang et al. 2016).

Initial environmental concentrations of Se in the water matrices used for this experimental work were 0.14 ± 0.03 μg $L^{-1}$ in freshwater and ~0.31 μg $L^{-1}$ for seawater (unpublished). Consequently, the $^{75}Se$ radiotracer spikes (~0.3 ng $L^{-1}$) to the water matrices were $10^3$-fold lower than environmental concentrations. The expected concentrations of potential Se radionuclide releases by hypothetical nuclear power plant accidents also would be orders of magnitude lower than environmental concentrations. For example, the Fukushima Dai-ichi accident discharged into the coastal environment $^{137}Cs$ activities ranging between 10 Bq $L^{-1}$ and 68 000 Bq $L^{-1}$ (i.e., equivalent to ~0.003 ng $L^{-1}$ and 20 ng $L^{-1}$; Buesseler et al. 2017). Although no such data exists for Se or Sn radionuclides, one may reasonably assume that the expected releases would be in the ultra-trace concentration levels. Accordingly, the results obtained from adsorption experiments suggest that dissolved Se radionuclides released into the Gironde Estuary or the Rhône River would mostly remain in solution within the estuarine reaches, independent from the turbidity and salinity gradients, continuously diluted with seawater during estuarine mixing, before reaching the coastal waters. The potential radiological risk associated to the beta and gamma emissions of dissolved Se radionuclides would depend on its potential bioavailability to aquatic organisms (i.e., Se biomethylation, Amoroux et al. 1997; nutrient-type behaviour; Measures and Burton 1980; Cutter and Cutter 1995).

### 4.2. Tin estuarine reactivity

Radiotracer sorption kinetics of Sn at ultra-trace levels (~3 ng $L^{-1}$) showed efficient adsorption of >86% of spiked Sn for both, the Gironde Estuary and the Rhône River sediments, generally increasing with sediment concentration. The applied spike concentration matches the orders of magnitude of environmental total dissolved Sn freshwater concentrations in the Garonne-Gironde fluvial-estuarine system (average 9.79 ± 0.97 ng $L^{-1}$ at La Réole, N~160, unpublished data), in other river systems (6 – 10 ng $L^{-1}$; Weber 1985; van den Berg et al. 1991), and in the Atlantic Ocean (0.36 – 3.56 ng $L^{-1}$; Byrd and Andreae 1982, 1986).

In this study, experimental distributions between the dissolved and particulate phases in the first 4-6h of contact produced preliminary $\log_{10}$ Kd values ranging from 4.8 to 6.6 L $kg^{-1}$. These values fall

within the range of natural $\log_{10}$ Kd values in the Garonne River at the La Reole site (average 6.2 L $kg^{-1}$; unpublished) and in the Gironde Estuary (4.8 to 6.2 L $kg^{-1}$; Pougnet 2018). These results suggest that field observations and laboratory experiments reflect similar Sn solid/liquid partitioning, with high Sn particle affinities widely independent from the salinity gradient. The few published studies report Sn conservative geochemical behaviour along estuarine salinity and turbidity gradients, despite the difficulties in evaluating dissolved inorganic Sn concentrations in the presence of higher-concentrated dissolved organo-tin species (Andreae et al. 1983; Byrd and Andreae 1986; van den Berg et al. 1981). Some studies report a non-conservative behaviour, proposing dissolution kinetics of atmospheric Sn-containing particles and estuarine scavenging as potential explanations to the deviation of the conservative trend (Andreae et al. 1983).

The differences in $^{113}$Sn desorption obtained between sediment types (Table 2, Fig. 5) suggest stronger adsorption of Sn onto Rhône River sediments than onto Gironde Estuary sediments. Duan et al. (2014) reported that ~90% of total Sn was present in the residual fraction of sediments from the Changjiang River Estuary. Preliminary parallel selective extractions applied to sediments from the Gironde Estuary and the River Rhône (Gil-Díaz et al. unpublished) confirm that Sn mainly belongs to the residual fraction (~86 and ~75%, respectively). Only 10-18% were extracted with the amorphous Fe/Mn oxides (i.e., ascorbate-fraction), and ~14% and ~25%, respectively occurred in the acid-soluble fraction (i.e., including phyllosilicates and sulphides, amorphous and crystalline Fe/Mn oxides and carbonates carrier phases; Huerta-Díaz and Morse 1990; Gasparon and Matschullat 2006). Tin mineral phases include sulphides, iron and calcium structures (*www.mindat.org*). Comparing results of XRD analyses for both sediments suggests (i) higher contents of carbonate minerals (i.e., especially calcite and siderite, Fig. 2), and (ii) potentially more abundant kaolinite and feldspar phases in the Rhône River (Fig. S1), coinciding with the higher acid-soluble Sn fraction in the former. Within the acid-soluble fraction, a main carrier phase could be related to Fe/Mn oxides (e.g., Dulnee et al. 2013), though little differences in Fe/Mn oxides can be withdrawn from the XRD results (Fig. 2). Accordingly, the stronger particle affinity of Sn incubated with Rhône River sediments may potentially be due to (i) preferential Sn adsorption to carbonate phases, or (ii) adsorption onto Fe/Mn oxide crystalline phases, presenting variable proportions between Garonne and Rhône River sediments. Nevertheless, the observed differences in adsorption and desorption behaviour of Sn also suggest different Kd values for both sediments, which should be accounted for when developing radionuclide dispersion scenarios.

The results on $^{113}$Sn adsorption and desorption kinetics suggest that, in the hypothetical case of a nuclear power plant accidental release to the aquatic environment, most of the Sn radionuclides may be rapidly adsorbed onto SPM and partly exported to the sediment, whatever the hydrological condition and related SPM concentrations. Accordingly, Sn radionuclide fate will directly depend on sediment dispersion and storage, desorption experiments showed low Sn dissolution. This implies, that Sn radionuclide effects to biota will be mostly linked to the bioaccessibility of particulate Sn. In the Rhône River the fate of Sn radionuclides would mainly depend on the site of emission and the downstream

morphology of the river (e.g. storage structures favour sedimentation) and hydrology (floods may favour transport to the Mediterranean). Radionuclide dispersion between the prodelta and the adjacent shelf are currently being assessed by numerical modelling approaches (Estournel et al. unpublished). Long Sn half-lives implying long environmental persistence of Sn radionuclides, together with long particle residence times (1-2 years or more) in the Gironde Estuary and the upstream migration of the MTZ towards the city of Bordeaux during Summer must be considered, when developing Sn radionuclide dispersion and radioprotection scenarios in the Gironde Estuary.

## 5. CONCLUSION

The present work is the first to address the biogeochemical behaviour of Se and Sn simulating contrasting salinity and turbidity conditions as they may occur in the river-sea continuum of the Garonne-Gironde fluvial-estuarine system and the Rhône River. The experimentally determined solid-liquid partitioning, expressed by Kd values are a prerequisite for the conceptual development of dispersion scenarios and management strategies anticipating potential accidental radionuclide releases. Different series of sorption experiments with stable and radioactive isotopes suggest that laboratory-Kd values of soluble elements such as Se may vary with the spiked concentrations, but elements presenting high particulate affinities (e.g. Sn) may show more independent, constant solid/liquid partitioning. Further work on Kd values under contrasting environmental conditions (including salinity, turbidity and redox conditions) is needed to develop precise models of radionuclide dispersion in aquatic systems.

The observed dominance of the dissolved fraction in Se radionuclide partitioning, independent from salinity and even in highly turbid conditions (>1000 mg $L^{-1}$) as those in the Gironde Estuary, clearly suggests that Se radionuclide dispersion would follow water transport towards the sea and that interactions with or uptake by living organisms should be foreseen. Contrastingly, Sn radionuclide releases would rapidly and widely irreversibly enter the particulate phase in both systems, independent from their respective sediment loads, and then follow the respective sediment dynamics. Sediment dynamics in the Gironde Estuary imply Sn radionuclide retention within the estuary, potentially during several years, and upstream migration into the reaches of the Bordeaux agglomeration during the dry seasons. Potential expulsion to the coastal ocean would depend on combined effects of seasonal freshwater discharges and tidal cycles. The scenario for the Rhône River suggests that Sn radionuclide dispersion will depend on the site of potential release, and implies possible retention of Sn radionuclides in reservoir sediments, discharge-related transport to the Mediterranean coast. Low reactivity and desorption efficiency suggest that transport and persistence of Sn radionuclides along the pro-delta and continental shelf in the Gulf of Lions may involve various sedimentation/erosion cycles.

## ACKNOWLEDGEMENTS

This study is a scientific contribution to the French National Project AMORAD (ANR-11-RSNR-0002) from the National Research Agency, allocated in the framework programme "Investments for the Future". This study was partially funded by the AMORAD Project (ANR-11-RSNR-0002). The authors gratefully acknowledge Franck Gîner from the IRSN in Cadarache for providing wet sediments from the SORA station in the Rhône River, Beate Oetzel from AGW-KIT for the XRD analyses, Christian Marquardt from INE-KIT for buying the radioactive standard solutions, and Markus Lenz from FHNW for quantifying environmental concentrations of dissolved Se in freshwater samples from La Réole. We also acknowledge the access to the INE-KIT controlled area to perform the radiotracer experiments.

## REFERENCES

Abe, Y., Iizawa, Y., Terada, Y., Adachi, K., Igarashi, Y., Nakai, I. (2014). Detection of uranium and chemical state analysis of individual radioactive microparticles emitted from the Fukushima nuclear accident using multiple synchrotron radiation X-ray analyses. Analytical Chemistry, 86(17), 8521-8525.

Aloisi, J. C., Monaco, A. (1975). La sédimentation infralittorale. Les prodeltas nord-méditerranéens. Comptes Rendus Académie Science Paris, 280, 2833-2836.

Amouroux, D., Donard, O. F. (1997). Evasion of selenium to the atmosphere via biomethylation processes in the Gironde estuary, France. Marine Chemistry, 58(1-2), 173-188.

Andreae, M. O., Byrd, J. T., Froehlich, P. N. (1983). Arsenic, antimony, germanium, and tin in the Tejo Estuary, Portugal: modeling a polluted estuary. Environmental Science and Technology, 17(12), 731-737.

Asai, S., Hanzawa, Y., Okumura, K., Shinohara, N., Inagawa, J., Hotoku, S., Suzuki, K., Kaneko, S. (2011). Determination of 79Se and 135Cs in spent nuclear fuel for inventory estimation of high-level radioactive wastes. Journal of Nuclear Science and Technology, 48(5), 851-854.

Asai, S., Toshimitsu, M., Hanzawa, Y., Suzuki, H., Shinohara, N., Inagawa, J., Okumura, K., Hotoku, S., Kimura, T., Suzuki, K., Kaneko, S. (2013). Isotope dilution inductively coupled plasma mass spectrometry for determination of 126Sn content in spent nuclear fuel sample. Journal of Nuclear Science and Technology, 50(6), 556-562.

Buesseler, K., Dai, M., Aoyama, M., Benitez-Nelson, C., Charmasson, S., Higley, K., et al. (2017). Fukushima Daiichi–derived radionuclides in the ocean: transport, fate, and impacts. Annual Review of Marine Science, 9, 173-203.

Byrd, J. T., Andreae, M. O. (1982). Tin and methyltin species in seawater: concentrations and fluxes. Science, 218(4572), 565-569.

Byrd, J. T., Andreae, M. O. (1986). Geochemistry of tin in rivers and estuaries. Geochimica et Cosmochimica Acta, 50(5), 835-845.

Castaing, P. (1981). Le transfert à l'océan des suspensions estuariennes: cas de la Gironde (Vol. 12). Original typescript.

Castaing, P., Allen, G. P. (1981). Mechanisms controlling seaward escape of suspended sediment from the Gironde: a macrotidal estuary in France. Marine Geology, 40(1-2), 101-118.

Castaing, P., Jouanneau, J. M. (1979). Temps de résidence des eaux et des suspensions dans l'estuaire de la Gironde. Journal Recherche Océanographie IV, 41-52.

Chang, Y., Zhang, J., Qu, J., Zhang, G., Zhang, A., Zhang, R. (2016). The behavior of dissolved inorganic selenium in the Changjiang Estuary. Journal of Marine Systems, 154, 110-121.

Cutter, G. A., Cutter, L. S. (1995). Behavior of dissolved antimony, arsenic, and selenium in the Atlantic Ocean. Marine Chemistry, 49(4), 295-306.

Cuvin-Aralar, M. L. A., Furness, R. W. (1991). Mercury and selenium interaction: a review. Ecotoxicology and Environmental Safety, 21(3), 348-364.

DIREN - National Hydrographic Databank (2015). Ministère de l'Écologie, du Développement Durable et de l'Énergie. <http://www.hydro.eaufrance.fr/> Last accessed on the 19/06/18.

Doxaran, D., Froidefond, J. M., Castaing, P., Babin, M. (2009). Dynamics of the turbidity maximum zone in a macrotidal estuary (the Gironde, France): Observations from field and MODIS satellite data. Estuarine, Coastal and Shelf Science, 81(3), 321-332.

Duan, L. Q., Song, J. M., Yuan, H. M., Li, X. G., Li, N., Ma, J. K. (2014). Distribution, chemical speciation and source of trace elements in surface sediments of the Changjiang Estuary. Environmental Earth Sciences, 72(8), 3193-3204.

Dulnee, S., Banerjee, D., Merkel, B. J., Scheinost, A. C. (2013). Surface complexation and oxidation of SnII by nanomagnetite. Environmental Science and Technology, 47(22), 12852-12859.

Eichenberger, E. (1986). The interrelation between essentiality and toxicity of metals in the aquatic ecosystem. Metal Ions in Biological Systems, 20, 67-100.

Froidefond, J.M., Jegou, A.M., Hermida, J., Lazure, P., Castaing, P. (1998). Variability of the Gironde turbid plume by remote sensing, effects of climatic factors. Oceanologica Acta, 21(2), 191-207.

Gasparon, M., Matschullat, J. (2006). Trace metals in Antarctic ecosystems: results from the Larsemann Hills, East Antarctica. Applied Geochemistry, 21(9), 1593-1612.

Huerta-Diaz, M. A., Morse, J. W. (1990). A quantitative method for determination of trace metal concentrations in sedimentary pyrite. Marine Chemistry, 29, 119-144.

Jouanneau, J. M., Latouche, C. (1981). The Gironde Estuary. Contributions to Sedimentology, 10.

Jouanneau, J.M., Weber, O., Cremer, M., Castaing, P. (1999). Fine-grained sediment budget on the continental margin of the Bay of Biscay. Deep-Sea Research Part II: Topical Studies in Oceanography, 46(10), 2205-2220

Ludwig, W., Dumont, E., Meybeck, M., Heussner, S. (2009). River discharges of water and nutrients to the Mediterranean and Black Sea: major drivers for ecosystem changes during past and future decades?. Progress in Oceanography, 80(3), 199-217.

Marion, C., Dufois, F., Arnaud, M., Vella, C. (2010). In situ record of sedimentary processes near the Rhône River mouth during winter events (Gulf of Lions, Mediterranean Sea). Continental Shelf Research, 30(9), 1095-1107.

Measures, C. I., Burton, J. D. (1978). Behaviour and speciation of dissolved selenium in estuarine waters. Nature, 273(5660), 293.

Measures, C. I., Burton, J. D. (1980). The vertical distribution and oxidation states of dissolved selenium in the northeast Atlantic Ocean and their relationship to biological processes. Earth and Planetary Science Letters, 46(3), 385-396.

Minas, M., Minas, H. J. (1989). Primary production in the Gulf of Lions with considerations to the Rhone River inputs. Water Pollution Research Reports, 13, 112-125.

Morewitz, H. A. (1981). Fission product and aerosol behavior following degraded core accidents. Nuclear Technology, 53(2), 120-134.

Ollivier, P., Hamelin, B., Radakovitch, O. (2010). Seasonal variations of physical and chemical erosion: A three-year survey of the Rhone River (France). Geochimica et Cosmochimica Acta, 74(3), 907-927.

Pont D. (1997) Les débits solides du Rhône à proximité de son embouchure : données récentes (1994–1995). Revue de Géographie de Lyon, 72, 23–33.

Pont, D., Simonnet, J. P., Walter, A. V. (2002). Medium-term changes in suspended sediment delivery to the ocean: consequences of catchment heterogeneity and river management (Rhône River, France). Estuarine, Coastal and Shelf Science, 54(1), 1-18.

Pougnet, F. (2018). Etat de la qualité des eaux de l'estuaire de la Gironde: cas du cadmium et des butylétains (Doctoral dissertation, Université de Bordeaux).

Schäfer, J., Blanc, G., Lapaquellerie, Y., Maillet, N., Maneux, E., Etcheber, H. (2002). Ten-year observation of the Gironde tributary fluvial system: fluxes of suspended matter, particulate organic carbon and cadmium. Marine Chemistry, 79(3-4), 229-242.

Seyler, P., Martin, J. M. (1991). Arsenic and selenium in a pristine river-estuarine system: the Krka (Yugoslavia). Marine Chemistry, 34(1-2), 137-151.

Sottolichio, A., Castaing, P. (1999). A synthesis on seasonal dynamics of highly-concentrated structures in the Gironde estuary. Comptes Rendus de l'Académie des Sciences-Series IIA-Earth and Planetary Science, 329(11), 795-800.

van den Berg, C. M. G., Khan, S. H., Daly, P. J., Riley, J. P., Turner, D. R. (1991). An electrochemical study of Ni, Sb, Se, Sn, U and V in the estuary of the Tamar. Estuarine, Coastal and Shelf Science, 33(3), 309-322.

van den Berg, C. M. (1993). Complex formation and the chemistry of selected trace elements in estuaries. Estuaries, 16(3), 512-520.

van der Sloot, H. A., Hoede, D., Wijkstra, J., Duinker, J. C., Nolting, R. F. (1985). Anionic species of V, As, Se, Mo, Sb, Te and W in the Scheldt and Rhine estuaries and the Southern Bight (North Sea). Estuarine, Coastal and Shelf Science, 21(5), 633-651.

Weber, G. (1985). The importance of tin in the environment and its determination at trace levelsDie Bedeutung des Zinns in der Umwelt und seine Bestimmung im Spurenbereich. Fresenius' Zeitschrift für Analytische Chemie, 321(3), 217-224.

Yao, Q. Z., Zhang, J., Qin, X. G., Xiong, H., Dong, L. X. (2006). The behavior of selenium and arsenic in the Zhujiang (Pearl River) estuary, South China Sea. Estuarine, Coastal and Shelf Science, 67(1-2), 170-180.

## 2. Transfer of Sn and Se to wild living bivalves

### 2.1. Bioaccumulation in wild oysters and mussels

Given the dominance of the dissolved phase in Se partitioning and the higher particle affinity of Sn, the aim of this section is to study the potential transfer of these elements to bivalves in coastal systems. Total Sn and Se soft tissue contents in wild oysters from the Gironde Estuary mouth and the Arcachon Bay (Comprian site; ***Figure 72***) as well as in wild mussels from the Rhône River mouth were compared. Furthermore, data on Cs bioaccumulation is also provided in this context, given its importance after radionuclide nuclear power plant accidental releases to the environment (highly persistent and soluble in the estuary salinity gradient).

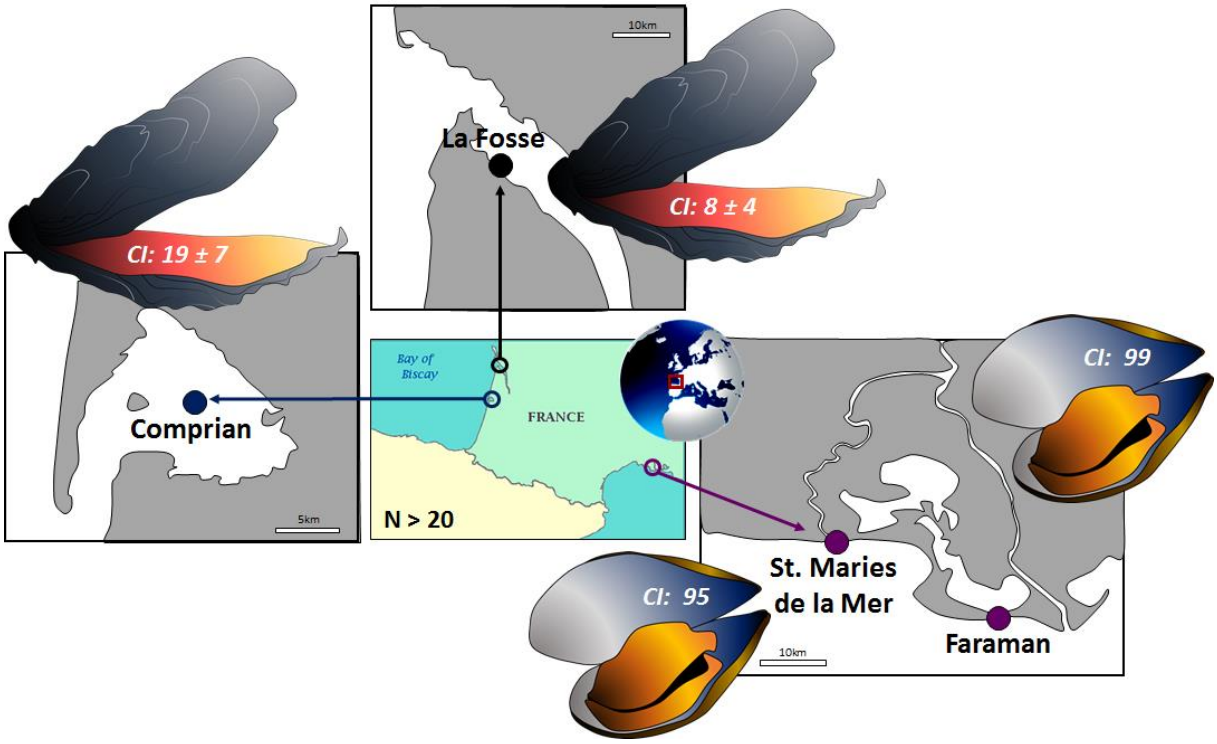


**Figure 72. Sampling sites used for comparison between Cs, Sn and Se bioaccumulation in wild organisms:** two sites in the Atlantic Ocean (La Fosse in the Gironde Estuary mouth and Comprian in the Arcachon Bay) and two sites in the Mediterranean Sea (St. Maries de la Mer in the "Petit" Rhône River mouth and Faraman in the "Grand" Rhône River mouth). Condition indexes (CI) are also given.

- *Sample collection and Condition Index*

Briefly, samples of wild oysters (N=20) were collected in April 2014 at the La Fosse site in the Gironde Estuary mouth and in April 2015 at the Comprian site in the Arcachon. Samples of wild mussels (N=80) from the Mediterranean Mussel Watch programme (MMW) were collected by the IRSN in March and May 2017 at the sites of St. Maries de la Mer and Faraman, then sent to the University of Bordeaux. Condition indexes (CI; ***Figure 72***) were calculated (***Equation 12***) (i.e., the proportion of soft tissue relative to the shell in mass; Lobel and Wright 1982) between comparative sites as a proxy of the organism's health status.

***Equation 12:***

$$CI = \frac{P_1 \cdot 1000}{P_2}$$

where, $P_1$ is the dry weight of the soft tissue (g), and $P_2$ is the dry shell weight (g), from Chávez-Villalba (2010).

- *Sample digestions and trace element analyses*

Freeze-dried, homogenised oyster tissues from La Fosse and Comprian, as well mussel tissues from St. Maries de la Mer and Faraman, were digested in closed plypropylene (PP) vessels with 1.4 mL $HNO_3$ (65% Suprapur® 14 M) and 2 mL HCl (30% Suprapur® 10 M) for 3 h at 90ºC in the hotplate (DigiPREP MS, SCP SCIENCE) and diluted with 13.6 mL of Milli Q® (Daskalakis et al. 1997; USEPA 2007).

Trace elements were analysed by external calibration with QQQ-ICP-MS (iCAP-TQ, THERMO®) using the KED-mode (He) for Cs and Sn and the $O_2$-mode for Se. Accuracies of parallel analyses of certified reference materials (CRM) used to verify the quality of the analysis (NIST 1643f, NCS DC 73307) and/or that of the digestion process (NIST 1566b) ranged between 91% and 116%, and recoveries were within the certified ranges (***Table 18***). Limits of detection (LOD) are also included in ***Table 18***.

**Table 18. Analytical performance of Cs, Sn and Se in dissolved (freshwater NIST 1643f) and particulate/biological (stream sediment NCS DC 73307 and oyster tissue NIST 1566b) certified reference materials (CRM).** Averages ± standard deviations (SD) are given for certified and measured values. Analytical limits of detection (LOD = 3·SD (n=10 blanks)).

| Element | NIST 1643f (µg $L^{-1}$) | | NCS DC 73307 (mg $kg^{-1}$) | | NIST 1566b (mg $kg^{-1}$) | | LOD (ng $L^{-1}$) |
|---|---|---|---|---|---|---|---|
| | Certified | Measured | Certified | Measured | Certified | Measured | |
| **Cs** | - | - | 5.10 ± 0.80 | 4.64 ± 0.14 | - | - | 0.12 |
| **Se** | 11.7 ± 0.1 | 11.4 ± 0.3 | 0.16 ± 0.03 | 0.15 ± 0.02 | 2.06 ± 0.15 | 2.16 ± 0.06 | 1.39 |
| **Sn** | - | - | - | - | 0.03 ± 0.01 | 0.03 ± 0.01 | 1.20 |
| ***Replica*** | ***N = 6*** | | ***N = 7*** | | ***N = 12*** | | ***N = 3*** |

- *Cs, Sn and Se soft tissue contents*

Results showed highest accumulations for Se (between 1100 – 4100 µg $kg^{-1}$ d.w.) and lower, relatively similar values for Cs and Sn (from 10 - 50 µg $kg^{-1}$ d.w., ***Table 19***) in both oysters and mussels. Systematically, oysters from La Fosse contained more trace elements than those of Comprian, with common Se/Sn ratios of 70-80 at both sites, whereas Se/Cs ratios differed from ~140 at La Fosse to ~210 at Comprian. Mussels in the Mediterranean coast showed relatively higher bioaccumulations of Cs and Sn in Faraman compared to St. Maries de la Mer (***Table 19***), with Se/Sn ratios of ~7 in Faraman and ~25 in St. Maries de la Mer, and Se/Cs ratios of ~76 in Faraman and ~51 in St. Maries de la Mer.

**Table 19. Total concentrations (µg $kg^{-1}$) of Cs, Sn and Se in wild oysters** (*Crassostrea gigas*, cf. *Magallana gigas*) from the La Fosse (Gironde Estuary mouth, N=20) and Comprian (Arcachon Bay, N=20) sites in the Atlantic coast, as well as wild mussels (*Mytilus galloprovincialis*) from the St. Maries de la Mer ("Petit" Rhône River mouth, N=80) and Faraman ("Grand" Rhône River mouth, N=80) sites in the Mediterranean coast. Errors correspond to standard deviations (SD).

| Coastline | | Site | Bivalve | Sampling date | Total soft tissue concentrations (µg $kg^{-1}$ d.w.) | | |
|---|---|---|---|---|---|---|---|
| | | | | | Cs | Sn | Se |
| Atlantic | | La Fosse | *C. gigas* | Apr. 2014 | 30.3 ± 31.7 | 49.5 ± 29.1 | 4160 ± 1380 |
| | | Comprian | *C. gigas* | Apr. 2015 | 7.46 ± 2.92 | 22.3 ± 10.5 | 1600 ± 650 |
| Mediterranean | | St. Maries de la Mer | *M. galloprovincialis* | Mar. 2017 | 15.5 ± 0.1 | 45.3 ± 30.3 | 1140 ± 170 |
| | | Faraman | *M. galloprovincialis* | Mar. 2017 | 21.6 ± 1.0 | 146 ± 117 | 1080 ± 30 |

- *Discussion on bioaccumulation of Sn, Se and Cs in oysters from the Atlantic coast (Gironde Estuary and Arcachon Bay) and mussels from the Mediterranean coast (St. Maries de la Mer and Faraman)*

Results on Cs, Sn and Se bioaccumulation in wild oysters and mussels provide a first insight into trace element differences and some potential site-dependent effects. Nevertheless, more samples covering more sites and longer periods would be needed to underpin specific site-dependent differences. From the data available, global trace element concentrations at all sites presented the following accumulation preferences: Se>Sn>Cs, which are higher than Te concentrations encountered in oysters from La Fosse (~2.08 µg $kg^{-1}$ d.w.; *Chapter 5*). Therefore, accidental releases of Se, Sn, Cs and Te radionuclides would be expected to show non-negligible bioaccumulations in wild bivalves,

especially for essential elements like Se and Sn, as well as for those mimicking metabolic pathways such as Cs (potassium channels, Bryan 1963). However, more information on radionuclide doses/activities and the biological half-lives of the different elements, required to eliminate them from the body, are necessary to reliably evaluate the corresponding radiological risk.

### 2.2. Organotropism in wild oysters from the Gironde Estuary

The aim of this approach is to understand the distribution of Cs, Sn and Se between biological organs as their accumulation can indicate storage or preferential uptake pathways, i.e., related to dissolved uptake through gills (direct pathway) or through ingestion of phytoplankton and particles (trophic pathway). Thus, a first evaluation of Cs, Sn and Se organotropism (i.e., gills, adductor muscle, mantle and digestive gland, ***Figure 73***) in five individuals from La Fosse (April 2014) was also performed. The organ samples (N = 5 for each organ) were pooled for the study to obtain sufficient sample masses. Otherwise, digestions and analyses were performed as aforementioned.

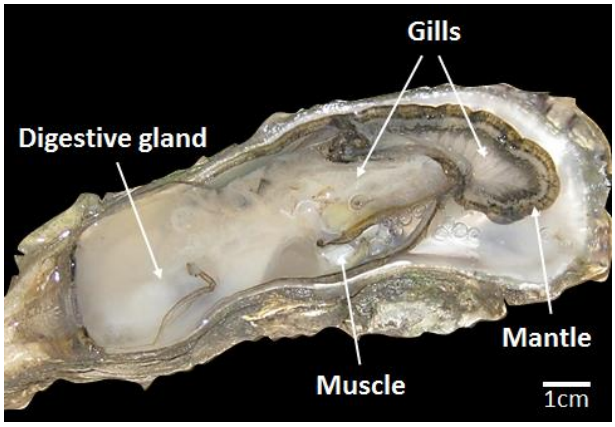


**Figure 73. Identification of oyster organs in a sample of *Crassostrea gigas*.**

Results showed highest accumulations of Se in the gills and the digestive gland, containing ~80% of total Se content in the whole soft tissue (***Figure 74***). In contrast, Sn and Cs accumulate to >50% in the mantle and ~30% in the digestive gland (***Figure 74***). In general, gills represent the fundamental interface for dissolved trace element uptake, whereas the digestive gland indicates uptake via particulate material and/or sequestration of trace elements in waste vesicles (lysosomes) as part of the detoxification and elimination mechanisms of xenobiotics (Marigómez et al. 2002). The presence of Se in the gills and the digestive gland is in accordance with its soluble nature and micronutrient character as it is likely accumulated in phytoplankton (explaining the trophic source). In contrast, Sn distribution between organs in wild oysters is different to that of Se, showing higher accumulation in the mantle and the digestive gland like Cs. The mantle is a storage organ for glycogen and lipids, but can also discard waste products from the haemolymph system or trace elements stored in lysosomes

(*https://www.nefsc.noaa.gov/*). This Sn distribution may suggest (i) the low influence of Sn accumulation through the direct pathway (gills) and potentially higher influence of the trophic pathway, and/or (ii) a fast redistribution between organs of Sn accumulation.

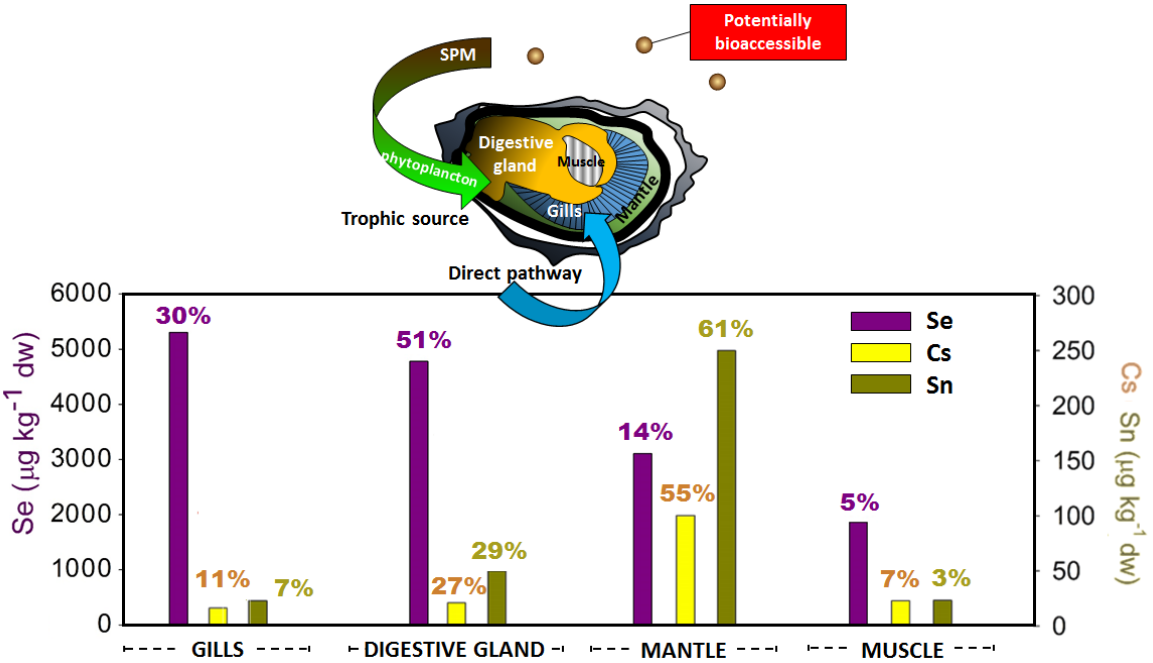


**Figure 74. Organotropism of Cs, Sn and Se.** Trace metal content in organs (gills, digestive gland, mantle and muscle) from a pool of wild oysters (N=5) from La Fosse (Gironde Estuary mouth, April 2014). Percentages indicate the relative contribution of each fraction to total metal content.

This organotropism approach provides a first insight on Se, Sn and Cs accumulation in wild oysters, suggesting differences between Se and Sn biological functions and common Sn and Cs accumulation. Complementary analyses (e.g. histopathological evindences) are required in order to better understand the biological distributions and roles of the studied elements.

## II. CONCLUSION

The outcomes of this chapter on contrasting trace element biogeochemical behaviours in the Garonne-Gironde fluvial-estuarine system and that of the Rhône River were as follows:

- Concentrations representative of environmental and radionuclide dissolved selenium (Se) discharges into contrasting salinity and turbidity environmental conditions suggest high mobility of Se related to a predominant transport in the dissolved phase. Bioaccumulation of Se (~1500 µg $kg^{-1}$ d.w.) in wild oysters and mussels of the Atlantic and Mediterranean coasts, particularly accumulating in gills and digestive glands, are in accordance with the essential character of Se in biological compartments and the potentially non-negligible influence of such dissolved discharges. The uptake of Se as a nutrient is probably regulated and active uptake may occur, specially for organic Se species.

- Sorption experiments using dissolved tin (Sn) concentrations representative of environmentally realistic levels under contrasting salinity and turbidity conditions as encountered in coastal systems suggest almost complete adsorption onto suspended particles, generally independent from the particle nature (Gironde vs Rhône sediments), particle concentrations (ranging from 10 mg $L^{-1}$ to 1000 mg $L^{-1}$) and salinity. Nevertheless, particulate Sn and/or the remaining low dissolved concentrations may be bioaccessible, because bioaccumulation of up to ~50 µg $kg^{-1}$ d.w) occurred in wild oysters and mussels of the Atlantic and Mediterranean coasts, particularly in storage organs such as the mantle. The contribution of organo-tin compounds to the total dissolved and tissue Sn concentrations remains unknown and should be investigated.

- A comparison between Gironde and Rhône fluvial-estuarine systems suggests relatively greater potential dissolution of adsorbed trace elements and radionuclides from the Gironde Estuary particles, given the higher Sn desorption after sediment exposure to clean freshwater and seawater. The higher Se and Sn bioaccumulation in Gironde Estuary oysters, compared to the wild oysters from the Arcachon Bay, despite comparable Sn/Se ratios, might reflect higher mobility/uptake and/or be related to dilution by growth in oysters from the Arcachon Bay.

- A comparison between field (i.e., natural) and laboratory (i.e., spiked) solid/liquid partitioning suggests comparable Kd values for highly particulate trace elements like Sn, though widely varying for more soluble elements like Se. These findings are relevant for the development of radionuclide dispersion scenarios in continent-ocean transition systems, as laboratory Kd are necessary for the understanding of the solid/liquid partitioning of spiked element (anthropogenic inputs) suggesting that such Kd values should be determined for concentration ranges that are realistic in view of potential discharges into the environment.

# DISCUSSION

# I. FUNDAMENTAL PARAMETERS FOR RADIONUCLIDE DISPERSION SCENARIOS

## 1. Inherited vs spiked solid/liquid partitioning (Kd)

Predictive models of radionuclide dispersion in aquatic environments require empirical information such as Kd values obtained from either field campaigns or from laboratory approaches. In fact, the IAEA (2004) summarises all known Kd values and other parameters, such as bioaccumulation factors in marine organisms, for many elements for radionuclide modelling purposes. Such is the concern on proper Kd determination that some models focus on estimating uncertainty- and sensitivity-based freshwater Kd using probability density functions (e.g., Ciffroy et al. 2009). Nevertheless, little is known about the similarities between field- and laboratory-based Kd values (Ciceri et al. 1988). In fact, field-based Kd values integrate inherited trace elements, including those in refractory mineral phases, whereas laboratory-based Kd values rather address solid/liquid partitioning of spiked elements (better simulating anthropogenic releases). Both values are generally assumed to be comparable (IAEA 2004), but may also differ as evidenced from some anthropogenic discharges and laboratory experiences, generally more soluble than the inherited element. Solid/liquid partitioning of stable and radioactive Cs and Sr (i.e., from global fallout and past nuclear tests in the atmosphere) in Japanese coastal waters suggests higher solubility of radioactive homologues (Uchida and Tagami 2017). Dumped nuclear wastes in the Arctic Seas also show a general high predominance of soluble radioactive elements (Fisher et al. 1999). Radionuclides from effluent waters of La Hague are easily transported by marine currents, i.e., not retained in coastal turbid waters (Salbu et al. 2003). Some experimentally determined Kd values for radioactive Cs and Fe were lower than respective field-Kd values (Ciceri et al. 1988) whereas the opposite was obtained for Co, Mn and Ag radionuclides, showing Kd values of several orders of magnitude higher than those obtained from field campaigns, attributed in this case to analytical errors during experimental conditions (Garnier-Laplace et al. 1997).

In this work, field observations provided inherited Kd values of Te and Sn in agreement with laboratory Kd values. In contrast, differences occurred for laboratory-based Se Kd values, showing variations of <1 order of magnitude of $\log_{10}$ Kd for spiked concentrations varying in $10^6$-fold (*Chapter 6*). Comparisons on Sb Kds in this regard were not addressed in this thesis, though Slowey et al. (1965) observed most of $^{125}$Sb in soluble form in the North Adriatic Sea and Strohal et al. (1975) quantified a small fixation rate of $^{125}$Sb radiotracer to inorganic particles in laboratory conditions. Nevertheless, $^{125}$Sb is also present in marine sediments (Tassi Pelati and Triulzi 1969), can be fixed into the particulate phase from $^{125}$Sb discharges from La Hague and Sellafield (Martin et al. 1994) or be transferred from radioactive debris to reactive natural particles (Robbins et al. 1992). Therefore, until now, radionuclide dispersion scenarios in the Garonne-Gironde fluvial estuarine system are based on field- and laboratory-based Kd values for Te and only field-based Kd behaviour for Sb. Dispersion scenarios of

accidental NPP discharges into the environment based on solid/liquid partitioning also must take into account complementary temporal aspects, including both radionuclide decays and the timescales of hydrological processes.

## 2. Temporal coupling between radionuclide decay time scales and hydrological processes

Hydrological processes are extremely important in determining the fate of radionuclide transport, as already foreseen for modelling of other radionuclides like $^{137}$Cs (Periáñez et al. 2016). In fact, previous chapters have shown the importance of seasonality on Sb and Te solid/liquid temporal partitioning in upstream watershed reaches in the Lot-Garonne River system as well as the relevance of hydrologically-controlled water and sediment dynamics, and residence times in the Gironde Estuary on Sb and Te estuarine particulate retention and transport. However, considering temporal scales of hydrological processes alone in radionuclide dispersion scenarios would overestimate the environmental fate of radionuclides in continent-ocean transition systems, as short-lived radionuclides may have already (at least partly) decayed within the timeframe of the hydrological process. Thus, dispersion scenarios of radionuclides in continent-ocean transition systems must take into account both temporal scales; those of hydrological processes and decay time series of the radionuclides of interest.

Temporal persistence of Sb and Te radionuclides after a hypothetical accidental release at time "t = 0" can be estimated from their fission yields and decay chains, as presented in ***Figure 13*** from Chapter 1. For this, one may assume the following:

- first order decay reactions for radioactive disintegration of individual radionuclides:

$$A \overset{k_A}{\rightarrow} B$$

$$\frac{dA}{dt} = -k_A \cdot [A]$$

*When* $[A] = [A_0]/2$, $t = t_{1/2}$, *thus:*

$$\frac{[A_0]}{2} = [A_0] \cdot e^{-k_A \cdot t_{1/2}}$$

$$-k_A \cdot t_{1/2} = \ln 1/2$$

$$k_A = \frac{\ln 2}{t_{1/2}}$$

- in a decay series, each radionuclide has incoming fluxes of atoms from parent radionuclides (when applicable) and outgoing fluxes of atoms due to natural decay through time. Therefore, the rate of change in concentration through time does not only depend on the initial

concentration and decay (half-lives) of the radioisotope itself but also on the concentration and decay rates of the parent radioisotopes. In the case of several elements, the equations would be:

$$A \overset{k_A}{\rightarrow} B \overset{k_B}{\rightarrow} C$$

$$\frac{dA}{dt} = -k_A \cdot [A]$$

$$\frac{dB}{dt} = k_A \cdot [A] - k_B \cdot [B]$$

$$\frac{dC}{dt} = k_B \cdot [B]$$

- initial concentrations are calculated as the product of the fission yields of each radioisotope and an estimated amount of $^{235}U$ atoms in a NPP fuel. This estimation can be relativised by expressing the produced or decayed atoms as a percentage of the initial $^{235}U$ concentration.
- the initial conditions (t = 0) correspond to the hypothetical, instantaneous release of radionuclides from a NPP point source, assuming that after this event there is no more production of radionuclides due to nuclear fission, only that coming from natural decay of parent radionuclides.
- all metastable forms are represented by 100% probability of occurrence.
- metastable forms appear only during decay reactions and not directly from the NPP fission reactions (no associated fission yield), thus, they are mathematically considered alike to the other radioisotopes in the model with a starting amount of atoms equal to zero.

Because the temporal units of half-lives range from ms to years, the chosen time step (Δt) to run the model has been adapted and allowed to vary accordingly through time so that the model converges and the radionuclide temporal resolution is appropriate. That is, the model starts with a small time step (6 min) so that the relevant fast decaying isotopes (t½ > 5 min) are well defined for the first hours after the NPP accident. The model progressively shifts to greater Δt (from 5h to 1000h for simulating the first year after the accident) as the t½ of the decaying elements increases. Such approximation results in successive radionuclide appearance and temporal persistence which may be compared with short-term hydrological processes at timescales relevant for tidal cycles and/or seasonal variability (***Figure 75***).

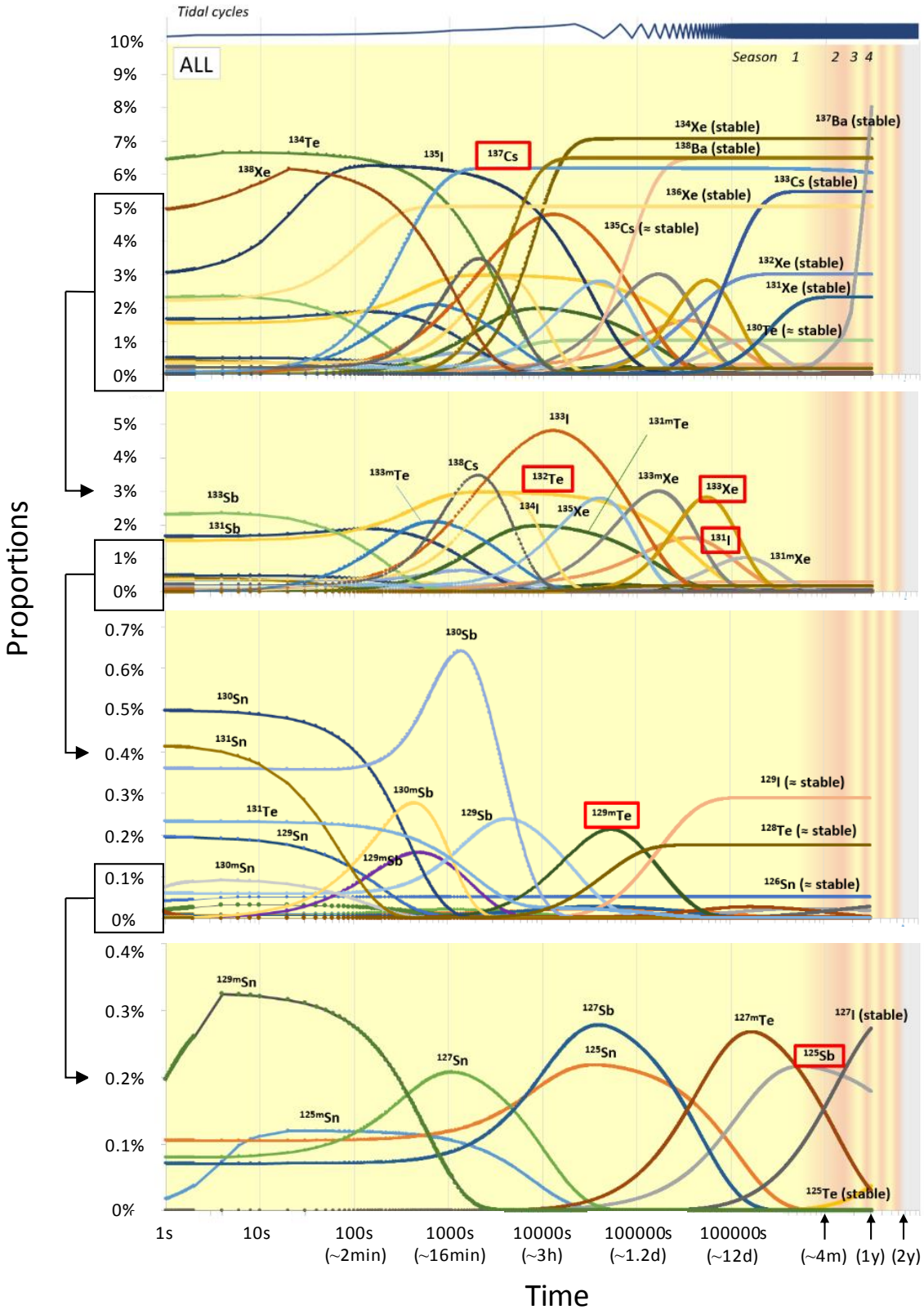


**Figure 75. Sb-Te radionuclide persistence after an instantaneous emission (t=0) up to ~1 year forecast from $^{235}$U in NPPs.** Each panel is a zoom of the lower scale of the previous graph. Radionuclides generally followed after NPP accidents are marked in red boxes. Hydrologically relevant time scales such as tidal semi-diurnal variability (top) or general 3-month seasonal variations (yellow-pink degraded background shading) are also shown.

This simulated succession of radionuclide decays represents the potential Sb and Te radionuclide environmental persistence after an instantaneous release at t = 0. In order to simulate more realistic NPP accidental releases, further parameters should be taken into account, mainly: (i) the fuel composition, that is, the amount of $^{235}U$ and $^{239}Pu$, as well as other fissionable elements present in the fuel, and their respective fission yields, (ii) the fuel burnup at the moment of the accident, and (iii) a continuous discharge as, for example, the FDNPP accident released radionuclides to the environment during 10 days. Such completion will necessarily increase the complexity, by generating numerous variations of scenarios and sub-scenarios, whereas the main objective of the present work was to set a general frame and produce a concept for the fundamental approach. As such, this first approach (***Figure 75***) allows to set the presence and succession of Sb and Te radionuclides in the context of hydrologically-relevant time scales, suggesting that the first month may show a non-negligible cocktail of radionuclides, whereas in the following months mostly $^{127m}Te$ and $^{125}Sb$ may predominate.

## II. MULTI-ELEMENT RADIONUCLIDE DISPERSION SCENARIOS IN THE GIRONDE ESTUARY

The results from this thesis allow to propose the following potential radionuclide dispersion scenarios for accidental dissolved releases from NPPs in continent-ocean transition systems such as the Garonne-Gironde fluvial estuarine system. These scenarios must take into account very different timescales: (i) radionuclide decay times ($t_{1/2}$), going along with potential changes in element-/isotope-specific geochemical and radioactive properties, (ii) the time required to reach solid/liquid partitioning equilibrium ($t_{S/L(eq)}$), (iii) the adsorption kinetics and extent of exchanges between the liquid and the solid phases, describing the partitioning of radionuclides, when equilibrium is not achieved, and (iv) the estuarine residence times of water (e.g., 18-86 days) and SPM (e.g., 1-2 years).

Radionuclides with half-lives longer than $t_{S/L(eq)}$ will be expected to present estuarine reactivity defined by the spiked Kd of the given element, as these radionuclides will likely reach partitioning equilibrium before decaying into their daughter radionuclides. In contrast, radionuclides with shorter half-lives than known $t_{S/L(eq)}$ will at least partly decay before reaching solid/liquid equilibrium. Assessing their sorption to the particulate phase must refer to the observed representative kinetic experiments estimating the time-dependent relative adsorption percentage of radionuclides onto estuarine SPM, the rest remaining in the dissolved phase. Furthermore, the natural decay of radionuclides implies that one chemical element transforms into another one, inducing changes in their geochemical behaviour and the evolution towards different equilibria. Consequently, this may even inverse the transfer direction between the dissolved and the particulate phases, depending on the respective particle affinities of the parent and daughter radionuclides. This further suggests that geochemical behaviour, transport and decay control radionuclide dispersion as a function of the intra-estuarine SPM and water dynamics/residence times.

Preliminary multi-element scenarios for Sb and Te radionuclide dispersion in the Gironde Estuary are proposed (***Table 20***) based on the information recovered in this thesis and the characteristic environmental dynamics of the Gironde Estuary.

**Table 20. Example of coupled timescales for Sb and Te radionuclide dispersion scenarios in the Gironde Estuary.** Assumed solid/liquid equilibrium times ($t_{S/L(eq)}$) for Te isotopes are ~5h in 1000 mg $L^{-1}$ (i.e., MTZ) and ~4 days in 100 mg $L^{-1}$ (i.e., average estuarine SPM), deduced from Te sorption kinetics (*Chapter 5*). Predicted fate is based on a single discharge, thus, scenarios for continuous/intermittent NPP discharges would, at least partly, derive from the following:

**SCENARIO A. Low discharge conditions:** upstream estuarine position of MTZ, between the Blayais NPP and the fluvial estuary, downstream average 100 mg $L^{-1}$ SPM, thus, $t_{S/L(eq)}$ ~ 4 days for Te, water residence times of ~86 days

*3 min ← 0* **: Time after the accidental release**

**Radionuclide decay**:

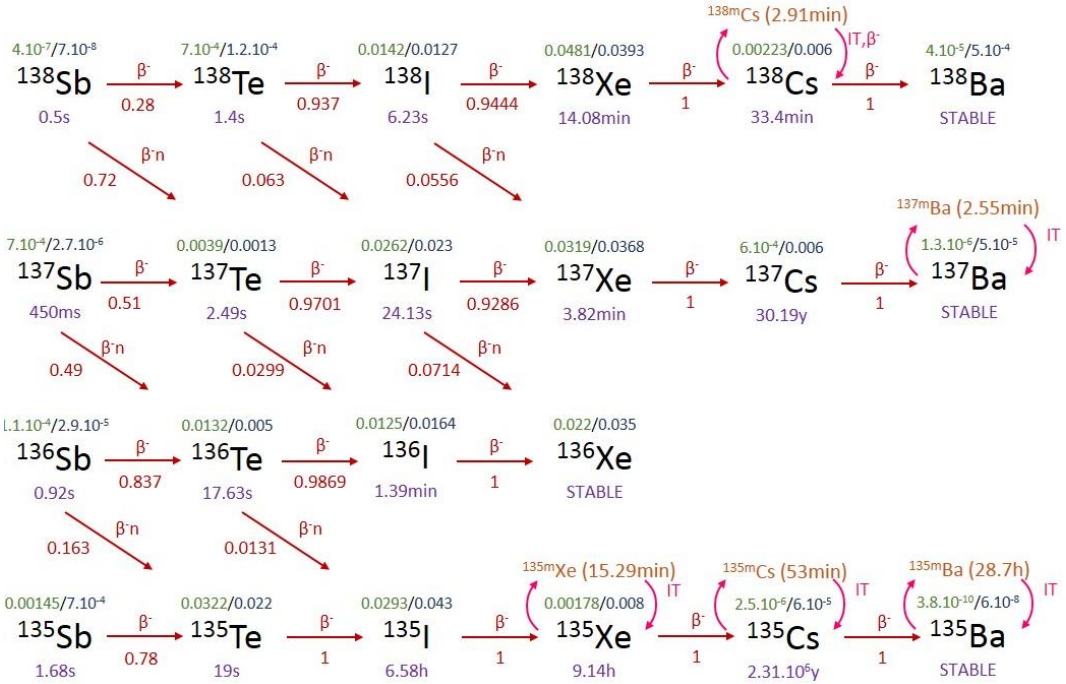


**Te fate**:
Fast decaying dissolved Te may decay into radioactive Xe, Cs and I within the estuary in the first minutes after the radionuclide release. The volatility or solubility of such daughter radionuclides in estuarine conditions is widely unknown.

**S/L (eq.) reached during timeframe?**
Te: No
Sb: No

**Estimated adsorption of the liquid discharge onto SPM**:
Te: unknown
Sb: unknown

**Estimated S/L distribution**:
Te: unknown
Sb: unknown

**Sb fate**:
Very fast decaying Sb radionuclides can produce respective Te daughter radionuclides in <3 min.

*(Table 20 Continued)*

*5 h ← 3 min*

**Radionuclide decay**:

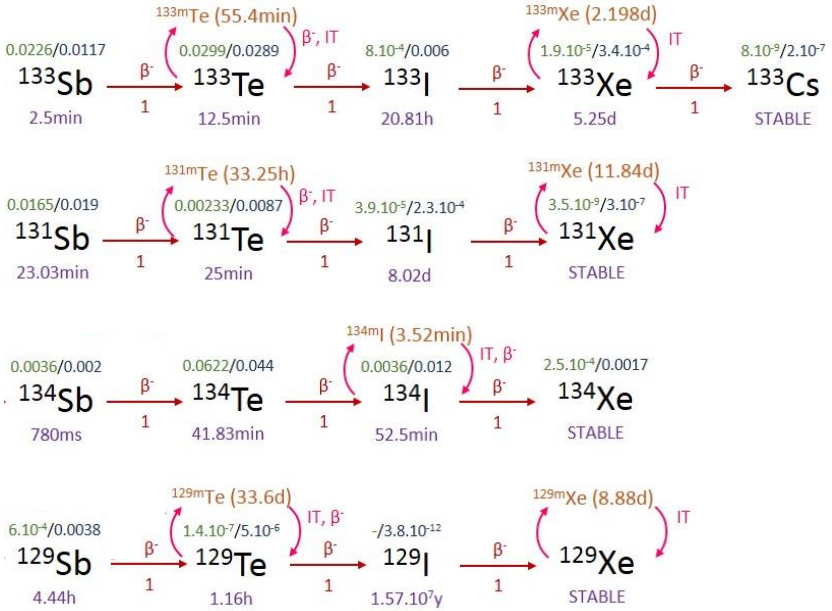


**Te fate**:

Within the first incoming (flow) or outgoing (ebb) tide (~6h), a fraction of Te radionuclides (~40%) will adsorb onto 100 mg $L^{-1}$ of SPM (***Figure 76***). Radioactive decay in both, the particulate and the dissolved phases within the estuarine water column will produce $^{133}$I, $^{131}$I and $^{129}$I radionuclides (commonly followed after NPP accidents). After 5h, ~75% of the remaining Te radionuclides (~1/32 of the initial quantity) in the dissolved phase may adsorb onto the SPM.

Radionuclide transport in the dissolved phase during the first hours after the accident will be directed towards the coast (i.e., during ebb) or towards the upstream estuary (i.e., during flow).

**S/L (eq.) reached during timeframe?**

Te: No

**Estimated adsorption of the liquid discharge onto SPM**:

Te: ~40% up to 75%

**Estimated S/L distribution**:

Te: unknown

**Sb fate**:

Important decay of Sb radionuclides into the more particle-active Te may contribute to Te radionuclide budget within the estuary, especially from $^{131}$Sb and $^{133}$Sb. Release of $^{129}$Sb will produce the commonly followed $^{129m}$Te, which will reach S/L (eq) within the first ~4 days after the accident. Its medium term half-life may contribute to its persistence within the estuary SPM for the following weeks (***Figure 76***).

*(Table 20 Continued)*

| | | | | |
|---|---|---|---|---|
| *4 d ← 5 h* | **Radionuclide decay**:<br> 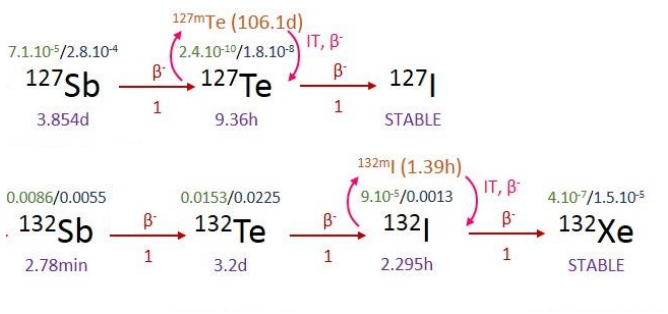 <br> | | | **Te fate**:<br>Within the first week after the accident, liquid discharges from the NPP to the estuary will be potentially retained inside the estuary (i.e., water residence times of up to 86 days). Thus, ~75% of $^{132}$Te and $^{127}$Te may adsorb onto the 100 mg $L^{-1}$ of SPM in the first 10h, and at least ½ of the initially discharged $^{132}$Te (commonly followed after an NPP accident) will reach S/L (eq.) in the first days, with ~90% as $Te_p$. |
| | **S/L (eq.) reached during timeframe?**<br>Te: Partially | **Estimated adsorption of the liquid discharge onto SPM:**<br>Te: ~75% | **Estimated S/L distribution**:<br>~90% of total Te as particulate Te | **Sb fate**:<br>Fast decay of $^{127}$Sb will produce $^{127}$Te and $^{127m}$Te, of which ~90% adsorbs onto the particulate phase (***Figure 76***). $^{132}$Sb decay will contribute to the $^{132}$Te estuarine budget. |
| *> 4 d* | **Radionuclide decay**:<br>Long-term half-lives: $^{130}$Te, $^{128}$Te, $^{123}$Te<br>Stable isotopes produced during fission: $^{126}$Te, $^{125}$Te, $^{124}$Te, $^{122}$Te | | | **Te fate**:<br>Draught conditions induce water residence times long enough to ensure that direct stable Te isotopes produced from nuclear fission follow a S/L redistribution according to natural Kd equilibrium ~1 week after the accident. |
| | **S/L (eq.) reached during timeframe?**<br>Te: Yes | **Estimated adsorption of the liquid discharge onto SPM:**<br>Te: >90% | **Estimated S/L distribution**:<br>~90% of total Te as particulate Te | **Sb fate**:<br>Medium-lived $^{125}$Sb can be potentially highly soluble (***Figure 76***), remaining inside the estuary (water residence times ~86 days), continuously transported to the coast, diluted and spread with oceanic currents to open ocean . |

*(Table 20 Continued)*

**SCENARIO B. High discharge conditions:** downstream estuarine position of the MTZ, between the Blayais NPP and the estuary mouth, implying a downstream average 1000 mg $L^{-1}$ SPM, thus, $t_{S/L(eq)}$ ~ 5h for Te, water residence times of ~18 days

*3 min ←0 : Time after the accidental release*

**Radionuclide decay**:

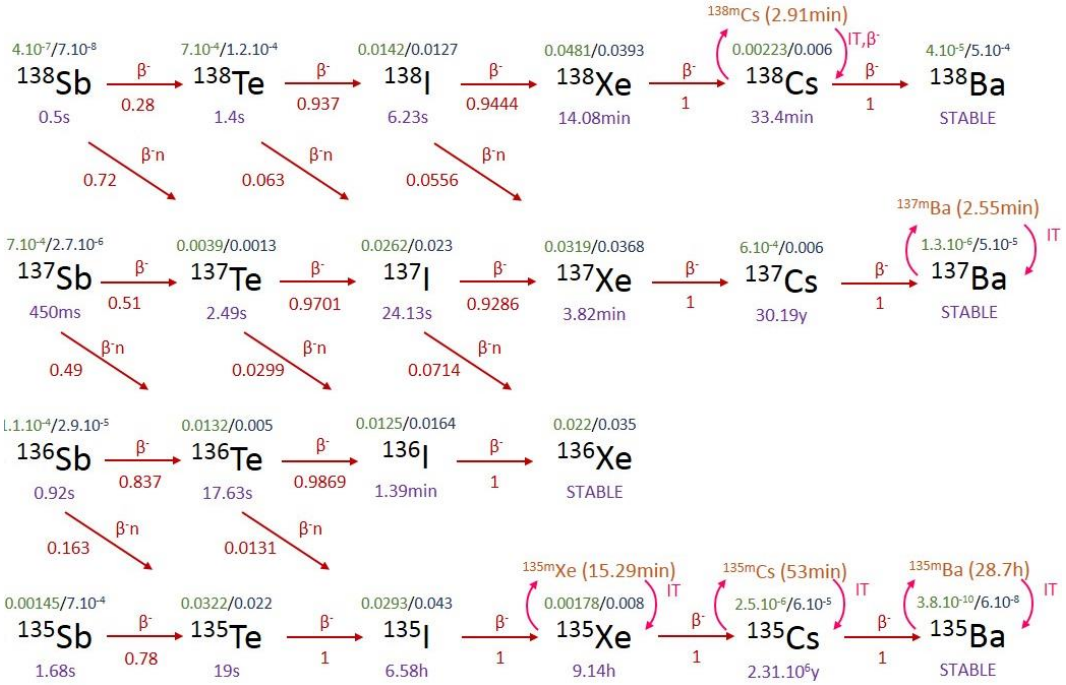


**Te fate**:

Idem to SCENARIO A

**S/L (eq.) reached during timeframe?**

Te: No

Sb: No

**Estimated adsorption of the liquid discharge onto SPM**:

Te: unknown

Sb: unknown

**Estimated S/L distribution**:

Te: unknown

Sb: unknown

**Sb fate**:

Idem to SCENARIO A

*(Table 20 Continued)*

*5 h ← 3 min*

**Radionuclide decay**:

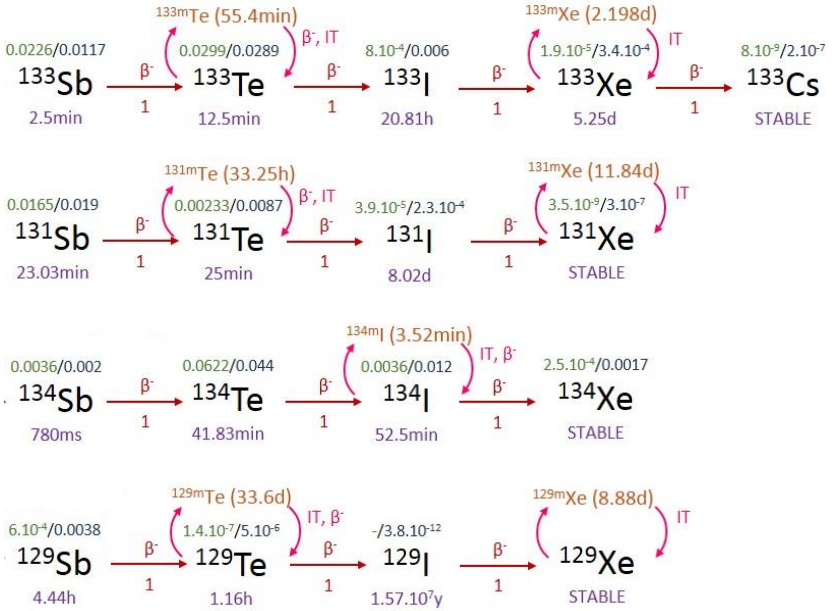


**Te fate**:

Within the first tide, ~90% of the dissolved Te radionuclides will adsorb onto the estuarine SPM (1000 mg $L^{-1}$). Thus, radioactive decay of Te radionuclides will take place mostly in the particulate phase, with expected re-dissolution for the commonly followed $^{133}$I, $^{131}$I and $^{129}$I radionuclides. Such decay may take place within the estuary reaches unless flood conditions are strong enough to expulse SPM to the coast. The produced dissolved radionuclides are expected to be transported to the coast in <18 days (i.e., estimated water residence time during floods). The production of Xe radionuclides (metastable forms) and stable Xe isotopes raises the question of solubility/volatility of this noble gas.

**S/L (eq.) reached during timeframe?**

Te: No

**Estimated adsorption of the liquid discharge onto SPM:**

Te: ~90%

**Estimated S/L distribution**:

Te: unknown

**Sb fate**:

Most Sb decay in the soluble phase may contribute to the estuarine Te radionuclide budget as even short water residence times are much longer than half-lives of these short-lived Sb radionuclides. The commonly followed $^{129m}$Te may, therefore, reach S/L (eq.) and adsorb to ~100% to the MTZ particles. Its half-life of 33.6 days suggests the potential transport of $^{129m}$Te in the MTZ towards the city of Bordeaux during the following draught conditions (***Figure 77***).

*(Table 20 Continued)*

<table>
<tr><td rowspan="3">4 d ← 5 h</td><td colspan="3">Radionuclide decay:<br> 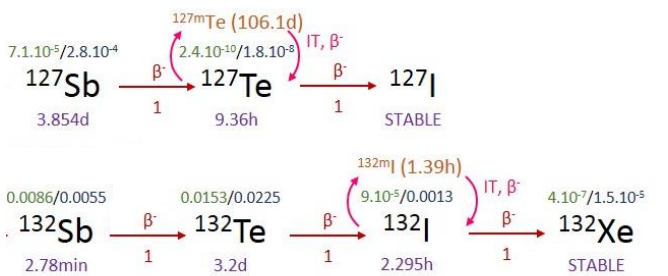
</td><td>Te fate:<br>Within the first week after the accident, ~90% of the NPP liquid discharge will be adsorbed in the MTZ with a solid/liquid distribution of ~100% of total Te as particulate Te. Therefore, decay into $^{132}$I will take place within the MTZ, and produce soluble stable and metastable I. The commonly followed $^{132}$Te will stay within the estuary MTZ unless flood conditions favour its coastal expulsion. Nevertheless, migration of the MTZ during the following dry season will most likely not transport these Te radionuclides towards the city of Bordeaux, because their half-lives are clearly shorter than the seasonal timescales (Figure 77).</td></tr>
<tr><td>S/L (eq.) reached during timeframe?<br>Te: Yes</td><td>Estimated adsorption of the liquid discharge onto SPM:<br>Te: ~90%</td><td>Estimated S/L distribution:<br>~100% of total Te as $Te_p$</td><td>Sb fate:<br>Both fast decays of $^{132}$Sb and $^{127}$Sb will further contribute to the Te radionuclide budget in the MTZ.</td></tr>
<tr><td rowspan="3">> 4 d</td><td colspan="3">Radionuclide decay:<br>Long-term half-lives: $^{130}$Te, $^{128}$Te, $^{123}$Te<br>Stable isotopes produced during fission: $^{126}$Te, $^{125}$Te, $^{124}$Te, $^{122}$Te</td><td>Te fate:<br>Flood conditions can also favour Te radionuclide S/L redistribution according to natural Kd equilibrium</td></tr>
<tr><td>S/L (eq.) reached during timeframe?<br>Te: Yes</td><td>Estimated adsorption of the liquid discharge onto SPM:<br>Te: >90%</td><td>Estimated S/L distribution:<br>~100% of total Te as $Te_p$</td><td>Sb fate:<br>Medium-lived $^{125}$Sb may be adsorbed in the MTZ to a certain extent, with 50% of the adsorbed fraction potentially mobile under suboxic conditions as occurring in the Soft Mud layer at the bottom of the water column in the MTZ, especially in the following dry season.</td></tr>
</table>

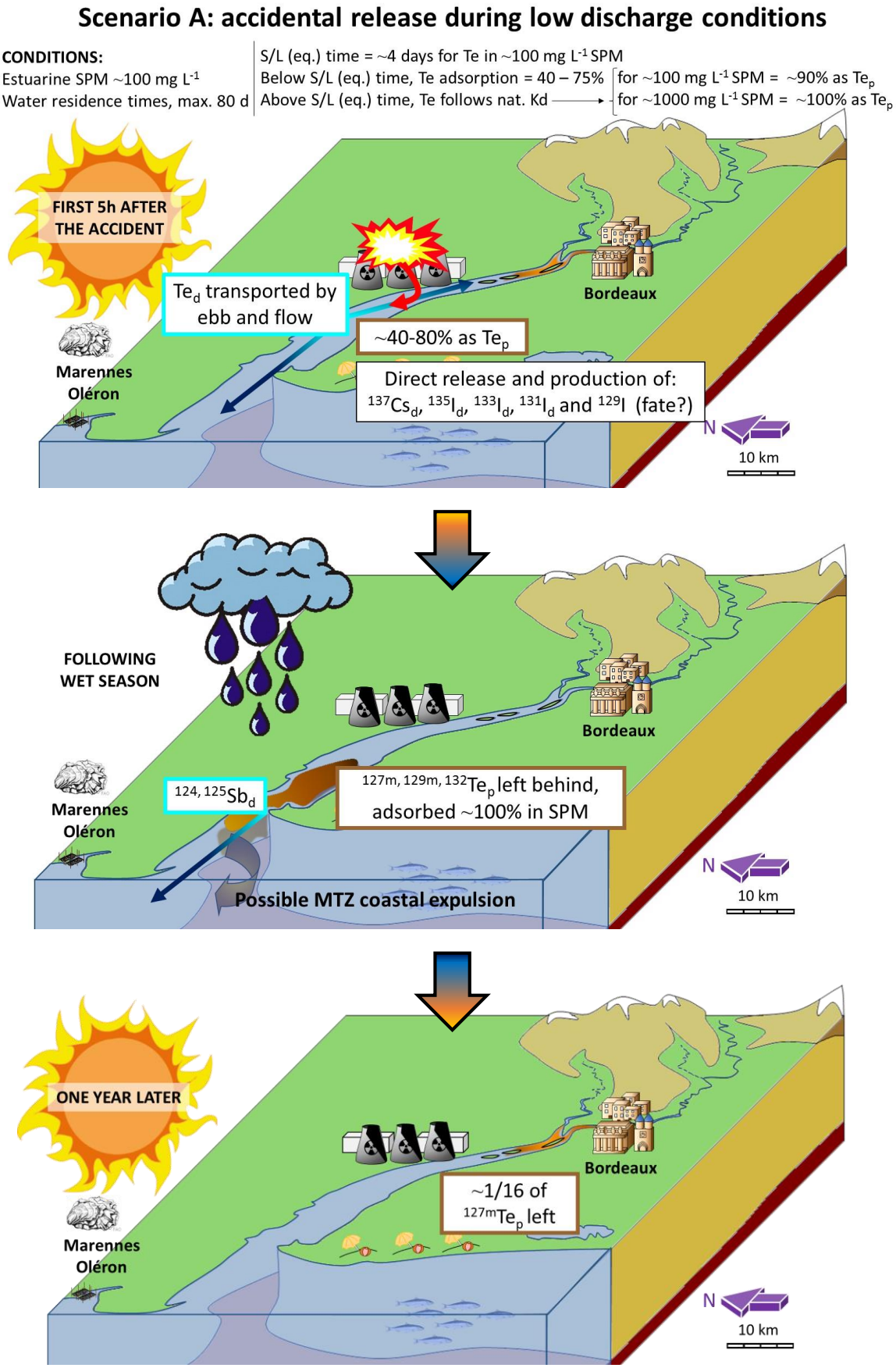


**Figure 76. Diagrams of proposed scenarios for accidental releases in low discharge conditions (Scenario A).** Each panel represents (from top to bottom) foreseen situations (i) during the first 5h, (ii) for the following dry/wet season, and (iii) one year after the accidental release.

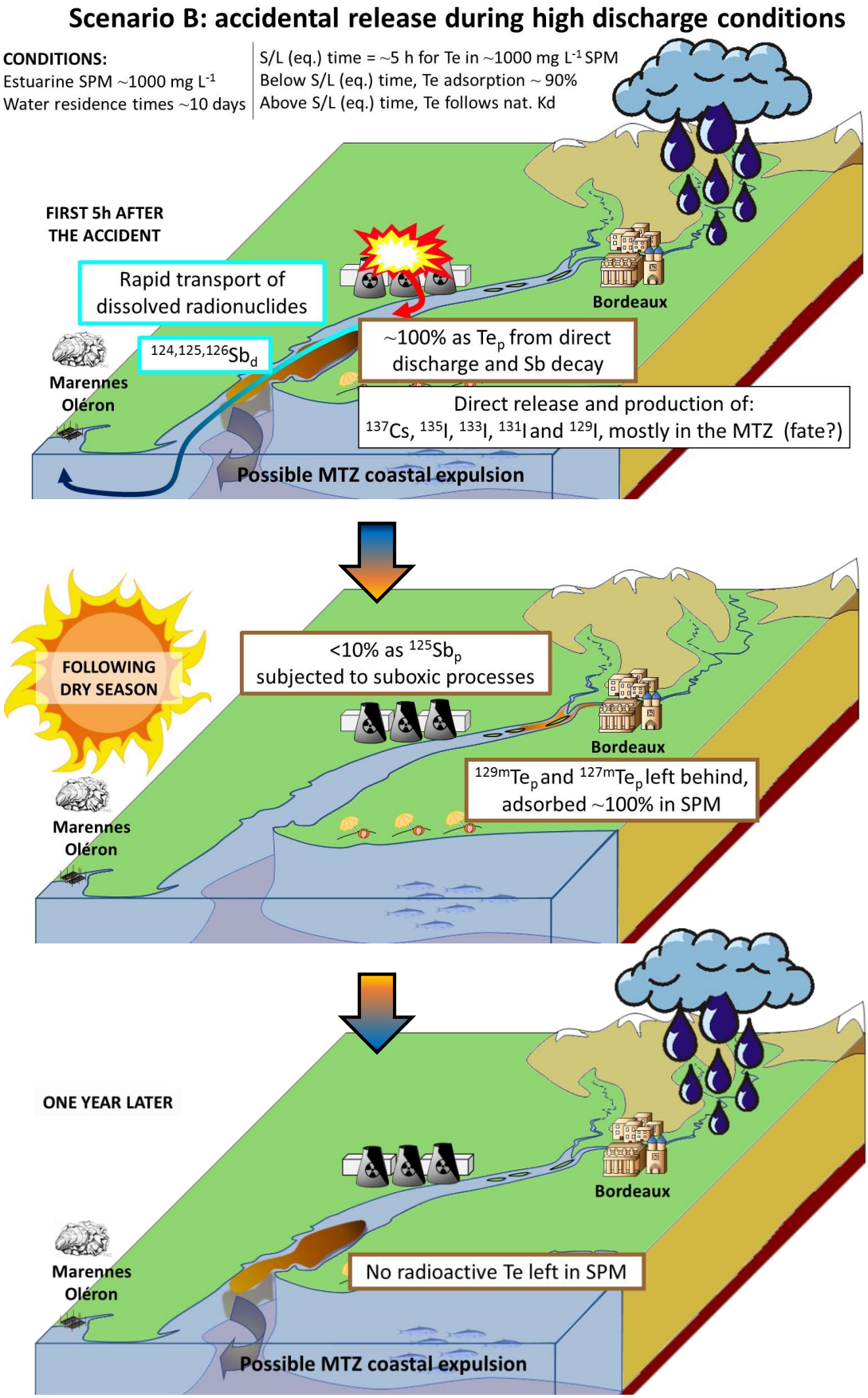


**Figure 77. Diagrams of proposed scenarios for accidental releases in high discharge conditions (Scenario B).** Each panel represents (from top to bottom) foreseen situations (i) during the first 5h, (ii) for the following dry/wet season, and (iii) one year after the accidental release.

Preliminary dispersion scenarios of hypothetical, liquid Sb and Te radionuclide discharges into the Gironde Estuary depend on the two extreme hydrological situations: low water (Scenario A, ***Table 20*** and ***Figure 76***) and high water discharges (Scenario B, ***Table 20*** and ***Figure 77***). Given the seasonal character of estuarine SPM and water discharges, the related estuarine residence times, the estuarine reactivity of both Sb and Te, and the potential transfer to wild organisms after radionuclide releases, the proposed scenarios globally suggest that:

- Scenario A: a hypothetical NPP accident during low discharge conditions may initially favour greater presence of dissolved Te radionuclides than Scenario B due to required longer times for solid/liquid equilibrium (~4 days). Particles retained within the estuary (negligible or inexistent expulsion during draught conditions) may join the MTZ due to tidal bottom currents, favouring the almost complete adsorption onto the particulate phase of any remaining Te radionuclides. The following rainy season would enable potential expulsion (under specific conditions) of radioactive MTZ particles to the coastal ocean. Within one year, the following draught conditions would transport the MTZ and the remaining radionuclides to the city of Bordeaux. However, these particles may be depleted in Te radionuclides given their relatively short half lives (***Figure 76***).

- Scenario B: an accident during high water discharge conditions may favour greater presence of particulate Te radionuclides in the MTZ, greater chance of storage of radionuclides in bottom sediments (i.e., sedimentation processes in estuarine/river bed and banks, etc.), and a potential upstream transport to the city of Bordeaux in the following dry season, especially for radionuclides like $^{129m}$Te and $^{127m}$Te (***Figure 77***). This type of scenario would imply higher decaying activity of medium-term radionuclides (including $^{125}$Sb) at Bordeaux compared to Scenario A.

These outcomes are somewhat counter-intuitive, because persistence and potential impact of contaminant and/or radionuclide spills would generally be expected to be lower under high discharge due to dilution and shorter residence times. In meso- to macrotidal, turbid estuaries such as the Gironde Estuary, the position of the MTZ (upstream or downstream from the accident) and its potential to fix the dissolved contaminants appears to be the main control of contaminant dispersal and persistence.

Accordingly, an accidental radionuclide release from the NPP of Golfech, upstream the Garonne River branch, would produce in all cases a B-type Scenario as the MTZ would always trap most, if not all, radionuclides. The only difference to an accidental event in the Blayais NPP would be the location of the MTZ and the transport time between the source and the MTZ, as (i) in draught conditions the

MTZ would trap relatively short-lived radionuclides in the fluvial estuary around Bordeaux, whereas (ii) in flood conditions the MTZ would trap most of the radionuclides in the downstream part of the estuary, with potential releases to the coast if specific conditions favour MTZ expulsion.

Potential radionuclide dispersion scenarios for the Rhône River system would suggest a more important role of the dissolved phase, compared to the scenarios presented for the Gironde Estuary, given the lower SPM concentrations at the Rhône River mouth. Furthermore, the weak tides in the western Mediterranean do not generate upstream-directed particle fluxes. These observations point to a relatively direct exportation of radionuclides to the sea, depending on hydrology, unless they are trapped in the reservoir sediments along the Rhône River. Again, the geographical position of the accident is an essential element for the development of reliable dispersion scenarios. Further research is required to conceptualise the different basic scenarios, including specific radionuclide-SPM interactions and their discharge into the highly saline Mediterranean Sea.

# GENERAL

# CONCLUSIONS AND PERSPECTIVES

# I. GENERAL CONCLUSIONS

The environmental behaviour of antimony (Sb) and tellurium (Te) in continent-ocean transition systems is poorly known and it is an important pre-requisite for the development of radionuclide dispersion scenarios in highly dynamic fluvial-estuarine systems hosting nuclear power plants. The present work aimed at contributing to the comprehensive knowledge of Sb and Te biogeochemical behaviour in the Garonne-Gironde fluvial estuarine system, producing original environmental information on Sb and Te reactivity, fluxes, solid/liquid partitioning and transfer to marine organisms. The study of trace element carrier phases in the solid phase and the related potential bioaccessibility using parallel selective extraction schemes has revealed the risk of major artefacts, when applying these commonly approved methods to 'new' elements.

The understanding of the environmental behaviour of anthropogenic releases, such as radionuclide discharges, into the aquatic system requires experimental setups addressing the respective behaviours of inherited and spiked Sb and Te. Comparison of Sb and Te behavior compared to that of other trace elements such as selenium (Se) and tin (Sn), as well as the compilation of both, field observations and laboratory outcomes, have substantially improved the conceptualisation of Sb and Te radionuclide dispersion scenarios in continent-ocean transition systems. The major conclusions of this work can be summarised as follows:

***1. Long-term monitoring of dissolved and particulate Sb and Te concentrations in the Garonne watershed allowed to identify contrasting geochemical behaviours between these two metalloids, including (i) regional background levels, (ii) anthropogenically influenced concentrations, (iii) seasonal variability, (iv) environmental solid/liquid partitioning, and (v) gross fluxes into the Gironde Estuary.***

- The long-term (14-years) study on Sb in the Lot-Garonne River watershed reports (i) a long-term trend in dissolved **Sb concentrations** potentially influenced by large-scale atmospheric Sb deposition, and (ii) particulate Sb concentrations presenting general high lithogenic background levels at the watershed scale. The latter was defined as a grain-size corrected, i.e. Th-normalised Sb concentration showing $Sb_p/Th_p$ ratios not higher than 0.54.

- Applying this lithogenic background, we have identified moderate to strongly contaminated concentrations at historically contaminated sites in the Riou Mort River watershed.

- Contrastingly, the long-term (2014-2017) study on Te in the same watershed showed no apparent recent anthropogenic influences neither for dissolved nor for particulate concentrations. Therefore, the measured dissolved (1.04 ± 0.32 ng $L^{-1}$) and particulate (48.2 ± 7.5 µg $kg^{-1}$)

concentration ranges are proposed as **Te regional average background concentrations** for the Lot-Garonne River watershed.

- Both, dissolved and particulate **Te concentrations showed a parallel seasonal pattern** at all study sites in the Lot-Garonne River system. Such original behaviour, combined with the identified high affinity of Te for the particulate phase, suggests that chemical and physical watershed weathering drives dissolved Te variability along the year and rapid adsorption to the particulate phase induces parallel variability. This seasonality contrasts to that observed for Sb, where only dissolved Sb varied in a seasonal manner.

- As a consequence, environmental **solid/liquid partitioning (Kd)** displayed greater variability for Sb (e.g., $\log_{10}$ Kd 3.1 and 5.1 L $kg^{-1}$) compared to that of Te ($\log_{10}$ Kd 4.3 to 5.7 L $kg^{-1}$). According to the aforementioned seasonal variability of Sb and Te dissolved and particulate concentrations, Sb watershed Kd shows a seasonal pattern, whereas the Kd of Te is more stable throughout the year. This points towards a stronger particle reactivity of Te and a rapid equilibration between the dissolved and the particulate phases. This study reports for the first time environmental Te solid/liquid partitioning (Kd) in freshwater systems. In contrast to Te, the partitioning of Sb is more complex and may reflect the balance between several potential control factors such as SPM abundance/quality, water discharges, water temperature, seasonal biological influences and/or changes in element speciation.

- Fluvial Sb dissolved and particulate concentrations at La Réole (median 0.16 ± 0.05 µg $L^{-1}$ and 2.8 ± 0.9 mg $kg^{-1}$, respectively) contribute to **average total gross fluxes** of 5.66 ± 2.96 t $y^{-1}$ (~50% particulate) entering the Gironde Estuary, with the highly concentrated Sb particles from Riou Mort generally contributing <3% to the total annual Sb flux. Lower total gross fluxes of ~90 ± 72 kg $y^{-1}$ were detected for Te, with varying contributions of 30% to 80% from the particulate phase.

***2. Oceanographic campaigns quantifying dissolved/particulate Sb concentrations and particulate Te concentrations along the Gironde Estuary salinity and turbidity gradients reveal contrasting geochemical non-conservative behaviour, suggesting addition/dissolution of Sb from the particulate phase and removal/adsorption of Te into the particulate phase.***

- Relatively lower Sb Kd values in the Gironde Estuary compared to the fluvial Kd imply increased **solubility of Sb**, potentially related to Sb release from particles by desorption and/or organic matter remineralisation.

- Field observations combined with laboratory experiments simulating contrasting salinity and turbidity conditions showed similar Te Kd values, supporting the partly scavenged behaviour of

Te in the Gironde Estuary. The experimentally quantified maximum Te adsorption capacity of estuarine bulk sediment of up to 50 mg $kg^{-1}$ is in line with the observed increase in **particulate Te** concentrations of estuarine SPM associated to longer residence times.

***3. The use of isotopically-labelled Sb, Te and Se adsorption experiments in bulk sediments of the Gironde Estuary allowed to identify both inherited and spiked solid fractionation of Sb, Se and Te.***

- **Inherited** Sb was mostly present in the operationally-defined residual fraction (~95%), showing <10% mobility in the ascorbate fraction simulating Sb behaviour in suboxic conditions in the presence of organic ligands. Inherited Se also showed important contributions to the residual fraction (~90%), with similar ~5% recoveries in the ascorbate and acid-soluble fractions. Contrastingly, inherited Te fractionation gave 50-70% in the residual fraction and 14% associated to the organic matter.
- As a general rule, all **spiked** Sb, Te and Se solid fractionations showed higher mobility than respective inherited elements. Spiked Sb and Se were extracted to >50% in the ascorbate fraction, with ~20% of Sb and ~10% of Se being potentially exchangeable (acetate fraction, F1). Spiked Te was highly present in the acid-soluble fraction (50-90%, F4) with only 10% attributed to the dissolution of amorphous Fe/Mn oxides (F2).

***4. Parallel selective extractions allowed to identify element-dependent artefacts for Sb, Te and Se solid fractionations associated to the reagents applied in each protocol for the F1 to F4 scheme.***

- Unexpected methodological artefacts were detected for both Sb and Se in the ascorbate fractions (F2) compared to the acid-soluble fractions (F4). There is evidence that the **acid-soluble fraction** underestimates the potentially reactive fraction, as supported by incomplete recoveries of spiked Sb and Se, maybe due to precipitation under acid conditions. The importance of this bias becomes evident from the 'residual' fractions of spiked Sb (90%), Se (80%) and Te (10-40%) although these spiked elements would generally not be expected to enter non-reactive phases. Consequently, the operationally-defined residual fraction would be overestimated when applying the commonly accepted extraction scheme to these elements.
- The use of organic complexants such as citrate or oxalate in other operationally-defined extractions (e.g. F2, **reducible fraction**) may probably extract more than the target phases, resulting in overestimation of the respective fraction. This artefact does not seem to occur for Te selective extractions.

- The **$H_2O_2$ fraction** (F3, oxidising) reflected an almost complete dissolution from the SPM of both inherited and spiked Se, probably related to the oxidation of Se species, inducing an overestimation of this fraction.

***5. Historical records of Sb and Te concentrations in wild oysters from the Gironde Estuary mouth reflect non-negligible Sb and Te biotransfer and no apparent recent trends revealing anthropogenic disturbances.***

- Historical samples (1984-2017) from soft tissues of wild oysters *Crassostrea gigas* (cf. *Magallana gigas*) in the Gironde Estuary mouth (**RNO/ROCCH**) showed stable concentration ranges of Te and Sb over time. This was attributed to either the absence of a measurable change in anthropogenic pressure and/or intense adsorption onto the estuarine particles, especially in the MTZ. Assuming that the dissolved fraction is generally more bioaccessible than the particulate phase and given the efficient mixing and pluri-annual residence times of estuarine particles, potential trends in anthropogenic release may be masked.

***6. The generally assumed similarities in the behaviours of the geochemical pairs Te and Se is not confirmed for the Gironde Estuary, as both, laboratory experiences and field observations showed marked differences between Te and Se.***

- Laboratory experiments revealed marked differences in (i) adsorption kinetics and isotherms, and (ii) distribution between preferential carrier phases (solid fractionation). Bioaccumulation in wild bivalves (oysters and mussels) also points towards differences in distribution between organs (no correlation), despite sometimes similar bioconcentration factors, suggesting independent mechanisms and regulations of Te and Se uptake, in relation with pathways and/or biological functions.

***7. Field-based and laboratory-based Kd values may be used indistinctly in radionuclide dispersion models for highly particulate trace elements (such as Te and Sn). However, field-based and laboratory-based Kds may considerably differ in more soluble elements (like Se and Sb).***

- Solid/liquid partitioning (Kd) values are a prerequisite for the conceptual development of radionuclide dispersion scenarios and management strategies anticipating potential accidental releases. Current predictive models use **field-based and laboratory-based Kds** indistinctly. Our field and laboratory experiences showed similar Kd values for the highly particle-active elements

Te and Sn. However, experimentally determined Kd values for Se spikes of 100 000 ng $L^{-1}$ and 0.3 ng $L^{-1}$ were widely different. Sediments adsorbed <5% of the spiked isotopically-labelled Sb, highlighting its affinity for the dissolved phase. Therefore, scenarios modelling the environmental dispersion of more soluble elements like Se and Sb should take into account laboratory-Kd values, determined for the concentration ranges and environmental conditions representative of the expected anthropogenic discharge.

***8. The use of isotopically-labelled radioactive elements like Se and Sn in adsorption experiments allow to simulate Se and Sn adsorption/desorption kinetics and Kd values at environmentally representative concentrations.***

- Selenium and Sn radiotracer experiments enabled the comparison of contrasting trace element reactivity with sediments from the **Gironde Estuary and the Rhône River**, at environmentally representative concentrations as expected for radionuclides after accidental releases. High Se solubility and high Sn adsorption onto the particulate phase imply that both systems present bulk sediments with abundant, strong sorption sites for Sn and weak or less abundant sorption sites for Se. Integrating such results into the development of radionuclide dispersion scenarios for the Gironde Estuary and the Rhône River systems reflects the transversal character of this work, potentially applicable to other continent-ocean transition systems.

***9. The coupling of multi-element radionuclide decays, corresponding adsorption kinetics and environmental hydrological processes at various timescales is a fundamental concept for the development of radionuclide dispersion scenarios (cf. aim of the AMORAD Project).***

- **Radionuclide decay chains** provide information on radionuclide persistence (half-lives) in the environment and that of the respective daughter radionuclides. The transformation from one element into another chemical element is a specificity of radionuclides, opposed to common biogeochemical studies. Such changes result not only in profound changes in radioactivity (type, intensity, half live, etc.) from the parent to the daughter element, but also in biogeochemical properties (solubility, bioavailability, etc.). The succession of these changing properties, occurring at variable timescales, must then be coupled to intrinsic dynamics of coastal systems to provide reliable support for short to medium term radiological risk assessment.
- **Environmentally representative kinetic experiments** allow to define fast adsorption capacities of bulk sediments and solid/liquid equilibrium times, fundamental for the correct use of Kd values and associated implications in radionuclide dispersion scenarios. Radionuclide solid/liquid

partitioning will follow that represented by the Kd value, when its half-life is greater than the time required to reach solid/liquid equilibrium.

- Considering **environmental forcing** such as tides, SPM and water residence times as well as seasonal processes such as the migration of the MTZ or the development of suboxic conditions in the MTZ is essential for radionuclide dispersion scenarios as their temporal frequencies (i) control the physical conditions that will allow radionuclides to reach or not solid/liquid equilibrium, and (ii) determine the mobility and fate of soluble or particulate radionuclides.

***10. The developed Sb and Te radionuclide dispersion scenarios for the Gironde fluvial estuarine system suggest (i) lower particulate retention of Te radionuclides during low discharge accidental releases compared to (ii) almost complete Te radionuclide retention in the MTZ during high discharge accidental releases, implying the risk of potential upstream transport of both Te and Sb radionuclides to the city of Bordeaux in the following dry season. The position of the MTZ with respect to the radionuclide source is a major condition for the dispersion scenario.***

- Concerning **radiation exposure pathways** to humans, the proposed scenarios suggest external potential risks related to dissolved or particulate radiation especially for the periods when the MTZ is present within the Bordeaux agglomeration during several months in the summer season. No information on exposure scenarios for aquatic organisms or humans in this area and related radiological risks is available/accessible.
- An accidental radionuclide release from the **Golfech NPP** would more or less rapidly reach the fluvial estuary near Bordeaux, depending on the discharge situation. In this configuration, the MTZ is necessarily downstream from the source and will work as a reactor, retarding and modifying the radionuclide transport to the sea.

Overall, the present work provides (i) a comprehensive knowledge on Sb and Te biogeochemical behaviour in fluvial-estuarine systems at several spatial and temporal scales, and (ii) key factors for the development of high resolution radionuclide dispersion scenarios including accurate quantification of radionuclide solid/liquid partitioning and the coupling of hydrological processes to radionuclide time scales. Consequently, this work constitutes (i) a contribution to research on Sb and Te biogeochemistry in continent-ocean transition systems, as well as (ii) a conceptual basis and guideline for the future development of more precise radionuclide dispersion scenarios in coastal environments.

# II. PERSPECTIVES

The present work contributes original knowledge on biogeochemical behaviours of Sb and Te in coastal systems and has set the conceptual frame for radionuclide dispersion scenarios. As such, this thesis has produced several key outcomes, supporting future lines of research for both, environmental studies and ongoing development of radionuclide dispersion models. Thus, the following perspectives are proposed:

- ***Analytical chemistry:***
  - Given the analytical challenges in the **quantification of dissolved Te concentrations in complex seawater matrices**, and the huge uncertainty/differences in the available literature, this work has proposed a dissolved Te value for the Atlantic coast of ~0.3 ng $L^{-1}$ by combining field particulate Te concentrations and laboratory-based Kd values. Further research should focus on the development of reliable techniques for the quantification of Te in seawater matrices to (i) produce fundamental knowledge on dissolved Te concentrations, as well as their spatial/temporal variations in coastal systems worldwide, (ii) stimulate the development and the commercialisation of certified reference materials for Te in seawater (and in biological matrices), not available today, and (iii) better understand Te reactivity and biogeochemical cycles in coastal salinity and turbidity gradients.

- ***Environmental solid/liquid partitioning (Kd):***
  - Solid/liquid partitioning of Sb and Te were variable, showing **contrasting seasonal patterns** over the years. Future environmental studies should aim at better understanding the causes of these observations, focusing on Sb/Te redox speciation, SPM quality and biological implications. Such approach should combine both, field and laboratory studies to (i) develop the appropriate analytical capacities for quantifying Sb and Te speciation at the ultra-trace level (e.g., hydride generation coupled to ICP-MS), (ii) characterise the reactivity of Sb and Te related to variability in SPM composition and abundance along different times of the year, and (iii) identify the roles of redox processes in Sb and Te speciation and the resulting availability to the biological compartment.

  - Furthermore, similar approaches should also be applied to coastal salinity and turbidity gradients of contrasting systems worldwide (including complementary parameters such as chlorophyll, nutrients, dissolved/particulate carbon contents, other redox-sensitive trace elements, etc.) so as to better understand the **driving processes controlling conservative vs non-conservative behaviour** of Sb and Te in transition waters.

- ***Solid fractionation:***
  - Element-dependent artefacts may occur when applying commonly used selective extraction protocols to new elements for which the protocols have not been tested. Future work should develop strategies to evaluate the **efficiency and reliability of selective extraction protocols before extending their use** to a wider group of target elements. For this, a battery of commonly applied protocols may be combined with information about the sample matrix and/or target carrier phases (Fe/Mn/Ca/Al extractions, sample mineralogy, etc.).

  - Evaluation of extraction protocols could also use a three-step approach combining a first selective extraction (e.g. F2) to withdraw the target carrier phase (e.g. Fe/Mn oxides), followed by spike experiments (ideally isotopically-labelled solutions) on the remaining bulk sediments and subsequent repetition of the initial extraction (here: F2), to **identify and quantify potential non-selectivity** of the applied reagents.

  - More importantly, it is critical to understand the mechanisms behind the **incomplete extraction of certain elements** like Sb and Se in the acid-soluble fractions, given that this bias may induce important underestimation of the potentially bioaccessible fraction in environmental applications.

- ***Environmental impacts of TCE's:***
  - Given (i) the yet unknown environmental impacts of recently increasing use of less studied TCEs (like Te) in new technologies, (ii) the absence of a defined historical trend for Te in biomonitoring organisms such as wild oysters at the Gironde Estuary mouth, and (iii) the high particle affinity of Te for the solid phase in aquatic environments, future works on **potential Te anthropogenic contamination** in highly sensitive continent-ocean transition systems such as estuaries should include less turbid coastal areas.

- ***Biological implications:***
  - Given the non-negligible bio-transfer quantified in this work, more work on the uptake pathways, accumulation and redistribution of Sb, Te and Se between different biological organs is required to **improve our understanding of the biological role of Sb and Te** in aquatic organisms such as wild oysters. Again, field observations should systematically be complemented by laboratory experiments using pertinent tracers, such as isotopically-labelled spikes, complemented by histopathological measurements.

- ***Radionuclide dispersion scenarios:***

  - Considerable progress in X-ray based microscopic solid phase analyses (XAS, XANES) allows nowadays to precisely assess redox state as well as binding sites and -mechanisms of certain trace elements in bulk sediments. Given the central role of solid/liquid partitioning in the development of radionuclide dispersion scenarios and the **non-negligible differences between field-Kd and laboratory-Kd values** observed for certain trace elements (e.g. Sb, Se), microscopic approaches in environmental and laboratory samples could facilitate future understanding of such Kd differences.

  - The next step in the development of Te and Sb radionuclide dispersion scenarios is to integrate the qualitative descriptions described in this work with a **mathematical model** accounting for the main environmental processes controlling the biogeochemical behaviour of Sb and Te. This would allow obtaining a more precise and quantitative view of their environmental fate in the Garonne-Gironde fluvial estuarine system, as well developing scenarios covering continuous radionuclide discharges over longer periods (e.g. days/weeks). Modelling should also take into account the radioactive dose emitted by Sb and Te radionuclides in order to better evaluate the radiological risk due to radionuclide dispersion.

  - Past accidental nuclear power plant releases have shown direct discharges into aquatic environments composed of a cocktail of short-, medium- and long-lived radionuclides. Better understanding of the biogeochemical behaviour of other less studied radionuclides such as Sn and Se, as well as the daughter radionuclides of Sb and Te, is required, especially for dynamic continent-ocean transition systems. In fact, such environments may constitute flushing and/or retaining areas of dissolved/particulate radionuclides along the land-sea continuum. As such, they control residence times and intermediate reservoirs, potentially transporting relatively short-lived radionuclides and the related radiation into inhabited areas (e.g., city of Bordeaux). Therefore, radiological risk assessment studies should thoroughly consider the **multi-component character of radionuclide discharges** and mobility coupled to environmental dynamics.

# RÉSUMÉ ÉTENDU

***Chapitre 1 : Introduction générale et contexte scientifique***

La production nucléaire semble aujourd'hui l'alternative la plus adéquate face à une demande mondiale en énergie éléctrique qui prévoit d'augmenter d'au moins deux-tiers d'ici 2035 (WNA 2015, 2018). Cependant, l'accident de la Centrale Nucléaire de Production d'Electricité (CNPE) de Fukushima Dai-ichi en 2011 a soulevé de nouvelles questions concernant la sûreté nucléaire des CNPE au 21ème siècle. En effet, la dispersion et les impacts inattendus des cocktails de radionucléides rejetés directement dans les milieux aquatiques restent peu connus. La haute densité en CNPE de la France (i.e., 58 réacteurs dans 19 CNPE ; IEA 2017), en lien directs avec les principaux cours d'eau tels que la Loire, la Seine, le Rhône ou la Garonne, ainsi que les zones côtières, la rend susceptible de subir un accident de type « Fukushima ».

Le **projet AMORAD** (« Amélioration des MOdèles de prévision de la dispersion et d'évaluation de l'impact des RADionucléides au sein de l'environnement »; ANR-11-RSNR-0002) a été créé en 2013 dans le cadre de l'évaluation du risque nucléaire en France. Il est soutenu par les programmes d'Investissement d'Avenir du Ministère de l'Enseignement Supérieur, de la Recherche et de l'Innovation ainsi que par l'Agence Nationale de la Recherche (ANR). L'objectif de ce projet est de déterminer les facteurs contrôlant la dispersion, les transferts entre compartiments environnementaux et les impacts des radionucléides sur l'Homme dans le but (i) d'augmenter la résolution modélisant le devenir des radionucléides dans l'environnement, (ii) de renforcer l'évaluation des risques radiologiques, et (iii) d'améliorer les protocoles de sécurité post-accidentels. Par conséquent, ce projet est structuré en plusieurs axes de recherche, comprenant un focus sur le milieu aquatique (*www.irsn.fr*).

L'axe Marin du projet AMORAD se découpe en quatre zones ateliers comprenant le Golfe de Gascogne (Océan Atlantique) et le Golfe du Lyon (Mer Méditerranéen). **Ce travail de thèse** s'inscrit dans l'axe Marin AMORAD, par l'étude de la dispersion des radionucléides rejetés directement sous forme liquide dans les zones de transitions continent-océan des systèmes fluviaux Lot-Garonne-Gironde (2 CNPE) et Rhône (4 CNPE), principaux apports d'eau et de particules vers ces zones ateliers respectives. Ces systèmes environnementaux présentent des conditions complexes de mélange entre les eaux douces et salines ainsi que des phénomènes hydrologiques à court et moyen terme (i.e., impliquant les cycles de marées, l'extension de l'intrusion marine, les débits saisonniers et la migration de la zone de turbidité) qui peuvent jouer des rôles non-négligeables sur la réactivité des radionucléides et leur devenir dans les milieux aquatiques.

Les radionucléides les plus communément enregistrés et étudiés après les accidents nucléaires (i.e., Tchernobyl et Fukushima) sont le césium (Cs) et l'iode (I), car ils présentent respectivement une longue demi-vie et une radiotoxicité non négligeable (e.g., Steinhauser et al. 2014, Buesseler et al.

2017). Cette étude s'intéresse à **l'antimoine (Sb) et au tellure (Te)** également enregistrés après les accidents. Ces radionucléides montrent des radioactivités non négligeables (Steinhauser et al. 2014) et présentent des temps de demie vie moyens à courts. Néanmoins, leur comportement biogéochimique en milieu aquatique reste encore peu connu en comparaison avec d'autres radionucléides.

Les radionucléides Sb et Te ayant un temps de demi-vie court, ils se sont entièrement dégradés dans le milieu naturel depuis les accidents de Tchernobyl et de Fukushima. Néanmoins, le comportement biogéochimique d'un élément est indépendant de sa masse atomique (forme stable ou radioactive). Ainsi, ce travail se focalise sur le comportement de l'isotope stable présent dans le milieu naturel. Les cycles biogéochimiques de Sb et Te sont relativement peu connus, particulièrement dans les milieux aquatiques côtiers. Ce manque d'information est principalement dû aux difficultés analytiques liées (i) aux faibles concentrations environnementales de Sb et de Te, et (ii) aux matrices complexes telles que les eaux saumâtres des eaux de transition et côtières. Cependant, la littérature fait souvent la comparaison entre le comportement biogéochimique de Sb et de l'arsenic (As) ainsi que de Te et du sélénium (Se), ces couples présentant des états d'oxydo-réduction semblables.

Ainsi, ce travail a pour **objectifs** spécifiques de :

- *Quantifier les concentrations et les flux dissous et particulaires* de Sb et Te le long du système fluvio-estuarien de la Gironde.
- *Caractériser les phases porteuses des éléments Sb, Te et Se hérités (naturels) et apportés (spike)* dans les sédiments naturels du système Garonne/Gironde ainsi que pour le Rhône.
- *Comprendre la réactivité et la cinétique d'adsorption et de désorption entre les phases dissoutes et particulaires* des éléments solubles (Sb, Se) ou avec une forte affinité vers les particules (Te, Sn) en conditions représentatives du milieu aquatique (i.e., gradient de salinité et turbidité estuarien de la Garonne/Gironde et du Rhône).
- *Vérifier le transfert de ces éléments vers les organismes aquatiques* comme les huîtres sauvages à l'embouchure de l'estuaire de la Gironde et extrapoler la potentielle exposition humaine par ingestion des radioéléments Sb et Te.

***Chapitre 2 : Approches méthodologiques***

Les objectifs de ce travail ont été étudiés principalement selon quatre approches :

- *Suivi mensuel à long terme de la contamination métallique du bassin versant de la Garonne.* Des prélèvements d'eau et particules ont permis de mieux comprendre le comportement

géochimique de Sb et Te dans le bassin versant de la Garonne, principal affluent de l'estuaire de la Gironde.

- *Missions de terrain ponctuelles dans l'estuaire de la Gironde.* La collecte et l'analyse d'échantillons d'eau et de particules au cours de quatre missions (nommées MGTS, «Métaux Gironde Transfert et Spéciation») le long des gradients de salinité et turbidité de l'estuaire de la Gironde ont permis d'étudier la réactivité de Sb et de Te dans ce compartiment très dynamique, pendant des conditions hydriques contrastées, variant de l'étiage à la crue.

- *Expérimentations en laboratoire.* Elles ont permis de réaliser : (i) des cinétiques d'adsorption et désorption des isotopes marqués (stables et radio-traceurs) afin de connaitre la vitesse d'interaction entre la phase dissoute et particulaire de Te et Se, dans le gradient de salinité et de turbidité des estuaires de la Gironde et du Rhône, ainsi que (ii) des extractions sélectives sur des sédiments des estuaires de la Gironde et du Rhône afin d'identifier les phases porteuses des éléments Sb, Te et Se hérités (naturels) et apportées (ajoutés).

- *Analyse des matrices biologiques.* Le transfert de Te et Se vers le biote (i) à l'embouchure de l'estuaire de la Gironde a été caractérisé par l'analyse des échantillons historiques (>30 ans) des huîtres sauvages prélevées grâce au suivi RNO/ROCCH, et (ii) à l'embouchure du Rhône avec des échantillons ponctuels de moules sauvages issus de l'IRSN.

Tous les résultats de ce travail sont présentés sous forme d'articles parmi lesquels certains ont déjà été publiés et d'autres sont prêts à être soumis à l'issue de cette thèse.

***Chapitre 3 : Le comportement biogéochimique de l'antimoine dans le système fluvio-estuarien de la Gironde***

Le présent chapitre est composé de deux publications concernant : (i) le suivi historique du comportement géochimique de Sb dans le bassin versant de la Garonne (*Environmental Chemistry, 2018*), et (ii) la réactivité de Sb le long du gradient de salinité et de turbidité de l'estuaire de la Gironde (*Marine Chemistry, 2016*).

La première publication présente les résultats d'un programme de surveillance à long terme dans le système fluvial Lot-Garonne. Une base de données sur 14 ans (2003-2016) presentant les concentrations d'antimoine dissous (<0,2 µm ; $Sb_d$) et particulaires ($Sb_p$) à cinq points d'échantillonnage stratégiques a permis : (i) d'observer une influence non négligeable des dépôts atmosphériques de Sb sur les concentrations de $Sb_d$ (~0,16 µg $L^{-1}$ en moyenne) dans le système de la rivière Lot-Garonne, (ii) d'identifier les tendances saisonnières de $Sb_d$, semblable à celle de As (Masson

et al. 2007), ainsi que (iii) de quantifier des concentrations de $Sb_p$ relativement élevées (de ~3 mg $kg^{-1}$ à ~10 mg $kg^{-1}$) par rapport à celles rapportées pour d'autres systèmes aquatiques français (~1 mg $kg^{-1}$ dans la Seine et le Rhône, ~3 mg $kg^{-1}$ dans la Loire). Une collecte supplémentaire d'échantillons d'eau filtrés à <0,02 µm représentant une période d'observation de 5 ans (2003-2007) a permis d'évaluer le faible rôle de la fraction colloïdale dans le transport de $Sb_d$ dans ce système. De plus, les flux totaux estimés suggèrent une prédominance (~70%) des apports de Sb issus de la Garonne central/amont (5,66 ± 2,96 t $an^{-1}$) entrant dans l'estuaire de la Gironde avec une contribution égale des flux dissous et particulaires.

Le deuxième article porte sur les résultats de Sb au cours de trois campagnes d'échantillonnage sur l'estuaire de la Gironde en 2014/2015 pour trois conditions hydriques différentes, i.e., étiage, débits intermédiaires et débits de crue (MGTS I-III). Un site d'étude de comparaison dans les eaux de transition du bassin d'Arcachon (hydrologiquement indépendant de l'estuaire de la Gironde) est également présenté. Les résultats suggèrent clairement que de longs temps de résidence dans le gradient de salinité et de turbidité favorisent le comportement additif non conservateur de Sb. Les coefficients de distribution ($log_{10}$ Kd ~ 3,5 - 4,4 L $kg^{-1}$) indiquent que la zone de turbidité maximale (ZTM ; présentant des matières en suspension, MES, ~1000 mg $L^{-1}$) piège ~90% de Sb total par rapport à ~50% en conditions moyennes de MES ≤ 100 mg $L^{-1}$.

***Chapitre 4 : Les phases porteuses de l'antimoine particulaire***

Les extractions sélectives sont largement utilisées sur les échantillons particulaires afin de mieux comprendre la mobilité et la réactivité / biodisponibilité potentielle des éléments traces par rapport aux concentrations totales particulaires. La première partie de ce chapitre décrit brièvement les connaissances actuelles concernant les protocoles d'extraction sélective et leurs mécanismes d'action.

La deuxième partie du chapitre présente un cas d'étude sur le fractionnement solide de Sb dans les sédiments naturels des estuaires de la Gironde et du Rhône. Connaissant la sensibilité de certains métaux traces aux milieux d'extraction et le comportement inconnu de Sb, ce travail représente une première approche sur les extractions parallèles de Sb avec différents réactifs ciblant la fraction oxyde de Fe/Mn (solutions d'hydroxylamine, d'oxalate et d'ascorbate, appelées « F2 ») et la fraction bioaccessible (solutions à 1M HCl et 1M $HNO_3$, appelées «F4»). Les résultats montrent une anomalie (F2 > F4) dépendant du sédiment et du protocole d'extraction, i.e., montrant une extraction plus importante de Sb avec les solutions oxalate et ascorbate pour les sédiments du système fluvio-estuarien Garonne/Gironde. Cette anomalie est probablement liée à la spéciation de Sb naturel et à la présence de complexants organiques dans la solution d'extraction tels que l'oxalate (Wenzel et al. 2001) et le citrate (Kostka et Luther 1994). La deuxième approche de cette étude consiste à comparer

le fractionnement de Sb naturel/hérité ($Sb_{nat}$) à celui de Sb en ajouté/apporté ($Sb_{ex}$) d'après des expériences d'adsorption par marquage isotopique sur les MES de la Garonne. Les résultats montrent une dissolution plus importante de la totalité de $Sb_{ex}$ (>50% associé à la fraction ascorbate) par rapport à $Sb_{nat}$ (présente à plus de 90% dans la fraction réfractaire). Les résultats de cette étude en laboratoire sont prêts à être soumis dans la revue scientifique à comité de lecture *Applied Geochemistry*, sous le titre « *Fractionation of inherited and spiked antimony (Sb) in fluvial/estuarine bulk sediments : unexpected anomalies in parallel selective extraction protocols* »

***Chapitre 5 : Le comportement biogéochimique du tellure dans le système fluvio-estuarien de la Gironde***

La première étude de ce chapitre montre la réactivité de Te dans le système fluvio-estuarien Lot-Garonne-Gironde à partir d'un suivi mensuel de quatre années (2014-2017). Les concentrations de Te dissous (<0,2 µm ; $Te_d$) et de particulaires ($Te_p$) ont été mesurées pour cinq points stratégiques d'échantillonnage dans le bassin versant de ce système. Ces résultats montrent des concentrations moyennes de ~1 ng $L^{-1}$ en $Te_d$ et ~50 µg $kg^{-1}$ en $Te_p$ suivant des patrons saisonniers parallèles, donnant donc des rapports solide/liquide environnementaux constants ($log_{10}$ Kd ~4,75 L $kg^{-1}$). De plus, ce suivi est complété par l'analyse des concentrations de particules issues de campagnes d'échantillonnages sur l'estuaire de la Gironde et couvrant une large gamme de conditions hydriques, d'étiage à crue (MGTS I à IV). Ces dernières montrent la forte affinité de Te envers la phase particulaire, dépendante des temps de résidence hydrique de l'estuaire. Un enregistrement historique des concentrations de Te dans les huîtres sauvages à l'embouchure de l'estuaire (1984-2017) est également analysé, relevant des valeurs relativement constantes (variant entre 1,33 et 2,89 µg $kg^{-1}$ de poids sec). Les résultats de cette étude de terrain ont été acceptés pour publication dans la revue scientifique *Environmental Chemistry*, sous le titre « *Tellurium behaviour in a major European fluvial-estuarine system (Gironde, France): fluxes, solid/liquid partitioning, and bioaccumulation in wild oysters* ».

La deuxième partie de ce chapitre approfondit la cinétique et les isothermes d'adsorption de $Te_d$ et $Se_d$, ainsi que leur fractionnement solide (naturel/hérité et en ajouté/apporté) dans les MES du système estuarien de la Gironde. Les résultats montrent différents comportements géochimiques entre Te et Se avec >90% de $Te_{ex}$ et <30% de $Se_{ex}$ adsorbés sur les particules estuariennes après 5h d'exposition. De plus, la valeur de Kd fluvial de Te est retrouvée dans le $log_{10}$ Kd déterminé expérimentalement dans l'eau de mer, ce qui suggère une affinité de la phase $Te_d$ vers le particulaire en condition estuarienne indépendant du gradient de salinité. Par conséquent, ~90% de la concentration totale de Te se retrouve dans la phase particulaire en conditions moyennes en MES (~100 mg $L^{-1}$) tandis que dans le bouchon vaseux (ZTM, ~1000 mg $L^{-1}$) >99% de la quantité totale de Te

sera piégé dans la phase particulaire. Les expériences de fractionnement solide montrent que $Te_{nat}$ et $Te_{ex}$ sont principalement associés à la fraction soluble dans l'acide, comprenant les oxydes, les carbonates, les monosulphures et les phases phyllosilicates amorphes et cristallins. Des artefacts méthodologiques ont été retrouvés uniquement pour les extractions de Se sur la fraction F2-ascorbate (comme pour le Sb) et F3-$H_2O_2$. Les résultats de cette étude de laboratoire sont prêts à être soumis dans la revue scientifique à comité de lecture *Applied Geochemistry*, sous le titre « *Tellurium and selenium sorption kinetics and solid fractionation under contrasting estuarine salinity and turbidity conditions* ».

***Chapitre 6 : Cinétique d'adsorption et désorption des radio-traceurs $^{75}$Se et $^{113}$Sn en conditions estuariennes : comparaison entre les systèmes Gironde et Rhône***

Ce chapitre présente des résultats expérimentaux de Kd pour des éléments présentant des affinités contrastés (phase dissoute et phase particulaire) obtenus avec des radiotraceurs de l´étain (Sn) et du Se pour des concentrations représentatives de l'environnement. Ces expériences ont été réalisées avec des sédiments naturels provenant de l'estuaire de la Gironde et de la rivière du Rhône dans des conditions estuariennes contrastées. De plus, le transfert biologique de Sn et de Se dans les huîtres sauvages de l'estuaire de la Gironde et dans les moules du Rhône a été quantifié et complétés par des informations préliminaires sur l'organotropisme.

Les résultats suggèrent une forte mobilité du Se impliquant une prédominance d'un transport en phase dissoute, ce qui est conforme à sa bioaccumulation dans les huîtres et les moules sauvages des côtes atlantiques et méditerranéennes, particulierèment dans les branchies et la glande digestive. A l'inverse, la quasi-totalité de Sn est adsorbé sur les particules en suspension, généralement indépendante de la nature des particules et des conditions expérimentales de turbidité et de salinité. La bioaccumulation de Sn dans les huîtres et les moules est moindre que celle du Se mais non-négligeable, montrant une plus forte accumulation dans le manteau. Une comparaison entre entre les Kd expérimentaux et ceux de terrain (données non publiées) et de laboratoire (Chapitre 5) suggère des valeurs de Kd comparables pour des éléments très particulaires tels que Sn, mais très variables pour des éléments plus solubles tels que Se. Ces différences entre Kd de terrain et de laboratoire pour un même élément doivent être considérées dans les scénarios de dispersion de radionucléides.

Les résultats de l'expérimentation avec les radiotraceurs sont prêts à être soumis dans la revue scientifique à comité de lecture *Journal of Environmental Radioactivity*, sous le titre « *Tin-113 and Selenium-75 radiotracer adsorption and desorption kinetics in contrasting estuarine salinity and turbidity conditions* ».

***Discussion, conclusions et perspectives du travail***

Ce travail fournit une meilleure caractérisation et compréhension environnementales des cycles biogéochimiques de Sb et Te dans les eaux de transition. De plus, les différentes approximations réalisées pour caractériser le comportement et la distribution de Sb et Te dans le système fluvio-estuarien de la Gironde (études de terrain et résultats de laboratoire) ont permis le développement des scenarios de dispersion de leurs homologues radioactifs. Ces scenarios prennent en compte trois **paramètres temporels fondamentaux** : (i) le temps nécessaire pour atteindre l'équilibre thermodynamique de Sb et Te entre la phase dissoute et particulaire le long des gradients de salinité et turbidité, (ii) la persistance environnementale des radionucléides, donnée par leur temps de demi-vie, et (iii) le temps de résidence des masses d'eau et particules dans l'estuaire de la Gironde.

Les **scénarios préliminaires de dispersion** des rejets hypothétiques accidentels de radionucléides de Sb et Te de la CNPE présente dans l'estuaire de la Gironde, à partir des valeurs experimentales des Kd de Sb et Te, suggèrent :

- Une libération accidentelle dans des conditions de crue favoriserait une adsorption et une rétention efficaces des radionucléides de Te et une retention partielle des radionucléides de Sb dans la ZTM, située en aval de l'estuaire. Une telle situation lie le devenir des radionucléides à la dynamique estuarienne de la ZTM qui entraînerait un long temps de résidence (environ 1 à 2 ans) et un transport en amont des radionucléides de Sb et Te vers l'agglomération bordelaise avec la migration saisonnière de la ZTM au cours de l'étiage suivant.
- En revanche, un relargage accidentel en conditions d'étiage, lorsque la position de la ZTM se situe en amont de la source ponctuelle, entraînerait une adsorption moins importante des radionucléides de Te dans la phase particulaire. De plus, les radionucléides de Sb auront une présence plus importante sous forme dissoute. Cette situation impliquerait donc une dispersion des radionucléides $Te_d$ et $Sb_d$ contrôlée par les temps de résidence des masses d'eau (jusqu'à environ 80 jours), avec une expulsion continue en zone côtière.

Les **conclusions** fondamentales de ce travail peuvent être résumées comme suit :

- La quantification des Sb et Te dissous et particulaires dans le système fluvio-estuarien de la Gironde reflète des comportements biogéochimiques très contrastés. En effet, des différences se retrouvent aux niveaux :
  - des teneurs environnementales (i.e., Sb à des niveaux traces et Te à des niveaux ultra-traces), plus fortement determinées par des activités anthropiques et des caractéristiques lithogeniques pour le Sb que le Te,

- des caractéristiques saisonnières (i.e., présent que pour $Sb_d$ et parallèle pour $Te_d$ et $Te_p$),
- des Kd naturels (i.e., $\log_{10} Kd_{Sb}$ entre 3.1 et 5.1 L $kg^{-1}$, $\log_{10} Kd_{Te}$ entre 4.3 et 5.7 L $kg^{-1}$) montrant une réactivité plus importante pour le Sb et une plus forte affinité de Te vers la phase particulaire,
- des phases porteuses dans les sédiments (i.e., Sb se retrouve en >90% et Te entre 50-70% dans la fraction réfractaire, avec une mobilité non négligeable de Sb associée à la dissolution des oxydes de Fe et Mn et une bioaccessibilité potentielle de Te depuis la fraction acide soluble),
- des flux bruts totaux dans l'estuaire de la Gironde (i.e., variant de 2800-10200 kg $an^{-1}$ pour le Sb et de 20-160 kg $an^{-1}$ pour le Te),
- des comportements biogéochimiques non-conservatifs le long du gradient de salinité et de turbidité (i.e., additif pour le Sb et de soustraction pour le Te),
- des facteurs de bioaccumulation non-negligeables chez les huîtres sauvages à l'embouchure de l'estuaire de la Gironde (i.e., de 60-140 pour Sb et de 2900-6300 pour Te), sans montrer des tendances spécifiques au cours du temps indiquant une influence de la contamination anthropique.

- La comparaison des phases porteuses de Sb, Te et Se hérités (naturels) et apportés (ajoutés) montre une mobilité/dissolution plus importante des éléments apportés (i.e., simulant un rejet anthropique en milieu aquatique) en conditions potentiellement retrouvables dans l'environnement (p.e., présentant des processus de diagenèse précoce avec des complexants organiques).

- Une batterie d'extractions selectives montre des artefacts associés à certains éléments, comme le Sb et le Se, risquant de produire des résultats et des interprétations biaisées. Ainsi, les réactifs d'extraction classiques, ne peuvent pas être utilisés systématiquement pour extraire de « nouveaux » éléments pour lesquels les protocoles n'ont pas été élaborés, adaptés ni testés.

- Les valeurs de partition solide/liquide (Kd) sont un prérequis au développement conceptuel de scénarios de dispersion de radionucléides. Les modèles prédictifs actuels utilisent des Kds détérminés à partir des données de terrain et de laboratoire indistinctement. Ce travail de thèse montre qu'une telle hypothèse est valable pour des éléments présentant de fortes affinités pour les particules (tels que Te et Sn). Cependant, les Kds basés sur le terrain et en laboratoire peuvent différer considérablement pour des éléments plus solubles (comme Se et Sb). Dans ce dernier cas, les scénarios devraient être basés sur des valeurs de Kd détérminées en laboratoire avec des concentrations et des conditions représentatives du rejet anthropique attendu et du milieu environnemental.

Cette étude fournit une base de référence pour d'autres recherches concernant la biogéochimie de Sb et Te dans les environnements fluvio-estuariens ainsi que les modèles de dispersion environnementale des homologues radioactifs. Ainsi, ces travaux permettent de proposer des **perspectives** concernant de futurs lignes de recherche telles que :

- *Sur le plan analytique* : (i) il est nécessaire de produire des matériaux certifiés de référence représentatifs des concentrations environnementales pour les matrices eau salée et biologiques afin de valider les analyses de Te dans ces types d'échantillons. De plus, (ii) il existe encore une grande incertitude concernant les teneurs de Te dissous dans les eaux saumâtres et dans l'océan. Ainsi, les développements analytiques futurs devraient se focaliser sur le dosage de cet élément trace dans ces matrices complexes.

- La distribution de Te dans le système fluvio-estuarien de la Gironde s'est révélée très affine de la phase particulaire. D'autres études s'interrogeant sur la c*ontamination anthropique actuelle de Te* dans le milieu aquatique devraient se focaliser dans des zones d'étude moins turbides afin de garder le signal anthropique potentiellement présent dans le système.

- *Concernant la prédiction des rejets anthropiques en milieu aquatique* : Une meilleure compréhension de la spéciation chimique (inorganique et/ou organique) des éléments traces rejetés dans l'environnement aquatique semble nécessaire. Une telle approche permettrait d'individualiser les impacts des formes moléculaires précises, montrant potentiellement un comportement indépendant à celui de l'élément cible naturel.

- *La suite aux scenarios de dispersion* des radionucléides de Sb et Te dans les systèmes fluvio-estuariens de la Gironde et du Rhône inclus dans ce travail de thèse serait le développement mathématique, rajoutant la dose émise dans chaque condition correspondante à la persistance et quantité des radionucléides rejetés. Cette approche permettrait de quantifier le risque radiologique des rejets accidentels hypothétiques de Sb et Te afin de renforcer la prise de décision post-accidentelle (objectif du projet AMORAD).

- Afin de *mieux caractériser l'exposition radioactive* d'après un cocktail de radionucléides rejetés pendant un accident nucléaire, des études complémentaires doivent être menées sur le comportement environnemental de nouveaux radionucléides encore peu étudiés. Il semblerait intéressant de continuer à étudier les radionucléides de l'étain (Sn) et du sélénium (Se) concernant : (i) leurs isotopes présentant des temps de demi-vies très variables (de court à long terme), (ii) leur potentielle mobilité environnementale dans le cadre de la gestion des déchets nucléaires, et (iii) leur rôle biologique, faisant partie des éléments bio-essentiels.

# REFERENCES

# A

**Abdou, M., Schäfer, J., Cobelo-García, A., Neira, P., Petit, J. C., Auger, D., et al. (2016).** Past and present platinum contamination of a major European fluvial–estuarine system: Insights from river sediments and estuarine oysters. Marine Chemistry, 185, 104-110.

**Abdou, M., Schäfer, J., Hu, R., Gil-Díaz, T., Garnier, C., Brach-Papa, C., et al. (2019).** Platinum in sediments and mussels from the northwestern Mediterranean coast: Temporal and spatial aspects. Chemosphere, 215, 783-792.

**Abril, G., Etcheber, H., Le Hir, P., Bassoullet, P., Boutier, B., Frankignoulle, M. (1999).** Oxic/anoxic oscillations and organic carbon mineralization in an estuarine maximum turbidity zone (The Gironde, France). Limnology and Oceanography, 44(5), 1304-1315.

**Agence Nationale de Sécurité (ANS 2016).** <https://www.asn.fr/Informer/Dossiers/La-surete-des-centrales-nucleaires/Le-parc-francais-des-centrales-nucleaires> Last accessed on the 14/12/2017

**Ah, Y., Car, M. (2016).** Mini Review Uranium-Thorium Decay Series in the Marine Environment of the Southern South China Sea. Journal of Geology and Geophysics, 5(246), 2.

**Al-Attar, A. F., Martin, M. H., Nickless, G. (1988).** A comparison between selenium and tellurium uptake and toxicity to Lolium perenne seedlings. Chemosphere, 17, 845-850.

**Alborés, A. F., Cid, B. P., Gómez, E. F., López, E. F. (2000).** Comparison between sequential extraction procedures and single extractions for metal partitioning in sewage sludge samples. Analyst, 125(7), 1353-1357.

**Allen, G.P. (1972).** Etude des processus sédimentaires dans l'estuaire de la Gironde. Mémoire IGBA. PhD Thesis, Bordeaux.

**Allen, G., Sauzay, G., Castaing, P., Jouanneau, J.M. (1977).** Transport and deposition of suspended sediment in the Gironde Estuary, France. In: estuarine processes (proc. Third int. estuarine research conf. Gavelston, U.S.A.: Oct. 7-9, 1975) Wiley, M. (ED.), 2, Circulation, Sediments and Transfer of Material in the Estuary, New York, U.S.A., Academic Press, 63-81.

**Allen, G. P., Salomon, J. C., Bassoullet, P., Du Penhoat, Y., De Grandpré, C. (1980).** Effects of tides on mixing and suspended sediment transport in macrotidal estuaries. Sedimentary Geology, 26, 69-90.

**Aliyu, A. S., Evangeliou, N., Mousseau, T. A., Wu, J., Ramli, A. T. (2015).** An overview of current knowledge concerning the health and environmental consequences of the Fukushima Daiichi Nuclear Power Plant (FDNPP) accident. Environment International, 85, 213-228.

**Aloisi, J. C., Monaco, A. (1975).** La sédimentation infralittorale. Les prodeltas nord-méditerranéens. Comptes Rendus Académie Science Paris, 280, 2833-2836.

**Alonso, A., González, C. (1991).** Modelling the chemical behaviour of tellurium species in the reactor pressure vessel and the reactor cooling system under severe accident conditions. Commission of the European Communities, Brussels.

**Ambe, S. (1987).** Adsorption kinetics of antimony (V) ions onto alpha-$Fe_2O_3$ surfaces from an aqueous solution. Langmuir 3, 489–493.

**Ames, D.E., Farrow, C.E.G.,** in Mineral deposits of Canada: a synthesis of major deposit types, district metallogeny, the evolution of geological provinces, and exploration methods, ed. W. D. Goodfellow, Geological Association of Canada, Special Publication 5, Mineral Deposits Division, **2007**, pp. 329–350.

**Amon, T. and Oberhummer, H. (2007).** Basic scientific information and facts about radiation. <http://www.radiationgames.net/0Nzm/CellTissueHumanBody6/O3aaklm/Radiation.htm> Last accessed on the 09/03/15

**An, Y.J., Kim, M. (2009).** Effect of antimony on the microbial growth and the activities of soil enzymes. Chemosphere, 74(5), 654-659.

**Anderson, H. L., Fermi, E., Grosse, A. V. (1941).** Branching Ratios in the Fission of Uranium (235). Physical Review, 59(1), 52.

**Andreae, M.O. (1983)** The determination of the chemical species of some of the "hydride elements" (arsenic, antimony, tin and germanium) in sea water: methodology and results. In Trace Metals in Sea Water (Eds. C.S. Wong, E. Boyle, K.W. Bruland, J.D. Burton, E.D. Goldberg). Springer Science + Business Media New York. DOI: 10.1007/978-1-4757-6864-0

**Andreae, M. O. (1984).** Determination of inorganic tellurium species in natural waters. Analytical Chemistry, 56(12), 2064-2066.

**Andreae, M. O., Byrd, J. T., Froehlich, P. N. (1983).** Arsenic, antimony, germanium, and tin in the Tejo Estuary, Portugal: modeling a polluted estuary. Environmental Science and Technology, 17(12), 731-737.

**Andreae, M. O., Froelich, P. N. (1984).** Arsenic, antimony, and germanium biogeochemistry in the Baltic Sea, Tellus, Series B, 36, 101–117.

**Arellano, M. (2001).**"Introducción al Análisis Clásico de Series de Tiempo", 5campus.com, Estadística. <http://www.5campus.com/leccion/seriest> Last accessed 11/11/18

**Arnot, J.A., Gobas, F.A.P.C. (2006).** A review of bioconcentration factor (BCF) and bioaccumulation factor (BAF) assessments for organic chemicals in aquatic organisms. Environmental Reviews, 14: 257-297

**ASN Annual Report.** Chapter 12. EDF Nuclear power plants. <https://www.google.com/url?sa=t&rct=j&q=&esrc=s&source=web&cd=10&ved=2ahUKEwjr4PHvrrPeAhXMyYUKHf-YATEQFjAJegQIAxAC&url=https%3A%2F%2Fwww.asn.fr%2Fannual_report%2F2006%2FPDF%2Fnuclear-power-plants-EDF.pdf&usg=AOvVaw08TLSnb93iD55nYUnZHvrf> Last accessed on the 01/11/18

**Audi, G., Bersillon, O., Blachot, J., Wapstra, A.H. (2003).** The NUBASE evaluation of nuclear and decay properties. Nuclear Physics, 729: 3-128

**Audry, S., Blanc, G., Schäfer, J. (2006).** Solid state partitioning of trace metals in suspended particulate matter from a river system affected by smelting-waste drainage. Science of the Total Environment, 363(1-3), 216-236.

**Audry, S., Grosbois, C., Bril, H., Schäfer, J., Kierczak, J., Blanc, G. (2010).** Post-depositional redistribution of trace metals in reservoir sediments of a mining/smelting-impacted watershed (the Lot River, SW France). Applied Geochemistry, 25(6), 778-794.

**Audry, S., Schäfer, J., Blanc, G., Bossy, C., Lavaux, G. (2004a).** Anthropogenic components of heavy metal (Cd, Zn, Cu, Pb) budgets in the Lot-Garonne fluvial system (France). Applied Geochemistry 19, 769-786

**Audry, S., Schäfer, J., Blanc, G., Jouanneau, J. M. (2004b).** Fifty-year sedimentary record of heavy metal pollution (Cd, Zn, Cu, Pb) in the Lot River reservoirs (France). Environmental Pollution, 132(3), 413-426.

**Austin, L. S., Millward, G. E. (1988).** Simulated effects of tropospheric emissions on the global antimony cycle. Atmos. Environ., 22, 1395. doi:10.1016/0004-6981(88)90164-3

**Averill, B.A. and Eldredge, P. (2012).** Chapter 20: Nuclear Chemistry. Principles of General Chemistry, v. 10. <http://2012books.lardbucket.org/books/principles-of-general-chemistry-v1.0/s24-nuclear-chemistry.html> Last accessed on the 07/03/15.

# B

**Ba, L. A., Döring, M., Jamier, V., Jacob, C. (2010).** Tellurium: an element with great biological potency and potential. Organic and Biomolecular Chemistry, 8(19), 4203-4216.

**Babula, P., Adam, V., Opatrilova, R., Zehnalek, J., Havel, L., Kizek, R. (2009).** Uncommon heavy metals, metalloids and their plant toxicity: a review. In Organic Farming, Pest Control and Remediation of Soil Pollutants (pp. 275-317). Springer, Dordrecht.

**Baesman, S.M., Bullen, T.D., Dewald, J., Zhang, D., Curran, S., Islam, F.S., Beveridge, T.J., Oremland, R.S. (2007).** Formation of tellurium nanocrystals during anaerobic growth of bacteria that use Te oxyanions as respiratory electron acceptors. Applied and Environmental Microbiology, 73(7), 2135-2143.

**Baeza, A., Corbacho, J. A., Rodríguez, A., Galván, J., García-Tenorio, R., Manjón, G., et al. (2012).** Influence of the Fukushima Dai-ichi nuclear accident on Spanish environmental radioactivity levels. Journal of Environmental Radioactivity, 114, 138-145.

**Baig, J. A., Kazi, T. G., Arain, M. B., Shah, A. Q., Sarfraz, R. A., Afridi, H. I., et al. (2009).** Arsenic fractionation in sediments of different origins using BCR sequential and single extraction methods. Journal of Hazardous Materials, 167(1-3), 745-751.

**Bajaj, M., Winter, J. (2014).** Se (IV) triggers faster Te (IV) reduction by soil isolates of heterotrophic aerobic bacteria: formation of extracellular SeTe nanospheres. Microbial cell factories, 13(1), 168.

**Baumann, Z., Casacuberta, N., Baumann, H., Masqué, P., Fisher, N. S. (2013).** Natural and Fukushima-derived radioactivity in macroalgae and mussels along the Japanese shoreline. Biogeosciences, 10(6), 3809-3815.

**Beaty, R. D., Manuel, O. K. (1973).** Tellurium in rocks. Chemical Geology, 12(2), 155-159.

**Belzile, N., Chen, Y. W. (2015).** Tellurium in the environment: A critical review focused on natural waters, soils, sediments and airborne particles. Applied Geochemistry, 63, 83-92.

**Belzile, N., Chen, Y.-W., Wang, Z. (2001).** Oxidation of antimony (III). by amorphous iron and manganese oxyhydroxides. Chemical Geology, 174, 379–387.

**Bekkali, N.** (2013). Modelos ARIMA y función de transferencia para series temporales (PFC). Universidad Politécnica de Valencia. <https://riunet.upv.es/bitstream/handle/10251/37010/Bekkali_Najib.pdf?sequence=1> Last accessed 12/11/18.

**Biver, M. (2011).** Some kinetic aspects of the mobilization of antimony from natural sources (Doctoral dissertation).

**Biver, M., Filella, M. (2016).** Bulk dissolution rates of cadmium and bismuth tellurides as a function of pH, temperature and dissolved oxygen. Environmental Science and Technology, 50(9), 4675-4681.

**Biver, M., Quentel, F., Filella, M. (2015).** Direct determination of tellurium and its redox speciation at the low nanogram level in natural waters by catalytic cathodic stripping voltammetry. Talanta, 144, 1007-1013.

**Blanc, G., Lapaquellerie, Y., Maillet, N., Anschutz, P. (1999).** A cadmium budget for the Lot-Garonne fluvial system (France). Hydrobiologia, 410, 331-341.

**Bolanz, M., Bläss, U., Ackermann, S., Ciobotă, V., Rösch, P., Tarcea, N., Popp, J., Majzlan, J. (2013).** The effect of antimonate, arsenate, and phosphate on the transformation of ferrihydrite to goethite, hematite, feroxyhyte, and tripuhyite. Clays and Clay Minerals, 61(1), 11-25.

**Boles, J.O., Lebioda, L., Dunlap, R.B., Odom, J.D. (1995).** Telluromethionine in structural biochemistry. SAAS Bulletin, Biochemistry and Biotechnology, 8, 29-34.

**Borsook, H., Davenport, H. W., Jeffreys, C. E., Warner, R. C. (1937).** The oxidation of ascorbic acid and its reduction in vitro and in vivo. Journal of Biological Chemistry, 117(1), 237-279.

**Bordas, F., Bourg, A. C. (1998).** A critical evaluation of sample pretreatment for storage of contaminated sediments to be investigated for the potential mobility of their heavy metal load. Water, Air, and Soil Pollution, 103(1-4), 137-149.

**Broche, P., Devenon, J. L., Forget, P., de Maistre, J. C., Naudin, J. J., Cauwet, G. (1998).** Experimental study of the Rhone plume. Part I: physics and dynamics. Oceanologica Acta, 21(6), 725-738.

**Brookins, D. G. (1988).** Tellurium. In Eh-pH Diagrams for Geochemistry (pp. 20-21). Springer, Berlin, Heidelberg.

**Bruneau, A., Fortier, M., Gagne, F., Gagnon, C., Turcotte, P., Tayabali, A., et al. (2015).** In vitro immunotoxicology of quantum dots and comparison with dissolved cadmium and tellurium. Environmental Toxicology, 30(1), 9-25.

**Bryan, G. W. (1963).** The accumulation of $^{137}Cs$ by brackish water invertebrates and its relation to the regulation of potassium and sodium. Journal of the Marine Biological Association of the United Kingdom, 43(2), 541-565.

**Bryan, G.W., Langston, W.J. (1992).** Bioavailability, accumulation and effects of heavy metals in sediments with special reference to United Kingdom estuaries: a review. Environmental Pollution, 76, 89-131.

**Budisa, N., Steipe, B., Demange, P., Eckerskorn, C., Kellermann, J., Huber, R. (1995).** High-level biosynthetic substitution of methionine in proteins by its analogs 2-aminohexanoic acid, selenomethionine, telluromethionine and ethionine in Escherichia coli. European Journal of Biochemistry, 230(2): 788-796

**Buesseler, K., Dai, M., Aoyama, M., Benitez-Nelson, C., Charmasson, S., Higley, K., et al. (2017).** Fukushima Daiichi–derived radionuclides in the ocean: transport, fate, and impacts. Annual Review of Marine Science, 9, 173-203.

**Buffle, J., Leppard, G. G. (1995).** Characterization of aquatic colloids and macromolecules. 1. Structure and behavior of colloidal material. Environmental Science and Technology, 29(9), 2169-2175.

**Buffle, J., Van Leeuwen, H. P. (1992).** Environmental particles. Vol. 1. (IUPAC Environmental analytical and physical chemistry series).

**Bureau de Recherches Géologiques et Minières (BRGM, 2014).** Carrières de France, exploitations actives. <http://www.brgm.fr/actualite/brgm-sim-presentent-carte-carrieres-france> Last accessed on the 13/07/2015.

**Buschmann, J., Sigg, L. (2004).** Antimony (III) binding to humic substances: influence of pH and type of humic acid. Environmental Science and Technology, 38(17), 4535-4541.

**Butterman, W. C., Carlin Jr, J. F. (2004).** Mineral commodity profiles: Antimony (No. 2003-19).

**Byrd, J. T. (1990).** Comparative geochemistries of arsenic and antimony in rivers and estuaries. Science of the Total Environment, 97, 301-314.

# C

**Cal-Prieto, M. J., Carlosena, A., Andrade, J. M., Muniategui, S., López-Mahía, P., Prada, D. (2000).** Study of Chemical Modifiers for the Direct Determination of Antimony in Soils and Sediments by Ultrasonic Slurry Sampling-ETAAS with D~ 2 Compensation. ATOMIC SPECTROSCOPY-NORWALK CONNECTICUT-, 21(3), 93-99.

**Calmet D, Bouisset P, Charmasson S, Kerboul C. (1994).** Protection and nuclear safety institute permanent observatory of marine radioactivity along the French coast of the Mediterranean Sea. In: Cigna A, Delfanti R, Serro L, editors. The radiological exposure of the population of the European community to radioactivity in the Mediterranean Sea. Marina-Med project. Rome, Italy: Proceedings of a seminar: EUR 155564 EN, pp. 415]425.

**Canfield, D.E. (1989).** Reactive iron in marine sediments. Geochimica et Cosmochimica Acta, 53, 619-632.

**Carbol, P., Solatie, D., Erdmann, N., Nylen, T., Betti, M. (2003).** Deposition and distribution of Chernobyl fallout fission products and actinides in a Russian soil profile. Journal of Environmental Radioactivity, 68(1), 27-46.

**Carlin, J. F. (2006).** Antimony recycling in the United States in 2000. US Department of the Interior, US Geological Survey.

**Casiot, C., Alonso, M. C. B., Donard, O. F., Potin-Gautier, M., Boisson, J. (1998).** Simultaneous speciation of arsenic, selenium, antimony and tellurium species in waters and soil extracts by capillary electrophoresis and UV detection. Analyst, 123(12), 2887-2893.

**Castaing, P., Allen, G.P. (1981).** Mechanisms controlling seaward escape of suspended sediment from the Gironde: a macrotidal estuary in France. Marine Geology, 40, 101-118.

**Castaing, P., Jouanneau, J.M. (1979).** Temps de résidence des eaux et des suspensions dans l'estuaire de la Gironde. Journal de Recherche Océanographique, IV, 41-52.

**Castelle, S. (2008).** Spéciation et réactivité du mercure dans le système fluvio-estuarien girondin. PhD Thesis. Bordeaux, p. 201

**Centre for Food Safety (2013).** The first Hong Kong total diet study: metallic contaminants. Report nº5. Food and Environmental Hygiene Department, Queensway, Hong Kong.

**Chang, S. C., Jackson, M. L. (1957).** Solubility Product of Iron Phosphate 1. Soil Science Society of America Journal, 21(3), 265-269.

**Charmasson, S., Barker, E., Calmet, D., Pruchon, A. S., Thébault, H. (1999).** Long-term variations of man-made radionuclide concentrations in a bio-indicator *Mytilus galloprovincialis* from the French Mediterranean coast. Science of the Total Environment, 237, 93-103.

**Chasteen, T. G., Bentley, R. (2003).** Biomethylation of selenium and tellurium: microorganisms and plants. Chemical Reviews, 103(1), 1-26.

**Chasteen, T. G., Fuentes, D. E., Tantaleán, J. C., Vásquez, C. C. (2009).** Tellurite: history, oxidative stress, and molecular mechanisms of resistance. FEMS Microbiology Reviews, 33(4), 820-832.

**Chávez-Villalba, J., Arreola-Lizárraga, A., Burrola-Sánchez, S., Hoyos-Chairez, F. (2010).** Growth, condition, and survival of the Pacific oyster *Crassostrea gigas* cultivated within and outside a subtropical lagoon. Aquaculture, 300, 128-136.

**Chen, Z., Xu, G.D., Chen, S., Zhang, J.H., Wang, M.M. (2014).** Hydrothermal synthesized nanostructure Bi–Sb–Te thermoelectric materials. Journal of Alloys and Compounds, 588, 384-387.

**Chester, R., Hughes, M. J. (1967).** A chemical technique for the separation of ferro-manganese minerals, carbonate minerals and adsorbed trace elements from pelagic sediments. Chemical geology, 2, 249-262.

**Choi, Y., Kida, S., Takahashi, K. (2013).** The impact of oceanic circulation and phase transfer on the dispersion of radionuclides released from the Fukushima Dai-ichi Nuclear Power Plant. Biogeosciences, 10(7), 4911-4925.

**Ciceri, G., Traversi, A. L., Martinotti, W., Queirazza, G. (1988).** Radionuclide partitioning between water and suspended matter: comparison of different methodologies. In Studies in Environmental Science (Vol. 34, pp. 353-375). Elsevier.

**Ciffroy, P., Durrieu, G., Garnier, J. M. (2009).** Probabilistic distribution coefficients (Kds) in freshwater for radioisotopes of Ag, Am, Ba, Be, Ce, Co, Cs, I, Mn, Pu, Ra, Ru, Sb, Sr and Th–implications for uncertainty analysis of models simulating the transport of radionuclides in rivers. Journal of Environmental Radioactivity, 100(9), 785-794.

**Claisse, D., Joanny, M., Quintin, J.-Y. (1992).** Le réseau national d'observation de la qualité du milieu marin (RNO). Analusis, M19–M22.

**Clark, R.S., Rowe, M.W., Ganapathy, R., Kuroda, P.K. (1967).** Iodine, uranium and tellurium contents in meteorites. Geochimica et Cosmochimica Acta, 31(10), 1605-1613

**Cobelo-García, A., Filella, M., Croot, P., Frazzoli, C., Du Laing, G., Ospina-Alvarez, N., Rauch, S., Salaun, P., Schäfer, J., Zimmermann, S. (2015).** COST action TD1407: network on technology-critical elements (NOTICE)—from environmental processes to human health threats. Environmental Science and Pollution Research, 22(19), 15188-15194.

**Cosma, C. (2002).** Some aspects of radioactive contamination after Chernobyl accident in Romania. Journal of Radioanalytical and Nuclear Chemistry, 251(2), 221-226.

**Costa, F. B., Yukimitu, K., Nunes, L. A. O., Figueiredo, M. S., Andrade, L. H. C., Lima, S. M., Moraes, J. C. S. (2016).** Spectroscopic properties of $Nd^{3+}$-doped tungsten–tellurite glasses. Journal of Physics and Chemistry of Solids, 88, 54-59.

**Coynel, A., Schäfer, J., Hurtrez, J. E., Dumas, J., Etcheber, H., Blanc, G. (2004).** Sampling frequency and accuracy of SPM flux estimates in two contrasted drainage basins. Science of the Total Environment, 330(1-3), 233-247.

**Coynel, A., Schäfer, J., Dabrin, A., Girardot, N., Blanc, G. (2007a).** Groundwater contributions to metal transport in a small river affected by mining and smelting waste. Water Research, 41, 3420-3428.

**Coynel, A., Blanc, G., Marache, A., Schäfer, J., Dabrin, A., Maneux, E., Bossy, C., Masson, M., Lavaux, G. (2009).** Assessment of metal contamination in a small mining- and smelting-affected watershed: high resolution monitoring coupled with spatial analysis by GIS. Journal of Environmental Monitoring, 11, 962-976.

**Cunha, R. L., Gouvea, I. E., Juliano, L. (2009).** A glimpse on biological activities of tellurium compounds. Anais da Academia Brasileira de Ciências, 81(3), 393-407.

**Cutter, G.A., Cutter, L.S. (1995).** Behaviour of dissolved antimony, arsenic and selenium in the Atlantic Ocean. Marine Chemistry, 49: 295-306

**Cutter, G.A., Cutter, L.S. (1998).** Metalloids in the high latitude North Atlantic: Sources and internal cycling, Marine Chemistry, 61, 25–36.

**Cutter, G.A., Cutter, L.S. (2006).** Biogeochemistry of arsenic and antimony in the North Pacific Ocean. Geochemistry Geophysics Geosystems 7, Q05M08, doi:10.1029/ 2005GC001159

**Cutter, G.A., Cutter, L.S. Featherstone, A.M., Lohrenz, S.E. (2001).** Antimony and arsenic biogeochemistry in the western Atlantic Ocean, Deep Sea Research, Part II, 48,

# D

**Dabrin, A., Schäfer, J., Blanc, G., Strady, E., Masson, M., Bossy, C., et al. (2009).** Improving estuarine net flux estimates for dissolved cadmium export at the annual timescale: application to the Gironde Estuary. Estuarine, Coastal and Shelf Science, 84(4), 429-439.

**Daskalakis, K.D., O'Connor, T.P., Crecelius, E.A. (1997).** Evaluation of digestion procedures for determining silver in mussels and oysters. Environmental Science and Technology, 31, 2303-2306.

**Davidson, C. M., Duncan, A. L., Littlejohn, D., Ure, A. M., Garden, L. M. (1998).** A critical evaluation of the three-stage BCR sequential extraction procedure to assess the potential mobility and toxicity of heavy metals in industrially-contaminated land. Analytica Chimica Acta, 363(1), 45-55.

**Dean, L. A. (1938).** An attempted fractionation of the soil phosphorus. The Journal of Agricultural Science, 28(2), 234-246.

**De Meio, R.H. Henriques, F.C. (1947).** Tellurium IV, excretion and distribution in tissues studied with a radioactive isotope. Journal of Biological Chemistry, 169, 609-623.

**DEI/SESURE Report n°2010-04 (IRSN).** Flux de radioactivité exportés par le Rhône en Méditerranée en 2008.

**Díaz-Vásquez, W. A., Abarca-Lagunas, M. J., Arenas, F. A., Pinto, C. A., Cornejo, F. A., Wansapura, P. T., et al. (2014).** Tellurite reduction by Escherichia coli NDH-II dehydrogenase results in superoxide production in membranes of toxicant-exposed cells. Biometals, 27(2), 237-246.

**DIREN - National Hydrographic Databank (2015).** Ministère de l'Écologie, du Développement Durable et de l'Énergie. <http://www.hydro.eaufrance.fr/> Last accessed on the 19/06/18.

**Dong, Z., Li, X., Liang, K., Mao, S., Huang, X., Yang, B., et al. (2007).** Telluroxides exhibit hydrolysis capacity. The Journal of Organic Chemistry, 72(2), 606-609.

**Duan, L. Q., Song, J. M., Li, X. G., Yuan, H. M. (2010).** The behaviors and sources of dissolved arsenic and antimony in Bohai Bay. Continental Shelf Research, 30(14), 1522-1534.

**Duan, L. Q., Song, J. M., Yuan, H. M., Li, X. G., Li, N., Ma, J. K. (2014).** Distribution, chemical speciation and source of trace elements in surface sediments of the Changjiang Estuary. Environmental Earth Sciences, 72(8), 3193-3204.

**du Bois, P. B., Salomon, J. C., Gandon, R., Guéguéniat, P. (1995).** A quantitative estimate of English Channel water fluxes into the North Sea from 1987 to 1992 based on radiotracer distribution. Journal of Marine Systems, 6(5-6), 457-481.

**du Bois, P. B., Guéguéniat, P. (1999).** Quantitative assessment of dissolved radiotracers in the English Channel: sources, average impact of la Hague reprocessing plant and conservative behaviour (1983, 1986, 1988, 1994). Continental Shelf Research, 19(15-16), 1977-2002.

**Durán-Toro, V., Gran-Scheuch, A., Órdenes-Aenishanslins, N., Monrás, J. P., Saona, L. A., Venegas, F. A., et al. (2014).** Quantum dot-based assay for Cu2+ quantification in bacterial cell culture. Analytical Biochemistry, 450, 30-36.

# E

**Egnatuk, C. M., Wang, T. F. (2015).** Differentiating special nuclear materials through computationally generated gamma-ray spectra. Journal of Radioanalytical and Nuclear Chemistry, 304(3), 1211-1217.

**Eichengreen, B. (1945).** Institutions and economic growth: Europe after World War II. Economic growth in Europe since, 38-72.

**Element Collection Inc.: Gray, T., Mann, N., Whitby, M. (2007).** Periodic Table of Isotopes. < http://periodictable.com/Isotopes/051.123/index.p.full.html> Last accessed on the 10/03/2015

**Enders, R., Jekel, M. (1996).** Adsorption and Coprecipitation of Antimony (III) in the Precipitation of Several Metylhydroxides. Vom Wasser, 86, 141-156.

**Endo, S., Tanaka, K., Kajimoto, T., Thanh, N. T., Otaki, J. M., Imanaka, T. (2014).** Estimation of β-ray dose in air and soil from Fukushima Daiichi Power Plant accident. Journal of Radiation Research, 55(3), 476-483.

**Esparza Catalán, C.** SERIES TEMPORALES, Laboratorio de Estadística, CSIC. <http://humanidades.cchs.csic.es/cchs/web_UAE/tutoriales/PDF/SeriesTemporales.pdf> Last accessed 11/11/18

**Espegren, F., Glänneskog, H., Foreman, M. R. S., Ekberg, C. (2018).** Chemical interaction between sea-salt and tellurium, between 300 and 1180 K. Journal of Radioanalytical and Nuclear Chemistry, 1-9.

**Essington, M.E., Vergeer, K.A. (2015).** Adsorption of antimonate, phosphate, and sulfate by manganese dioxide: competitive effects and surface complexation modeling. Soil Science Society of America Journal, 79, 803-814.

**Eyrolle-Boyer, F., Antonelli, C., Renaud, P., Tournieux, D. (2015).** Origins and trend of radionuclides within the lower Rhône River over the last decades. Radioprotection, 50(1), 27-34.

# F

**Fehr, M. A., Rehkämper, M., Halliday, A. N., Wiechert, U., Hattendorf, B., Günther, D., et al. (2005).** Tellurium isotopic composition of the early solar system—A search for effects resulting from stellar nucleosynthesis, 126Sn decay, and mass-independent fractionation. Geochimica et Cosmochimica Acta, 69(21), 5099-5112.

**Feldmann, J., Hirner, A. V. (1995).** Occurrence of volatile metal and metalloid species in landfill and sewage gases. International Journal of Environmental Analytical Chemistry, 60(2-4), 339-359.

**Fennema, O. R. (1996).** Food Chemistry 3rd.

**Ferreira, S. L., dos Santos, W. N., dos Santos, I. F., Junior, M. M., Silva, L. O., Barbosa, U. A., et al. (2014).** Strategies of sample preparation for speciation analysis of inorganic antimony using hydride generation atomic spectrometry. Microchemical Journal, 114, 22-31.

**Filella, M. (2010).** 8: Alkyl Derivatives of Antimony in the Environment. In Organometallics in environment and toxicology (pp. 267-301).

**Filella, M. (2011).** Antimony interactions with heterogeneous complexants in waters, sediments and soils: a review of data obtained in bulk samples. Earth-science reviews, 107(3-4), 325-341.

**Filella, M. (2013).** Food for thought: a critical overview of current practical and conceptual challenges in trace element analysis in natural waters. Water, 5(3), 1152-1171.

**Filella, M., Belzile, N., Chen, Y. W. (2002a).** Antimony in the environment: a review focused on natural waters: I. Occurrence. Earth-Science Reviews, 57(1-2), 125-176.

**Filella, M., Belzile, N., Chen, Y. W. (2002b).** Antimony in the environment: a review focused on natural waters: II. Relevant solution chemistry. Earth-Science Reviews, 59(1-4), 265-285.

**Filella, M., Belzile, N., Lett, M.C. (2007).** Antimony in the environment: a review focused on natural waters. III. Microbiota relevant interactions. Earth-Science Reviews, 80(3-4), 195-217.

**Filella, M., Rodríguez-Murillo, J. C. (2017).** Less-studied TCE: are their environmental concentrations increasing due to their use in new technologies?. Chemosphere, 182, 605-616.

**Filella, M., Williams, P. A. (2012).** Antimony interactions with heterogeneous complexants in waters, sediments and soils: a review of binding data for homologous compounds. Chemie der Erde-Geochemistry, 72, 49-65.

**Filella, M., Williams, P. A., Belzile, N. (2009).** Antimony in the environment: knowns and unknowns. Environmental Chemistry, 6(2), 95-105.

**Filgueiras, A.V., Lavilla, I., Bendicho, C. (2002).** Chemical sequential extraction for metal partitioning in environmental solid samples. Journal of Environmental Monitoring, 4(6), 823-857.

**Fisher, N. S., Fowler, S. W., Boisson, F., Carroll, J., Rissanen, K., Salbu, B., et al. (1999).** Radionuclide bioconcentration factors and sediment partition coefficients in Arctic Seas subject to contamination from dumped nuclear wastes. Environmental Science and Technology, 33(12), 1979-1982.

**Fleming, A. (1932).** On the specific antibacterial properties of penicillin and potassium tellurite. Journal of Pathology of Bacteria, 35, 831-842

**Fleming, A., Young, M.Y. (1940).** The inhibitory action of potassium tellurite on coliform bacteria. Journal of Pathology of Bacteria, 51, 29-35.

**Foo, K. Y., Hameed, B. H. (2010).** Insights into the modeling of adsorption isotherm systems. Chemical Engineering Journal, 156(1), 2-10.

**FRANCAISE, République. LOI N 2015-992** Du 17 Août 2015 Relative À La Transition Énergétique Pour La Croissance Verte. 2017

**Franke, K. W., Moxon, A. L. (1936).** A comparison of the minimum fatal doses of selenium, tellurium, arsenic and vanadium. Journal of Pharmacology and Experimental Therapeutics, 58(4), 454-459.

**Froidefond, J.M., Jegou, A.M., Hermida, J., Lazure, P., Castaing, P. (1998).** Variability of the Gironde turbid plume by remote sensing, effects of climatic factors. Oceanologica Acta, 21(2), 191-207.

**Freundlich, H. (1907).** Over the adsorption in solution, Journal of Physical Chemistry, 57 (1907), 385–471.

**Furuta, N., Iijima, A., Kambe, A., Sakai, K., Sato, K. (2005).** Concentrations, enrichment and predominant sources of Sb and other trace elements in size classified airborne particulate matter collected in Tokyo from 1995 to 2004. Journal of Environmental Monitoring, 7(12), 1155-1161.

# G

**Gandon R, Bailly du Bois P et Baron Y (1998).** Caractère conservatif de l'antimoine 125 dans les eaux marines soumises à l'influence des rejets de l'usine de retraitement des combustibles irradiés de La Hague. Radioprotection, 33(4), 457-482

**Garg, S.P., Singh, I.S., Sharma, R.C. (2003).** Long term lung retention studies of 125Sb aerosols in humans. Health Physics, 84(4), 457-468.

**Garnier-Laplace, J., Fournier-Bidoz, V., Baudin, J. P. (1997).** Etat des connaissances sur les échanges entre l'eau, les matières en suspension et les sédiments des principaux radionucléides rejetés en eau douce par les centrales nucléaires. Radioprotection, 32(1), 49-71.

**Gaspard, J. P. (1982).** Physisorption and Chemisorption. In Interfacial Aspects of Phase Transformations (pp. 103-118). Springer, Dordrecht.

**Gasparon, M., Matschullat, J. (2006).** Trace metals in Antarctic ecosystems: results from the Larsemann Hills, East Antarctica. Applied Geochemistry, 21(9), 1593-1612.

**Gebel, T. (1999).** Metalle/antimon, In: Wichmann-Schlipköter-Fülgraff (Ed.). Umweltmedizinisches, Handbuch, p. 17.

**Germain P, Masson M et Baron Y (1990).** Contribution aux recherches sur les movements des élèments à l'état de traces dans les eaux côtières de la Manche par l'étude de la distribution spatiale de traceurs radioactifs industriels dans les moules et les fucus. Rapport CEA-R-5534

**Gillain, G., Brihaye, C. (1985).** A routine speciation method for a pollution survey of coastal sea-water. Oceanologica Acta, 8(2), 231-235.

**Gleyzes, C., Tellier, S., Astruc, M. (2002).** Fractionation studies of trace elements in contaminated soils and sediments: a review of sequential extraction procedures. TrAC Trends in Analytical Chemistry, 21(6-7), 451-467.

**Gmelin, C.G. (1824)** Versuche über die Wirkungen des Baryts, Strontians, Chroms, Molybdaens, Wolframs, Tellurs, Titans, Osmiums, Platins, Iridiums, Rhodiums, Palladiums, Nickels, Kobalts, Urans, Ceriums, Eisens und Mangans auf den tierischen Organismus. Tübingen, p. 43.

**Goldberg, E. D., Arrhenius, G. O. S. (1958).** Chemistry of Pacific pelagic sediments. Geochimica et Cosmochimica Acta, 13(2-3), 153-212.

**Goldfarb, R. J. (2014).** Tellurium: The Bright Future of Solar Energy. US Department of the Interior, US Geological Survey.

**Goles, G.G., Anders, E. (1962).** Abundances of iodine tellurium and uranium in meteorites. Geochimica et Cosmochimica Acta, 26(7), 723-737.

**Gommy, C. (1997).** Optimisation d'un schéma de spéciation des métaux Pb, Zn, Cd et Cu: Application à des sols pollués du Nord de la France. Thèse, Université de Technologie de Compiègne, France.

**Groenenberg, J. E., Römkens, P. F., Zomeren, A. V., Rodrigues, S. M., Comans, R. N. (2017).** Evaluation of the single dilute (0.43 M) nitric acid extraction to determine geochemically reactive elements in soil. Environmental Science and Technology, 51(4), 2246-2253.

**GRNC Groupe Radioécologie Nord Cotentin (1999).** Inventaire des rejets radioactifs des installations nucléaires. Rapport final, volume 1. IRSN, Fontenay aux Roses.

**Grousset, F.E., Jouanneau, J.M., Castaing, P., Lavaux, G., Latouche, C. (1999).** A 70-year record of contamination from industrial activity along the Garonne River and its tributaries (SW France). Estuarine, Coastal and Shelf Science, 48, 401-414.

**Gu, B., Schmitt, J., Chen, Z., Liang, L., McCarthy, J. F. (1994).** Adsorption and desorption of natural organic matter on iron oxide: mechanisms and models. Environmental Science and Technology, 28(1), 38-46.

**Guegueniat, P., Kershaw, P., Hermann, J., du Bois, P. B. (1997).** New estimation of La Hague contribution to the artificial radioactivity of Norwegian waters (1992–1995) and Barents Sea (1992–1997). Science of the Total Environment, 202(1-3), 249-266.

**Guérin, T., Chekri, R., Vastel, C., Sirot, V., Volatier, J.-L., Leblanc, J.-C., Nöel, L. (2011).** Determination of 20 trace elements in fish and other seafood from the French market. Food Chemistry, 127, 934-942

**Guntay, S., Powers, D. A., Devell, L. (1997).** The Chernobyl reactor accident source term: Development of a consensus view (No. IAEA-TECDOC--964 (V. 2)).

**Gupta, S. K., Chen, K. Y. (1975).** Partitioning of trace metals in selective chemical fractions of nearshore sediments. Environmental letters, 10(2), 129-158

# H

**Hall, G. E. M., MacLaurin, A. I., Pelchat, J. C., Gauthier, G. (1997).** Comparison of the techniques of atomic absorption spectrometry and inductively coupled plasma mass spectrometry in the determination of Bi, Se and Te by hydride generation. Chemical Geology, 137(1-2), 79-89.

**Hall, G.E.M., Pelchat, J-C. (1997).** Analysis of geological materials for bismuth, antimony, selenium and tellurium by continuous flow hydride generation inductively coupled plasma mass spectrometry. Part 1. Mutual hydride interferences. Journal of Analytical Atomic Spectrometry, 12, 97 – 102

**Han, C., Li, Z., Li, W.J., Chou, S.L., Dou, S.X. (2014).** Controlled synthesis of copper telluride nanostructures for long-cycling anodes in lithium ion batteries. Journal of Materials Chemistry A, 2(30), 11683-11690.

**Hansen, K. (1853).** Versuche über die Wirkung des Tellürs auf den lebenden Organismus. Annalen 86: 208–215.

**Harada, T., Takahashi, Y. (2009).** Origin of the difference in the distribution behavior of tellurium and selenium in a soil–water system. Geochimica et Cosmochimica Acta, 72(5), 1281-1294.

**Harmens, H., Norris, D., Mills, G. (2013).** Heavy Metals and Nitrogen in Mosses: Spatial Patterns in 2010/2011 and Long-Term Temporal Trends in Europe. ICP Vegetation Programme Coordination Centre. Centre for Ecology and Hydrology, Bangor, UK p. 63

**Hayashi, T., Hoshii, Y., Namiki, M. (1983).** On the yellow product and browning of the reaction of dehydroascorbic acid with amino acids. Agricultural and Biological Chemistry, 47(5), 1003-1009.

**Hayes, S. M., McCullough, E. A. (2018).** Critical minerals: A review of elemental trends in comprehensive criticality studies. Resources Policy.

**Henkel, S., Kasten, S., Poulton, S. W., Staubwasser, M. (2016).** Determination of the stable iron isotopic composition of sequentially leached iron phases in marine sediments. Chemical Geology, 421, 93-102.

**Herath, I., Vithanage, M., Bundschuh, J. (2017).** Antimony as a global dilemma: Geochemistry, mobility, fate and transport. Environmental Pollution, 223, 545-559.

**Hirner, A. V., Feldmann, J., Krupp, E., Gruemping, R., Goguel, R., Cullen, W. R. (1998).** Metal (loid) organic compounds in geothermal gases and waters. Organic Geochemistry, 29(5-7), 1765-1778.

**Hirose, K. (2016).** Fukushima Daiichi Nuclear Plant accident: Atmospheric and oceanic impacts over the five years. Journal of Environmental Radioactivity, 157, 113-130.

**Honda, M. C., Kawakami, H., Watanabe, S., Saino, T. (2013).** Concentration and vertical flux of Fukushima-derived radiocesium in sinking particles from two sites in the Northwestern Pacific Ocean. Biogeosciences, 10(6), 3525-3534.

**Holwell, D. A., McDonald, I. (2007).** Distribution of platinum-group elements in the Platreef at Overysel, northern Bushveld Complex: a combined PGM and LA-ICP-MS study. Contributions to Mineralogy and Petrology, 154(2), 171-190.

**Hudson-Edwards, K.A., Houghton, S.L., Osborn, A. (2004).** Extraction and analysis of arsenic in soils and sediments. TrAC Trends in Analytical Chemistry, 23(10-11), 745-752.

**Huerta-Diaz, M. A., Morse, J. W. (1990).** A quantitative method for determination of trace metal concentrations in sedimentary pyrite. Marine Chemistry, 29, 119-144.

# I

**Iguchi, Y., Baba, T., Kawakami, H. (2006).** Study for Nuclide Transfer Ratio of Particles Generated by Thermal Cutting. In 14th International Conference on Nuclear Engineering (pp. 443-449). American Society of Mechanical Engineers.

**Institut de Radioprotection et Sûreté Nucléaire (IRSN 2007).** IRSN's viewpoint on the safety and radiation protection of French nuclear power plants in 2007. DSR Report No. 271.

**Institut de Radioprotection et Sûreté Nucléaire (IRSN 2009).** Incidents et accidents. <https://www.irsn.fr/FR/connaissances/Installations_nucleaires/La_surete_Nucleaire/echelle-ines/Pages/2-Incidents-accidents.aspx#.W6CqK_k6-00> Last accessed on the 04/08/2018

**Institut de Radioprotection et Sûreté Nucléaire (IRSN 2013).** - <http://www.irsn.fr/FR/connaissances/Environnement/radioactivite-environnement/radioecologie/Pages/3-origines_des_radionucleides.aspx#.WkvC-XnjLIU> Last accessed on the 09/08/2018

**Institut de Radioprotection et Sûreté Nucléaire (IRSN 2014).** <http://www.irsn.fr/FR/connaissances/Installations_nucleaires/La_surete_Nucleaire/risque-nucleaire/phases-accident-nucleaire/> Last accessed on the 12/06/2018

**Institut de Radioprotection et Sûreté Nucléaire (IRSN 2018).** <http://www.irsn.fr> Last accessed on the 09/02/2018

**Intergovernmental Panel on Climate Change (IPCC 2017)** <http://www.ipcc.ch/> Last accessed on the 03/02/2018

**International Atomic Energy Agency (IAEA 2004).** Sediment distribution coefficients and concentration factors for biota in the marine environment. International Atomic Energy Agency: Vienna, Austria.

**International Atomic Energy Agency (IAEA 2017).** International Nuclear and Radiological Event Scale. <https://www.iaea.org/topics/emergency-preparedness-and-response-epr/international-nuclear-radiological-event-scale-ines> Last accessed on the 04/08/2018

**International Chernobyl Project. (1991).** The International Chernobyl Project: technical report: assessment of radiological consequences and evaluation of protective measures. International Atomic Energy Agency. ISBN 92-0-129191-4 Vienna

**International Commision on Radiological Protection (ICRP 2012).** Compendium of Dose Coefficients based on ICRP Publication 60. ICRP Publication 119. Ann. ICRP 41(Suppl.).

**International Energy Agency (IAE 2017)**. Key world energy statistics <https://www.iea.org/topics/electricity/> Last accessed on the 03/02/2018.

**Ito, K., Watanabe, M., Kamiya, M. (2003).** Evaluation of the evaporation behavior of Pd, Mo, Te, and Sb in simulated low level radioactive liquid waste. Journal of Radioanalytical and Nuclear Chemistry, 255(2), 391-395.

**Izrael, Y.A. (2002).** Radioactive fallout after nuclear explosions and accidents. Elsevier, Saint Louis.

# J

**Jackson, M. L. (1958).** Soil chemical analysis. Engle-wood Cliffs. NT Prentice Hall Inc.

**Jalón-Rojas, I., Schmidt, S., Sottolichio, A. (2015).** Turbidity in the fluvial Gironde Estuary (southwest France) based on 10-year continuous monitoring: sensitivity to hydrological conditions. Hydrology and Earth System Sciences, 19, 2805-2819.

**Jamier, V., Ba, L. A., Jacob, C. (2010).** Selenium-and Tellurium-Containing Multifunctional Redox Agents as Biochemical Redox Modulators with Selective Cytotoxicity. Chemistry-A European Journal, 16(36), 10920-10928.

**Jenne, E. A. (1968).** Chapter 21 in Trace Inorganics in Water, RF Gould (ed.), American Chemical Society Advances in Chemistry Series, 73, 337.

**Jouanneau, J.M. (1982).** Matières en suspension et oligo-éléments métalliques dans le système estuarien Girondin: comportement et flux. PhD Thesis. Bordeaux, p. 150

**Jouanneau, J.M., Latouche, C. (1981).** The Gironde Estuary. In: Contributions to Sedimentology, Vol. 10. Stuttgart, 1-115.

**Jouanneau, J.M., Weber, O., Cremer, M., Castaing, P. (1999).** Fine-grained sediment budget on the continental margin of the Bay of Biscay. Deep-Sea Research Part II: Topical Studies in Oceanography, 46(10), 2205-2220.

# K

**Kabata-Pendias, A. (2011).** Trace Elements in Soils and Plants. CRC Press, Taylor and Francis Group.

**Kameník, J., Dulaiova, H., Buesseler, K. O., Pike, S. M., Šťastná, K. (2013).** Cesium-134 and 137 activities in the central North Pacific Ocean after the Fukushima Dai-ichi Nuclear Power Plant accident. Biogeosciences, 10(9), 6045-6052.

**Kanda, J. (2013).** Continuing $^{137}Cs$ release to the sea from the Fukushima Dai-ichi Nuclear Power Plant through 2012. Biogeosciences, 10(9), 6107-6113.

**Kanisch, G., Aust, M. O. (2013).** Does the Fukushima NPP disaster affect the caesium activity of North Atlantic Ocean fish?. Biogeosciences, 10(8), 5399-5410.

**Keon, N. E., Swartz, C. H., Brabander, D. J., Harvey, C., Hemond, H. F. (2001).** Validation of an arsenic sequential extraction method for evaluating mobility in sediments. Environmental Science and Technology, 35(13), 2778-2784.

**Kersten, M., Förstner, U. (1987).** Cadmium associations in freshwater and marine sediment. Cadmium in the Aquatic Environment, 51-88.

**Kleykamp, H. (1985).** The chemical state of the fission products in oxide fuels. Journal of Nuclear Materials, 131(2-3), 221-246.

**Knoll, G. F. (1989).** Radiation detection and measurement. Edition John Wiley & Sons USA.

**Kojima, S., Arinobu, T., Kosuda, C., Kato, M., Furukawa, M. (2012).** Radiochemical analysis of fission and neutron activation products released from the Fukushima Daiichi Nuclear Power Plant accident (2).

**König, S., Lorand, J. P., Luguet, A., Pearson, D. G. (2014).** A non-primitive origin of near-chondritic S–Se–Te ratios in mantle peridotites; implications for the Earth's late accretionary history. Earth and Planetary Science Letters, 385, 110-121

**Kostka, J. E., Luther III, G. W. (1994).** Partitioning and speciation of solid phase iron in saltmarsh sediments. Geochimica et Cosmochimica Acta, 58(7), 1701-1710.

**Kotrly, S., Sucha, L. (1985).** Handbook of chemical equilibria in analytical chemistry. Horwood. Halsted Press.

**Krachler, M., Emons, H., Zheng, J. (2001).** Speciation of antimony for the 21st century: promises and pitfalls. TrAC Trends in Analytical Chemistry, 20(2), 79-90.

**Krachler, M., Shotyk, W. (2004).** Natural and anthropogenic enrichments of molybdenum, thorium and uranium in a complete peat bog profile, Jura Mountains, Switzerland. Journal of Environmental Monitoring, 6, 418–426.

**Krachler, M., Zheng, J., Koerner, R., Zdanowicz, C., Fisher, D., Shotyk, W. (2005).** Increasing atmospheric antimony contamination in the northern hemisphere: snow and ice evidence from Devon Island, Arctic Canada. Journal of Environmental Monitoring, 7, 1169-1176

**Krupka, K. M., Serne, R. J. (2002).** Geochemical Factors Affecting the Behavior of Antimony, Cobalt, Europium, Technetium, and Uranium in Vadose Zone Sediments (No. PNNL-14126). Pacific Northwest National Lab.(PNNL), Richland, WA (United States).

**Kryshev, I. I., Kryshev, A. I., Sazykina, T. G. (2012).** Dynamics of radiation exposure to marine biota in the area of the Fukushima NPP in March–May 2011. Journal of Environmental Radioactivity, 114, 157-161.

**Kusakabe, M., Oikawa, S., Takata, H., Misonoo, J. (2013).** Spatiotemporal distributions of Fukushima-derived radionuclides in nearby marine surface sediments. Biogeosciences, 10(7), 5019-5030.

# L

**Lai, L., Jin, J. C., Xu, Z. Q., Mei, P., Jiang, F. L., Liu, Y. (2015).** Necrotic cell death induced by the protein-mediated intercellular uptake of CdTe quantum dots. Chemosphere, 135, 240-249.

**Lajtha, K., Driscoll, C.T., Jarrell, W. M., Elliott, E.T. (1999).** Soil phosphorus. Standard soil methods for long-term ecological research, 115-142.

**Lanceleur, L., Schäfer, J., Chiffoleau, J. F., Blanc, G., Auger, D., Renault, S., et al. (2011).** Long-term records of cadmium and silver contamination in sediments and oysters from the Gironde fluvial–estuarine continuum–Evidence of changing silver sources. Chemosphere, 85(8), 1299-1305.

**Lanceleur, L., Schäfer, J., Blanc, G., Coynel, A., Bossy, C., Baudrimont, M., Glé, C., Larrose, A., Renault, S., Strady, E. (2013).** Silver behaviour along the salinity gradient of the Gironde Estuary. Environmental Science and Pollution Research, 20, 1352-1366.

**Langmuir, I. (1918).** The adsorption of gases on plane surfaces of glass, mica and platinum. Journal of the American Chemical Society, 40(9), 1361-1403.

**Langston, W.J., Burt, G.R. and Pope, N.D., 1999.** Bioavailability of metals in sediments of the Dogger Bank (central North Sea): a mesocosm study. Estuarine, Coastal and Shelf Science, 48, 519-540.

**Lapaquellerie, Y., Maillet, N., Jouanneau, J.-M., Coakley, J.P., Latouche, C. (1996).** Flux de matières en suspension et de cadmium dans le Lot. Hydroécologie Appliquée, 8, 173-191.

**Lapaquellerie, Y., Jouanneau, J.M., Maillet, N., Latouche, C. (1995).** Pollution en Cd dans les sédiments du Lot (France) et calcul du stock de polluant. Environmental Technology, 16, 1145-1154.

**Larner, A. J. (1996).** Alzheimer's disease, Kuf's disease, tellurium and selenium. Medical Hypotheses, 47(2), 73-75.

**Larrose, A., Coynel, A., Schäfer, J., Blanc, G., Massé, L., Maneux, E. (2010).** Assessing the current state of the Gironde Estuary by mapping priority contaminant distribution and risk potential in surface sediment. Applied Geochemistry, 25(12), 1912-1923.

**Latouche, C. (1992).** La pollution par le cadmium des huîtres sauvages de l'Estuaire de la Gironde. Origine. Mécanismes responsables de la fixation du cadmium. Ichtyophysiol. Acta, 15, 139-152.

**Lauwers, L.F., Roelants, A., Rossel, P.M., Heyndrickx, B., Baute, L. (1990).** Oral antimony intoxication in man. Critical Care Medicine, 18, 324-326

**Leal, J. J., Narro-García, R., Desirena, H., Marconi, J. D., Rodríguez, E., Linganna, K., De la Rosa, E. (2015).** Spectroscopic properties of tellurite glasses co-doped with $Er^{3+}$ and $Yb^{3+}$. Journal of Luminescence, 162, 72-80.

**Lee, M., Bae, W., Chung, J., Jung, H. S., Shim, H. (2008).** Seasonal and spatial characteristics of seawater and sediment at Youngil bay, Southeast Coast of Korea. Marine Pollution Bulletin, 57(6-12), 325-334.

**Lee, D. S., Edmond, J. M. (1985).** Tellurium species in seawater. Nature, 313(6005), 782.

**Le Floch, J.F. (1961).** Propagation de la marée dynamique dans l'estuaire de la Seine et la Seine Maritime. PhD Thesis, Paris, p. 507

**Lehto, J., Paatero, J., Pehrman, R., Kulmala, S., Suksi, J., Koivula, T., Jaakkola, T. (2008).** Deposition of gamma emitters from Chernobyl accident and their transfer in lichen–soil columns. Journal of environmental radioactivity, 99(10), 1656-1664.

**Leigh, K., Bouldin, J., Buchanan, R. (2012).** Effects of exposure to semiconductor nanoparticles on aquatic organisms. Journal ofT, 2012.

**Lekhi, P., Cassis, D., Pearce, C. M., Ebell, N., Maldonado, M. T., Orians, K. J. (2008).** Role of dissolved and particulate cadmium in the accumulation of cadmium in cultured oysters (*Crassostrea gigas*). Science of the Total Environment, 393(2-3), 309-325.

**Leuz, A.-K., Mönch, H., Johnson, C.A. (2006).** Sorption of Sb(III) and Sb(V) to Goethite: influence on Sb(III) oxidation and mobilization. Environmental Science and Technology, 40, 7277-7282.

**Leverett, P., Reynolds, J.K., Roper, A.J., Williams, P.A. (2012).** Tripuhyite and schafarzikite: two of the ultimate sinks for antimony in the natural environment. Mineralogical Magazine, 76, 891-902.

**Limousin, G., Gaudet, J. P., Charlet, L., Szenknect, S., Barthes, V., Krimissa, M. (2007).** Sorption isotherms: a review on physical bases, modeling and measurement. Applied Geochemistry, 22(2), 249-275.

**Liu, C. K., Faller, S. H., Kuroda, P. K. (1990).** Ruthenium-103, iodine-131, tellurium-132, and cesium-137 in air after the Chernobyl event. Radiochimica Acta, 50(3), 159-168.

**Liu, R., Xu, W., He, Z., Lan, H., Liu, H., Qu, J., Prasai, T. (2015).** Adsorption of antimony (V) onto Mn (II)-enriched surfaces of manganese-oxide and FeMn binary oxide. Chemosphere, 138, 616-624.

**Lobel, P.B., Wright, D.A. (1982).** Relationship between body zinc concentration and allometric growth measurements in the mussel *Mytilus edulis*. Marine Biology, 66, 145-150.

**Lombi, E., Holm, P. E. (2010).** Metalloids, soil chemistry and the environment. In MIPs and Their Role in the Exchange of Metalloids (pp. 33-44). Springer, New York, NY.

**Lopez-Sanchez, J. F., Rubio, R., Rauret, G. (1993).** Comparison of two sequential extraction procedures for trace metal partitioning in sediments. International Journal of Environmental Analytical Chemistry, 51(1-4), 113-121.

**Loring, D., Rantala, R. (1992).** Manual for the geochemical analyses of marine sediments and suspended particulate matter. Earth-Science Reviews, 32, 235–283.

**Lozano, R. L., Hernández-Ceballos, M. A., Adame, J. A., Casas-Ruíz, M., Sorribas, M., San Miguel, E. G., Bolívar, J. P. (2011).** Radioactive impact of Fukushima accident on the Iberian Peninsula: evolution and plume previous pathway. Environment International, 37(7), 1259-1264.

# M

**Ma, Y. and Uren, N.C. (1995).** Application of a new fractionation scheme for heavy metals in soils. Communications in Soil Science and Plant Analysis, 26, 3291-3303.

**Mahdy, M. A., Mahdy, I. A., El Zawawi, I. K. (2015).** Characterization of Pb24Te76 quantum dot thin film synthesized by inert gas condensation. Spectrochimica Acta Part A: Molecular and Biomolecular Spectroscopy, 134, 302-309.

**Marigómez, I., Soto, M., Cajaraville, M. P., Angulo, E., Giamberini, L. (2002).** Cellular and subcellular distribution of metals in molluscs. Microscopy Research and Technique, 56(5), 358-392.

**Marion, C., Dufois, F., Arnaud, M., Vella, C. (2010).** In situ record of sedimentary processes near the Rhône River mouth during winter events (Gulf of Lions, Mediterranean Sea). Continental Shelf Research, 30(9), 1095-1107.

**Martin, J. M., Wollast, R., Loijens, M., Thomas, A., Mouchel, J. M., Nieuwenhuize, J. (1994).** Origin and fate of artificial radionuclides in the Scheldt estuary. Marine Chemistry, 46(1-2), 189-202.

**Marwede, M., Reller, A. (2012).** Future recycling flows of tellurium from cadmium telluride photovoltaic waste. Resources, Conservation and Recycling, 69, 35-49.

**Masson, M., Schäfer, J., Blanc, G., Dabrin, A., Castelle, S., Lavaux, G. (2009).** Behavior of arsenic and antimony in the surface freshwater reaches of a highly turbid estuary, the Gironde Estuary, France. Applied Geochemistry, 24, 1747-1756

**Masson, M., Lanceleur, L., Tercier-Waeber, M.-L., Schäfer, J., Hezard, T., Larrose, A., Bossy, C., Blanc, G. (2011a).** Distribution and reactivity of oxyanions (Sb, As, V, Mo) in the surface freshwater reaches of the Gironde Estuary (France). Applied Geochemistry, 26, 1222-1230

**Masson, M., Blanc, G., Schäfer, J., Parlanti, E., Le Coustumer, P. (2011b).** Copper addition by organic matter degradation in the freshwater reaches of a turbid estuary. Science of the Total Environment, 409(8), 1539-1549.

**Masson, M., Van Weers, A.W., Groothuis, R.E.J., Dahlgaard, H., Ibbett, R.D., Leonard, K.S. (1995).** Time series for seawater and seaweed of $^{99}$Tc and $^{125}$Sb originating from releases of La Hague. Journal of Marine Systems, 6, 397-413.

**Maugeri, E. A., Neuhausen, J., Eichler, R., Piguet, D., Schumann, D. (2014).** Thermochromatography study of volatile tellurium species in various gas atmospheres. Journal of nuclear materials, 452(1-3), 110-117.

**McFarlane, J. (1996).** Fission product tellurium chemistry from fuel to containment (No. PSI--97-02).

**McPhail, D.C. (1995).** Thermodynamic properties of aqueous tellurium species between 25 and 350. Geochimica et Cosmochimica Acta, 59(5), 851-866.

**Mecklenburg, S., Shaaban, S., Ba, L. A., Burkholz, T., Schneider, T., Diesel, B., Kiemer, A.K., Röseler, A., Becker, K., Reichrath, J., Stark, A., Tilgen, W., Abbas, M., Wessjohann, L.A., Sasse, F., Jacob, C. (2009).** Exploring synthetic avenues for the effective synthesis of selenium-and tellurium-containing multifunctional redox agents. Organic and Biomolecular Chemistry, 7(22), 4753-4762.

**Mehra, O. P., Jackson, M. L. (1960).** Iron oxide removal from soils and clays by a dithionite–citrate system buffered with sodium bicarbonate. In Clays and clay minerals: proceedings of the Seventh National Conference (pp. 317-327).

**Meybeck, M., Pasco, A., Ragu, A. (1993).** Etablissement des flux polluants dans les rivières: pourquoi, comment et à quel prix. 4ème Rencontre de l'Agence Régionale pour l'Environnement Provence Alpes Coˆ te d'Azur. Toulon: ARPE, PACA, 1993; pp. 55–67.

**Meybeck, M., Pasco, A., Ragu, A. (1994).** Etablissement des flux polluants dans les rivières : pourquoi, comment et à quel prix. '4ème Rencontres de l'Agence Régionale pour l'Environnement. In 'Provence-Alpes-Côte d'Azur. Colloque scientifique sur les charges polluantes véhiculées par les fleuves et les rivières en Méditerranée'. Collection 1991–1992–1993

**Meybeck, M., Ragu, A. (1995).** River Discharges to the Oceans. An Assessment of Suspended Solids, Major Ions, and Nutrients. (UNEP Nairobi)

**Middelburg, J. J., Hoede, D., van der Sloot, H. A., van der Weijden, C. H., Wijkstra J. (1988).** Arsenic, antimony and vanadium in the North Atlantic Ocean, Geochimica et Cosmochimica Acta, 52, 2871–2878.

**Miller, J. (2012).** The current status of nuclear power in the world. Presentation. ASME Energy Committee Colloquium II, California.

**Mishkin, F.S., White, E.N. (2002).** US stock market crashes and their aftermath: implications for monetary policy (No. w8992). National bureau of economic research.

**Mitsunobu, S., Takahashi, Y., Sakai, Y., Inumaru, K. (2009).** Interaction of synthetic sulfate green rust with Antimony(V). Environmental Science and Technology, 43, 318-323.

**Monrás, J. P., Collao, B., Molina-Quiroz, R. C., Pradenas, G. A., Saona, L. A., Durán-Toro, V., et al. (2014).** Microarray analysis of the Escherichia coli response to CdTe-GSH Quantum Dots: understanding the bacterial toxicity of semiconductor nanoparticles. BMC genomics, 15(1), 1099.

**Montperrus, M., Bohari, Y., Bueno, M., Astruc, A., Astruc, M. (2002).** Comparison of extraction procedures for arsenic speciation in environmental solid reference materials by high-performance liquid chromatography–hydride generation-atomic fluorescence spectroscopy. Applied Organometallic Chemistry, 16(7), 347-354.

**Mork, K.A., Hall, R.E. (1980).** Energy prices, inflation, and recession, 1974-1975. The Energy Journal, 1(3), 31-63.

**Moss, R. L., Tzimas, E., Kara, H., Willis, P., Kooroshy, J. (2011).** Critical metals in strategic energy technologies. JRC-scientific and strategic reports, European Commission Joint Research Centre Institute for Energy and Transport.

**Mukhopadhyay, R., Bhattacharjee, H., Rosen, B. P. (2014).** Aquaglyceroporins: generalized metalloid channels. Biochimica et Biophysica Acta (BBA)-General Subjects, 1840(5), 1583-1591.

**Müller G (1969).** Index of geoaccumulation in sediments of the Rhine river. The Journal of Geology 2, 108–118

**Müller, K., Daus, B., Morgenstern, P., Wennrich, R. (2007).** Mobilization of antimony and arsenic in soil and sediment samples–evaluation of different leaching procedures. Water, Air, and Soil Pollution, 183(1-4), 427-436.

# N

**Nagao, S., Kanamori, M., Ochiai, S., Tomihara, S., Fukushi, K., Yamamoto, M. (2013).** Export of 134 Cs and 137 Cs in the Fukushima river systems at heavy rains by Typhoon Roke in September 2011. Biogeosciences, 10(10), 6215-6223.

**Nakata, K., Sugisaki, H. (Eds.). (2015).** Impacts of the Fukushima nuclear accident on fish and fishing grounds. Tokyo: Springer Japan.

**Nelson, S.A. (2014).** Weathering and Clay Minerals. Tulane University. <http://www.tulane.edu/~sanelson/eens211/weathering&clayminerals.htm> Last accessed on the 05/11/18

**Nicolet, J.-P. and Erdi-Krausz, G. (2003).** Guidelines for radioelement mapping using gamma ray spectrometry data. IAEA-TECDOC-1363. Vienna

**Nieboer, E., Richardson, D. H. (1980).** The replacement of the nondescript term 'heavy metals' by a biologically and chemically significant classification of metal ions. Environmental Pollution Series B, Chemical and Physical, 1(1), 3-26.

**Nishio, T., Koike, I., Hattori, A. (1982).** Denitrification, nitrate reduction, and oxygen consumption in coastal and estuarine sediments. Applied and Environmental Microbiology, 43(3), 648-653.

**Nolan, C., Whitehead, N., Teyssie, J. L. (1991).** Tellurium—speciation in seawater and accumulation by marine phytoplankton and crustaceans. Journal of Environmental Radioactivity, 13(3), 217-233.

# O

**Oberli, F., Gartenmann, P., Meier, M., Kutschera, W., Suter, M., Winkler, G. (1999).** The half-life of 126Sn refined by thermal ionization mass spectrometry measurements. International Journal of Mass Spectrometry, 184(2-3), 145-152.

**Ojebuoboh, F. (2008).** Selenium and tellurium from copper refinery slimes and their changing applications. World of Metallurgy-ERZMETALL, 61(1), 255-261.

**Okkenhaug, G., Zhu, Y. G., Luo, L., Lei, M., Li, X., Mulder, J. (2011).** Distribution, speciation and availability of antimony (Sb) in soils and terrestrial plants from an active Sb mining area. Environmental Pollution, 159(10), 2427-2434.

**Ollivier, P.R., Bahrou, A.S., Marcus, S., Cox, T., Church, T.M., Hanson, T.E. (2008).** Volatilization and precipitation of tellurium by aerobic, tellurite-resistant marine microbes. Applied and environmental microbiology, 74(23), 7163-7173.

**Ollivier, P., Hamelin, B., Radakovitch, O. (2010).** Seasonal variations of physical and chemical erosion: A three-year survey of the Rhone River (France). Geochimica et Cosmochimica Acta, 74(3), 907-927.

**Orsini, L., Bermond, A. (1993).** Application of a sequential extraction procedure to calcareous soil samples: preliminary studies. International Journal of Environmental Analytical Chemistry, 51, 97-108.

# P

**Papastefanou, C., Manolopoulou, M., Charalambous, S. (1988).** Radiation measurements and radioecological aspects of fallout from the cherbonyl reactor accident. Journal of Environmental Radioactivity, 7(1), 49-64.

**Pérez, J. M., Calderón, I. L., Arenas, F. A., Fuentes, D. E., Pradenas, G. A., Fuentes, E. L., et al. (2007).** Bacterial toxicity of potassium tellurite: unveiling an ancient enigma. PLoS One, 2(2), e211.

**Pérez-Moreno, S. M., Gázquez, M. J., Pérez-López, R., Bolivar, J. P. (2018).** Validation of the BCR sequential extraction procedure for natural radionuclides. Chemosphere, 198, 397-408.

**Periáñez, R. (2005).** Modelling the transport of suspended particulate matter by the Rhone River plume (France). Implications for pollutant dispersion. Environmental Pollution, 133(2), 351-364.

**Periáñez, R., Bezhenar, R., Brovchenko, I., Duffa, C., Iosjpe, M., Jung, K. T., et al. (2016).** Modelling of marine radionuclide dispersion in IAEA MODARIA program: Lessons learnt from the Baltic Sea and Fukushima scenarios. Science of the Total Environment, 569, 594-602.

**Petticrew, M. (2003).** Why certain systematic reviews reach uncertain conclusions. BMJ, 326, 756. doi:10.1136/BMJ.326.7392.756

**Phillips, D.J.H. (1977).** The use of biological indicator organisms to monitor trace metal pollution in marine and estuarine environments—a review. Environmental Pollution (1970), 13, 281–317.

**Pickering, W.F. (1986).** Metal ion speciation; soils and sediments (a review). Ore Geology Reviews, 1, 83-146.

**Pierart, A., Shahid, M., Séjalon-Delmas, N., Dumat, C. (2015).** Antimony bioavailability: knowledge and research perspectives for sustainable agricultures. Journal of Hazardous Materials, 289, 219-234.

**Pierce, M.L., Moore, C.B. (1982).** Adsorption of arsenite and arsenate on am-$Fe(OH)_3$. Water Research, 16, 1247–1253.

**Pinel-Raffaitin, P., Pécheyran, C., Amouroux, D. (2008).** New volatile selenium and tellurium species in fermentation gases produced by composting duck manure. Atmospheric Environment, 42(33), 7786-7794.

**Pontillon, Y., Ducros, G., Malgouyres, P. P. (2010).** Behaviour of fission products under severe PWR accident conditions VERCORS experimental programme—Part 1: General description of the programme. Nuclear Engineering and Design, 240(7), 1843-1852.

**Poulton, S. W., Canfield, D. E. (2005).** Development of a sequential extraction procedure for iron: implications for iron partitioning in continentally derived particulates. Chemical Geology, 214(3-4), 209-221.

**Povinec, P. P., Aoyama, M., Biddulph, D., Breier, R., Buesseler, K., Chang, C. C., et al. (2013).** Cesium, iodine and tritium in NW Pacific waters-a comparison of the Fukushima impact with global fallout. Biogeosciences, 10(8), 5481-5496.

**Presley, B. J., Kolodny, Y., Nissenbaum, A., Kaplan, I. R. (1972).** Early diagenesis in a reducing fjord, Saanich Inlet, British Columbia—II. Trace element distribution in interstitial water and sediment. Geochimica et Cosmochimica Acta, 36(10), 1073-1090.

# Q

**Qi, C., Liu, G., Chou, C.-L., Zheng, L. (2008).** Environmental geochemistry of antimony in Chinese coals. Science of the Total Environment, 389, 225-234.

**Qi, P., Pichler, T. (2016).** Sequential and simultaneous adsorption of Sb(III) and Sb(V) on ferrihydrite: implications for oxidation and competition. Chemosphere, 145, 55-60.

**Qin, H.-B, Takeichi, Y., Nitani, H., Terada, Y., Takahashi, Y. (2017).** Tellurium distribution and speciation in contaminated soils from abandoned mine tailings: comparison with selenium. Environmental Science & Technology, 51(11), 6027-6035.

**Quentel, F., Filella, M., Elleouet, C., Madec, C.L. (2006).** Sb(III) oxidation by iodate in seawater: a cautionary tale. Science of the Total Environment 355, 259–263.

**Quevauviller, P. (1998).** Method Performance Studies for Speciation Analysis. Royal Society of Chemistry, Cambridge, UK.

**Quevauviller, P., Ure, A., Muntau, H., Griepink, B. (1993).** Improvement of analytical measurements within the BCR-programme: single and sequential extraction procedures applied to soil and sediment analysis. International Journal of Environmental Analytical Chemistry, 51(1-4), 129-134.

**Quintin, J.-Y., Sottolichio, A., Derriennic, H., Schmidt, S., et al. (2012).** Surveillance Ecologique du site du Blayais-Année 2012. RST DYNECO/AG/13-02. http://archimer. ifremer. fr/doc/4200/434022.

# R

**Rajput, M. U., Ali, N., Hussain, S., Mujahid, S. A., MacMahon, D. (2012).** Beta decay of the fission product 125Sb and a new complete evaluation of absolute gamma ray transition intensities. Radiation Physics and Chemistry, 81(4), 370-378.

**Ramos-Ruiz, A., Field, J. A., Wilkening, J. V., Sierra-Alvarez, R. (2016).** Recovery of elemental tellurium nanoparticles by the reduction of tellurium oxyanions in a methanogenic microbial consortium. Environmental Science and Technology, 50(3), 1492-1500.

**Reemtsma, T., These, A., Springer, A., Linscheid, M. (2008).** Differences in the molecular composition of fulvic acid size fractions detected by size-exclusion chromatography–on line Fourier transform ion cyclotron resonance (FTICR–) mass spectrometry. Water research, 42(1-2), 63-72.

**Reguigui, N. (2006).** Gamma Ray Spectrometry, Practical Information.

**Reimann, C., de Caritat, P.D. (2000).** Intrinsic flaws of element enrichment factors (EFs) in environmental geochemistry. Environmental Science and Technology, 34(24), 5084-5091.

**Reimann, C., de Caritat, P.D. (2012).** Chemical elements in the environment: factsheets for the geochemist and environmental scientist. Springer Science and Business Media.

**Reimann, C., Matschullat, J., Birke, M., Salminen, R. (2010).** Antimony in the environment: lessons from geochemical mapping. Applied Geochemistry, 25(2), 175-198.

**Ren, J. L., Zhang, X. Z., Sun, Y. X., Liu, S. M., Huang, D., Zhang, J. (2016).** Antimony and arsenic biogeochemistry in the East China Sea. Deep Sea Research Part II: Topical Studies in Oceanography, 124, 29-42.

**Rizzi, M., D'Aloia, M., Castagnolo, B. (2010).** Semiconductor detectors and principles of radiation-matter interaction. Journal of Applied Sciences(Faisalabad), 10(23), 3141-3155.

**Rizwan, U. (2015).** Development of Gamma-Ray Spectroscopy Techniques for Fundamental and Applied Research (Doctoral dissertation, Science: Department of Chemistry). Simon Fraser University, Canada.

**Robbins, J. A., Lindner, G., Pfeiffer, W., Kleiner, J., Stabel, H. H., Frenzel, P. (1992).** Epilimnetic scavenging of Chernobyl radionuclides in Lake Constance. Geochimica et Cosmochimica Acta, 56(6), 2339-2361.

**Robert, S., Blanc, G., Schäfer, J., Lavaux, G., Abril, G. (2004).** Metal mobilization in the Gironde Estuary (France): the role of the soft mud layer in the maximum turbidity zone. Marine Chemistry, 87, 1-13.

**Roper, A. J., Williams, P. A., Filella, M. (2012).** Secondary antimony minerals: phases that control the dispersion of antimony in the supergene zone. Chemie der Erde-Geochemistry, 72, 9-14.

**Rose-Weston, L., Brenan, J. M., Fei, Y., Secco, R. A., Frost, D. J. (2009).** Effect of pressure, temperature, and oxygen fugacity on the metal-silicate partitioning of Te, Se, and S: Implications for earth differentiation. Geochimica et Cosmochimica Acta, 73(15), 4598-4615.

**Rosenberg, E., Ariese, F. (2001).** Quality control in speciation analysis. In Trace element speciation for environment, food and health. Ebdon, L., Pitts, L., Cornelis, R., Crews, H., Donard, O.F.X. and Quevauviller, Ph. (eds), The Royal Society of Chemistry, Cambridge, UK.

# S

**Saegusa, J., Oishi, T., Kawasaki, K., Yoshizawa, M., Yoshida, M., Sawahata, T., Honda, T. (2000).** Determination of gamma-ray efficiency curves for volume samples by the combination of Monte Carlo simulations and point source calibration. Journal of Nuclear Science and Technology, 37(12), 1075-1081.

**Salbu, B., Skipperud, L., Germain, P., Guegueniat, P., Strand, P., Lind, O. C., Christensen, G. (2003).** Radionuclide speciation in effluent from La Hague reprocessing plant in France. Health Physics, 85(3), 311-322.

**Saleh, M.A., Wilson, B.L. (1998).** Analysis of metal pollutants in the Houston Ship Channel by inductively coupled plasma/mass spectrometry. Ecotoxicology and Environmental Safety, 44, 113-117.

**Salminen, R., Batista, M.J., Bidovec, M., Demetriades, A., De Vivo, B., De Vos, W., Duris, M., Gilucis, A., et al. (2005).** Geochemical Atlas of Europe. Part 1 – Background Information, Methodology and Maps.

**Sanders, J. G., Windom, H. L. (1980).** The uptake and reduction of arsenic species by marine algae. Estuarine and Coastal Marine Science, 10(5), 555-567.

**Sanial, V., Buesseler, K. O., Charette, M. A., Nagao, S. (2017).** Unexpected source of Fukushima-derived radiocesium to the coastal ocean of Japan. Proceedings of the National Academy of Sciences, 201708659.

**Santschi, P. H., Bollhalder, S., Zingg, S., Lück, A., Farrenkothen, K. (1990).** The self-cleaning capacity of surface waters after radioactive fallout. Evidence from European waters after Chernobyl, 1986-1988. Environmental Science and Technology, 24(4), 519-527.

**Santschi, P.H., Lenhart, J.J. and Honeyman, B.D. (1997).** Heterogeneous processes affecting trace contaminant distribution in estuaries: the role of natural organic matter. Marine Chemistry, 58, 99-125.

**Schäfer, J., Blanc, G., Lapaquellerie, Y., Maillet, N., Maneux, E., Etcheber, H. (2002).** Ten-year observation of the Gironde tributary fluvial system: fluxes of suspended matter, particulate organic carbon and cadmium. Marine Chemistry, 79, 229-242.

**Scheinost, A.C., Rossberg, A., Vantelon, D., Xifra, I., Kretzschmar, R., Leuz, A.-K., Funke, H., Johnson, C.A. (2006).** Quantitative antimony speciation in shooting range soils by EXAFS spectroscopy. Geochimica et. Cosmochimica Acta 70, 3299–3312.

**Schiøtte, L., Compston, W., Bridgwater, D. (1989).** U–Th–Pb ages of single zircons in Archaean supracrustals from Nain Province, Labrador, Canada. Canadian Journal of Earth Sciences, 26(12), 2636-2644.

**Schneider, R., Wolpert, C., Guilloteau, H., Balan, L., Lambert, J., Merlin, C. (2009).** The exposure of bacteria to CdTe-core quantum dots: the importance of surface chemistry on cytotoxicity. Nanotechnology, 20(22), 225101.

**Schroeder, H.A., Buckman, J., Balassa, J.J. (1967).** Abnormal trace elements in man: tellurium. Journal of chronic diseases, 20(3), 147-161.

**Schwertmann, U. (1964).** Differenzierung der Eisenoxide des Bodens durch Extraktion mit Ammoniumoxalat-Lösung. Zeitschrift für Pflanzenernährung, Düngung, Bodenkunde, 105(3), 194-202.

**Seaborg, G.T. and Loveland, W. (1990).** The Elements Beyond Uranium. Wiley, New York

**Seyedmohammadi, S., DiNezza, M. J., Liu, S., King, P., LeBlanc, E. G., Zhao, X. H., et al. (2015).** Molecular beam epitaxial re-growth of CdTe, CdTe/CdMgTe and CdTe/CdZnTe double heterostructures on CdTe/InSb (1 0 0) substrates with As cap. Journal of Crystal Growth, 425, 181-185.

**Shortland, A. (2002).** An antimony bead from Jerablus Tahtani. Historical Metallurgy, 36(1), 1-5.

**Shotyk, W., Cheburkin, A.K., Appleby, P.G., Fankhauser, A., Kramers, J.D. (1996).** Two thousand years of atmospheric arsenic, antimony, and lead deposition recorded in an ombrotrophic peat bog profile, Jura Mountains, Switzerland. Earth and Planetary Science Letters, 145, E1-E7.

**Shotyk, W., Krachler, M., Chen, B. (2004).** Antimony in recent, ombrotrophic peat from Switzerland and Scotland: Comparison with natural background values (5,320 to 8,020 14C yr BP) and implications for the global atmospheric Sb cycle. Global Biogeochemical Cycles, 18(1).

**Shuman, L. M. (1982).** Separating Soil Iron-and Manganese-Oxide Fractions for Microelement Analysis 1. Soil Science Society of America Journal, 46(5), 1099-1102.

**Shuman, L.M. (1983).** Sodium hypochlorite methods for extracting microelements associated with soil organic matter. Soil Science Society of America Journal, 47, 656-660.

**Siddick, Z.H., Newman, R.A. (1988).** Use of platinum as a modifier in the sensitive detection of tellurium in biological samples. Analytical Biochemistry, 172(1), 190-196.

**Sigleo, A.C., Helz, G.R. (1981).** Composition of estuarine colloidal material: major and trace elements. Geochimica et Cosmochimica Acta, 45, 2501–2509.

**Smichowski, P. (2008).** Antimony in the environment as a global pollutant: a review on analytical methodologies for its determination in atmospheric aerosols. Talanta, 75(1), 2-14.

**Smith, C. L., De Laeter, J. R., Rosman, K. J. R. (1977**). Mass spectrometric isotope dilution analyses of tellurium in meteorites and standard rocks. Geochimica et Cosmochimica Acta, 41(5), 676-681.

**Smith, A. R., Thomas, K. J., Norman, E. B., Hurley, D. L., Lo, B. T., Chan, Y. D., et al. (2014).** Measurements of fission products from the Fukushima Daiichi incident in San Francisco Bay Area air filters, automobile filters, rainwater, and food. Journal of Environmental Protection, 5, 207-221.

**Song, J. H. (2018).** An assessment on the environmental contamination caused by the Fukushima accident. Journal of environmental management, 206, 846-852.

**Sonzogni, A.A. (2013).** Chart of Nuclides NuDat 2.6 - National Nuclear Data Center. Brookhaven National Laboratory. <http://www.nndc.bnl.gov/nudat2/reCenter.jsp?z=51&n=68> Last accessed on the 10/03/15.

**Sottolichio, A., Castaing, P. (1999).** A synthesis on seasonal dynamics of highly-concentrated structures in the Gironde estuary. Comptes Rendus de l'Académie de Sciences – Série IIa: Sciences de la Terre et des Planètes, 329, 795-800.

**Speakman, S.** Basics of X-Ray Powder Diffraction: Training to Become an Independent User of the X-Ray SEF at the Center for Materials Science and Engineering at MIT. Online] [Cited: April 6, 2017.] http://prism. mit. edu/xray/oldsite/Basics% 20of% 20X-Ray% 20Powder% 20Diffraction. pdf.

**Stangherlin, E.C., Favero, A.M., Zeni, G., Rocha, J.B., Nogueira, C.W. (2006).** Exposure of mothers to diphenyl ditelluride during the suckling period changes behavioral tendencies in their offspring. Brain Research Bulletin, 69(3), 311-317.

**Steinhauser, G., Brandl, A., Johnson, T. E. (2014).** Comparison of the Chernobyl and Fukushima nuclear accidents: a review of the environmental impacts. Science of the Total Environment, 470, 800-817.

**Sterckeman, T., Douay, F., Baize, D., Fourrier, H., Proix, N., Schvartz, C. (2004).** Factors affecting trace element concentrations in soils developed on recent marine deposits from northern France. Applied Geochemistry, 19(1), 89-103.

**Strady, E., Blanc, G., Baudrimont, M., Schäfer, J., Robert, S., Lafon, V. (2011).** Roles of regional hydrodynamic and trophic contamination in cadmium bioaccumulation by Pacific oysters in the Marennes-Oléron Bay (France). Chemosphere, 84(1), 80-90.

**Stumm, W., Sulzberger, B. (1992).** The cycling of iron in natural environments: considerations based on laboratory studies of heterogeneous redox processes. Geochimica et Cosmochimica Acta, 56(8), 3233-3257.

**Sulzberger, B., Suter, D., Siffert, C., Banwart, S., Stumm, W. (1989).** Dissolution of Fe (III)(hydr) oxides in natural waters; laboratory assessment on the kinetics controlled by surface coordination. Marine Chemistry, 28(1-3), 127-144.

**Sun, H.W., Shan, X.Q., Ni, Z.M. (1982).** Selective separation and differential determination of antimony (III) and antimony (V) by solvent extraction with N-benzoyl-N-phenylhydroxylamine and graphite furnace atomic adsorption spectrometry using a matrix modification technique. Talanta 29, 589–593.

**Sung, W. (1995).** Some observations on surface partitioning of Cd, Cu and Zn in estuaries. Environmental Science and Technology, 29, 1303.

**Sutherland, R. A. (2010).** BCR®-701: A review of 10-years of sequential extraction analyses. Analytica Chimica Acta, 680(1-2), 10-20.

# T

**Tack, F.M.G., Verloo, M.G. (1996).** Impact of single reagent extraction using $NH_4OAc$-EDTA on the solid phase distribution of metals in a contaminated dredged sediment. Science of the Total Environment, 178, 29-36.

**Tagami, K., Uchida, S., Ishii, N., Zheng, J. (2013).** Estimation of Te-132 distribution in Fukushima Prefecture at the early stage of the Fukushima Daiichi nuclear power plant reactor failures. Environmental Science and Technology, 47(10), 5007-5012.

**Takayanagi, K., Cossa, D., Martin, J. M. (1996).** Antimony cycling in the western Mediterranean, Marine Chemistry, 54, 303–312.

**Tang, S., Cai, Q., Chibli, H., Allagadda, V., Nadeau, J. L., Mayer, G. D. (2013).** Cadmium sulfate and CdTe-quantum dots alter DNA repair in zebrafish (Danio rerio) liver cells. Toxicology and Applied Pharmacology, 272(2), 443-452.

**Tapia, J., Audry, S. (2013).** Control of early diagenesis processes on trace metal (Cu, Zn, Cd, Pb and U) and metalloid (As, Sb) behaviors in mining-and smelting-impacted lacustrine environments of the Bolivian Altiplano. Applied Geochemistry, 31, 60-78.

**Taylor, A. (1996).** Biochemistry of tellurium. Biological Trace Element Research, 55(3), 231-239.

**Tessier, A., Campbell, P.G.C., Bisson, M. (1979).** Sequential extraction procedure for the speciation of particulate trace metals. Analytical Chemistry, 51(7), 844-851.

**Thakur, P., Ballard, S., Nelson, R. (2012).** Radioactive fallout in the United States due to the Fukushima nuclear plant accident. Journal of Environmental Monitoring, 14(5), 1317-1324.

**Thakur, P., Ballard, S., Nelson, R. (2013).** An overview of Fukushima radionuclides measured in the northern hemisphere. Science of the Total Environment, 458, 577-613.

**Thanabalasingam, P., Pickering, W.F. (1990).** Specific sorption of antimony (III) by the hydrous oxides of Mn, Fe, and Al. Water, Air, Soil Pollution, 49, 175– 185.

**Thébault, H., Rodríguez y Baena, A. M., Andral, B., Barisic, D., Albaladejo, J. B., Bologa, A. S., et al. (2008).** $^{137}$Cs baseline levels in the Mediterranean and Black Sea: a cross-basin survey of the CIESM Mediterranean Mussel Watch programme. Marine Pollution Bulletin, 57(6-12), 801-806.

**Thomson S. (1926).** Antimonyall Cupps: Pocula Emetica or Calices Vomitorii. British Medical J. 1 (no 3406, April 10th, 1926) 669-671

**Tian, H., Zhou, J., Zhu, C., Zhao, D., Gao, J., Hao, J., et al. (2014).** A comprehensive global inventory of atmospheric antimony emissions from anthropogenic activities, 1995–2010. Environmental Science and Technology, 48(17), 10235-10241.

**Tighe, M., Lockwood, P. (2007).** The importance of non-crystalline hydroxide phases in sequential extractions to fractionate antimony in acid soils. Communications in Soil Science and Plant Analysis, 38, 1487–1501.

**Tighe, M., Lockwood, P., Wilson, S. (2005).** Adsorption of antimony (V) by floodplain soils, amorphous iron (III) hydroxide and humic acid. Journal of Environmental Monitoring, 7, 1177–1185.

**Tipping, E., Hetherington, N.B., Hilton, J., Thompson, D.W., Bowles, E., Hamilton-Taylor, J. (1985).** Artefacts in the use of selective chemical extraction to determine distributions of metals between oxides of manganese and iron. Analytical Chemistry, 57(9), 1944-1946.

**Tschan, M., Robinson, B.H., Schulin, R. (2009**). Antimony in the soil-plant system – a review. Environmental Chemistry, 6(2), 106-115.

**Tsumune, D., Tsubono, T., Aoyama, M., Uematsu, M., Misumi, K., Maeda, Y., Yoshida, Y., Hayami, H. (2013).** One-year, regional-scale simulation of $^{137}$Cs radioactivity in the ocean following the Fukushima Daiichi Nuclear Power Plant accident. Biogeosciences Discussions, 10(4).

**Turner, R. J., Borghese, R., Zannoni, D. (2012).** Microbial processing of tellurium as a tool in biotechnology. Biotechnology Advances, 30(5), 954-963.

**Turner, R.J., Weiner, J.H., Taylor, D.E. (1999).** Tellurite-mediated thiol oxidation in *Escherichia coli*. Microbiology, 145(9), 2549-2557.

# U

**Uchida, S., Tagami, K. (2017).** Comparison of coastal area sediment-seawater distribution coefficients (Kd) of stable and radioactive Sr and Cs. Applied Geochemistry, 85, 148-153.

**Uddin, M. S., Hermanne, A., Sudár, S., Aslam, M. N., Scholten, B., Coenen, H. H., Qaim, S. M. (2011).** Excitation functions of α-particle induced reactions on enriched $^{123}$Sb and $^{nat}$Sb for production of $^{124}$I. Applied Radiation and Isotopes, 69(4), 699-704.

**UiO Chemical Institute.**
**<**https://www.mn.uio.no/kjemi/forskning/grupper/miljovitenskap/miljovitenskapbloggen/tokamak.html> Last accessed on the 16/09/18.

**Ungureanu, G., Santos, S., Boaventura, R., Botelho, C. (2015).** Arsenic and antimony in water and wastewater: overview of removal techniques with special reference to latest advances in adsorption. Journal of Environmental Management, 151, 326-342.

**United Nations Scientific Committee on the Effects of Atomic Radiation (UNSCEAR, 2008)**. Sources and effects of ionizing radiation. Report Vol. I: sources. United Nations publications, New York.

**Ure, A. M., Quevauviller, P., Muntau, H., Griepink, B. (1993).** Speciation of heavy metals in soils and sediments. An account of the improvement and harmonization of extraction techniques undertaken under the auspices of the BCR of the Commission of the European Communities. International journal of environmental analytical chemistry, 51(1-4), 135-151.

**U.S. Environmental Protection Agency (1999).** Integrated Risk Information System (IRIS) on Antimony. National Center for Environmental Assessment, Office of Research and Development, Washington, DC.

**U.S. Environmental Protection Agency (2000).** Methods for measuring the toxicity and bioaccumulation of sediment-associated contaminants with freshwater invertebrates. Second edition. EPA 600/R-99/064

**U.S. Environmental Protection Agency (Revised in 2007).** Determination of Trace Metals By SW-846. Method 6020A. Inductively Coupled Plasma-Mass Spectrometry. EPA, Connecticut.

**U.S. Geological Survey (2014).** Antimony statistics, in Kelly, T.D., and Matos, G.R., comps., Historical statistics for mineral and material commodities in the United States: U.S. Geological Survey Data Series 140, accessed [18/08/18], at http://minerals.usgs.gov/minerals/pubs/historical-statistics/.

**U.S. Geological Survey (2018).** Antimony. By Kateryna Klochko, In U.S. Geological Survey Mineral Commodity Summaries, January 2018. <https://minerals.usgs.gov/minerals/pubs/commodity/antimony/> Last accessed on the 25/09/18

**U.S. Geological Survey (2018).** Tellurium. By C. Schuyler Anderson, In U.S. Geological Survey Mineral Commodity Summaries, January 2018. <https://minerals.usgs.gov/minerals/pubs/commodity/selenium/> Last accessed on the 25/09/18

# V

**van den Berg, C. M. G., Khan, S. H., Daly, P. J., Riley, J. P., Turner, D. R. (1991).** An electrochemical study of Ni, Sb, Se, Sn, U and V in the estuary of the Tamar. Estuarine, Coastal and Shelf Science, 33(3), 309-322.

**van der Sloot, H. A., Hoede, D., Wijkstra, J., Duinker, J. C., Nolting, R. F. (1985).** Anionic species of V, As, Se, Mo, Sb, Te and W in the Scheldt and Rhine estuaries and the Southern Bight (North Sea). Estuarine, Coastal and Shelf Science, 21(5), 633-651.

**Vernon, R. (1976).** Oil Crisis. United States.

**Vink, B.W. (1996).** Stability relations of antimony and arsenic compounds in the light of revised and extended Eh-pH diagrams. Chemical Geology, 130(1-2), 21-30.

**Viñas, P., Lopez-Garcia, I., Merino-Merono, B., Hernandez-Cordoba, M. (2005).** Ion chromatography-hydride generation-atomic fluorescence spectrometry speciation of tellurium. Applied Organometallic Chemistry, 19 (8): 930-934.

**Vojteková, V., Poperníková, Z., Abusenaina, A.M.M. (2014).** Antimón v rôznych zložkách životného prostredia. Chemické listy, 108, 125-140.

# W

**Walbran, B.B., Robins, E. (1978).** Effects of central nervous system accumulation of tellurium on behavior in rats. Pharmacology Biochemistry and Behavior, 9(3), 297-300.

**Walling, D.E., Webb, D.W. (1985).** Estimating the discharge of contaminants to coastal waters by rivers. Marine Pollution Bulletin, 16,488 - 492.

**Wallschläger, D., Feldmann, J. (2010).** 10: Formation, Occurrence, Significance, and Analysis of Organoselenium and Organotellurium Compounds in the Environment. In Organometallics in environment and toxicology (pp. 319-364).

**Walter H. Adey and Karen Loveland (2007).** CHAPTER 6 - The Input of Organic Energy: Particulates and Feeding, In Dynamic Aquaria (Third Edition), Academic Press, London, Pages 93-100

**Wang, S. (2011).** Tellurium, its resourcefulness and recovery. JOM, 63(8), 90.

**Wang, X., Guan, W. (2012).** Large-scale synthesis of flower-like Te nanocrystals with uniform branches by a surfactant-assisted method. Nanoscience Methods, 1(1), 86-92.

**Webb, B.W., Phillips, J.M., Walling, D.E., Littlewood, I.G., Watts, C., Leeks, G.J.L. (1997).** Load estimation methodologies for British river and their relevance to the LOIS RACS (R) program. Science of the Total Environment 194, 379-389.

**Weber, G. (1985).** The importance of tin in the environment and its determination at trace levels. Die Bedeutung des Zinns in der Umwelt und seine Bestimmung im Spurenbereich. Fresenius' Zeitschrift für Analytische Chemie, 321(3), 217-224.

**Weber, T. W., Chakravorti, R. K. (1974).** Pore and solid diffusion models for fixed-bed adsorbers. AIChE Journal, 20(2), 228-238.

**Wedepohl, K.H. (1995).** The composition of the continental crust. Geochimica et Cosmochimica Acta, 59, 1217–1232.

**Wehmeier, S., Raab, A., Feldmann, J. (2004).** Investigations into the role of methylcobalamin and glutathione for the methylation of antimony using isotopically enriched antimony (V). Applied Organometallic Chemistry, 18(12), 631-639.

**Wenzel, W.W., Kirchbaumer, N., Prohaska, T., Stingeder, G., Lombi, E., Adriano, D.C. (2001).** Arsenic fractionation in soils using an improved sequential extraction procedure. Analytica Chimica Acta, 436(2), 309-323.

**Whitehead, N.E., Ballestra, S., Holm, E., Huynh-Ngoc, L. (1988).** Chernobyl radionuclides in shellfish. Journal of Environmental Radioactivity, 7, 107-121.

**Wilson, S. C., Lockwood, P. V., Ashley, P. M., Tighe, M. (2010).** The chemistry and behaviour of antimony in the soil environment with comparisons to arsenic: a critical review. Environmental Pollution, 158(5), 1169-1181.

**Wilson, N., Webster-Brown, J. (2009).** The fate of antimony in a major lowland river system, the Waikato River, New Zealand. Applied Geochemistry, 24, 2283-2292.

**World Health Organization (2003).** Antimony in Drinking-water, Background document for development of WHO Guidelines for Drinking-water Quality. <http://www.who.int/water_sanitation_health/dwq/chemicals/antimony.pdf> Last accessed on the 10/07/2015

**World Nuclear Association (WNA, 2015).** WNA Library. <http://www.world-nuclear.org/Information-Library/> Last accessed on the 10/02/15

**World Nuclear Association (WNA 2018).** Nuclear Power in France. <http://www.world-nuclear.org/information-library/country-profiles/countries-a-f/france.aspx> Last accessed on the 26/05/2018

**World Nuclear Association (WNA 2018).** Nuclear radiation and Health effects. < http://www.world-nuclear.org/information-library/safety-and-security/radiation-and-health/nuclear-radiation-and-health-effects.aspx> Last accessed on the 04/08/2018.

**World Nuclear Association (WNA 2018).** Nuclear Power Reactors. <http://www.world-nuclear.org/information-library/nuclear-fuel-cycle/nuclear-power-reactors/nuclear-power-reactors.aspx> Last accessed on the 23/09/2018.

**World Nuclear Association (WNA 2018).** Chernobyl accident. <http://www.world-nuclear.org/information-library/safety-and-security/safety-of-plants/chernobyl-accident.aspx> Last accessed on the 05/08/2018.

**Wu, X., Song, J., Li, X. (2014).** Occurrence and distribution of dissolved tellurium in Changjiang River estuary. Chinese Journal of Oceanology and Limnology, 32(2), 444-454.

# X

**Xi, J., He, M., Lin, C. (2009).** Adsorption of antimony(V) on kaolinite as a function of pH, ionic strength and humic acid. Environmental Earth Sciences, 60, 715-722.

**Xi, J., He, M., Lin, C. (2011).** Adsorption of antimony(III) and antimony(V) on bentonite: kinetics, thermodynamics and anion competition. Microchemical Journal, 97,85-91.

# Y

**Yaffe, L., Day, A. E., Greer, B. A. (1953).** The Fission Yield of $Te^{134}$. Canadian Journal of Chemistry, 31(1), 48-54.

**Yamada, A., Miyagishima, N., Matsunaga, T. (1997).** Tellurite removal by marine photosynthetic bacteria. Journal of Marine Biotechnology, 5, 46-49.

**Yang, G., Pointeau, V., Tevissen, E., Chagnes, A. (2017).** A review on clogging of recirculating steam generators in Pressurized-Water Reactors. Progress in Nuclear Energy, 97, 182-196.

**Ylipieti, J., Rissanen, K., Kostiainen, E., Salminen, R., Tomilina, O., Täht, K., Gilucis, A., Gregorauskiene, V. (2008).** Chernobyl fallout in the uppermost (0–3 cm) humus layer of forest soil in Finland, North East Russia and the Baltic countries in 2000–2003. Science of the Total Environment, 407(1), 315-323.

**Yoon, B. M., Shim, S. C., Pyun, H. C., Lee, D. S. (1990).** Hydride generation atomic absorption determination of tellurium species in environmental samples with in situ concentration in a graphite furnace. Analytical Sciences, 6(4), 561-566.

**Yuan, G., Li, Y., Bao, N., Miao, J., Ge, C., Wang, Y. (2014).** Facile synthesis and thermoelectric studies of n-type bismuth telluride nanorods with cathodic stripping Te electrode. Materials Chemistry and Physics, 143(2), 587-594.

# Z

**Zangi, R., Filella, M. (2012).** Transport routes of metalloids into and out of the cell: a review of the current knowledge. Chemico-Biological Interactions, 197(1), 47-57.

**Zayed, J., Philippe, S. (2009).** Acute oral and inhalation toxicities in rats with cadmium telluride. International Journal of Toxicology, 28(4), 259-265.

**Zeien, H.U., Brümmer, G.W. (1989).** Chemische Extraktionen zur Bestimmung von Schwermetallbildungformen in Boden. Mitt. Dtsch. Bodenk. Gesell., 59, 505-510.

**Zeldowitsch, J. (1934).** Adsorption site energy distribution. Acta Physicochimica URSS, 1, 961-973.

**Zeng, C., Ramos-Ruiz, A., Field, J. A., Sierra-Alvarez, R. (2015).** Cadmium telluride (CdTe) and cadmium selenide (CdSe) leaching behavior and surface chemistry in response to pH and $O_2$. Journal of Environmental Management, 154, 78-85.

**Zhang, L. S., Combs, S. M. (1996).** Using the installed spray chamber as a gas-liquid separator for the determination of germanium, arsenic, selenium, tin, antimony, tellurium and bismuth by hydride generation inductively coupled plasma mass spectrometry. Journal of Analytical Atomic Spectrometry, 11(11), 1043-1048.

**Zhou, Y., Li, L., Tan, Q., Li, J. F. (2014).** Thermoelectric properties of Pb-doped bismuth telluride thin films deposited by magnetron sputtering. Journal of Alloys and Compounds, 590, 362-367.

**Zhou, Q., Maurice, P. A., Cabaniss, S. E. (2001).** Size fractionation upon adsorption of fulvic acid on goethite: Equilibrium and kinetic studies. Geochimica et Cosmochimica Acta, 65(5), 803-812.

# SCIENTIFIC PRODUCTION

## PUBLICATIONS

### *Published/accepted:*

1. **Gil-Díaz T**., Schäfer J., Pougnet F., Abdou M., Dutruch L., Eyrolle-Boyer F., Coynel A., Blanc G. (2016). Distribution and geochemical behaviour of antimony in the Gironde Estuary: A first qualitative approach to regional nuclear accident scenarios. Marine Chemistry, 185: 65 – 73

2. **Gil-Díaz T**., Schäfer J., Coynel A., Bossy C., Dutruch L., Blanc G. (2018). Antimony in the Lot-Garonne River system: A fourteen-year record of solid/liquid partitioning and fluxes. Environmental Chemistry, *in press* (DOI:10.1071/EN17188)

3. **Gil-Díaz T.,** Schäfer J., Dutruch L., Bossy C., Pougnet F., Abdou M., Lerat-Hardy A., Pereto C., Derriennic H., Briant N., Sireau T., Knoery J., Blanc G. Tellurium behaviour in a major European fluvial-estuarine system (Gironde, France): fluxes, solid/liquid partitioning, and bioaccumulation in wild oysters. Environmental Chemistry, *in press* (DOI: 10.1071/EN18226)

### *To be submitted:*

1. **Gil-Díaz T.**, Schäfer J., Filella M., Dutruch L., Bossy C.. Fractionation of inherited and spiked antimony (Sb) in fluvial/estuarine bulk sediments : unexpected anomalies in parallel selective extraction protocols. *To be submitted to Applied Geochemistry*

2. **Gil-Díaz T.**, Schäfer J., Keller V., Eiche E., Dutruch L., Möβner C., Lenz M., Eyrolle-Boyer F. Tellurium and selenium sorption kinetics and solid fractionation under contrasting estuarine salinity and turbidity conditions. *To be submitted to Applied Geochemistry*

3. **Gil-Díaz T.,** Heberling F., Eiche E., Fuss M., Böttle M., Keller V., Schäfer J. Tin-113 and Selenium-75 radiotracer adsorption and desorption kinetics in contrasting estuarine salinity and turbidity conditions. *To be submitted to Journal of Environmental Radioactivity*

## ORAL PRESENTATIONS IN INTERNATIONAL CONFERENCES (5)

**2017** **Gil-Díaz T.**, Keller V., Schäfer J., Eiche E., Mößner C., Pougnet F., Dutruch L., Bossy C., Coynel A., Blanc G.Preliminary results on estuarine Te reactivity: application for potential Te radionuclide environmental dispersion scenarios in the Gironde Estuary (France). 27th Goldschmidt, 13 – 18th August 2017, Paris (France).

**Gil-Díaz T.**, Schäfer J., Eyrolle-Boyer F., Pougnet F., Abdou M., Coynel A., Dutruch L., Bossy C., Derriennic H., Blanc G. Temporal coupling of radioactive dispersion and estuarine processes: case study of a multielement radionuclide accidental release in the Gironde Estuary (France). 14th International Estuarine Biogeochemistry Symposium (IEBS), 4 – 7th June 2017, Rimouski (Canada). *Price of excellence to student oral communication*.

**Gil-Díaz T.**, Schäfer J., Eiche E., Möβner C., Eyrolle-Boyer F., Coynel A., Blanc G. Tellurium (Te) reactivity in estuarine gradients and implications for accidental radionuclide release scenarios. 1st Workshop on Environmental Concentrations, Cycling and Modeling of Technology Critical Elements (COST ACTION TD 1407), 18-19th January, Rehovot (Israel).

**2016** **Gil-Díaz T.,** Schäfer J., Hu R., Pougnet F., Bossy C., Dutruch L., Derriennic H., Filella M., Blanc G. Effects of selective extraction schemes on redox-sensitive Sb: implications for environmental quantitative Sb radionuclide dispersion scenarios. 18th International Conference on Heavy Metals in the Environment (ICHMET), 12-15th September 2016, Ghent (Belgium).

**Gil-Díaz T.**, Schäfer J., Pougnet F., Husson A., Dutruch L., Eyrolle-Boyer F., Coynel A., Gardes T., Bossy C., Blanc G. A preliminary approach to multiple radionuclide NPP accidental release and dispersion in the Gironde Estuary (France). 32nd International Conference on Environmental Geochemistry and Health (SEGH), 4-8th July 2016, Brussels (Belgium)

## POSTER PRESENTATIONS IN INTERNATIONAL CONFERENCES (7)

**2018** **Gil-Díaz T.**, Schäfer J., Dutruch L., Keller V., Eiche E., Mößner C., Lenz M., Abdou M., Gardes T., Rementeria A., Zaldibar B., Eyrolle-Boyer F. Tellurium and selenium reactivity in estuarine gradients and bioaccumulation in wild oysters. Workshop on Technology Critical Elements in exosystem and human health (COST ACTION TD 1407), 19-20th April 2018, Tallinn (Estonia).

**2017** **Gil-Díaz T**., Keller V., Schäfer J., Eiche E., Mößner C., Pougnet F., Dutruch L., Bossy C., Coynel A., Blanc G. Tellurium environmental behaviour at the continent-ocean interface: preliminary scenarios for hypothetical radionuclide releases. 27th Goldschmidt, 13 – 18th August 2017, Paris (France).

**2016** Gardes T., **Gil-Díaz T.**, Schäfer J., Pougnet F., Abdou M., Coynel A., Bossy C., Dutruch L., Husson A., Derriennic H., Blanc G. Behaviour of inorganic tin along the Gironde fluvial-estuarine continuum: implications for dispersion and fate scenarios of accidental radionuclide release. 32nd International Conference on Environmental Geochemistry and Health (SEGH), 4 – 8th July 2016, Brussels (Belgium).

**Gil-Díaz T.**, Schäfer J., Pougnet F., Husson A., Bossy C., Dutruch L., Derriennic H., Coynel A., Blanc G. Antimony diagenetic implications for radionuclide accidental release scenarios in the Gironde Estuary (France). 15th International Symposium on Oceanography of the Bay of Biscay (ISOBAY 15), 22-24th June 2016, Bilbao (Spain).

**Gil-Díaz T.**, Schäfer J., Pougnet F., Abdou M., Dutruch L., Eyrolle-Boyer F., Coynel A. Antimony fate modelling approach for regional nuclear risk assessment. SETAC Europe 26th Annual Meeting, 22 – 26th May 2016, Nantes (France).

**2015** **Gil-Díaz T.**, Makni L., Schäfer J., Pougnet F., Abdou M., Mikolaczyk M., Petit J.C.J., Coynel A., Dutruch L., Bossy C., Husson A., Chiffoleau J.-F., Derriennic H., Blanc G. Inorganic antimony in the Gironde fluvial-estuarine continuum and bioaccumulation in wild oysters

at the estuary mouth: a preliminary approach to the fate of regional accidental radionuclide releases. 3rd International Workshop on Antimony in the Environment, 6 – 9th October 2015, Leipzig (Germany).

**Gil-Díaz T.**, Makni L., Schäfer J., Pougnet F., Abdou M., Mikolaczyk M., Coynel A., Dutruch L., Bossy C., Husson A., Derriennic H., Blanc G. Spatiotemporal distribution of dissolved and particulate inorganic antimony along the Gironde fluvial-estuarine continuum: a preliminary approach to regional nuclear accident scenarios. 13th International Estuarine Biogeochemistry Symposium (IEBS), 7 – 10th June 2015, Bordeaux (France).

## INVITED ORAL PRESENTATIONS AND DISSEMINATION ACTIVITIES (9)

**2018** **Object: Invited scientific communication at the Swiss Federal Institute of Aquatic Science and Technology (EAWAG)**

**Talk:** Geochemical behaviour of Sb and Te in transition waters: an approach to Sb and Te radionuclide dispersal scenarios in case of accidental nuclear power plant releases
**Place:** seminar room at EAWAG (Zürich, Switzerland)
**Date:** 3rd October 2018

**Object: Seminars 2017/2018 from the Institute for Nuclear Waste Disposal (KIT INE)**

**Talk:** Geochemical behaviour of Sn, Sb, Se and Te in transition waters: an approach to Sn, Sb, Se and Te radionuclide dispersal scenarios in case of accidental nuclear power plant releases
**Place:** seminarraum, Bau 714, KIT (Karlsruhe, Germany)
**Date:** 9th August 2018

**Object: "Sciences et Environnements" Doctoral School's PhD Day (JDED – EDSE)**

**Talk:** Tellurium and selenium reactivity in estuarine gradients and bioaccumulation in wild oysters (*poster communication*)
**Place:** Le Haut Carré Agora (Talence, France)
**Date:** 2-3rd May 2017

**Object: Day of Scientific Exchange at EPOC Laboratory (JEST)**

**Talk:** Selenium and Tellurium environmental behaviour at the continent-ocean interface: preliminary scenarios for hypothetical radionuclide releases (*poster communication*)
**Place:** Seminar room at Meriadeck (Bordeaux, France)
**Date:** 5-6th April 2018

**2017** **Object: Science Fair (Open House Day)**

**Talk:** Metals used in energy production: consequences in the aquatic environment (*french oral communication*)
**Place:** Arcachon Marine Station (Arcachon, France)
**Date:** 7th October 2017

**Object: Day of Scientific Exchange at EPOC Laboratory (JEST)**

**Talk:** Preliminary approach to radionuclide dispersion scenarios from potential accidental releases in the Gironde Estuary (case study of Sb) (*french oral communication*)
**Place:** Seminar room at the Casino of Arcachon (Arcachon, France)
**Date:** 3-4th May 2017

**Object: Invited scientific communication for the Marine Research Axis to the 4th meeting of the AMORAD Project**

**Talk:** Preliminary approach to Sb radionuclide accidental releases and dispersion in the Gironde Estuary
**Place:** Fontenay-aux-Roses, Paris (France)
**Date:** 10th February 2017

2016

**Object: Mineralogy/Geochemistry Seminars 2016/2017 from the Applied Geosciences Institute (KIT)**

**Talk:** Scenarios on the behaviour of multiple radionuclides (Sn, Sb, Se, Te) in the Gironde Estuary (France) in case of Nuclear Power Plant accidental release – a preliminary approach
**Place:** room 157, Geb. 50.40, KIT (Karlsruhe, Germany)
**Date:** 11th November 2016

**Object: Marine Research Axis meeting (AMORAD Project)**

**Talk:** Avancements sur les scénarios du devenir de rejets accidentels de radionucléides dans l'interface continent-océan (*french oral communication*)
**Place:** Fontenay-aux-Roses, Paris (France)
**Date:** 11-12th October 2016

## CO-SUPERVISION OF STUDENT RESEARCH PROJECTS (7)

2018

**Madhushri Varunji (Master 1)**. Introduction to Research Internship on environmental trace metals at continent-ocean interfaces. Master in Marine Environment and Resources (MER), University of Bordeaux, France (8 – 26th January, 2018)

2017

**Jean-Baptiste Kucharski (Master 1)**. Extractions sélectives des oxydes de Fe et Mn : comportement environnemental ou dépendance du protocole ? Master en Sciences de la Mer, University of Bordeaux, France (May - June, 2017)

**Virginia Keller (L3)**. Behaviour of Selenium and Tellurium along saline gradients in estuaries – case study Gironde (« Verhalten von Selen und Tellur entlang saliner Gradienten im Ästuar – Fallbeispiel Gironde »). Bachelor thesis in Geoecology (B.Sc.), Institute of Applied Geosciences, Karlsruhe (Germany) July 2017. *Bachelor (3rd year) research internship at UBx (March-April 2017) in collaboration with the Karlsruhe Institute of Technology (KIT).*

**2016**

**Rouyu Hu (Master 1)**. Introduction to Research Internship on selective extractions of Sb from fluvial and estuarine particles. Master in Marine Environment and Resources (MER), University of Bordeaux, France (January 2016)

**Sarker Mohammed Khalil Ibrahim (Master 1).** Introduction to Research Internship on adsorption kinetics of Te on estuarine particles. Master in Marine Environment and Resources (MER), University of Bordeaux, France (January 2016)

**Thomas Gardes (Master 2).** Comportement biogéochimique de l'étain inorganique dans le continuum Lot-Garonne-Gironde : Première approximation du devenir de rejets accidentels de radionucléides des centrales nucléaires. Thèse de Master en STEE, Spécialité Océanographie, Parcours Enregistrement sédimentaire et Paléoclimat. University of Bordeaux, France (February - June, 2016)

**2015**

**Linda Makni (Master 1)**. Comportement et bioaccumulation de l'antimoine inorganique dans l'estuaire de la Gironde: première approximation du devenir de rejets accidentels de radionucléides. Thèse de Master en Géosciences, Spécialité Dynamique Terrestre et Risques Naturels. Université de Montpellier, Montpellier, France (May - June, 2015)

*“Never take things for granted”*

*FGC*